AUGUST 1978

analytical chemistry

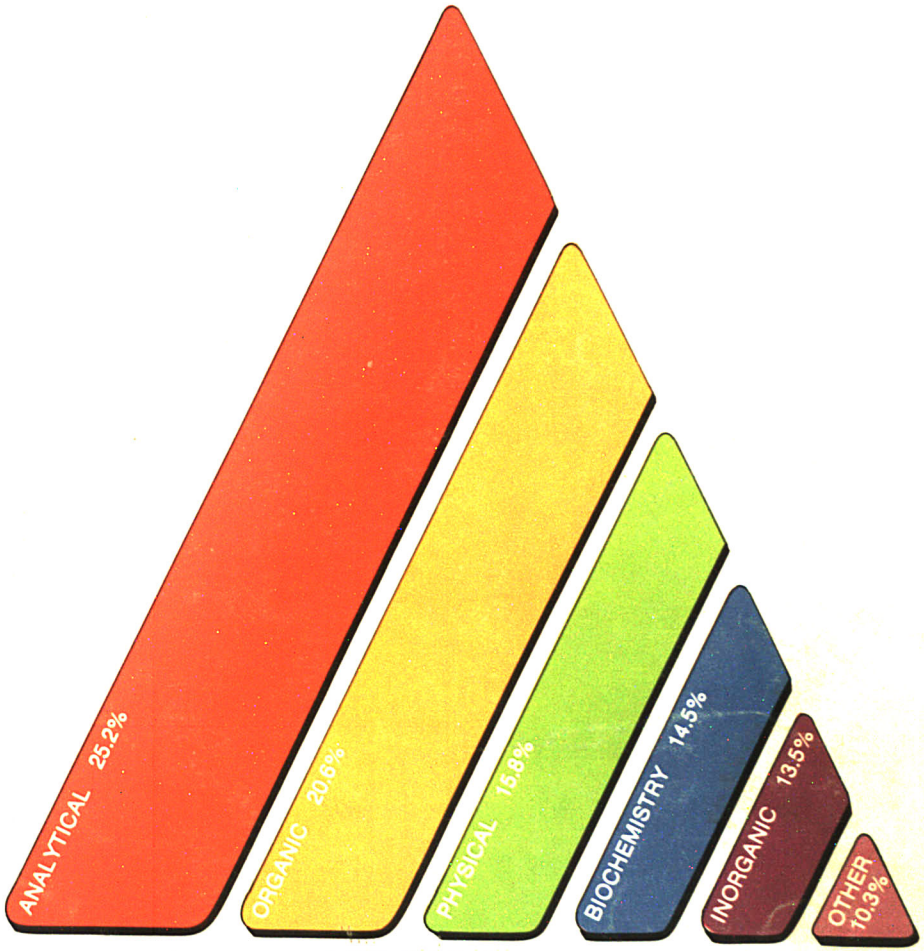

Academic Chemistry Job Openings in 1978

New Omniscribe® Series B-5000

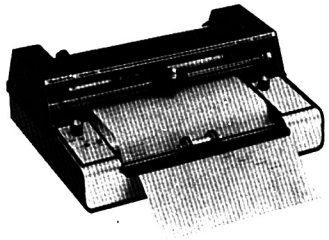

from
$395*
Single Pen
$645*
Dual Pen
*U.S. Domestic Price Only

One and Two Pen 10" Strip Chart Recorders

- Self-aligning sprocketless paper drive
- Non-contact feed back element
- 6 switch selectable chart speeds, field adjustable for Eng/Met scaling
- Over 160 models to select from

*A registered trademark of Houston Instrument

houston instrument | DIVISION OF BAUSCH & LOMB
"the recorder company"

CIRCLE 97 ON READER SERVICE CARD

Optimize performance with Houston Instrument modular flexibility

Omnigraphic® Model 2000
X-Y Recorder

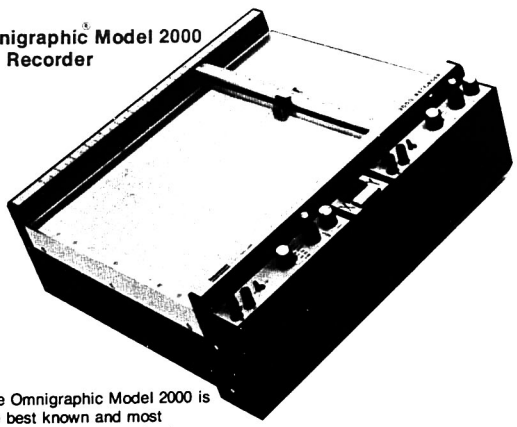

The Omnigraphic Model 2000 is the best known and most versatile X-Y recorder in the world. It outperforms all others and still beats their price. If you're looking at X-Y's, consider these Omnigraphic features.

- 11" X 17" or 8½" X 11"
- 30 in/sec speed (40 in/sec available)
- ±0.2% accuracy
- Best common mode rejection
- Same servo response on both axes
- Best price/performance available
- Prices from $950*

Send for free "Designer's Choice" catalog today.

*Registered trademark of Houston Instrument

*U.S. Domestic Price only

houston instrument | DIVISION OF BAUSCH & LOMB
ONE HOUSTON SQUARE
(512) 837-2820
AUSTIN, TEXAS 78753
TWX 910-874-2022
EUROPEAN HEADQUARTERS Rochesterlaan 6 B240 Gistel Belgium Phone 059/277446 Telex Bausch 81388
"the recorder company"

Point plot, record log of signal, and many other functions with the Model 3000 Omnigraphic® strip chart recorder.

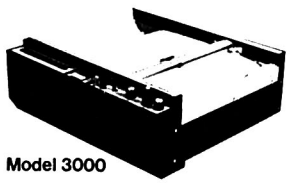

Model 3000

- 16 different input modules
- Wide speed range, push button selectable
- 1 or 2 pen models
- Rack mount available
- Prices start at $990*

Send for free literature

*A registered trademark of Houston Instrument
*U.S Domestic Price only

houston instrument | DIVISION OF BAUSCH & LOMB
"the recorder company"

For rush literature requests or local sales office information only, persons outside Texas call toll free 1-800-231-5205

CIRCLE 98 ON READER SERVICE CARD

CIRCLE 99 ON READER SERVICE CARD

Visit us at Booth 1010 at the WESCON Show

TOC in water to a precision of ±10 parts per BILLION?

Yes. [And find it FAST]

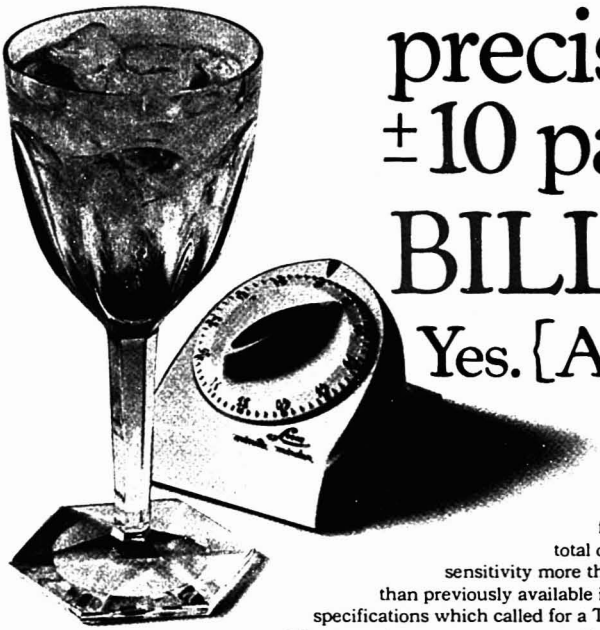

Developed in response to EPA's public proposal Ci-76-0923, the field-proven Dohrmann* DC-54 total organic carbon analyzer provides sensitivity more than an order of magnitude higher than previously available instruments. It exceeds the EPA specifications which called for a TOC analyzer with ±10 ppb precision while preserving response to purgeables.*

These characteristics make the DC-54 ultra-low-level TOC analyzer ideally suited for drinking water analysis.

Existing DC-50 and DC-52 TOC analyzers can be readily converted to these specifications by merely adding the sampling module and accessories of the DC-54.

The DC-54 uses the proven methodology of ultraviolet promoted chemical oxidation followed by reduction to methane and flame ionization detection. Analysis time is less than 9 minutes. The range of the DC-54 is 0 to 10,000 ppb (μg C-litre).

Remember Dohrmann does it all—from drinking water to waste water. And we support you with a Dohrmann field sales and service staff, factory-trained and dedicated to your needs.

Call Leon Hiam to find out more. To receive literature, write or circle the reader service number below.

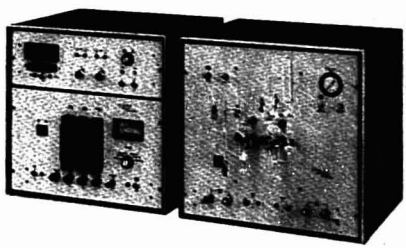

*Cited as the method for organic carbon analysis in the Federal Register, EPA Interim Primary Drinking Water Regulations, Part II, Thursday, February 9, 1978, p. 5780, paragraph 141.55, Analytical Methods (6).

ENVIROTECH | **DOHRMANN**

3240 Scott Boulevard
Santa Clara, CA 95050

CALL TOLL FREE (800) 538-7708

In Alaska, California, Hawaii, Puerto Rico, call collect (408) 249-6000.

CIRCLE 51 ON READER SERVICE CARD

There are lots of good reasons to use Whatman Advanced Ion Exchange Celluloses for separations of nucleic acids, proteins, enzymes. Here are ten of them:

- **Faster Kinetics of Exchange.** Whatman microgranular AIEC's absorb 6.5 times more bovine serum albumin in 5 minutes than conventional DEAE cellulose. Desorb rapidly, thoroughly.
- **Higher Polyelectrolyte Capacity.** For example, Grade DE 52 absorbs approximately 500 mg of bovine serum albumin in 20 minutes.
- **Greater Accessibility of Exchange Sites.** With no loss of dimensional stability. Hence superior protein capacity and kinetics of adsorption.
- **Greater Uniformity of Substitution.** Greater than conventional ion exchange celluloses. Excellent reproducibility of results.
- **Uniform Charge Density.** Thus, greater protein loadings, sharper elution bonds, better selectivity.
- **Easier Handling, High Dimensional Stability.** Available wet (pre-swollen) or dry. Rigorous control of physical form.
- **Optimized Range.** DEAE (anion) or CM (cation). Both wet or dry, microgranular or fibrous. Select best form for the particular application.
- **Narrow Particle Size Range.** For easier column packing, better packed-column reproducibility, higher packing densities, more predictable flow rates.
- **Dependable Reproducibility.** Whatman AIEC's are always the same, batch-to-batch, so performance is predictable, reproducible.
- **Whatman Quality.** Painstaking, meticulous manufacture, rigorous quality control.

Whatman Advanced Ion Exchange Celluloses. At your laboratory supply dealer or from **Whatman Inc.** ■ 9 Bridewell Place, Clifton, New Jersey 07014 ■ (201) 777-4825

CIRCLE 234 ON READER SERVICE CARD

Whatman

Volume 50, No. 9, August 1978
ANCHAM
50(9) 815A–916A/1233–1408 (1978)
ISSN 0003-2700

Published monthly with review issue added in April and Laboratory Guide in August by the American Chemical Society, from 20th and Northampton Sts., Easton, Pa. 18042. Executive and Editorial headquarters, American Chemical Society. 1155 16th St. N.W., Washington, D.C. 20036 (202) 872-4600. Second class postage paid at Washington, D.C., and at additional mailing offices.

1978 Subscription prices—including surface postage

	1 yr	2 yr	3 yr
MEMBERS:			
Domestic	$10.00	$18.00	$25.00
Foreign	19.00	36.00	52.00
NONMEMBERS—PERSONAL:			
Domestic	14.00	26.00	38.00
Foreign	23.00	44.00	65.00
INSTITUTIONAL:			
Domestic	14.00	26.00	38.00
Canada	23.00	44.00	65.00
Other foreign	29.00	54.00	77.00

Airmail and air freight rates are available from Membership & Subscription Services, ACS, P.O. 3337, Columbus, Ohio 43210 (614) 421-7230.

New and renewal subscriptions should be sent with payment to the Office of the Controller at the ACS Washington address.

Subscription service inquiries and changes of address (include both old and new addresses with ZIP code and *recent mailing label*) should be directed to the ACS Columbus address noted above. Please allow six weeks for change of address to become effective.

Claims for missing numbers will not be allowed if loss was due to failure of notice of change of address to be received in the time specified; if claim is dated (a) North America: more than 90 days beyond issue date, (b) all other foreign: more than one year beyond issue date; or if the reason given is "missing from files".

Microfiche subscriptions are available at the same prices but are mailed first class domestic and airmail foreign. Inquiries and payments to Microform Program, ACS Washington address.

Single issues, current year, $3.00 except review issue and Labguide, $4.00; **back issues and volumes; microfilm editions** from volume 1 to present: *write or call* Special Issues Sales, ACS Washington address (202) 872-4365.

analytical chemistry

CONTENTS

Our cover illustrates data from an ACS survey. See Professor Laitinen's editorial, page 1233. For more information on analytical chemistry in academe, see REPORTS *on pages 849 A and 852 A*

Briefs

Determination of Lead in a Chloride Matrix with the Graphite Furnace 1234

Detection of less than 20 pg of lead in 1% $NaCl_2$ or $MgCl_2$ solutions is demonstrated after molybdenum coating of the graphite furnace tubes and adding NH_4NO_3 as a matrix modifier.

D. C. Manning and Walter Slavin,* The Perkin-Elmer Corporation, Norwalk, Conn. 06856 *Anal. Chem., 50 (1978)*

Determination of Silver in Precipitation by Furnace Atomic Absorption Spectrometry 1239

The determination of precipitable silver at levels down to 1×10^{-6} μg/mL is described. The method is accurate to better than ±20% for triplicate analyses.

J. D. Sheaffer and Gerald Mulvey, Department of Atmospheric Science, Colorado State University, Fort Collins, Colo. 80523, and **R. K. Skogerboe,*** Department of Chemistry, Colorado State University, Fort Collins, Colo. 80523 *Anal. Chem., 50 (1978)*

Chemiluminescence Fiber Optic Probe for Hydrogen Peroxide Based on the Luminol Reaction 1242

The detectability and response time of the CL fiber optic probe are significantly better than observed with enzyme electrodes. The detection limit is close to 10^{-6} M peroxide.

Thompson M. Freeman and W. Rudolf Seitz,* Department of Chemistry, University of New Hamsphire, Durham, N.H. 03824 *Anal. Chem., 50 (1978)*

Determination of Trace Amounts of Alkyls and Hydrides by Metastable Transfer Emission Spectrometry 1247

Metastable transfer emission spectrometry can detect gaseous alkyls and hydrides with sensitivities of less than 1 ppb.

D. G. Sutton,* J. E. Melzer, and G. A. Capelle, Aerophysics Laboratory, The Ivan A. Getting Laboratories, The Aerospace Corporation, El Segundo, Calif. 90245 *Anal. Chem., 50 (1978)*

Determination of Microgram Amounts of Some Transition Metals in Seawater by Methyl Isobutyl Ketone–Nitric Acid Successive Extraction and Flameless Atomic Absorption Spectrophotometry 1250

The detection limits for Ag, Cd, Cr, Cu, Fe, Ni, Pb, and Zn are 0.02, 0.003, 0.05, 0.05, 0.20, 0.10, 0.03, and 0.03 μg/L, respectively, with mean RSD ranging from 18 to 25%.

Tsu Kai Jan* and David R. Young, Southern California Coastal Water Research Project, El Segundo, Calif. 90245 *Anal. Chem., 50 (1978)*

Aluminum Determination by Atomic Emission Spectrometry with Calcium Atomization Inhibition Titration 1253

The calcium flame emission technique allows aluminum determination at less than 0.1 ppm with accuracy and precision of a few percent and sufficient specificity for many applications.

J. H. Liu and C. O. Huber,* Department of Chemistry, University of Wisconsin—Milwaukee, Milwaukee, Wis. 53201 *Anal. Chem., 50 (1978)*

Determination of Trace Metals by Microwave Plasma Spectrometry with an Atmospheric Pressure Helium Discharge 1257

A recently designed 2450-MHz resonant cavity for generating microwave-induced plasmas is evaluated for metallic element determinations.

Andrew T. Zander and Gary M. Hieftje,* Department of Chemistry, Indiana University, Bloomington, Ind. 47401 *Anal. Chem., 50 (1978)*

Quantitative Detection of Trace Impurities in Gases by Infrared Spectrometry of Cryogenic Solutions 1260

Improved sensitivity and specificity of infrared spectrometry is discussed as applied to the determination of trace impurities in various carrier or solvent gases.

Samuel M. Freund,* William B. Maier II, Redus F. Holland, and Willard H. Beattie, University of California, Los Alamos Scientific Laboratory, P.O. Box 1663, Los Alamos, N.M. 87545 *Anal. Chem., 50 (1978)*

Photoacoustic Spectroscopy Applied to Systems Involving Photoinduced Gas Evolution or Consumption 1262

Systems studied include oxygen consumption in the photooxidation of rubrene and gas evolution in the heterogeneous photocatalytic oxidation of acetic acid.

Robert C. Gray and Allen J. Bard,* Department of Chemistry, The University of Texas at Austin, Austin, Tex. 78712 *Anal. Chem., 50 (1978)*

X-ray Microanalysis of a Natural Mordenite-Containing Rock and Its Ion-Exchange Derivatives 1265

The chemical composition of natural mordenite and its ion-exchange derivatives are determined by X-ray microanalysis. Crystal particles smaller than 0.5 μm are used.

János Papp,* Erzsébet Czárán, and András Jánossy, Central Research Institute for Chemistry of the Hungarian Academy of Sciences, P.O. Box 17, 1525 Budapest, Hungary *Anal. Chem., 50 (1978)*

* Corresponding author.

ORION is ready to prove which pH electrode is all wet.

You've been hearing about the advantages of our gel-filled, epoxy body, pH electrode: No messy refilling with KCl. Unbreakable in normal use. Plus the fast, stable response you demand in pH measurements.

Now along comes "Ol' Thirsty". Claims the wet way is the best way - that "refreshable" electrodes are faster and more stable. Who to believe?

We think talk is cheap; it's performance that counts. That's why we've come up with a no-risk offer that will let you prove to yourself which is the better electrode. In the real world of your laboratory. In your samples. With your pH meter.

Here's our offer. Call your laboratory supply dealer and order one of our 91-05 combination pH electrodes. It fits most Beckman, Corning, and ORION meters. Check our electrode's performance for thirty days against the "thirsty" one you now use - even if it cost two or three times more than our $36 suggested list price. We're confident you'll get as good or better stability and speed of response with our electrode.

If we're wrong, send us your test results and the electrode by October 15, 1978. We'll refund your purchase price AND send you free one gallon of KCl to keep Ol' Thirsty on his feet.

Why put up with the mess of an electrode that's all wet? ORION GX series electrodes give you the convenience of a no-refill, no-break pH electrode, with no sacrifice in performance.

ORION RESEARCH

380 PUTNAM AVE., CAMBRIDGE, MA 02139 U.S.A.
Call us toll-free at (800) 225-1480

CIRCLE 157 ON READER SERVICE CARD

Briefs

Energy-Dispersive X-ray Spectrometric Analysis of Environmental Samples after Borate Fusion 1268

An automated fusion procedure for sample preparation is investigated to overcome particle-size and sample inhomogeneity effects in the analysis of environmental samples by energy-dispersive x-ray spectrometry.

P. A. Pella,* K. E. Lorber, and K. F. J. Heinrich, Institute for Materials Research, Analytical Chemistry Division, National Bureau of Standards, Washington, D.C. 20234

Anal. Chem., 50 (1978)

Calculated X-ray Diffraction Data and Quantitative X-ray Diffractometry 1272

An equation is given to relate k_{ij}, the quantitation constant, to the calculated XRD parameters, ASF_J and $I_{i,J}^{rel}$. A diffractometer constant, κ, is introducted to allow interlaboratory comparison of experimental $k_{i,J}$ values.

Stephen Altree-Williams, Division of Occupational Health and Radiation Control, Health Commission of New South Wales, P.O. Box 163, Lidcombe, Australia 2141 *Anal. Chem., 50 (1978)*

Resistive-Pulse Particle-Sizing Instrument 1275

A particle size analyzer is tested with seven latex standards. Diameter estimates have a mean relative standard deviation of 1.2%.

A. W. Venolia, Fruit and Vegetable Chemistry Laboratory, Science and Education Administration, U.S. Department of Agriculture, Pasadena, Calif. 91106 *Anal. Chem., 50 (1978)*

Isotopic Determination of Silver in Picomole Quantities by Surface Ionization Mass Spectrometry 1279

An anion exchange procedure for the quantitative separation of Ag from natural samples is described. The isotopic composition of picomole quantities of Ag is measured with a precision of 0.1%.

William R. Kelly,* Fouad Tera, and G. J. Wasserburg, The Lunatic Asylum of the Charles Arms Laboratory, Division of Geological and Planetary Sciences, California Institute of Technology, Pasadena, Calif. 91125 *Anal. Chem., 50 (1978)*

Characterization of Metal Surfaces by Secondary Ion Mass Spectrometry and X-ray Photoelectron Spectroscopy 1286

The behavior of clusters up to Ag_5^+ and In_4^+, ejected from polycrystalline Ag and In surfaces under low flux argon ion bombardment, is investigated.

R. W. Hewitt, A. T. Shepard, W. E. Baitinger, and Nicholas Winograd,* Department of Chemistry, Purdue University, West Lafayette, Ind. 47907, and **G. L. Ott and W. N. Delgass,** School of Chemical Engineering, Purdue University, West Lafayette, Ind. 47907 *Anal. Chem., 50 (1978)*

Effect of Argon Ion Bombardment on Metal Complexes and Oxides Studied by X-ray Photoelectron Spectroscopy 1290

Although most of the metal centers in the complexes and oxides are reduced, some are oxidized or exhibit no change depending upon the ligands and central metal atoms present.

Yoshio Umezawa and Charles N. Reilley,* Department of Chemistry, University of North Carolina, Chapel Hill, N.C. 27514 *Anal. Chem., 50 (1978)*

Standards for pH Measurements in Isotonic Saline Media of Ionic Strength $I = 0.16$ 1295 ■

Attempts to improve the measurement of pH in clinical media of ionic strength 0.16, based on a matching of liquid-junction potentials through a selection of new standard reference solutions, are described.

Roger G. Bates,* Carmen A. Vega, and D. R. White, Jr., Department of Chemistry, University of Florida, Gainesville, Fla. 32611 *Anal. Chem., 50 (1978)*

Differential Pulse Polarographic Determination of Molybdenum at Parts-per-Billion Levels 1300

The method is based on the electrochemical reduction of the complex, dioxobis(8-quinolinolato)molybdenum(VI).

Paula Bosserman and Donald T. Sawyer,* Department of Chemistry, University of California, Riverside, Calif. 92521, and **Albert L. Page,** Department of Soil and Environmental Sciences, University of California, Riverside, Calif. 92521

Anal. Chem., 50 (1978)

Differential Pulse Polarography of Phenylarsine Oxide 1303

The polarographic reduction of phenylarsine oxide is pH dependent. The detection limit of PAO is 10^{-8} M at pH 7.3 with a RSD of 1.7%, and a maximum sensitivity of 450 μA/mM.

J. H. Lowry,* R. B. Smart, and K. H. Mancy, Department of Environmental & Industrial Health, The Environmental Chemistry Laboratory, 2530 School of Public Health I, The University of Michigan, Ann Arbor, Mich. 48109 *Anal. Chem., 50 (1978)*

Determination of Ammonia and Other Nitrogen Compounds by Polarography 1309

The method is applied to water and brine samples and to the testing of reagent grade chemicals. Sensitivity is below 1 ppm.

J. D. McLean,* V. A. Stenger, R. E. Reim, M. W. Long, and T. A. Hiller, The Dow Chemical Company, Analytical Laboratories, Midland, Mich. 48640 *Anal. Chem., 50 (1978)*

■ Supplementary material available.

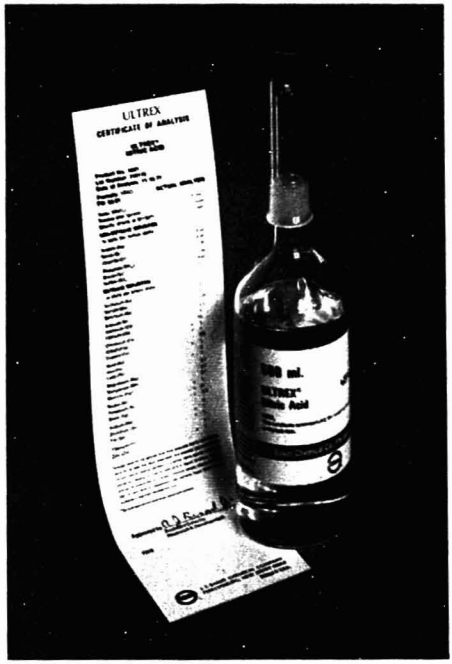

ULTREX®

Ultra-High Purity Acids

For Exacting Trace Element Analysis

Low blanks are essential for ultra-trace analysis. They permit the scientist to utilize the full sensitivity of his instrumentation. Chemists performing atomic absorption spectroscopy, for example, are facing problems of high blank values with increasing frequency. This need prompted the development of J. T. Baker's own advanced low blank acids. These ULTREX acids are produced and packaged in specially designed pre-leached containers, and offer **100% Metal Analysis** to identify and assure extremely low levels of key metallic impurities to meet the exacting needs of the trace element analyst.

Example: The specification for lead in reagent grade Nitric Acid is 200 ppb (parts per billion). J. T. Baker's ULTREX Nitric Acid had a lead content of less than 1 ppb . . . and the certificate of analysis provided lists lot values for more than 25 trace elements.

ULTREX acids

- Provide low blank values for metals
- Tested and controlled for the most common impurities, including a total metal analysis.
- Delivered with a certificate of analysis reporting actual analytical values.
- Analyzed according to the methods delineated in the certificate
- In stock — available for off-the-shelf delivery

For your exacting trace element analysis needs, consider the J. T. Baker line of ULTREX acids (acetic, hydrochloric, hydrofluoric, nitric, perchloric and sulfuric) providing reliable, superior alternative to in-house purification. For more information, contact:

J. T. Baker Chemical Co.
222 Red School Lane
Phillipsburg, New Jersey 08865
Telephone (201) 859-2151

CIRCLE 18 ON READER SERVICE CARD

Briefs

Electrocatalysis of Dihydronicotinamide Adenosine Diphosphate with Quinones and Modified Quinone Electrodes 1315

Dihydronicotinamide adenosine diphosphate is oxidized electrocatalytically by coupling to electrogenerated *o*-quinones, in solution or to the surface of a chemically modified quinone electrode.

Daniel Chi-Sing Tse and Theodore Kuwana,* Department of Chemistry, The Ohio State University, Columbus, Ohio 43210
Anal. Chem., 50 (1978)

Enzymatic Determination of Nitrate: Electrochemical Detection after Reduction with Nitrate Reductase and Nitrite Reductase 1319

The subsequent reduction of nitrate to ammonia is carried out by the dual-enzyme system nitrate and nitrite reductases. The detection range is 5×10^{-5}–1×10^{-2} M using an air-gap electrode to monitor the ammonia.

Chih-Hen Kiang, Shia S. Kuan, and George G. Guilbault,* Department of Chemistry, University of New Orleans, New Orleans, La. 70122
Anal. Chem., 50 (1978)

Enzymatic Determination of Nitrate: Fluorometric Detection after Reduction with Nitrate Reductase 1323

Nitrate is reduced by nitrate reductase with the subsequent oxidation of NADH to NAD^+. The rate of disappearance of NADH is monitored by fluorometry, with detection ranges from 50 ppb to 7.5 ppm.

Chih-Hen Kiang, Shia S. Kuan, and George G. Guilbault,* Department of Chemistry, University of New Orleans, New Orleans, La. 70122
Anal. Chem., 50 (1978)

Determination of Polypropylene Glycol Extracted from Polymers into Food-Simulating Solvents 1325

Combining the classical Zeisel alkoxyl reaction with high-efficiency GLC, the method is used to determine the amount and molecular weight of polypropylene glycol. All 1,2-oxypropylene compounds can be determined to 0.05 ppm.

Tore Ramstad,* T. J. Nestrick, and R. H. Stehl, Dow Chemical U.S.A., Midland, Mich. 48640
Anal. Chem., 50 (1978)

Preparation and Chromatographic Applications of an Amide Resin 1328

A new complexing resin containing a tertiary amide group is synthesized. It selectively retains U(VI), Th(IV), and Zr(IV) from an aqueous solution of pH 3.0, and Au(III) and Pd(II) from an HCl solution.

Gene M. Orf and James S. Fritz,* Ames Laboratory—U.S. Department of Energy and Department of Chemistry, Iowa State University, Ames, Iowa 50011
Anal. Chem., 50 (1978)

Characterization of the Ion-Exchange Membrane Detector for Liquid Chromatography and Its Application to the Separation of Quaternary Ammonium Compounds 1330

The detector has a useful linear range of 2.5 orders of magnitude, and a precision of better than 1% standard error.

John G. Dorsey, Mark S. Denton, and T. W. Gilbert,* Department of Chemistry, University of Cincinnati, Cincinnati, Ohio 45221
Anal. Chem., 50 (1978)

Evaluation of a Computer-Controlled Stopped-Flow System for Fundamental Kinetic Studies 1333

A computer-controlled stopped-flow instrument is used for a fully automated kinetic study of the Fe(III)-thiocyanate reaction and rate constants are evaluated for a proposed mechanism.

Glen E. Mieling and Harry L. Pardue,* Department of Chemistry, Purdue University, West Lafayette, Ind. 47907
Anal. Chem., 50 (1978)

In-Situ Chemically-Modified Surfaces for Normal-Phase Liquid Chromatography 1337

Three short-chainlength trichlorosilane modified silica gels are prepared by an in-situ process. Detailed investigations of efficiency and selectivity of these modified materials are reported.

R. K. Gilpin* and W. R. Sisco, Research Division, McNeil Laboratories, Camp Hill Road, Fort Washington, Pa. 19034
Anal. Chem., 50 (1978)

Determination of 5-Hydroxyindole-3-acetic Acid in Urine by High Performance Liquid Chromatography 1342

By checking the accuracy of calibration curves and preventing 5-HIAA decomposition, HPLC combined with aromatic adsorption chromatography results in 99.9% recovery and a detection limit of 0.1 μg/mL.

Nermin Fornstedt, Department of Clinical Chemistry, University Hospital, S-750 14 Uppsala, Sweden
Anal. Chem., 50 (1978)

High Performance Liquid Chromatography with Metal-Solute Complexes 1346

Cu(II) complexes are used for the separation of aromatic amines. The presence of Cu(II) results in a large increase in the selectivity ratios of the solutes studied.

Francis K. Chow and Eli Grushka,* Department of Chemistry, State University of New York at Buffalo, Buffalo, N.Y. 14214
Anal. Chem., 50 (1978)

Problems with Product Performance or Research Data?

HOW ACCURATE ARE YOUR POLYMER CHARACTERIZATIONS?

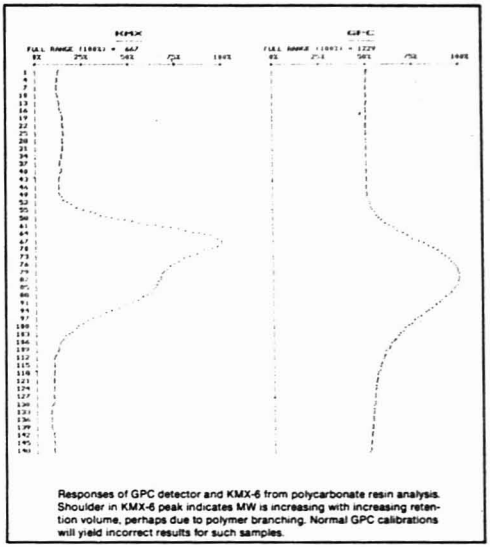

Responses of GPC detector and KMX-6 from polycarbonate resin analysis. Shoulder in KMX-6 peak indicates MW is increasing with increasing retention volume, perhaps due to polymer branching. Normal GPC calibrations will yield incorrect results for such samples.

If you're doing polymer characterizations, and you're *not* routinely measuring absolute molecular weight (MW) and MW distributions, there's a strong probability that your results are either incomplete or inaccurate. The fact is, MW and MW distributions are second in importance only to the actual chemical composition in influencing the physical properties of a polymer.

GPC Measures Size. Until recently, gel permeation chromatography (GPC) was the only method available to determine these parameters. The problem is, GPC measures molecular size, not molecular weight. To provide MW data, it has to rely on error-prone column calibrations and assumptions on the relationship of hydrodynamic size to MW.

KMX-6 Measures Weight. Now, with the Chromatix KMX-6, you can rapidly and directly measure absolute (not relative) molecular weight. Furthermore, you can connect the KMX-6 to a conventional GPC, and it will give you on-line MW distributions as well.

Independent of Column Calibrations. In providing MW and MW distributions, the KMX-6 is completely independent of GPC column

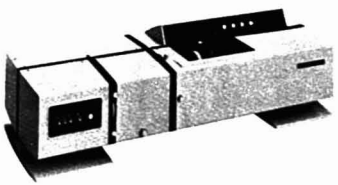

calibrations. This makes it especially useful for the analysis of aqueous polymers, such as dextrans, since it is insensitive to changes in column calibrations due to fluctuations in solvent pH and ionic strength.

Handles Linear and Branched Polymers. Unlike conventional stand-alone GPC, the KMX-6 is not influenced by inconsistencies in the molecular size/weight relationship and thus can be used with both linear and branched polymers, and mixtures thereof. Furthermore, it has enhanced sensitivity to higher weight fractions such as microgel, which usually cannot be detected by GPC methods. It can also operate at high temperatures for the analysis of polyolefins.

Laser Light Source. Technologically, the rapid direct-measurement capability of the KMX-6 is based on the marriage of a coherent light source to proven light scattering techniques. By using a laser source, the KMX-6 overcomes the classical problems formerly associated with light scattering. In particular, very small and dilute samples can now be used. Also, sample clarification requirements have been greatly minimized by the extremely small volume (0.1 μl) illuminated by the laser.

Call or write Chromatix for full details, or Circle **37** for LS-3 Application Note *Measurement of Polyolefin MW and MW Distributions*, **38** for LS-4 *Measurement of MW of Water Soluble Polymers*, **39** for LS-5 *MW Distributions of Water Soluble Polymers*, **40** for brochure, **41** for technical representative to call.

chromatix

560 Oakmead Parkway
Sunnyvale, CA 94086
Phone: (408) 736-0300
TWX: 910-339-9291

D6903 Neckargemünd 2
Unterestrasse 45a
West Germany
Phone: (06223) 7061/62
Telex: 461-691

Briefs

Correspondence

Weigh to go!

People are putting more miles on the Ohaus 10.10-10 than on any other portable. Because no other balance this small (10" x 3¼" x 3⅞") is this tough.

But it's not until you snap off the hard plastic lid that you really start moving.

The "Approach to Weight" indicator saves time, since it warns you that a predetermined weight is approaching.

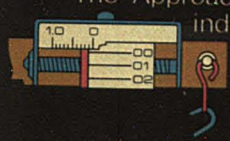

And, you get the precision of a micrometer poise that rotates to adjust settings 0.01 to 1 g.

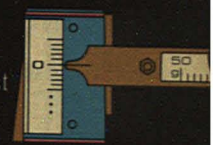

The Ohaus 10.10-10. At this price, it's the only weigh to go!

For full details, contact Ohaus Scale Corporation, 29 Hanover Road, Florham Park, N.J. 07932.

CIRCLE 156 ON READER SERVICE CARD

49.75

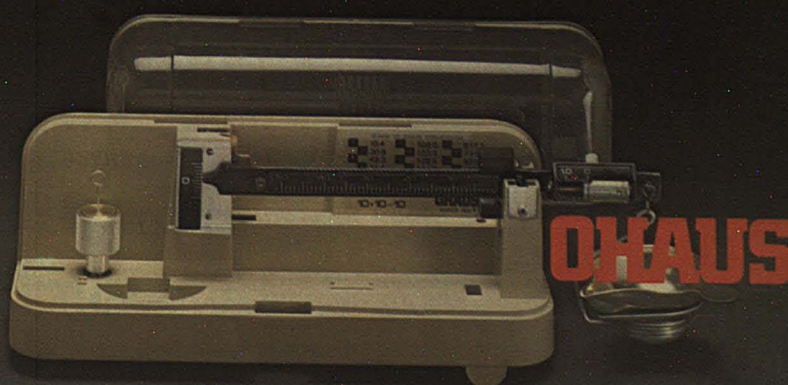

Measuring up since 1907

Briefs

Aids for Analytical Chemists

Matheson
Lyndhurst, N.J. 07071

East Rutherford, N.J. 07073/Morrow, Georgia 30260/La Porte, Texas 77571
Gloucester, Massachusetts 01930/Joliet, Illinois 60434/Gonzales, Louisiana 70737
Cucamonga, California 91730/Newark, California 94560/Bridgeport, N.J. 08014
Dorsey, Maryland 21227/Whitby, Ontario, Canada L1N 5R9
Edmonton, Alberta, Canada T5B 4K6/B2431 Oevel, Belgium
6056 Heusenstamm, West Germany

CIRCLE 140 ON READER SERVICE CARD

ANALYTICAL PROFILES OF DRUG SUBSTANCES, Volume 7

Edited by KLAUS FLOREY

CONTENTS: *S. A. Benezra and T. R. Bennett*, Allopurinol. *P. K. Bhattacharyya and W. M. Cort*, Amoxicillin. *C. G. Eckhart and T. McCorkle*, Chlorpheniramine Maleate. *W. C. Schoenleber et al.*, Dihydroergotoxine Methanesulfonate. *D. D. Hong*, Diphenoxylate Hydrochloride. *C. A. Janicki and R. K. Gilpin*, Droperidol. *D. H. Szulczewski and W.-H. Hong*, Epinephrine. *C. S. Lee and L. Z. Benet*, Ethambutol Hydrochloride. *J. Kirschbaum*, Fluoxymesterone. *G. Satzinger et al.*, Hexetidine. *C. E. Orzech et al.*, Hydroflumethiazide. *J. Tsau and N. DeAngelis*, Hydroxyzine Dihydrochloride. *S. A. Benezra and P. R. B. Foss*, 6-Mercaptopurine. *M. K. C. Chao et al.*, Phenobarbital. *C. Papastephanou and M. Frantz*, Sulfamethazine. *K. Florey*, Thiostrepton. *G. J. Manius*, Trimethoprim. *C. Papastephanou*, Tubocurarine Chloride.

1978, 528 pp., $24.00/£15.60 ISBN: 0-12-260807-0

ANALYTICAL METHODS FOR COAL AND COAL PRODUCTS Volume I

Edited by CLARENCE KARR, JR.

Analytical Methods for Coal and Coal Products is a comprehensive multivolume reference that will fill the need for an authoritative single source on methods of analysis and characterization of coal and the numerous products and waste materials derived from the use of coal. The nineteen chapters in Volume One, prepared by researchers with expertise in their specific disciplines, are of particular interest to analytical chemists, managers of analytical laboratories, fuel chemists, and chemists and chemical engineers working with coal in industry and research organizations. Both the theory and practical laboratory details of the various analytical methods are thoroughly covered and there is extensive cross-referencing.

SECTION HEADINGS: Physical Properties of Coal. Proximate and Ultimate Analysis of Coals. Trace Elements in Coal and Coal Products. Coal-Derived Liquids.

1978, 592 pp., $49.50/£32.15 ISBN: 0-12-399901-4

POLYCYCLIC HYDROCARBONS AND CANCER

VOLUME I: ENVIRONMENT, CHEMISTRY AND METABOLISM

Edited by HARRY V. GELBOIN and PAUL O. P. TS'O

FROM THE PREFACE:

[These volumes are] a comprehensive summary of the present state of knowledge in polycyclic aromatic hydrocarbon research, particularly in relation to cancer, and bring together information from many diverse disciplines in the Environmental, Chemical, Biological, and Medical Sciences.

SECTION HEADINGS: Energy Sources. Environment: Occurrence and Monitoring. Tobacco Carcinogenesis. Epidemiology. Chemistry, Carcinogenicity and Theory. Metabolism and Activation. Enzymology. Pharmacokinetics.

1978, 432 pp., $37.50/£24.35 ISBN: 0-12-279201-7

VOLUME II: Molecular and Cell Biology

1978, 480 pp., $42.00/£27.30 ISBN: 0-12-279202-5

Send payment with order and save postage and handling charges. *Prices are subject to change without notice.*

ACADEMIC PRESS, INC.

A Subsidiary of Harcourt Brace Jovanovich, Publishers

111 FIFTH AVENUE, NEW YORK, N.Y. 10003
24-28 OVAL ROAD, LONDON NW1 7DX

CIRCLE 3 ON READER SERVICE CARD

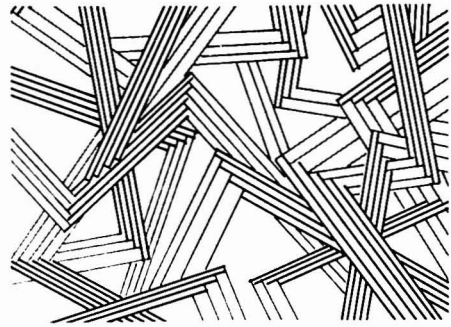

Copolymers, Polyblends, and Composites

Advances in Chemistry Series No. 142

Norbert A. J. Platzer, *Editor*

A symposium sponsored by the Division of Industrial and Engineering Chemistry, and co-sponsored by the Division of Polymer Chemistry, the Division of Organic Coatings and Plastics Chemistry, and the Division of Cellulose, Wood, and Fiber Chemistry of the American Chemical Society.

This timely collection of thirty-eight papers is comprehensive and unique in its coverage of the latest research results on copolymers, polyblends, and composites which are used to toughen brittle polymers with elastomers, to reinforce rubbers with active fillers, and to strengthen or stiffen plastics with fibers or minerals.

Specific topics include:

- determination of MWD in homopolymers; liquid-liquid phase transition phenomena
- grafting kinetics of ABS; rubber-modified polymers; block copolymers; laminating resins; vinylene carbonate
- polymerization and copolymerization behavior; covulcanization of elastomer blends

482 pages (June 1975) $34.50 clothbound (ISBN 0-8412-0214-1).

SIS/American Chemical Society
1155 16th St., N.W./Wash., D.C. 20036

Please send _____ copies of *No. 142 Copolymers, Polyblends, and Composites* at $34.50 per book.

☐ Check enclosed for $_____. ☐ Bill me.
Postpaid in U.S. and Canada, plus 40 cents elsewhere.

Name _____

Address _____

City _____ State _____ Zip _____

HARD WORKING ECONOMY OR HIGH PERFORMANCE VERSATILITY— THE CHOICE IS YOURS.

No matter which Gould strip chart recorder you choose, you get rugged design and outstanding reliability. Both the Model 105 and the Model 110 are at home in your plant or in the lab and both offer 99.9% linearity, 10 chart speeds and sealed follow-up elements.

The Model 105 recorder features a die-cast flat bed design, easy loading z-fold paper, one or two channels, 1 mV full scale to 10 volt measurement range, multicolor felt tip writing and English or metric chart speeds.

The Gould Model 110 offers the additional versatility of plug-in amplifiers covering a wide range of fixed and multispan voltages and temperatures. The Model 110 features a lifetime guaranteed fine line thermal pen, roll paper and is available for rack mounting or portable operation.

It all depends on what your application calls for, hard-working economy or high performance versatility. Gould has both.

For complete information contact Gould Inc., Instruments Div., 3631 Perkins Ave., Cleveland, Ohio 44114. (216) 361-3315.

For brochure call toll free: (800) 325-6400, ext 77. In Missouri: (800) 324-6600.

CIRCLE 81 ON READER SERVICE CARD

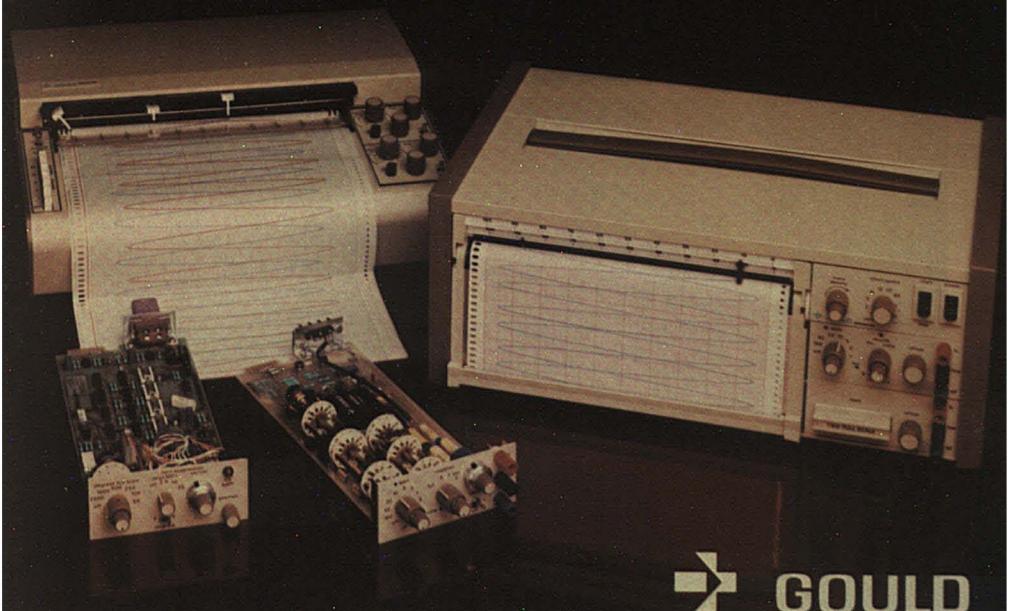

GOULD

The R-600 control panel is simple to operate, easy to understand.

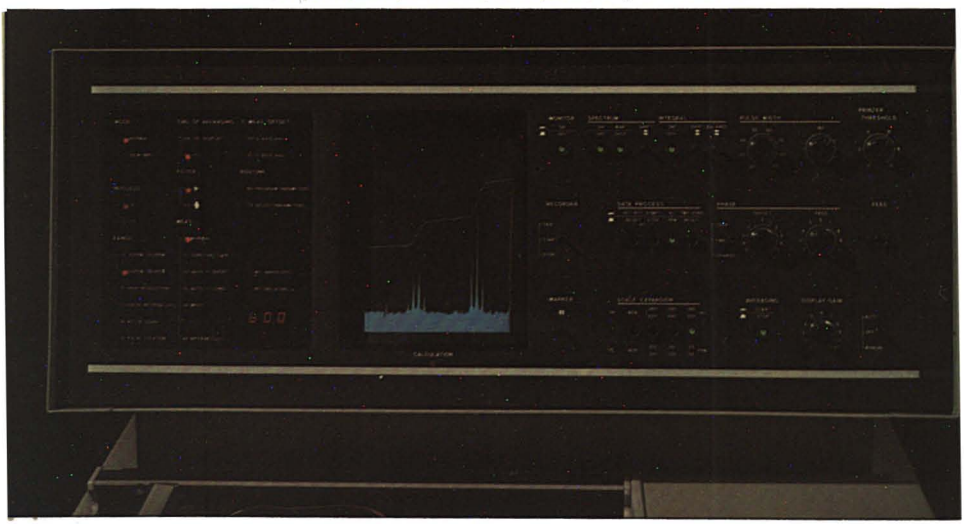

NOW... EFFORTLESS FT NMR

Perkin-Elmer's Model R-600 is a high-performance, low-cost instrument for routine proton observation at 60 MHz. It's the first commercially available NMR spectrometer with a dedicated digital microcomputer that doesn't require a computer expert. The R-600 utilizes the proven R-24 Series magnet system. And because it's a permanent magnet NMR, there are no special requirements for water or power. Just plug it in.

So it's easy to operate, easy to install. And with an extremely low price tag and operating cost, it's also easy on your budget.

MULTIPLE USES

All you need are microgram samples to get routine spectra from the Model R-600. Consequently, you can apply NMR in many new areas. You can get unequivocal identification of many LC and GC fractions. You can use NMR to analyze trace amounts of impurity or isolated natural product when these are all you have available.

MULTIPLE SAVINGS

Even if you have a complex FT NMR spectrometer now, you still need the Model R-600. Your large unit is usually tied up with time-consuming ^{13}C experiments. Besides, adapting it to proton capability would be tedious or costly. Adding a Model R-600 will give you the extra NMR you need, save money, and get your work done on time.

With superb sensitivity, the R-600 lets you run routine experiments on a small scale. Your sample requirements drop from milligram sizes to 500 micrograms or less. But you'll still get the same quality spectra.

SIMPLE OPERATION

Not only is the microcomputer easy to operate, it also does most of the work. And the R-600 is the first FT NMR with controls arranged for operation like a conventional continuous wave instrument. Programming was designed by an NMR spectroscopist, so operational parameters and commands are user oriented. With just ten keys, the control panel simplifies setting the operating conditions and readout of the measurements.

EASY T_1

The Model R-600 has other advantages. For instance, its two Auto-T_1 modes enable you to run a complete T_1 experiment while specifying the fewest parameters. There's also a solvent suppression mode to minimize interfering peaks such as water.

GET ALL THE FACTS

Learn how the Model R-600 can simplify your NMR life. Request our literature describing its long list of benefits. Ask for a demonstration. Write Perkin-Elmer Corp., Main Ave., MS-12, Norwalk, CT 06856. Or call Tom Proulx or Jim Hannon at 203-762-1778.

PERKIN-ELMER

Expanding the world of analytical chemistry

CIRCLE 170 ON READER SERVICE CARD

Report

Flow Injection Analysis

D. Betteridge
Chemistry Department
University College of Swansea
Swansea SA2 8PP, UK

Since Skeggs' classic work (*1*) it has been generally assumed that air segmentation of the flowing stream and attainment of a "steady state" signal are essential parts of continuous flow analysis (CFA). Recently, Růžička and Hansen (*2*) in Copenhagen and Stewart et al. (*3–5*) in Washington, D.C., have independently performed similar experiments of injecting the sample directly into the carrier stream, and have proved that analysis without air segmentation is not only possible but also advantageous. They have termed it flow injection analysis (FIA); this is the name used in this REPORT rather than "nonsegmented continuous flow analysis", which has wider implications.

Skeggs may justly be considered the Henry Ford of analysis because of his revolutionary conception of continuous flow analysis. The improvement in sample throughput coupled with its accuracy, reproducibility, and reliability has resulted in its widespread use.

However, the basic thinking behind the approach was to perform normal chemical procedures on a conveyor belt principle. Thus, in a colorimetric procedure, appropriate amounts of sample and reagent are brought together and mixed by successive inversions until a "steady state" is reached when its absorbance is measured. Air segmentation is used to prevent carry-over of samples and to assist in the mixing; the proportionating pump, through which the sample reactant and buffer solutions are drawn, is a vital part of the apparatus.

By contrast in FIA, there is no air segmentation, the sample is introduced as a plug via a valve or syringe, mixing is mainly by diffusion-controlled processes, and the response curves do not reach the steady state plateau, but have the form of sharp peaks. The absence of air segmentation leads to a higher sample throughput. The presence of a sample-carrier interface, over which concentration gradients develop during the course of analysis has opened up new analytical possibilities for continuous flow analysis. The reproducibility is good, and there is no sample carry-over. There is no need to introduce and remove air bubbles, and an expensive high-quality pump is not necessary. The requisite apparatus can be easily assembled from existing standard laboratory equipment, easily manufactured or purchased as a complete unit. The available options are discussed in the next section.

Experimental

The basic apparatus is shown as a block diagram in Figure 1. The essential parts are: a means to propel the carrier, a sample injection system, a detector and something to display the output, and linking tubing. There are many ways in which these components can be manufactured or combined. One of the simplest is what might be termed the "basic LEGO" model devised by Růžička and Hansen (*6*). The basic components are made of Plexiglas, tubing is 0.4–1-mm i.d. polypropylene, and connections are made by pushing the tubing into slightly tapered holes in the components. The whole, mounted neatly on a LEGO board (Figure 2), is ideally suited for teaching and occasional determination. This apparatus was developed by improving the connections and inlet system (*7*). The fully developed system is commercially available from BIFOK (Figure 3). Stewart used modified HPLC apparatus operated at 500 psi and with 0.2–0.4-mm i.d. tubing (*3–5*). In our laboratory we have used stainless steel tubing (0.8 mm i.d.), Swagelok connections and a standard chromatography valve, and controlled the injection and data processing with a microprocessor. One of our objectives is to improve the precision of 1–2%, which is easily obtained with all of the apparatus mentioned by a factor of 10.

Other combinations can give perfectly satisfactory results, which indicates that wide variations in the important parameters can be tolerated. However, as shown in the section on theory, there are optimum conditions for operation, and on both theoretical and practical grounds a tubing of 0.5 mm i.d. is best. Larger diameter tubing leads to increasing dispersion, whereas with the smaller diameter the tubing may easily be blocked and high-pressure pumps are required for operation. The remaining discussion is concerned with specific components.

Pressure Head. In most applications 0.5–1-mm i.d. tubing and flow rates of 0.5–5 mL min^{-1} are employed so that the flow can be maintained by

0003-2700/78/0350-832A$01.00/0

a peristaltic pump or constant head device. With a fast revolving multiroller pump, pulsation is never a problem—a consequence of having no compressible air bubbles. With some pumps it is a minor problem that can easily be suppressed (*8*). Stewart has encountered and overcome pulsation in high-pressure systems (*9*).

Injection Port. The first of the inlet systems devised by Růžička and Hansen to gain widespread acceptance is the simple flap valve illustrated in Figure 4a. Typically, the sample volume is 0.1–0.2 cc. Because of the pressure surge it is desirable to have a length of tubing between the port and the carrier reservoir to act as a buffer. For the last year Růžička and Hansen have preferred a simple rotary valve (Figure 4b) that dispenses 30–100 μL; this is incorporated in the BIFOK apparatus. Both valves have a repeatability of 1% and permit sampling every 10 s. With a chromatography valve, samples of 6 μL have been routine in our laboratory.

Detectors. In the earliest experiments, in which spectrophotometric determinations were employed, a standard tubular flow cell (vol 18 μL) and spectrophotometer were used to detect the sample peak after colour development. This remains a convenient method, although the standard flow cell can be replaced with a Plexiglas block 4 × 1 × 1 cm through which a hole ca. 1 mm has been drilled and

polished. This enables push-pull connections to be made with polypropylene tubing, which fits into a standard cuvette holder, giving a flow cell that retains the flow pattern and has an effective volume of 8 μL.

Several novel detectors have been developed for use with FIA; these are also cheap and easy to assemble.

Ion-Selective Electrodes. Růžička and Hansen have mounted an ion-selective electrode (ISE) and a reference electrode in a tubular container held at an angle of ca. 30°. The effluent stream flows onto the indicator electrode and then onto the reference electrode. An outflow tube is positioned so that the reference electrode is in a pool of effluent. Signals are obtained that are proportional to the function measured, provided the gap between the electrodes is gauged correctly (*10*). Furthermore, it is possible to use a series of electrodes and a cas-

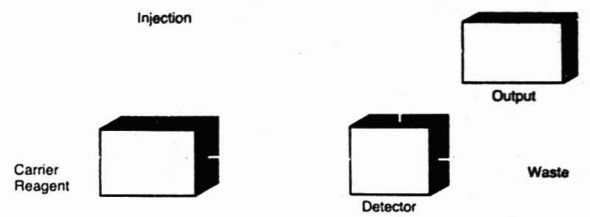

Figure 1. Block diagram of basic FIA apparatus

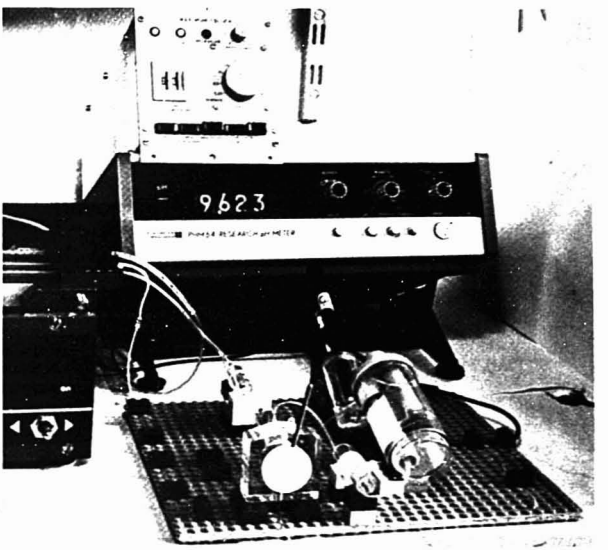

Figure 2. "Basic LEGO" apparatus with potentiometric detector

Carrier pumped from reader's left to right, through rotary valve (Figure 3B) and ISE detector as described in text. Peak integrator situated above voltmeter

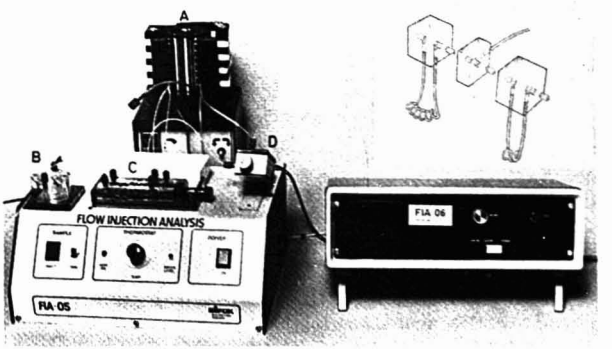

Figure 3. BIFOK FIA system

A, pump; B, rotary valve; C, Plexiglas block connectors and polypropylene tubing (see inset); D, detector

INTRODUCING TOTAL CHEMICAL ANALYSIS. ONE BUTTON AND TWO MINUTES AWAY.

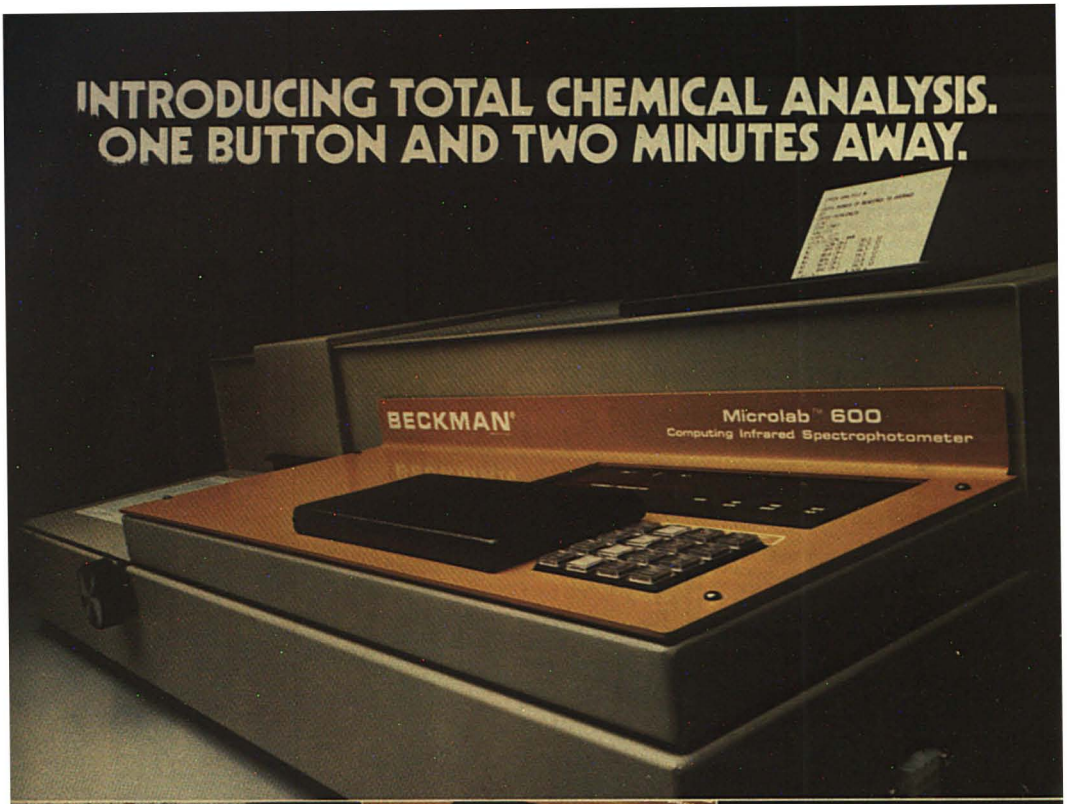

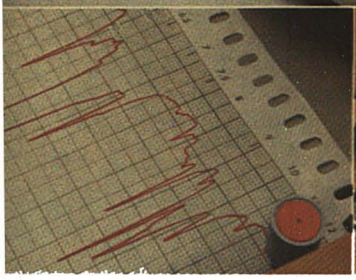

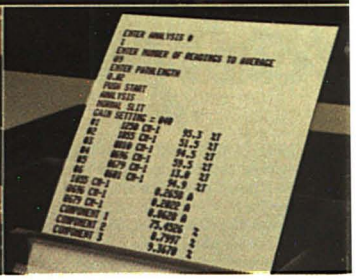

Rapid precise qualitative and quantitative final answers by IR analysis are now available at the push of a button on the new Microlab™ 600 Computing Infrared Spectrophotometer.

High precision double beam optics under self-contained automatic computer control analyze most solid, liquid, and gaseous multi-component samples in under two minutes.

Once you've entered your analysis protocol using the Microlab keyboard, the complete analytical procedure is stored right on board for immediate one-button recall.

No outside computational power is needed. Microlab optimizes your scanning parameters, computes quantitative final answers, and reports a complete analysis in analog (chart), digital, and printer modes while storing your program for future use.

High speed, precision, and repeatability are accompanied by features like Repetitive Scanning with selectable Cycle, Time Delay and Wavelength Span, Peak Pick Routine and Automatic Gain Set.

And finally, operator training time is reduced to a minimum by the teaching printer that instructs the user, inquires, and reports on completed operational steps.

So don't wait two minutes more to start saving hours of analysis time. Get complete information. Contact your local Beckman Representative or Scientific Instruments Division, Beckman Instruments, Inc., P.O. Box C-19600, Irvine, CA 92713.

Innovation in IR since 1940.

BECKMAN®

CIRCLE 27 ON READER SERVICE CARD

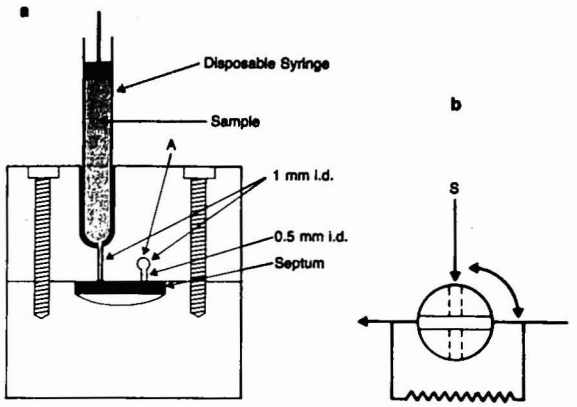

Figure 4. Simple valves for sample injection

(a) Cross section of flap valve. Carrier flows through A. On depression of syringe, septum is forced down, and sample occupies resulting depression. Septum regains original position and forces sample into carrier stream. Constructed from Plexiglas blocks held together by nylon screws. (b) Rotary valve. Sample placed in wider tube of known volume. When rotated through 90°, carrier diverted through larger diameter tubing, and sample enters carrier stream

cading effluent to obtain a measure of several species in the same sample. Under these dynamic conditions it is not necessarily the case that the potential is that which would be obtained if a conventional measurement were made. It may also be true that the sample matrix affects the rate of equilibration. However, in all cases so far reported, in which the calibrants have been properly matched samples, good calibration curves have been obtained.

Potentiometric Detectors. In principle it is possible to detect a sample peak by differential potentiometry, with one electrode in the carrier stream before the point of injection. The difficulty is that the potential difference is very sensitive to the radial position of the electrode downstream from the injection point. If it just pokes through the side of the tubing, it is not very sensitive to concentration changes. (It seems as though there is a "dead" layer on the walls of the tube.) If it is placed midstream it interferes with the flow characteristics and gives irreproducible results. This led Nagy et al. to abandon FIA and resort to a mixing chamber (*11*). However, the difficulties have been overcome by Karlberg and Thelander, who have placed the last part of the tubing in a vertical position inside a small cup. The indicator electrode is a platinum wire centrally placed in the mouth of the tube, and a reference electrode is placed in the cup (*12*).

Photometric/Refractometric Detector. A flow cell has been manufactured with a 3-cm path length, a light emitting diode (LED) at one end, and a photodiode at the other (*13*). The total component cost including the associated electronics is less than $25. Insofar as the LED can be selected to cover most of the visible spectrum, it makes a spectrophotometer redundant. The sensitivity extends to the ppb region.

Because the sample plug has a parabolic head and tail, it acts as a lens if there is a difference in refractive index between carrier and sample. By virtue of the design of the detector, where the light beam is along the axis of flow, it functions as a differential refractometer as well as a photometric detector. It is capable of better discrimination than an Abbe refractometer and is almost as sensitive as a conventional differential refractometer.

Photometric detectors with the light beam normal to the flow may also function as refractometers, as is evidenced by the small negative peaks exhibited on many FIA peaks. However, this does not pose any problems in practice.

Dielectric Detector. A conductimetric detector based on a semiconductor oscillator chip has been exhibited (*14*). It is cheap, but the optimum design has yet to be achieved. However, it has digital output, which is advantageous if a microprocessor is to be used to process the results.

In addition to these, detectors that are in routine use for monitoring HPLC effluent may be used.

Air bubbles generally interfere and must be removed. This can often be achieved by having the cell on an incline rather than horizontal.

Solvent Extraction

Karlberg et al. have elegantly demonstrated that solvent extraction by FIA is a most attractive procedure (*15*). By use of a teepiece with a carefully positioned platinum side tube, the aqueous carrier containing the sample is interspersed alternately with very small segments of organic solvent. Extraction takes place across the aqueous-nonaqueous interface, and the two phases are separated after extraction by a second teepiece. Wall drag causes convection in both phases, increasing the rapidity of attaining equilibrium concentration distribution.

Dialysis

A simple but effective dialyser, consisting of a dialysing membrane clamped between two Plexiglas blocks, has been reported and proved quite satisfactory for analysis of blood samples, etc. (*6*).

Applications and Theory

The applications of FIA known to the author are summarised in Table I, page 842 A. Determinations that have been demonstrated in workshops are included, since it is probable that full accounts will soon be published. The order is roughly chronological, thus emphasising the trend to lower flow rates and shorter lengths of tubing, which has accompanied improvement in understanding of the theoretical principles underlying the method. The range of conditions under which satisfactory results can be obtained emphasises the robustness of the technique. However, a knowledge of the theory aids in the selection of optimum conditions; therefore, it will be briefly reviewed.

First, two conceptual errors that have given rise to needless controversy must be disposed of. One relates to the notion that turbulent flow is essential. This is stated in the early papers of Růžička et al. (*2*, *16*), but they soon realised that laminar flow is preferable. In fact, a Reynolds number (RE) of 2000, which is usually taken to be the onset of turbulent conditions, corresponds to a flow rate in 1-mm diameter tubing of 93 mL min^{-1}. Therefore, it is unlikely that FIA has ever been carried out with turbulent flow. However, incipient turbulence can be caused by projections and coiled tubes; in the high-pressure systems an RE of 2000 is approached. Thus, the

point has been a matter of dispute (*39, 40*).

The other error arose from the initial stress laid on the mechanical aspect of flow injection, which was emphasised by the terminology adopted. Critics have not been slow to point out that some forms of nonsegmented CFA predate 1974 (*7*). However, the analytical significance of maintaining the integrity of the sample plug and allowing mixing to be controlled by diffusion processes had escaped earlier workers. This is illustrated by Nagy et al. who performed the experiment of injecting a sample into a flowing stream in a large diameter open tube with the object of measuring the potential of the sample downstream—clearly FIA (*11*). Unfortunately, they used electrodes that protruded into the stream. This gave rise to erratic results, from which they concluded that the open tube must be abandoned in favour of a mixing chamber. They noted a further disadvantage of the open tube: "The reproducibility of the measurements was impeded by a concentration gradient perpendicular to the flow." It is the essence of flow-injection analysis that this concentration gradient is a key source of analytical information and that it is essential to maintain the integrity of the plug and to limit mixing to diffusion-controlled processes.

Růžička and Hansen's first experiments were not performed with this in mind. They thought, in accord with conventional concepts, that turbulent flow assisted in dispersion of the sample and that the great increase in sample throughput and simplicity of apparatus were the most appealing features of the method. However, they soon recognised that turbulent flow was not needed. A hint that the mixing process was diffusion controlled was provided by a set of key experiments (*24*) and was strengthened by the discovery of Sir Geoffrey Taylor's paper, "Dispersion of Soluble Matter in Solvent Flowing Slowly Through a Tube" (*41*). Further study has led to a statement of theory that is almost definitive and is certainly the starting point for all concerned with the method (*7*). It makes clear that what is really important about FIA is the chemistry that happens between the points of injection and detection, not the improved mechanics of injection and throughput.

One can see how confusion and controversy arose, and the historian of science can only note that yet again we have an instance of the inventors not realising immediately the totality of what they had discovered and of others being within a whisker of getting there first.

Basic Principles. Between the points of injection and detection the sample plug will have been physically dispersed to some degree, and in addition some chemical reactions may have taken place. The peak detected will reflect both processes.

The physical dispersion is brought about partly by longitudinal flow which gives rise to parabolic head and tail and partly by radial diffusion (Figure 5). (It is analogous to chromatography without partitioning and without a stationary phase to disturb the flow pattern.) The relative importance of these processes depends upon the flow rate, the radius of the tube, the time of the analysis, and the magnitude of the diffusion coefficient.

The precise relationships are given in Table II, which summarises the treatment of Růžička and Hansen (*7*).

Basic Models and Equations. The peak obtained generally fits the *C*-curve equation (Table II), but to evaluate the role of the empirical parameters, it is necessary to develop other equations. One is due to Taylor, who elucidated the significance of diffusion (*41*). In any flowing stream in a pipe the velocity at the walls is zero, and that at the centre is twice the mean. Thus, if a sample plug is placed in the stream, it assumes a parabolic shape by the process of convection. If this were the only means of dispersion, some of the sample would stick to the walls, and the plug would have an infinitely long tail. However, the molecules can diffuse away from (and back to) the walls and thus gain some longitudinal motion as they join the main stream. The diffusion can be longitudinal, i.e., in the direction of flow or radial—perpendicular to the direction of flow. Taylor showed that while these processes always occur, dispersion by longitudinal diffusion can be ignored relative to that caused by the main flow pattern, whereas radial diffusion is always important in narrow tubes, and at low flow rates it may even be the major mechanism for dispersion. Under diffusion-controlled conditions, the peak shape is Gaussian. FIA generally is carried out just outside Taylor conditions, but Taylor's argument leads to the following practical conclusions: mixing will be complete without recourse to mechanical stirring; the concentration gradients in a given sample plug are both reproducible and predictable; and the peak shape will be influenced by differences in the sample and carrier matrices, because the whole of the plug, matrix and analyte, is diffusing into the carrier.

Another useful equation is that for the "tank-in-series" model. This is exactly analogous to the concept of the height equivalent to a theoretical plate model of chromatography. It postulates that the tube between the points of injection and detection consists of a number, *N*, of imaginary tanks. These are in series and the simple mathematical models used to account for the distribution of a sample

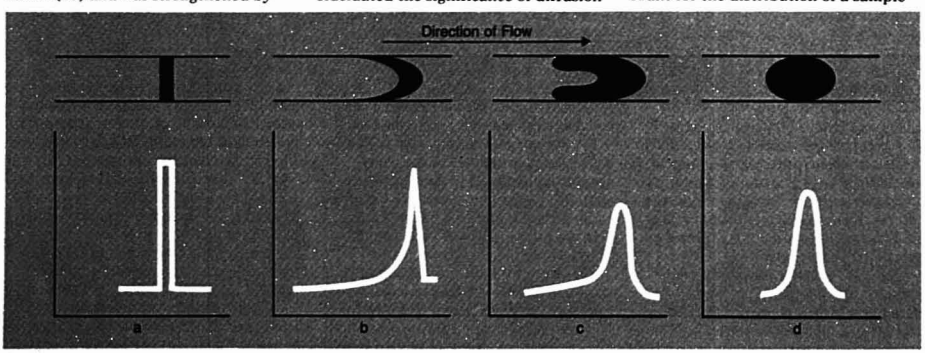

Figure 5. Diagramatic representation of effects of convection and radial diffusion on concentration profiles of samples monitored at a suitable distance downstream from injection

(a) No dispersion. (b) Dispersion predominantly by convection. (c) Dispersion by convection and diffusion. (d) Dispersion predominantly by diffusion

the Varian CDS-111...a powerful chromatography data system that is easy to use

The CDS-111 efficiently uses the capabilities of advanced microprocessor technology to save the chemist's time and to make it easier to quantitate analysis results.

Simple controls

The controls are simple and straightforward, easier to use than many hand calculators. Four switches and a small keyboard provide complete control. For example, to run a typical analysis, from injection through calculations and printed report, all you need to do is: press the "start" button, make your injection when the "ready" light comes on and, after the last peak elutes, press the compute button to get your complete report. It's that simple on the outside because the CDS-111 does so much more on the inside.

Presets handle most chromatograms

For most chromatograms you don't have to program the CDS-111 at all. It has been preset at the factory so that the critical peak measuring parameters are automatically set up when you switch on the power. The presets provide initial monitoring and adjustment to instrument signal noise, detection and processing of peaks, automatic updating of peak measuring parameters if peaks become broader, perpendicular and tangent peak separation, trapezoidal baseline correction and reporting of area percent . . . all automatically!

It's easy to set and change parameters to handle unusual chromatograms

Whenever you encounter an unusually complex analysis, it is easy to override the automatic preset parameters and manually set exactly the values that you need.

It speaks the language of chemistry

The CDS-111 doesn't speak abstract computerese. It speaks the language of chemistry. For example, if there is no reference peak at a time when a reference peak is expected the CDS-111 doesn't vaguely say "error" and leave you guessing; it says "NORP." It is specific and understandable.

And the CDS-111 is really helpful when recalculation is required. It not only tells you if an error has occurred, it tells you what the error is so that you can easily correct it and recalculate, in most cases, *without having to reinject.*

"Must" peak gives extra protection

To detect errors and provide extra protection for the system, the first reference peak can be designated as a "must" peak. Then, in each analysis, the "must" peak must occur within a prescribed time window and be within prescribed size limits. If the "must" peak fails to meet either of these criteria, an error is detected, a message is printed and the alarm count is incremented. If the alarm count reaches a significant level the CDS-111 can terminate the analysis. The "must" peak can detect faults or errors in all system components. It will detect incorrect flow rates, wrong detector, wrong sample, a deteriorating column, a plugged or leaking syringe, anything that causes the "must" peak to fail to meet its criteria.

It has a nine-method memory

Once a method is set up, the CDS-111 will store it for instant call up. The CDS-111 will hold up to nine complete analytical methods in memory, each programmed to optimize a specific analysis and automatically control the entire chromatography system —chromatograph, automatic sampler, valving and external devices —in automatic, closed loop operation.

As a result, you don't have to reprogram every time you run a different sample. You can simply call up the method file that you set up and stored the first time you ran the analysis.

The CDS-111 makes chromatography automation available to every lab

It interfaces simply with both gas and liquid chromatographs. Two different basic models are available, so you can choose a system that best meets your particular needs and budget.

To have a Varian technical representative contact you circle **Reader Service No. 225**

For more information circle **Reader Service No. 226**

Varian Instrument Division, 611 Hansen Way, Box D-070, Palo Alto, California 94303

varian

The CDS-111 is priced to provide more performance per dollar than any other chromatography data system available today.

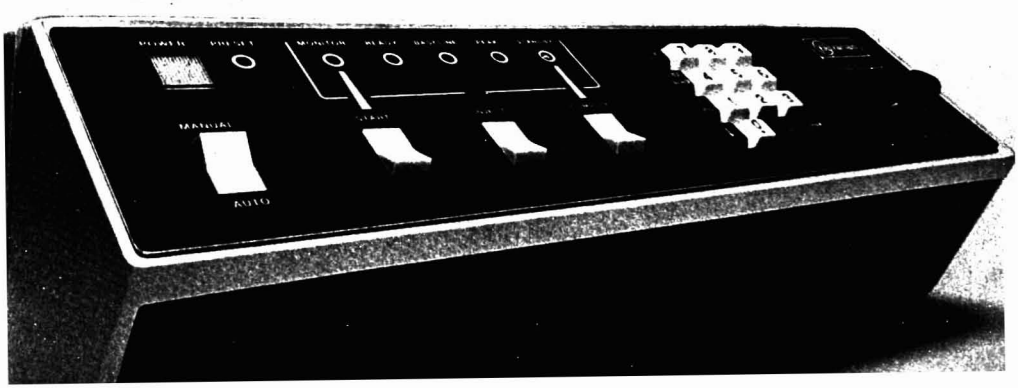

INTRODUCING
the Varian 5000 family of liquid chromatographs

It makes LC responsive and simple

The Varian 5000 Series is a family of powerful microcomputer-CRT-based liquid chromatographs that make LC easy for anyone.

It makes tough separations seem simple. The helpful CRT continuously displays *all* instrument conditions. Tells you everything you need to know, right now. Responds to you. Helps you build programs. Prompts and leads you. Makes LC easier than ever before.

It comes with full support. With your Model 5000 you receive a commitment from Varian to provide strong, continuing support—training, service and applications assistance—that will assure successful solution of your liquid chromatography problems.

Price/performance. There are six basic models in the 5000 Series: from simple isocratic to completely automatic gradient systems. Each is designed to offer unbeatable price/performance; to provide a new level of LC capability at system prices lower than most LC components.

Upward expandability. 5000 Series chromatographs are upward expandable and offer many options. You can configure a 5000 that is exactly right for your laboratory. Later, as your needs change, you can add whatever new capability you require.

For full details on a 5000 that may be exactly right for you, circle Reader Service Number 223.

To have a Varian representative contact you, circle Reader Service Number 224.

See it at the National ACS Show in Miami, September 10-15, 1978

varian

introduced into the first tank can be used to account for the physical dispersion of sample as a function of time. The actual "size" of the tank is a function of tube dimensions and flow rate. The shape of the distribution predicted by the tank-in-series model is shown in Figure 6. For high N it becomes Gaussian, i.e., indistinguishable from Taylor's model, but for $N = 1$ a very different shape is found. The application of this model to FIA has led to some radical developments that are described below.

Dispersion. An empirical definition of dispersion is given in Table II. The tank-in-series model is used for all except the narrow tube for which Taylor's equation is most appropriate. The practical conclusions to be drawn from the detailed studies with respect to flow rate and tube length are shown in the table. It was also found that the optimum for the tube diameter is 0.5 ∓ 0.2 mm i.d. In this range a reasonable flow rate can be maintained without difficulty, reagent consumption is not excessive, and a variety of chemistries is available to the analyst.

With limited dispersion the sample integrity is maintained to a high degree. This is the ideal when FIA is used as a sample inlet system for the measurement of pH, pCa, etc., of the sample. The justification of measuring pH, etc., this way lies in the small sample size (ca. 30 μL), the short time of measurement (ca. 10 s) as the "steady state signal" is not required, and the possibility of performing several determinations in sequence on the same sample. The theory suggests that in order to gain maximum sensitivity and minimum analysis time, it is better to use a short narrow tube than a mixing chamber. With the mixing chamber and the typical parameters shown in Table II, the analysis time

Table II. Basic Equations and Guidelines for FIA

	equation	comment
BASIC MODELS AND EQUATIONS		
(a) general curve for FIA the *C*-curve	$C = \frac{1}{2\pi\delta}\, e^{-(1-\pi^2\delta/4\delta}$	
(b) dispersion is controlled by radial diffusion. Taylor's equation	$C = \frac{M}{\pi r^2}\frac{1}{2\sqrt{\pi\delta L^2}}\, e^{-(1-x)^2/L^2\delta}$	(i) $\delta = \underline{D}t/L^2$ (ii) holds when $T \geq r^2/3.8^2\, D_c$
(c) tank in series there are N imaginary tanks between the points of injection and detection	$C = \frac{1}{t_i}\left(\frac{t}{t_i}\right)^{N-1}\frac{1}{(N-1)!}\, e^{-t/t_i}$ for $N = 1$ $C = \frac{1}{t_i}\, e^{-t/t_i}$	(i) $T = Nt_i$ and for $N > 10$, $\delta = 1/2\ T^2/N$ (ii) reactor volume = $V_R = QL/F$ if r is constant (iii) for low N dispersion is skew, and for high N, it is Gaussian; therefore, long narrow tubes result in symmetric peaks, and shorter tubes give asymmetric peak. If the tube is equivalent to 1 tank, there is an exponential rise and fall
DISPERSION (Figure 5)		
(a) definitions	(i) $D = \frac{C_s^*}{C^{max}} = \text{const}\,\frac{H_s^*}{H}$ (ii) $D_t = D_t D_t D_d$ (iii) $D_t = \frac{C_s^{max}}{C^{max}} = \text{const}\,\frac{H_s}{H}$	a simple practical method of measuring sample dispersion. In spectrophotometry H is recorded peak height, H_s^* is the peak height with cell full of undispersed coloured solution the total dispersion is the product of the dispersion in the injection system, D_i, the flow tube, D_t, and the detector, D_d. D_d is assumed to be 1
(b) limited dispersion $D_t = 1 - 3$	For $r = 0.2$ mm and L as small as possible, have 1 tank and $D_t \approx D_t$ Then rise curve $C = C_s^*(1 - e^{-kS})$ fall curve $C = C_s^*\, e^{-kS}$ and $S_{1/2}$ = vol to give $C^{max} = \frac{1}{2}C_s^* = \frac{0.693}{k}$	(i) corresponds to $D \approx D_t = 2$ (ii) sample volume should be approx $S_{1/2}$ and sample zone should pass through less than half its length before reaching the detector (iii) flow rate and L should be a minimum typical values: $S_{1/2} = 28$ μL for $Q = 0.5$ mL min^{-1}, $L = 22$ cm, $r = 0.2$ mm
(c) medium dispersion $D_t \approx 3 - 10$ (diffusion controlled)	(i) $D_t = \frac{2}{W_s}F\sqrt{T}\sqrt{t_i}$ (ii) $D_t = \frac{2}{W_s}F\sqrt{T}\sqrt{t_i}(1 - 2^{-n})$ where $n = \frac{S}{S_{1/2}}$ and $e^{-0.693n} \approx 2^{-n}$	(i) Gaussian curve assumed, hence $N = (2\ L/W)^2$ and $t_i = L/N$ (ii) dispersion increases linearly with pumping rate but as square root of travelled distance or residence time typical values: see Table I
(d) large dispersion (mixing chamber)	(i) $\frac{CV_m}{C_s^*S} = e^{-t/T}$ (ii) $D_m = \frac{V_m}{S}$ (iii) $t_{1/2} = 0.693\,\frac{V_m}{Q}$	(i) $C = C^{max}$ at $t = 0$ (ii) It takes ca. 4 $t_{1/2}$ for baseline to return to 4% typical values: $S = 0.1$ mL, $V_m = 2.5$ mL, $Q = 5$ mL min^{-1}, $D_m = 25$ and $t_{1/2} = 0.35$ min

Symbols other than those defined above:

C = concentration (mol L^{-1})
C_s^* = concentration of injected sample (mol/L)
C^{max} = concentration of element of fluid at peak maximum (at $t = T$) (mol L^{-1})
C_s^{max} = concentration of element of fluid at peak maximum, extrapolated to $t = 0$ (mol L^{-1})
D = dispersion (dimensionless)
$\underline{D}$ = axial dispersion coefficient (cm^2 s^{-1})
D_c = molecular diffusion coefficient (cm^2 s^{-1})
δ = dispersion number (dimensionless)
d = tube diameter (mm)
F = linear flow velocity (mm/s)
H = peak height at $t = T$ (mm)
H_s^* = peak height recorded with flow cell filled with solution of concentration C_s^* (mm)
H_s = peak height extrapolated to $t = 0$ (mm)
L = total length of a line (cm)
l_i = length of a mixing stage (mm)
M = mass of injected material (mol)
N = number of mixing stages (dimensionless)
Q = pumping rate (mL min^{-1})
R_e = Reynolds number ($R_e = 21.2\ Q/d$) (dimensionless)
r = tube radius (mm)
S = sample volume (μL)
$S_{1/2}$ = sample volume necessary to reach 50% of C_s^* at C^{max} (μL)
T = mean resident time (s)
t = time (s)
t_i = mean resident time in one tank (s)
$t_{1/2}$ = half wash time (s)
V_m = mixing chamber volume (μL)
V_p = volume of plug flow section of a tube (μL)
V_R = reactor volume (μL)
W = reduced peak width (at $t = T$) (mm)
W_s = reduced peak width extrapolated to $t = 0$
x = distance from peak maximum (cm)

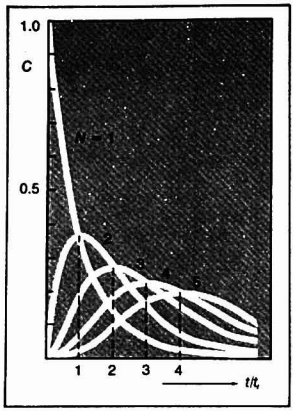

Figure 6. *C*-curves obtained for tank-in-series model at various values of *N*

is 1.5 min, and the peak height is reduced to 0.04 ($1/D_t$) of that for pure sample. With the same sample size and flow rate, but using a 50-cm tube of 0.5 mm, the analysis time is 3.6 s and the reduction in peak height is 0.5. Thus, compared with the mixing chamber, the narrow tube increases sample throughput by a factor of 25 and the sensitivity by 10. These figures are, of course, only illustrative, but the validity of the argument has been confirmed experimentally.

Medium dispersion ($D = 3 - 10$) has been used for most of the applications listed in Table I. For many systems the extent and rate of chemical interaction have to be taken into account. In a sample application such as spectrophotometric determination, the peak height is diminishing as the colour-forming reaction is progressing. If the chemical reaction is slow, it is best to select flow conditions where the reaction is incomplete, but reproducible. It is also possible to use the chemistry going on across the interface to analytical advantage, as discussed below.

Large dispersion is best accomplished with a mixing chamber which corresponds to one tank.

Sample Size. Taylor's theory does not take account of sample size, although it is a parameter of analytical importance and has a marked effect on peak shape (Figure 7). Růžička and Hansen take it into account by considering the dispersion arising from the inlet system, D_i, separately from that due to the flow, D_f. It follows that the sample size has more influence on the peak shape when the total dispersion is low ($D_i \geq D_f$).

Viscosity and Refractive Index. All the theories discussed so far assume that the viscosity and refractive index of the sample and carrier are identical. If they are not, changes in the peak pattern will be evident. Differences in viscosity will affect the peak height; changes in refractive index may, with a photometric detector, result in a small negative peak and distortion of the peak. Within a series of known samples, these effects can be countered by calibration, preferably with matching the physical properties of carrier and sample.

Novel Applications. Many of the determinations recorded in Table I can be carried out by air segmented continuous flow analysis at higher cost and lower sampling rate (*40*), but others exploit reactions across the interface between sample and carrier and/or the mode of sample dispersion. These latter, most of which are in their infancy, will be briefly reviewed.

Multielement Trace Analysis. If the carrier stream and sample plug are at different pH at the point of injection, a well-defined pH gradient will be developed as the sample disperses within the carrier. Most colour-forming reactions of analytical interest are pH dependent and pH-absorbance curves for a given metal ion-reagent combination are characteristic of the metal ion. Thus, if the sample consists of a mixture of metal ions and the carrier a solution of reagent, the extent of colour formation at any point across the interface will be dependent on the pH at that point. In other words, the interface contains sufficient chemical information to enable several metals to be detected and determined. There remains the problem of extracting that information, but the feasibility of the approach has been demonstrated for mixture of lead (II) and vanadium (V) with PAR (Figure 8) (*34*).

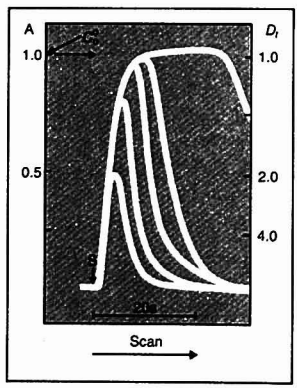

Figure 7. Curves obtained by injection of 59, 108, 206, 403, and 795 L C_c^* correspond to absorbance of nondiluted dye solution

Titrimetry (*25*). In the above application it appears from the peak profile that, in effect, the carrier works into the sample reacting with it along the way. If a complex is being formed, or an acid is reacting with a base, a gradient "titration" is being performed (*42*). The points of inflection on the peak will correspond to the steepest part of the concentration gradient, i.e., the ends of the interface and the peak width will be a function of sample concentration. However, in view of the time it takes to achieve the requisite degree of mixing, it is easier to inject the sample, concentration C_A, into a mixing chamber of volume V, through which the flow rate is f_A and to add titrant concentration, C_B at flow rate, f_B. Then t_{eq} is defined as the peak width at some constant potential and is given by (*25*):

$$t_{eq} = \frac{V}{f_A} 2.3 \log C_A^* - \frac{V}{f_A} 2.3 \log C_B \frac{f_{B \cdot n}}{f_A}$$

for the reaction $A + nB = AB_n$.

In view of the comments above on mixing chambers, it must be emphasised that the role of the chamber is to achieve a "stretched out" concentration gradient more rapidly than in an open tube, because the width of the peak, not its height, is measured. By these means acid-base and complexiometric microtitrations have been performed.

Turbidimetry. In turbidimetric methods published so far, it has been noted that there is a problem of build-up of precipitate on the walls of the tube. One approach to overcome this is illustrated by the determination of sulphate. The carrier solution is alkaline and contains barium and EDTA such that an excess of carrier dissolves the precipitate. The sample is made acid so that during the initial stage of mixing and as the sample passes the detector, the carrier is neutralised and precipitation occurs. On further mixing the precipitate redissolves (*35*). There are many further examples where the momentary disturbance of the pH and or complexing power of the carrier or sample can be exploited.

Potentiometry. Karlberg and Thelander have shown that the potential changes across the interface if the carrier is an oxidant and the sample a reductant or vice versa (*15*). The differential potential between carrier and sample plug is easily measured and is a function of sample concentration.

Kinetic. Since FIA is faster than segmented continuous flow analysis, faster reactions can be used for analytical purposes. For example, in our laboratory we have found that the reaction between cobalt (II) and PAR is

Compare Varian's AA-775 with any other AA on the market...

Compare:

☐ **Rapid sequential-element analysis (or sequential multi-element analysis):**
Four lamps, ready to go—no warm-up, no waiting.

☐ **Calibration accuracy with the rational method:**
Unique calibration algorithm with five standards for unsurpassed accuracy (patent applied for). What's more, the calibration can be established on the mean of 'n' measurements. Flame or flameless.

☐ **Standard additions in real time:**
Complete and immediate computation of 'standard additions' results using a simple calibration routine and up to five calibration values. This calibration is stored and utilized for the rest of the sample run.

☐ **Sample weight compensation:**
Automatic correction for differences between the specified sample weight and the actual sample weight.

☐ **The best gas control system yet:**
Controls and monitors all 10 vital functions including liquid level in the drain trap and flame gas flow rates. Yet it's easy to use, and safe.

☐ **Automatic sampling:**
Sampling accessories permitting automatic calibration and unattended operation for both flame and flameless modes.

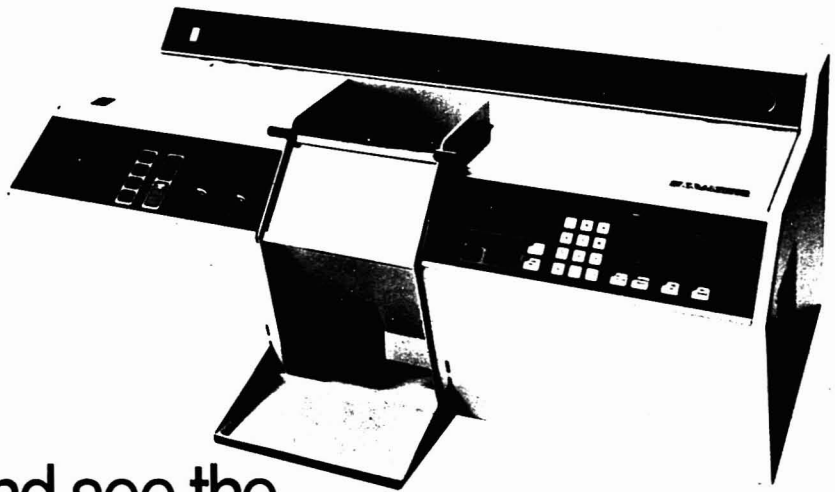

and see the AA-775 win hands down!

☐ **Fast change from flame to furnace and back:**
Conversion from one mode to the other takes three minutes!

☐ **Plus:**
A highly developed double-beam optical system; simultaneous background correction (it's DB too); statistics available for display and calibration; extensive error diagnosis and self test; simple operation; and superior performance.

Compare the AA-775. Contact Varian Associates of Canada, Ltd., 45 River Drive, Georgetown, Ontario, L7G 2J4
or use the Reader Service Card.
Circle **218** for detailed information.
Circle **219** to have a Varian representative call.

varian

Table I. Applications of FIA

	determination	detector	carrier stream/conditions	flow rate, mL min^{-1}	tubing: length, cm	tubing: i.d., mm [a]	sensitivity	sample throughput, per hour	ref
1.	PO_4^{3-}	(a) spec (phosphomolybdate)	NH_4MoO_3 (0.005 M), HNO_3 (0.4 M)	18	250	1	ppm		2
		(b) spec (molybdenum blue)	(i) as for (a)	18	250	1	ppm	200–250	
			(ii) ascorbic acid (1%)	1.5[b]	50	0.5	ppm	120	40
2.	NH_3, NH_4^+	air gap electrode	NaOH (0.05 M)	10	150	1	10^{-3}–10^{-2} M	60	2
3.	P in plant material, e.g., beans	spec (molybdenum blue)	(i) NH_4MoO_3 (0.005 M), HNO_3 (0.4 M), ethanol (5%)	18	230	1	ppm	420	16
			(ii) ascorbic acid (5%)	1.8					
4.	N in plant digests	(a) spec (indophenol blue)	(i) phenol (5%), NaOH (12%), ethanol (33%)	8.6	170+	1	1–2%	180	17
			(ii) alkaline NaOCl	8.6[b]	550				
		(b) air gap electrode	NaOH (1 M)	8.6	490		1–2%	110	
5.	Cl^- in brackish waters	spec . $[Hg(SCN)_2/Fe(III)]$	$Hg(SCN)_2$ (0.0626%), $Fe(NO_3)_3$ (3.03%),	8.6	500	1	1–5 × 10^{-3} M	200	16
			HNO_3 (0.047 M), ethanol (15%)	0.6	50	0.5	1–5 × 10^{-3} M	120	40
6.	P and N in plant digests	spec (molybdenum blue and indophenol blue)	as above in 3 and 4 split stream enables first P and then N to be determined			1		200	19
7.	PO_4^{3-} and Cl^- in blood sera	spec (molybdenum blue, $[Hg(SCN)_2/Fe(III)]$	sample dialysed before addition of colour-forming reagents						6
			(a) PO_4^{3-}: (i) H_2SO_4, (ii) NH_4MoO_3,	all 5	70 + 180	1		50	
			(iii) ascorbic acid	(i) and (ii) 2.4	30 + 70	1		125	
			(b) Cl^-: (i) H_2SO_4, (ii) H_2O,	(iii) 4.0					
			(iii) $Hg(SCN)_2$/Fe(III)						
8.	K, Na, NO_3^-	K^+, Na^+, NO_3^- electrodes		4.0	85	1	10^{-5}–10^{-3} M	125	8
9.	glucose in blood sera	kinetic (single point) glucose dehydrogenase	(i) glucose dehydrogenase (5.2 kV·L^{-1}), mutarotase (0.11 kV·L^{-1}), NaCl (0.15 M), NAD (1.1 × 10^{-3} M) at pH 7	2.0	53 for dialysis + 112	1	10^{-3}–10^{-2} M	60	20
			(ii) NaCl (0.14 M)	2.0					
10.	NO_3^- in soil extracts, wastewaters, etc.	NO_3^- electrode	borax (0.01 M), NaOH (0.01 M), glycerine (0.2%)	3	106	1	10^{-5}–10^{-2} M	90	21
11.	N, P, and K in fertilizers	elec, K^+, NO_3^-	for N: phenol (2.5%), NaOH (1.5 M) (16.5%)	NO_3^-, K, 3.2	50	0.5	1–10%	NO_3, 85; K, 115	22
		spec, PO_4^{3-}, NH_4^+	Others as above	PO_4^{3-}, 0.6	50	0.75	1–10%	120	
				NH_4^+, 1.8 + 1.2	52 + 70	0.86	1–10%	90	
12.	Trypsin	spec (N-benzoyl-*L*-arginine-*p*-nitroanalide hydrochloride)			3048	30 AWG	50–260 ppm	100	5
13.	pH	elec		1.5	5	0.5		180	7
14.	heavy metals	stripping voltammetry	1 mL, 90-s plating, 140-s stripping				10^{-9}–10^{-5} M		7
15.	SO_4^-	turbidimetric	(i) $BaCl_2$, $2H_2O$ (5%), polyvinylalcohol (0.05%)	5.9	112–204	1	ppm	180	23
		($BaSO_4$)	(ii) HCl (0.01 M)	5.9					
16.	glycerol/H_2O	spec	H_2O, bromothymol blue (0.001%)	4	140	1	10–80%		24
17.	Ca/EDTA strong acid/strong base titration	titrations, large dispersion	a. EDTA, 5 × 10^{-4} M	0.84	(i) mixing chamber 0.98 mL		10^{-3}–10^{-2} M	50	25
			b. NaOH, 10^{-3} M	1.35	(ii) 25	0.75			

	determination	detector	carrier stream/conditions	flow rate, mL min^{-1}	tubing		sensitivity	sample throughput, per hour	ref
					length, cm	i.d., mm [a]			
18.	Pb, Cu, Cd, and Zu in pharmaceutical products	turbidimetric (thioacetamide)	(i) thioacetamide, (ii) NaOH, glycerol, [a] and (iii) buffer [a]	(i) and (ii) 1.6	250		ppm		26
19.	NH_4^+ in amino acids	elec	(i) NaOH (0.5 M) (ii) NH_4^+ (5 ppm)	3.3 0.3	250		ppm		27
20.	strong acids and bases, HCOOH, CH_3COOH, CH_3NHCH_2OH	elec (titration)	(i) H_2O (ii) buffer	4.5 0.4	300		5×10^{-3}–1 M		28
21.	caffeine	spec/solvent extraction	(i) alkaline soln (ii) tetrapyridyl ammonium bromide (0.1%) in CCl_4	1.6 1.6	200		70–100 ppm	60	15
22.	Fe(III) ascorbic acid	pot	Ce(IV) soln	1.0	80		$1–20 \times 10^{-3}$ M	45–60	12
23.	N in pharmaceutical products	spec	(i) alkaline buffer (ii) sodium salicylate (15%), $Na_2Fe(CN)_5NO.2H_2O$ (0.03%) (iii) NaOCl (0.4% active Cl_2)	1.4 1.4 [b] 1.4 [b]	250+ 660 + 330		ppm	15–30	29
24.	SO_4^{2-} in dextran	nephelometry ($BaSO_4$)	as 15. Dextran >10% interferes, but FIA preferable to static method						29
25.	glucose	pot (enzymatic oxidation)	buffer, pH 6 pass through immobilised glucose oxidase in a reactor	2.5				120	30
26.	NO_3^-	NO_3^- electrode	buffer, pH 9.5	2	30			120	31
27.	Cl^-, Br^-, I^-	titration (Ag^+)	(i) H_2O (ii) $NaNO_3$ (0.1 M), $AgNO_3$ (10^{-3} M)	1.8 1.8 [b]	100	0.7			31
28.	Al	spec (Aluminon)	Aluminon soln	2.4				100	32
29.	viscosity	(i) spec (ii) refractometer (iii) dielectric	H_2O	2 or 8	70	0.8	1–100 cP	30–100	33
30.	refractive index	flow cell with LED one end and photodiode at other		2.9	215	0.86		100	13
31.	Pb and V(I) mixtures	spec	4-(2-pyridylazo) resorcinol, 10^{-3} M, pH 9.9 buffer	2.5	215	0.86	10^{-6}–10^{-4} M	100	34
32.	Ag	spec/solvent extraction (dithizone)	(i) dithizone in CCl_4 (7×10^{-5} M) (ii) aqueous				$5–30 \times 10^{-5}$ M		7
33.	SO_4^{2-}	turbidimetric ($BaSO_4$)	Ba(II) (0.02 M), EDTA (0.025 M) at pH 10 samples at pH 2	2.9	124	0.86	40–100 ppm		35
34.	NO_3^-	UV spec				1	1–30 ppm	120	36
35.	Ca in animal feeds (cresolphthalein complexone, CPC)	spec	(i) H_2O (ii) CPC (0.01%) (iii) 2-amino-2-methylpropan-1-ol (9%)	19.5 0.80 2.0	70+ 370+ 410+	1	0.5–5%	300	38
36.	protein in plant material	spec	(i) HCl, 0.6 M (ii) borax buffer, 10–10.5 [b] (iii) 2,4,6-trinitrobenzene sulphuric acid 0.15% [b]	3 3 3	60+ 40+ 200	1	40–160 ppm	120	37

[a] When not stated, usually 1 mm. [b] Added after the sample injection point.

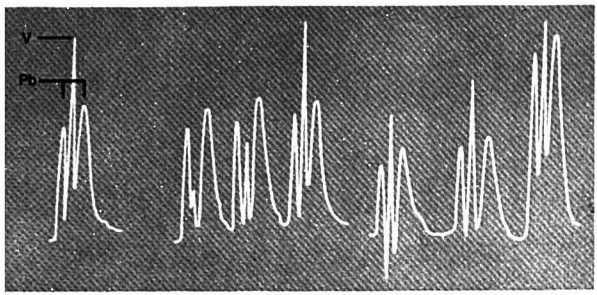

Figure 8. Different reactions of Pb (II) and V ($\overline{V}$) with PAR
In inner regions of sample plug pH is ca. 2, and only V ($\overline{V}$) reacts with PAR. In outer regions pH is higher (PAR carrier is at pH 9), and only Pb (II) reacts with PAR

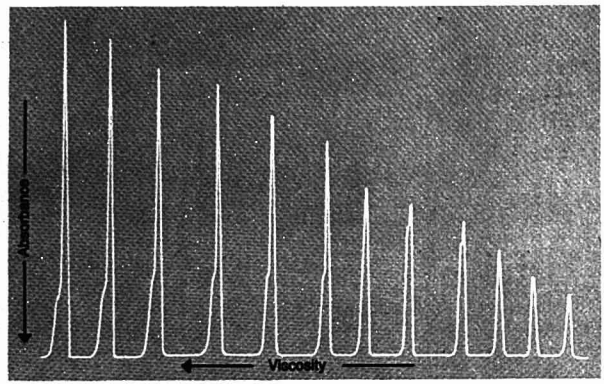

Figure 9. Peak profiles obtained by injecting glycerol water mixtures into water carrier stream coloured with methyl orange
Detector, spectrometer (525 nm). Flow rate, 7.17 cm s^{-1}. Sample size, 200 μL. Length of 0.86-mm i.d. tubing between injection and detection, 200 cm. Peak height linearly relates to log viscosity

faster than the corresponding reaction with nickel. By using two detectors in series or by stream splitting, mixtures of nickel and cobalt can be determined.

It is also possible to extract much more kinetic information from the chemical reaction which takes place as the sample is physically dispersed. The possibilities for analytical development are indicated by the single point determination (*20*) and a stopped flow procedure for the enzymatic determination of glucose (*7*).

Viscosity and Diffusion Coefficients. The viscosity can be measured in two ways: by the time taken for the sample to reach the detector under conditions of low dispersion or the peak height under conditions of medium dispersion. The former is dependent upon the Poiseuille equation and is, in principle, an absolute method. The latter is based on Taylor's equation and really measures the diffusion coefficient. The simplest illustration is to inject a sample into a coloured carrier stream. The absorbance of the sample plug at some point downstream is then a direct measure of the dispersion of the sample into the carrier (Figure 9). For any given system a calibration curve can be constructed relating log viscosity to peak height. Sample sizes of 6 μL have been used routinely for samples 1–20 cP, and the carrier serves to keep the apparatus clean. It appears to be an attractive method for measuring diffusion coefficients, which are mainly determined by extremely time-consuming methods and which have biochemical significance. These studies have shown up the importance of chemical interaction (mainly by hydrogen bonding) in the mixing process. It is evident that the theories of dispersion, discussed above, which do not take into account solvent–solvent interactions have limitations. For systems in which hydrogen bonding is minimised, e.g., toluene carrier, a linear relationship has been found for viscosity and time-to-peak maximum.

Other Nonsegmented Systems. FIA is only one form of nonsegmented continuous flow analysis. A narrow definition of the method has been adopted to keep this article within bounds. Thus, several important closely related methods have been omitted, notably the work of Mottola et al. (*43–46*) with a recycling system and that of Pungor et al. (*47, 48*) on potential measurement, both of which have helped to open up an examination of the potentialities of nonsegmented CFA.

Conclusions

The advantages of FIA are speed, simplicity of apparatus, and the potential for some novel analyses. The disadvantages are the inability to perform lengthy operations and the difficulty in automatically performing different determinations on the same sample.

At present, FIA is useful to those who perform straightforward analyses routinely. The saving in time is useful, and it is easy to switch from one determination to another either with the replaceable units in the BIFOK instrument or by making up separate units for different determinations. It is a godsend to teachers of analytical chemistry. With simple apparatus, easily manufactured by the departmental workshop, the principles of continuous flow analysis can be demonstrated, spectrophotometers can be spared the hammering given by a class of students, analysis time is greatly shortened, and so many results are obtained in such a short time that ideas of precision and elementary statistics are introduced naturally.

For the more complex analyses we can expect further instrumental development. Procedures for dialysis and solvent extraction already exist, and other analytical operations will probably be adopted for FIA. In our laboratory we are applying microprocessors to the control of the sample introduction and the analysis and to processing the results. It is clear that it is feasible to perform several determinations on the same sample. All of these developments depend on exploiting chemistry, and thinking old problems through in a new way.

In some respects the relationship of FIA to other systems of CFA is analogous to the position of the microprocessor in the realm of computers. One development in automatic analysis has been a fully computerised device capable of performing several determinations on the one sample. There is no way in which FIA could mimic this system because excessive dispersion of the sample would take place during

Varian UV-Vis spectrophotometers for every need.

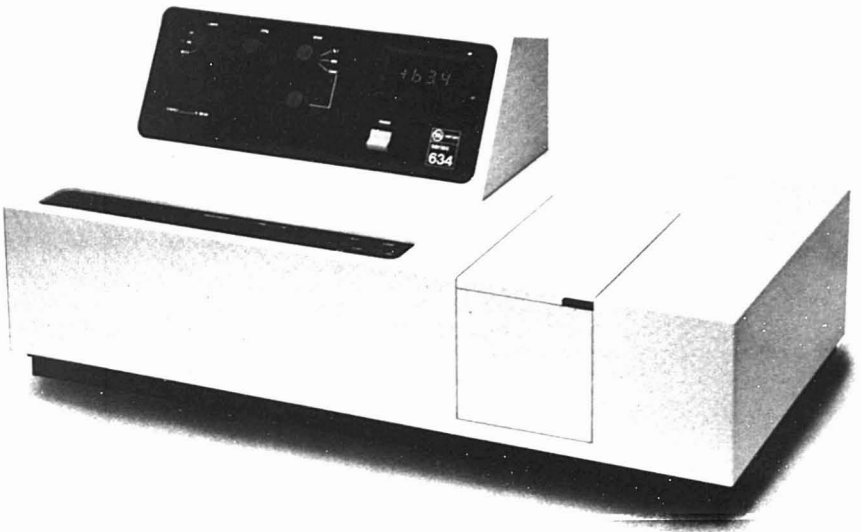

Choose Varian's UV-Vis spectrophotometer ...join thousands of happy users.

The Series 634 Spectrophotometers offer outstanding value in low-priced instruments. Take a look at their versatility. Thousands have chosen to buy Series 634 over all competitors.

Digital readout. This is standard on both instruments for all three operating modes: absorbance, transmission, and concentration. And there's automatic decimal positioning in the absorbance and %T modes.

Versatile wavelength ranges. Series 634 covers the 190 to 900-nm range—unsurpassed in low-priced instruments. Choose the model that fits your needs and budget. *All* Series 634 spectrophotometers measure up to 900 nm so you can do those important analyses at higher wavelengths.

Choice of wavelength scanning. Both manual and automatic scanning are available. Automatic scanning is simple with pushbutton selection of four speeds. Automatic scanning is standard on the Model 634S and an integral part of the instrument.

Recorder compatibility. Unlike some spectrophotometers, Series 634 is compatible with standard laboratory recorders that can also be used with other instruments. You're not locked in to a one-use recorder, an important feature for the budget-limited lab. And when it comes to a fine, all-round recorder to do best by your Series 634, Varian has that, too.

Sample compartment versatility. The key is size. The extra large compartment lets you handle a wide range of sample accessories of different sizes and shapes. Three sided access plus a large beam separation make it easy to use. With Series 634 you can measure many samples that other low-priced instruments can't handle.

These are just a few highlights of this versatile, low-priced spectrophotometer. We haven't even touched on its outstanding performance, so you'll want to know more.

Circle **220** for a Series 634 data package.

Circle **221** if you'd like to see a representative.

varian

Varian Instrument Division, 611 Hansen Way, Box D-070, Palo Alto, California 94303

the course of analysis. It may be, however, that the speed, flexibility, and low cost of FIA make it worthwhile in some instances to perform a sequence of individual determinations—by analogy, have a number of dedicated microcomputers rather than everything on a main frame computer. There is little doubt that in the long run FIA will affect the philosophy of automatic analysis. In the short term, as with microprocessor development, we may expect a flurry of methods that are no more than the straightforward adaptation of existing continuous flow methods. The real developments will come about by full realisation of the chemical potential of the system. Hopefully, FIA will excite students, be of practical value to analysts, and by virtue of its simplicity bring about an improved understanding and use of all continuous flow systems.

Literature Cited

(1) L. T. Skeggs, *Am. J. Clin. Pathol.*, **13**, 451 (1957).
(2) J. Růžička and E. H. Hansen, *Anal. Chim. Acta*, **78**, 17 (1975); Danish Patent Application No. 4846/84, Sept. 1974; U.S. Patent 4,022,575.
(3) K. K. Stewart, G. R. Beecher, and P. E. Hare, *Fed. Proc.*, **33**, 1439 (1974).
(4) G. R. Beecher, K. K. Stewart, and P. E. Hare, 168th Meeting ACS, Div. Agric. and Food Chem., Symp. on Chemical & Biological Methods for Protein Quality Determination, Paper No. 22, 1974.
(5) K. K. Stewart, G. R. Beecher, and P. E. Hare, *Anal. Biochem.*, **70**, 167 (1976).
(6) J. Růžička and E. H. Hansen, *Anal. Chim. Acta*, **87**, 353 (1976).
(7) J. Růžička and E. H. Hansen, *ibid.*, **99**, 37 (1978).
(8) H. Bergamin F°, B. F. Reis, and E.A.G. Zagatto, *ibid.*, **97**, 427 (1978).
(9) K. K. Stewart, *Anal. Chem.*, **49**, 2125 (1977).
(10) J. Růžička, E. H. Hansen, and E. A. Zagatto, *Anal. Chim. Acta*, **88**, 1 (1977).
(11) G. Nagy, Zs. Feher, and E. Pungor, *ibid.*, **52**, 47 (1970).
(12) B. Karlberg and S. Thelander, *Analyst*, **103**, in press (1978).
(13) D. Betteridge, E. L. Dagless, B. Fields, and N. Graves, *ibid.*, in press.
(14) D. Betteridge, E. L. Dagless, P. David, and D. R. Deans, Workshop at SAC-77 Conf., Birmingham, England, Jul. 1977.
(15) B. Karlberg and S. Thelander, *Anal. Chim. Acta*, **98**, 1 (1978).
(16) J. Růžička and J.W.B. Stewart, *ibid.*, **79**, 79 (1975).
(17) J. Růžička, H. B. Filho, and E. A. Zagatto, *ibid.*, **81**, 371 (1976).
(18) J. Růžička, J.W.B. Stewart, and E. A. Zagatto, *ibid.*, p 387.
(19) J.W.B. Stewart and J. Růžička, *ibid.*, **82**, 137 (1976).
(20) E. H. Hansen, J. Růžička, and B. Rietz, *ibid.*, **89**, 241 (1977).
(21) E. H. Hansen, A. K. Ghose, and J. Růžička, *Analyst*, **102**, 705 (1977).
(22) E. H. Hansen, F. J. Krug, A. K. Ghose, and J. Růžička, *ibid.*, p 714.
(23) F. J. Krug, H. B. Filho, E.A.G. Zagatto, and S. S. Jørgensen, *ibid.*, p 503.
(24) D. Betteridge and J. Růžička, *Talanta*, **23**, 409 (1976).
(25) J. Růžička, E. H. Hansen, and H. Mosback, *Anal. Chim. Acta*, **92**, 219 (1977).
(26) E. Bylund, R. Anderson, and J. Carlsson, Proc. Workshop on Flow Injection Analysis, No. 1, Swedish Chemical Society, Uppsala, Sweden, 4–5 Oct. 1977.
(27) B. Karlberg and I. Dahl, *ibid.*, No. 2.
(28) O. Åström, *ibid.*, No. 3.
(29) J. Lindberg and B. Ander, *ibid.*, No. 7.
(30) L. Gorton, *ibid.*, No. 8.
(31) R. Lundin and T. Anfält, *ibid.*, No. 11.
(32) P. Holmqvist, *ibid.*, No. 13.
(33) D. Betteridge, E. L. Dagless, P. David, and D. R. Deans, Abstract SAC-77 Conf., Birmingham, England, Jul. 1977.
(34) D. Betteridge and B. Fields, *Anal. Chem.*, **50**, 654 (1978).
(35) D. Betteridge, D. Beetlestone, and P. Sweet, unpublished results, March–May 1978.
(36) J. Slanina, F. Bakker, A.G.M. Bruijn-Hes, and J. J. Möls, *Z. Anal. Chem.*, **289**, 38 (1978).
(37) L. Sodeck, J. Růžička, and J.W.B. Stewart, *Anal. Chim. Acta*, **97**, 327 (1978).
(38) W. D. Basson and J. F. Van Staden, *Analyst*, **103**, 296 (1978).
(39) M. Margoshes, *Anal. Chem.*, **49**, 17 (1977).
(40) J. Růžička, E. H. Hansen, H. Mosback, and F. J. Krug, *ibid.*, p 1858.
(41) G. Taylor, *Proc. Roy. Soc. Ser. A.*, **219**, 186 (1953).
(42) B. Fleet and A.Y.W. Ho, in "Ion-Selective Electrodes", E. Pungor, Ed., pp 17–37, Akademiai Kiado, Budapest, Hungary, 1973.
(43) V.V.S.E. Dutt and H. A. Mottola, *Anal. Chem.*, **47**, 357 (1975).
(44) V.V.S.E. Dutt, A. Eskander-Hanna, and H. A. Mottola, *ibid.*, **48**, 1207 (1976).
(45) V.V.S.E. Dutt and H. A. Mottola, *ibid.*, **49**, 319 (1977).
(46) V.V.S.E. Dutt and H. A. Mottola, *ibid.*, p 776.
(47) Zs. Feher, G. Nagy, K. Toth, and E. Pungor, *Analyst*, **99**, 899 (1974).
(48) E. Pungor, Zs. Feher, and G. Nagy, *Pure Appl. Chem.*, **44**, 595 (1975).

D. Betteridge is a reader in the Department of Chemistry of the University College of Swansea (Wales). He received his BS and PhD degrees from the University of Birmingham, studying under R. Belcher and T. S. West. Dr. Betteridge's research interests include photoelectron spectrometry, photoacoustic and acoustic emission spectroscopy, flow injection analysis, analytical applications of microprocessors, and the history of the teaching of analytical chemistry.

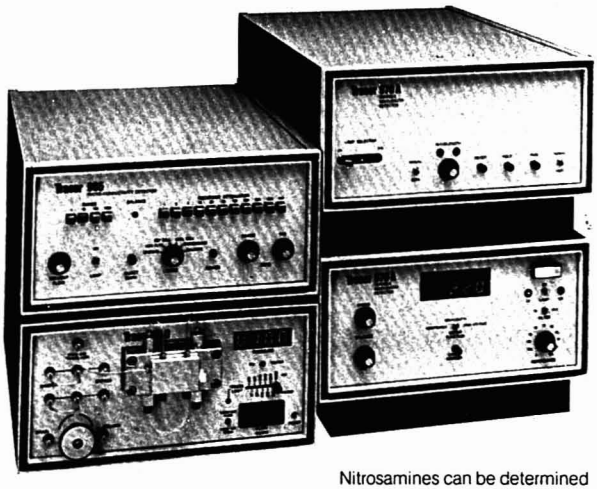

The Series 900 Liquid Chromatograph by Tracor is the most dynamic liquid chromatograph available today. The Series 900 features Tracor's patent pending 965 Photo-Conductivity detector. This unique detector features unusually high sensitivity and selectivity for compounds which contain chlorine, nitrogen and some sulfur compounds. Two chromatograms of polychlorinated biphenyls are shown using the 965 Photo-Conductivity Detector. This mixture gives no response at 254 nm on a UV absorbance detector. Isochratic runs using the same solvent mixture allow for the determination of the different PCB mixtures by the different peak ratios.

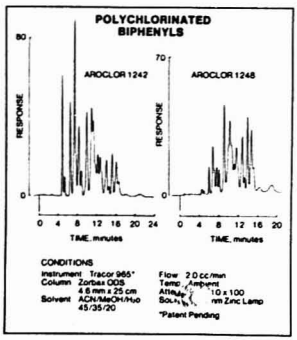

Nitrosamines can be determined at the residue level with the use of the Tracor 965 Photo-Conductivity Detector. Two nitrosamine mixtures, 10 ng and 5 ng respectively, are shown using an isochratic solvent mixture.

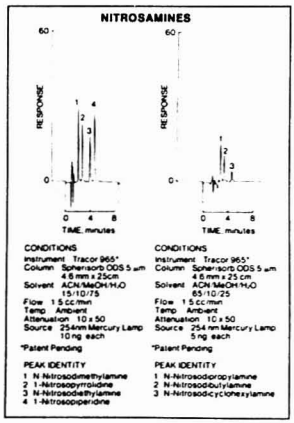

With the use of a dual pen recorder, the output of the Tracor 970A variable wavelength detector and the Tracor 965 Photo-Conductivity Detector can be recorded using the detectors in series. A chromatogram containing several polynuclear hydrocarbons and two chlorinated pesticides shows the selectivity of chlorinated pesticides over hydrocarbons on the Tracor 965 Photo-Conductivity Detector. The UV absorbance detector responds to the polynuclear hydrocarbons and gives no response to the pesticides. The effluent from the variable wavelength detector is passed to the Photo-Conductivity Detector with very little band spreading where the pesticides are detected. (Recycling of the solvent mixture for continuous use of an isocratic solvent mixture is recommended for the Photo-Conductivity Detector. This recycling is possible with the use of an ion-exchange cartridge in the system before the high pressure pump.)

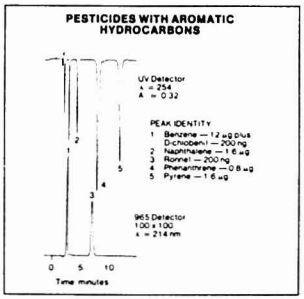

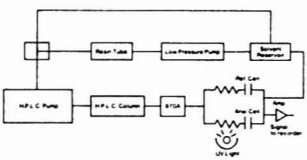

Liquid Chromatography by Tracor

Tracor Instruments

Tracor, Inc. 6500 Tracor Lane Austin, Texas 78721 Telephone 512:926 2800 TELEX 77-6414

CIRCLE 202 ON READER SERVICE CARD

Report

Janet Osteryoung
National Science Foundation
Washington, D.C. 20550

Survey of Analytical Chemistry Faculty in Graduate Departments of Chemistry in the United States and Canada

Analytical chemists in the U.S. have assumed for the last five years or so that their numbers were increasing in graduate chemistry departments in this country. To provide some facts pertinent to this assumption, I have surveyed the *ACS Directory of Graduate Research* to identify analytical chemists in graduate chemistry departments in the U.S. and Canada and to explore how their numbers have changed in various categories over time. The results of the survey may be summarized by saying that there has been a pronounced increase of analytical chemists in graduate departments, that the increase is much greater than that of all chemistry faculty, and that the increases pervade all types of institutions.

Data for the survey were obtained from the 1971, 1975, and 1977 editions of the *ACS Directory of Graduate Research*, which lists members of the faculties of graduate chemistry departments in the U.S. and Canada by institution. The listing for each faculty member includes a list of publications and theses supervised, areas of research interest, some biographical information, and an italicized word or short phrase describing the primary broad classification of the individual as a chemist. Because the material for the Directory comes from the departments themselves, this last item is a fairly accurate representation of the attitude of the chemist himself about his professional identification. In this study, this description, unmodified by consideration of publication titles, etc., was used to categorize people. With the exception of *Inorganic–Analytical*, descriptions including the word *analytical* were used to identify analytical chemists. In addition, a very few individuals categorizing their interest as *Chemical Instrumentation* or *Electrochemistry* were placed in this group. Individuals who have their primary professional identification as analytical chemists but who choose for the Directory another description such as *Mass Spectroscopy* were not included. Only departments appearing in all three years of the survey were included. A few institutions that changed dramatically over that time period due to substantial reorganization were not included. Summaries of the data are presented in Table I and Figure 1. The survey sample included 195 schools. During this time period, about 40% of the departments increased in size, whereas the remainder either held constant or decreased in size. During the time period 1971–75, 32% of the expanding departments increased in number of analytical faculty, 57% remained constant, and only 10% decreased. In the same period, 31% of schools that remained the same or decreased in total number of faculty also increased in number of analytical faculty. Fifty-two percent of these schools remained constant in numbers of analytical faculty, and 17% decreased. Clearly, the pressure to increase the numbers of analytical faculty was expressed uniformly across universities, and the response was as impressive among those schools experiencing severe financial pressures as among those undergoing expansion. Considering the difficulties in contracting the size of a department, this in itself is remarkable. The period 1975–77 naturally expresses changes of a smaller magnitude. In 1971–75, 32% of the 195 schools increased the number of analytical faculty, 14% decreased, and 54% remained the same.

Table I. Total Numbers of Faculty

	1971	1975	1977
all 195	4587	4669	4719
top 20	710	702	698
next 58	1623	1607	1647

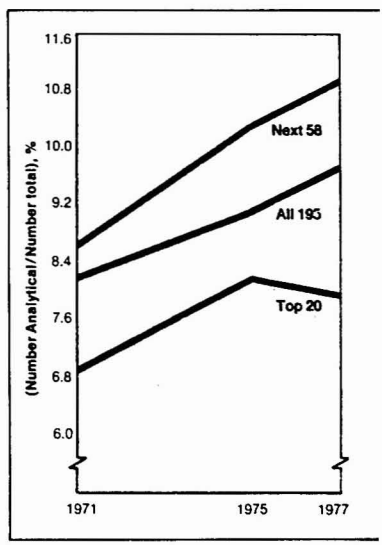

Figure 1. Percentage increases in analytical faculty at schools with graduate chemistry departments in the U.S. and Canada. See Table IV

Table II. Roose-Andersen Report Ranking of Graduate Chemistry Faculties

TOP 20

Harvard	Illinois	Wisconsin	Purdue
Cal Tech	California, Los Angeles	Yale	California, San Diego
California, Berkeley	Chicago	Princeton	Ohio State
Stanford	Columbia	Northwestern	Texas
MIT	Cornell	Iowa State (Ames)	Indiana

NEXT 58

Michigan	Colorado	Iowa (Iowa City)	Wayne State	Nebraska
Minnesota	Oregon	Kansas	Arizona State	New Hampshire
Rockefeller	Brown	Louisiana State	Cincinnati	Rensselaer
Florida State	Florida	Massachusetts	Delaware	Rutgers
Johns Hopkins	Notre Dame	North Carolina	Emory	Syracuse
Michigan State	Rochester	Oregon State	Georgia Tech	Tennessee
Penn State	Arizona	Pennsylvania	Houston	Texas A & M
Rice	Buffalo	Pittsburgh	Illinois Institute of Technology	Tulane
Washington (Seattle)	California, Davis	Southern California	Kansas State	Virginia
Brandeis	California, Riverside	Utah	Maryland	Virginia Polytech
Carnegie Mellon	Duke	Vanderbilt	N.Y.U.	Washington State
Case Western Reserve	Georgia	Washington (St. Louis)		

For 1975–77, the corresponding numbers are 26%, 11%, and 63%. Between 1971 and 1975, the increase in number of faculty was 82 while the increase in analytical faculty was 49, or 60% of the net increase. The fraction of analytical faculty increased from 8.2 to 9.1%. In the period 1975 to 1977, the increase was 50 faculty, whereas the increase in analytical faculty was 34 (68%). The fraction of analytical faculty in 1977 was 9.7%.

Although these numbers demonstrate strong and sustained growth in the role of the field of chemical analysis in graduate chemistry departments, it is a common perception that analytical chemistry is not well represented at the "best schools" and that these schools have not been a part of the phenomenon described above. For this reason, it is instructive to examine schools in some quality grouping. For this purpose, the 1970 ranking of graduate chemistry faculties by the Roose-Andersen Report was used. This is somewhat unsatisfactory because the ranking is for U.S. schools only and because reputation lags so far behind current performance, but it provides some basis for examining trends in the better schools in comparison with all schools. The *Top 20* and *Next 58* are taken from this report and listed in Table II. Summaries of data for all schools and for schools by category are given in Tables I and III–V. In addition, the data of Table IV are represented graphically in Figure 1. Clearly, the growth patterns are similar in each category. The growth rate has been greatest in the *Next 58* schools, but the *Top 20* have increased in numbers of analytical faculty while decreasing in overall numbers. This is more remarkable when one considers that 7 of the *Top 20* (35% of the schools representing 30% of the faculty) have no analytical chemist on the faculty. Of the *Next 58* only 13 (22% representing 17% of the faculty) and of the remaining 117 only 21 (18% representing 16% of the faculty) have no analytical chemist. It is not possible based on this cursory examination to identify causal factors that account for the phenomenon of strong growth in the area of academic analytical chemistry. However, it is clearly the collective wisdom of academic chemistry departments based on the most meaningful vote, allocation of resources, that the subdiscipline of analytical chemistry has been undervalued in the recent past and that the strength of the discipline as a whole will be improved by providing a larger fraction of resources to analytical chemistry.

Table III. Numbers of Analytical Faculty

	1971	1975	1977
all 195	374	423	457
top 20	49	57	55
next 58	139	166	179

Table IV. Analytical Faculty as % of Total Faculty

	1971	1975	1977
all 195	8.2	9.1	9.7
top 20	6.9	8.1	7.9
next 58	8.6	10.3	10.9

Table V. Number in 1977 Minus Number in 1971

	total faculty	analytical faculty
all 195	132	83
top 20	−12	6
next 58	24	40

Janet Osteryoung is associate professor of civil engineering at Colorado State University. She obtained the PhD degree in chemistry at Caltech with Fred Anson in 1967. She is currently on leave from CSU while temporary Program Director for Chemical Analysis, National Science Foundation. Her research interests include electroanalytical methods development, especially for toxic substances in the environment.

The Model 4202 Dual-Channel Signal Averager

No matter what you call your experiment—
• AUGER • ESCA • NMR • ESR • EPR • ION DETECTION • CYCLIC VOLTAMMETRY • MICROWAVE SPECTROSCOPY • MOLECULAR BEAM STUDIES • IR SPECTROSCOPY • TIME OF FLIGHT MASS SPECTROSCOPY • KINETICS
ask PARC about their NEW Model 4202.

You'll get all these outstanding features!

- Dual Input signal channels for processing two simultaneous signals.
- 3 switch selectable averaging modes (Linear Summation, Exponential, Normalized) —choose the one that best fits your type of signal.
- Huge memory of 2048 28-bit words—lets you average for hours without memory overflow.
- Variable Sampling Rates (5 μs to .9 s) to accommodate slow and fast signals.
- Division & Subtraction of curves stored in separate memory halves for data normalization and baseline (blank) subtraction.
- Analog & Digital outputs for X-Y plotters and computer peripherals.
- Transient Capture
- 4 Histogram Modes: Multichannel Scaling, Time Interval Distribution, Event Correllogram & Latency Histogram.

Low Cost—the Model 4202's domestic price is $5495 including vertically-mounted CRT. A rack-mounted version including side-mounted CRT is $5595. You can purchase the Model 4202 without CRT for a low $4495.

Write to EG&G Princeton Applied Research, P.O. Box 2565, Princeton, NJ 08540; or phone 609/452-2111 to arrange a demonstration or additional information.

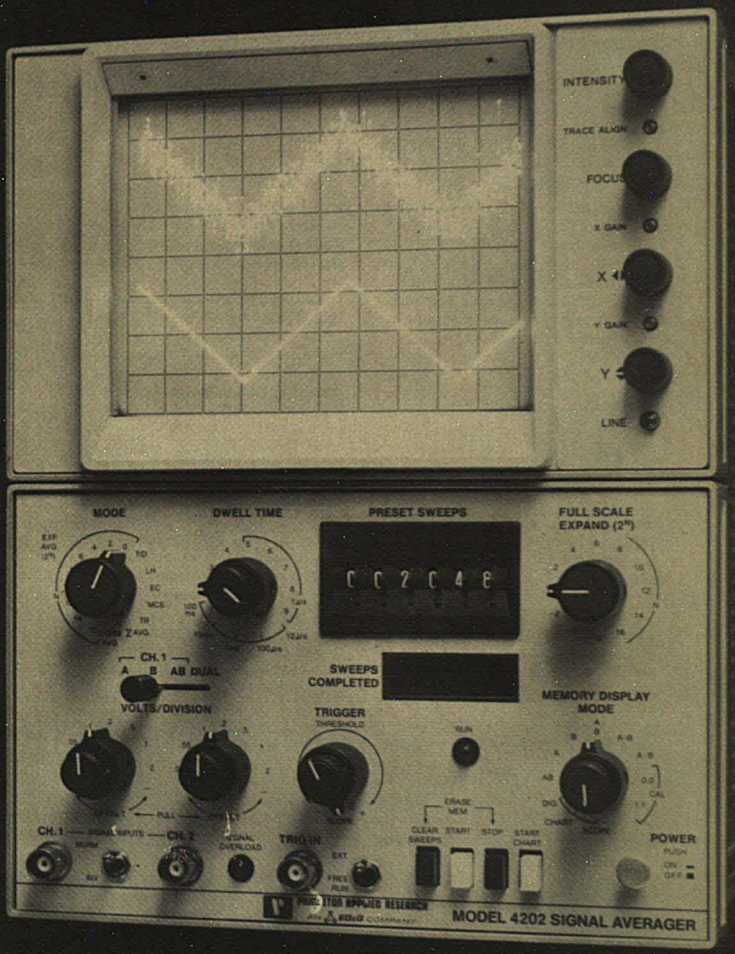

SYSTEM MANUFACTURERS: Contact us for OEM applications.

453

EG&G
PRINCETON APPLIED RESEARCH

Circle 171 For Information Only

Report

H. A. Laitinen
University of Florida
Gainesville, Fla. 32604

Professional Status of Academic Analytical Chemistry

In an article entitled "Reputational Ratings of Doctoral Programs" [*Science*, **199**, 1310 (1978)], R. T. Hartnett, M. J. Clark, and L. L. Baird, who are research psychologists at Educational Testing Service, Princeton, N.J., examined doctoral programs in three fields in 25 institutions. This study differed from the surveys conducted by the American Council on Education in 1964 and 1969 in covering a smaller number of institutions and programs in greater detail. The fields (chemistry, history, and psychology) were chosen to permit a comparison of the ratings of subspecialties with those of the fields as a whole. In each discipline, each faculty respondent was asked to rate the quality of the faculty in his or her own subspecialty as well as in the whole department in the institutions under study.

The correlations of ratings of the subspecialties with the ratings of total programs are given in Table I. To quote the original article, "In chemistry departments, a close relation between sub-specialty faculty ratings is also the usual case, but there is one glaring exception—analytical chemistry".

An inquiry to Dr. Hartnett led to the scatter diagram shown in Figure 1, in which it emerges that four departments out of the 25 surveyed had high overall ratings but showed up poorly in analytical chemistry. Indeed, if these four were omitted in calculating a new Pearson correlation coefficient, the new value of r became 0.85.

It is apparent that the "normal" situation is for a good correlation between analytical chemistry and chemistry as a whole, but that a relatively few excellent chemistry departments have chosen to ignore or downgrade analytical chemistry as a graduate discipline. It might be remarked that several departments showing overall excellence are also outstanding in analytical, and that in others analytical is relatively stronger than the department as a whole. This situation was clearly evident in the survey carried out by G. A. Rechnitz several years ago [ANAL. CHEM., **43** (4), 51A (1971)] as well as that of Janet Osteryoung in the current issue (page 849 A).

The occasional noncorrelation between overall quality and excellence in analytical would be of little concern, except that several highly rated chemistry departments that are weak in graduate analytical chemistry tend to serve as models for developing departments.

It appears to this writer that there are two basic reasons why a few otherwise excellent departments failed to develop strong analytical research programs. The first is that analytical research, which deals with improvements in methodology, can be ignored if research in other areas is content to use state-of-the-art methodology, i.e., to rely on others for its advancement. The other reason is that modern analytical chemistry is itself a complex

Table I. Correlations of Ratings of Subspecialties with Ratings of Total Programs, CGS/ETS Survey 1975. All Ratings Pertain to Quality of Faculty

discipline and subspecialty	range in no. of raters[a]	Pearson r
chemistry		
analytical	15–33	0.40
biochemical	11–39	0.94
inorganic	35–63	0.94
organic	80–121	0.98
physical	70–151	0.98
history		
ancient	8–23	0.94
medieval	15–35	0.91
modern	52–131	0.99
american	75–169	0.98
third world	24–68	0.95
psychology		
educational	1–4	0.79
measurement	1–6	0.91
personality	6–19	0.88
developmental	9–40	0.85
experimental	64–168	0.98
organizational	7–18	0.54
clinical	26–97	0.78
social	21–72	0.88

[a] Refers to the number of ratings supplied by respondents for the subspecialty faculty of a given institution. Thus, the analytical chemistry faculty of one institution was rated by 33 respondents, of another by 15.

0003-2700/78/0350-852A$01.00/0

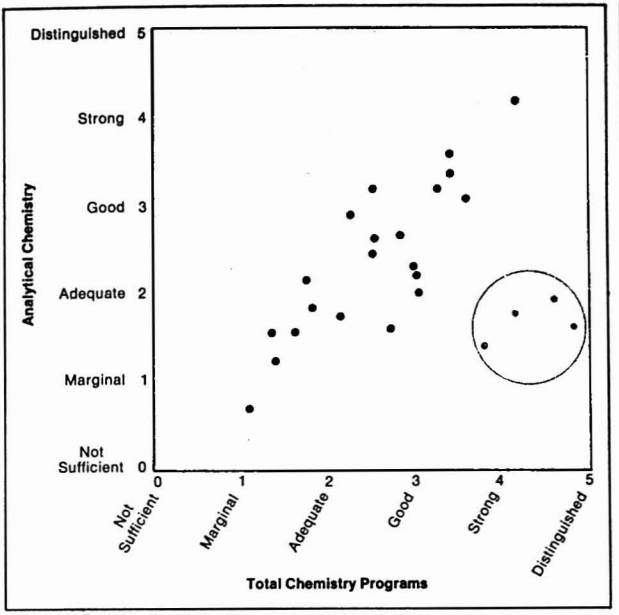

Figure 1. Ratings of total chemistry and analytical chemistry programs

area with several subdisciplines, so to have a truly viable analytical program is difficult if a department is strongly oriented around individual research programs of limited number.

Of course, analytical advances are made by chemists of many types, and even without an identifiable analytical graduate program, a department may be making significant contributions to analytical research. Conversely, analytical chemists are making significant contributions to other areas of chemistry through the use of their methodology. It comes down to a self-definition, in which a chemist chooses to associate professionally with colleagues of kindred interests. This association takes various forms, such as joining professional societies or divisions of them, choosing a publication medium, participating in research symposia, and the like. A given chemist, of course, can have more than one professional identification such as analytical chemistry plus spectroscopy, electrochemistry, chromatography, computers, etc.

Despite this blurring of professional identities, analytical chemists do have a commonality in possessing at least an awareness of many diverse approaches to problem-solving, and their contribution consists of choosing the method or combination of methods leading to the most efficient solution to the problem at hand. As pointed out by Janet Osteryoung, the analytical community has felt for the past several years that it is gaining strength in graduate departments, and this feeling has been confirmed by her study. Correspondingly, the demand for PhD analytical chemists in industry and government as well as academic institutions has grown in recent years to the point that emerging PhD's in other areas of chemistry are belatedly discovering an interest in analytical. This is surely acceptable, *provided* that the necessary diversity of background and experience and interest in dealing with analytical problem-solving is present. Just because an organic chemist has had experience in interpreting IR, MS, or NMR spectra in identifying structures does not qualify him as an analytical chemist, unless he has the interest and competence to deal with impurities and mixtures. Likewise, the experimental physical chemist may or may not qualify for an analytical-oriented position depending upon his attitude and experience in analytically significant measurements. It is said that imitation is the sincerest form of flattery, and the analytical profession can take pride because it is growing by accretion as well as by internal nourishment.

16 PRODUCTION 12 QUALITY 67 INDIVIDUAL FOR ONLY

When you look at a Hamilton Microliter® Syringe, it looks like just a simple syringe. Some glass, a needle, and a plunger. Just one moving part. But, looks can be deceiving.

Producing a syringe to the quality standards we've set for ourselves is no simple task. It begins with a concept: To make the finest precision syringe that it is possible to make. To achieve that goal requires a commitment to quality.

That means starting with only quality materials: pharmaceutical grade glass and fine stainless steel. It also means trained craftsmen. Here are a few of the operations through which a Microliter® syringe goes.

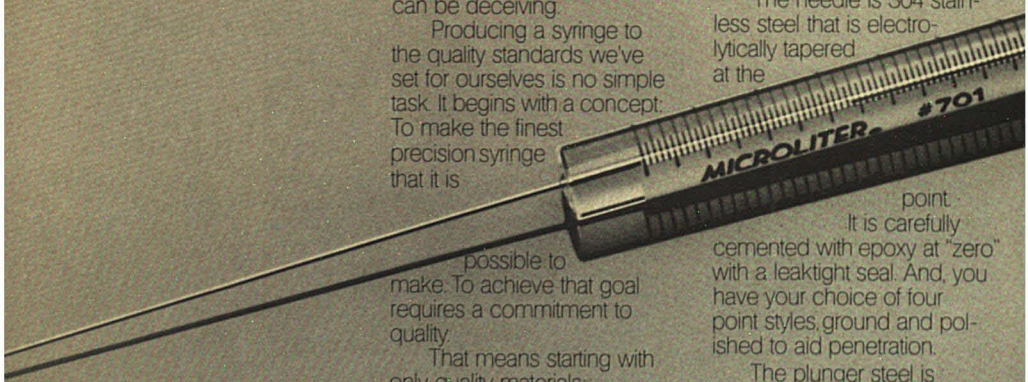

The barrel is annealed to relieve strains, the flange is formed lovingly by hand, and the graduations are carefully etched into the glass by ionic reaction with silver nitrate...in all, some 36 individual operations are performed on the glass.

The needle is 304 stainless steel that is electrolytically tapered at the point. It is carefully cemented with epoxy at "zero" with a leaktight seal. And, you have your choice of four point styles, ground and polished to aid penetration.

The plunger steel is straightened by precision machines and centerless ground. The button is permanently staked onto the plunger.

Each syringe is individually assembled and the plunger fitted by hand to exceedingly close tolerances. Then they are tested for leaks with acetone at five

STAGES, CONTROL CHECKS, OPERATIONS $18.00.

atmospheres pressure.

Altogether there are 67 individual production operations and quality control checks. You can't produce a quality syringe without every single step. That's why the scientific community has relied on the accuracy of Hamilton syringes for two decades. And that's a reputation we don't take lightly.

And, finally, the price. A Microliter® 701N was $18.00 in 1958...and it's still $18.00 in 1978. Only by constantly developing our manufacturing skills and improving our speed of production have we been able to offset the rising costs of material and labor.

That's what you can't see when you look at a Hamilton Syringe. The concept. The commitment. The pride. But, they're more important to the quality of a syringe than the materials used or production process. They are what has made Hamilton syringes the world's standard precision liquid measuring device.

For a free copy of our current catalog, write to Dept. A, Hamilton Company, Post Office Box 10030, Reno, Nevada 89510.

HAMILTON

CIRCLE 100 ON READER SERVICE CARD

September 10–15, 1978

176th ACS National Meeting

Miami Beach

The Fall National Meeting of the American Chemical Society will be held in Miami Beach, September 10–15, 1978. As usual the annual meeting will feature a myriad of technical sessions and professional and social activities that will bring thousands of people in the chemical profession to this southern city. In all, 27 of the Society's 29 divisions and a number of committees will participate in the five days of technical sessions. The technical program will include over 3000 papers to be presented at almost 400 planned sessions.

The most important event at Miami Beach for the readers of ANALYTICAL CHEMISTRY is the celebration of the 50th anniversary of the JOURNAL. The Analytical Chemistry Division will mark the occasion with the 50th Anniversary Symposium dedicated to Lawrence T. Hallett, a former editor. The symposium is scheduled for Wednesday morning and will be presided over by Herbert A. Laitinen, current editor of ANALYTICAL CHEMISTRY. The community that has nurtured the JOURNAL over the years will have an opportunity to hear eight distinguished speakers survey the history of the JOURNAL and the discipline which helped put the JOURNAL in its place today. G. E. Peace, Jr., will survey the origin of the JOURNAL during the late 19th century. Sidney Siggia will follow with a review of the many contributions of Lawrence T. Hallett during the early years when Dr. Hallett was editor. The next five speakers will review the developments in the field of analytical chemistry in each of the last five decades, concluding with the 1970's. Finally, the concluding remarks prepared by I. M. Kolthoff, the man regarded by many as the father of modern analytical chemistry, will be read by one of his former students, Vernon Stenger. The entire proceedings of the symposium will be published in the A pages of ANALYTICAL CHEMISTRY in the November and December 1978 issues.

Other programs of the Analytical Chemistry Division include three symposia with three sessions each and six general sessions. A total of 103 papers will be presented at these sessions. Among the symposia topics are: image detectors in chemistry (15 papers), novel approaches to trace drug analysis (15 papers), and sample injection techniques into unsegmented flows (12 papers). The six general sessions will cover the areas of electroanalytical chemistry, chromatography, spectroscopy, and general analytical chemistry.

In addition to these programs for which the Analytical Division is the primary sponsor, the Division will participate in a number of symposia cosponsored with other divisions. These are: Symposium on Trace Analysis of Nitrogen and Sulfur Pollutants in the Atmosphere (five sessions), joint with the Division of Environmental Chemistry; Symposium on Analytical Chemistry of Petroleum Hydrocarbons in the Marine/Aquatic Environment (three sessions), joint with the Division of Petroleum Chemistry, Inc.; Symposium on *A Century of Chemistry at the U.S. Geological Survey* (four sessions), joint with the Division of the History of Chemistry; Symposium on Chemical Oceanography in the Academic Curriculum (one session), joint with the Division of Chemical Education, Inc.; Symposium on High-Efficiency Radiochemical Separations (two sessions), joint with the Division of Nuclear Chemistry and Technology.

All sessions sponsored by the Analytical Chemistry Division will be held in the Miami Beach Convention Center, except the program jointly sponsored with the Division of Nuclear Chemistry and Technology. That symposium will be held at Doral Beach, which is some distance north from the convention center. There will be a shuttle bus service.

The Analytical Chemistry Division social hour and dinner ($11) will be held Tuesday, September 12 at 6:00 and 7:00 p.m., respectively, at Hotel

Here are a few of the hundreds of hotels and thousands of apartment buildings where some three million Miami Beach visitors find lodging every year

Fontainbleau. Interested persons are urged to purchase tickets in advance. For further information on the advance ticket puchase and the room number, see *Chem. Eng. News*, August 7.

Several ACS courses given in conjunction with the meeting before and after the meeting will be of interest to analytical chemists. For more information, see pages 866 A and 868 A.

The detailed technical program given below includes all the Analytical Division sessions and those cosponsored by the Division.

Preregistration forms and housing information are contained in *Chem. Eng. News*, June 26, 1978. The complete technical program for the meeting will appear in *Chem. Eng. News*, August 7, 1978.

DIVISION OF ANALYTICAL CHEMISTRY

D. M. Hercules, *Chairman*
A. J. Cunningham, *Secretary*

MONDAY MORNING

SECTION A

Miami Beach Convention Center
Symposium on Image Detectors in Chemistry *Joint with Division of Physical Chemistry*
Yair Talmi, *Presiding*

9:00—1. Image Detectors in Chemistry, An Overview. **Y. Talmi.**
9:20—2. Computer Processing of Spectroscopic Data. Applications in Liquid Chromatography. **D. B. Pautler, J. C. Spavins, M. L. Malczewski, M. J. Milano.**
9:50—3. A Dual-Beam Linear Photodiode Array Spectrometer System for Liquid Chromatographic Separation Methods Development. **W. Nunn, R. E. Dessy.**
10:25—Intermission.
10:40—4. Versatility of an Optical Multichannel Analyzer as an HPLC Detector. **J. R. Jadamec, W. A. Saner, R. W. Sager.**
11:10—5. Multidimensional, Multicomponent Fluorescence Analysis with a Video Fluorometer. **J. B. Callis, D. W. Johnson, G. F. Christian, E. R. Davidson.**
11:45—Discussion.

SECTION B

Miami Beach Convention Center
Symposium on Novel Approaches to Trace Drug Analysis
L. A. Sternson, *Presiding*

9:00—Introductory Remarks.
9:05—6. Drug Analysis by HPLC. **B. L. Karger, R. W. Giese, R. Eksteen, N. Tanaka.**
9:45—7. The Use of Immobilized Enzymes in the Analysis of Biological Fluids. **P. W. Carr, R. S. Shifreen.**
10:25—Intermission.
10:35—8. The Use of Chemical Derivatization in the HPLC Analysis of Anti-Neoplastic Agents. **L. A. Sternson.**
11:10—9. Fluorescence Methods of Clinical Drug Analysis. **G. G. Guilbault.**
11:35—10. A Sensitive Gas Chromatographic Method for the Simultaneous Determination of Ritalin and Its Metabolite Ritalinic Acid in Plasma Using N-P FID Detector. **B. L. Hungund, M. Hanna, B. G. Winsberg.**

SECTION C

Miami Beach Convention Center
General: Electroanalytical Chemistry
D. C. Johnson, *Presiding*

9:00—11. Immobilized Oxidase Enzymes as Electrochemical Sensors. **V. S. Srinivasan, G. Sittampalam.**
9:20—12. Comparison of Ion-Sensitive Electrode Selectivity with Ion-Exchange and Ion-Pairing Liquid Chromatography Retention. **R. F. Hirsch, U. Jingjit, E. Rachlin, K. Regan.**
9:40—13. Fast, Simple Analysis of Serum Glucose. **J. L. Buteyn, C. O. Huber.**
10:00—14. Photo-Electrochemical Determination of Nitrosamines. **D. C. Johnson, B. G. Snider.**
10:20—Intermission.
10:30—15. Simultaneous Determination of the Isomers of Nitrophthalic Acid by Differential Pulse Polarography. **P. M. Surana.**
10:50—16. A Comparison of DC, Pulse and Differential Pulse Detection in Flow-Through Tubular Electrodes. **D. C. Johnson, P. L. Meschi, E. C. Lewis, J. H. Larochelle.**
11:10—17. Evaluation of Errors Introduced During Potentiometric Titrations Using Silver Sulfide Membrane Due to Electrode Nonspecificity. **W. R. Hussein.**
11:30—18. Deposition Discriminating Stripping Analysis of Metals in Aqueous Solution. **B. Vassos, G. Martinez.**

MONDAY AFTERNOON

SECTION A

Miami Beach Convention Center
Symposium on Image Detectors in Chemistry *Joint with Division of Physical Chemistry*
Yair Talmi, *Presiding*

2:00—19. A High Resolution Grating Microspectrofluorometer with Topographic Option for Studies in Living Cells. **J. G. Hirschberg, A. W. Wouters, E. Kohen, J. S. Ploem, C. Kohen.**
2:30—20. Analytical Applications of the Laser Microprobe Using Electronic Imaging Detection. **T. H. Briggs.**
3:00—21. Evaluation of an Echelle Spectrometer with an Image Dissector for Simultaneous Multielement Determinations. **H. L. Pardue, H. L. Felkel.**
3:30—Recess.
3:45—22. Use of the OMA for Analyzing Light Intensity Gradients from the Absorption Optical System of the Ultracentrifuge. **D. L. Rockholt, E. G. Richards.**
4:15—23. Electro-Optical Ion Detector for Simultaneous Monitoring of all Ion Species over a Wide Range. **H. G. Boettger, C. E. Giffin, D. D. Norris, W. J. Dreyer.**
4:45—Discussion.

SECTION B

Miami Beach Convention Center
Symposium on Novel Approaches to Trace Drug Analysis
L. A. Sternson, *Presiding*

2:00—24. Evaluation of Vidicons as Multiwavelength Detectors for Drug Determinations. **H. L. Pardue, A. E. McDowell.**
2:35—25. Microorganisms as Novel Sources of Reagents for the Determination of Drugs in Biological Fluids. **R. V. Smith.**
3:10—Intermission.
3:20—26. Plastic Electrode as an Analytical Tool. **T. Higuchi.**
3:55—27. Drugs in Blood by Liquid Chromatography. **P. T. Kissinger.**
4:30—28. Dipstick for Morphine in Urine. **J. G. Montalvo, Jr., C-G. Lee, R. Wawro, L. Truxillo, R. Curran, C. Iannaccone, D. Eyer.**

SECTION C

Miami Beach Convention Center
General: Electroanalytical Chemistry
P. Zuman, *Presiding*

2:00—29. Chemically Modified Pt Electrodes Bearing Electroactive Ferrocene Molecules. **J. R. Lenhard, R. W. Murray.**
2:20—30. Chemical Modification of Metal Oxide Electrodes Using Cyanuric Chloride. **T. Kuwana, A.W.C. Lin.**
2:40—31. Electrocatalysis of NADH Using Quinones and Modified Quinone Electrodes. **T. Kuwana, D. C-S. Tse.**

You should be getting more...

Recovery

Reproducibility

Resolution

Sephasorb™ HP Ultrafine

is an exciting new adsorbent for liquid chromatography giving you new ways of achieving your separation with maximum reproducibility and complete recovery.

- Novel selectivity for difficult separations
- Catalytically inert for excellent recovery
- High chemical stability for use over a wide pH range (pH 2–12)
- Reusable many times without loss in activity for economical use
- Highly reproducible retention times
- Narrow bead size distribution for excellent resolution
- Porous bead for good capacity
- Rigid spherical bead for excellent flow properties

Get more information and applications from our booklet "Sephasorb™ HP Ultrafine. Chromatography in organic solvents" available free on request.

Pharmacia Fine Chemicals
Division of Pharmacia, Inc.
Piscataway, New Jersey 08854
Phone (201) 469-1222

Pharmacia Fine Chemicals

CIRCLE 164 ON READER SERVICE CARD

3:00—32. Ferric-EDTA Reduction Kinetics at the Glassy Carbon Electrode. **R. A. Petersen, C. O. Huber.**
3:20—Intermission.
3:30—33. Polarographic Reduction of Aminobenzaldehydes and Pyridine Carboxaldehydes. **J. F. Rusling, P. Zuman.**
3:50—34. Keto-Enol Equilibria, Hydration, and Polarographic Reduction of 1,2-Diketones. **N. Sleszynski, P. Zuman.**
4:10—35. Electrochemical Reduction of Benzyl Halides: Radical vs. Carbanion Formation. **D. A. Kock, D. E. Bartak.**
4:30—36. Catalytic Electroreduction of O_2 Using Water Soluble Iron Porphrin. **T. Kuwana, P. Forshey.**

TUESDAY MORNING

SECTION A

Miami Beach Convention Center
Symposium on Image Detectors in Chemistry *Joint with Division of Physical Chemistry*
Yair Talmi, *Presiding*

9:00—37. A Multimicroprocessor Controlled, Vidicon, Stopped-Flow Spectrophotometer. **E. Carlson, C. G. Enke.**
9:30—38. Time-Resolved Resonance Raman and Fluorescence-Line Narrowing Spectroscopy. **M. A. El-Sayed.**
10:00—39. Picosecond Time-Resolved Photometer. **W. Yu.**
10:30—Intermission.
10:45—40. Using TV Imaging Systems for Picosecond Fluorescence and Absorption Time-Resolved Kinetic Studies of Photosynthetic and Photovisual Systems. **F. Pellegrino, R. R. Alfano.**
11:15—41. A Three-Dimensional (λ, I, τ) Picosecond Spectrometer. **P. M. Rentzepis.**
11:45—Discussion.

SECTION B

Miami Beach Convention Center
Symposium on Novel Approaches to Trace Drug Analysis
G. G. Guilbault, *Presiding*

9:00—42. Use of Phosphorimetry for Drug Analysis. **J. D. Winefordner.**
9:35—43. Direct Analysis of Urine for Steroids and Dopamine Metabolites by Mass-Analyzed Ion Kinetic Energy Spectrometry. **T. K. Joseph, P. T. Kissinger, R. W. Kondrat, T. Kruger, R. G. Cooks.**
10:10—44. High Resolution Ion Exchange Chromatography Applied to a Study of Acetaminophen Metabolism in Man. **J. E. Mrochek, C. D. Scott.**
10:45—Intermission.
10:55—45. In Vitro Studies on the Metabolic Oxidations of Aliphatic Amines to Chemically Reactive Species. **N. Castagnoli, N. P. McGraw, B. Ho.**
11:30—46. Analysis of Erythromycin. III. Determination of Erythromycin by Ion-Pair Extraction with ^{35}S-Methyl Orange. **R. V. Smith, R. G. Harris, D. D. Maness, A. Martin.**
11:55—Concluding Remarks.

TUESDAY AFTERNOON

SECTION A

Miami Beach Convention Center
General: Spectroscopy
G. T. Bastiaans, *Presiding*

2:00—47. Precise Elemental Analysis of Heteropoly Anions via Plasma Emission Spectrometry. **G. J. Bastiaans, M. A. Fernandez.**
2:20—48. Determination of Non-Metals by Inductively Coupled Argon Plasma (ICAP) Spectroscopy. **A. F. Ward, L. F. Marciello.**
2:40—49. Characterization of Metal Alloys Using Inductively Coupled Argon Plasma Optical Emission Spectroscopy. **A. F. Ward, L. F. Marciello.**
3:00—50. Simultaneous Analysis of As, Se, Sn and Sb by Hydride Generation with Microwave Induced Plasma Atomic Emission. **W. B. Robbins, J. A. Caruso, F. L. Fricke.**
3:20—Intermission.
3:30—51. Determination of Cadmium, Copper, Lead and Manganese in Human Kidney Cortex Using Zeeman Effect Flameless Atomic Absorption Spectrometry. **P. A. Pleban, K. H. Pearson, R. J. Shamberger.**
3:50—52. Quantitation of Selenium, Manganese, Iron, Copper, and Zinc in Human Kidney Tissue by X-ray Fluorescence. **G. S. Kuntz, R.L.R. Towns.**
4:10—53. An Investigation of Satellite Structure Found in X-ray Photoelectron Spectroscopy (ESCA). **J. C. Carver, H. Razzavi.**
2:00—*Divisional Business Meeting,* Convention Center.
6:00—*Divisional Social Hour.* Hotel Fontainbleau.
7:00—*Divisional Dinner.* Hotel Fontainbleau.

SECTION B

Miami Beach Convention Center
General: Chromatography
H. A. Moye, *Presiding*

2:00—54. A Simple GC–MS Method for Simultaneous PGE_1 and PGE_2 Analysis Based on Concurrent Elution and Selected Ion Monitoring. **A. Ferretti.**
2:20—55. A Gas Chromatographic Microanalytical Procedure for the Analysis of Oxalate Ion in Human Urine. **H. A. Moye, R. Garman.**
2:40—56. Therapeutic Monitoring of Anticonvulsant Drugs in Psychiatric Patients: Simultaneous Gas-Chromatographic Determination of Celontin, Zarontin, Phenobarbital, Dilantin, Tegretol, and Primidone in Presence of Mesantoin, Kemadrin, Prolixin, and Haldol in Plasma. R. Varma.
3:00—57. Determination of Disopyramide in Serum by HPLC. **C. R. Ghosh, H. G. Lankford.**
3:30—58. High Pressure Liquid Chromatography of Unsaturated and Cyclopropane Fatty Acids. **R. A. Miller, N. E. Bussell.**
3:50—59. Analysis of Hydroxyl Fatty Acids by High Pressure Liquid Chromatography. **N. E. Bussell, R. A. Miller.**
4:10—60. Thin-Layer Chromatographic Separation of Conjugated Bile Acids. **A. K. Batta, S. Shefer, G. Salen.**
4:30—61. Separation of Some Cholesterol Derivatives by Thin Layer Chromatography. **H. J. Issaq, N. Risser, J. Bowden.**
2:00—*Divisional Business Meeting,* Convention Center.
6:00—*Divisional Social Hour.* Hotel Fontainbleau.
7:00—*Divisional Dinner.* Hotel Fontainbleau.

WEDNESDAY MORNING

SECTION A

Miami Beach Convention Center
Symposium on Sample Injection Techniques into Unsegmented Flows
H. A. Mottola, *Presiding*

9:00—Introductory Remarks: An Overview. **H. A. Mottola.**
9:20—62. Flow Injection Analysis. Principle and Theory of the Method. Design of a Programmable Microanalyzer. **J. Ruzicka, E. H. Hansen.**
10:10—Intermission.
10:25—63. Flow Injection Analysis. New Analytical Methods Based on the Use of Spectrophotometric and Potentiometric Flow-Through Detectors. **E. H. Hansen, J. Ruzicka.**
11:15—64. Theory and Practice of Continuous-Flow Analysis: Comparison of Flow Injection Analysis

with Modern Segmented Flow. **M. Margoshes.**

SECTION B

Miami Beach Convention Center

50th Anniversary Symposium: The Journal and the Science

H. A. Laitinen, *Presiding*

9:00—Introductory Remarks.
9:10—65. Edward Hart, Ph.D.—The Man Behind the Journal. **G. E. Peace, Jr.**
9:30—66. L. T. Hallett: The Early Years. **S. Siggia.**
9:40—67. Analytical Chemistry: The Journal and the Science, 1929–1939. **V. A. Stenger.**
10:00—68. Analytical Chemistry: The Journal and the Science, the 1940's. **H. A. Laitinen.**
10:20—Intermission.
10:40—69. Analytical Chemistry in the 1950's. **L. B. Rogers.**
11:00—70. 50 Years of Analytical Chemistry—The Journal and the Science—the 1960's. **J. D. Winefordner.**
11:20—71. Analytical Chemistry: The Journal and the Science in the 1970's and Beyond. **B. R. Kowalski.**
11:40—Concluding Remarks. **I. M. Kolthoff.**

WEDNESDAY AFTERNOON

SECTION A

Miami Beach Convention Center

Symposium on Sample Injection Techniques into Unsegmented Flows

H. A. Mottola, *Presiding*

2:00—72. Injection Technique as a New Approach for Dynamic Flow-Through Analysis with Electroanalytical Sensors. **E. Pungor, Zs. Fehér, G. Nagy, K. Tóth.**
2:35—73. Design and Characteristics of Membrane Covered Electrochemical Sensors for Use in Unsegmented Flows. **D. N. Gray, F. E. Semersky, B. Watson.**
3:10—Intermission.
3:25—74. Analysis of Elution Patterns in Unsegmented Flow Using a Novel pH Monitor. **R. C. Barabino, M. H. Keyes.**
4:10—75. Analytical Chemistry at the Interface. **D. Betteridge, E. L. Dagless, P. David, D. R. Deans, B. Fields, P. Sweet.**

SECTION B

Miami Beach Convention Center

General: Spectroscopy

P. N. Keliher, *Presiding*

2:00—76. Study of the Interference of Organic Compounds with the 2,4-Xylenol Spectrophotometric Method for Nitrate. **G. Norwitz, J. Farino, P. N. Keliher.**
2:20—77. Calibration of Circular Dichrometers in the Visible and Ultraviolet Regions. **J. L. Scott, V. C. Zadnik, K. H. Pearson.**
2:40—78. Photo-Acoustic Spectroscopy: Spectral Analysis of Solid and Liquid Samples. **J. W-p. Lin, L. P. Dudek.**
3:00—79. Some Inter-Related Parameters that Influence the Accuracy of Atomic Absorption Determination of Mercury in the Atmosphere. **J. C. Hilborn, G. F. Dowd.**
3:20—Intermission.
3:30—80. The Determination of Molybdenum in Engine Lubricating Oils by Atomic Absorption Spectrophotometry. **C. S. Saba, K. J. Eisentraut.**
3:50—81. Origin, Distribution, and Bioaccumulation of Selenium in Kentucky and Barkley Lakes. **B. E. McClellan, K. Frazer, J. Vargo, R. Aulick.**
4:10—82. Elevated Temperature ^{13}C FT-NMR Studies of Coal Products. **L. T. Taylor, H. C. Dorn, T. Glass.**
4:30—83. New Reagents for Characterization of Functional Groups by ^{19}F NMR. **H. C. Dorn, P. Szabo, K. Koller, T. Glass.**

THURSDAY MORNING

SECTION A

Miami Beach Convention Center

Symposium on Sample Injection Techniques into Unsegmented Flows

H. A. Mottola, *Presiding*

9:00—84. Closed-Loop Systems and Other Ancillary Concepts in Sample Injection Techniques into Unsegmented Flows. **H. A. Mottola.**
9:35–85. Repetitive Determination of Heavy Metals by Sample Injection in a Closed-Loop System. **C-M. Wolff, J-P. Schwing.**
10:10—Intermission.
10:25—86. Extraction by Flow-Injection Analysis. **B. I. Karlberg, S. Thelander.**
11:00—87. Automated Loading of Discrete Samples in Unsegmented Continuous Flow Analysis. **K. K. Stewart, G. R. Beecher.**
11:35—88. On the Design and Optimization of Chemiluminescence Analysis in Flowing Systems. **W. R. Seitz.**

SECTION B

Miami Beach Convention Center

General: Chromatography

9:00—89. Identification of Insoluble Coatings and Impregnations by Pyrolysis and Gas Chromatography. **J. Kovar.**
9:20—90. Characterization of Polyethers and Polyurethanes via Reaction Gas Chromatography. **S. Siggia, D. Gibian.**
9:40—91. High Performance Aqueous Gel Permeation Chromatography of Water Soluble Polymers. **T. Hashimoto, Y. Kato, H. Sasaki, M. Aiura.**
10:00—92. The Analysis of Epoxy Resin Formations. **J. E. Twichell, J. Q. Walker.**
10:20—Intermission.
10:30—93. HPLC Determination of Acrylamide Monomer in Polyacrylamide and in Environmental Samples. **N. E. Skelly, E. R. Husser.**
10:50—94. Optimization of Ternary Solvent Systems for HPLC. **B. R. Belinky.**
11:10—95. Applications of the Ion Exchange Membrane Detector for Liquid Chromatography. **J. G. Dorsey, T. W. Gilbert.**
11:30—96. A Capillary Gas Chromatographic Inlet for the Analysis of Trace Concentration of Compounds. **S. M. Sonchik, J. Q. Walker.**

THURSDAY AFTERNOON

SECTION A

Miami Beach Convention Center

General

N. E. Skelly, *Presiding*

2:00—97. Use of Polymer Supported Functional Groups for the Selective Concentration of Specific Inorganic Species from Complex Fluids. **S. Siggia, M. Colella, D. Gibian.**
2:20—98. Investigations into the Mechanisms of Separation of Solvent Refined Coal on Bio-Beads by Way of Model Compounds. **D. W. Hausler, J. Hellgeth, L. T. Taylor.**
2:40—99. Evaluation of Methods for Determination of Sulfide in Coal Gasification Wastewater. **J. K. Olson, H. H. Schobert.**
3:00—100. Direct Head Gas Analysis for Isolation of Volatile Trace Organics in Aqueous Environmental Samples. **S. L. Friant, I. H. Suffet.**
3:30—Intermission.
3:40—101. Continuous Monitoring of Total Hardness at the Part per Billion Level. **F. R. Whiteley, M. J. Gaertner.**
4:00—102. Reversed Phase HPLC Separations in the Presence of Metal Chelate Additives. **B. L. Karger, W. S. Wong, R. L. Viavattene, J. N. LePage, G. Davies.**

4:20—103. Determination of Acid Content of Bitumen by Catalytic Thermometric Titrimetry. **A. Nadjafi, E. J. Greenhow.**

Division of Environmental Chemistry

H. E. Allen, *Chairman*
R. L. Jolley, *Secretary*

MONDAY MORNING

SECTION E

Miami Beach Convention Center
Symposium on Trace Analysis of Nitrogen, Sulfur, and Halogen Compounds in the Atmosphere
W. M. Cooke, *Presiding*

9:00—Introduction. **W. M. Cooke.**
9:10—28. A View of the Importance of Measurements of Atmospheric Sulfur Compounds. **J. P. Friend.**
9:40—29. Spurious Sulfate Formation on Collected Ambient Aerosol Samples. **B. W. Loo, R. C. Gatti, A. J. Ramponi, R. K. Stevens, K. E. Noll, H. E. Allen.**
10:05—30. A Comparison of Sulfuric Acid Measurement Methods. **L. W. Richards, K. R. Johnson, L. S. Shepard.**
10:30—Break.
10:45—31. Sulfate in Diesel Exhaust. **W. R. Pierson, D. E. McKee.**
11:10—32. Aerosol Sulfur in the Eastern United States. **J. W. Winchester.**
11:30—33. Characterization of the Miami Aerosol. **K. A. Hardy, R. Patterson.**

MONDAY AFTERNOON

SECTION E

Miami Beach Convention Center
Symposium on Trace Analysis of Nitrogen, Sulfur, and Halogen Compounds in the Atmosphere
R. K. Stevens, *Presiding*

2:00—62. Analysis of Sulfur-Containing Air Samples Collected at Cedar Island, N.C. **R. S. Braman, J. M. Ammons.**
2:25—63. Trace Analysis of Sulfur Gases Using Solid Adsorbent Preconcentration and Gas Chromatography. **M. S. Black.**
2:45—64. Direct Measurements of Emission Rates of Some Atmospheric Biogenic Sulfur Compounds. **V. P. Aneja, J. H. Overton, Jr., L. T. Cupitt, J. L. Durham, W. E. Wilson.**
3:05—Break.
3:20—65. $^{34}S/^{32}S$ Studies of Biogenic Sulfur Emissions at Wallops Is., Va. **D. R. Hitchcock, M. S. Black.**
3:45—66. On the Nature of Diurnal Variation of Sulfates at Rural Sites in the Eastern United States. **G. T. Wolff, P. R. Monson, M. A. Ferman.**
4:10—67. A Study of the Emissions of SO_2, H_2SO_4, and Sulfate from a Coal-Fired Boiler Incorporating a Wet-Limestone Scrubber. **J. B. Homolya, J. L. Cheney.**

TUESDAY MORNING

SECTION E

Miami Beach Convention Center
Symposium on Trace Analysis of Nitrogen, Sulfur, and Halogen Compounds in the Atmosphere
W. M. Cooke, *Presiding*

9:00—97. Measurement of Atmospheric Nitrogen Compounds. **Chester W. Spicer.**
9:25—98. Comparison of Nitrates Collected by Hi-Vol and Dichotomous Samplers. **R. K. Stevens, T. G. Dzubay, D. T. Mage, R. Burton, G. Russwurm, D. Rickel.**
9:45—99. A Laboratory Feasibility Study to Determine and Develop a Sampling and Analytical Technique for Measuring Nitric Acid Vapors at Atmospheric Concentrations. **R. J. Hare, M. T. Wininger, W. D. Ross, J. Tesch, R. E. Sievers.**
10:05—100. Measurement of Nitrogen-Containing Trace Gases in the Troposphere by In-situ Long-Path Infrared Absorption Spectroscopy. **P. L. Hanst, E. C. Tuazon, A. M. Winer, R. A. Graham, J. N. Pitts, Jr.**
10:25—Break.
10:40—101. Nitrite in Airborne Particulates. **L. D. Hansen, B. E. Richter, D. J. Eatough.**
11:00—102. Determination of Volatile Nitrosamine in Air. **P. J. Jimenez, F. M. Perry, Jr., E. W. Day, Jr.**
11:20—103. Sampling and Analysis for Acrylonitrile in Ambient Air. **J. Going, P. Kuykendall, J. Onstot, K. Thomas, S. Long.**

TUESDAY AFTERNOON

SECTION E

Miami Beach Convention Center
Symposium on Trace Analysis of Nitrogen, Sulfur, and Halogen Compounds in the Atmosphere
P. L. Hanst, *Presiding*

2:00—131. Global Budgets and Distributions of Selected Halocarbons, Hydrocarbons, N_2O, and SF_6. **H. B. Singh.**
2:25—132. Tropospheric and Lower Stratospheric Profiles of Halocarbons and Related Chemical Species. **D. R. Cronn, D. E. Harsch, E. Robinson.**
2:50—133. Total Stratospheric Elemental Chlorine Content—Initial Results. **W. W. Berg, S. N. Gitlin, F. E. Grahek.**
3:15—Coffee Break.
3:30—134. Boundary Layer Hydroxyl Measurements by a ^{14}C Tracer Technique. **J. C. Sheppard, M. J. Campbell, B. Au.**
3:50—135. A Program for Determining the Atmospheric Lifetime of Fluorocarbons. **D. M. Cunnold, F. N. Alyea, R. G. Prinn.**
4:15—136. Global Measurements of Trace Halocarbons in the Atmosphere. **R. A. Rasmussen.**

WEDNESDAY MORNING

SECTION E

Miami Beach Convention Center
Symposium on Trace Analysis of Nitrogen, Sulfur, and Halogen Compounds in the Atmoshpere
P. L. Hanst, *Presiding*

9:00—160. An Approach to Accurate Determinations of Ambient Halocarbons by Electron Capture Detection. **P. G. Simmonds, J. E. Lovelock.**
9:25—161. Atmospheric Photodissociation of HOCl. **M. J. Molina, L. T. Molina.**
9:50—162. Atmospheric Chemistry of HOCl. **P. L. Hanst, J. W. Spence, E. O. Edney.**
10:15—Break.
10:30—163. The Interaction of Odd Hydrogen and Odd Chlorine Photochemistry and Their Roles in the Catalytic Destruction of Stratospheric Ozone. **J. Fishman, P. J. Crutzen.**
10:55—164. Reactions of Importance to Stratospheric Chlorine Chemistry. **J. P. Jesson, L. C. Glasgow, C. Miller, D. L. Filkin.**

Division of Petroleum Chemistry, Inc.

B. J. Dropesky, *Chairman*
R. C. Hahn, *Secretary*

TUESDAY MORNING

SECTION C

Miami Beach Convention Center
Symposium on Analytical Chemistry of Petroleum in the Marine/Aquatic Environment
E. W. Novotny, *Presiding*

9:00—Introductory Remarks. **E. W. Novotny.**

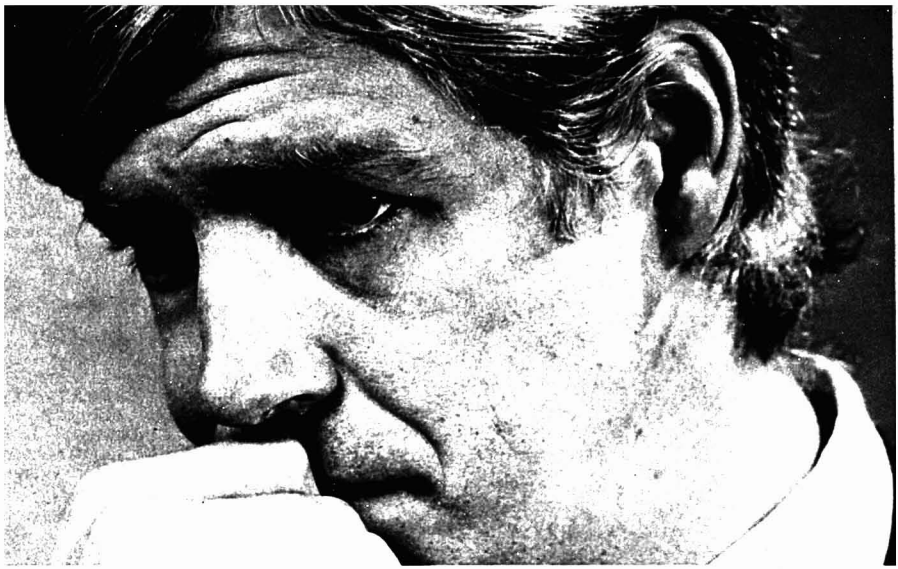

A Jarrell-Ash Plasma AtomComp gives you 2880 elements an hour.

[That'll make a dent in your workload!]

Today's metal workloads are bigger than ever. That's why you owe it to yourself to investigate what **Plasma AtomComp™** can do for you.

This distinguished family of plasma emission spectrometers provides all the sensitivity of atomic absorption and atomic emission instruments. But with far greater **capability.** Up to 48 elements simultaneously, in up to 60 samples, in as little as 60 minutes.

That's almost **10 times** greater capability than even the most advanced AA workhorses.

Plus — Plasma AtomComp provides remarkable range — automatic analysis over a dynamic concentration range of **100,000** without having to change a single parameter! Outstanding convenience — it is computer controlled. And versatile printout — % or ppm or ppb or any other units you desire.

Whatever your field — water, wastewater, air, soils, foods, feeds, petroleum, biologicals — if a high-throughput workload is your problem, Jarrell-Ash is your answer. Jarrell-Ash plasma spectrometry. The **truly multi-element** approach. Send for literature today.

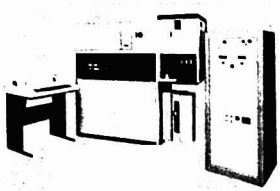

CIRCLE 112 ON READER SERVICE CARD

Jarrell-Ash Division
Fisher Scientific Company

590 Lincoln Street
Waltham, Massachusetts 02154
Phone (617) 890-4300

9:05—32. An Overview of the Biogeochemistry of Fossil Fuel Hydrocarbons in Marine/Aquatic Environments. **J. W. Farrington.**
9:50—33. Recent Advances in the Determination of Petroleum Hydrocarbons in Zooplankton and Macrofauna. **J. S. Warner, R. M. Riggin, A. P. Graffeo.**
10:20—34. Advances in High Resolution Glass Capillary Gas Chromatography. **S. P. Cram, F. J. Yang.**
10:50—35. Methods of Analysis for Polynuclear Aromatic Hydrocarbons in Environmental Samples. **R. J. Pancirov, T. D. Searl, R. A. Brown.**
11:20—36. Analytical Chemistry of Petroleum—An Overview of Practices in Petroleum Industry Laboratories with Emphasis on Biodegradation. **L. Petrakis, D. M. Jewell, W. F. Benusa.**

TUESDAY AFTERNOON

Miami Beach Convention Center
Symposium on Analytical Chemistry of Petroleum in the Marine/Aquatic Environment
F. Weiss, *Presiding*

2:00—Introductory Remarks. **F. Weiss.**
2:05—37. The Solubility Behavior of Polynuclear Aromatic Hydrocarbons in Aqueous Systems. **W. E. May, S. P. Wasik.**
2:35—38. The Multiple Gas-Phase Equilibration Method and Its Application to Environmental Studies. **C. D. McAuliffe.**
3:05—39. Comparison of Extraction Methods for Hydrocarbons in Marine Sediment. **D. W. Brown, L. S. Ramos, M. Y. Uyeda, W. D. MacLeod, Jr.**
3:35—40. The Role of Nonhydrocarbons in the Analysis of Virgin and Biodegraded Petroleum. **D. M. Jewell.**
4:05—41. Application of Trace Analytical Techniques to a Study of Hydrocarbon Composition upon Dispersion of Petroleum in a Flowing Seawater System. **R. M. Bean, J. W. Blaylock, R. G. Riley.**
4:35—42. Determination of Aromatic and PAH Content of Oily Waters. **I. Lysyj, E. C. Russell.**

WEDNESDAY MORNING

SECTION A

Miami Beach Convention Center
Symposium on Analytical Chemistry of Petroleum in the Marine/Aquatic Environment
L. Petrakis, *Presiding*

9:00—Introductory Remarks. **L. Petrakis.**
9:05—43. Oil Spill Identification and Remote Sensing. **A. P. Bentz.**
9:50—44. Hydrocarbons in the Sediments of the Bermuda Region: Lagoonal to Abyssal Depths. **J. N. Butler, T. D. Sleeter.**
10:20—45. Polycyclic Aromatic Hydrocarbons in Marine/Aquatic Sediments. **R. A. Hites, R. E. Laflamme, J. G. Windsor, Jr.**
10:50—46. Distribution of Aromatic Hydrocarbons from Selected Atlantic, Gulf of Mexico, and Pacific OCS Areas. **E. B. Overton, J. L. Laseter.**
11:20—47. A Comparison of Methods for the Analysis of Hydrocarbons in Marine Sediments. **J. L. Lake, C. W. Dimock, C. B. Norwood.**

Division of History of Chemistry (Prime Division)

N. D. Heindel, *Chairman*
R. M. Hawthorne, *Secretary-Treasurer*

WEDNESDAY MORNING

Miami Beach Convention Center
Symposium on *A Century of Chemistry at the U.S. Geological Survey, I. May, Chairman*
I. May, *Presiding*

9:00—Introductory Remarks.
9:10—15. History of X-ray Fluorescence Analysis and the Present State-of-the-Art at the U.S. Geological Survey. **H. J. Rose, Jr.**
9:30—16. An Automated Glass Fusion Technique for the Determination of Total Volatile Content of Rocks. **V. G. Mossotti, B. S. King.**
9:50—17. A Fully-Focusing X-ray Spectrometer with Applications to Geochemical Analysis. **J. R. Lindsay, R. R. Larson, H. J. Rose, Jr., R. W. Werre.**
10:10—Intermission.
10:30—18. William Francis Hillebrand, the Survey's First Chemist. **I. May.**
10:50—19. Determination of Platinum, Palladium, and Rhodium in Geologic Materials by Fire Assay and Atomic Absorption Spectroscopy Using Electrothermal Atomization. **F. O. Simon, P. J. Aruscavage, R. Moore.**
11:10—Organic Geochemistry—A U.S. Geological Survey Tradition. **I. A. Breger.**
11:30—21. Nuclear Methods in Geochemistry. **J. J. Rowe.**

WEDNESDAY AFTERNOON

Miami Beach Convention Center
Symposium on *A Century of Chemistry at the U.S. Geological Survey, I. May, Chairman*
J. J. Rowe, *Presiding*

2:00—22. Isotopic Chemistry at the U.S. Geological Survey. **B. R. Doe.**
2:20—23. The U.S.G.S. Effort in the Application of Stable Isotopes to Geochemistry. **I. Friedman.**
2:40—24. Frank Wigglesworth Clarke, 1847–1931. **M. Fleischer.**
3:00—Intermission.
3:20—25. A Brief History of Analytical Atomic Emission Spectroscopy in the Washington Laboratory of the U.S. Geological Survey. **D. W. Golightly, C. S. Annell.**
3:40—26. Improved Detection Limits for Selected Elements of Geochemical Significance by Emission Spectrography. **J. L. Seeley, C. Heropoulos, P. J. Lamothe, R. E. Mays.**
4:00—27. A Background Correction System for the Analysis of Geochemical Samples Using an Inductively Coupled Plasma. **P. J. Lamothe, J. L. Seeley.**
4:20—28. Simultaneous Determination of Major, Minor, and Trace Elements in Geochemical Materials by Direct-Reading Emission Spectrometry. **J. L. Seeley, P. J. Lamothe.**

THURSDAY MORNING

Miami Beach Convention Center
Symposium on *A Century of Chemistry at the U.S. Geological Survey, I. May, Chairman*
R. J. Pickering, *Presiding*

9:00—29. History of Change, Water-Quality Activities of the U.S. Geological Survey. **W. H. Durum.**
9:20—30. Centralization and Automation of Water Analyses in the Water Resources Division of the U.S. Geological Survey. **W. A. Beetem, R. L. McAvoy.**
9:40—31. The Use of Standard Reference Water Samples by the U.S. Geological Survey. **L. J. Schroder, M. J. Fishman, L. C. Friedman, G. Darlington.**
10:00—Intermission.
10:20—32. Programs to Assure the Quality of Water-Quality Data by the U.S. Geological Survey. **L. C. Friedman.**
10:40—33. Recent Trends in the Use of Simultaneous Multielement Techniques for the Analysis of Natural Water Samples: Part I, Plasma Emission Methods. **H. E. Taylor, R. K. Skogerboe.**

11:00—34. Recent Trends in the Use of Simultaneous Multielement Techniques for the Analysis of Natural Water Samples: Part II, Atomic Absorption Spectrometry–Anodic Stripping Voltammetry. **R. K. Skogerboe, H. E. Taylor, K. R. O'Keefe.**
11:20—35. Analysis of Natural Waters Applied to Mineral Exploration. **W. H. Ficklin, W. R. Miller, G. A. Nowlan.**

THURSDAY AFTERNOON

Miami Beach Convention Center
Symposium on *A Century of Chemistry at the U.S. Geological Survey, I. May, Chairman*
B. P. Fabbi, *Presiding*

2:00—36. W. F. Hillebrand, the Father of Standard Samples in Geology. **F. J. Flanagan.**
2:20—37. Geochemical Studies of U.S. Coal Resources Related to Coal Usage and the Environment. **F. O. Simon, P. Zubovic.**
2:40—38. Analytical Methodology for Geochemical Exploration—Pioneered by the U.S. Geological Survey. **F. N. Ward.**
3:00—39. Selective Extraction of Trace Metals from Halide Acid Solutions Using Aliquat 336 in Methyl Isobutyl Ketone. **J. G. Viets, J. R. Clark.**
3:20—Intermission.
3:40—40. Atomic Absorption Determination of Cobalt, Nickel, and Copper in Geological Materials. **R. F. Sanzolone, T. T. Chao, G. L. Crenshaw.**
4:00—41. Determination of Uranium and Thorium after Complete Sample Decomposition and Anion-Exchange Separation. **D. M. Hopkins.**
4:20—42. Induction-Coupled Plasma Multi-Element Analysis of Geologic Materials Using a Selective Extraction Technique. **J. M. Motooka, E. L. Mosier, S. J. Sutley, J. G. Viets.**

Division of Chemical Education, Inc.

H. A. Bent, *Chairman*
J. A. Bell, *Secretary*

THURSDAY MORNING

Miami Beach Convention Center
Symposium on Chemical Oceanography in the Academic Curriculum
T. C. Loder, *Presiding*

9:00—Introductory Remarks.
9:05—32. Teaching Chemical Oceanography? One Approach that Works! **T. C. Loder.**
9:20—33. Chemistry Backgrounds and Quality of Incoming Oceanography Graduate Students. **I. W. Duedall.**
9:40—34. Enriching the Chemistry Curriculum with Recent Advances in Chemical Oceanography. **R. W. Zuehlke.**
10:00—35. Teaching Chemical Oceanography with a Biological Bias. **J. H. Sharp.**
10:20—36. MSC 521—A Core Course in Chemical Oceanography at the University of South Florida. **K. A. Fanning, P. R. Betzer.**
10:40—37. The Undergraduate Marine Chemistry Laboratory Program at the College of Charleston. **W. F. Kinard.**
11:00—38. Guidelines for Future Instruction in Chemical Oceanography. **R. W. Baier.**
11:20—39. The Teaching of Marine Chemistry to Undergraduate Students—A Viewpoint from the United Kingdom. **P. S. Liss.**
11:40—40. Global Chemical Models and Oceanography. **W. W. Hay.**

Division of Nuclear Chemistry and Technology

B. J. Dropesky, *Chairman*
R. L. Hahn, *Secretary*

THURSDAY MORNING

Doral Beach
Symposium on High Speed and High Efficiency Radiochemical Separations *Joint with Division of Analytical Chemistry*
E. P. Horwitz, Organizer, *Presiding*

9:00—Introductory Remarks.
9:05—63. Rapid Radiochemical Separation Procedures for Studies on Short-Lived Nuclides. **N. Trautmann.**
9:45—Discussion.
9:50—64. Rapid Automated Nuclear Chemistry. **R. A. Meyer, E. A. Henry, O. G. Lien, H. G. Hicks, S. G. Prussin, P. C. Stevenson.**
10:15—Discussion.
10:20—Intermission.
10:30—65. A Rapid Separation System for Short-Lived Actinides and Transactinides. **E. K. Hulet, R. W. Lougheed, J. M. Nitschke.**
10:55—Discussion.
11:00—66. The Rapid Separation of the Lanthanides on High-Efficiency Bonded-Phase Ion Exchangers. **R. M. Cassidy, S. Elchuk.**
11:25—Discussion.

THURSDAY AFTERNOON

SECTION A

Doral Beach
Symposium on High Speed and High Efficiency Radiochemical Separations
E. P. Horwitz, *Presiding*

2:00—67. SISAK—A Technique for Fast On-Line Radiochemical Separations. **J. Rydberg, G. Sharnemark.**
2:40—Discussion.
2:45—68. Facility for Short Half-Life Fission Product Studies Using a ^{252}Cf Source. **R. J. Gehrke, R. C. Greenwood, R. A. Anderl, V. J. Novick, J. D. Baker.**
3:10—Discussion.
3:15—Intermission.
3:20—69. A Rapid Rare Earth Separation System. **J. D. Baker, D. H. Meikrantz, R. J. Gehrke, R. C. Greenwood.**
3:45—Discussion.
3:50—70. Laboratory Centrifugal Contactor for Rapid Liquid-Liquid Extraction. **R. A. Leonard, G. J. Bernstein, A. A. Ziegler, R. H. Pelto, M. J. Steindler.**
4:15—Discussion.
4:20—71. Separation of Actinides by High Pressure Liquid Chromatography and Determination of Their Production Cross Sections in the Reactions of $^{136}Xe + ^{238}U$ and $^{238}U + ^{238}U$. **M. Schädel, W. Brüchle, H. Gäggler, J.-V. Kratz, G. Herrman, N. Trautmann.**
4:45—Discussion.

J. J. Kirkland

Du Pont Scientist Receives Tswett Medal

J. J. Kirkland of Du Pont Co. received the commemorative Tswett Medal for his outstanding contributions in the field of liquid chromatography in ceremonies marking the 75th

anniversary of the chromatographic sciences in Tallinn, Estonia, Soviet Union. The medal was presented to Dr. Kirkland by the Soviet Union Scientific Council for Chromatography at a symposium dedicated to the discovery of chromatography by the Russian botanist, M. S. Tswett, in 1903. Dr. Kirkland addressed the symposium on recent developments in the field of size-exclusion liquid chromatography.

Dr. Kirkland's research in liquid chromatography was significant in the development of a line of Du Pont's liquid chromatography systems that are now widely used in both academic and industrial research. He has published more than 50 articles and has written two books on liquid chromatography. He serves on several editorial advisory boards for journals and is also a current member of the advisory board of ANALYTICAL CHEMISTRY. Other major awards earned by Dr. Kirkland include the 1972 American Chemical Society Chromatography Award; the 1973 ACS Delaware Section Award; and the 1974 Chromatography Forum, Steven Dal Nogare Award in Chromatography.

Andre D'Arcangelo Joins AC Staff

Andre D'Arcangelo joined the editorial staff of ANALYTICAL CHEMISTRY as an editorial assistant in June. Mr. D'Arcangelo received a BA degree in biochemistry from the Catholic University of America in Washington, D.C., in February 1978. Before joining the editorial staff, he worked briefly in the research labs at the National Cancer Institute. In addition to his responsibilities in the editorial review process, Mr. D'Arcangelo is NEW PRODUCTS editor.

Andre D'Arcangelo

Correction

The price of the nuclear magnetic resonance spectrometer purchased by the University of Missouri-St. Louis and Washington University under a joint NSF grant was $155 000. The price was incorrectly quoted on page 752 A of the July issue.

Call for Papers

XXI Colloquium Spectroscopicum Internationale—8th International Conference on Atomic Spectroscopy

Cambridge, England. July 1–6, 1979. The conference is cosponsored by the Royal Society, the International Union of Pure and Applied Chemistry, the Chemical Society, and the Institute of Physics and is organized by the Association of British Spectroscopists. Papers encompassing all branches of spectroscopy with particular emphasis on analytical chemistry are invited. Prospective authors should submit abstracts of no more than 50 words by September 4, 1978, to Association of British Spectroscopists, P.O. Box 109, Cambridge, CB1 2HY, United Kingdom. Authors of accepted papers will receive special abstract forms on which to submit a 300-word extended abstract in English, French, or German for publication in the Official Conference Book of Abstracts.

Meetings

The following meetings are newly scheduled in ANALYTICAL CHEMISTRY. *The 1978 meetings listed earlier appear in the July issue*

- **4th European Electro-optics Conference and Exhibition.** Oct. 10–13. Jaarbeurs Congress Hall, Utrecht, The Netherlands. Organized by Sira Institute on Behalf of the European Electro-Optics Assn. *Contact: R. Keiller, Sira Institute Ltd., South Hill, Chislehurst, Kent BR7 5EH, UK*
- **3rd Annual Analytical Chemistry Symposium of the Baton Rouge Analytical Instrument Discussion Group.** Oct. 12–13. Baton Rouge Riverside Centroplex. *Contact: Marty Fontenot; BRAIDG Symposium Registration Chairman, Ciba Geigy Corp., P.O. Box 11, St. Gabriel, La. 70776*
- **25th National Vacuum Symposium of American Vacuum Society.** Nov. 28–Dec. 1. San Francisco. *Contact: E. N. Sickafus, Program Chairman, Ford Motor Co., Scientific Research Laboratory, Room 2859, Dearborn, Mich. 48121. 313-323-1502*
- **3rd Annual Toxic Substances Control Conference.** Dec. 4–6. Washington, D.C. *Contact: Government Institutes, Inc., 4733 Bethesda Ave., N.W., Washington, D.C. 20014. 301-656-1090*
- **Symposium on Pulsed Nuclear Magnetic Resonance in Solids.** Dec. 18–19. Queen Elizabeth College, U. of London. *Contact: J. A. S. Smith, Dept. of Chemistry, Queen Elizabeth College, Campden Hill Rd., London, W8, UK*

Short Courses

ACS Courses. For more information, contact: Department of Educational Activities, American Chemical Society, 1155 Sixteenth St., N.W., Washington, D.C. 20036. 202-872-4508

Toxicology for Chemists
Washington, D.C. Aug. 21–23. Frederick Sperling. $430, ACS members; $500, nonmembers

Capillary Gas Chromatography
Miami Beach, Sept. 9–10; San Francisco, Dec. 1–2. Stuart Cram and Milos Novotny. $250, ACS members; $300, nonmembers

High-Pressure Liquid Chromatography Workshop
Miami Beach, Sept. 9–10; Houston, Oct. 4–5; Atlanta, Oct. 26–27. David Freeman. $250, ACS members; $300, nonmembers

Statistics for Experimental Design
Miami Beach, Sept. 9–10; Houston, Oct. 4–5; Boston, Nov. 3–4. John Hromi. $200, ACS members; $240, nonmembers

Effective Writing for Scientists and Engineers
Miami Beach. Sept. 13–15. Henrietta Tichy and Sylvia Fourdrinier. $230, ACS members; $280, nonmembers

Laboratory Safety: Recognition and Management of Hazards
Miami Beach. Sept. 13–15. Norman V. Steere and Maurice Golden. $280, ACS members; $330, nonmembers

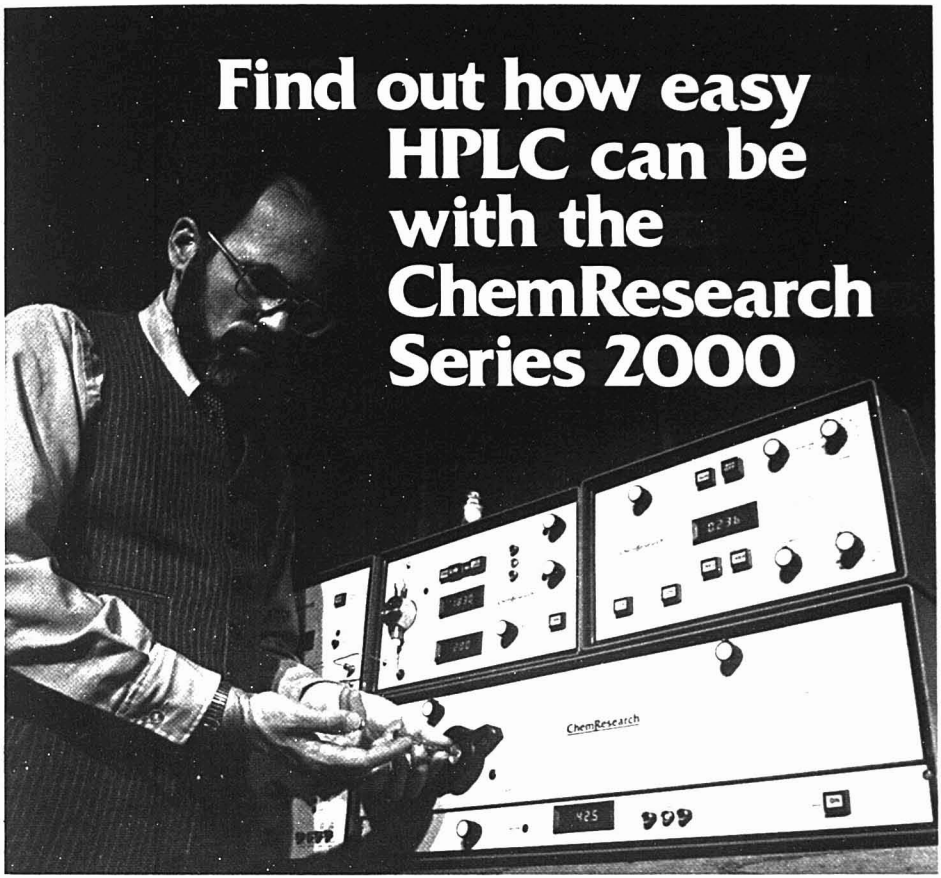

Designed with the operator in mind, the ChemResearch Series 2000 has many conveniences to make high performance liquid chromatography easy. LED readouts monitor 15 operating parameters. Valve and column plumbing are mounted on the oven door, providing easy access for column or sample loop changes. A precisely reproducible injection mark is made automatically every time the valve is operated. Pressure and temperature limit controls with alarms protect the instrument and operator. And a valve protects against air locks during solvent changes.

Modular construction makes it easy to adapt the Series 2000 to your HPLC needs. You can choose from two high-sensitivity detectors, giving you the option of multi-wavelength or variable UV/visible absorbance. You can choose an isocratic version and later add a single gradient module that's programmable for concave, convex, or linear gradients for both solvent and flow. Easy choices that give you the versatility you need for practically any separation.

Solvent delivery is monitored by an advanced feedback control which produces an exceptionally smooth flow by compensating for valve action, system compressibility, and other irregularities. In fact, the single piston ChemResearch pump delivers solvent as smoothly as most dual piston pumps.

The solvent, injection valve, and column are maintained at the same temperature in the forced-air oven to provide better reproducibility and to prevent precipitation of samples which require heat to remain in solution. Temperatures are precisely controlled within ± 1°C throughout the oven chamber, which accomodates two 25 or 50 cm columns.

Make your HPLC easier—send for ChemResearch literature today. Or dial direct, toll free (800) 228-4250 (continental U.S.A. except Nebraska). Instrumentation Specialties Company, P.O. Box 5347, Lincoln, Nebraska 68505.

ChemResearch

CIRCLE 107 ON READER SERVICE CARD

Thermal Methods of Analysis
Miami Beach. Sept. 14–15. Wesley W. Wendlandt and Ilya M. Sarasohn. $200, ACS members; $240, nonmembers

Thin-Layer Chromatography
Miami Beach, Sept. 14–15; Boston, Nov. 2–3. Victor W. Rodwell and Donald J. McNamara. $200, ACS members; $240, nonmembers

Microprocessors & Minicomputers—Interfacing and Applications
Blacksburg, Va. Sept. 16–21. Raymond Dessy and the Chemistry Dept. Instrument and Design Group from VPI&SU. $455, ACS members; $515, nonmembers

Gas Chromatography–Mass Spectrometry
Houston, Oct. 4–5; San Francisco, Nov. 29–30. J. Throck Watson and O. David Sparkman. $200, ACS members; $240, nonmembers

Maintaining and Troubleshooting Chromatographic Systems Workshop
Houston, Oct. 6–7; Atlanta, Oct. 21–22. John Q. Walker, Minor T. Jackson, Jr., and M.P.T. Bradley. $230, ACS members; $280, nonmembers

Solving Problems with Modern Liquid Chromatography
Boston. Oct. 28–29. J. J. Kirkland and Lloyd R. Snyder. $230, ACS members; $280, nonmembers

Gas Chromatography
Boston. Nov. 2–3. Roy A. Keller and Michael F. Burke. $200, ACS members; $240, nonmembers

Interpretation of Mass Spectra
Boston, Nov. 3–4; San Francisco, Nov. 29–Dec. 1. Don C. DeJongh. $200, ACS members; $240, nonmembers

Microprocessors & Minicomputers—Interfacing and Applications
Blacksburg, Va. Dec. 10–15. Raymond Dessy and the Chemistry Dept. Instrument and Design Group from VPI&SU. $455, ACS members; $515, nonmembers

Liquid Chromatography, Theory & Practice
Blacksburg, Va. Dec. 11–14. Herold McNair. $450, ACS members; $510, nonmembers

---

Aerosol Measurement
U. of Minnesota. Aug. 16–18. $300. *Contact:* Joe Kroll, Dept. of Conferences, 211 Nolte Center, 315 Pillsbury Drive, S.E., U. of Minnesota, Minneapolis, Minn. 612-373-3685

Process Chromatography (GC and LC)
Baton Rouge Riverside Centroplex. Oct. 9–12. $250. *Contact:* Patricia McDowell, Baton Rouge Analytical Instrument Discussion Group, P.O. Box 14233, Baton Rouge, La. 70808. 504-766-5580

Advanced Atomic Absorption Spectroscopy
Baton Rouge Riverside Centroplex. Oct. 9–12. $200. *Contact:* Patricia McDowell, Baton Rouge Analytical Instrument Discussion Group, P.O. Box 14233, Baton Rouge, La. 70808. 504-766-5580

Analyze this:

THE INTERFACE THAT PUTS LC WHERE GC/MS IS TODAY!
This first commercial LC/MS Interface now makes possible mass spectral analysis of materials difficult or impossible to analyze with a GC/MS system—and also provides a sensitive (nanogram level) universal detector for liquid chromatography.

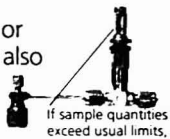

If sample quantities exceed usual limits, split option provides an effective zero dead volume transfer of the allowable quantity of solution.

Flash vaporizer heats samples for such a short time that vaporization is attained without decomposition of test materials.

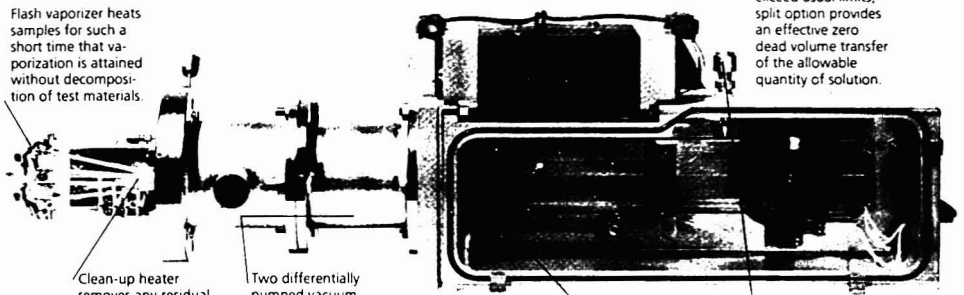

Clean-up heater removes any residual sample to prevent any interference peak in the next belt cycle.

Two differentially pumped vacuum locks complete removal of solvent and also protects mass spectrometer's vacuum. Less than 10^{-7} g/sec of solvent enters the mass spectrometer.

Continuous belt Interface is the mechanism for maintaining high yields With belt interlock features for utmost safety.

The LC/MS accepts as much as 1.2 to 2.0 cc/min of volatile non-polar solvents such as hexane or methylene chloride. Water solutions are handled in amounts of 0.1 to 0.3 cc/min.

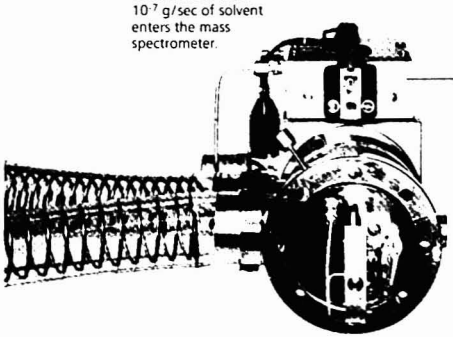

Infrared reflector improves evaporation of solvent.

The LC/MS Interface can be installed in the field on any Finnigan GC/MS with differential pumping, or can be ordered with a new Finnigan system.

finnigan Instruments
A DIVISION OF FINNIGAN CORPORATION
845 W. Maude
Sunnyvale, California 94086
(408) 732-0940
Telex: 346399

CIRCLE 75 ON READER SERVICE CARD

Molecular Absorption Spectroscopy (IR, UV, Fluorescence)
Baton Rouge Riverside Centroplex. Oct. 9–12. $200. *Contact:* Patricia McDowell, Baton Rouge Analytical Instrument Discussion Group, P.O. Box 14233, Baton Rouge, La. 70808. 504-766-5580

Basic Organic Mass Spectral Interpretation and GC/MS
Airport Holiday Inn, Newark, N.J. Oct. 23–27. D. De Jongh and G. Ouchi. $400. *Contact:* Ann Woolley, Finnigan Institute, 11750 Chesterdale Rd., Bldg. #5, Cincinnati, Ohio 45246. 513-772-5500

For Your Information

The American Nuclear Society (ANS) announces the availability of the **"KWIC Index of Nuclear Instrumentation and Analysis in the Physical Sciences Research in Progress—1977"**, an original compilation of prepublication research information. The index identifies nearly 550 current research projects in progress in the following areas of nuclear instrumentation: instrumented systems with small sources, radiation detectors, radiation dosimetry, isotope tracer and analysis techniques, and radiation processing. Each project title is listed under all significant key words, which are alphabetically arranged down the center of each page with surrounding context. Copies are available at $20 (56 pages) each from ANS, 555 N. Kensington Ave., La Grange Park, Ill. 60525.

"Compendium of Analytical Nomenclature" compiles analytical nomenclature and symbols approved by the Council of the International Union of Pure and Applied Chemistry. The compendium is available from Pergamon Press, Fairview Park, Elmsford, N.Y. 10523, at $25 a copy for hardbound and $15 for paperbound.

The **Hazardous Chemical Safety School,** developed by the J. T. Baker Chemical Co., will be held throughout the country on a regional basis through September 1978. The two-day seminar/workshop covers the fundamentals of hazardous chemical safety. The principal areas are flammable solvents, corrosive chemicals, toxic chemicals, insidious hazards related to chemicals, compressed gases, and cryogenic chemicals. A set of 40 slides with a script is provided with the manual for use by the participants in their in-house safety training programs. Attendance is limited to 50, and the tuition is $245. For further information on schedules, contact: Patty Morton, Safety Training, J. T. Baker Chemical Co., Phillipsburg, N.J. 08865 (201-454-2500).

Esterline Angus Instrument Corp., a subsidiary of Esterline Corp., announces the formation of Esterline Process Control Systems Division. The new division will be responsible for the sales of high technology products and systems for monitoring and control in the process industries. The product line includes process analyzers, transmitters and transducers, electronic analog and digital data processors and controllers, and integrated monitoring and control systems. For additional information, contact: Esterline Process Control Systems, Division Esterline Angus Instrument Corp., Box 24000, Indianapolis, Ind. 46224 (317-244-7611).

Gilson manufactures an extensive line of quality equipment and instrumentation for liquid chromatography. Shown here are three of our most popular and well-accepted instruments. For complete details on these units as well as many other items to make your LC work more precise and productive, call, write, or circle the reader service number below.

CHROMATOGRAPHIC COMPATIBLES FROM GILSON

CIRCLE 85 ON READER SERVICE CARD

Micro-Fractionator, Model FC-80. This diminutive, low cost fraction collector is ideal for use with small and medium size LC columns. Can be operated in *cold room*. Model FC-80 weighs only 13 lbs (6 kg) and occupies a bench span of only 11½" X 6" (29 cm X 15 cm). Move it anywhere, or store it in a drawer when you don't use it. A wide range of tube sizes may be used—up to 80 13 X 100 mm or 12 X 75 mm or 10 X 75 mm. It is a combination drop counting or time fractionator.

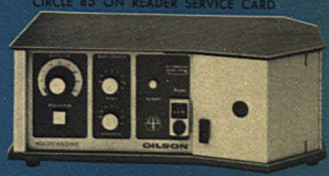

CIRCLE 86 ON READER SERVICE CARD

Double-beam UV/VIS Monitor. (Model HM shown.) Gilson has paid painstaking attention to the critical parameters of UV/VIS design. Column resolution is maintained by our unique blown quartz cell with its high bubble-clearing capabilities. High sensitivity is assured by maintaining long light paths and using low noise electronics. Cells are easily interchangeable and include Kel-F 8 µl volume, 10 mm light path cells for HPLC. Internal heater allows cold room operation.

Peristaltic Pumps. Our MINIPULS line of miniature pumps have long set the performance standard. They are available in 1, 4, 8 and 16 channel models. All feature high torque motors, extremely stable electronic speed control, pump heads with 10 rollers to minimize pulsation, and chemically resistant tubing that can be replaced while the motor is running. Widest flow range: from 1 ml to 1300 ml/hr for all pumps except the HP16 (0.5 to 650 ml/hr). *Multichannel pumps generate gradient for ion exchange chromatography and density gradient centrifugation.* Optional models are available with flow ranges from very slow to very high.

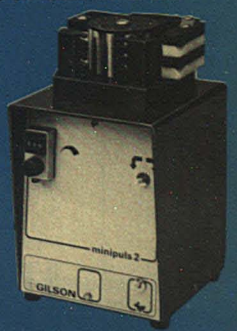

CIRCLE 87 ON READER SERVICE CARD

Demonstration of these fine instruments is available upon request through a network of qualified GME representatives.

GILSON®

Gilson Medical Electronics Inc.
P.O. Box 27 • Middleton, Wisconsin 53562 • Phone (608) 836-1551

Your companion in chromatography

News

In July, **Chemical Abstracts Service added 21 new topics to its *CA Selects,*** a biweekly current-awareness publication. Some of the new titles and subscription rates for 26 issues are: Analytical Chemistry, $50; Computers in Chemistry, $55; Environmental Pollution, $55; Mössbauer Spectroscopy, $50; Pollution Monitoring, $50; and Trace Element Analysis, $50. Thirty-six previous titles are still available. Each biweekly series contains the complete Chemical Abstracts abstracts and citations for recent papers, patents, and other publications in a particular area. Contents are selected by searching CAS's computer-readable information base with a special search profile developed for the topic. Additional information and complimentary issues may be obtained by writing the Marketing Dept., Chemical Abstracts Service, P.O. Box 3012, Columbus, Ohio 43210.

Gas chromatography, liquid chromatography, maintaining and troubleshooting chromatographic systems, laboratory automation, and **electroanalytical chemistry** are some of the many **short course topics the ACS Educational Department is now offering on a "house call" basis.** For many years, ACS has conducted short courses in analytical chemistry and related fields covering a wide range of topics at levels from introductory to highly technical. Now, an organization can schedule the same courses, with the same instructors and teaching materials, right at or near their own headquarters at great savings in time and money. For scheduling and pricing information, call or write: Department of Educational Activities, 1155 Sixteenth St., N.W., Washington, D.C. 20036 (202-872-4507).

American manufacturers of laboratory, diagnostic and health safety and equipment are invited to participate in LABEX INTERNATIONAL 79, scheduled for March 12–16, 1979, at the National Exhibition Centre, Birmingham, England. The biennial event is sponsored by the Scientific Manufacturers' Association of Great Britain and the British Laboratory Ware Association. Further details on booth space, shipping, customs, travel, and accommodations can be obtained from Kallman Associates, U.S. Representative-LABEX, 30 Journal Square, Jersey City, N.J. 07306 (201-653-3304).

How in the world can four metal rods help in food production and environment protection?

To meet the demands of a growing world population, science and industry have in the recent past assumed major roles in agricultural productivity. Their assistance has led to improved irrigation methods, more efficient machinery for handling soils and crops, high yield strains of grain and more effective measures toward pest control. These developments have helped to produce more food, but one hangs like a dark threatening cloud — pesticides.

Those that are dense and water insoluble, migrate within the water system as far as lakes and seas where they quickly settle. Aquatic flora and fauna incorporate these chemicals only to be ingested by progressively higher life forms until finally the food chain ends at man. Most pesticides show toxic effects at concentration levels so low that a serious analytical problem is posed in their quantitative determination.

Easily degradable pesticides may be the ultimate answer. But for the present, research must be concentrated on the removal of existing compounds from human tissue and the monitoring of transmittal agents such as water systems, agricultural products and fish.

What instrumentation can characterize pesticides in plant/animal tissues and water samples at the required trace levels? Extranuclear Laboratories, Inc. offers SIMULSCAN 200 GC/MS which, with its simultaneous CI/EI ionization spectra, is ideally suited for analysis in biological studies. Shown are the simultaneous CI/EI spectra from the same GC peak of the pesticide 0,0-diethyl 0, p-nitrophenyl phosphorothionate.

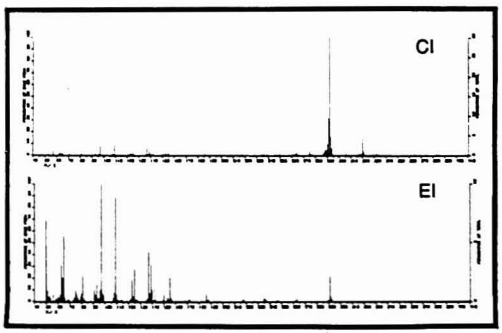

Organic analysis at low levels

SIMULSCAN 200 GC/MS provides simultaneous but separate CI/EI spectra for the same sample, combining the structural and fingerprint characteristics of EI with the high sensitivity and simpler molecular ion structure of CI. In the chemical ionization mode, the system's negative ion capabilities are of particular value in the analysis of pesticides.

And the four metal rods? They're the heart of our quadrupole mass spectrometers.

Extranuclear Laboratories, Inc.
P.O. Box 11512 / Pittsburgh, Pennsylvania 15238 (412) 782-3884
Telex: 812-378 Extralab Pgh

Extranuclear Laboratories will hold their annual Fall School In Mass Spectrometry during the week of Nov.6. For information call and ask for ext. 11.

CIRCLE 63 ON READER SERVICE CARD

SULFUR IN COAL & COKE IN 2 MINUTES...

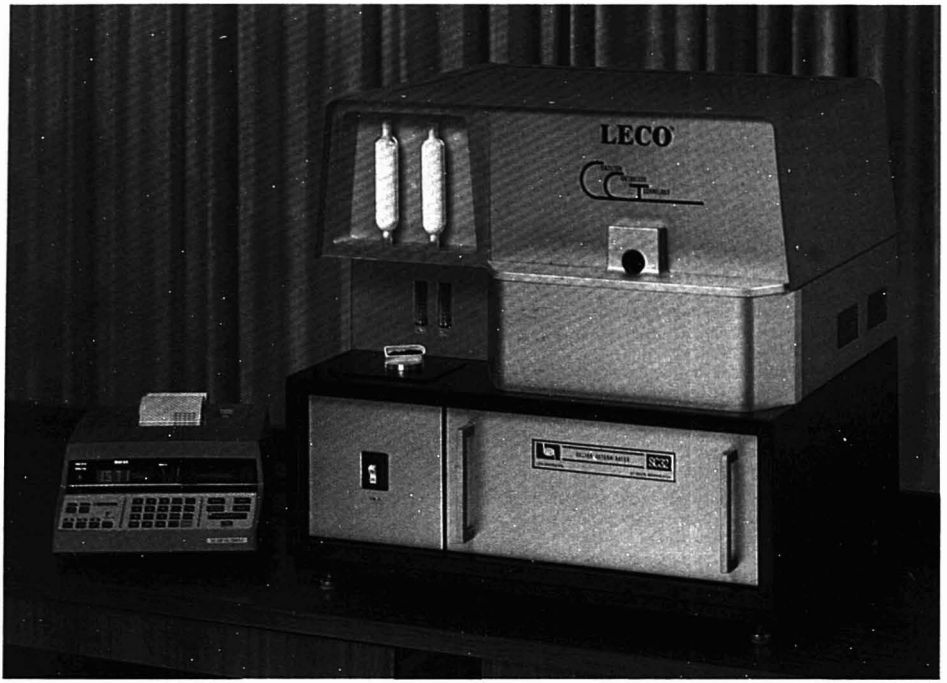

with the LECO® SC-32

- Accuracy ±2 percent of Sulfur content
- Microprocessor Technology
- Large Sample (up to 1 gram)
- Integral Diagnostic Program (lab technician can easily perform service)
- Solid State IR Detection (no standard solutions)

CONTACT LECO TODAY!

LECO CORPORATION 3000 Lakeview Ave. St. Joseph, MI 49085, U.S.A. Phone: (616) 983-5531

LECO®

CIRCLE 125 ON READER SERVICE CARD

Irwin H. Suffet
Department of Chemistry
Environmental Studies Institute
Drexel University
Philadelphia, Pa. 19104

Patrick R. Cairo
Research and Development
Philadelphia Water Department
Philadelphia, Pa. 19107

In Search of the Cause of Legionnaires' Disease

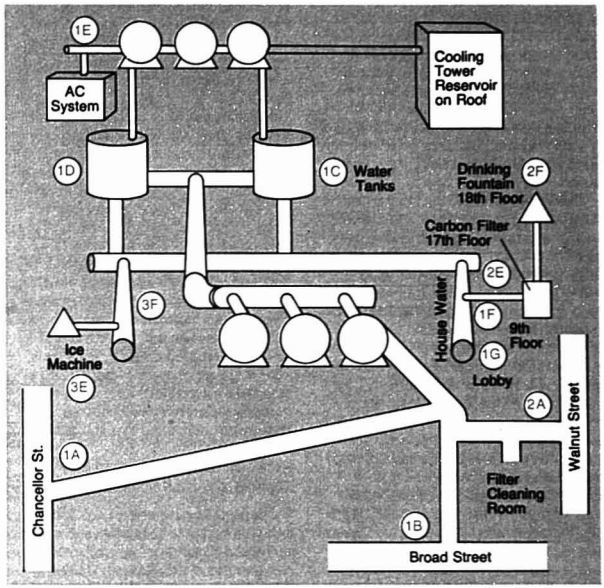

Figure 1. Schematic diagram of water system of convention center hotel

Transmission of disease occurs through a vector, e.g., insect, water, soil, air, or food. The cause (etiologic agent) and the vector of Legionnaires' disease, which occurred in Philadelphia, July 21–24, 1976, were being sought by the Center for Disease Control (CDC) (Atlanta, Ga.) and the Philadelphia Health Department. Yet, three weeks after the outbreak of the disease, no agent or vector had been found. Theories abounded!

Symptoms of Legionnaires' disease closely resembled those of pneumonia. Thus, to separate victims from background cases of pneumonia that would normally develop in a city the size of Philadelphia, CDC selected both clinical and epidemiologic characteristics. Persons were classified as victims of the disease if they possessed fever and chest x-ray evidence of pneumonia or a temperature greater than 102 °F and a cough. To further narrow the definition, they had to have attended the American Legion Convention or have visited the convention center hotel between July 1 and the onset of illness. Statistical analysis of 182 suspected cases ultimately revealed that a typical victim became ill seven days after arriving in Philadelphia and had a temperature rise to 102–105 °F. Since these symptoms could be produced by numerous types of microorganisms and toxins, the investigation was broadened to include all possible environmental factors.

A cross-connection survey of the convention center's water system, conducted on August 8, 1976, showed many violations. Either the wastewater or the air conditioning system could have contaminated the hotel drinking water system. A cross-connection could bring toxic substances into the water supply or perhaps bring organic compounds that would react in a synergistic manner with compounds commonly found in part-per-billion quantities in drinking water. Also, possibly, an agent from a cross-connection, such as dichromate (an antifouling chemical in the air conditioning system), could change a set of trace organics in some unknown fashion into toxic substances. In addition to helping victims of Legionnaires' disease, protection of the people remaining in the hotel was also a major concern. Would there be a subsequent outbreak? Were cross-connections or toxic compounds involved? The Philadelphia Water Department, asked to investigate the environmental systems of the hotel, reviewed with health agencies their findings and learned that a thorough evaluation of the trace organics in the hotel drinking water system had not been undertaken. Thus, an effort in cooperation with Drexel University was initiated immediately to study the drinking water and the air conditioning systems.

How to study water entering and circulating in a 50-year-old hotel was a major problem. Drinking water entering the hotel could come from two treatment plants, each obtaining its water from different surface water supplies, the Schuylkill and Delaware Rivers. The two water sources then intermix within the distribution system and enter the hotel through two water

0003-2700/78/0350-875A$01.00/0

mains. Where should samples be taken? How could representative samples be obtained? What isolation methods were readily available, and which should be used? How could the source of water entering the hotel be determined? How could a comparison of analyses performed at different locations be made? It should be emphasized that a comprehensive trace organic survey of any site in a complex water distribution system had never been accomplished. No protocol or standard methods existed for this type of study, and adaptation of laboratory methods to field locations was necessary.

The effect of chlorination and detention time on the trace organic content of a drinking water has only recently been studied and still is not fully understood. Data from many water treatment plants indicate that each drinking water may be unique in composition and chemical reactivity. Studies of collected samples show that even treated water is of ever-changing quality. Recent studies at one of Philadelphia's Water Treatment Plants showed a variation in trace organic content during a week of continuous composite sampling. The chlorinated material also has been shown to change with time. In fact, the rate of change may be different for each sample. Furthermore, at a specific location in a complex water distribution system, such as the one servicing the hotel, the water may be comprised of a changing mixture of river sources since water flow is controlled by consumption.

Sample Site Selection

With limited time available, the choice of sampling sites was extremely important. To ensure that no possible contamination source would be missed, sampling locations were chosen to follow the path of the water through the hotel distribution system (Figure 1) from one water main (1B) to the tanks on the 19th floor (1C, 1D) and then down through the other floors (9th and lobby, 1F and 1G). All these samples were collected simultaneously on 8/25/76. In addition, a cross-connection with the air conditioning system (1E) on the 19th floor was sampled on 8/25/76. Two special sites at the input and output water from a drinking water fountain outside of a ballroom on the 18th floor (2E, 2F) and at an ice machine on the 2nd floor (3E, 3F) were sampled along with the cooling and condenser water from the air conditioning system on 8/27/76. The second water main (1A) also was sampled on 8/27/76. These sites were representative of the location where attendees at the Legionnaires' conference could obtain water that might be a vector of the disease.

Representative Samples and Choice of Isolation Method

No sample sites are ideal, no isolation method is totally efficient, and no method of obtaining a representative sample is time tested. Consequently, one must make choices based upon the state-of-the-art at that time and the pragmatic considerations of manpower and equipment available. The investigation reported here has enabled the development of an analytical protocol for the study of future emergency water problems.

The decision was made to utilize a composite sampling method to obtain representative samples throughout the hotel's distribution system. Eight-hour composite samples were collected during midweek working days. Macroreticular resin (MRR) XAD-2 and continuous liquid-liquid extraction (CLLE) were the isolation methods used. They have been used successfully in identification of trace organics in drinking water in Philadelphia since 1975 (*1*). The MRR and CLLE equipment was operational, and the manpower was experienced in its use. These isolation methods are useful for analysis of the "neutral"-type organics, boiling between 40 and 230 °C. Figure 2 shows the sampling apparatus at a location in the hotel's subbasement where a water main sample (2A) was collected.

Comparison of Samples Collected at Different Locations

A gas chromatographic "profile" method was used to compare samples (*2, 3*), and selected samples were run by GC/MS to identify the components of these samples. The analytical approach used to study the trace organics present in the hotel's water system is shown in Figure 3. Of prime importance is the GC profile evaluation in which the question of possible contamination may be considered. A GC profile is a fingerprint of a complex group of trace organics present in the extracted water and constitutes an information pattern of the sample. By plotting peak area or height proportional to a standard on a relative retention time scale, many GC profiles can be compared to obtain an understanding of the spatial changes in the hotel's water system. A unique GC profile computer program was used to study the difference in the trace organics between samples. It must be emphasized that differences between GC profiles can be caused by different compounds or different relative concentrations of a mixture of compounds in a sample. GC profiles are used to observe peak changes and to aid in the selection of samples to best utilize severely limited GC/MS analysis time.

A cursory evaluation of the GC profiles of the organics present through the distribution system showed it to be extremely useful in demonstrating differences between samples. When GC/MS was used to identify a compound, its identity was considered confirmed if it matched the mass spectrum of a pure reference compound and if its relative retention time on a 20% SE-30 packed column was the

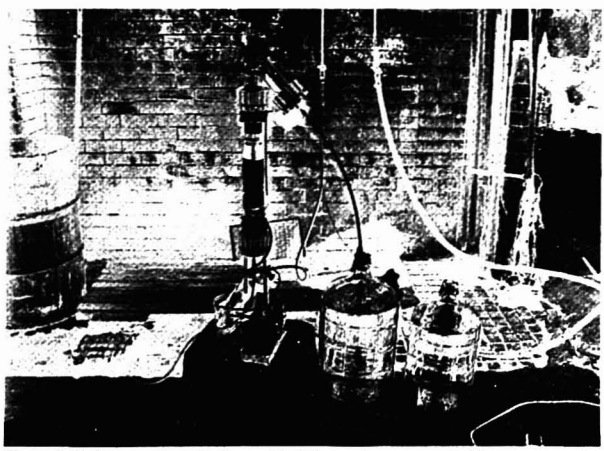

Figure 2. On-line sample collection and isolation system as operated in screen washing room located in subbasement of hotel

Walnut Street water main (2A) sample collected at this point. Continuous composite sample after dechlorination and pH adjustment fed continuously to on-line MRR-XAD-2 macroreticular resin sampler; at overflow, sample collected for subsequent continuous liquid-liquid extraction

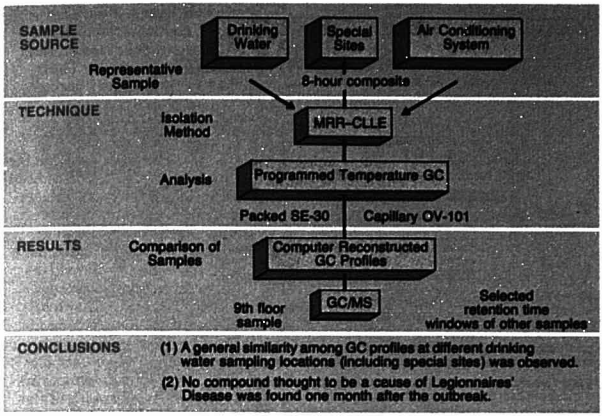

Figure 3. Analytical approach for identification of trace organics

same as the reference compound. In addition, tentative identifications were made where reference compounds were not commercially available but the mass spectrum of a peak matched uniquely characteristic literature mass spectra. When needed, computer-assisted interpretation was provided by Cornell University's Mass Spectral Identification System PBM and STIRS.

Was There a Difference Between Samples?

A detailed GC profile analysis was performed on the organics in the drinking water samples and air conditioning system. Figure 4 shows "spiked" GC profiles of samples obtained at various locations by the MRR sampling method. Each spike represents a GC peak, with the height of the peak representative of the size of the original GC peak—either small, medium, or large (relative heights on the GC peak profiles are respectively, 0.2, 0.5, and 1.0 units). A reproducibility of ±0.015 RRT units was obtained during this study.

Two phenomena were observed in drinking water samples with these spiked profiles:

- A general similarity among GC profiles of MRR samples at different drinking water sampling locations (including special sites) is obvious. The CLLE samples were very similar to the MRR samples except for concentration differences (CLLE collection volumes were around 30 L at a 10:1 water:solvent ratio, whereas MRR volumes were around 100 L).
- Minute changes could be seen less distinctly. Comparison with the original chromatograms showed that sometimes shoulders on peaks could be seen, and at other times these were obscured by large peaks. This is demonstrated more clearly by simulated 3-D profiles, with peak heights and widths of the profile actually measured (Figure 5).

The CLLE samples from the air conditioning system were the only samples to appear quite different from the drinking water system. With an equivalent sample volume, more and higher GC peaks of different RTT's were observed.

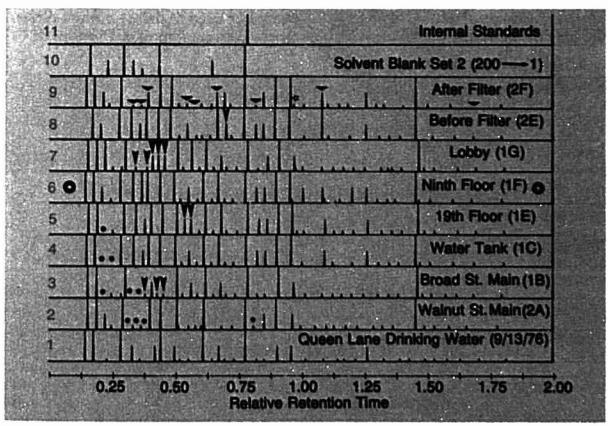

Figure 4. GC profiles on SE-30 of drinking water samples from convention center hotel

Water samples collected by MRR-XAD-2 macroreticular resin column over 8-h period on 8/23/76 and 8/27/76. Sample 1 from one of the water treatment plants that feeds water to the hotel. Sample 2 collected on 8/27/76 and listed as 2A to show it was not collected on 8/23/76. ▼ Missing in 9th floor, present in sample. ★ Missing in sample, present in 9th floor. ☆ Minor peak in carbon filter effluent, not in influent. Peak lowered in intensity in effluent of carbon filter as compared to influent to carbon filter. Internal standards were 2-ethyl-1-hexanol (RRT: 0.78) dibutyl phthalate (2.00). All samples eluted with 200 mL ether evaporated to 1 mL

GC/MS Identification of Trace Organics in the Drinking Water and Air Conditioning System

The 9th floor samples were chosen as reference GC profiles for the hotel drinking water system since they contained the most GC peaks of the largest concentration. Thus, it was reasoned that if a compound that could have caused Legionnaires' disease was in the drinking water, it would be found in this sample or in a sample where a GC peak was missing from the profile of the 9th floor (● Figure 4).

A detailed GC/MS analysis was completed with a 6% SE-30 column on the 9th floor MRR and CLLE samples and on selected samples at RRT's where GC peaks were missing from the 9th floor MRR sample. Also, a complete GC/MS analysis was run on the MRR samples for the drinking water fountain with the carbon filter. The carbon filter had been installed on this fountain for an *unknown period of time*. Table I shows GC/MS results for the 9th floor MRR and CLLE samples. GC/MS analysis of the selected samples where GC peaks were missing from the 9th floor sample (Figure 4) showed that RRT shifts due to changes in relative concentrations

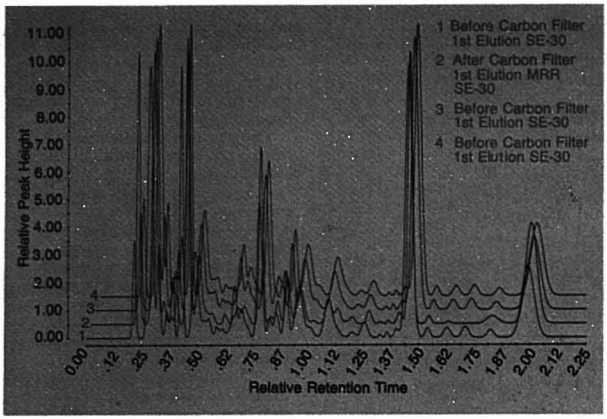

Figure 5. GC profiles of drinking water samples taken before and after a carbon filter on a drinking water fountain

Chromatograms same as sample numbers 8 and 9 from Figure 4. *Before* sample plotted as 1st, 3rd, and 4th chromatograms, respectively

of mixtures of compounds eluting as single peaks was the primary reason for differences. Benzene (19th floor) and a branched C8 alkene (19th and lobby) were the only compounds in these samples that were not found in the 9th floor sample. Two possibilities are that they were obscured by a larger peak or were added in water distribution. GC/MS of these CLLE samples added further confirmation of these components. Other CLLE samples were too dilute to allow GC/MS analysis.

GC/MS analysis of the trace organics present in the carbon filter influent showed a set of compounds which was similar to those found in the drinking water system (Table I). Two new compounds were observed: phenylacetic acid and 1,2:3,5-di-*O*-isopropylidene-*D*-xylofuranose. This may be accounted for by the fact that the influent sample to the carbon filter was collected two days after the drinking water samples. GC/MS analysis of the trace organics present in the carbon filter effluent showed the same compounds that were present in the influent except for the addition of trichloroethylene, diethyl phthalate, 2-dichlorobenzene isomers, dichloroacetonitrile, toluene, a dichloropropene isomer, and a C9 branched hydrocarbon. These compounds have previously been observed in Philadelphia's drinking water and are apparently being displaced by others that are adsorbed.

Most of the compounds found in the hotel drinking water system have been identified in drinking waters throughout the United States and are also part of the variable complement of trace organics found in Philadelphia's drinking water. Thus, it was evident that these could not be the cause of Legionnaires' disease. 1,1-Dichloroethane, a C5 alkene, methyl bromide, and phenanthrene or anthracene are compounds that had never been isolated in any other Philadelphia drinking water sample, but a search of the toxicological significance of these compounds indicated that these should not have led to the disease.

Table I shows the GC/MS analysis of the air conditioning system. Diethyl sulfate is an additional compound to the drinking water sample mixture of compounds. Since this compound was not found in any of the drinking water samples, contamination caused by a cross-connection at the time of sampling is unlikely. Once again, no obvious solution to Legionnaires' disease was found.

Capillary Column GC

The decision was made to select several samples and run capillary column GC. Its high resolving power would be used to detect minute differences between samples. Portions of

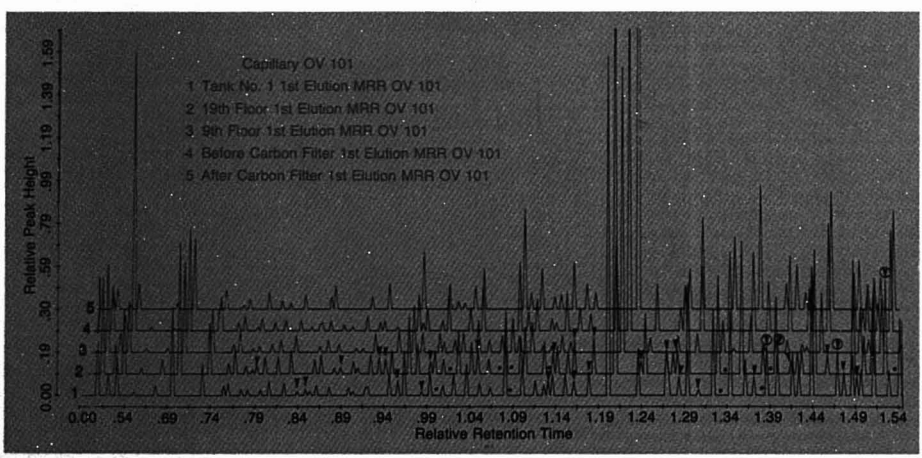

Figure 6. Portions of capillary GC profiles on OV-101 of drinking water samples from convention center hotel

These chromatograms from same samples as numbers 4, 5, 6, 8, and 9 from Figure 4. ▼ Missing in 9th floor, present in sample. ★ Missing in sample, present in 9th floor. (▼) If peaks are very large, they are circled

Table I. Compounds Identified by GC/MS in Bellevue-Stratford Samples Taken by Macroreticular Resin (MRR) and by Continuous Liquid-Liquid Extraction (CLLE)[a]

	drinking water	air conditioning system	
	9th floor (MRR)	chill (CLLE)	condenser (CLLE)
HALOGENATED			
bromoform	X[b]	X	
carbon tetrachloride	X		
chloroform	X		
dibromochloromethane	X	X	
dichlorobromomethane	X		
dichlorobenzene isomer	X		
tetrachloroethylene	X	X	X
trichloroacetone	X[c]		
dichloropropene isomers	2[d]		
dichloroacetonitrile	X		
chloro-methyl-butene isomers	4		
1,1,1-trichloroethane		X	
1,1-dichloroethane		X	
1,2-dichloroethane	X		
methyl bromide	X		
AROMATIC			
acetophenone	X		
benzaldehyde	X[c]		X
ethyl benzene or xylene isomers	4	1	2
toluene	X		
m- or *p*-tolunitrile	X[c]		
dimethyl or ethyl phenol isomer	X		
dimethyl or ethyl benzaldehyde isomers[e]	2		
C5-benzene isomer	X		
phenanthrene or anthracene	X		
MISCELLANEOUS			
2,3:4,6-di-*O*-isopropylidene-*L*-sorbofuranose	X[c]		
dibutyl phthalate	X[c]		
tributyl phosphate	X[c]		
dihydroactinidiolide	X[c]		
C5 alkene	X		
C6 branched hydrocarbon	X		
C7-9 branched hydrocarbons		X	
ethanol		X	
acetone		X	
diethyl sulfate		X	
triethyl phosphate			X
TENTATIVES			
ethyl sorbate	X		
1 (2 or 4-chlorophenyl) ethanol	X		
1,1,2-trichloroethane			X

[a] All impurities found in the blank are not listed. [b] X = compound identified. [c] Confirmed by GC/MS in 9th floor CLLE. [d] Any number = number of isomers identified. [e] May also be mixed with a C4-benzene isomer.

GC profiles with true relative heights are shown in Figure 6. Approximately 125 peaks per sample were isolated by using capillary columns compared with 35 peaks on packed columns.

After a detailed examination of the capillary GC runs, it became clear that there was very little difference in the type and amount of trace organics throughout the hotel's drinking water system! Less than 10% of the approximately 125 peaks showed any noticeable variation compared with the ninth floor. Only 4 peaks on capillary GC, at RRT 1.41, 1.43, 1.49, and 1.55, were considered to be significant. Thus, our preliminary analysis with an SE-30 packed column was confirmed by capillary GC. GC profile evaluation was an effective method for examination of the trace organics throughout the hotel's drinking water system. It enabled determining similarities of samples and thus provided a screening method for subsequent GC/MS work.

The Disease Agent

In January 1977, six months after the outbreak of Legionnaires' disease, CDC reported that it had isolated a previously unidentified microorganism that is believed to be the cause of the disease. As detailed in the *New England Journal of Medicine* (4), after months of fruitless efforts, a gram-negative, nonacid-fast bacillus was isolated from lung tissues of victims by inoculating guinea pigs and then transferring their spleen suspensions to embryonated eggs. Cultivating the organism on artificial media required several more months of effort until finally a procedure was established which permitted testing of a large number of disease victims. Once confident that this bacterium was indeed the agent, CDC set out to find whether similar outbreaks of pneumonia in the past had been caused by this organism. Using serum specimens stored from previous outbreaks in 1966 at a hospital in Washington, D.C., and in 1968 in Pontiac, Mich., CDC concluded that the sera contained significant numbers of antibodies to implicate the bacterium. By November 1977 CDC reported (5) that confirmed sporadic cases of Legionnaires' disease had been found in 24 states of the United States as well as England and Spain.

The Disease Vector

Although medical authorities are confident that they have identified the agent, the mode of transmission of the disease remains a mystery. Person-to-person spread was quickly ruled out when secondary infections to families of the Philadelphia victims did not occur. Similarly, food, tobacco, and alcohol were dismissed as possible vectors. Transmission through water is unlikely, for although the epidemiologic investigation has shown that water consumption was higher than normal for victims, one-third of the cases denied drinking any water; in fact, a group never entered the hotel. The vector now believed to be the best possibility is air transmission or a soil- or dirt-borne organism. This hypothesis is predicated on the fact that many victims spent considerable time in the lobby of the hotel. A low grade or intermittent exposure of the organism may have resulted from some type of construction-related activity that would have disturbed the niche of the bacterium, causing its entry into the air environment of the hotel and its surroundings. Further work is still needed before the mode of transmission is conclusively demonstrated.

Discussion

Although the organic profile of the hotel water system did not uncover the vector for Legionnaires' disease, significant experience was gained in the development and testing of an analytical protocol to be used in responding to emergency water problems. Cross-connection incidences have been the cause of numerous gastrointestinal diseases and, in some cases, even deaths. Though in most instances microorganisms are the agents of the disease, toxic chemicals have been responsible for some occurrences. By responding promptly with thorough analytical surveys, the cause of the problem may be quickly found and corrective steps taken before serious health problems develop.

A second benefit of the investigation of the hotel water system has been the demonstration of the versatility of the isolation steps. Although designed for use in a laboratory environment, the apparatus was easily adapted to very hostile environments. These steps can be used in the field to conduct trace organic surveys of complex water distribution networks, thus obviating the need for bringing large volumes of water back to the laboratory. Finally, the role of the analytical chemist in a team of disease investigators was once again demonstrated.

Acknowledgment

The authors acknowledge the continued support of the Philadelphia Water Department for this research under the leadership of Water Commissioner Carmen F. Guarino and J. V. Radziul, chief of research. The authors thank James Coyle, Philadelphia Water Department, who coordinated the field sampling program; Lewis Brenner, Philadelphia Police Department Laboratory; and Bruce Schultz and Areta Wowk of Drexel University for GC profile work and GC/MS.

References

(1) I. H. Suffet, L. Brenner, and J. V. Radziul, "GC/MS Identification of Trace Organic Compounds in Philadelphia Waters", in "Identification and Analysis of Organic Pollutants in Water", L. H. Keith, Ed., Chap. 23, pp 375–97, Ann Arbor Science, Ann Arbor, Mich., 1976.
(2) E. R. Glaser, B. Silver, and I. H. Suffet, *J. Chromatogr. Sci.*, **15**, 22 (1977).
(3) I. H. Suffet and E. R. Glaser, *ibid.*, **16**, 12 (1978).
(4) J. E. McDade et al., *New England J. Med.*, **297**, No. 22 (Dec. 1, 1977).
(5) Center for Disease Control, "Morbidity and Mortality Report", "Sporatic Cases of Legionnaires' Disease—United States", Vol 26, No. 45, Nov. 11, 1977.

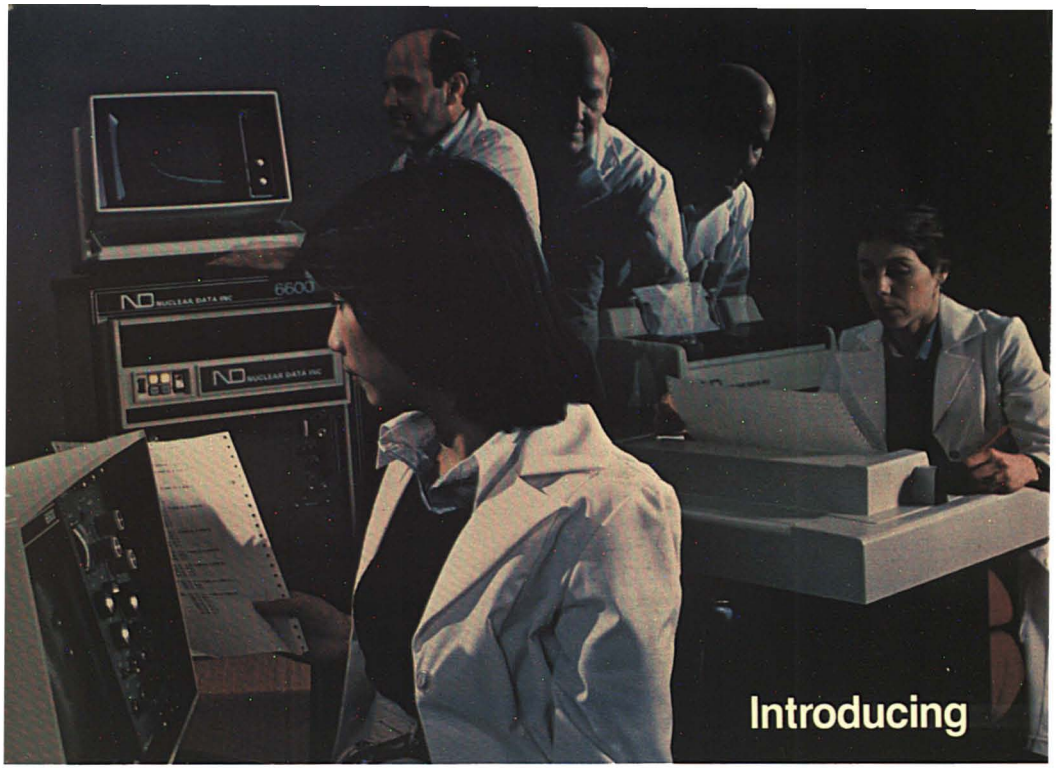

The ND6600 X-Ray Analysis System And Maryann And John And Cindy And . . .

That's right, multiple users performing multiple tasks simultaneously using the powerful hardware and software capabilities of the ND6600 Laboratory Computer System. While other X-ray data systems perform only single tasks, the ND6600 accomplishes a multitude of computerized tasks for multiple independent users.

The 6600 system combines the efficiency of distributed processing with the exclusive, synchronous COMBUS to meet requirements in all areas of spectroscopy. The system simultaneously acquires, processes and displays data from a variety of radiation sources (up to 24 separate experiments) over an essentially infinite range of energies. Analyses can be performed on the basis of pulse height for energy dispersive data and multichannel scaling (pulse counting) for wavelength dispersive data. ND6600 X-ray analysis capabilities include:

Qualitative X-Ray Analysis: KLM markers can be independently displayed on each user's spectrum. All possible element assignments for a set of spectral peaks are listed and each assignment is tested for the probability of the element being present using all defined lines for the element.

Tube-Excited Quantitative X-Ray Analysis: Fundamental Parameters matrix correction software accounts for line enhancement and absorption effects and includes provisions for thin and micro-sample analysis. Automatic background removal and deconvolution are standard.

Electron-Excited Quantitative X-Ray Analysis: Deconvolution and ZAF correction software based on Frame C automatically performs analysis for electron column applications.

Ask for literature on the ND6600 X-Ray Analysis System including sample reports, data displays and typical applications.

CIRCLE 146 ON READER SERVICE CARD

Golf and Meacham Roads
Schaumburg, Illinois 60196
Tel: 312 884-3621

Bonameser Strasse 44
6000 Frankfurt/Main 50
Federal Republic of Germany
Tel: 529952

Nuclear Data Inc

AUGUST 1978

VALID THROUGH DECEMBER 1978

ADVERTISED PRODUCTS:

	7	8	9	10	11	12	13	14	15	16	17
18	19	20	21	22	23	24	25	26	27	28	
29	30	31	32	33	34	35	36	37	38	39	
40	41	42	43	44	45	46	47	48	49	50	
51	52	53	54	55	56	57	58	59	60	61	
62	63	64	65	66	67	68	69	70	71	72	
73	74	75	76	77	78	79	80	81	82	83	
84	85	86	87	88	89	90	91	92	93	94	
95	96	97	98	99	100	101	102	103	104	105	
106	107	108	109	110	111	112	113	114	115	116	
117	118	119	120	121	122	123	124	125	126	127	
128	129	130	131	132	133	134	135	136	137	138	
139	140	141	142	143	144	145	146	147	148	149	
150	151	152	153	154	155	156	157	158	159	160	
161	162	163	164	165	166	167	168	169	170	171	
172	173	174	175	176	177	178	179	180	181	182	
183	184	185	186	187	188	189	190	191	192	193	
194	195	196	197	198	199	200	201	202	203	204	
205	206	207	208	209	210	211	212	213	214	215	
216	217	218	219	220	221	222	223	224	225	226	
227	228	229	230	231	232	233	234	235	236	237	
238	239	240	241	242	243	244	245	246	247	248	
249	250	251	252	253	254	255	256	257	258	259	

NEW PRODUCTS:

401	402	403	404	405	406	407					
408	409	410	411	412	413	414	415	416	417	418	
419	420	421	422	423	424	425	426	427	428	429	
430	431	432	433	434	435	436	437	438	439	440	
441	442	443	444	445	446	447	448	449	450	451	
452	453	454	455	456	457	458	459	460	461	462	
463	464	465	466	467	468	469	470	471	472	473	
474	475	476	477	478	479	480	481	482	483	484	
485	486	487	488	489	490	491	492	493	494	495	

READER SURVEY:

301	302	303	304	305	306	307					
308	309	310	311	312	313	314	315	316	317	318	
319	320	321	322	323	324	325	326	327	328	329	
330	331	332	333	334	335	336	337	338	339	340	
341	342	343	344	345	346	347	348	349	350	351	

TO VALIDATE THIS CARD, PLEASE CHECK ONE ENTRY FOR EACH CATEGORY BELOW:

Intensity of product need:
- ☐ 1. Have salesman call
- ☐ 2. Need within 6 mos.
- ☐ 3. Future project

Primary field of work:
- ☐ A. Energy
- ☐ B. Environmental
- ☐ C. Medical/Biological
- ☐ D. Drug/Cosmetic
- ☐ E. Forensic/Narcotic
- ☐ F. Textile/Fiber
- ☐ G. Metals
- ☐ H. Pulp/Paper/Wood
- ☐ I. Soaps/Cleaners
- ☐ J. Paint/Coating/Ink
- ☐ K. Electrical/Electronic
- ☐ L. Instrument Dev./Des
- ☐ M. Plastic/Polymer/Rub
- ☐ N. Agricultural/Food
- ☐ O. Inorganic Chemicals
- ☐ P. Organic Chemicals

Primary area of employment:

INDUSTRIAL
- ☐ A. Research/Development
- ☐ B. Quality/Process Control

MEDICAL/HOSPITAL
- ☐ C. Research/Development
- ☐ D. Clinical/Diagnostic

GOVERNMENT
- ☐ E. Research/Development
- ☐ F. Regulate/Investigate

COLLEGE/UNIVERSITY
- ☐ G. Research/Development
- ☐ H. Teaching

INDEPENDENT/CONSULTING
- ☐ I. Research/Development
- ☐ J. Analysis/Testing

This copy of Analytical is:
- ☐ 1. Personally addressed to me in my name.
- ☐ 2. Addressed to other person or to my firm.

NAME: _____

TITLE: _____

FIRM: _____

STREET: _____

CITY: _____

STATE: _____ ZIP: _____

PHONE: (___ ___ ___) ___ ___ ___ - ___ ___ ___ ___

FIRST CLASS
Permit #27346
Philadelphia, PA

BUSINESS REPLY MAIL

NO POSTAGE NECESSARY IF MAILED IN THE UNITED STATES

POSTAGE WILL BE PAID BY:

analytical chemistry

P.O. BOX #7826
PHILADELPHIA, PA 19101

FIRST CLASS
Permit #27346
Philadelphia, PA

BUSINESS REPLY MAIL

NO POSTAGE NECESSARY IF MAILED IN THE UNITED STATES

POSTAGE WILL BE PAID BY:

analytical chemistry

P.O. BOX #7826
PHILADELPHIA, PA 19101

YOUR "READER SURVEY" VIEWS ARE VITAL

Analytical Chemistry frequently presents a Reader Survey section that provides you with an opportunity to indicate your interests and activities. Your answers help us in planning editorial material that will be useful to you in your work.

To express your Reader Survey views, simply circle your answers on one of these adjacent reply cards and drop it in the mail. No postage is required.

AUGUST 1978

VALID THROUGH DECEMBER 1978

ADVERTISED PRODUCTS:										
7	8	9	10	11	12	13	14	15	16	17
18	19	20	21	22	23	24	25	26	27	28
29	30	31	32	33	34	35	36	37	38	39
40	41	42	43	44	45	46	47	48	49	50
51	52	53	54	55	56	57	58	59	60	61
62	63	64	65	66	67	68	69	70	71	72
73	74	75	76	77	78	79	80	81	82	83
84	85	86	87	88	89	90	91	92	93	94
95	96	97	98	99	100	101	102	103	104	105
106	107	108	109	110	111	112	113	114	115	116
117	118	119	120	121	122	123	124	125	126	127
128	129	130	131	132	133	134	135	136	137	138
139	140	141	142	143	144	145	146	147	148	149
150	151	152	153	154	155	156	157	158	159	160
161	162	163	164	165	166	167	168	169	170	171
172	173	174	175	176	177	178	179	180	181	182
183	184	185	186	187	188	189	190	191	192	193
194	195	196	197	198	199	200	201	202	203	204
205	206	207	208	209	210	211	212	213	214	215
216	217	218	219	220	221	222	223	224	225	226
227	228	229	230	231	232	233	234	235	236	237
238	239	240	241	242	243	244	245	246	247	248
249	250	251	252	253	254	255	256	257	258	259

NEW PRODUCTS:										
401	402	403	404	405	406	407				
408	409	410	411	412	413	414	415	416	417	418
419	420	421	422	423	424	425	426	427	428	429
430	431	432	433	434	435	436	437	438	439	440
441	442	443	444	445	446	447	448	449	450	451
452	453	454	455	456	457	458	459	460	461	462
463	464	465	466	467	468	469	470	471	472	473
474	475	476	477	478	479	480	481	482	483	484
485	486	487	488	489	490	491	492	493	494	495

READER SURVEY:										
301	302	303	304	305	306	307				
308	309	310	311	312	313	314	315	316	317	318
319	320	321	322	323	324	325	326	327	328	329
330	331	332	333	334	335	336	337	338	339	340
341	342	343	344	345	346	347	348	349	350	351

TO VALIDATE THIS CARD, PLEASE CHECK ONE ENTRY FOR EACH CATEGORY BELOW:

Intensity of product need:
- ☐ 1. Have salesman call
- ☐ 2. Need within 6 mos.
- ☐ 3. Future project

Primary field of work:
- ☐ A. Energy
- ☐ B. Environmental
- ☐ C. Medical/Biological
- ☐ D. Drug/Cosmetic
- ☐ E. Forensic/Narcotic
- ☐ F. Textile/Fiber
- ☐ G. Metals
- ☐ H. Pulp/Paper/Wood
- ☐ I. Soaps/Cleaners
- ☐ J. Paint/Coating/Ink
- ☐ K. Electrical/Electronic
- ☐ L. Instrument Dev./Des
- ☐ M. Plastic/Polymer/Rub
- ☐ N. Agricultural/Food
- ☐ O. Inorganic Chemicals
- ☐ P. Organic Chemicals

Primary area of employment:
INDUSTRIAL
- ☐ A. Research/Development
- ☐ B. Quality/Process Control

MEDICAL/HOSPITAL
- ☐ C. Research/Development
- ☐ D. Clinical/Diagnostic

GOVERNMENT
- ☐ E. Research/Development
- ☐ F. Regulate/Investigate

COLLEGE/UNIVERSITY
- ☐ G. Research/Development
- ☐ H. Teaching

INDEPENDENT/CONSULTING
- ☐ I. Research/Development
- ☐ J. Analysis/Testing

This copy of Analytical is:
- ☐ 1. Personally addressed to me in my name.
- ☐ 2. Addressed to other person or to my firm.

NAME: _____

TITLE: _____

FIRM: _____

STREET: _____

CITY: _____

STATE: _____ ZIP: _____

PHONE: (___ ___ ___) ___ ___ ___ - ___ ___ ___ ___

NEW! PRECISION LIQUID DISPENSERS

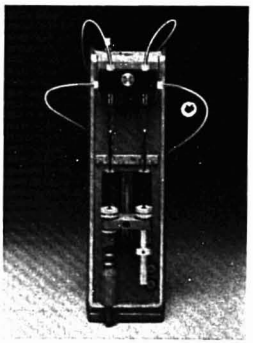

Single and Dual Channel Dispensers

Now you can solve almost all of your liquid dispensing problems with Hamilton's new and improved, low-cost Precision Liquid Dispensers (PLD). Designed for industrial R&D, quality control, and filling operations, with accuracy and precision where strict tolerances are required.

Check these features:
- ☐ New, improved valve system.
- ☐ Longer valve life saves downtime.
- ☐ Easy cleaning and changing.
- ☐ Simple, trouble-free operation.
- ☐ Weight-balanced, rugged construction.
- ☐ Operates in any position or environment.
- ☐ Pneumatic (non-electric) operation.
- ☐ Ideal for operations where oxygen or flammables are present, or in most extremes of temperature or viscosity.
- ☐ Under standard conditions, precision is ±.05%, accuracy is ±1%.

If you have a liquid dispensing problem, call the experts. We'll send out a trained sales engineer or put you in touch with one of our dealers. Write for literature to John Nadolny, Hamilton Company, P.O. Box 10030, Reno, Nevada 89510, or call (702) 786-7077.

HAMILTON

CIRCLE 94 ON READER SERVICE CARD

CAMAC
ANSI/IEEE-583

With the advent of KineticSystems new mini crate, now you can realize all the advantages of the CAMAC computer interface standard within a small stand-alone 8010 microcomputer system.

This new mini crate 8010 offers you both an economical way to automate your process and limitless capabilities for expansion. It is specifically designed for your small process systems and those remote applications with limited requirements.

Twelve stations within the crate provide for one double-width controller plus ten single-width I/O modules. The right-hand enclosed portion of the crate contains two Minifloppy disk drives and the microcomputer of your choice.

As with our standard 25-station CAMAC crate and with all our modules, the mini 8010 microcomputer system complies with the CAMAC specifications for computer-automated monitoring and control. CAMAC offers you modular expansion, computer independence, fast access of remote points, and distributed intelligence and control.

We can provide a CAMAC 8010 microcomputer system tailored to your needs from a full line of stocked I/O modules and equipment as well as software to handle them. Write or call today for more information.

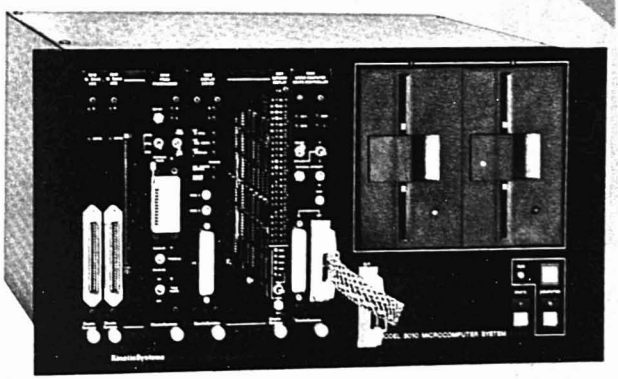

the start of a beautiful process control system

KineticSystems Corporation

Dept. AC88, 11 Maryknoll Drive • Lockport, Illinois 60441 • (815) 838 0005 • TWX 910 638 2831
6 Chemin de Tavernay • 1218 Geneva, Switzerland • (022) 98 44 45 • Telex 28 9622

CIRCLE 119 ON READER SERVICE CARD

New Products

Recorder Calibrator

Model HC-25 quickly checks the performance of both strip chart and x-y recorders. It evaluates span calibration, dead zone, chart speed or time base accuracy, linearity, and overshoot. The calibrator provides more than 80 output range spans from 0.1 to 15 mV via function switch with six output recorder functions, and time markers that can be set from 0.1 to 99 s/in. at variable amplitudes from 0 to 100 mV/in. Houston Instrument **419**

Purge and Trap Sampler

The HP 7675A purge and trap sampler concentrates traces of volatile organic compounds to levels detectable by GC and GC/MS. It uses the dynamic headspace technique of analysis in which the sample is continuously purged by gas flowing through it. Volatile organics in water are transferred to the gaseous phase and then adsorbed on a trap where they are heated and backflushed onto the analytical column. The unit is programmable, allowing the user to select purge time, trap desorption time, and temperature. Prices start at $3500. Hewlett-Packard Co. **410**

The XL-200 superconducting FT–NMR spectrometer with multitasking data system incorporates a high-performance data management system that affords unique multitasking capability and high sample throughput. It is equipped with a wide-bore 47-kg superconducting magnet for high-resolution studies of ^{1}H at 200 MHz and ^{13}C at 50.3 MHz. The superconducting solenoid is housed in a low-loss dewar unit that allows the system to operate over three months with only 25 L of liquid helium. The data management system employs two processing units—one 32 bits wide and specializing in high-speed data collection and spectrometer control, and the other programmed in a high-level language and providing flexible data manipulation. Prices start at $149 500. Varian Associates **401**

Autosampler for Atomic Absorption

The IL254 FASTAC (flame/furnace autosampling technique with automatic calibration) automatically presents up to 95 samples either to an atomic absorption burner system or to the IL555 controlled-temperature furnace atomizer. It differs from other furnace autosamplers in that the sample passes through a nebulizer and mixing chamber and is presented to the furnace as an aerosol. Advantages provided are controllable analytical sensitivity, good precision, low sample carryover, and high speed. Instrumentation Laboratory Inc. **412**

The TN-4000 spectroscopic analysis system, a multichannel analyzer, features multiple-processor technology, independent data memories, and an interactive operator's control console. Complete software packages providing automated, quantitative analysis are available for neutron activation analysis and gamma-ray spectroscopy. The system is offered with a selection of central processing units and may be configured with as many as eight independently accessed data memories, providing analytical power of up to eight separate analyzers in one centrally controlled system. Spectral data and system information are dynamically displayed on a 9-in. fully alphanumeric CRT. Tracor Northern, Inc. **402**

X-ray Energy Spectrometer

Sigma-X is a microprocessor-based x-ray energy spectrometer employing several radioisotopes to induce x-ray fluorescence. Nondestructive multielement analyses are performed within 60 s per assay. The microprocessors are programmed for dedicated analytical applications (i.e., stainless steel, copper alloys, urinalysis, etc.). A simple insertion of a preprogrammed microprocessor PC board changes the dedicated application. The spectrometer is equipped with a 16-sample capacity sample changer and a fail-safe interlocked radioisotope source shutter with provision for vacuum operation. Kevex Corp. **408**

GPC Columns

These columns are packed with Spherogel, a polystyrene-divinylbenzene gel. The degree of cross-linking provides good stability, As a result, many solvents can be used without problems of swelling or loss of column efficiency. The columns are 30 cm long with an i.d. of 0.8 cm. Seven different pore diameters are available covering the molecular weight range of 100 to 5 × 10^6. Typical efficiencies are in excess of 20 000 plates per meter. Altex Scientific, Inc. **420**

The Microlab P microprocessor-controlled hand pipet can be used as a universal repeating dispenser, transfer pipet, automatic buret for microtitration, dispenser for exponential dilution, and repeating diluter. It has a motorized plunger controlled by a programmable microprocessor. Ten steps are programmable. Volume, speed, and functions are selected on a separate keyboard command module. Gas-tight syringes with volumes from 50 to 5000 μL may be used, and volumes from 0.5 to 5000 μL may be dispensed. Full scale dispensing takes 2–10 s. Accuracy is better than 1.0%, and reproducibility is better than 0.3%. Hamilton Co. **405**

The E-900 data acquisition system can accumulate a single or multiscan time-averaged EPR spectrum, store spectra complete with all parameter information on tape, and print out file header information of selected spectra. It also can display up to three spectra, perform X-Y scale shift, linear baseline correction, differentiation, integration, noise spike deletion, and *g*-value calculation. It has a read/write memory of 23K bytes, and a magnetic tape storage of 250K bytes with program editing, programming, plotting, and matrix manipulation. Varian Instrument Division **403**

Acid Spill Neutralizer

Neutrasol Low Na^+ is designed to treat hazardous acid spills occurring in areas sensitive to metal ion contamination. Total metal content of this liquid is less than 0.08%. It initiates a controlled neutralization reaction as well as a color change indicating pH of the reaction mixture. Moderate foaming accompanies the treatment serving to suppress hazardous fume release and promote controlled reaction rates. Return of the spill mixture to a blue color signifies complete neutralization of the acid. J. T. Baker Chemical Co. **416**

UV Detector for HPLC

The SP8300 detector may be used with any liquid chromatograph. It is virtually flow insensitive and can be used at 0.0025 AUFS with pulsing pumps. Short-term noise is less than 50 × 10^{-6} AU. Baseline stability is enhanced by line voltage control circuitry that eliminates the effects of voltage fluctuations on lamp intensity. Operation at 254 nm is standard, and optional wavelengths of 280, 312, 365, 436, and 546 are available. Full scale sensitivity ranges from 0.0025 to 1.28 AU. The detector cell volume is 10 μL. Spectra-Physics **417**

Column Oven for Liquid Chromatography

The LC-100 column air bath oven is a self-contained module that can hold up to eight 30-cm columns with diameters from 3.5 mm to 2.54 cm. Temperatures from 10 to 99 °C can be controlled to within 1 ± 0.5 °C. Higher column efficiencies, shorter runs with better separation, reduced system back pressures, increased sample/eluent solubility, and improved retention time precision can be obtained. Perkin-Elmer Corp. **409**

UV Detector for LC

Model LC-15 features high-sensitivity, 0.002 absorbance units full scale with stable baselines, subnanogram level detection of strong UV-absorbing compounds, and digital display of absorbance. The instrument has a primary detection capability at 254 nm. Optional wavelength filter kits of 280, 350, 410, 440, and 550 nm are also available. Convenience features include recorder marker, polarity switch, zero calibration and testing switches, variable time constant selector, and recorder-independent integrator output terminals. Perkin-Elmer Corp. **415**

New Products

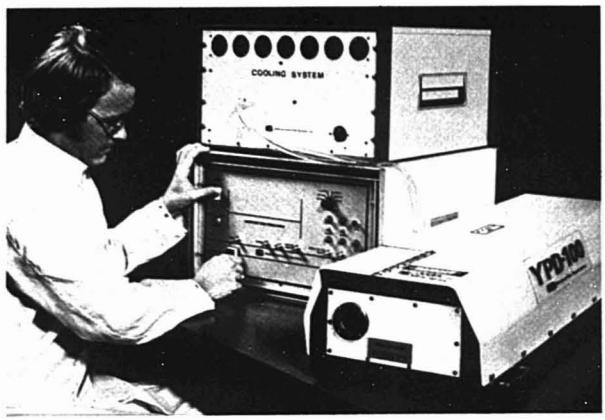

Model YPD-100 pulsed Nd:YAG-pumped dye laser is capable of producing a peak power output of 0.5 MW over a 500–900-nm range. It consists of three basic units: a laser head assembly, a power supply, and a cooling unit. The system has application in underwater illumination (photography, bottom sounding), chemistry (Raman spectroscopy, fluorescent microscopy), pollution studies (in situ and remote), medical research, and laser Doppler velocimetry. Priced under $30 000. International Laser Systems, Inc. **404**

HPLC Detectors

Three HPLC ChroMonitor detectors can measure the majority of chemical compounds utilizing UV/VIS. The 770 eliminates prism changes and uses a tungsten lamp. Light scattering is eliminated, and a low drift and good signal-to-noise ratio is maintained. The 785 is a dual-beam, flow-through spectrophotometer with continuously variable wavelengths from 195 to 750 nm. A deuterium lamp is the source needed for the wavelength ranges. The 790 is a dual-beam unit operating on the log ratio method and yields a larger dynamic range. Micromeritics Instrument Corp. **411**

X-ray Energy Spectrometer

Model 007 Fusion-X features five solid state lithium drifted x-ray detectors, multiplexed to detect and characterize laser-induced nuclear fusion events. High-powered focused laser beams are used for the generation of fusion energy by imploding microspheres containing fusile materials. Characteristic x rays are emitted during each burst of fusion energy. These x rays are detected by solid state detectors and analyzed by an x-ray energy spectrometer. A gate valve is incorporated in the detector assembly subsystem to allow windowless detector operation. The removal of the beryllium window makes it possible to detect and analyze low-energy x rays. Kevex Corp. **413**

Liquid Sampler for GC

The MS-1 automatic syringe is designed to simplify the injection process and produce more precise results than can be obtained with ordinary injection techniques. It can be used with the Sigma Series chromatographs. The sampler accepts a sealed vial containing the sample and once installed, the sample is injected at the push of a button. Between sample injections, solvent flush is accomplished by forcing the cleaning flush through the system under pressure, rather than relying on the small vacuum created by ordinary syringe plungers. Perkin-Elmer Corp. **418**

Chemicals

Gas Mixtures

Gas mixtures of benzene in air zero gas and nitrogen zero gas, and gas mixtures of acrylonitrile are prepared according to calibration standards set by OSHA. Benzene calibration mixtures are available in aluminum cylinders; a number of cylinder sizes are offered. Acrylonitrile mixtures are available in air ultra zero or in inert background gases, and are prepared in steel cylinders. Matheson **422**

For more information on listed items, circle the appropriate numbers on one of our Readers' Service Cards

It's not green cheese!

So what is the moon made of? Data provided by the Apollo, Surveyor and Luna missions give us the answer. To find out, fill in the coupon below and send for a copy of **The Chemical Composition of the Lunar Surface** by Anthony Turkevich, University of Chicago reprinted from Accounts of Chemical Research, March 1973 9 pages with cover

0214/10405

The Chemical Composition of the Lunar Surface **$2.00**

Anthony L. Turkevich

Name

Address

Zip

Mail **With Remittance** To:
Journals Department
American Chemical Society
1155 16th Street, N.W.
Washington, D.C. 20036

Join the Barnes Special-of-the-Month Club and save on analytical accessories.

Each month in 1978 Barnes is featuring a special on IR analytical accessories. Offers include 10 and 20% discounts on transmission windows and cells, free gifts and useful application notes.

Each offer will be effective for one month only. To know about them in advance, join the Barnes Special-of-the-Month Club. Simply send us your name, title, organization. Clip out this ad and return it to us. We'll send you Barnes latest Infrared Analytical Accessories Catalog as well. You can't get the specials until Barnes gets your name, so act now! Write Barnes Engineering Co., 30 Commerce Rd., Stamford, Ct. 06904; or call us toll-free at (800) 243-3498.

BARNES

Name_____

Title_____

Address_____

City/State/Zip_____

AC-8

CIRCLE 26 ON READER SERVICE CARD

Thermolyne's Type 1900 Hot Plate ranks No. 1 in temperature control accuracy . . . that's what over a half million satisfied users tell us. You **get** what you set . . . every time. Full-power response brings plate to desired temperature quickly . . . then automatically cycles to accurately maintain that setting. No lag or overshoot . . . just "right-on" control.

Contact your Lab Supply Dealer or write to:

SYBRON | Thermolyne

Thermolyne Corp., a subsidiary of Sybron Corp., 2555 Kerper Blvd., Dubuque, IA 52001

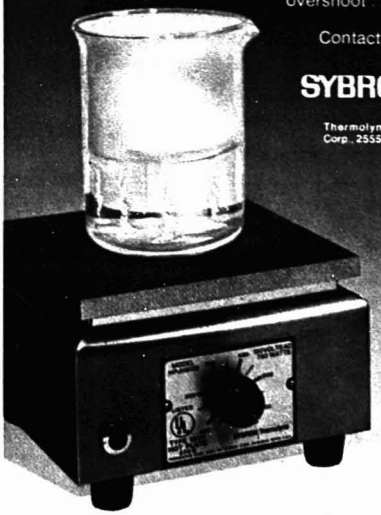

Our Hot Plates don't just get hot

. . . they accurately control solution temperatures

CIRCLE 201 ON READER SERVICE CARD

WHAT'S NEW IN BALANCES?

THE NEW METTLER CATALOG WILL TELL YOU.

Mail to Mettler Instrument Corporation, Box 71, Hightstown, NJ 08520

Please send me a copy of your new catalog.

NAME _____

TITLE _____

COMPANY _____

ADDRESS _____

CITY _____

STATE _____ ZIP _____

The new Mettler catalog shows and describes the latest Mettler electronic balances as well as ever-popular Mettler mechanicals. Models for the lab or industrial plant. Top loaders and analyticals.

Get your copy by mailing the above coupon.

Mettler

CIRCLE 141 ON READER SERVICE CARD

REAGENT CHEMICALS

American Chemical Society Specifications 5th Edition

Analytical chemists—update your reference shelf by ordering this indispensable handbook of the latest ACS specifications for 320 reagent chemicals.

This valuable tool includes 15 new items from two supplements of the 4th edition, plus 36 new reagents, such as calcium sulfate, quinoline, benzoyl chloride, lactose, silver diethyldithiocarbamate, and many more.

The fifth edition also contains for the first time:

- flame and flameless atomic absorption methods
- new colorimetric test for arsenic
- polarographic and chromatographic procedures
- Karl Fischer method for water

By returning the green card in the back of the book, you will receive *free* reprints of two future supplements to be announced in *Analytical Chemistry.*

Limited stock of 2nd edition available at $3.50.

685 pages (1974) Clothbound $40.00. Postpaid in U.S. and Canada, plus 40 cents elsewhere.

Order from:
Special Issues Sales
American Chemical Society
1155 Sixteenth St., N.W.
Washington, D.C. 20036

Manufacturers' Literature

Optimizing Analyses by Use of Splitless Injection on Capillary Columns. Application Note AN 228-5 describes the technique and the HP glass capillary inlet system used for analyzing complex chemical mixtures. Retention time and quantitative reproducibility are shown. 6 pp. Hewlett-Packard **430**

Electronic Balance. The Mettler A30 is described. Ranges of 0–30 g with an additional 30 g available with 0.1-mg readability. Standard equipment includes automatic stability detector and a four-position switch for adjusting the measuring cycle. 2 pp. Mettler Instrument Corp. **431**

Dual-Element Determinations with an Atomic Absorption Spectrophotometer. A report detailing the success of the IL751 spectrophotometer in 25 analytical laboratories for sample analysis of fresh water and wastewater, effluents, steel, foods, nonferrous alloys, air filter particulates, blood serum, biological cells, plating baths, plants, glass, soils, plastics, geologicals, and brines. 4 pp. Instrumentation Laboratory Inc. **432**

Amino Acid Analyzer. A method for plasma and urine analysis is described for the Durrum Model D-500 in Application Report #2. Includes tables of data selected from teletype printouts, the automatic procedure and standard deviations of the calibration standard. 6 pp. Durrum Instrument Corp. **433**

Polarographic Wet Chemistry System. Describes a total free or total residual chlorine system that utilizes the polarographic sensor technique. Data sheet PDS-E 400 contains sections on system components, system description, and operation. 2 pp. National Sonics Div., Envirotech Corp. **434**

Analyzers. Describes and illustrates the company's complete line of analyzers. Explains their function to ensure the safe and waste-free use of EtO in medical, pharmaceutical, and food plant sterilizers. 10 pp. Foxboro Co. **435**

Chromatography. Two issues of the series *Chromatography Newsletters*, CHN-9 and CHN-10, feature articles on advanced technology applications in liquid and gas chromatography. 15 and 16 pp. Perkin-Elmer **436**

Calibration Standards. Information to assist in developing dynamic primary standards. 66 pp. Analytical Instrument Development, Inc. **442**

Rapid Kinetics Spectrophotometry. Amino acid analysis of biological fluids and articles on applications of rapid kinetics are discussed. 4 pp. Durrum Instrument Corp. **443**

Metering Pump. Reciprocating, explosion proof, and peristaltic pumps are described. Flow rates of 1.6–4800 mL/h and pressures to 5000 psig. Information on complete solvent delivery systems for isocratic and HPLC systems is also available. 12 pp. Laboratory Data Control **444**

Spectrophotometer Accessory. Data sheet available that details spectral enhancement, kinetic measurements, and quantitative analysis on the Derivative/Log A accessory for the Cary 219. 4 pp. Varian **445**

UV Spectroscopy. Two articles entitled "Examples of Application of Multi-Component Analysis Unit for M556 Double Wavelength/Double Beam Spectrophotometer" (ADS-105) and "Further Applications of Integrating Sphere Model 200" are available. 8 and 6 pp. Perkin-Elmer **446**

Liquid Chromatography. Three application notes in "LC at work" series: #40, "Reverse Phase Ion Pair Chromatography of High Molecular Weight Quaternary Amines"; #41, "Determination of Free Fatty Acids by HPLC"; #42, "HPLC Analysis of Δ-THC and Metabolites in Biological Fluids". 6, 5, and 4 pp. Varian **447**

Portable Thermometer. Specifications on the digital thermometers, Models 721 and 521, and information on their surface, liquid emersion, and air temperature probes are given. 4 pp. Precision Digital **448**

Spilled Mercury. The handling of spilled mercury and the dangers of poisoning associated with it are discussed in bulletin BD-108. 2 pp. Wilmad Glass Co. Inc. **449**

Transient Waveform Recording. Specific research and testing applications employing transient waveform recorders are described. Includes applications for kinetic studies such as stopped flow and temperature jump. 22 pp. Physical Data, Inc. **450**

For more information on listed items, circle the appropriate numbers on one of our Readers' Service Cards

---

Spectrometer Leak Detectors. The 936 Series of instruments are described: Model 936-70 for automated, liquid nitrogen-free, trapless production testing; the 936-60 for all-purpose, conventional leak testing; and the 936-65 for ultrasensitive, repetitive leak testing. 20 pp. Varian **437**

Fluorometry. Discussions of fluorometer use in algae and chlorophyll analysis, fluorescent dyes as tracers, flow measurements, sewer infiltration, time of travel studies, and particulate matter and clarity. 6 pp. Turner Designs **438**

Surface Analysis. A summary of features of the Model 525-BX ISS/SIMS is presented along with techniques for pinpointing causes of corrosion, catalyst poisoning, and other surface anomalies. 8 pp. 3M Co. **439**

Laboratory Instruments. Amino acids, fast chemical reactions, and ions in biological solutions are featured together with their major applications. 4 pp. Durrum **440**

Moisture Monitor. Accurate measurement of trace moisture in gas streams is discussed on the Model 303. Du Pont Co. **441**

Automated Analysis. A special issue of *Environmental and Process Newsletter* deals with automated analysis in tertiary oil recovery processes and measurement of nutrients in wastewater and seawater. 6 pp. Technicon Industrial Systems **451**

Spectroradiometer System. Describes the Model 550/555 which integrates the features of the Model 550 radiometer/photometer with the Model 555-61 monochromator for a high-efficiency measurement system capable of providing radiometric measurements of both continuous and pulsed sources as a function of wavelength. 6 pp. EG & G Inc. **452**

Analytical Testing Services. Describes various testing and consulting services available including gas analyses, mass spectrometry, gas and liquid chromatography, leak detection, and industrial hygiene. 15 pp. Gollob Analytical Service **453**

High-Intensity Light Systems. Features complete line of lamp housings, arc lamps, arc lamp power supplies, and optics for the generation and control of high-intensity light. 16 pp. Schoeffel Instrument Corp. **454**

Radioimmunoassay. RackGamma II, a two-channel version of the Model 1270 RIA instrument, enables users to count gamma emitting isotopes in addition to ^{125}I. 9 pp. LKB Instruments, Inc. **455**

Manufacturers' Literature

Liquid Scintillation Counter. Gives operational details and technical specifications of the RackBeta liquid scintillation counters which feature automatic operation and flexibility to meet requirements in both research and clinical applications. 8 pp. LKB Instruments, Inc. **456**

Catalogs

Constant-Temperature Baths and Circulators. An antidrift temperature control concept is illustrated and described. Model specification charts are included. 3 pp. Haake Inc. **459**

Laboratory Products. Included are electrophoresis products, thin-layer chromatography products, laboratory aids, and laboratory filtration supplies. Gelman Instrument Co. **460**

Laboratory Supplies. Comprehensive catalog 478 includes lab-ware vessels, filtering devices, tubing and fittings, coatings, lubricants, goggles, lens cleaning stations, first aid products, fire extinguishers, lab furniture, mixers, and heating equipment. 108 pp. General Scientific Equipment Co. **461**

Valves and Connectors. Variable bore and high-pressure valves and fittings featured. 20 pp. Omnifit Inc. **465**

Balances. A comprehensive and descriptive catalog on Sartorius balances and scales. 26 pp. Brinkmann Instruments, Inc. **466**

Chromatography Products. Lists supplies and equipment for gas, thin-layer, and high-performance liquid chromatography as well as high-purity lipids and other chemical standards, isotope-labeled compounds, and derivatization reagents. 192 pp. Applied Science Laboratories, Inc. **474**

Metering Pumps. Describes valveless metering pumps with flow rates up to 1000 mL/min. 6 pp. Fluid Metering, Inc. **475**

Liquid Transfer Products. Features the full pipet line, diluter-dispensers, and accessories. 10 pp. Scientific Manufacturing Industries **476**

Laboratory Supplies and Equipment. Contains many items of interest to laboratory workers including cleaning supplies and equipment, glassware, plasticware, and safety equipment. 120 pp. Interex Corp. **477**

Defining and Solving Analytical Problems

Applied Problem Solving Through Creative Thinking. J. D. Reid. 200-page manual + 6 audiotape cassettes (5.7 hours). Dept. of Educational Activities, American Chemical Society, 1155 16th St., N.W., Washington, D.C. 20036. 1978. $155. Additional manuals: 1–9 copies, $13 each; 10–49 copies, $10.50 each; 50 or more, $9.75 each

Reviewed by Rudolph H. Stehl, Analytical Laboratory, Bldg. 574, Dow Chemical, Midland, Mich. 48640

The precept under which the ACS has prepared this course is, "It is an art that can be learned by studying techniques developed to aid in our attack on problems." And like the field of modern analytical chemistry itself, the successful person is part artist, part scientist. While the underlying science can be taught and learned, success is also very dependent on the artistry associated with the application to real problems.

This course, arranged to be accomplished in eight sessions, is covered by six 30–72-min tape cassettes, 30 sections of text material, and numerous problem-solving and evaluation periods. The suggested time for lectures, discussions, problem-solving exercises, and review requires a minimum of 18 hours.

This course is not primarily designed for the individual scientist. It is, or could be, of greater value to group leaders, beginning section leaders, project leaders, or those with aspirations of technical management roles in industry, academics, or government. Some of the techniques described are, of course, practicable to the individual chemist, but many require the participation of interested, if not willing coworkers.

The author has developed a detailed and logical progression of topics that cover the nature of the scientific process and the nature of various methods of defining and solving problems (brainstorming or deferred judgment, shared participation, panel consensus, and the Delphi method). Included are exercises in problem solving and several other "aids" such as mnemonic memory peg methods. The course concludes with several sections on "selling" the ideas created by these processes to others and a short section on organizational planning and team building. An appendix includes supplemental reading and problem material, and both general and specific references are given for further study. Eight reprints of selected articles are also provided.

For the modern organizational chemist faced with a bewildering array of research, engineering, safety, health, and environmental considerations and questions, this course provides only a brief introduction into how to identify and solve the various problems. It does, however, afford the group leader, manager, or director (or those hopeful of those positions) the opportunity to learn about and practice some of the various techniques by which researchers can solve problems. It does not devote more than the first quarter of the course to the creative process itself.

This course can be recommended for study by those people and organizations who hope to weld the scientist and manager into an effective team.

Aquametry, Pt. I: A Treatise on Methods for the Determination of Water. 2nd Ed. J. Mitchell, Jr., and D. M. Smith. xi + 632 pages. John Wiley & Sons, Inc., 605 Third Ave., New York, N.Y. 10016. 1977. $29.95

Reviewed by H. E. Taylor, Geological Survey, Denver Federal Center, Box 25046, Denver, Colo. 80225

Published as volume 5 in the Wiley-Interscience series on chemical analysis, this monograph provides a very comprehensive survey of the methods and techniques for the determination of water. Part I includes an introductory chapter on the structure and physical properties of water, and the remainder of the volume is dedicated to the detailed description and evaluation of virtually every meaningful technique for its determination. Included are chapters on chemical, gravimetric, physical, thermal, spectrophotometric, infrared, nuclear magnetic resonance, radiochemical, and other miscellaneous techniques. Parts II and III of volume 5 (not reviewed) are dedicated to electrometric techniques and Karl Fischer methods, respectively.

Each chapter is well documented and starts with some basic fundamental theory of the principle involved. A section on the description and characteristics of the instrumentation or apparatus required for the determination is followed by extensive applications information with detailed examples. The scope of applications includes the determination of both bound and unbound water in a wide variety of sample types including atmospheric, geologic, agricultural, biological, and general industrial.

This treatise is unique in character, since it provides the reader with a compendium of information not generally available in standard texts on analytical chemistry or in monographs on particular techniques (i.e., IR, UV, or NMR). The authors have written a very systematic and well-documented text, with easily interpreted figures and illustrations. Many new references and citations have been included with the second edition, making this monograph current with modern technology.

Optoacoustic Spectroscopy and Detection. Yoh-Han Pao, Ed. xi + 244 pages. Academic Press Inc., 111 Fifth Ave., New York, N.Y. 10003. 1977. $19

Reviewed by R. N. Kniseley and J. F. McClelland, Ames Laboratory, Iowa State University, Ames, Iowa 50011

The stated purpose of this book is to provide an introduction to the principles and methods of optoacoustic spectroscopy. The book contains eight chapters dealing primarily with analytical gas-phase measurements. The final chapter treats the recently developing condensed matter applications. The chapters are written in a readily understandable fashion by workers in the field or in fields closely related, thus providing a useful source of information on a growing area of research through 1976.

The first three chapters cover the physics of signal generation and detection, energy deexcitation and transfer mechanisms following optical absorption, and design of the measurement apparatus. Sections of particular interest in these chapters include discussions of optimum optoacoustic system design, practical design considerations, excitation via intensity and wavelength modulation, and comparisons of the optoacoustic method with other analytical techniques. Chapters 4 and 5 survey tunable incoherent and laser light sources for the ultraviolet–visible and infrared spectral regions, respectively. In chapter 4 most of the discussion concerns lasers and related

topics such as second harmonic generation. Incoherent sources and monochromators are treated in less complete detail, which is unfortunate since this area is important in the optoacoustic spectroscopy of condensed samples. Chapter 5 deals exclusively with laser sources, which is reasonable because of the low power of conventional incoherent infrared sources. Many of the laser sources discussed in chapters 4 and 5 are pulsed rather than CW and may not be practical for modulation waveforms approximating a sinewave. Some discussion might have been given to this aspect since most of the material in the other chapters does not encompass pulsed excitation.

The final three chapters contain considerable information on experimental methods and results obtained by optoacoustic measurements. The experimental results presented encompass both research studies where the special capabilities of the optoacoustic method were used to obtain new information and exploratory investigations where advantages of the method were demonstrated by comparison with results using other techniques. Chapter 6 discusses gas-phase measurements in the infrared for vapor identification and quantitation. Small and large molecule gases, multicomponent mixtures, and molecular relaxation rates are included in this chapter. Gas-phase spectroscopy in the visible and ultraviolet regions is treated in chapter 7. The signal amplitude and phase are discussed, followed by illustrative spectra of both signal components for various gases. These results demonstrate some of the unique capabilities of the optoacoustic technique in the ultraviolet and visible regions where more varied and complicated processes are associated with deexcitation relative to the infrared.

The final chapter covers condensed phase measurements including signal theory and experimental methods, and presents extensive data for this sample type. The theoretical and experimental sections differ from the earlier gas-phase material due to the different signal generation sequence occurring with condensed samples. The theory presented uses a simplified model appropriate for an introductory treatment. The data include numerous spectra from studies related to physics, chemistry, biology, and medicine, which also demonstrate some unique capabilities. This section unfortunately does not include interesting recent work that has occurred since 1976.

In conclusion, this book might have benefited from having an introductory chapter that could help to integrate the chapters in terms of an overall picture. For instance, some chapters use the term *photoacoustic* rather than *optoacoustic*, which will confuse some readers. Only in the last chapter does the reader learn that the term *photoacoustic* was instituted to prevent confusion with the acoustooptic effect which involves the interaction of light with acoustic waves in a crystal.

Liquid Chromatography Detectors (Journal of Chromatography Library, Vol. 11). R.P.W. Scott. vii + 248 pages. Elsevier North-Holland, Inc., 52 Vanderbilt Ave., New York, N.Y. 10017. 1977. $34.50

Reviewed by Ronald E. Majors, Varian Instrument Div., 2700 Mitchell Dr., Walnut Creek, Calif. 94598

The last several years have seen great advancements in the reliability and reproducibility of LC pumping systems and in the efficiency and stability of LC columns, but compared with gas chromatography, the detector is still the weakest link in the LC system. Much work is in progress on detector research to improve performance, especially sensitivity. However, R.P.W. Scott has been able to present an admirable treatise which does relate to us how to get the most information, be it sensitivity or selectivity, out of our currently commercially available and experimental detectors as well as several earlier, now obsolete, commercial detectors.

The book is divided into four standalone parts: general detector characteristics, bulk property detectors, solute property detectors, and use of detectors. For each part individual chapters then cover specific properties, detectors, or techniques. Each chapter dealing with individual detection principles begins with a general theoretical coverage, followed by the means of practical application of the theory, and finally, when applicable, details of a commercially available detector, complete with photograph.

In the first part, general detector characteristics are discussed. A very good coverage of the criteria for detector specification is presented. In addition to the normal definitions of dynamic range, noise, drift, sensitivity, etc., some guidelines for evaluating and minimizing detector characteristics that affect column performance, like cell volumes and connecting tubing dimensions, are discussed. The influence of detector amplifier and recorder time constants on peak shape is covered as well as the types of filters that can be used to enhance signal-to-noise. For those less interested in covering the details of the units of measurements and symbols derived in the first 36 pages, a useful summary of detector specification criteria is presented in chapter 4. This summary could serve as a guide (but probably won't!) to instrument manufacturers for items to specify in setting detector specifications. In fact, in later chapters when covering commercial detectors, the author uses this format to summarize specifications derived from manufacturers' literature or by his own experimental determinations.

The second part covers bulk property detectors, which as a group are the least-used LC detectors because of their general lack of sensitivity. Unfortunately, the refractive index (RI) detector, the most widely used of this type, is given equal coverage to dielectric constant and electrical conductivity detectors, which see almost no use. Expansion of the RI section to include more details of the popular Fresnel type of commercial detector would have been useful. Lesser-known bulk property detectors (e.g., vapor pressure detector) are given some coverage at the end of this part.

The third part covering solute property detectors was justly given a third of the book. Such detectors are selective, usually sensitive, and are the most widely used today. Of the detectors covered, the ultraviolet absorption and fluorescence detectors probably account for 80–90% of those currently in actual use. A good general coverage of the principles of operation of both fixed and variable wavelength UV detectors is presented. A detailed coverage of the microadsorption detector, commercially unavailable for several years, and the spray impact detector, which still remains a research curiosity, was unwarranted, whereas infrared and radioactivity monitors commercially available for several years remained unnoticed. Experimental electrochemical detectors are covered, but commercial versions have only become available recently. Historical details of the transport detector (moving wire-FID) were amply provided, but this could be expected since the author was a codeveloper of this device. Unfortunately, the moving wire-FID detector has gone by the wayside, having been dropped by the manufacturer over a year ago. Nevertheless, the details provided here could spur some LC'ers to dust off the detector and have another go at it.

Part 4, "The Use of Detectors in LC", is probably the most useful sec-

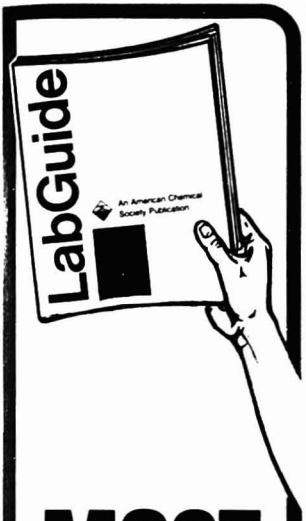

MOST USED

...because it's most useful.

The annual ACS **LabGuide** is the definitive directory to scientific instruments, equipment, chemicals, services, books, trade names, manufacturers and their sales offices.

It leads all others in editorial pages, in advertising pages, and in reader usage: **more than 70,000 inquiries every year.**

Now for the short of it.

New short columns with economical disposable cartridges and quick disconnect fittings for fast replacement mean More Performance at Lower Cost... MPLC*

HPLC costs less with our new short column concept. Optimum results can be obtained in routine separations when a few thousand plates are sufficient. Quality routine separations come easy with our new short columns packed with 10 micrometer sorbants and operating at low flow rates. So whenever a few thousand plates are sufficient, you should consider use of MPLC short columns.

Short columns use the same sorbants. Short columns use the same 10 μm sorbants found in our tall columns. A separation developed in research with our tall columns can be performed on a routine basis by short columns. Columns are 4.6 mm x 10 cm. Packing itself is placed in a disposable cartridge. In turn, the cartridges are connected to the LC system through a holder with quick disconnect low dead volume fittings.

*MPLC is a trademark of Brownlee Labs

Save the hardware, change the cartridge. Because we save end fittings and use a reusable cartridge holder, costs are cut to about half that of standard 25 cm analytical columns.

Nine different sorbants. Nine different LiChrosorb* sorbants cover reverse phase, adsorption, polar bonded and ion exchange modes of LC.

All short cartridges are tested for both efficiency and peak skewness. A computer printout listing cartridge serial number and type, test conditions and test results is included with each cartridge.

More information. For a complete description of these new Brownlee columns write for the new four page brochure. Please address Rheodyne Inc., 2809 Tenth St., Berkeley, CA 94710. Phone (415) 548-5374.

LiChrosorb is a registered trademark of E. Merck, Darmstadt, West Germany

RHEODYNE

THE LC CONNECTION COMPANY

CIRCLE 174 ON READER SERVICE CARD

tion for the practitioner. The long list of detectors discussed in the first three quarters of the book is distilled down to the six commercially available detectors: UV, RI, fluorescence, conductivity, electron capture, and the wire transport detector. Guidelines for selection of the appropriate detector are given. The reviewer found chapter 3 on practical hints on detector operation particularly helpful. Some special detector techniques such as differential and vacancy chromatography and aspects of qualitative and quantitative analysis are discussed. Chapter 5 on spectroscopic detectors covers LC/UV, and LC/MS interface, which utilizes a moving belt to transport the sample into the MS ionization source, is discussed.

All in all, the book accomplishes what it purported to do. It gives liquid chromatographers an overview of most detection possibilities with the section on actual use covering only the main ones. Those detectors that are research curiosities or obsolete detectors were presented to stimulate research to develop improved designs or improve existing designs. At times the author gets into minute details of construction that would probably not interest the average chromatographer. The text is relatively error free, is quite readable despite its photographic reproduction, and provides an adequate number of examples. Its coverage of basic principles will not let it quickly become obsolete in this field of intense activity. It is recommended to any liquid chromatographer who desires to have a thorough knowledge of detection principles, who would like to get the most information from his available detectors, or who is interested in pursuing development of a new detector.

New Books

Colorimetric Determination of Nonmetals. 2nd Ed. David F. Boltz and James A. Howell, Eds. xxii + 543 pages. John Wiley & Sons, Inc., 605 Third Ave., New York, N.Y. 10016. 1978. $33.95

Prior to his untimely death in 1976, David F. Boltz (editor of the first edition) had done much of the work toward this edition, including the five chapters he contributed. Although written by different authors, all chapters are organized uniformly into sections on separations (where applicable), methods of determination, and applications. Most of the procedures are described in sufficient detail to allow duplication without further reference. The elements covered in 12 chapters are boron, bromine, carbon, chlorine, fluorine, iodine, nitrogen, oxygen, phosphorus, selenium and tellurium, silicon, and sulfur.

A Critical Review of Equilibrium Data for Proton and Metal Complexes of 1,10-Phenanthroline, 2,2′-Bipyridyl and Related Compounds (IUPAC Chemical Data Series, No. 17). W.A.E. McBryde. x + 78 pages. Pergamon Press Inc., Maxwell House, Fairview Park, Elmsford, N.Y. 10523. 1978. $11

Because of their remarkable properties as ligands, the heterocyclic bases, 1,10-phenanthroline and 2,2′-bipyridyl and a host of their derivatives have been extensively studied by analytical chemists as well as inorganic chemists. Certain complexes of these ligands with intense color and characteristic stabilities find a number of useful applications as colorimetric reagents. This book compiles, from the published data, the equilibrium association constants characteristic of the reactions of these compounds with hydrogen ions and metal ions in solution. Although the compilation is devoted mainly to aqueous solutions, some values determined in nonaqueous and mixed solvents are also included. A coded designation of the experimental method by which each constant was determined is given, but readers are advised to consult the original literature for details.

8080A/8085 Assembly Language Programming. Lance A. Leventhal. xxvii + 344 pages. Osborne & Associates Inc., P.O. Box 2036, Berkeley, Calif. 94702. 1978. $7.50

The book assumes the reader's familiarity with microcomputers in general and in particular with chapters 6 and 7 of another book, "An Introduction to Microcomputers: Volume 1—Basic Concepts", also published by Osborne and Associates. The contents of the 16 chapters include: introduction to assembly language programming, assemblers, the 8080A and 8085 assembly language instruction sets, examples of simple programs, program loops, character-coded data, code conversion, examples of arithmetic problems, tables and lists, subroutings, input–output, interrupts, problem definition and program design, debugging and testing, documentation and redesign, and sample projects. Most of the chapters provide a set of exercise problems.

Worked Examples in X-Ray Analysis. 2nd Ed. R. Jenkins and J. L. de Vries. 135 pages. Springer-Verlag New York Inc., 175 Fifth Ave., New York, N.Y. 10010. 1978. $9.80

This book with 49 problems and answers is intended as a supplement to existing texts in the fields of x-ray spectrometry and x-ray powder diffraction. As such, it assumes the reader's familiarity with the basic theory. All of the problems are presented with worked answers side by side and are divided into five major sections dealing with spectra, instruments, counting statistics, quantitative analysis, and miscellaneous. Within each of the five sections, examples of three types are found, i.e., either of a general nature or dealing specifically with x-ray spectrometry or x-ray diffractometry. The examples are rated A, B, and C in the order of increasing difficulty.

Continuing Series

Systematic Materials Analysis, Vol. IV. J. H. Richardson and R. V. Peterson, Eds. xviii + 493 pages. Academic Press, Inc., 111 Fifth Ave., New York, N.Y. 10003. 1978. $49.50

The series provides brief discussions on a broad range of instrumental methods available to the materials analyst. As such, the scope of each chapter treating a particular instrumental technique is limited to a discussion sufficient for the analyst to understand the operation and capabilities of the instrument. The techniques covered in volume IV by 14 contributors include atomic absorption and atomic fluorescence flame photometry, ion microprobe, mass spectrometry, molecular weight determinations, neutron diffractometry, particulate characterization, polarimetry, polarography, methods for the detection of noncentrosymmetry in solids, thermal analysis, and transmission electron microscopy.

Encyclopedia of Electrochemistry of the Elements, Vol. 11. Allen J. Bard and Henning Lund, Eds. xii + 344 pages. Marcel Dekker, Inc., 270 Madison Ave., New York, N.Y. 10016. 1978. $75

Volume 11 initiates the organic section which in five volumes will complete this long-standing series on electrochemistry of the elements. The 15th and final volume will be published in 1979. Volume 11 contains

"Trace concentrations. That's all AA is good for."

Fiction

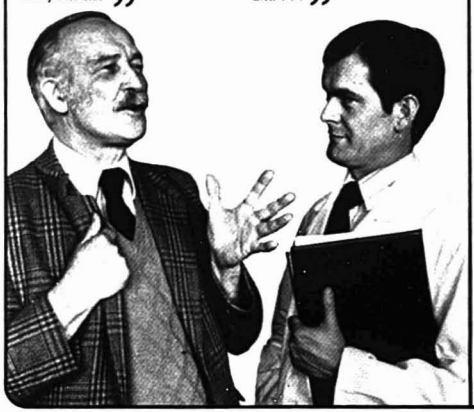

Fact

Results of analysis of elements in cement and geological samples. *Analyst (1977),* **102,** *64.*

Sample	Analyte	Certified Element Content (%)	Results of Replicate Determinations (%)*
BCS 372 Portland Cement	CaO	65.8	66.2, 66.4, 66.2, 66.4
	Mn_2O_3	0.06	0.055, 0.054, 0.055, 0.055
	SiO_2	21.3	21.3, 21.2, 21.1, 21.2
	TiO_2	0.33	0.328, 0.326, 0.326, 0.328
BCS 267 Silica Brick	SiO_2	95.9	95.9, 95.8, 95.9
	TiO_2	0.17	0.165, 0.162, 0.168
BCS 303 Iron Ore Sinter	Fe	36.0	36.4, 36.1, 36.1
	Al_2O_3	6.81	6.74, 6.79, 6.76

**Determined using Pye Unicam SP1900, SP2900 or SP190 Series AA Spectrophotometers*

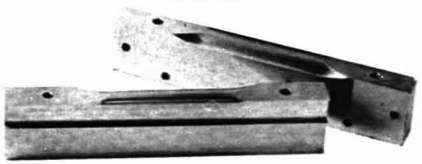

Pye Unicam laminar flow burners

The above results kill the myth that atomic absorption is only good for trace concentrations. The cement analysis shows very high and very low concentrations in the same sample. Silica brick has extraordinarily high levels of SiO_2. The iron ore sinter demonstrates aluminium analysis - notoriously difficult for other spectrophotometers. A micro-dissolution method needing only 10 mg of sample - specially developed by Pye Unicam - was used for the silica brick and iron ore sinter analyses. Copper in brass was also analysed at the 58% level with 0.34% precision.

The precision of these results was only possible because of the unique design of Pye Unicam spray chambers and burners. The inert PTFE and penton lined spray chamber contains a fully adjustable impact bead and brings high efficiency to the platinum iridium nebuliser with its tantalum annulus. The burners have a stable laminar flow with very high solids handling capacity.

Pye Unicam capability in atomic absorption does not just mean the supply of outstanding spectrophotometers and accessories. There are demonstration and application facilities for all interested in AA. There is a comprehensive package of AA literature. Write, 'phone or use the reader reply service today for further information.

PHILIPS

Pye Unicam

A SCIENTIFIC INSTRUMENT COMPANY OF PHILIPS

York Street Cambridge CB1 2PX England
Telephone (0223) 58866 Telex 817331

CIRCLE 172 ON READER SERVICE CARD

two review chapters, hydrocarbons and hydroxy compounds, each contributed by five different authors. The chapter on hydrocarbons is divided into sections on alkanes, aliphatic alkenes, aliphatic alkynes, alkylaromatic hydrocarbons, polycyclic aromatic hydrocarbons, and miscellaneous hydrocarbons. Within each of these sections and the chapter on hydroxy compounds, the organization is as follows: electrode potentials and voltammetric properties, electrochemical studies, and applied electrochemistry. Each section includes tables of available thermodynamic, kinetic, voltammetric, and other electrochemical data, and a critical discussion on the known electrochemical reactions. The literature citations include a few from 1976, but in the main the bibliography does not seem to extend much beyond 1974. The book is reproduced from typewritten text.

Automated Immunoanalysis, Part 1. Robert F. Ritchie, Ed. xii + 333 pages. Marcel Dekker, Inc., 270 Madison Ave., New York, N.Y. 10017. 1978. $34.50

This book is devoted to automated immunonephelometry and radioimmunoassays. The chapters are written by authors from various teaching hospitals and a leading manufacturer of automated clinical instruments. Most chapters present a concise discussion of the basic chemistry that forms the basis for the technique and the mechanics of the instrumentation, sufficient to allow the intended audience, the clinical worker, to appreciate the principles behind the particular analytical technique. Topics covered in the 15 chapters include optical considerations in nephelometry, automated precipitin analysis, enhancing effects of nonionic polymers on immunochemical reactions, analytical variables for specific protein analysis, comparison immunochemical techniques, reference materials for plasma protein analysis, albumin, automated determination of immunoglobulins, automated immunochemical analysis of serum IgA in a Red Cross donor population, IgM, transferrin, automated immunochemical analysis of human low-density lipoproteins, interpretation of data: complement consumption detected by multivariant analysis, physiological and pathophysiological study of blood coagulation system function by plasma fibrinogen chromatography, and automated nephelometric analysis of haptens. The book is a good quality photo-offset copy of typewritten text.

U.S. Government Publications

Order copies of the following PREPAID at the price shown by SD Cat. No. from Superintendent of Documents, U.S. Government Printing Office, Washington, D.C. 20402. Foreign remittances must be in U.S. exchange and include an additional 25% of the publication price to cover mailing costs

Standard X-Ray Diffraction Powder Patterns: Section 14, Data for 68 Substances. M. C. Morris et al. 143 pages. 1977. $2.75. SD Cat. No. 003-003-01842-2. NTIS No. NBS-MN-25-Sec. 14

Standard x-ray diffraction patterns are presented for 68 substances. Twenty-seven of these are experimental data obtained with an x-ray diffractometer, and 41 are calculated. All d-values are assigned Miller indices determined by comparison with computed interplanar spacings consistent with space group extinctions. The densities and lattice constants are calculated. The calculated diffraction patterns are computed from published crystal structure data. Both peak height and integrated intensities are reported for the calculated patterns.

Procedures Used at the National Bureau of Standards to Determine Selected Trace Elements in Biological and Botanical Materials. R. Mavrodineanu, Ed. 295 pages. 1977. $7.50. SD Cat. No. 003-003-01858-9. NTIS No. NBS-SP-492

This volume consists of 13 papers describing the analytical procedures selected at the National Bureau of Standards (NBS) for the determination of Ag, Al, As, Be, Bi, Ca, Cd, Cr, Cu, Fe, Hg, K, Mg, Mn, Mo, Na, Ni, Pb, Pt, Sb, Se, Te, Tl, V, and Zn in biological and botanical materials. The procedures are used for the certification of various substances issued by NBS as Standard Reference Materials. The specific analytical methods include sample preparation, neutron activation analysis, spark source mass spectrometric isotope dilution, atomic absorption and flame emission spectrometry, molecular absorption spectrometry, fluorescence spectrometry, and polarography. Further details on sample preparation, purity of reagent, and problems associated with blanks are given in 16 additional papers that are reproduced in the appendix to this volume.

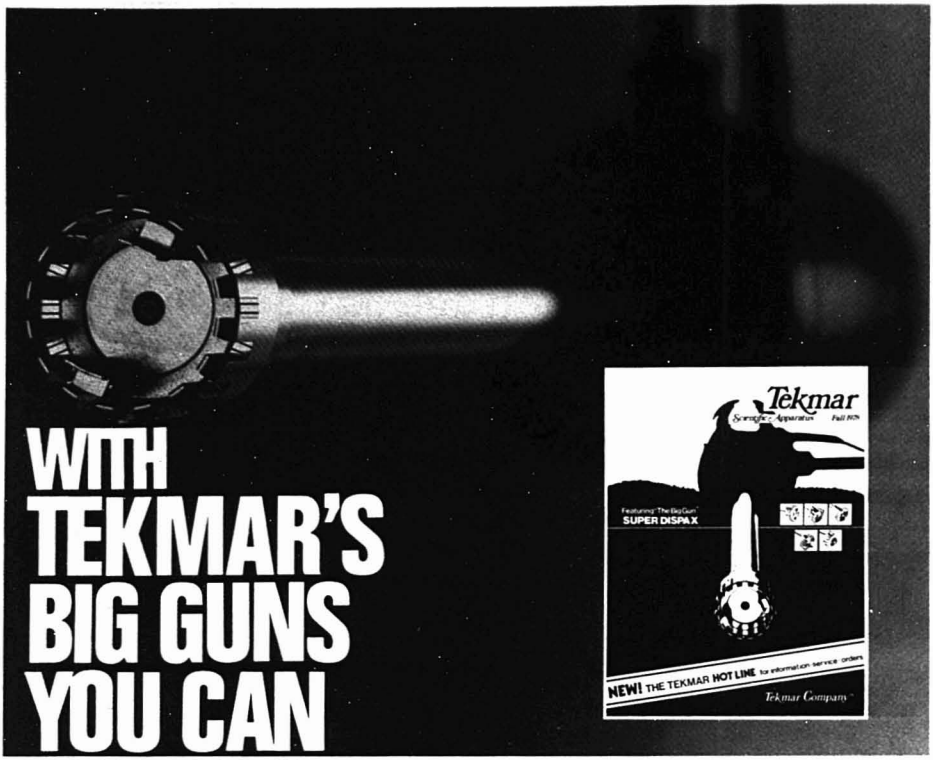

WITH TEKMAR'S BIG GUNS YOU CAN DISPERSE EMULSIFY HOMOGENIZE SHRED BLEND & CUT

Tekmar's Super Dispax units range in size from the SDT Tissumizer which can be hand-held to in-line units capable of 300 gallon per minute flow rates. All fully guaranteed by Tekmar.

Whatever your job, Tekmar can recommend the appropriate unit for your application.

All of the units are based on the rotor-stator principle. Liquid and solid pump through the rotor-stator generator and are subjected to shear, impact, collision, and cavitation effects which disperse, disrupt, emulsify, homogenize, or shred . . . as needed.

Tekmar also offers a complete line of accessories to supplement the use of our homogenizers.

But, best of all, when we sell them, they stay in operation, with few service problems with any size from large to small.

Interested? Circle the Reader Service No. for the full story, or call us collect in Cincinnati.

Tekmar Company

P.O. Box 37202 Cincinnati, Ohio 45222 Tel: (513) 761-0633

To receive our latest catalog, use the Reader Service No. 203

Instrumentation in Forensic Drug Chemistry

Forensic chemistry: The application of chemistry to legal problems

A hospital clinical chemistry laboratory receives a sample of stomach contents obtained from a comatose patient suspected to be suffering from a drug overdose. In a matter of several hours or less, phenobarbital and seconal are identified. The physician is informed, and appropriate treatment results in the recovery of the patient.

This rapid identification of drugs is accomplished by chemical ionization mass spectrometry coupled to a computer-based spectral search system. The system was developed by G.W.A. Milne and H.M. Fales of the National Institutes of Health, and N.C. Law of Suburban Hospital in Bethesda, Md., and is currently in routine use at Suburban Hospital. The facility serves Washington, D.C., area hospitals and receives about 500 cases per year.

This is just one of the many examples presented at the International Symposium on Instrumental Applications in Forensic Drug Chemistry, held May 29–30, 1978, in Arlington, Va. The symposium, sponsored by the Drug Enforcement Administration, focused on the advancements of instrumental techniques in applications to forensic chemistry. Leading researchers from the United States and six foreign nations presented papers during the four sessions that covered spectroscopy, computer applications, chromatographic advances, and special topics.

Drug abuse is a major problem faced by law enforcement officials today, and identification of drugs and related compounds is an important part of the forensic chemist's job. Although the example given by Dr. Milne was of a clinical application of drug identification, laboratory techniques used in various drug-related problems, such as emergency drug overdoses, drug monitoring, or metabolism studies, can also be used in forensic cases. For example, the analysis of an illicit drug mixture by an extremely sensitive and specific analytical technique can provide valuable information regarding the history of the illicit material.

Mass spectrometry is currently in wide use as a method for both qualitative and quantitative determinations in forensic drug analysis. Its high sensitivity and structural specificity are the main reasons for its increasing utility in the identification of therapeutic and illicit drugs, their metabolites, and related substances. Often the materials being analyzed are complex mixtures, and this has led to the widespread use of gas chromatography coupled to mass spectrometry (GC/MS), an extremely powerful tool available to the forensic chemist.

One example of this was presented by M. G. Horning of Baylor College of Medicine in Houston, who reported on the routine quantification of drugs in the picogram range by a GC/MS/computer system with selected ion detection. The procedure involves stable isotope-labeled internal standards. Quantification is based on the ratio of stable isotope to sample. The method is extremely sensitive and specific. Specificity is improved even further when the chemical ionization mode is used and if two or more ions are monitored for the drug and internal standard.

Many of the techniques available today for drug identification employ computers for collecting and analyzing data. Several systems currently in use and reported during the symposium involve a retrieval-type search system for qualitative identification of drugs. As in the system used at Suburban Hospital, compounds are identified by comparison of their spectroscopic data to those of known compounds. As these systems are improved and the data bases enlarged, they will become more and more important in forensic drug analysis.

The high resolving power and sensitivity of chromatographic methods have made them useful in forensic work. Among the methods, gas chromatography (GC) is the most efficient and sensitive and is a well-established part of the forensic laboratory. While the development of GC has now reached a plateau, high-performance liquid chromatography (HPLC) is undergoing many new developments that will be of importance to the forensic chemist. HPLC is especially valuable for polar, involatile, or thermally unstable compounds not amenable to GC. One of the most active areas of research in HPLC is in the improvement of detection systems. Ultraviolet and fluorescence spectrometric, and electrochemical detectors are most commonly used today. A promising technique, the on-line coupling of HPLC to a mass spectrometer as a detection system, was discussed by P. J. Arpino of Ecole Polytechnique. This technique provides good sensitivity and a wide range of applications and as an identification method is capable of analyzing nanogram amounts.

R. L. Williams of the Metropolitan Police Forensic Science Laboratory in London reported that his laboratory has been successful in constructing several low-cost liquid chromatographs designed for a specific application. With isocratic elution, it is possible to operate a particular system under the optimum conditions for the analysis of a specific group of drugs. According to Williams, there is a great need for dedicated systems such as this that can rapidly do a number of similar analyses. He sees a promising future for this through the use of liquid chromatography.

Irving Sunshine of the Cuyahoga County Coroner's Lab in Cleveland, Ohio, discussed the application of immunoassay techniques to the detection of drugs in biological samples. These techniques are very sensitive and have made it possible to test for substances previously difficult or impossible to measure. The two most often used are radioimmunoassay and enzyme immunoassay. The rapid speed of the analysis and the minimal technical skill involved make these very attractive in routine drug identification. Specificity is, however, a limiting factor, since structurally related compounds and metabolites may also give positive results. As a possibility for future development, Dr. Sunshine suggested immunoassay techniques as HPLC detection systems.

As laws are continually being broadened and revised to counter the alarming increase in crime rates, law enforcement agencies will be looking more and more to the scientific community for advice and technical support in their efforts. The development of new and improved analytical techniques will play a very important role in meeting the future needs of the forensic scientist.

Deborah C. Stewart

Three simultaneous LDH reaction rates versus a blank, using the Automatic Cuvette Programmer with individual sample offset separating the traces. A Reference Compensator maintained the drift-free baseline.

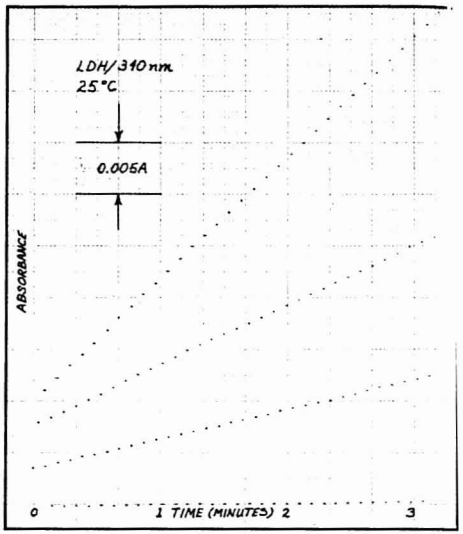

Gilford's Automatic Cuvette Programmer makes repositioning of microcuvettes a pushbutton routine.

Positioning Accuracy Helps Ensure Measurement Accuracy

For accurate, repeatable results, precise sample positioning is critical. Particularly if you want to use flow-through or microcuvettes. With such cuvettes and the associated microapertures, positioning inconsistencies would be translated into apparent absorbance errors on the recorder chart.

The four-cuvette Gilford system makes the necessary precision automatic, positioning cuvettes within 0.025mm time after time. No bother, no special (and expensive) optics required.

Manual or Automatic, Positioning is Convenient and Fast

You can select a single cuvette position just by pushing a button, or choose a combination of positions for automatic operation. You can monitor any or all four cuvettes for precise dwell times of 2 to 99 seconds. And positioning itself is quick, just 1½ seconds between adjacent positions. Thus if you have all four cuvette positions selected, and have chosen a dwell time per cuvette of two seconds, you'll get a second reading on any given sample within 14 seconds. More readings per sample per unit time means that you can more accurately follow the progress of a reaction.

Design of the Programmer Makes Recordings More Meaningful

Individual recorder offset controls for cuvette positions 2, 3, and 4 serve two functions: they let you separate overlapping traces for clarity in presentation; and they let you use the most sensitive recorder scale for the sample with the least activity. There's no need to adjust sample concentration so that all the samples you're measuring have similar absorbance characteristics.

Accessories to the Gilford Automatic Cuvette Programmer include an auxiliary timer for long-term assays and an analog multiplexer that allows you to monitor parameters like sample temperature in sequence with absorbance.

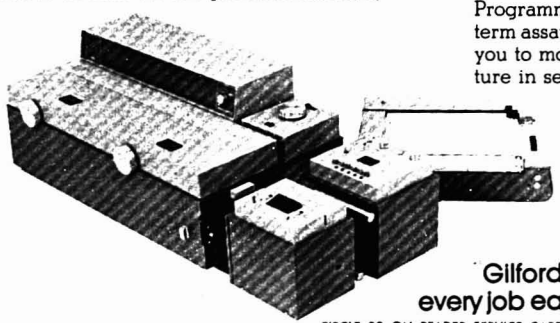

gilford INSTRUMENT
Oberlin, Ohio 44074
(216) 774-1041 Telex: 98-0456
Paris (Malakoff), France
Düsseldorf, W. Germany
Teddington, Middx., England
Toronto (Mississauga), Canada

Gilford Research Spectrophotometers: every job easier, every result more accurate.

CIRCLE 83 ON READER SERVICE CARD

A. B. Harvey
Chemical Diagnostics Branch
Naval Research Laboratory
Washington, D.C. 20375

Coherent Anti-Stokes Raman Spectroscopy

CARS

Nearly two decades ago the discovery of the optical maser or the laser, as it is now called, ushered in a new era. The laser introduced scores of exciting fields of endeavor that affect physics, chemistry, biology, and engineering. One such field is nonlinear optics, which arose almost immediately with the advent of the laser and grew very rapidly in the years to follow (*1*). As we shall soon see, the fields of nonlinear optics and nonlinear spectroscopy are dependent on lasers because of the high electric field strengths available from these intense sources.

In Figure 1 we depict how a medium is polarized or how a dipole moment is induced in a medium in the presence of high electric fields of a laser beam. In its most simplistic mathematical form, the polarization can be expressed as an expansion in the field strength as follows:

$$P = aE + bE^2 + cE^3 + \dots \quad (1)$$

where P is the polarization, E is the field strength, a is the linear coefficient, and b, c, etc., are the nonlinear coefficients. It is readily seen that if $a > b > c > \dots$, then at low fields, terms in Equation 1 beyond the first are negligibly small, and we are left with the linear term that characterizes ordinary linear optics. However, at greater and greater field strengths the higher-order or nonlinear terms begin to contribute significantly to the overall polarization. Let us now consider the first nonlinear term, which is dependent on the square of the electric field strength:

$$P^{(2)} = bE^2 \quad (2)$$

If the electric field of the electromagnetic radiation is expressed as a simple sinusoidal function, $E = E_0 \cos \omega t$, where E_0 is the amplitude, ω is the circular frequency (in units of radians/s) of the alternating field, and t is time, and is inserted into Equation 2, then the relation becomes:

$$P^{(2)} = bE_0^2 \cos^2 \omega t \quad (3)$$

which by the trigonometric identity yields:

$$P^{(2)} = \frac{b}{2} E_0^2[1 + \cos 2\omega t] \quad (4)$$

Thus, if the second-order coefficient is nonzero, the presence of strong fields at frequency ω allows for the creation of a new frequency at twice the fundamental, 2ω. The intensity of the new frequency is very dependent on the magnitude of the second-order nonlinear coefficient, b. This doubling process is now a routine operation and is very useful in producing new laser frequencies. For example, the fundamental frequency output of the Nd:YAG laser at 1060 nm in the infrared can be easily doubled in appropriate crystals to produce green output (532 nm) at efficiencies typically about 30%. This output can be doubled again in another crystal to produce ultraviolet radiation (266 nm) again at high efficiency. These frequencies are used in the CARS (coherent anti-Stokes Raman spectroscopy) experiments to be discussed in this report.

It should be mentioned that the field strengths in Equation 2 need not be identical. Thus, Equation 3 can be written more generally as:

$$P^{(2)} = b(E_0' \cos \omega_1 t)(E_0'' \cos \omega_2 t) \quad (5)$$

where E_0' and E_0'' are the field strengths at frequencies ω_1 and ω_2, respectively. Again by trigonometric identity we can see that new frequencies at $\omega_1 + \omega_2$ and $\omega_1 - \omega_2$ are generated. In addition to the sum and difference frequencies, it can be shown that under the proper conditions the

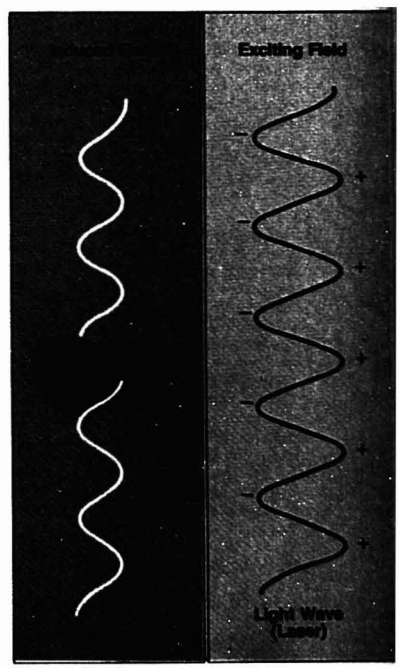

Figure 1. Creation of an induced field in matter by the presence of the intense electric field of a laser

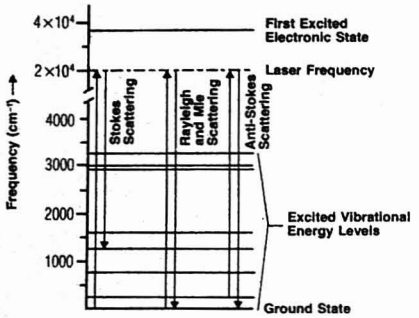

Figure 2. Energy level diagram for typical molecule depicting Stokes and anti-Stokes Raman shifts

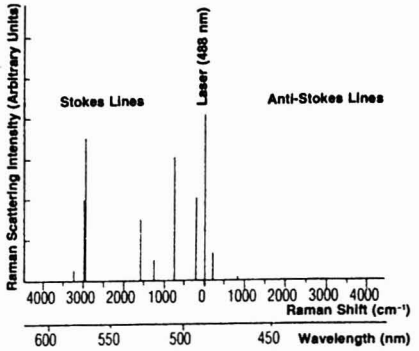

Figure 3. Stokes and anti-Stokes Raman lines for energy level scheme illustrated in Figure 2
Note lack of anti-Stokes lines except for small Raman shifts

fundamental frequency can be broken up into two photons of longer wavelength. This forms the basis of the parametric oscillator, which is a very useful tunable coherent laser source (2).

If we now proceed to the third-order term, we see that additional new frequencies or harmonics arise. By analogy with the second-order term, the third harmonic or triple the fundamental can be generated. As a matter of fact, one can use successive nonlinear processes to effectively produce very high harmonic frequencies. For example, the 28th harmonic of the Nd:YAG laser beam has been produced at frequencies that lie in the deep vacuum ultraviolet at 38.0 nm (3).

The third-order term can be made responsible for other processes. For example, if two laser beams at frequency ω_1 and ω_2 are coupled in a medium, new frequencies at $2\omega_1 - \omega_2$ and $2\omega_1 + \omega_2$ are created. It is the former process that we wish to discuss during the remainder of this report. However, our interest in $2\omega_1 - \omega_2$ is not to generate new frequencies, but to detect this emission, the intensity of which, when plotted against frequency (usually ω_2), forms the basis for a new kind of Raman spectroscopy, which we call CARS. This nonlinear method, which has been reviewed extensively by a number of authors in recent months (4), is only one of many nonlinear Raman processes, most of which are just emerging as useful spectroscopic tools.

In normal Raman spectroscopy a laser is focused in a sample, and the scattered light is collected at right angles to the laser beam. A monochromator is employed to separate the frequency components of the inelastically scattered photons. Figure 2 shows that the frequency difference between the red shifted photons (the Stokes lines) and the laser frequency is a measurement of the vibrational frequencies of the medium. The blue shifted photons (or the anti-Stokes lines) are displaced to higher frequency from the laser frequency again by an amount equal to the vibrational frequencies in the medium. The anti-Stokes lines are usually much weaker than the corresponding Stokes transitions in ordinary Raman spectroscopy because molecules must be thermally populated to vibrational levels above the ground state (see Figure 3).

Thus, ordinary Raman scattering is a method of examining vibrational spectra and is frequently complementary with information obtained from infrared spectroscopy (5). For example, Raman spectroscopy can be used to observe homonuclear diatomic molecules or important vibrational frequencies in polyatomic molecules where the modes are weak or inactive in the infrared spectrum. Raman spectroscopy is also useful for examining spectra in aqueous solution, a medium that is very opaque on the infrared region. Unfortunately, however, normal Raman spectroscopy has many drawbacks that some of the new nonlinear Raman processes like CARS may indeed overcome. A few of these disadvantages include very small scattering cross sections that are particularly bothersome for low-pressure gas-phase spectra. Another problem is interference from fluorescence or luminescence in the sample. Furthermore, resolution in normal Raman spectroscopy is limited by the monochromator and not the laser.

In the CARS process the emission is in the anti-Stokes region, although Stokes output is also possible and useful. If ω_1 is the frequency of one laser beam and ω_2 the other ($\omega_1 > \omega_2$), then the anti-Stokes emission occurs at $\omega_3 = 2\omega_1 - \omega_2$. This emission, which is basically a mixing of three photons to

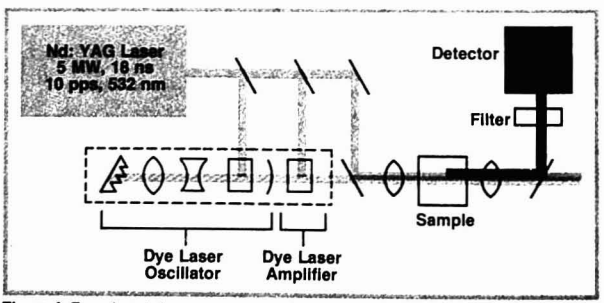

Figure 4. Experimental arrangement for CARS apparatus used in making measurements at NRL
Two input laser beams and CARS output do not appear to be focused or completely overlapped. This effect is for illustrative purposes only

Swagelok®

Tube Fittings (1/16″ to 1″) Install them. Forget them.

Swagelok® Tube Fittings make their seal and grip the tubing in a patented way that allows you to forget tubing connections as a source of trouble in your system. They offer the industry's widest choice of standard sizes, shapes and materials to meet your needs exactly. *And they're locally available, off the shelf, from your Full Service Distributor.*

Patented

CRAWFORD FITTING COMPANY
29500 Solon Road, Solon, Ohio 44139
Crawford Fittings (Canada), Ltd., Ontario

CIRCLE 33 ON READER SERVICE CARD

produce a fourth, takes place in any medium as a result of the third-order nonlinear coefficient (c in Equation 1) and hence does not require thermal population as in normal Raman spectroscopy. Consequently, when the difference in frequency between the two laser beams is equal to a Raman resonance frequency (i.e., when $\omega_1 - \omega_2 = \omega_R$), then the conversion efficiency to ω_3 ($= \omega_1 + \omega_R$) is greatly enhanced. The character of the emitted radiation is very different from normal Raman scattering (see Figure 4). First, the output is coherent or laser-like (unlike normal Raman scattering, which is scattered into 4π steradians for unpolarized exciting light). Second, the process can be quite efficient (as much as 1% of the intensity at ω_2), several orders of magnitude greater than conventional Raman scattering. Third, the CARS beam is created in the anti-Stokes region, which has important advantages over normal (Stokes-shifted) Raman effect.

Mathematical Formulation

Quantitative description of CARS cannot be derived here, but the theoretical development can be found elsewhere (*6*). However, it is useful to discuss the various dependences of CARS as they relate to quantitative, qualitative, and instrumental diagnostics. The intensity of the CARS signal can be described approximately by the following relation for focused laser beams.

$$P_3 \approx \left(\frac{2}{\lambda_1}\right)^2 \left(\frac{4\pi^2\omega_3}{n_3 c^2}\right)^2 |3\chi^{(3)}|^2 P_1^2 P_2 \qquad (6)$$

$\chi^{(3)}$ is called the third-order nonlinear susceptibility, the more usual terminology for the coefficient "c" in Equation 1. $\chi^{(3)}$ is a complex number composed of a resonant and nonresonant part as indicated below:

$$\chi^{(3)} = \chi^{\mathrm{Res}} + \chi^{\mathrm{NR}} \qquad (7)$$

with the resonant term equal to:

$$3\chi^{\mathrm{Res}} = \frac{2Nc^4}{\hbar n \omega 2^4}\left(\frac{d\sigma}{d\Omega}\right) \times \frac{\omega_R \Delta_j}{\omega_R{}^2 - (\omega_1 - \omega_2)^2 - i\Gamma(\omega_1 - \omega_2)} \qquad (8)$$

and where P_i is the power at ω_i, n is refractive index, N is number density, $d\sigma/d\Omega$ is the normal Raman cross section, the product $N\Delta_j$ is the difference in population in the lower and upper states involved in the transition, and Γ is the normal Raman line width. The remainder are well-known quantities.

From Equations 6–8 it is clear that CARS differs from normal Raman effect in that the signal is dependent on the square of the number density or concentration of the resonant material. It is also dependent on the cube of the overall laser intensity and inversely as the square of the line width and the square of the normal Raman cross section (the inherent intensity of the normal Raman band). Equation 8 is shown for only one resonance. Actually, all resonant materials have many possible transitions. Thus, Equation 8 should really be summed over all the resonances in the medium. This sum becomes squared in Equation 6, resulting in a complicated, but readily understood interaction among resonances. On the other hand, if there is no resonant material present (for example, pure argon gas), or if we are off resonance, a residual signal is generated via the nonresonant susceptibility, χ^{NR} and/or from distant resonances. This fact is probably the most serious drawback for CARS because at low concentrations of resonant material, the nonresonant background arising from the diluent interferes with the measurement of the resonant signal. Nonetheless, there are many applications where CARS is very useful in obtaining spectroscopic information that would be inaccessible by normal Raman spectroscopy.

Spectroscopic Applications

One of the most useful applications of normal Raman spectroscopy is in the analysis of biological samples (*7*). However, fluorescence has been a notoriously severe interference. In Figure 5 we show two representative CARS spectra of molecules never before recorded by normal Raman spectroscopy because of fluorescence interference (*8*). These two examples are Rhodamine 6G and Rhodamine B, which are such strong fluorescers that they are among the most potent dyes used in dye lasers.

In Figure 6 the CARS spectra of D_2 and N_2 at the center of an electrical discharge are displayed (*9*). These spectra were recorded with no interference from the strong blue emission emanating from the discharge. From the relative intensities of the various Q-branches it is possible to measure the temperature of the gases. Since electrical excitation preferentially excites vibrational modes in these molecules, it is not surprising that the vibrational temperature is found to be much greater than the rotational/translational temperature. In D_2, for example, $T_v \approx 1050$ K, whereas T_r is determined to be near ambient (~400 K). On the other hand, the vibrational temperature in N_2 is much greater than D_2 and is in fact found to be non-Boltzmann. This fact explains why N_2 is a much better energy storage medium for lasers than D_2.

CARS can also be used to measure

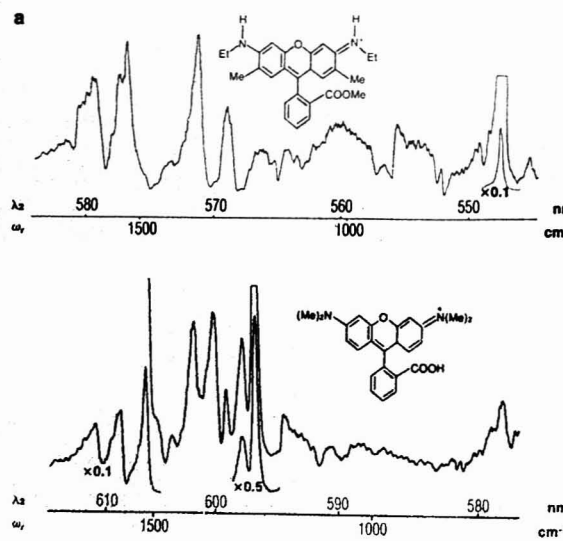

Figure 5. Portion of CARS spectra of two highly fluorescent dyes in solution (~10^{-5} M): a) Rhodamine-6G and b) Rhodamine-B

Normal Raman spectra of these materials have never been reported because of intense laser-induced fluorescence background. Resonance enhancement with electronic transitions in these materials allows one to record CARS spectra at much lower concentration levels. These spectra were recorded by L. Carreira and L. Goss at the University of Georgia

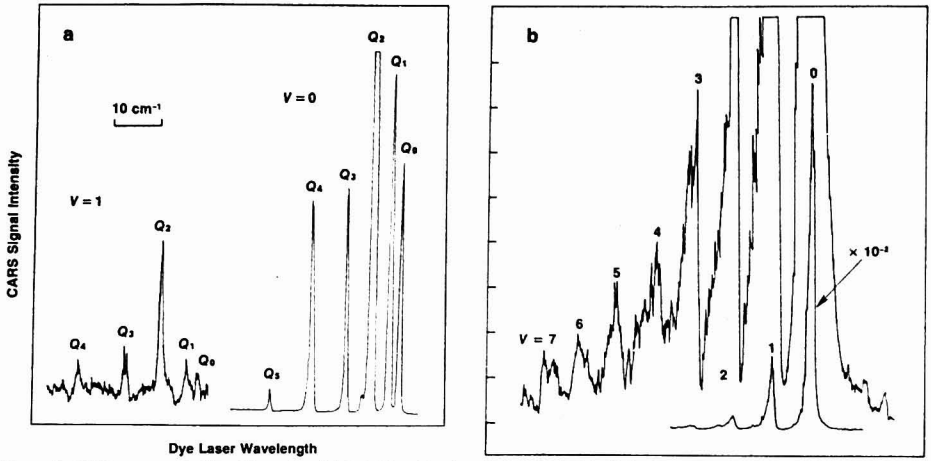

Figure 6. CARS spectra of a) D_2 (48 torr) and b) N_2 (10 torr) in glow region of electrical discharge

Relative intensities of Q branches are measurements of temperature

temperature in flames and other hot gases, and again the technique is not hindered by background radiation. Figure 7 is an example of such. Here a CARS spectrum of N_2 was used to measure temperature in a flat flame burner (methane/air at 1 atm pressure). In this example, the dye laser was spectrally scanned over several minutes to achieve the spectrum displayed. For many practical combustion experiments where turbulence is prevalent, spectra must be recorded in a single shot. Such spectra can be recorded with a broad band dye laser and a monochromator to spectrally separate the anti-Stokes frequencies. An example (*10*) of this is illustrated in Figure 8.

Another important application of CARS is in the analysis of photochemical processes. In Figure 9 we show the CARS spectrum of photochemical decomposition products. In this experiment a portion of ω_1 (at 532 nm) is doubled a second time to produce a third beam at 266 nm. These three coherent beams (the probing CARS beams at ω_1 and ω_2 and the photolysis beam at 266 nm) are spatially and temporarily overlapped in 15 torr of benzene vapor. Normally, radiation at 266 nm would not bring about photodecomposition in benzene vapor, but under the intense field strengths available in these coherent sources, two photons of 266-nm radiation excite the molecule to energy levels in the vacuum ultraviolet region. From the figure, spectral frequencies associated with saturated, olefinic, and acetylenic hydrocarbons, which are known photochemical products of single photon vacuum ultraviolet excitation, are evident. It is interesting to note that in these experiments the primary laser radiation is an infrared laser beam at 1060 nm. All other coherent sources were generated from this laser. With it we produced coherent or laser beams ranging from the visible region to the ultraviolet. It was even possible to carry out vacuum ultraviolet processes without vacuum ultraviolet radiation. The resultant chemistry and spectroscopy was the direct result of nonlinear optics and nonlinear properties in matter. It is also of value to note that in the 8–15-ns duration of the laser pulses and at 15 torr pressure, the benzene molecule has been photolyzed and analyzed in a nearly collision-free environment. Thus, the spectrum shown in Figure 9 may actually be a composite of many transient species as well as stable molecules.

Clearly, the advent of the laser has greatly extended the resolution capabilities of absorption and emission spectroscopy because of the extreme spectral purity inherently available in

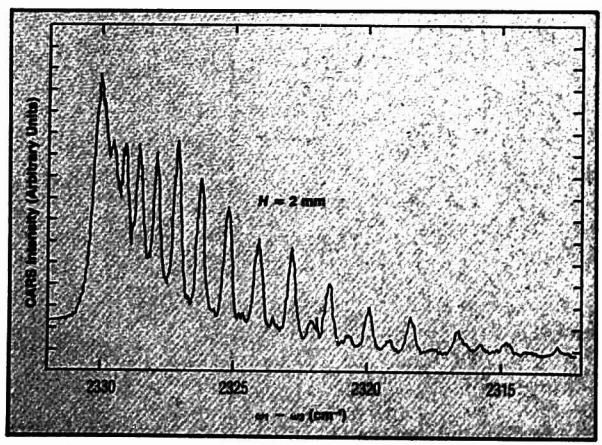

Figure 7. Spectrum of N_2 in laboratory flat flame burner (methane/air)[2]

Normal Raman spectra usually reveal unresolved band envelope curve fitted with calculated spectra to extract temperature data. Pressure = 1 atm; P_{ω_1} = 3 mW; P_{ω_2} = 0.1 mW; 110-min scan; resolution = 0.4 cm^{-1}

these light sources. Normal spontaneous Raman spectroscopy has benefited enormously from the laser in sensitivity and sample size, but resolution has lagged. This is because in normal Raman scattering, resolution is determined by the monochromator employed rather than the spectral width of the exciting laser. Thus, high resolution by conventional Raman spectroscopy is ~0.1–0.01 cm^{-1} with routine scanning at ~5 cm^{-1}. On the other hand, resolution of CARS spectra is usually limited only by the laser line width and, of course, the spectral width of the molecular transition. Hence, "routine" CARS spectra are recorded at ~0.4 cm^{-1} with high resolution at 10^{-3}–10^{-4} cm^{-1}. In Figure 10 the CARS spectrum of ν_1 in methane is displayed under high-resolution solution conditions (*11*). This band is nearly featureless under most "high"-resolution Raman spectrometers. Also since CARS emission is collected in the forward direction, the doppler width is considerably narrowed.

Summary and Conclusions

CARS is a new, nonlinear Raman spectroscopy that has many advantages over normal Raman spectroscopy in biological chemistry, combustion and gas laser diagnostics, high-resolution Raman spectroscopy, and as a general spectroscopic tool for photochemical analysis and chemical kinetics measurements, especially on the nanosecond and picosecond scale. It will probably never replace normal Raman spectroscopy for which there is commercial equipment. Conventional Raman spectroscopy is also less costly, is easier to employ, and has wider applicability than CARS. At present, CARS is progressing somewhat in proportion to advances in laser technology. The most serious drawback for CARS, however, is the problem of interferences caused by the nonresonant or residual background that limits the sensitivity of the technique to ~1% in solution or ~10–1000 ppm in gaseous mixtures. Nonetheless, CARS will undoubtedly continue to prove itself as an important specialized tool for diagnostic applications where other techniques are more difficult or impossible to use. Furthermore, the problems with background interference may be solved. Already some favorable samples have been examined by CARS to 10^{-7} M by means of electronic resonance enhancement. Clearly, there will be additional advances made to improve the technique.

Finally, CARS is only one of several even newer nonlinear Raman spectroscopies that may have even greater applicability than CARS. These nonlinear Raman techniques will be reviewed as they pertain to chemical

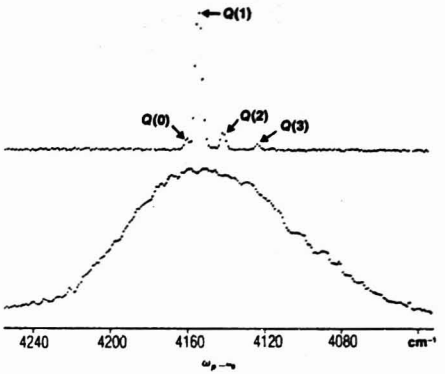

Figure 8. CARS spectra as recorded simultaneously by dual-spectrum optical multichannel analyzer

Upper and lower traces are for H_2 sample and reference gases, respectively. Reference anti-Stokes linewidth is 25 Å

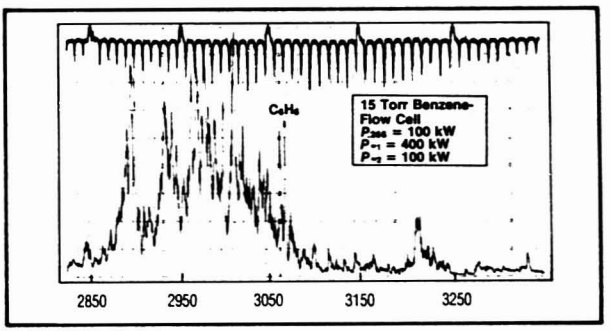

Figure 9. Spectrum obtained by superimposing three laser beams

Fourth harmonic of Nd:YAG laser (266 nm) effects photochemical decomposition of benzene vapor via a two-photon process, and two CARS beams probe photochemical products

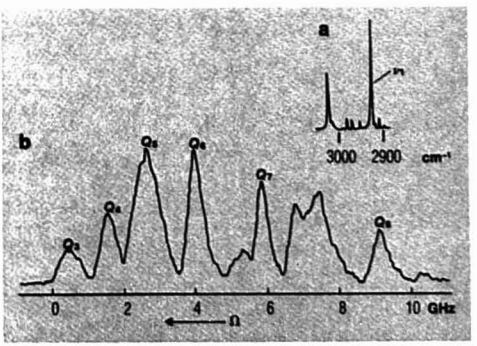

Figure 10. High-resolution capability of CARS, which is clearly much superior to that obtained with conventional Raman techniques

a) Spectrum of spontaneous Raman scattering of CH_4; b) CARS spectrum of Q branch of ν_1 vibration of CH_4: resolution, 40 MHz; pressure, 20 torr

and analytical applications in a future publication (*12*).

Acknowledgment

I extend my gratitude to a number of my friends and colleagues with whom I have collaborated in CARS over the past several years. These include R. Byer, S. Harris, and R. Begley (formerly) at Stanford; G. Klauminzer at Molectron Corp., J.-P. Taran at ONERA in France; R. DeWitt, W. Shaub, S. Lemont, R. Gammon, and J. McDonald at NRL; W. Sanders (Catholic University); W. Tolles at the Naval Postgraduate School; and especially J. Nibler (Oregon State University) who spent a very productive sabbatical year at NRL. I also thank L. Carreira and L. Goss (University of Georgia) for allowing me to illustrate their spectra prior to publication.

References

(1) N. Bloembergen, "Nonlinear Optics", Benjamin, Reading, Mass., 1965; C. Flynzanis, "Quantum Electronics—A Treatise", H. Rabin and C. Tang, Eds., Vol 1, Academic Press, New York, N.Y., 1975; F. Zernike and J. E. Midwinter, "Applied Nonlinear Optics", Wiley, New York, N.Y., 1973; A. Yariv, "Introduction to Quantum Electronics", 2nd ed., Wiley, New York, N.Y., 1975.

(2) R. L. Byer and R. L. Herbert, "Parametric Oscillation and Mixing", in "Nonlinear Infrared Generation", Y.-R. Shen, Ed., p 81, Springer-Verlag, Berlin, Germany, 1977.

(3) J. Reinjes et al., *Appl. Phys. Lett.*, **30**, 480 (1977).

(4) W. M. Tolles, J. W. Nibler, J. R. McDonald, and A. B. Harvey, *Appl. Spectrosc.*, **31**, 253 (1977); J. W. Nibler, W. M. Shaub, J. R. McDonald, and A. B. Harvey, "Coherent Anti-Stokes Raman Spectroscopy", in "Vibrational Spectra and Structure", J. R. Durig, Ed., Vol 6, Elsevier, New York, N.Y., 1977; J. W. Nibler and A. B. Harvey, "Applications of CARS", in "Analytical Raman Spectroscopy", W. Keifer, Ed., Wiley-Interscience, New York, N.Y., 1977; A. B. Harvey and J. W. Nibler, *Appl. Spectrosc. Rev.*, in press (1978); J. W. Nibler and G. V. Knighten, "Coherent Anti-Stokes Raman Spectroscopy", in "Topics in Applied Physics", A. Weber, Ed., Chap. 7, Springer-Verlag, 1977; H. C. Andersen and B. S. Hudson, "Coherent Anti-Stokes Raman Scattering", in "Molecular Spectroscopy", D. A. Long, Ed., Vol 5, Chemical Society, London, England, 1977.

(5) N. B. Colthup, L. H. Daly, and S. E. Wiberly, "Introduction to Infrared and Raman Spectroscopy", 2nd ed., Academic Press, New York, N.Y., 1975.

(6) R. N. DeWitt, A. B. Harvey, and W. M. Tolles, "Theoretical Development of Third-Order Susceptibility as Related to Coherent Anti-Stokes Raman Spectroscopy (CARS)", NRL Memorandum Report 3260, April 1976; Ref. (4a) and references therein.

(7) B. S. Hudson, *Ann. Rev. Biophys. Bioeng.*, **6**, 135 (1977).

(8) L. A. Carreira and L. P. Goss, in press.

(9) J. W. Nibler, J. R. McDonald, and A. B. Harvey, *Opt. Commun.*, 18, 371 (1976); W. M. Shaub, J. W. Nibler, and A. B. Harvey, *J. Chem. Phys.*, **67**, 1883 (1977).

(10) W. B. Roh, P. Schreiber, and J.-P.E. Taran, *Appl. Phys. Lett.*, **29**, 174 (1976); W. B. Roh and P. W. Schreiber, *Appl. Opt.*, **17**, xx (1978).

(11) M. R. Aliev, D. N. Kozlov, and V. V. Smirnov, *JETP Lett.*, **26**, 31 (1977).

(12) A. B. Harvey, Ed., "Chemical Applications of Nonlinear Spectroscopy", Academic Press, to be published in 1979.

Albert B. Harvey is head of the Naval Research Laboratory's Chemical Diagnostics Branch. His research interests include optical diagnostics of chemical systems, kinetics of gas phase reactions, chemical lasers and energy transfer, and novel methods of trace analysis and control.

Gilson presents a masterwork of precision and performance for **liquid column chromatography...** The Model HM Holochrome

VARIABLE WAVELENGTH DETECTOR

- **UV-VIS · DUAL BEAM**
- **HOLOGRAPHIC MONOCHROMATOR— 190 to 600 nm.**
- **INTERCHANGEABLE FLOW CELLS — INCLUDES AN 8 μl VOLUME 10 mm LIGHT PATH CELL FOR HPLC APPLICATIONS**

This Model HM uses a stabilized Deuterium light source and the newest precision Holographic grating monochromator to provide continuous digital wavelength adjustment from 190 to 600 nanometers, without changing light sources.

Holographic Monochromator Reduces Light Dispersion

A monochromator provides greater flexibility, narrower bandwidth, and longer life than interference filters. The use of a holographically constructed concave grating simplifies the optics. This eliminates some lenses and mirrors that would normally be required with a conventional flat plane grating monochromator, thus reducing light dispersion.

High Sensitivity, Low Noise

Full-scale sensitivity can be set from .01 to 2 AU. The combination of high sensitivity and narrow bandwidth results in superior peak resolution as well as wide sensitivity range. Gilson UV/VIS Holochrome monitor utilizes integrated circuit electronics and light intensity sufficient to maintain low noise levels with long light path. Noise is less than .0002 AU.

Flow Cells for HPLC and Gravity Systems

Pressure limit 35 kg/cm² (500 psi)

KEL-F FOR HPLC
10 mm light path—8 μl volume
BLOWN QUARTZ FOR BUBBLE-FREE OPERATION
10 mm light path—70 μl volume
2.5 mm light path—32 μl volume
Gilson HM flow cells optimize bubble-free operation, long light path, small cell volume, and minimum peak broadening.

Two Recorder Outputs For Tall and Short Peaks

Two recorder outputs can be set at different sensitivity levels (for example .01 and 2 AU). In this way, both tall and short peaks can be recorded simultaneously with optimum resolution.

GILSON COLUMN MONITORS ARE CONSTRUCTED FOR COLD ROOM OPERATION

CALL OR WRITE:

Gilson Medical Electronics, Inc.
Serving research laboratories for more than a quarter of a century

U.S.A. MANUFACTURING PLANT
P.O. Box 27, Middleton, Wisconsin 53562
Telephone 608/836-1551 Telex No. 26-5478

EUROPEAN MANUFACTURING PLANT
Gilson Medical Electronics, Inc. (FRANCE) S.A.
Boite Postale 45, 95400 Villiers-le-bel
Arnouville-LesGonesse, FRANCE
Telephone 990 54-41 Telex No. 69-1182F

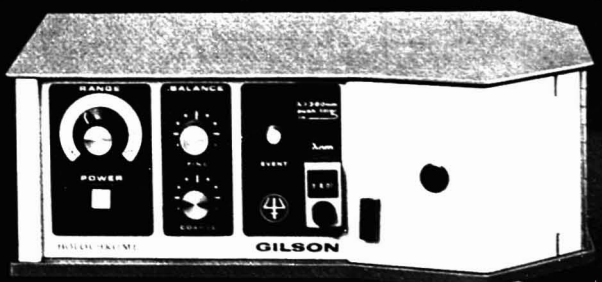

HPLC

Circle #89 for informational literature
Circle #90 for demonstration

LABORATORY SERVICE CENTER

INDEX TO ADVERTISERS IN THIS ISSUE

INDEX TO ADVERTISERS IN THIS ISSUE

** *Company so marked has advertisement in Foreign regional edition only.*

Advertising Management for the American Chemical Society Publications

CENTCOM, LTD.

Thomas N. J. Koerwer, President; James A. Byrne, Vice President; Clay S. Holden, Vice President; Benjamin W. Jones, Vice President; Robert L. Voepel, Vice President; C. Douglas Wallach, Vice President, 25 Sylvan Rd. South, Westport, Connecticut 08880 (Area Code 203) 226-7131

ADVERTISING SALES MANAGER
James A. Byrne

SALES REPRESENTATIVES

Atlanta, GA . . . Robert E. Kelchner, CENTCOM, Ltd. Telephone: 203-226-7131

Boston, MA . . . Don Davis, CENTCOM, LTD. Telephone 203-226-7131

Chicago . . . Thomas Hanley, CENTCOM, LTD., 540 Frontage Rd., Northfield, Ill. 60093. 312-441-6383.

Cleveland . . . James Pecoy, CENTCOM, LTD., Suite 205, 18615 Detroit Ave., Lakewood, Ohio 44107. 216 228-8050.

Houston . . . Robert LaPointe, CENTCOM, LTD., 415-692-0949.

Denver . . . Clay S. Holden, CENTCOM LTD., 213-776-0552.

Los Angeles 90045 . . . Clay S. Holden, CENTCOM, LTD., Newton Pacific Center, 3142 Pacific Coast Highway, Suite 200, Torrance, CA 90505, 213-325-1903

New York 10017 . . . Don Davis, Richard L. Going, CENTCOM LTD., 60 East 42nd St., 212-972-9660

Philadelphia . . . Richard L. Going, CENTCOM LTD., GSB Building, Suite 510 1 Belmont Avenue Bala Cynwyd, Pa. 19004. Telephone: 215-667-9666

San Francisco, CA . . . Robert LaPointe, CENTCOM, LTD., Room 235, 1499 Bayshore Highway, Burlingame, CA 94010. Telephone: (415) 692-0949

Westport 06880 . . . Don Davis, CENTCOM, LTD., 25 Sylvan Rd. So., 203-226-7131.

Manchester, England . . . Jill E. Loney, Technomedia Ltd., 216, Longhurst Lane, Mellor, Stockport, SK6 5PW, Telephone: 061-427-5660

Reading, England . . . Malcolm Thiele, Technomedia Ltd., Wood Cottage, Shurlock Row, Reading, RG10 OOE. Telephone 073-581-302

Tokyo, Japan . . . Haruo Moribayashi, International Media Representatives Ltd., 1, Shibe-Kotohiracho, Minato-ku Tokyo. Telephone: 502-0656

Verviers, Belgium . . . Andre Jamar, Etablissements Andre Jamar, 1 Rue Mallar, 4800 Verviers. Telephone (087) 22-53-85.

PRODUCTION DEPARTMENT

Production Director
Joseph P. Stenza

Advertising Production Assistant
Barbara Autderheide

analytical chemistry

Published by the
AMERICAN CHEMICAL SOCIETY
1155 16th Street, N.W.
Washington, D.C. 20036

Books and Journals Division
Director: D. H. Michael Bowen
Editorial: Charles R. Bertsch
Magazine and Production: Bacil Guiley
Research and Development: Seldon W. Terrant
Circulation Development: Marion Gurfein

Manuscript requirements are published in the January 1978 issue, page 189. Manuscripts for publication (4 copies) should be submitted to ANALYTICAL CHEMISTRY at the ACS Washington address.

The Status of Academic Analytical Chemistry

On p 849 A of the current issue, Dr. Janet Osteryoung of the National Science Foundation describes a survey of analytical chemistry faculty in graduate chemistry departments in the United States and Canada. This survey was carried out by comparing trends in the numbers of analytical chemists compared with chemists as a whole, as determined by examination of the 1971, 1975, and 1977 editions of the ACS Directory of Graduate Research. To quote her summary, "There has been a pronounced increase of analytical chemists in graduate departments, the increase is greater than that of all chemistry faculty, and the increases pervade all types of institutions".

On p 852 A, we carry a follow-up of an article by Rodney T. Hartnett et al. in *Science*, **199**, 1310 (1978) in which the peer ratings of faculty quality in three specialties (chemistry, history, and psychology) are compared with corresponding ratings of subspecialties in each field in 25 diverse institutions. The striking conclusion was that with the single exception of analytical chemistry, the subspecialty ratings correlated reasonably well with the ratings of the three specialties as a whole. Upon closer scrutiny, it turned out that the poor correlation for analytical chemistry resulted from four departments of the 25 being weak in graduate analytical chemistry while being exceptionally strong in chemistry as a whole.

According to the third annual survey of academic openings carried out by the ACS (*Chem. Eng. News*, June 19, 1978, p 39) analytical chemistry rates first in the number of vacancies. Of the 310 available positions reported in 324 schools surveyed, 78 will be in analytical chemistry as compared with 64 in organic chemistry, 49 in physical chemistry, 45 in biochemistry, and 42 in inorganic chemistry.

These studies reinforce the feeling that academic analytical chemistry has been on the upswing during the recent past and also that in a few departments of high quality, analytical chemistry is being relatively neglected. Other departments of recognized excellence have maintained high quality analytical programs and, of course, in several notable departments, analytical chemistry is well in advance of the department as a whole. All of this might seem too trivial to deserve special mention except for the fact that the top-rated departments tend to serve as models for less prestigious ones. Those responsible for deciding the future of graduate programs would be well advised to look more deeply than just at a few top-rated chemistry departments before concluding that analytical chemistry need not play a significant role.

H. A. Laitinen

Determination of Lead in a Chloride Matrix with the Graphite Furnace

D. C. Manning and Walter Slavin*

The Perkin-Elmer Corporation, Norwalk, Connecticut 06856

We report conditions permitting the accurate and sensitive determination of lead in a chloride matrix using the graphite furnace. By comparison with some previous procedures, we achieve this analysis by using ramp atomization, area integration, molybdenum coating of the pyrolytically-coated graphite tubes and by adding NH_4NO_3 as a matrix modifier. We are able to detect less than 20 pg Pb in solutions containing 1% NaCl or $MgCl_2$, which is equivalent to 0.1 μg Pb/g of the solid salt.

Lead is probably the most frequent determination performed in the graphite furnace, and a chloride matrix is probably the most ubiquitous. In several such studies, workers have independently found that the presence of magnesium greatly intensifies the chloride interference on lead. We have chosen to use several alkali and alkaline earth chlorides as models in our interference studies on lead with the expectation that techniques which will control these interferences will control the interference of chloride in the presence of most other cations.

We have attempted to evaluate experimentally and compare the various proposals and suggestions in the literature relating to the interference of chloride in the determination of lead. The literature is often contradictory, and some of these contradictions are illuminated. Most of our experiments used $MgCl_2$ as the test matrix since several authors have reported this to be the most troublesome.

Interferences, especially their degree, are very dependent upon the design of the system. Indeed, the effects of a potential interferent upon the Pb absorption vary significantly during the life of an individual graphite tube, as found by Fuller (*1*), which we have confirmed.

In early applications work with the furnace, Fernandez and Manning (*2, 3*) found that the presence of NaCl reduced the apparent lead found. Studying this interference, Ediger (*4, 5*) introduced the concept of "matrix modification" by suggesting that the drying or charring properties of the sample matrix be deliberately altered by chemical additions. If NaCl is a major matrix material, it will produce a large background signal unless it is driven off in the ashing cycle. However, many analyte metals are lost at temperatures lower than that which will drive off the NaCl. Ediger proposed the addition of NH_4NO_3 to convert the NaCl to products which can be driven off in the ashing step, below 500 °C.

Many workers have studied the lead–chloride system both theoretically and experimentally (*6–17*). The molecular absorption spectra of various gaseous metal halides have been published (*17–21*) and have shown that the background signal observed when NaCl is a major matrix material is not simply light scattering but includes molecular absorption by the NaCl molecule.

Lead was determined in waters of low salinity by Regan and Warren (*22*), and potential interferences were studied by adding 100 μg/mL Ca, Mg, Sr, and Ba to HCl and HNO_3 solutions. The worst interferences resulted from the Mg in HCl solution. These authors found that addition of 1% ascorbic acid to each of the interference solutions reduced all of the interferences to less than 7%. It was shown that the presence of calcium broadened and shortened the peaks, while the presence of chloride reduced the total peak area.

Fuller (*1*) states that oxalic acid decomposes completely to CO_2 below 300 °C and that when oxalic acid and PbO are heated together in an inert atmosphere at 300 °C, free Pb is produced. Thus, he found that 1% oxalic acid removed the characteristic interference of 0.1% $MgCl_2$ on the Pb absorption signal.

Hodges (*23*) found considerable loss of Pb signal when 475 μg/mL $MgCl_2$ was added to 0.1 μg/mL Pb solution. The effect was completely removed when 2% H_3PO_4 was added. However, urine samples treated with H_3PO_4 produced erratic results. When the graphite cylinder was pretreated by 10 firings with a 1% ammonium molybdate solution, the background absorption was greatly reduced and orthophosphoric acid then suppressed the interferences in urine analysis for Pb.

Significant interferences in the determination of Pb, Cd, and Se in samples containing 5% HCl were found by Henn (*24*). For Pb, these interferences were controlled by adding 200 μg/mL Mo to samples and standards. The furnace tubes were preconditioned by several firings with the Mo solution.

In a study of Pb in NaCl solutions, Frech and Cedergren (*13*) found that nonatomic absorption caused by 2 μL of 2% NaCl was observed alone and in the presence of 1.3 M NH_4NO_3 or 2 M HNO_3. The nonatomic absorption disappeared above about 1000 °C for NaCl alone, while both treatments accomplished removal of the NaCl at about 500 °C. Hydrogen was not sufficiently effective as a suppressor for the Pb–NaCl system. Without NaCl, no Pb was lost while ashing up to 900 °C. When Pb was determined in NaCl, with and without 2 M HNO_3, Pb was not lost in ashing below 630 °C. However, even in 2 M HNO_3, not all the Pb appeared to be measured.

In another study of the determination of lead in waters of low salinity with the graphite furnace, Thompson et al. (*25*) found a considerable suppression of signal for many of the components typically found in polluted water. However, these authors were not able to find any improvement when hydrogen was added to the nitrogen gas as suggested by Frech (*15*) or when ascorbic and oxalic acid were added as suggested by Regan and Warren (*22*) or when ammonium nitrate was added to the sample as suggested by Ediger (*5*). These authors found that they could reduce the interference from the various sample constituents by treating the graphite tube with lanthanum. Solutions of lanthanum nitrate hexahydrate were heated to high temperature in the tube, and the tube was then used for the Pb determination. Presumably this alters the surface of the tube with a layer of lanthanum carbide.

In spite of these problems, several authors have shown that lead can be determined if certain precautions are taken. Shaw and Ottaway (*26*) found that interferences in the determination of Pb were serious only in a chloride medium. They developed a graphite furnace method for Pb in steel and iron by dissolving the sample in nitric acid. Barnett and McLaughlin (*27*) also determined very low levels of Pb by

0003-2700/78/0350-1234$01.00/0

Table I. Experimental Conditions

λ 217 nm, slit 4 (0.7 nm)	
Pb EDL	
D_2 background correction used	
furnace:	step 1 (dry), 110 °C for 20 s
	step 2 (char), ramp 15 s, 550 °C for 15 s
	step 3 (atomize), ramp 9 s, 2500 °C for 9 s
	argon flow, 12 mL/min
	15-s integration

avoiding a chloride medium and choosing nitric acid for dissolution. Frech (*28*) developed a method for very low concentrations of Pb (less than 1 μg/g) in steels. The steel was dissolved in 2.5% HCl and 1% HNO_3 (aqua regia) in which the sample is 0.25%. Using 5 μL of this solution, it proved possible to ash the sample in the temperature range from about 660 to 740 °C. In this temperature range, Frech found that the chloride could be driven off prior to atomization and that no lead was lost for these specific materials.

McArthur (*29*) reported the effects of chloride on the Mn determination with results that are very similar to our observations for Pb. He found that NH_4NO_3 largely removed the effect.

EXPERIMENTAL

The Perkin-Elmer Model 603 atomic absorption spectrophotometer was used with the Model HGA-2200 graphite furnace with the Temperature Ramp Accessory. The Model AS-1 Auto Sampler was used to improve precision and to reduce the fatigue associated with the large number of samples that were run. All furnace sample dosage volumes were 20 μL. When a specific weight of lead (i.e. 2 ng) is referred to, we mean amount present in a single 20-μL dosage.

The analytical experimental conditions are as indicated in Table I. Using the Pb electrodeless discharge lamp (EDL) which is many times brighter than Pb hollow cathode lamps (*30*), we found the 217.0-nm line to be preferable. The 217.0-nm line lies just outside the strong molecular absorption band of NaCl (*18–20*).

In this study it proved always necessary to use the deuterium background corrector when there were significant amounts of chloride matrix present. Throughout this study, the background signal was recorded simultaneously with the analytical signal on a Perkin-Elmer Model 56 two-pen recorder using the deuterium arc as the light source. To record automatically the absorption signal with no sample present, we used a circuit described by Epstein (*31*). Most measurements were repeated in triplicate. A recording pyrometer, the Ircon Modline Model 2000, was used during all of these experiments. Integrated absorbance readings were printed using the Perkin-Elmer PRS-10 Printer Sequencer.

In this study, we frequently found samples where quantitation by measuring peak area (*32, 33*) produced less apparent analytical interference than did the measurement of peak height. To obtain optimum signals for peak area required somewhat different conditions than were optimum for peak height. Except for determination of concentrations within ten times the detection limit, we used area integration throughout the study.

The gas flow meter was approximately calibrated for argon flow. A flow of "12" was approximately 12 mL/min, "20" was about 24 mL/min and "30" was about 45 mL/min. This is the flow through the graphite tube during atomization.

RESULTS

Since there is important interaction between the various parameters that have been studied in the lead–chloride system, experiments were conducted to study separately the effect of each of the potential parameters.

Furnace Parameters. Our furnace conditions are similar to those recommended (*34*) for Pb. We find that a short (9-s) ramp atomization provides some separation between the background and the Pb absorption peak and thus reduces the problems associated with large background signals.

An investigation of the rate of heating in the atomization step (550 to 2000 °C) showed that approximately 140 °C/s maximized the integrated lead signal. As the heating increased the signals became smaller reaching 25% of the maximum at 700 °C/s. At heating rates slower than 140 °C/s, the peaks became broad. This was independent of the presence of $MgCl_2$ matrix. This result was found with ordinary graphite sample tubes as well as with tubes that were pyrolytically coated.

The char temperature was studied using a solution containing 2 ng Pb, 5% oxalic acid, and 0.4% $MgCl_2$ with an atomization ramp time of 9 s. No lead was lost in charring below 690 °C while the loss was significant at 920 °C. The lead absorption signal was insensitive to changes in char times of 5 to 45 s, or to the use of ramp charring. The background signal in the atomization step remained constant for all the variations in char parameters, including charring at 920 °C where one third of the lead was lost.

The use of gas stop instead of a low argon flow through the furnace tube during atomization increased peak area by about 15%. With real samples that contain a considerable matrix not destroyed during the charring step, operation with gas stop may be impractical since the windows collect a coating which must be removed.

Graphite Tube Surface Treatment. Manning and Ediger (*35*) showed that pyrolytically coating the graphite furnace tubes provided about 70% increase in sensitivity for Pb when either peak height or peak area was used for quantitation. Recent work in our laboratories (*36*) indicates that this increase comes about by reducing the Pb vapor lost through the walls of the porous graphite tubes.

Treating the surface of the graphite tube with carbide-forming elements has been reported by Runnels et al. (*37*) who thereby improved the sensitivity and precision of the beryllium determination. The authors examined the surface of molybdenum-treated tubes by x-ray diffraction and found that the inner surface was coated uniformly with molybdenum carbide. Thompson et al. (*25*) used a lanthanum pretreatment technique to reduce interferences on lead determination in stream and waste water. Cioni et al. (*38*) heated titanium dioxide in the furnace to provide a layer that prevented Ba from reacting with the graphite. Without the coating, there were interferences in the determination of Ba in silicate rocks.

Several workers (*23, 24*) have observed that treating or altering the sample tube surface with molybdenum reduces the effect of chloride interferences on lead. Ortner and Kantuscher (*39*) compared foil linings of tungsten and tantalum with treating the furnaces with salts of the same metals. The salt treatment produced metal carbide surfaces which produced a better environment for the determination of silicon.

The early days of our study were plagued by difficulties in repeating observations from day-to-day and by differences from one graphite tube to another and between pyrolytic and nonpyrolytic graphite tubes. During this time Fuller (*1*) observed that the surface condition of the graphite furnace tubes has a great effect upon the degree of interference of $MgCl_2$ on the determination of Pb. In a new graphite tube or a pyrolytically-coated graphite tube, $MgCl_2$ strongly inhibited Pb absorption, while a used tube that had become coated with soft graphite exhibited much less interference. This helps to explain the lack of reproducibility of the $MgCl_2$ interference and the variety of results found by different workers (*11, 22–24*).

We investigated the treatment of the tube surface as suggested by Henn (*24*) and Hodges (*23*) as a control for this variability. Molybdenum was used to coat graphite tubes which had not received a pyrolytic graphite coating as well as tubes that had received a prior coating of pyrolytic graphite.

A molybdenum solution was made by dissolving 9.2 g of $(NH_4)_6Mo_7O_{24}{\cdot}4H_2O$ in 40 mL of 5% NH_4OH and diluting to

Table II. Durability of Molybdenum Coating

sequence	integrated absorbance, abs-s						($MgCl_2$, %)
	0	0.2	0.4	0.8	1.2	1.6	
1	0.73	0.72	0.76	0.87	0.74	0.57	
2	0.79	0.82	0.86	0.90	0.87	0.82	
3	0.75	0.75	0.77	0.98	0.87	0.80	
4	0.77	0.78	0.81	0.86	0.88	0.83	
5	0.76	0.78	0.80	1.01	0.88	0.79	
6	0.79	0.78	0.80	0.86	0.88	0.88	
7	0.79	0.79	0.79	0.94	0.85	0.88	
8	0.79	0.81	0.83	0.86	0.87	0.90	

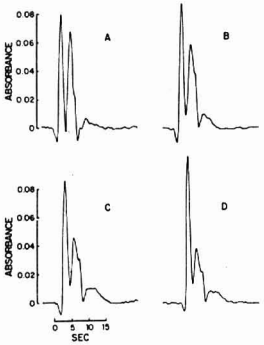

Figure 1. Effect of successive molybdenum treatments on a pyrolytically-coated graphite tube. The test solution was 20 μL of a solution containing 0.2 ng Pb, 1% NaCl, and 4% NH_4NO_3. The instrumental conditions were as given in Table I. Segment A is the absorbance before molybdenum treatment. B is the same solution after a single molybdenum treatment of the tube. C resulted after the second treatment and D after the third

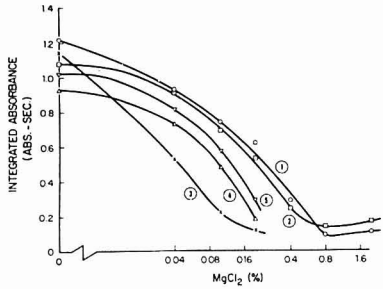

Figure 2. Interference of $MgCl_2$ on Pb absorbance in various graphite tubes. The test solution contained 2 ng Pb and varying amounts of $MgCl_2$. The mean integrated absorbance (abs-s) of six consecutive firings was used for each data point shown. Curve 1 represents a pyrolytically-coated tube that also received the molybdenum treatment while curve 3 is a pyrolytically-coated tube without the treatment. An ordinary graphite tube that received the treatment is shown as curve 2, while curves 4 and 5 are ordinary tubes without treatment. Curve 4 was made with a previously unused tube while curve 5 utilized a well-used tube

50 mL in a volumetric flask. This results in approximately 10% Mo (w/v). A tube is conditioned by introducing 25 μL of the molybdenum solution through the sample introduction hole and using the furnace program shown in Table I, except that during step 3 the purge gas is stopped to reduce the convection of the vaporized molybdenum out of the sample tube. The treatment is repeated for three sequences.

Figure 1 shows the effect of successive molybdenum treatments. A tube which had previously received a pyrolytic coating was fired with a solution containing 1% NaCl, 4% NH_4NO_3, and 0.2 ng Pb. The resulting recorder tracing is shown in Figure 1A. The tube was given a single molybdenum conditioning as described above, and 20 μL of the same salt solution was again fired, with the result shown in Figure 1B. The tube was molybdenum-conditioned a second time, and the 1% salt solution again fired with results shown in Figure 1C. The conditioning was again repeated, and the resulting tracing is shown in Figure 1D. Two further conditionings and firings produced no apparent change in the tracings which are not shown here.

The first peak in each tracing is produced by lead and varies only slightly as the conditionings are repeated. The pattern following the lead peak is caused by residual uncompensation of the background.

Figure 2 summarizes the effect of $MgCl_2$ on the lead signal when using tubes with and without the described treatment. Five tubes were investigated: two pyrolytically coated tubes, one having been molybdenum-treated and an untreated tube as a control; three standard tubes, one having been molybdenum-treated, and two untreated controls, one unused and one previously used extensively. Solutions containing 2 ng Pb and 0 to 1.8% $MgCl_2$ were run in the several tubes. While integrated peak area is shown, a plot of peak height showed similar results. The improvement realized by molybdenum coating is greater for pyrolytically-coated tubes (curves 1 and 3) than for ordinary graphite tubes (curves 2, 4, and 5). There is a small but real difference between a used and unused tube. This confirms the observations reported by Fuller (*1*). The precision with the molybdenum-coated tubes was generally better than 2%, expressed as a coefficient of variation, while the uncoated tubes provided precision often several times poorer.

One factor that is important in determining the value of the molybdenum surface treatment is how long it lasts. We treated several tubes and then made a large number of repeated runs to see the change with time. A typical example is shown in Table II. The solutions contained 2 ng Pb. Since this test was also associated with a matrix modification experiment, all solutions also contained 5% (w/v) NH_4NO_3. Each solution was run in triplicate or quadruplicate before moving to the next solution (higher $MgCl_2$ content). At the end of the sequence a water blank was run to check the baseline. The eight sequences represent 208 individual firings of the tube. The test was discontinued after 208 firings although the tube was still satisfactory and was used for other tests. There was no change in the results that could be attributed to deterioration of the molybdenum coating. The first sequence in the series of eight shows results different from the seven following. This indicates that a short run-in may be necessary for the molybdenum coating.

Matrix Modification. Several workers have shown that adding various substances to a solution containing chloride

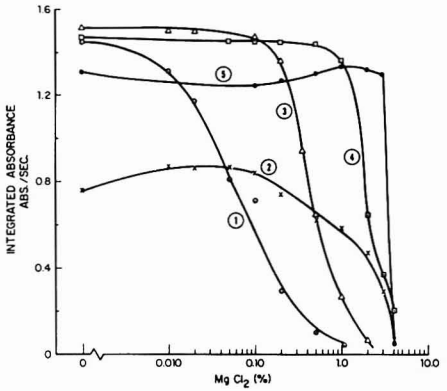

Figure 3. Effect of several matrix modifiers on the $MgCl_2$ interference in the determination of lead. The test solution contained 2 ng Pb and varying amounts of $MgCl_2$. (1) No modifier. (2) H_3PO_4 2% v/v. (3) Sucrose 5% w/v. (4) NH_4NO_3 5% w/v. (5) Oxalic acid 5% w/v

reduces the chloride interference on lead. Substances which have been proposed are: dicarboxylic acids (*1*, *22*), nitric (*13*) and phosphoric (*23*, *40*) acids, ammonium nitrate (*5*), and sucrose (*22*). We have investigated the relative efficiencies of several of these materials, and summarize our results in Figure 3. The experimental samples contained 2 ng Pb and concentrations of $MgCl_2$ varying from 0 to 4%. Three replicates of each solution were run and the means of the integrated absorbance were plotted after correcting for blank values. A new pyrolytically-coated tube, treated with molybdenum solution, was used for each different matrix modifier sequence.

Figure 3 shows the suppressive effect of $MgCl_2$ on lead in the absence of a matrix modifier, and also the effect of separately adding H_3PO_4 2% w/v, NH_4NO_3 5% w/v, oxalic acid 5% w/v, and sucrose 5% w/v. The addition of orthophosphoric acid produced greater background signals than corresponding amounts of the other substances, and for this reason a smaller amount was added. Also preliminary experiments indicated that there was little improvement by using larger concentrations of H_3PO_4.

In addition to the substances included in Figure 3 other organic acids were investigated: citric, L-ascorbic, tartaric, and maleic. These provided results similar to oxalic acid, in some cases giving slightly less protection. In an attempt to look at other organic materials with properties similar to sucrose, a six-carbon chain alcohol, sorbitol, was selected. This material is very similar to sucrose in its carbon, hydrogen, and oxygen content, as well as being water soluble. When it was used as a matrix modifier, however, the results were only slightly improved (40% to 50%) compared to no matrix modification, and clearly less than the effect produced by sucrose. The protection mechanism therefore appears to involve more than merely the constituents of the substance added.

An examination of matrix modification substances used with NaCl revealed that NH_4NO_3 was slightly superior to the dicarboxylic acids in protecting against interference. Therefore NH_4NO_3 was chosen for subsequent experiments with NaCl. Figure 4 shows the effect of varying the concentration of NH_4NO_3 on the lead signal and 1% NaCl background signal. The background only signal (top tracing) was obtained simultaneously with the lead absorption signal (bottom tracing) by using a two-pen recorder, with the second pen recording a signal from the spectrometer reference beam. The reference beam signal was recorded as percent absorption, with 100% corresponding to complete beam attenuation. The background is greatly reduced (from 93% to 27%) as the amount of NH_4NO_3 is increased. In the absorbance signal, the matrix provides a second broad peak which is not appreciably altered as the NH_4NO_3 is increased. The second peak must be excluded from quantitative measurements at low concentrations of lead.

Calcium chloride also produces a significant inhibition in the Pb absorbance signal in the furnace. Using the experi-

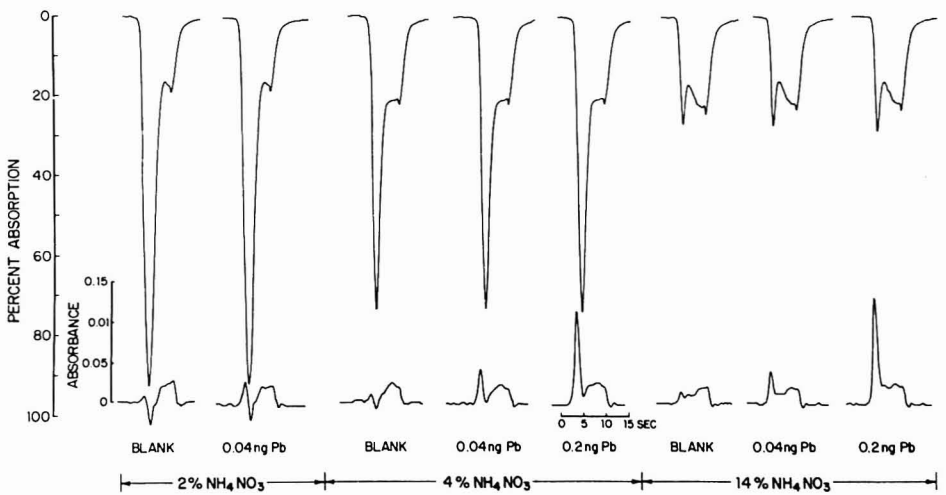

Figure 4. Effect of NH_4NO_3 on the Pb absorbance signal in an NaCl matrix. The test solution contained 1% NaCl and the Pb and NH_4NO_3 shown in the figure. The upper curve is the background absorption. The conditions were as in Table I except that the 12 mL/min of argon flowed for a 6-s atomization period after the 9-s ramp

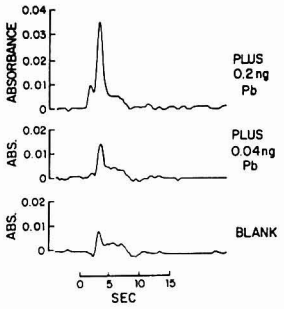

Figure 5. Absorbance of solutions containing 1% $MgCl_2$ and 4% NH_4NO_3. The analytical conditions were as in Table I. The absorbance expansion was 5X. The blank absorbance corresponds to 0.009, the 0.04 ng Pb addition to 0.014, and the 0.2 ng addition to 0.035. Corrected for the blank, the 0.04 addition yielded an absorbance of 0.005, the 0.2 addition an absorbance of 0.026. The blank contained about 0.07 ng Pb

mental conditions of Table I and a pyrolytically-coated tube that had been molybdenum-treated, varying concentrations of $CaCl_2$ were analyzed. The test solutions contained 2 ng Pb, varying amounts of $CaCl_2$, and 4% (w/v) NH_4NO_3. The interference of up to 3% w/v $CaCl_2$ was controlled by 4% NH_4NO_3. The background signals were recorded during these experiments. When 3.3% $CaCl_2$ was atomized, the background absorbance was greater than 2. Nevertheless, the peak absorbance signal proved to be analytically useful. This is because the ramp atomization separates the background signal from the Pb absorbance signal. As we found in the case of the $MgCl_2$ experiments discussed earlier, very high concentrations of $CaCl_2$ produced a trailing second peak on the Pb absorbance signal. As before, it was an uncompensated baseline upset and did not correspond with Pb.

Pb Detection Limit in NaCl and $MgCl_2$. We have established the approximate detection limit for Pb in NaCl and $MgCl_2$ matrices using the recommended procedure. We have not established the limiting amount of the salt matrix that can be accommodated in the graphite furnace, but we have shown that a 20-μL sample containing 1% NaCl or $MgCl_2$ (0.2 mg) can be handled using 4% (w/v) NH_4NO_3.

Numerous experiments showed that variation of the NH_4NO_3 between 2 and 15% (w/v) produced no significant effect upon the Pb signal with the 1% NaCl matrix, although as reported in an earlier portion of this paper, the background signal varied with the amount of NH_4NO_3 added.

Figure 5 shows tracings of a blank and solutions containing additions of 0.04 and 0.2 ng Pb to 1% $MgCl_2$ and 4% NH_4NO_3. Correcting the two additions for the absorbance of the blank, that is, the amount of Pb in the 1% NaCl and 4% NH_4NO_3, yields absorbances that are linear with the concentration of Pb. Approximately 0.07 ng Pb is indicated as present in the 0.2-mg $MgCl_2$ blank sample, or about 0.35 μg Pb/g $MgCl_2$.

In both the NaCl and $MgCl_2$ experiments we could have detected as little as 20 pg Pb or 0.1 μg Pb/g of the solid salt. This is still about 10× poorer than the detection limit one can achieve in simple aqueous solutions (*34*).

CONCLUSION

Many hundreds of results on many different graphite tubes with different histories show that we can quantitatively measure very small amounts of Pb in a chloride matrix.

To do it:

(1) We use a short atomization ramp that separates the residual background due to the NaCl from the lead absorbance.

(2) We coat the interior of the graphite tubes with molybdenum to get reproducible signals for Pb in this matrix.

(3) We add 4% NH_4NO_3 as a matrix modifier to remove much of the chloride matrix during the char cycle at temperatures well below those that cause loss of Pb.

ACKNOWLEDGMENT

We thank R. Ediger, F. Fernandez, R. Beaty, Sabina Slavin, and W. B. Barnett for many valuable discussions and suggestions.

LITERATURE CITED

(1) C. W. Fuller, *At. Absorp. Newsl.*, **16**, 106 (1977).
(2) D. C. Manning and F. J. Fernandez, *At. Absorp. Newsl.*, **9**, 65 (1970).
(3) F. J. Fernandez and D. C. Manning, *At. Absorp. Newsl.*, **10**, 65 (1971).
(4) R. Ediger, G. Peterson, and J. D. Kerber, *At. Absorp. Newsl.*, **13**, 61 (1974).
(5) R. D. Ediger, *At. Absorp. Newsl.*, **14**, 127 (1975).
(6) B. V. L'vov, *Spectrochim. Acta, Part B*, in press.
(7) W. C. Campbell and J. M. Ottaway, *Talanta*, **21**, 837 (1974).
(8) C. W. Fuller, *Analyst (London)*, **99**, 739 (1974).
(9) J. Aggett and A. J. Sprott, *Anal. Chim. Acta*, **72**, 49 (1974).
(10) R. E. Sturgeon, C. L. Chakrabarti, and C. H. Langford, *Anal. Chem.*, **48**, 1792 (1976).
(11) J. M. Ottaway, *Proc. Anal. Div., Chem. Soc.*, **13**, 185 (1976).
(12) W. Frech and A. Cedergren, *Anal. Chim. Acta*, **83**, 83 (1976).
(13) W. Frech and A. Cedergren, *Anal. Chim. Acta*, **88**, 57 (1977).
(14) W. Frech, G. Lundgren, and S. E. Lunner, *At. Absorp. Newsl.*, **15**, 57 (1976).
(15) W. Frech and A. Cedergren, *Anal. Chim. Acta*, **82**, 93 (1976).
(16) E. J. Czobik and J. P. Matousek, *Anal. Chem.*, **50**, 1 (1978).
(17) J. W. McLaren and R. C. Wheeler, *Analyst (London)*, **102**, 542 (1977).
(18) M. J. Adams, G. F. Kirkbright, and P. Rienvatana, *At. Absorp. Newsl.*, **14**, 105 (1977).
(19) B. R. Culver and T. Surles, *Anal. Chem.*, **47**, 920 (1975).
(20) M. W. Pritchard and R. D. Reeves, *Anal. Chim. Acta*, **82**, 103 (1976).
(21) S. Yasuda and H. Kakiyama, *Anal. Chim. Acta*, **84**, 291 (1976).
(22) J. G. T. Regan and J. Warren, *Analyst (London)*, **101**, 220 (1976).
(23) D. J. Hodges, *Analyst (London)*, **102**, 66 (1977).
(24) E. L. Henn, "Flameless Atomic Absorption Analysis: An Update", **ASTM STP 618**, 54–64 (1977).
(25) K. C. Thompson, K. Wagstaff, and K. C. Wheatstone, *Analyst (London)*, **102**, 310 (1977).
(26) F. Shaw and J. M. Ottaway, *Analyst (London)*, **99**, 184 (1974).
(27) W. B. Barnett and E. A. McLaughlin, *Anal. Chim. Acta*, **80**, 285 (1975).
(28) W. Frech, *Anal. Chim. Acta*, **77**, 43 (1975).
(29) J. M. McArthur, *Anal. Chim. Acta*, **93**, 77 (1977).
(30) W. B. Barnett, J. W. Vollmer, and S. M. DeNuzzo, *At. Absorp. Newsl.*, **13**, 33 (1976).
(31) M. S. Epstein, *At. Absorp. Newsl.*, **16**, 75 (1977).
(32) B. V. L'vov, "Atomic Absorption Spectrochemical Analysis", Adam Hilger, London, 1970.
(33) P. Schrammel, *Anal. Chim. Acta*, **72**, 414 (1974).
(34) Perkin-Elmer Corp. "Analytical Methods for Atomic Absorption Spectrophotometry Using the HGA Graphite Furnace", No. 993-9312, March 1977.
(35) D. C. Manning and R. D. Ediger, *At. Absorp. Newsl.*, **15**, 42 (1976).
(36) E. Wiedeking, to be published.
(37) J. H. Runnels, R. Merryfield, and H. B. Fisher, *Anal. Chem.*, **47**, 1258 (1975).
(38) R. Cioni, A. Mazzucotelli, and G. Ottonello, *Anal. Chim. Acta*, **82**, 415 (1976).
(39) H. M. Ortner and E. Kantuscher, *Talanta*, **22**, 581 (1975).
(40) J. P. Matousek and K. G. Brodie, *Anal. Chem.*, **45**, 1606 (1973).

RECEIVED for review March 13, 1978. Accepted May 22, 1978.

Determination of Silver in Precipitation by Furnace Atomic Absorption Spectrometry

J. D. Sheaffer[1] and Gerald Mulvey[2]

Department of Atmospheric Science, Colorado State University, Fort Collins, Colorado 80523

R. K. Skogerboe*

Department of Chemistry, Colorado State University, Fort Collins, Colorado 80523

A procedure for the determination of silver in precipitation at levels down to 1×10^{-6} μg/mL using furnace atomic absorption and evaporative preconcentration is described. The method is shown to produce results which are precise to better than ±20% for triplicate analyses. Collaborative test and spike-recovery results also indicate that the accuracy is in this range. Results are presented which indicate the validity of the sample storage procedures used and problems which may be associated with such procedures. The method has been used for the analysis of precipitation samples to demonstrate the occurrence of significant increases in the silver content of snowfall 100 km or more downwind of silver iodide seeding locations.

The effectiveness of silver iodide as a weather modification agent has been extensively studied. It has been demonstrated that seeding with relatively small amounts of silver iodide, under proper dispersion conditions, can measurably increase precipitation from certain orographic and cumulus formations (*1*). Higher concentrations of silver in seeded vs. unseeded precipitation is considered partial evidence of an effective seeding operation. Similarly, the silver content of precipitation in downwind locations is an important indication of inadvertent (extended area) seeding effects.

The concentration of silver in natural, unseeded, precipitation is usually on the order of 10^{-6}–10^{-5} μg/mL (*2*, *3*). Silver levels reported in seeded precipitation range upward to, but rarely exceed, 10^{-3} μg/mL (*4*). Warburton (*3*) measured silver in snow collected 80 km downwind of a seeding program in the Sierra Mountains and noted that seeding approximately doubled the silver background level of 4×10^{-6} μg/mL. The determination of these ultratrace concentration levels requires an analytical method of unusually high sensitivity. Methods used to successfully determine concentrations of silver in precipitation include neutron activation analyses (NAA) and furnace atomic absorption spectroscopy (FAAS) (*4*, *5*). Although NAA and FAAS are very sensitive methods, a preconcentration step is often required to bring silver concentrations to measurable levels. Preconcentration has been done by solvent extraction and cation exchange methods (*4*, *5*). These techniques are time consuming and require great care, elaborate cleaning, very pure reagents, and frequent monitoring of efficiency.

One analyst has avoided many of these problems by using evaporative preconcentration with FAAS (*6*). Relatively large volumes of precipitation are injected directly into a graphite furnace, evaporated to dryness, and atomized. The furnace configurations of many FAAS systems are too small for efficient application of this preconcentration technique. The present report describes the use of an oversize graphite tube furnace in a flameless atomization system and includes procedural innovations for rapid evaporative preconcentration and analysis of silver in precipitation.

Table I. Summary of Instrumentation and Operating Conditions

spectrophotometer	Varian-Techtron, Model AA5
atomization unit	Varian-Techtron, Model 63
furnace conditions	
dry	5 s at ~120 °C
ash	5 s at ~300 °C
atomize	5 s at ~2000 °C
background correction	Varian-Techtron, Model BC6, with H_2 continuum lamp
furnace	special, long tube, fabricated from Poco Graphite, No. FX9 (see Figure 1)
sheath gas	argon, welding grade at 5 L/min plus 10% methane in argon at 0.1 L/min during ash and atomize steps
analytical wavelength	328.1 nm
recorder	Coleman, Model 65, strip chart recorder

EXPERIMENTAL

Apparatus. The atomic absorption system and operating conditions used are summarized in Table I. The standard graphite tube furnace was replaced by the oversize unit shown in Figure 1. The internal volume of this furnace is nominally 0.2 mL. A small indentation was drilled opposite the injection port to facilitate control of the localization of samples injected.

Reagents. All nitric acid used was doubly redistilled in quartz and stored in Teflon bottles prior to use. Dilutions of this acid were made with distilled-deionized water previously stored in polyethylene bottles. The silver blank of 3 M acid prepared from these reagents was consistently less than 2×10^{-6} μg/mL. Analytical standards were prepared from AR grade $AgNO_3$ dissolved in 3 M HNO_3 and stored in Teflon bottles. A 0.1% (w/v) solution of paraffin in AR grade cyclohexane was used as a pretreatment dip for the furnaces.

Procedures. Falling snow samples were collected in plastic bags held 1 m above the ground by support frames. Samples were retrieved as soon as snowfall stopped and were held frozen until analyzed. Rainfall samples were collected in acid washed, 1-L polyethylene bottles fitted to the stems of 30-cm diameter polyethylene funnels set 1 m above the ground. Each rain water collection bottle was spiked with 10 mL of 3 M HNO_3 prior to collection to inhibit losses of silver through wall adsorption. Rainfall samples were frozen as soon as possible after collection and retained in that form for storage. Sample collections were made by cooperative observers previously made aware of procedures necessary to preserve the samples and avoid contamination.

In preparation for analysis, snow samples were thoroughly mixed in the bags and a fraction of each was transferred to smaller bags for melting at room temperature. A volume of 3 M HNO_3

[1] Present address, Environmental Research and Technology, Inc. Fort Collins, Colo. 80521.
[2] Present address, Meteorology Research, Inc., Altadena, Calif.

0003-2700/78/0350-1239$01.00/0

sufficient to provide a 1% (v/v) acid concentration in the anticipated melt water volume was added to each sample on initiation of melting. Rainfall samples were allowed to completely melt in the collection bottles to avoid silver fractionation associated with freezing. Aliquots of each sample type were subsequently transferred to smaller plastic bags (Baggies) retained in beakers. All samples were kept covered except during the final analysis preparation step.

Sample furnaces were dipped in cyclohexane solutions of paraffin and allowed to air dry. The resulting paraffin film prevented seepage of the water into the graphite lattice and was instrumental in confining sample aliquots to the central region of the furnace during evaporation. Samples were transferred to the furnaces by sequential injections of 50 μL each with an Eppendorf pipet. To evaporate each injection, the furnaces were placed in an aluminum vee-notch holder device designed to hold up to 50 furnaces and situated on a hot plate. Evaporation of successive injections at ~80 °C was typically continued until 1.0 mL of sample had been delivered. Preparation of approximately 40–50 sample furnaces in this manner required about 2 h. Following such preparation, sample furnaces were stored sealed in individual plastic vials until analyzed.

For analysis, the furnaces were individually inserted into the work head of the atomizer and run through the atomization cycle under conditions stipulated in Table I. The individual response characteristic of each furnace was subsequently determined by injection and analysis of a series of standard solutions. This approach compensated for slight differences between furnaces and/or furnace alignment in the optical path.

RESULTS AND DISCUSSION

Sample Storage. The very low silver content of natural precipitation samples requires the use of containers that neither contribute a silver blank nor adsorb silver from aqueous solution at the typical 10^{-5} μg/mL level. The silver concentrations of small quantities of 3 M HNO_3, 0.03 M HNO_3, and distilled-deionized water were monitored for ten days during storage at room temperature in new acid washed polyethylene bottles. No increases were observed in the $<2.0 \times 10^{-6}$ μg/mL silver blank levels. Similar tests were performed on several brands of plastic bags. One brand (Baggies) showed no evidence of a silver blank and was selected for use in snow collection and analytical work.

Strumpler (7) has reviewed the problem of container wall adsorption of ions in aqueous solution. His report indicates good stability for low silver concentrations (5×10^{-4} μg/mL) stored in polyethylene containers at room temperature with HNO_3 at a pH of 2. In tests performed in this laboratory, silver concentrations (3×10^{-5} g/mL and 9×10^{-5} g/mL) were monitored during storage at pH 1.5 (0.03 M HNO_3) in polyethylene containers at room temperature. No measurable loss of silver occurred during the first ten days. However, at termination of the experiment (28 days), concentrations had decreased about 15%. Another series of tests showed no silver adsorption by the plastic bags from acidified (pH 1.5) or neutral aqueous silver solutions after 12-h storage at room temperature.

In other reports (8, 9), water samples were frozen to provide additional stability at low concentrations of solute ions. The present studies indicated that considerable "fractionation" of dissolved impurities occurred when acidified (pH 1.5), low concentration, silver solutions were frozen and stored at −20 °C. After several weeks of such storage, it was noted that a few milliliters of liquid remained unfrozen. The unfrozen liquid was highly acidic and analysis showed very high silver concentrations indicating that the unfrozen liquid contained most of the silver present in the sample. It is inferred from this that freezing preserves such silver solutions by confining the Ag ions to highly localized and acidic zones rather than by immobilization of individual ions. Moreover, the entire sample must be melted to reconstitute a solution representative of the original concentration.

Table II. Results of Rainwater Storage Check Experiment

storage time, days	Ag concentration ± std dev[a] (μg/mL × 10^5) for sample numbers			
	A	B	C	D
0	1.4 ± 0.3	2.9 ± 0.5	4.4 ± 0.5	8.7 ± 0.5
155	1.0 ± 0.3	2.7 ± 0.6	4.9 ± 0.5	9.6 ± 1.2
225	1.3 ± 0.1	2.8 ± 0.3	[b]	8.0 ± 0.6
230	1.1 ± 0.2	2.6 ± 0.3	3.4 ± 0.5	8.2 ± 0.9

[a] Determined by three replicate measurements. [b] Not determined.

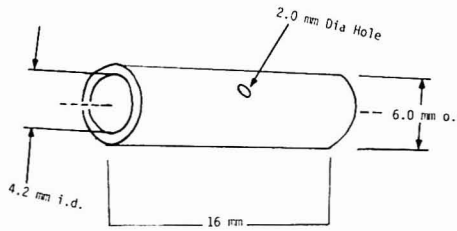

Figure 1. Dimensions of tube furnace used

To check the general validity of the storage procedures used, four rainfall samples, acidified to pH 1.5, were analyzed within 24 h of collection, and then stored frozen at −20 °C. At intervals, each was removed, completely thawed, sampled, analyzed, and returned to the freezer. The results summarized in Table II indicate that statistically significant reductions in the measured silver concentrations were not observed after several months of storage. Since the procedure used involved successive freezing and thawing, the data also indicate that losses of silver due to these processes are negligible. In view of the above results, it was inferred that the storage of snow samples in the frozen state should also be valid. A few partially thawed and refrozen snow samples were received. These samples were acidified, melted completely, and thoroughly mixed in the collection bag before a portion was removed for analysis. The data in Table II also indicate that the analytical precision is typically better than ±20% of the amount present and tends to improve at higher concentrations.

Development of the Method. Attempts to preconcentrate silver by the dithizone solvent extraction method (4) were met with many problems. A rather high and persistent silver blank level (1.5×10^{-4} μg/mL) in the chelating solution (10^{-4} M prepurified dithizone in CCl_4) resulted in a net transfer of silver from the organic phase for most precipitation samples. As a result, nonlinear and often irreproducible extraction efficiencies were observed for the range of silver concentrations of interest. Silver levels in the extracts also tended to be unstable with concentrations decreasing to 50% or less within 1 h. Also, satisfactory cleaning of the extraction equipment required extensive soaking and rinsing with hot concentrated nitric acid. The method was consequently abandoned and emphasis placed on the development of procedures requiring use of minimal reagents to avoid such problems.

Development of the enlarged furnace (Figure 1) was based on the need for a unit with a larger sample volume. The dimensions selected were also influenced by an evaluation of the effect of tube length on the analytical response. It was noted that the silver absorbance per unit concentration increased with increasing tube length, attained a maximum at 15–17 mm length, and dropped off for longer tubes. The absorbance increases observed may be attributed to the combined increases in optical path and residence time therein. Measurements with an optical pyrometer indicated that

Table III. Summary Results of the Collaborative Test Program

sample no.	Ag concn[a] added	analysis results for lab no. indicated: 1[b] concn[a]	1[b] percent recovery[e]	2[c] concn[a]	2[c] percent recovery[e]	3[d] concn[a]	3[d] percent recovery[e]	present work concn[a]	present work percent recovery[e]
1	0	60	...	<10	...	3	...	6 ± 3	...
	8	40	...	14	>50	8	63	8 ± 3	25
2	0	150	...	<10	...	4	...	6 ± 1	...
	24	<30	...	29	>79	26 ± 3	92	28 ± 5	92
3	0	80	...	<10	...	3	...	5 ± 1	...
	40	70	...	20	>25	39 ± 7	98	49 ± 4	110
4	0	50	...	<10	...	<3	...	7 ± 1	...
	80	120	88	97	>108	93 ± 4	112	96 ± 13	111

[a] All silver concentrations are given in $\mu g/mL \times 10^6$; where given, ± values refer to standard deviations for 2 or 3 replicate analyses. [b] Lab cites detection limit of 3×10^{-5} $\mu g/mL$; preconcentration by cation exchange method (*5*) used. [c] Lab cites a detection limit of 1×10^{-5} $\mu g/mL$. Preconcentration by evaporation used. [d] Lab cites a detection limit of 3×10^{-6} $\mu g/mL$. Preconcentation by evaporation used. [e] Percent recovery = 100 (concn in spiked sample − residual concn)/spike concn.

furnace surface temperatures in excess of ~1700 K were required to maximize absorbance. This agrees well with the results reported by Woodriff et al. (*4*). The dropoff in absorbance with tube lengths greater than ~17 mm was due largely to the inability to uniformly heat these to this temperature level in less than 10 s. Heating for longer periods caused rapid decay of the furnaces.

These larger furnaces permitted the delivery of larger sample volumes for the multiple evaporation steps required. Although the successive evaporations could be carried out in the FAAS unit itself, the use of a hot plate allowed the more economical processing of numerous samples simultaneously. The furnaces used are also sufficiently large to permit convenient mounting in the atomization work head without serious disruption of instrument alignment.

After using particular furnaces for a few analyses, it was noted that their interiors were deteriorated sufficiently that samples wet the surfaces unevenly with concomitant losses in measurement precision. Treatment of the furnaces with paraffin as described above effectively alleviated this problem without contributing to the silver blank. Similarly, the introduction of methane in the sheath gas during the ashing and atomization steps as a means of pyrolyzing the tube surfaces also extended their useful life. Thus, each furnace could be used for 15–20 or more analyses.

Studies indicated that repetitive injections to obtain large volumes (1.0 mL) using low concentration silver standards produced absorption responses equivalent to those obtained when equivalent amounts of silver were injected in a single small volume (5 μL) at concentrations 200 times higher. Since the injection volume did not significantly affect the response for an absolute amount of silver, sample absorbance signals were calibrated by injection of smaller volumes of standards covering the appropriate silver mass ranges. Variations in alignment, furnace condition, and support electrode contact necessitated calibration of each furnace for each sample run. This was usually done by bracketting the Ag mass in the sample with standards. As noted above, triplicate sample analyses involving the entire procedure were typically reproducible to ±20% at the 1×10^{-5} $\mu g/mL$ level and improved to ±10% at ten times that level. This compares favorably with an average relative standard deviation of 40% reported by Woodriff et al. (*4*). The detection limits attainable were largely determined by reagent blanks; these were typically less than 1×10^{-6} $\mu g/mL$.

Validation of the Method. To demonstrate the integrity of the method, a limited collaborative study was carried out. Four rainfall samples, preserved as stipulated above, were divided into aliquots and known concentrations of silver were added to one aliquot from each sample. Portions of these eight samples were sent to three other laboratories involved in the determination of silver in precipitation. Each laboratory was also provided with a concentrated silver standard (10^4 $\mu g/mL$ in 3 M HNO_3) and instructed to utilize this in the preparation of standards for the check analyses. Each laboratory used FAAS as the quantitation technique but Lab 1 relied on preconcentration by cation exchange prior to analysis (*5*). The results summarized in Table III indicate that the laboratory relying on chemical preconcentration consistently reported anomalously high results suggesting a contamination problem. The method used by Lab 2 lacked adequate sensitivity; their results were reasonable but somewhat inconsistent. The results of Lab 3 and the present work agree quite well and demonstrate reasonable accuracies as indicated by the recoveries. Although these data are limited, they definitely imply that the present method provides a general means for determination of Ag at the concentration levels required. They are also partially indicative of the problems encountered when chemical preconcentration procedures are used. As indicated above, such usage is probably best avoided for Ag analyses.

Application of the Method. The determination of silver in precipitation was for the general purpose of assessing the extended area cloud seeding effects. Rainfall samples from convective thundershower systems were collected during the summers of 1973–74 in the plains area 30–100 km downwind of the National Hail Research Experiment (*10*) cloud seeding area near Sterling, Colo. The sporadic nature of summer rain showers, coupled with the limited attention that cooperative observers could provide, resulted in sample bottles sometimes being left unattended for several days or more prior to or following rainfall. Consequently, many of the samples contained appreciable quantities of dust, plant material, and insects; all of these can serve as significant sources of Ag. The rainfall analysis results thus showed considerable variation in silver concentration. The concentrations in the seed and no-seed samples proved to be statistically equivalent.

Snow samples were collected during the winters of 1974–75 and 1975–76 in an area near the Palmer Lake Divide between Denver and Colorado Springs. This area is 90–395 km downwind of orographic cloud seeding experiments near Climax and Wolf Creek Pass, Colo. (*2*). The snow samples were of consistently high quality; an occasional pine needle or small amount of dust were the only visible impurities. These impurities were easily separated from the snow by manual means. The comparatively better sample quality was the result of several factors determined by the snow cover and temperature regimes, i.e., minimal dust contamination, no insects, and closer attention by cooperative observers.

The analysis results for each storm group were averaged to obtain a single datum per storm (*11*). Samples which contained snowfall from two or more storms were rejected from the data set. The resulting data set was subdivided in seeded and nonseeded subsets of 14 and 43 averaged measurements, respectively. Seeded samples were those collected when substantial seeding occurred in conjunction with favorable winds for transport of seeding material to the sampling area.

Evaluation of each data subset via the Half-Normal Method described by Daniel (*12*) indicated that both fit a log-normal (Geometric) rather than a normal distribution. Evaluation for the presence of outliers resulted in the rejection of 1 and 5 inordinately high values from the seeded and nonseeded subsets, respectively, at the 95% confidence level. The remaining data in these subsets of 13 and 38 average measurements were also shown to fit a log-normal rather than a normal distribution. This is consistent with the stochastic behavior of trace substances in natural systems as pointed out by Rustagi (*13*) and Ahrens (*14*). The geometric mean and standard deviation of the seeded subset were determined to be $1.7 \times 10^{-5} \pm 0.3 \times 10^{-5}$ μg Ag/mL; the values for the nonseeded subset were $7.8 \times 10^{-6} \pm 2.4 \times 10^{-6}$ Ag/mL. The difference between these means was determined to be significant at the 95% confidence level. This effectively indicates that seedling resulted in a mean increase in the silver content of the snowfall by approximately a factor of 2 as previously noted by Warburton (*3*). In this context, the results suggest the occurrence of extended area seeding effects at distances approximating 100 km or more when meteorological conditions are favorable. This is supported by the analysis of the silver data and the associated meteorology presented by Mulvey and Sheaffer (*11*).

The accurate determination of Ag at these concentration levels is more than a trivial problem. Results obtained in the present study have indicated that precautions must be taken to avoid contamination. The presence of appreciable amounts of Ag in many reagents and the difficulty of purifying these further argues for the use of a minimal reagent approach such as that adopted herein. The accumulation of the majority of the Ag and the acid preservative in the portion of an aqueous sample which does not freeze at −20 °C emphasizes the necessity of completely thawing such samples in order to obtain a representative sample of the original for analysis. Finally, the analysis of rainfall for the present purpose must be based on the utilization of a sample collection system which remains closed until precipitation starts and closes soon after it ends. Otherwise, contamination by fugitive dust and insects will render the data highly suspect.

LITERATURE CITED

(1) L. O. Grant and A. M. Kahan, "Weather Modification for Augmenting Orographic Precipitation"; J. Simpson and A. S. Dennis, "Cumulus Clouds and their Modification", in "Weather and Climate Modification", W. N. Hess, Ed., John Wiley and Sons, New York, N.Y., 1974.
(2) E. Bollay Associates, Final Report, Bureau of Reclamation Contract No. 14-06-D-5573, 20 pp, 1965.
(3) J. A. Warburton, Proceedings of International Conference on Weather Modification, Canberra, Australia, 1971, p 185.
(4) R. Woodriff, R. B. Culver, D. Schrader, and A. B. Super, *Anal. Chem.*, **45**, 230 (1973).
(5) J. A. Warburton, and L. G. Young, *Anal. Chem.*, **44**, 2043 (1972).
(6) D. A. Segar, Department of Commerce, NOAA Laboratories, Miami, Fla., personal communication, 1976.
(7) A. W. Strumpler, *Anal. Chem.*, **45**, 2251 (1973).
(8) A. W. Strumpler, *Atmos. Environ.*, **10**, 33 (1975).
(9) J. Wisnuski, Proceedings of the Fourth Conference on Weather Modification, 516 (1974).
(10) J. E. Dye, C. Knight, and T. W. Cannon, Proceedings of the Fourth Conference on Weather Modification, Fort Lauderdale, Fla., 1974.
(11) G. Mulvey and J. D. Sheaffer, submitted to *J. Appl. Meteorol.*
(12) Cuthbert Daniel, *Technometrics*, **1**, 311 (1959).
(13) J. S. Rustagi, *Arch. Environ. Health*, **8**, 68 (1964).
(14) L. A. Ahrens, *Geochim. Cosmochim. Acta*, **5**, 49 (1954).

RECEIVED for review March 30, 1978. Accepted May 12, 1978.

Chemiluminescence Fiber Optic Probe for Hydrogen Peroxide Based on the Luminol Reaction

Thompson M. Freeman and W. Rudolf Seitz*

Department of Chemistry, University of New Hamsphire, Durham, New Hampshire 03824

A chemiluminescence (CL) fiber optic probe for hydrogen peroxide based on the luminol reaction has been constructed by immobilizing peroxidase in a polyacrylamide gel on the end of a fiber optic. When the probe is immersed in a solution of peroxide in the presence of excess luminol, CL is generated as peroxide diffuses into the peroxidase phase. The fiber optic transmits CL to a detector. The theory of CL fiber optic probes has been developed assuming a first-order reaction in the enzyme phase. However, the peroxide probe shows response which is second order in peroxide. The detection limit is close to 10^{-6} M peroxide. The time required to reach steady state varies with peroxide concentration. At 10^{-5} M H_2O_2, steady state is reached in about 4 s. Under the conditions usually employed, the CL intensity is limited by the rate of mass transfer from solution to the surface of the enzyme phase rather than by the activity of the peroxidase.

In this paper we report a new approach to using immobilized enzymes for analytical purposes, the chemiluminescence (CL) fiber optic probe. This approach is applicable to any enzyme-catalyzed process that leads to the production of light. The enzyme catalyst is immobilized on the surface of a fiber optic. When the fiber optic is immersed in a solution of substrate, light will be generated as substrate diffuses into the immobilized enzyme phase. This light is transmitted through the fiber optic to a photomultiplier tube. The light level will reach a steady state when the rate at which substrate diffuses into the enzyme phase equals the rate at which substrate reacts in the enzyme phase. If the light-producing reaction is first order in substrate, then steady-state CL will be proportional to substrate concentration.

CL fiber optic probes offer several potential advantages for chemical analysis. By immobilizing the enzyme catalyst, it is possible to reuse the enzyme many times. Often immobilization leads to an increase in enzyme stability. The advantages of immobilization have been well documented and have led to considerable work to develop analytical methods utilizing immobilized enzymes (*1–3*). The main advantages of CL methods are low detection limits and wide linear dynamic ranges with simple instrumentation (*4, 5*). It should

0003-2700/78/0350-1242$01.00/0

be pointed out that CL fiber optic probes are only one of several possible analytical configurations involving CL catalyzed by immobilized enzymes. For instance, immobilized enzymes can also be used as sensors in flow systems by having the analyte flow over the immobilized phase which is positioned opposite a light detector. An example of this has been reported by Hornby (6). Also, an ATP assay has been developed by injecting sample into a solution containing firefly luciferase immobilized on a glass rod (7).

The CL fiber optic probe is similar in many ways to enzyme electrodes. Both involve a thin layer of enzyme over the surface of a sensor. However, there are several important differences. The enzyme electrode requires not only that substrate diffuse into the enzyme phase but also that product diffuse to the surface of the electrode. The time required to reach steady state depends on the thickness of the enzyme layer. In the CL fiber optic probe, the reaction of substrate is detected directly via the light generated, and there is no need for product to diffuse to the surface of the fiber optic. As a result, response time is independent of the thickness of the enzyme layer, and it is not necessary to prepare a thin layer of enzyme. It is, however, necessary to use an immobilized phase which is transparent to the CL emitted. This limits the number of possible enzyme phases suitable for CL fiber optic probes.

The system chosen for this study was the luminol reaction catalyzed by peroxidase.

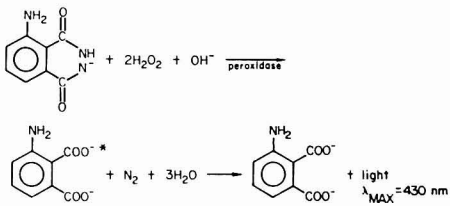

If luminol is in excess, the CL intensity will reflect the amount of peroxide. This system was chosen because peroxidase is inexpensive and available with high specific activity. Also, the authors have previous experience working with luminol and coupling enzymatic processes to the formation of hydrogen peroxide (8, 9). However, it should be emphasized that the advantages of the CL fiber optic probe approach will be more significant for some of the bioluminescence reactions, particularly the firefly reaction used to determine adenosine triphosphate (10) and bacterial bioluminescence used to determine NADH (11). For both these reactions, enzyme cost, availability, and stability are important considerations which have limited analytical usage.

THEORY

The intensity observed using a CL fiber optic probe is proportional to the number of molecules reacting per unit time in the enzyme phase. Because this differs from other enzyme probes, a brief theoretical treatment relating the observed signal to enzyme activity in the immobilized phase will be presented. Initially, it will be assumed that mass transfer in solution is efficient enough so that the concentration of substrate at the surface of the enzyme phase equals the substrate concentration in the bulk of the solution. In practice, the solution is stirred so that mass transfer in solution should be considerably more efficient than mass transfer in the enzyme phase, which occurs by diffusion; however, if the activity of the immobilized enzyme is high enough, the substrate may be reacted at the surface rapidly enough to cause significant concentration depletion at the surface. It is also assumed that the enzyme-catalyzed reaction follows

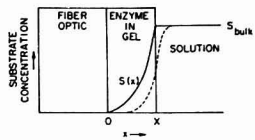

Figure 1. Model of CL fiber optic probe. The substrate concentration profile assuming mass transfer to the probe surface is fast enough to be neglected is designated by the smooth line. The dotted line shows the profile if the reaction at the surface of the probe is rapid enough to deplete the surface concentration of substrate

Michaelis–Menten kinetics and that the substrate concentration is much smaller than K_m, the Michaelis constant. In this case, the rate of the enzyme-catalyzed reaction is proportional to substrate concentration.

The model of the system is illustrated in Figure 1. At steady state, i.e., when the rate of substrate entering the enzyme phase equals the rate at which substrate reacts, the distribution of substrate within the enzyme phase is given by the following equation (12):

$$S(x) = S_{bulk} \frac{\cosh \sqrt{\frac{V_{max}}{K_m \bar{D}_s}}\, x}{\cosh \sqrt{\frac{V_{max}}{K_m \bar{D}_s}}\, X} \quad (1)$$

The terms in Equation 1 are defined as follows: $S(x)$ = substrate concentration at position x in the enzyme phase (mol/L); S_{bulk} = substrate concentration in bulk solution (mol/L); X = membrane thickness (cm); V_{max} = rate of substrate conversion in the gel under conditions of excess substrate (mol/L-s); K_m = Michaelis constant (mol/L); $\bar{D}_s$ = diffusion coefficient for substrate in gel (cm²/s).

What we are actually interested in is the number of moles reacting per unit time V. For Michaelis–Menten kinetics with $[S] << K_m$, where $[S]$ = substrate concentration

$$R = \frac{V_{max}}{K_m}[S]V \quad (2)$$

where R is the rate of the reaction (mol/L-s). V is obtained by replacing $[S]$ with the effective amount of S. For the gel, the effective amount of $[S]$ is the surface area of the gel times the integral of $S(x)$ from 0 to X:

$$V = \frac{V_{max}}{K_m} A \int_0^X S(x)\, dx \quad (3)$$

Substituting Equation 1 into Equation 3

$$V = \frac{V_{max}}{K_m} A \int_0^X S_{bulk} \frac{\cosh \sqrt{\frac{V_{max}}{K_m \bar{D}_s}}\, x}{\cosh \sqrt{\frac{V_{max}}{K_m \bar{D}_s}}\, X} dx \quad (4)$$

Rearranging

$$V = \frac{V_{max}}{K_m} A S_{bulk} \frac{1}{\cosh \sqrt{\frac{V_{max}}{K_m D_s}}\, X} \int_0^X \cosh \sqrt{\frac{V_{max}}{K_m \bar{D}_s}}\, x\, dx \quad (5)$$

Evaluating the integral yields

$$V = \frac{V_{max}}{K_m} AS_{bulk} \frac{\sinh\sqrt{\frac{V_{max}}{K_m \bar{D}_s}}\, X}{\cosh\sqrt{\frac{V_{max}}{K_m \bar{D}_s}}\, X} \cdot \frac{1}{\sqrt{\frac{V_{max}}{K_m \bar{D}_s}}} \quad (6)$$

which can be rearranged to

$$V = \sqrt{\frac{V_{max} \bar{D}_s}{K_m}}\, AS_{bulk} \frac{\sinh\sqrt{\frac{V_{max}}{K_m \bar{D}_s}}\, X}{\cosh\sqrt{\frac{V_{max}}{K_m D_s}}\, X} X \quad (7)$$

For large values of $\sqrt{(V_{max}/K_m D_s)}\, X > 2$ assuming diffusion coefficients are equal in solution and in the gel, the sinh and cosh terms are essentially equal, and drop out of the equation. This corresponds physically to the situation where essentially all the substrate is reacted before it has a chance to diffuse to the opposite end, i.e., the sensor end of the enzyme layer.

The CL intensity will be proportional to the rate of the reaction:

$$I_{CL}\left(\frac{\text{photons}}{\text{second}}\right) = \phi_{CL}\left(\frac{\text{photons emitted}}{\text{molecule reacting}}\right)\phi_{det}\left(\frac{\text{photons detected}}{\text{photons emitted}}\right) V\left(\frac{\text{molecules reacting}}{\text{second}}\right) \quad (8)$$

where ϕ_{CL} is the chemiluminescence efficiency and ϕ_{det} is the detection efficiency. From these equations, it is possible to estimate the photon flux for a given set of conditions.

As expected I_{CL} is proportional to the bulk substrate concentration. The most interesting aspect of these equations is the fact that the intensity is proportional to the square root of the enzyme activity. Thus variations in activity will affect CL intensity but not to the extent that they would in solution.

If the enzyme phase is very active, the substrate may react so rapidly that there will be significant depletion of substrate at the surface of the enzyme phase. In this case we need to define a new variable, $S_{surface}$, the surface concentration of substrate. If the solution is stirred, then it is possible to apply the Nernst diffusion layer concept, commonly employed in electrochemical theory for stirred solutions. The equation is:

$$V' = \frac{AD_s(S_{bulk} - S_{surface})}{\delta} \quad (9)$$

where V' is the number of moles reaching the surface per second, $S_{surface}$ is the surface concentration of substrate, and δ is the thickness of the Nernst diffusion layer.

Equation 7 must now be modified so that the S_{bulk} term is replaced by $S_{surface}$. At steady state, the number of moles reaching the enzyme phase per unit time will equal the number of moles reacting in the enzyme per unit time, i.e., $V = V'$. By rearranging Equation 7 using $S_{surface}$ in place of S_{bulk} and assuming the sinh and cosh terms are equal, we get an expression for $S_{surface}$:

$$S_{surface} = \frac{V}{\sqrt{\frac{V_{max} \bar{D}_s}{K_m}}\, A} \quad (10)$$

By plugging into Equation 9, solving for V, and rearranging, one gets:

$$V = \frac{\sqrt{\frac{V_{max} \bar{D}_s}{K_m}} \cdot A(D_s/\delta) S_{bulk}}{\sqrt{\frac{V_{max} \bar{D}_s}{K_m}} + \frac{D_s}{\delta}} \quad (11)$$

The relative magnitude of the two terms in the denominator reflects the relative rates of mass transfer to the enzyme surface and reaction in the enzyme phase. If D_s/δ is large, Equation 11 reduces to Equation 7. On the other hand if $\sqrt{V_{max} D_s/K_m}$ is much larger than D_s/δ, then mass transfer to the enzyme surface determines steady-state intensity. In this case, the observed signal will be independent of enzyme activity but will depend on the value of δ which is a function of the manner in which the solution is stirred.

EXPERIMENTAL

Preparation of Enzyme Phase. Two procedures were used to prepare the immobilized enzyme phase. For some experiments, a weighed amount of horseradish peroxidase (Sigma Type I, EC 1.11.1.7, specific activity approximately 1080 units/mg at 25 °C was dissolved in 0.1 M KOH–H_3BO_3 buffer along with luminol (Aldrich). The buffer pH and luminol concentration were chosen to be the same as in the peroxide solution to be analyzed, typically pH 9 and 10^{-3} M. This solution served as the enzyme phase and was separated from the solution phase by a dialysis membrane (average pore radius, 24 Å).

Most experiments involved peroxidase immobilized by physical entrapment in a polyacrylamide gel. The procedure for preparing the gel was adapted from a literature method reported to give a clear gel (*13*). The gel was formed from a solution of 50 mL of either 0.1 M KOH–H_3BO_3 buffer or 0.1 M phosphate buffer containing luminol, 0.12 g *N,N*-methylenebis(acrylamide) (Aldrich), and 2.38 g acrylamide (Aldrich). The buffer pH and luminol concentrations were chosen to be the same as those in the peroxide solution, typically pH 9 and 10^{-3} M luminol. The solution was filtered to remove undissolved solids. Enzyme gels were prepared by adding a weighed amount of peroxidase to the acrylamide buffer–luminol solution. Approximately 1 mg/mL of both riboflavin and potassium persulfate were added to photosensitive polymerization. Polymerization was carried out in a water-saturated nitrogen environment by irradiating with a mercury lamp until a solid gel formed. The thickness of the gel was 1 mm. Response is independent of gel thickness so this is not an important variable. The gel layer appeared to be uniform.

Peroxide solutions were prepared by dilution of 30% H_2O_2 in 0.1 M KOH–H_3BO_3 or 0.1 M phosphate buffer and luminol. All solutions contained 0.5 g/L EDTA to tie up any trace metals that might otherwise catalyze luminol CL in the solution producing a background signal.

Apparatus. A diagram of the apparatus is shown in Figure 2. Ten mL of sample are added to a 15-mL beaker on a magnetic stirrer. To keep the beaker position and stirring constant, a piece of cardboard was taped onto the stirrer, and a hole was cut to just fit the beaker. Also, the beaker was glued into position on the stirrer and emptied by drawing solution out with a syringe.

The polyacrylamide gel containing peroxidase was held on the end of a fiber optic by a piece of Nylon mesh from a stocking. The Nylon mesh was held between two 0.5-inch long concentric pieces of Tygon tubing which slipfitted onto the fiber optic. In some experiments, a dialysis membrane was placed between the gel and the Nylon mesh. When using a peroxidase solution as the enzyme phase, a dialysis membrane sandwiched between two pieces of Nylon mesh was fitted between the two concentric pieces of Tygon.

The fiber optic was 2 feet long with a $^1/_8$-inch diameter (Corning, numerical aperture, 0.63, acceptance angle 39°, transmittance 0.63 at 500 nm). A light-tight shield was placed around the enzyme end of the optic to exclude ambient light. The other end of the fiber optic was placed in front of a 9558 QA

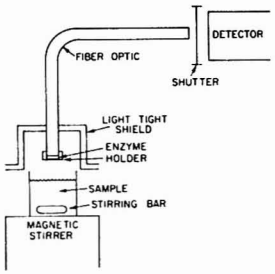

Figure 2. Diagram of apparatus comprising CL fiber optic probe

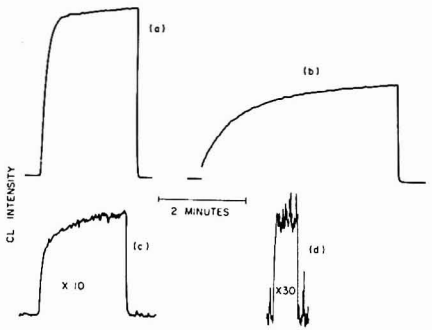

Figure 3. Typical data showing CL intensity vs. time for various conditions: (a) pH 9, 10^{-3} M luminol, 10^{-4} M H_2O_2; (b) pH 10, 10^{-3} M luminol, 10^{-4} M H_2O_2; (c) pH 8, 10^{-3} M luminol, 10^{-4} M H_2O_2, and (d) pH 9, 10^{-3} M luminol, 10^{-5} M H_2O_2. All data for a polyacrylamide gel containing 1 mg/mL horseradish peroxidase

photomultiplier, S20 response, operated at 1800 volts from a Fluke 412B high voltage power supply. Light intensity as a function of time was recorded on a Heath SR-255A/B stripchart recorder. A shutter was interposed between the end of the fiber optic and the detector to protect the photomultiplier from excess light when the enzyme end of the fiber optic was removed from solution. The shutter was opened immediately after inserting the probe into solution. In some experiments, the photomultiplier was cooled with dry ice to reduce dark current.

Procedures. Measurements of CL intensity vs. peroxide concentration were done by making standard additions of peroxide to a 10-mL solution of buffer and luminol. In experiments observing the effect of pH or luminol concentration on CL intensity, separate gels were prepared for each measurement. Each gel was prepared in the presence of the pH and luminol concentration of the planned measurement.

A crude qualitative study of the effect of temperature on the probe was done by cooling the probe and solutions with an ice bath measuring the solution temperature just before the fiber optic was inserted in the solution.

RESULTS AND DISCUSSION

Effect of pH and Luminol Concentration. The most important variable influencing the peroxide CL fiber optic probe is pH. It is necessary to compromise between the optimum pH for peroxidase activity and the optimum pH for maximum CL intensity from luminol (*10, 11*). The problem is illustrated by typical data for 10^{-4} M peroxide at pH's 8, 9, and 10 shown in Figure 3. At pH 8, the CL intensity reaches steady state within a few seconds, reflecting high peroxidase activity; however, sensitivity is low because the CL efficiency of luminol is low at this pH. At pH 10, on the other hand, sensitivity is good but peroxidase activity is low. As a consequence, peroxide diffuses further into the gel before it is completely reacted, and it takes much longer to reach steady state. The best compromise is to work at a pH where steady state is still reached in about 30 s and sensitivity is still satisfactory.

Table I. Relative CL Intensity from 10^{-4} M H_2O_2 at Different pH's and Luminol Concentrations[a]

	luminol, M		
pH	10^{-2}	10^{-3}	10^{-4}
8	0.003	0.089	...
9	0.88	0.99	0.56
10	1.00	0.72	0.10

[a] All values are normalized relative to the intensity for 10^{-2} M luminol at pH 10.

Luminol concentration is another important variable. The effects of luminol concentration and pH are summarized in Table I. The optimum conditions are 10^{-3} M luminol at pH 9.

Since both pH and luminol concentration affect CL intensity, it was decided that all enzyme gels should be prepared at the same pH and luminol concentration as planned for the solution. Otherwise there would be concentration gradients across the gel, and sensitivity would tend to change with time until concentrations in the two phases equalized. In fact the gradual increase in intensity with time for 10^{-4} M hydrogen peroxide at both pH 8 and 9 is attributed to luminol depletion in the zone where the reaction takes place.

Figure 3 also shows typical data for 10^{-5} M H_2O_2 at pH 9 and 10^{-3} M luminol. At lower peroxide concentrations, the response time is much faster, approximately 3 s to reach steady state. Also, there is no gradual increase in intensity since the amount of peroxide is too small to cause significant luminol depletion.

Precision and the Effect of Stirring. Steady-state CL intensity increases as the rate of stirring increases. Because of this, measures were taken to keep the beaker in the same position on the magnetic stirrer at all times. However, precision was still limited by variations in stirring. The variation between replicate measurements on the same solution was typically on the order of 10% RSD.

Another measure that was attempted to reduce the effect of stirring was to interpose dialysis membrane between the gel and solution. In one experiment using the same gel, the presence of a dialysis membrane caused the signal from 10^{-4} M H_2O_2 to decrease by a factor of 0.62. The precision improved from 9% to 5% RSD, and there was an increase in response time.

The dependence of steady-state CL intensity on stirring indicates that the rate of mass transfer to the surface of the enzyme phase does influence response. The peroxide is reacting so rapidly in the enzyme phase that there is significant substrate depletion at the surface of the enzyme phase.

Effect of Temperature. A rather crude experiment cooling the probe and solution to 0 °C, did not cause an observable change in steady-state CL intensity or in response time. Since enzyme activity would vary significantly with temperature, this also indicates that mass transfer to the surface of the enzyme phase is the primary factor affecting steady-state CL.

Effect of Enzyme Level. As would be expected for a mass transfer controlled system, steady-state CL and the time required to reach steady state were independent of the amount of peroxidase in the enzyme phase for levels from 0.5 mg/mL to 3 mg/mL. For 0.1 mg/mL enzyme, there was a slight decrease in steady-state CL intensity but the time required to reach steady state increased from 30 to 120 s. At these

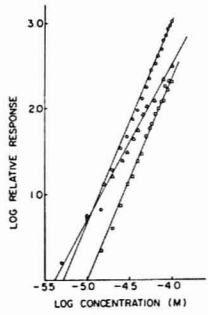

Figure 4. Log CL Intensity vs. log peroxide concentration for three probes: (O) 1 mg/mL horseradish peroxidase in a polyacrylamide gel, (□) 1 mg/mL horseradish peroxidase in solution, and (Δ) 0.1 mg/mL horseradish peroxidase in a polyacrylamide gel

reduced levels of enzyme, apparently surface depletion of peroxide is less, and enzyme activity is a significant factor in determining response time.

Response to Peroxide Concentration. Figure 4 shows log intensity vs. log concentration hydrogen peroxide for 1 mg/mL and 0.1 mg/mL enzyme in polyacrylamide gel and for enzyme in solution separated from the peroxide solution by dialysis membrane. The slope of the log-log plot for the 1 mg/mL enzyme in the gel is 2.3 and 2.35 for the enzyme solution, considerably greater than first order. This came as a surprise. Since the intensity of luminol CL is linearly proportional to hydrogen peroxide concentration with a variety of other catalysts and cooxidants (*14*, *15*) first-order response was also expected with peroxidase. However, the peroxidase–luminol reaction has been studied and found to involve two peroxides per photon emitted (*16*). Thus, second-order kinetics in peroxide under conditions where peroxide is in much smaller concentrations than other reagents is not unreasonable.

The fact that observed response is somewhat greater than second order is at least qualitatively consistent with a system where there is significant substrate depletion at the enzyme surface. Since the process consuming substrate in the enzyme phase is second order in substrate while the mass transfer process supplying substrate to the surface is first order, the extent of surface depletion will be relatively greater at higher substrate concentrations. As a result, the flux to the enzyme surface will be relatively greater at high concentrations and we would expect a response greater than second order. At 0.1 mg/mL peroxidase in a gel, the reaction in the enzyme phase is slower, substrate depletion at the enzyme surface is less, and as would be expected the slope of the calibration is closer to 2.0.

The fact that surface depletion is greater at high peroxide levels may also account for the observation that steady-state response is reached more slowly at higher levels of peroxide.

The log-log plots for the gels are not straight lines. The shape of this curve is reproducible and is observed at both pH 8 and 9 at luminol concentrations from 10^{-4} to 10^{-3} M. The origin of this behavior is not known. For a solution enzyme phase, the plot is considerably straighter. The fact that intensity is greater for the gel than the solution enzyme phase is because there is a Nylon mesh behind the dialysis membrane used to separate the solution enzyme phase from the peroxide solution. This mesh blocks some of the CL from the detector causing a reduction in intensity.

The minimum detectable concentration is 10^{-6} M. There is no background emission so the detection limit depends on the magnitude of the signal relative to the detector noise.

CONCLUSIONS

This paper has demonstrated the possibility of doing a chemiluminescence analysis using immobilized enzymes. The detectability and response time of the CL fiber optic probe are significantly better than observed with enzyme electrodes. The detection limit is not nearly as low as observed using ferricyanide-catalyzed luminol CL (*14*), mainly as a consequence of having to make a compromise between optimum conditions for luminol efficiency and optimum conditions for peroxidase activity.

Using the fiber optic probe is quite convenient. Measurements can be easily made at a rate of more than one per minute, particularly when working at 10^{-5} M H_2O_2. However, with a system like peroxidase–luminol where response is mass transfer limited, precision is poor because it is difficult to maintain reproducible mass transfer. Better precision would be observed in a system designed for more constant mass transfer, e.g., a flow system. It should, however, be pointed out that mass transfer limited systems are desirable in that response is independent of enzyme activity and other variables such as temperature that affect enzyme activity. Also the precision in terms of concentration is better than the precision in terms of peak height because the response is second order.

The peroxide probe based on luminol can potentially be coupled to other enzymatic processes that yield peroxide, e.g., glucose analysis using glucose oxidase. However, the fact that response is greater than first order is not convenient. Since peroxide is a reactant in other CL reactions, we plan to investigate the possibilities of other peroxide probes before attempting to couple to other reactions. We did not further evaluate the analytical properties of our present probe because we expect other systems will give better response to peroxide.

LITERATURE CITED

(1) L. D. Bowers and P. W. Carr, *Anal. Chem.*, **48**, 544A (1976).
(2) H. H. Weetall, *Anal. Chem.*, **46**, 602A (1974).
(3) O. R. Zaborsky, "Immobilized Enzymes", CRC Press, Cleveland, Ohio, 1973.
(4) W. R. Seitz and M. P. Neary, *Anal. Chem.*, **44**, 188A (1974).
(5) W. R. Seitz and M. P. Neary, in "Methods of Biochemical Analysis", D. Glick, Ed., Vol. 23, Interscience, New York, N.Y., 1976, pp 161–189.
(6) W. Hornby, presented at the Summer Symposium on Immobilized Enzymes in Analytical Chemistry, Amherst, Mass., June 1977.
(7) Y. Lee, I. Jablonski, and M. DeLuca, *Anal. Biochem.*, **80**, 496 (1977).
(8) D. C. Williams III, G. F. Huff, and W. R. Seitz, *Clin. Chem. (Winston-Salem, N.C.)*, **22**, 372 (1976).
(9) D. C. Williams and W. R. Seitz, *Anal. Chem.*, **48**, 1478 (1976).
(10) B. L. Strehler, in "Methods of Biochemical Analysis", D. Glick, Ed., Vol. 16, Interscience, New York, N.Y., 1968, pp 99–179.
(11) S. E. Brolin, E. Borglund, L. Tegner, and G. Wettermark, *Anal. Biochem.*, **42**, 124 (1971).
(12) W. J. Blaedel, T. R. Kissel, and R. C. Boguslaski, *Anal. Chem.*, **44**, 2030 (1972).
(13) G. P. Hicks and S. J. Updike, *Anal. Chem.*, **38**, 726 (1966).
(14) D. T. Bostick and D. M. Hercules, *Anal. Chem.*, **47**, 447 (1975).
(15) V. Patrousky, *Talanta*, **23**, 553 (1976).
(16) M. J. Cormier and P. M. Prichard, *J. Biol. Chem.*, **243**, 4706 (1968).

RECEIVED for review January 3, 1978. Accepted May 8, 1978. Work supported by Grant No. 671 from the Central University Research Fund of the University of New Hampshire.

Determination of Trace Amounts of Alkyls and Hydrides by Metastable Transfer Emission Spectrometry

D. G. Sutton,* J. E. Melzer, and G. A. Capelle[1]

Aerophysics Laboratory, The Ivan A. Getting Laboratories, The Aerospace Corporation, El Segundo, California 90245

Experiments in which the newly developed analytical technique, metastable transfer emission spectrometry (MTES), was used indicate that this method can be effectively used to detect and measure small concentrations of metal and semimetal alkyls and hydrides in the gas phase. The molecules trimethylbismuth (TMB) and germane (GeH_4) were used for the prototype systems. However, many other molecules in these two classes can also be detected. Both TMB and GeH_4 have been measured in a flowtube device to concentrations of less than 10^7 molecules/cm^3, or an equivalent detectivity in the sample gas of better than 1 ppb. The flowtube detection device and its application to various problems are discussed. Other classes of compounds that should be detectable with our device are identified.

The recent development (*1*) of the new qualitative and quantitative measurement technique, metastable transfer emission spectrometry (MTES), has made it possible to detect various atomic vapors in a gas flow to concentrations of as low as 10^4 atoms/cm^3. This technique has been adapted, with no increase in experimental complexity, to permit the detection and measurement of many gas-phase molecules. The technique involves the mixing of a flow of sample gas, which contains traces of the molecule to be measured, with active nitrogen (*2*). The active nitrogen breaks apart the molecule and electronically excites one of its constituent atoms, e.g., Bi in the case of trimethylbismuth (TMB). Emission from the atoms is then monitored. The spectrum identifies the atom(s) present, and the intensities (I) of one or more of the emission lines are used as a measurement of the concentration of the emitting species:

$$I = K'(\mathrm{A}) \tag{1a}$$

or

$$I_{\mathrm{Bi}} = K'_{\mathrm{Bi}}(\mathrm{Bi}) \tag{1b}$$

In the case of TMB, K' and K'_{Bi} are constants. If there is no other source of the atom, its concentration is then, within limits, directly proportional to the concentration of the original parent molecule (M) present

$$(\mathrm{A}) = K''(\mathrm{M}) \tag{2}$$

Thus, from Equation 1,

$$I = K(\mathrm{M}) \tag{3a}$$

where $K = K'K''$ is a constant. For TMB,

$$I_{\mathrm{Bi}} = K_{\mathrm{Bi}}(\mathrm{TMB}) \tag{3b}$$

The simple form of this equation has been verified over a large range of concentrations for several alkyls and hydrides. Limitations on the validity of Equation 3 will be discussed subsequently.

[1] Present address, EG&G, Inc., 130 Robin Hill Road, Goleta, Calif. 93017.

EXPERIMENTAL

The experimental setup is shown in Figure 1. The apparatus described in ref. 1 was used with two modifications. The furnace unit of the prior apparatus, which was used for vaporizing solid samples, was replaced by a system for handling gaseous species. In addition, the flowtube section was mounted horizontally and viewed end-on. A different and more accurate calibration method was also employed.

The sample gas, which contains small amounts of a molecule to be measured, is flowed at a known rate through a calibrated orifice, or through a capillary if smaller flows are needed, into the flowtube system. N_2 gas can be added to this sample flow, either before injection into the system or at the injection point by means of the outer coaxial jacket surrounding the sample injector. This N_2 flow is used especially when the sample flows are small, e.g., when the capillary is used, to positively sweep the sample into the reaction zone. Coaxial N_2 flow is initially adjusted to optimize the measured intensity for a given configuration and sample molecule. It is then adjusted as necessary throughout the experiment to compensate for changes in the sample gas flow, i.e., to keep the total flow constant in order to ensure that the mixing dynamics that occur downstream upon injection of the active nitrogen remain reasonably constant. The partial pressure in the flowtube, which is a result of the sample plus N_2 sweeping flow, is a sufficiently accurate diagnostic for adjusting the carrier N_2 flow. This partial pressure is typically about one third of the total flowtube operating pressure. Active nitrogen is also injected into the flow and accounts for the balance of the 2- to 5-Torr flowtube pressure. It is prepared by passing a flow of pure nitrogen gas contained in a 12-mm o.d. quartz tube through a 70-W microwave discharge upstream of the injection point. The discharge is confined to that portion of the 12-mm quartz tube surrounded by a McCarroll type cavity (*3*).

The glow that results in the mixing region and extends downstream is observed photoelectrically (RCA Model 1P28) through a monochromator. Normally, the glow consists primarily of atomic emission, with a weaker background of N_2 emission resulting from the Lewis–Rayleigh afterglow. Significant emission from other molecular species is seen only occasionally. The intensity of one of the atomic lines provides a qualitative measure (Equation 2) of the concentration of the parent molecule from which it was derived, if there are no other sources of that atom in the system and if the active nitrogen concentration remains relatively constant and unperturbed by the sample gas in the observation area. A simple calibration over the concentration range of interest in order to verify Equation 3 is all that is necessary to quantify the measurements for any particular experimental setup and sample gas.

For TMB, calibration consisted of the preparation of a dilute "standard" mixture of 1 part TMB in 10^4 parts of N_2. Further dilution gave irreproducible results. This mixture was then passed through the capillary (the orifice provided too large a flow) at a known rate, and the signal I_{Bi} was measured. The use of the known pumping speed of our system (3.25 L/s) enabled the TMB concentration in the observation area to be calculated. By means of Equation 3b, the calibration was thus effected. When such dilute mixtures and low flows of TMB were used, it was necessary to allow the system sufficient time to reach a steady-state equilibrium point before calibration data were taken. Experimentally we observed that with TMB, 15 min or more were necessary at very low flows. Although the TMB mixtures were made with N_2, such standard mixtures could also be made with other diluent gases, or with multiple trace samples in order to

0003-2700/78/0350-1247$01.00/0

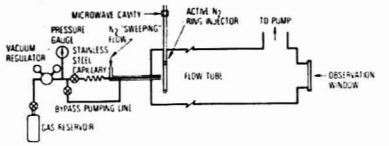

Figure 1. Flowtube device for detection of gas-phase species by MTES

duplicate more accurately the unknown gas that would ultimately be run in the system. The coaxial N_2 sweeping flow could similarly be replaced by other gases. Normally, when true unknowns are run, the trace substances are present in concentrations much smaller than 1:10^4; hence, for maximum sensitivity, the larger flow afforded by the use of the orifice (0.005-cm radius hole) could be used. These larger flows would require no additional sweeping flow; thus, high sensitivity could be obtained with direct atmospheric sampling while maintaining the same system pressure.

RESULTS AND DISCUSSION

When the orifice is used, the flow is controlled by means of the upstream pressure (P_1). If $P_1 < 2P_2$, where P_2 is the downstream (flowtube) pressure, sonic flow conditions exist (*4*) and the flow rate through the orifice is directly proportional to P_1. For flow through the capillary, the flow rate is again controlled by the pressure, but the relation is more complex. Poiseuille flow normally develops (*5*), and the flow rate dN/dt of molecules through the capillary can be given with good accuracy by the expression

$$\frac{dN}{dt} = \frac{\pi a^4 (P_1 + P_2)(P_1 - P_2)}{16\eta k T l}\left(1 + \frac{4\zeta}{a}\right) \qquad (4)$$

where a is the inside radius of the capillary tube, l is its length, P_1 and P_2 are the respective upstream and downstream pressure, η is the viscosity of the gas flowing through the capillary, and

$$\zeta = \frac{2\eta}{P_1 + P_2}\left(\frac{\pi}{2}\frac{kT}{m}\right)^{1/2} \qquad (5)$$

is the slip coefficient. The last term of Equation 4 (in parentheses) is a slip correction factor (*5*), which compensates for the fact that the velocity of the molecules flowing down the narrow tube is not zero at the walls. Reasonably long lengths of stainless-steel capillary tubing of $a = 0.005$ cm are readily available commercially; for these experiments, a relatively short length ($l = 15$ cm) is sufficient.

For convenience, Equation 4 may be rewritten as

$$\frac{dN}{dt} = \frac{\pi a^4}{16\eta k T l} Z \qquad (6)$$

where

$$Z = (P_1 + P_2)(P_1 - P_2)\left[1 + \frac{4\eta}{a(P_1 + P_2)}\right]\left(\frac{2\pi kT}{m}\right)^{1/2} \qquad (7)$$

A steady flow of the sample gas, in this case 1 part TMB in 10^4 parts N_2, was established through the capillary. The flow was then shunted to a known volume at the same pressure (P_2). By the measurement of the time required for a small pressure rise in the known volume, it was possible to determine the flow rate (dN/dt). Measurements were taken for several values of P_1. dN/dt was then plotted vs. $Z(P_1,P_2)$ (Figure 2).

Clearly, a straight line resulted, demonstrating that the dependence of the flow on pressure given by Equation 6 is indeed valid. For this plot, P_1 was varied from 40 to 310 Torr. The initial concentration of the sample species in the flowtube observation zone is calculated from dN/dt and the pumping

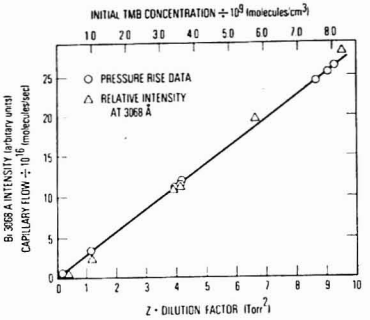

Figure 2. Capillary flow rate and intensity of Bi 3068-Å emission plotted vs. Z and initial TMB concentration

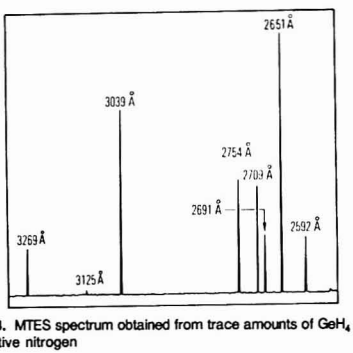

Figure 3. MTES spectrum obtained from trace amounts of GeH_4 mixed with active nitrogen

speed of the flowtube system.

Various flows of the TMB sample through the capillary and into the flowtube were established, and the signal intensity (I) produced by Bi emission at 3068 Å was measured to check the validity (i.e., the simple linearity) of Equation 3. I_{Bi} was plotted vs. Z. The result was again a straight line, as predicted, and, when the intensity scale was normalized at one point to coincide with Figure 2, the lines merged. Thus, at least for TMB, I_{Bi} is indeed proportional to the TMB concentrations, within the limits described previously, and Equation 3 holds. The range of linearity for TMB concentration measurements with our apparatus was from 10^{10} TMB/cm^3 to 10^7 TMB/cm^3. At higher concentrations, the plots showed some curvature, presumably because of active nitrogen depletion. With added difficulty, the measurements could be extended above 10^{10}/cm^3 in the current device by a careful calibration of the nonlinear portion of the curve. Signal-to-noise considerations prevented the measurement of concentrations below 10^7/cm^3. Lower concentrations could probably be measured with an optimized system with respect to f number, spectral slit width, and detector sensitivity. A concentration of 10^7 TMB/cm^3 was detected with a spectral slit width of 16 Å FWHM. The reduction of the slit width to 1.6 Å resulted in poorer detectivity by a factor of 14; the upper limit of 10^{10}/cm^3 remained, of course, unchanged.

Germane (GeH_4), a gas at room temperature, was also studied with the use of the MTES system. Dilutions of up to 2:10^5 of GeH_4 in N_2 were used, and the intensity of the 2651-Å Ge emission line was monitored. A spectrum of the emission that results when active nitrogen is mixed with a gas flow containing trace amounts of GeH_4 is shown in Figure 3.

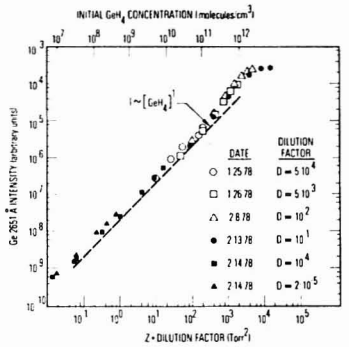

Figure 4. Intensity of Ge 2651-Å emission plotted vs. Z and initial GeH_4 concentration

Note that there is a relatively featureless background, clear of any significant spectral interferences. This featureless background is generally the case when MTES is used. If there are any spectral interferences, they are normally atomic lines resulting from other trace materials present. In a manner similar to that described for TMB, the validity of Equation 3 for GeH_4 was verified. These results are plotted in Figure 4, where a log–log format was used to accommodate the large dynamic range of the detection system. The emission intensity at 2651 Å is proportional to the initial GeH_4 concentration over a range of 5 orders of magnitude. The dashed line in Figure 4 was drawn with a slope of 1 and parallels the loci of data points.

Note that GeH_4 was detected at concentrations below 10^7 GeH_4/cm^3 or with about 0.1 ppb of GeH_4 in the sample gas flow. As before, this was achieved with a 16-Å spectral slit width. The effective upper limit of detection, determined as the highest concentration where the linear relation given by Equation 3 still holds, is approximately 10^{11} GeH_4/cm^3, as can be seen from Figure 4. With most trace molecules, this point was indicated by a bending over of the curve towards the x-axis, resulting from depletion of the active nitrogen. However, an interesting variation was observed with GeH_4. At concentrations between 10^{10} and 10^{11} GeH_4/cm^3, the intensity of the Ge 2651-Å emission line actually increased with the GeH_4 concentration at a rate increasingly faster than linear before finally saturating. Clearly, some secondary reaction was involved, but no specific mechanism is suggested at this time. The onset of saturation was indicated visually by a constriction of the pale yellow Lewis–Rayleigh afterglow and the appearance of new colors.

A number of other substances were put into the MTES system as "trace molecules", primarily to determine if they could be detected by means of the method; minimum and maximum detectable concentrations were not measured. All the materials tested were detected. Among them were AsH_3, PH_3, SiH_4, $Al(CH_3)_3$, $Ga(C_2H_5)_3$, and $Ge(C_2H_5)_4$. With the exception of PH_3, all of these materials yield clean atomic line spectra when added to active N_2. PH_3 and active nitrogen produce the PN $A^1\Sigma \rightarrow X^1\Sigma$ band system.

All of the "trace molecules" investigated thus far in the MTES apparatus exhibit a concentration region wherein the relation between the atomic emission intensity and the molecular concentration is linear, i.e., a region where Equation 3 holds. The exact kinetic sequence that occurs when a trace molecule is mixed with active nitrogen is not presently known; in fact, the reaction mechanism almost certainly differs for different molecular species (*6*, *7*). It appears, however, that the general process involves the stripping down of the molecule to the central atom, probably by successive attacks on the N atoms present in the active nitrogen. Subsequent (one-step) excitation of the stripped atom by bimolecular collision with the $N_2(A^3\Sigma_u^+)$ would then account for the observed fluorescence (*8*, *9*). It is unimportant whether the stripping reaction is first order or a more complex function of the active nitrogen concentration. Since MTES requires that the active nitrogen concentration be essentially constant, the analysis is valid as long as the overall kinetics are linear in the concentration of the sample molecule, which has been the case over a reasonably large concentration range for all molecules investigated thus far. As mentioned previously, however, deviations from linearity (other than simple saturation) have been observed with GeH_4. At high concentrations of sample gas, it is probable that secondary reactions with intermediate products of the stripping process may begin to play an important role. In any case, when working with a new molecule, the linearity expressed in Equation 3 should be verified empirically in the concentration range of interest.

The absolute accuracy achieved on a concentration measurement will depend on many factors, including the nature of the unknown, the background matrix in which it is embedded, spectral interferences, and, of course, the accuracy of the calibration standards. Reproducibility normally will be one of the prime considerations affecting accuracy. Similar flow conditions must be maintained in the device throughout an experiment, including keeping the active nitrogen production rate constant. Gross changes in the flow or composition of the sample and carrier gas must also be avoided, which is especially important if they contain species such as O_2, which can reduce detectivity both by quenching active nitrogen and by reacting with free atoms.

Throughout the experiments with TMB and GeH_4, the results were cross-checked, which included running identical concentrations on different days and comparing results obtained in the same experiment but using two calibration standards that differed in concentration by several orders of magnitude. Within the limits of applicability for the method, as described previously, it has been possible to achieve routinely an accuracy of ±15% (for 80% of the measurements) for all but the smallest concentrations.

CONCLUSIONS

Quantitative detection of a gaseous alkyl (TMB) and a hydride (GeH_4) at 1 ppb or less was demonstrated. Spectra were obtained that indicate that our process will be generally applicable to many molecules belonging to these two classes of compounds. In particular, tetraethyllead probably can be detected at concentrations well below the toxic level. Similar evidence exists in the literature that strongly indicates that a wide variety of metal carbonyls (*10*) and halides (*11*) could be detected and measured directly with our technique.

In a previous publication (*1*), we reported the detection of Bi atoms at a concentration of $10^4/cm^3$. It is probable that the reported sensitivity ($10^7/cm^3$) of the identical technique to trimethylbismuth is limited by the ability of active nitrogen to effect the decomposition of the metal complex. An auxiliary discharge or pyrolytic techniques applied to the gas flow containing the sample may improve the detectivity of the order of 10^2 to 10^3. As an alternative method, the sample may be passed through the same microwave discharge used to prepare the active nitrogen; however, design changes would be required to avoid the loss of metal downstream of the discharge.

Our technique looks promising for many applications. Three of the most obvious uses are: (1) as an alarm system for toxic gases of the types in question, (2) a method of analyzing feedstock gases used in the manufacture and doping of solid-state electrical components, and (3) a method of

analyzing combustion effluents.

ACKNOWLEDGMENT

The authors gratefully acknowledge the helpful suggestions of their colleague, Karl R. Westberg.

LITERATURE CITED

(1) G. A. Capelle and D. G. Sutton, *Appl. Phys. Lett.*, **30**, 407 (1977).
(2) A. N. Wright and C. A. Winkler, "Active Nitrogen", Academic Press, New York, N.Y., 1968.
(3) F. C. Fehsenfeld, K. M. Evenson, and H. P. Broida, *Rev. Sci. Instrum.*, **36**, 294 (1965).
(4) A. H. Shapiro, "The Dynamics and Thermodynamics of Compressible Fluid Flow", Vol. I, Ronald Press, New York, N.Y., 1953.
(5) L. B. Loeb, "The Kinetic Theory of Gases", Dover Publications, New York, N.Y., 1961.
(6) H. A. Dewhurst and G. D. Cooper, *J. Am. Chem. Soc.*, **82**, 4220 (1960).
(7) R. Storr, A. N. Wright, and C. A. Winkler, *Can. J. Chem.*, **40**, 1296 (1962).
(8) C. J. Duthler and H. P. Broida, *J. Chem. Phys.*, **59**, 167 (1973).
(9) D. H. Stedman, J. A. Meyer, and D. W. Setser, *J. Chem. Phys.*, **48**, 4320 (1968).
(10) W. R. Brennen and G. B. Kistiakowski, *J. Chem. Phys.*, **44**, 1695 (1966).
(11) L. F. Phillips, *Can. J. Chem.*, **41**, 73 (1963); also, **41**, 2060 (1963).

RECEIVED for review April 14, 1978. Accepted May 22, 1978.

Determination of Microgram Amounts of Some Transition Metals in Seawater by Methyl Isobutyl Ketone–Nitric Acid Successive Extraction and Flameless Atomic Absorption Spectrophotometry

Tsu Kai Jan* and David R. Young

Southern California Coastal Water Research Project, El Segundo, California 90245

A method is presented for the analysis of trace metals in seawater at concentrations below 1 μg/L. The method utilizes a methyl isobutyl ketone (MIBK) extraction procedure followed by a nitric acid back extraction step (to stabilize the metal complexes), and analysis by flameless atomic absorption spectrophotometry. The detection limits for Ag, Cd, Cr, Cu, Fe, Ni, Pb, and Zn are 0.02, 0.003, 0.05, 0.05, 0.20, 0.10, 0.03, and 0.03 μg/L, respectively. For those metals occurring below 1 μg/L, triplicate analyses of three different seawater samples yield mean relative standard deviations ranging from 18 to 25%.

Flameless atomic absorption spectrometry is being widely utilized for metals determinations in aqueous samples because of its low detection limits (on the order of 1 μg/L) and its relative ease of operation. However, concentrations of most trace metals in seawater are often considerably below this level. In addition, certain of the dissolved solids in seawater (totaling about 3.5 g/L) may cause serious interferences in the determination of such elements as Ag, Cd, Cu, Pb, and Zn. Hence, a sample preparation technique is necessary to preconcentrate trace elements from seawater and separate them from the interfering components. Many studies (*1–6*) have been reported to serve this purpose, but ion exchange and MIBK extraction are the two methods most generally used. The Chelex-100 cation-exchange method of Riley and Taylor (*1*) requires a large sample size and gives low recovery efficiencies for Cr and Cu, two metals of great interest to marine ecologists (*7*). Brooks et al. (*3*) developed an APDC-MIBK extraction technique for the determination of six elements in saline water by flame atomic absorption spectrophotometry. However, their work did not include three metals of primary concern (Ag, Cd, Cr); it also was limited by the instability of the metal complexes formed (less than one day). Therefore, we have attempted to overcome these difficulties by developing a revised procedure for the determination of Ag, Cd, Cr, Cu, Fe, Ni, Pb, and Zn in seawater. This procedure involves an APDC-MIBK extraction step followed by back extraction with 4 N nitric acid. The metals complexes in the acid extract were found to be stable for more than one week, with the exception of the Ag complex, which is stable only for about 3 days. Here we present the details of this procedure, and compare the results with those obtained by the Chelex-100 ion exchange and APDC-MIBK single extraction methods.

EXPERIMENTAL

Apparatus. A Varian-Techtron atomic absorption spectrophotometer (model AA-6), equipped with a carbon rod atomizer (model 63) and a background corrector (model BC-6), was used for all trace metal measurements. Two and one-half μL of treated sample solution was injected into the graphite tube using a Unimetrics micropipetter (model 8010), and absorbance peaks were recorded in the peak-read mode. The instrumental settings for each element are given in Table I. A Beckman Model H-5 pH meter with glass electrode was used for pH adjustments and a Burrell wrist action shaker was used for the extractions.

Reagents and Materials. The following analytical reagent grade chemicals were used without further purification: Ammonium hydroxide, concentrated and 1 N solutions; 5% ammonium acetate buffer solution, pH adjusted to 5.5 with acetic acid; metal standard solutions, which were made from dilutions of 1000 ppm stock solutions (Varian-Techtron). Nitric acid was double distilled from Vycor (G. Frederick Smith Chemical Co.). MIBK was double distilled and 1% ammonium pyrrolidine dithiocarbamate aqueous solution (APDC) was freshly prepared and then purified by redistilled MIBK. Distilled deionized water (DDW) was used for all rinses and dilutions. Chelex-100 resin (Bio-Rad Laboratories) was purified with 1 N HNO_3 solution and then successively treated with 1 N NH_4OH solution and CH_3COONH_4 buffer to convert it to an ammonium form.

The seawater samples were collected in Nalgene polyethylene bottles and filtered through a 0.4-μm Nuclepore membrane filter packed with polypropylene separators. The filtered samples were acidified with concentrated HNO_3 to a pH of 2 and preserved by refrigeration. Nalgene Teflon beakers with Teflon covers and Teflon separatory funnels were used for sample preparations. Glass chromatography columns, 2 cm in diameter fitted with

0003-2700/78/0350-1250$01.00/0

Table I. Instrumental Settings for AAS of Metals in Seawater Extracts

element	Ag	Cd	Cr	Cu	Fe	Ni	Pb	Zn
wavelength, nm	328.1	228.8	357.9	324.7	248.3	232.0	217.0	213.9
lamp current, mA	3	5	5	3	5	5	5	5
spectral slit, nm	0.5	0.5	0.2	0.5	0.2	0.2	1.0	0.5
dry,[a] 50 s	3.5	3.5	3.5	3.5	3.5	3.5	3.5	3.5
ash,[a] 20 s	5.0	4.0	6.0	6.0	6.0	6.0	4.0	4.0
atomize[a] 2 s	6.5	7.0	7.5	7.0	8.0	8.0	6.5	6.5
N_2 gas, L/min	4	4	4	4	4	4	4	4
H_2 gas, L/min	-	-	1	-	-	-	-	-

[a] Arbitrary dial settings on the M-63 power supply.

Table II. Effect of Nitric Acid Concentration on Metals Determination

element	μg added[a]	relative recovery[b] 2 N	4 N	6 N
Ag	0.037	1.0	1.0	1.5
Cd	0.020	1.2	1.0	1.1
Cr	0.025	1.2	1.0	0.83
Cu	0.100	1.0	1.0	1.3
Fe	0.100	0.61	1.0	0.75
Ni	0.100	0.88	1.0	0.84
Pb	0.050	0.21	1.0	0.81
Zn	0.250	0.79	1.0	0.75

[a] Filtered island control seawater (200 mL) spiked with metal standard solution. [b] Results are mean values obtained from 3 replicates (corrected for unspiked values) and are determined relative to the recovery obtained using 4 N HNO_3 as the back extraction reagent.

Teflon stopcocks, were used for the ion-exchange procedure. All laboratory wares were cleaned in 6% HNO_3 solution (analytic reagent) for more than 24 h and rinsed with DDW.

Calibration Standards. Internal standards were prepared for the MIBK single extraction method by adding incremental amounts of the eight elements in seawater; these were treated with the regular samples. Standards for the MIBK-HNO_3 successive extraction and Chelex-100 ion-exchange methods were prepared in acid solution, and spiked seawater samples with standards were processed along with the nonspiked samples to make the necessary corrections.

Procedure. For the APDC-MIBK extraction, a 200-mL seawater sample in a Teflon beaker containing 2 mL of 1% APDC is heated to incipient boiling at a pH of about 4. The purpose of heating the sample is to make the complexation of Cr(III) with APDC possible, but care must be taken to avoid extensive boiling, or poor recovery will be observed. After cooling to room temperature, 7 mL of MIBK is added to the sample and the mixture is transferred into a polyethylene bottle and shaken for 25 min on a mechanical shaker. After allowing the layers to separate in a separatory funnel for 20 minutes, the bottom (aqueous) layer is discarded and the organic layer is drained into a polyethylene bottle.

For the acid back extraction, 5 mL of 4 N HNO_3 is pipetted into the MIBK extract obtained from the previous step, and the mixture is shaken for 20 min. After transferring the mixture into a Teflon separatory funnel and standing for 20 minutes, the acid layer is drained into a polyethylene bottle and preserved in a refrigerator until analyzed. Analytical blanks are determined by filtering 200 mL of DDW through a 0.4-μm filter and then processing it with the regular samples.

For the Chelex-100 ion-exchange procedure, 1 L of sample is adjusted to a pH of 7.6 ± 0.2 and passed through an exchange column, which is filled to a depth of 4 cm of Chelex-100 resin, with the flow rate not exceeding 5 mL/min. After rinsing the column with 250 mL of DDW, 25 mL of 4 N HNO_3 is used to elute the metals at a flow rate not exceeding 1 mL/min, and the eluate is collected in a polyethylene bottle for subsequent analysis. Analytical blanks are determined by passing 1 L of pre-filtered DDW through a Chelex-100 column and then processing it with the regular samples.

Table III. Analytical Blanks and Detection Limits

element	analytical blank,[a] μg/L	detection limit,[b] μg/L
Ag	<0.02	0.02
Cd	<0.003	0.003
Cr	<0.05	0.05
Cu	<0.05	0.05
Fe	0.40	0.20
Ni	<0.10	0.10
Pb	<0.03	0.03
Zn	0.06	0.03

[a] Mean of 4 determinations. [b] For a 200-mL seawater sample using 5 mL of 4 N HNO_3 as the back extraction reagent.

Table IV. Recovery of Metals from Spiked Seawater

element	μg added[a]	μg found[b] mean	SD[c]	av. recovery, %
Ag	0.037	0.007	0.0007	19
	0.185	0.024	0.0006	13
Cd	0.020	0.016	0.0025	80
	0.100	0.081	0.0085	81
Cr	0.025	0.020	0.0026	80
	0.125	0.117	0.0279	94
Cu	0.100	0.103	0.0219	103
	0.500	0.373	0.0528	75
Fe	0.100	0.069	0.0095	69
	0.500	0.381	0.0796	76
Ni	0.100	0.080	0.0081	80
	0.500	0.391	0.0099	78
Pb	0.050	0.035	0.0023	70
	0.250	0.163	0.0329	65
Zn	0.050	0.059	0.0064	118
	0.250	0.192	0.0439	77

[a] Filtered island control seawater (200 mL) spiked with metal standard solution. [b] After correcting for concentration measured in unspiked sample. [c] SD = standard deviation, $n = 3$.

RESULTS AND DISCUSSION

Effect of HNO_3. A preliminary test was first conducted to determine the extraction efficiencies obtained by using various strengths of nitric acid in the back extraction step. Table II lists the relative recoveries of trace elements from spiked seawater. These results show that, in most cases, highest recoveries were obtained by using a 4 N HNO_3 solution. Therefore, this concentration of HNO_3 was selected for this study.

Analytical Blanks, Detection Limits, and Recoveries. Because of the very low concentrations of trace elements which usually occur in seawater, special care must be taken at all phases of the procedure to minimize contamination. Typical analytical blanks and detection limits for a 200-mL sample are given in Table III. To test the overall recovery, 200 mL of filtered seawater was spiked with known amounts of eight elements at two concentration levels and the metals were

Table V. Precision of the MIBK-HNO_3 Successive Extraction Method

	seawater A			seawater B[a]			seawater C[a]			mean RSD, %	
	mean	SD[b]	RSD,[c] %	mean	SD	RSD, %	mean	SD	RSD, %	<1 μg/L	>1 μg/L
Ag	<0.02	-	-	<0.02	-	-	<0.02	-	-	-	-
Cd	0.086	0.0044	5.1	0.049	0.0219	45	0.084	0.0061	7.3	19	-
Cr	0.08	0.026	33	0.09	0.006	6.7	0.11	0.017	15	18	-
Cu	0.32	0.0173	5.4	0.74	0.332	45	2.28	0.633	28	25	28
Fe	<0.20	-	-	1.35	0.203	15	2.23	0.045	2.0	-	8.5
Ni	0.14	0.0153	11	0.19	0.086	45	0.71	0.081	11	22	-
Pb	0.03	0.006	20	0.12	0.035	29	0.28	0.031	11	20	-
Zn	0.03	0.006	20	5.41	0.561	10	5.90	0.191	3.2	20	6.6

[a] Seawater B and C received pre-filtered (0.45 μ) and frozen; analytical blanks are listed in Table III. [b] SD = standard deviation, $n = 3$. [c] RSD = relative standard deviation.

Table VI. Trace Metals Analysis of Seawater (Sample D) Using MIBK-HNO_3 Successive Extraction and Chelex-100 Ion-Exchange Methods

	MIBK-HNO_3 extraction	ion exchange
Cd, μg/L	0.039	0.026
	0.038	0.044
	0.052	0.036
mean	0.043	0.035
SD[a]	0.008	0.009
% RSD[b]	19	26
Zn, μg/L	0.08	<0.2
	<0.03	<0.2
	0.06	<0.2
mean	<0.06	<0.2
SD	~0.015	-
% RSD	~25	-

[a] SD = standard deviation. [b] RSD = relative standard deviation.

determined using standards prepared in acidic solution. As indicated in Table IV, the recovery values for seven elements were greater than 65% and averaged 82%, while the recovery of Ag was less than 20%.

Precision. The precision of the MIBK-HNO_3 successive extraction method was evaluated by analyzing three water samples, each in triplicate, for eight elements; the results are given in Table V. Seawater A was collected at 33°24′05″ N, 118°9′30″ W, 18 km off the east end of Catalina Island, Calif. This is considered to be an "island control" station. Seawater B was taken at 51°44′ N, 02°23′ E, reported to be a "coastal control" site. Seawater C was sampled at 52°03′ N, 04°04′ E, in a region considered to be "polluted". Both seawater B and C were provided us by an International Council for the Exploration of the Sea working group as part of an international intercalibration program. As shown in Table V, for concentrations below 1 μg/L, the relative standard deviations (RSD) averaged 21% (range: 5.1–45%); for concentrations above 1 μg/L (only Fe and Zn in seawater B, and Cu, Fe, and Zn in seawater C), the mean RSD was 11% (range: 2.0–28%). Below 1 μg/L, the mean RSDs for Cd, Cr, Cu, Ni, Pb, and Zn were 19, 18, 25, 22, 20, and 20%, respectively, while above 1 μg/L, the mean RSDs for Cu, Fe and Zn were 28, 8.5 and 6.6%, respectively.

Comparison of Methods. To compare this method with that of the single MIBK extraction procedure (for Ag, Cr, Cu, Fe, Ni, and Pb) and Chelex-100 ion exchange (for Cd and Zn), two surface seawater samples were collected off the southern California coast (Seawater D at Ormond Beach, 34°07′30″ N, 119°10′45″ W; Seawater E in Santa Monica Bay, 33°55′30″ N, 118°33′15″ W). Both samples were filtered through a 0.4-μm Nuclepore filter within a few hours of collection, were acidified to a pH of 2, and were split into two aliquots for analysis by different methods. For seawater D, the ion-exchange procedure was utilized within a few days of collection, whereas the aliquot for the MIBK-HNO_3 successive extraction was processed the following week. Seawater E was analyzed by both the MIBK single extraction and MIBK-HNO_3 successive extraction methods the day after collection. As indicated in Tables VI and VII, the results for Cr, Cu, Fe, and Ni obtained by the different methods agreed within 10%; for Cd, within 19%. However, a variation of 32% was obtained for Pb analyzed by the different procedures. For most metals, the lowest RSD value was obtained with the MIBK-HNO_3 successive extraction method. One of the most significant

Table VII. Trace Metals Analysis of Seawater (Sample E) Using MIBK Single Extraction and MIBK-HNO_3 Successive Extraction Methods

method	Ag, μg/L	Cr, μg/L	Cu, μg/L	Fe, μg/L	Ni, μg/L	Pb, μg/L
MIBK-HNO_3	<0.02	0.14	0.78	3.28	0.59	0.29
extraction	<0.02	0.17	0.73	3.57	0.59	0.25
	<0.02	0.16	0.82	3.51	0.59	0.28
	<0.02	0.12	0.82	3.10	0.59	0.31
mean	<0.02	0.15	0.79	3.37	0.59	0.28
SD[a]	-	0.022	0.043	0.22	0.00	0.025
% RSD[b]	-	7.3	5.4	6.5	0.0	8.9
MIBK single	<0.01	0.11	0.95	3.40	0.51	0.32
extraction	<0.01	0.15	0.75	3.47	0.54	0.40
	<0.01	0.15	0.67	3.15	0.54	0.34
	<0.01	0.19	0.84	4.05	0.56	0.43
mean	<0.01	0.15	0.80	3.52	0.54	0.37
SD	-	0.033	0.120	0.380	0.021	0.051
% RSD	-	22	15	11	3.9	14

[a] SD = standard deviation. [b] RSD = relative standard deviation.

aspects of the new procedure is the significantly lower detection limit for seawater Zn (0.03 μg/L), primarily due to the lower analytical blank. This is important in the view of the extremely small concentrations (<0.1 μg/L) of dissolved Zn which can occur in unpolluted seawater (8).

Stability and Application. The stability of metals in the acid extract was observed by comparing the absorbance of these with metal standards prepared in acid solution over a two-week period. No measurable change was found for Cr and Cu after two weeks, or Cd, Fe, Ni, Pb and Zn after one week. However, the Ag level was stable for only about three days; after one week its signal decreased substantially. This probably is due to the absorption of Ag on the walls of the polyethylene container.

The MIBK-HNO_3 two-step successive extraction procedure described here appears to be a useful method for the analysis of Ag, Cd, Cr, Cu, Fe, Ni, Pb, and Zn in filtered seawater, with detection limits ranging from 0.003 to 0.2 μg/L. Because of the excellent stability of the final extract for all of these metals, this method is particularly useful when the analysis of more than one element in several seawater samples is desired.

ACKNOWLEDGMENT

We thank Patrick Hershelman, Jean Wright, and Mike Moore of this Project for their assistance in seawater sampling and processing.

LITERATURE CITED

(1) J. P. Riley and D. Taylor, *Anal. Chim. Acta*, **40**, 479 (1968).
(2) R. A. A. Muzzarelli and R. Rocchetti, *Anal. Chim. Acta*, **69**, 35 (1974).
(3) R. R. Brooks, B. J. Presley, and I. R. Kaplan, *Talanta*, **14**, 809 (1967).
(4) S. L. Sachdev and P. W. West, *Environ. Sci. Technol.*, **4**, 749 (1970).
(5) J. Nix and T. Goodwin, *At. Absorp. Newsl.*, **9**, 119 (1970).
(6) T. Kono and A. Nemori, *Bunseki Kagaku*, **24**, 419 (1975).
(7) D. R. Young, D. J. McDermott, T. C. Heesen, and T. K. Jan, in "Marine Chemistry in the Coastal Environment", ACS Symposium Series 18, T. M. Church, Ed., Washington, D.C., 1975, p 424.
(8) K. W. Bruland, G. A. Knauer, and J. H. Martin, *Nature (London)*, **271**, 741 (1978).

RECEIVED for review March 20, 1978. Accepted May 19, 1978. Contribution No. 111 of the Southern California Coastal Water Research Project.

Aluminum Determination by Atomic Emission Spectrometry with Calcium Atomization Inhibition Titration

J. H. Liu and C. O. Huber*

Department of Chemistry, University of Wisconsin—Milwaukee, Milwaukee, Wisconsin 53201

Aluminum inhibition effects on calcium flame emission were employed to study the determination of aluminum. The release effects of lanthanum on the calcium flame emission signal were also used. The latter technique involves the addition of calcium chloride followed by lanthanum chloride to the sample solution, while monitoring the calcium emission signal. The signal enhancement due to the lanthanum release is linearly related to aluminum concentration. A detection limit of 0.03 ppm Al was found. A variety of aluminum sample determinations compare well with those for established methods. The technique is promising in terms of speed, simplicity, and precision when compared to conventional methods available in the sub-ppm range. The unusual shapes of these "titration curves" yield unique information on some of the chemistry occuring during the millisecond time period during which a droplet evaporates, dehydrates, and then decomposes in the flame. Correlations are made between features of the titration curves and the releasing process which point to a mechanism involving an equilibrium reaction.

Aluminum is the third most abundant element in the Earth's crust. Its abundance and wide use make its determination important environmentally as well as economically. One example is the matter of "spent alum" disposal from water filtration processes. The possibility of aluminum-related effects on health has been discussed (*1*, *2*). There are few rapid, selective, and convenient methods for aluminum determination at sub-parts-per-million levels (*3*). Direct flame atomic absorption requires an acetylene–nitrous oxide flame and is somewhat limited in detection limit. Indirect atomic absorption measurement of aluminum by the enhancement of aluminum on the signals for iron, cobalt, nickel, and chromium were studied by Ottaway et al. (*4*). Their investigation resulted in increased sensitivity. We report a technique here which offers some analytical advantages. The technique is based on atomization inhibition titration (AIT) and subsequent release.

AIT is a procedure based upon "titrating" the sample (inhibitor) solution being aspirated into the flame with a monitor metal solution while observing the monitor metal signal (*5–7*). The technique allows observation of atomic absorption or emission signal vs. droplet composition. The method yields unique titration curve shapes with information not available by the more common techniques. It exploits, rather than merely accommodates, some of the drastic chemical processes occuring in the droplet during its approximately millisecond desolvation process. Calcium was selected as the flame emission monitor metal because it provides low detection limits and because formation of refractories with aluminum has been well documented. Analysis of the titration curves obtained can be used further to characterize some of the droplet desolvation chemical mechanisms which control the analytical signals.

EXPERIMENTAL

Apparatus. The Jarrell-Ash Model 82-516 spectrometer with an infusion pump for titrant insertion is used for flame measurement. For better signal-to-noise ratios and optical efficiency, a 620-nm (CaO emission band) interference filter replaces the monochromator (*6*). The hydrogen–air flame with a pre-mix chamber laminar flow burner provides the quiet, cool (below 2000 °C), relatively transparent flame, and the relatively uniform droplet size necessary.

All glassware used in these studies was acid-hardened by soaking in 3 N hydrochloric acid overnight to minimize errors due to leaching and solubility.

0003-2700/78/0350-1253$01.00/0

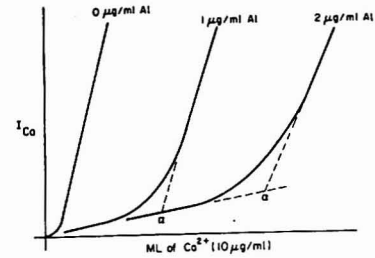

Figure 1. Atomization inhibition titration curve

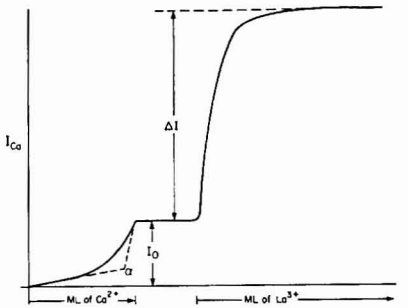

Figure 2. Atomization inhibition-release titration curve

Procedure. A 100-mL beaker containing 50 mL of sample served as the titration vessel. It was placed on a magnetic stirrer. Immediately after aspiration was started, titrant flow and recording were initiated simultaneously by a common switch. Titrant was added continuously with an infusion pump until well past the appropriate end point so that appropriate linear extrapolations could be made on the recorded titration curve. By use of the infusion pump, titration procedures could be arranged so that the most concentrated samples require about 2–3 min to reach the end point. The term "titration" used here refers to procedure. The technique does not involve stoichiometric reactions in the bulk titration solution—the usual case for titrations.

For potable and wastewater samples, acetylacetone was used to separate aluminum from interferences. Aluminum was extracted from a pH 5 acetate buffer with a 50% (v/v) acetylacetone solution in chloroform. A single extraction yields slightly over 90% of the aluminum in the organic phase so that 2–3 extractions were required (*8*). Aluminum was re-extracted from the organic phase by shaking with a 4 M HCl solution. The above procedure removed Ca, Mg, Zn, Cd, Mn, Co, Ni, Pb, Hg, Ti, Cr(III), U(VI), Fe(II) (*9*), and some of the interfering anions. Fluoride ion interfered with the separation procedure. When fluoride and aluminum were present at a molar ratio of 4:1, only 50% of the aluminum was reported to be extracted at pH 7 (*8*). In all experiments, standards were pH adjusted and saturated with acetylacetone in order to simulate extracted samples.

Reagents and Solutions. All solutions were prepared from reagent grade materials and double distilled water. Stock standard solutions were prepared as follows.

Calcium carbonate was dissolved in a slight excess of hydrochloric acid. The solution was boiled to expel carbon dioxide and, after cooling, made to predetermined volume with water.

Aluminum metal was dissolved in a slight excess of hydrochloric acid.

RESULTS AND DISCUSSION

Analytical Method. The formation of refractory compounds is related to flame temperature and environment (air–fuel ratio). Aluminum shows increasing inhibition as the air:hydrogen ratio increases, but at the highest ratio there is loss of sensitivity of Ca emission. Thus, an air-rich flame at an optimal air:hydrogen ratio (1:1 flow ratio at the burner plus chamber auxiliary air) is used. Titration curves for several aluminum concentrations with a continuously added Ca titrant solution containing 10 ppm as $CaCl_2$ are shown in Figure 1. The data show rather gradual change in slope (curvature) in the regions where inhibition ceases. Similar observations were made by Doty and Schrenk (*10*). The shape of the curve was affected by the nature of the anion. Using nitrate instead of chloride gives a less rounded curve and hence a more complete inhibition. For both aluminum nitrate and chloride solutions, however, the data contrast with the much sharper shifts found earlier in this laboratory for the analysis of silicate (*11*) and phosphate (*12*).

Linear extrapolations can be made, however, to locate the end point. The critical ratio, α [(Ca)/(Al) at end point] was found to be constant with constant flame conditions. Linearity was found for plots of volume of calcium titrant added to reach the ratio α vs. aluminum concentration. Blanks were necessary to compensate for the presence of aluminum in the solvent and the time lapse between initiation of titrant flow and the appearance of the titrant in the flame (about 2 s). The time lapse was dependent upon the aspiration rate and diameter of the aspiration tubing (*11*). The concentration range of this method at a particular flame setting was about tenfold. At higher concentrations identification of the linear segments of the curve (Figure 1) became difficult, but by selection of air–fuel ratios to control the flame temperature and flame chemical environment, concentration ranges from 0.1 to greater than 20 μg/mL could be accommodated.

The atom ratio of calcium to aluminum at the endpoint (α) of the titration was somewhat dependent on the air–fuel mixture ratio. α was generally around 0.33–0.35, with very slight increases as air:hydrogen ratio increases. As the flame went very lean, the value of α increased rapidly to 0.44, indicating that the flame chemical environment as well as flame temperature governs the critical ratio. Under most flame conditions (α = 0.33), the refractory mixed oxide formed corresponds to $2CaO{\cdot}3Al_2O_3$. Dinnin (*13*) has reported a Ca/Al refractory atom ratio of 0.5 using a hydrogen–oxygen flame. Rubesca (*14*) has collected these refractory particles and analyzed them by x-ray diffraction. He suggested that a number of mixed oxides were formed.

The importance of chemical environment in forming refractory oxide has been shown by Slavin (*15*), where he used Schlieren patterns to show that the exclusion of entrained oxygen from the flame profoundly affected the formation of refractory oxides. Elwell and Gidley pointed out that in an excess of oxygen in the flame the dissociation of oxides will be retarded in accordance with the mass action law (*16*). Aluminum atomic absorption was not found using an oxy-cyanogen flame (*17*), even though it has a much higher temperature than can be obtained with a nitrous oxide–acetylene flame (*18*, *19*) which does yield an Al signal.

Although titration curves such as in Figure 1 can be used for aluminum concentration measurements, accuracy of the extrapolations was limited by the amount of curvature. Within a suitable concentration range, calcium depression is proportional to aluminum concentration. Thus, determining aluminum by a release effect is feasible. La, Sr, Mg, glycerol and $HClO_4$, Ba, EDTA, and oxine have been reported to release Al from Ca; however, only Sr and La release totally (*13*). Experimental results show negligible La emission at 622 nm, and it was selected as the releaser.

Calcium was added until the critical ion ratio, α, was exceeded and a predetermined signal magnitude (I_0 in Figure 2) was attained. At this point, the addition of calcium was discontinued and the addition of lanthanum begun via an

Table I. Aluminum Determinations by AIT-RELEASE

sample	μg Al/mL ± estimated standard deviation	comparison value
synthetic wastewater	0.28	0.25[a]
synthetic wastewater	0.59	0.50[a]
Milwaukee tap water	0.021 ± 0.00[b]	0.03[c]
Milwaukee tap water	0.064 ± 0.004	0.05[c]
Milwaukee tap water	0.063 ± 0.014	0.05[c]
Al base alloy, NBS 85a	0.29 ± 0.03	0.25[d]
Al base alloy, NBS 86b	0.21 ± 0.02	0.18[d]

[a] Added as $AlCl_3$. [b] Three replicates. [c] As reported by water purification plant using Eriochrome cyanine R photometric method. [d] As reported by NBS.

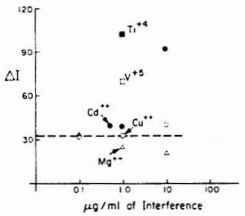

Figure 3. Interference level of various cations for determination of 0.1 μg/mL. Al, pH 5. With no interferences present, $\Delta I = 32$

infusion pump. With increasing lanthanum concentration, a distinct upward shift in emission intensity was obtained corresponding to the release of the calcium inhibited by the aluminum (ΔI in Figure 2). The magnitude of ΔI was found to increase with I_0, the signal when calcium addition is discontinued. It is therefore necessary to discontinue calcium addition at a constant I_0 value when making a series of measurements. With this precaution, values of I_0 between 0.1 and 0.2 (full scale 1.0) were suitable. Accuracy of the method can be expected to be independent of the mode of addition of reagents. The release (ΔI) is linearly related to the aluminum concentration. The AIT-release technique was applied to several samples (Table I). The sample solutions from the aluminum base alloys (~90% Al) were determined without the acetylacetone extraction step.

Silicates, phosphates, and sulfate interfere because they also form refractories with calcium, and lanthanum also releases those inhibition refractories. Accordingly, there is a signal enhancement when such anions are present. The effects of the cations of Fe, Cu, Zn, Mg, Cd, V, Ti, and H on the analytical signal were examined. With the exception of Fe and Zn, there was a measurable discrepancy for 100-fold excess of interference. The extent and relative concentrations are indicated in Figure 3. The acetylacetone solvent extraction prevents the interference of the refractory forming anions and of the alkaline earth cations.

When the release step is performed at lower pH, the magnitude of the release signal is increased. For 0.1 M HCl the signal size for conditions corresponding to Figure 3 is 48 and goes to 90 for 4 N HCl. The signal shape, however, is retained so that analytical measurements can be performed if the acidity is maintained constant.

Repetitive runs on 0.1-ppm Al samples provided the standard deviation and relative percent standard deviation data presented in Table II.

As examples of the accuracy and precision of the method, the results for known solutions are shown in Table III. The precision decreases with decreasing concentration of aluminum. For a sample containing 0.5 μg of Al (50-mL sample; 0.01 μg/mL Al), the relative standard deviation increases to 100%. The cause attributed to this is the presence of significant quantities of aluminum in all laboratory reagents and the laboratory environment. Samples of 0.02 μg/mL and 0.04 μg/mL of Al when exposed to the laboratory environment in open beakers for 24 h were found to contain 0.04 and 0.07 μg/mL of Al, respectively. A. J. Blotcky et al. (*21*) used activation analysis to show that even distilled and distilled-deionized water contains 0.01–0.03 μg/mL of Al.

Table II. Detection and Determination Limits by the AIT-Release Method

standard deviation[a]	±0.010 μg Al/mL
relative standard deviation, %[a]	9.63%
determination limit[b]	0.20
detection limit[b]	0.032
detection limit[c]	0.02

[a] Seven replicate runs, 0.100 μg Al/mL. [b] 95% C. I. and 5% RSD, see Parsons (*20*). [c] The concentration of a solution which yields a signal equal to twice the standard deviation of a series of measurements which is distinctly detectable above the baseline (definition recommended by the Scientific Apparatus Makers Association).

Table III. Accuracy and Precision for Determination of Al in H_2O by AIT-Release

no. of detmns	true value, μg/mL	mean determined μg/mL	s, μg/mL	% bias
4	0.12	0.12	0.006	
7[a]	0.10	0.10	0.009	
4	0.070	0.081	0.008	16
4	0.050	0.051	0.003	2
4	0.030	0.025	0.008	−17
4	0.010	0.009	0.009	−10

[a] Used to calculate detection limit (*20*).

Mechanism of the Release Effect. The mechanisms accounting for the shape of the titration curve (see Figure 2) can be stated as follows. Initially there is formation of refractory calcium aluminate. Therefore, inhibition of calcium emission is observed at calcium to aluminum ratios less than the critical ratio, α. When lanthanum is added to the solution, the reactions in the evaporating droplets are altered such that calcium is released and the signal is restored. In this part of the procedure, the response curve shows a shape which suggests an equilibrium process. Further examination of these curves showed that total lanthanum concentration divided by calcium signal intensity vs. total lanthanum concentration yields excellent linearity (minimum correlation coefficient of 0.997) for samples ranging from 0.1 to 0.5 μg/mL aluminum.

A simple equilibrium model can be suggested for the reactions occuring in the evaporating droplets for the release process:

$$\text{Ca·3Al} + \text{La} \underset{k_2}{\overset{k_1}{\rightleftharpoons}} \text{La·3Al} + \text{Ca} \qquad (1)$$

where the calcium aluminate refractory is represented as Ca·3Al. The rate of formation of free calcium is given by:

$$\frac{d(Ca)}{dt} = k_1[(Ca)_t - (Ca)][(La)_t - (La\cdot 3Al)] \qquad (2)$$

where $(Ca)_t$ and $(La)_t$ are total concentrations of refractory and free calcium, and lanthanum, respectively.

The rate of removal of free calcium is given by:

$$\frac{-d(Ca)}{dt} = k_2(La\cdot 3Al)(Ca) \qquad (3)$$

At equilibrium, the two rates are equal. On algebraic rearrangement:

$$\frac{[(La)_t(La\cdot 3Al)]}{(Ca)} = \frac{[(La)_t(La\cdot 3Al)]}{(Ca)_t} + \frac{k_2(La\cdot 3Al)}{k_1(Ca)_t} \quad (4)$$

Using $I_{Ca} = k(Ca)$ where I_{Ca} is the calcium signal intensity and k is the analytical constant, Equation 4 can be rearranged to:

$$\frac{[(La)_t(La\cdot 3Al)]}{I_{Ca}} = \frac{[(La)_t(La\cdot 3Al)]}{k(Ca)_t} + \frac{k_2(La\cdot 3Al)}{k_1 k(Ca)_t} \quad (5)$$

If it is assumed that the activity of solid La·3Al is constant and the lanthanum activity in the releasing complex can be neglected compared with the total concentration of lanthanum; such that $(La)_t - (La\cdot 3Al) \approx (La)_t$, then Equation 5 can be simplified. Two possibilities for such an assumption are: (1) decomposition of the La·3Al release complexes to provide more soluble reactant La, or (2) high activity of the soluble reactant lanthanum compared to the possibly solid phase La·3Al. Equation 5 then becomes:

$$\frac{(La)_t}{I_{Ca}} = \frac{(La)_t}{k(Ca)_t} + \frac{k_2(La\cdot 3Al)}{k_1 k(Ca)_t} \quad (6)$$

This equation correlates with the linearity of $(La)_t/I_{Ca}$ vs. $(La)_t$ observed experimentally.

During the release process, both $(Ca)_t$, the total calcium concentration and the aluminum concentration in the droplet are constant. Thus, the inverse slope of Equation 6, i.e., $k(Ca)_t$, should be linearly related to aluminum concentration for the various release experiments. This was found to be true experimentally over the range of 0.20 to 0.50 μg Al/mL.

The intercept in Equation 6 can be stated as

$$y_0 = \frac{k_2(La\cdot 3Al)}{k_1 k(Ca)_t} \quad (7)$$

Assigning unit activity to solid aluminum lanthanate and substituting $I_{max} = k(Ca)_t$, where I_{max} is the intensity signal for full release of calcium one obtains

$$\frac{k_2}{k_1} = y_0 I_{max} \quad (8)$$

By this method k_1/k_2 was evaluated over the range of 0.2 to 0.5 μg/mL aluminum yielding $k_1/k_2 = 7.0\ (s = \pm 0.8) \times 10^4$.

The corresponding $\Delta G°$ for the releasing equilibrium can be estimated using $T = 373$ K, the boiling point of the solvent. The value obtained is: −8.3 kcal/mol. Such a treatment illustrates the possible usefulness of atomic inhibition titration and atomic inhibition-release titration for examination of flame and flash evaporation processes.

Previously reported work on the release of magnesium from a fluoride refractory by addition of hydrochloric acid, in contrast to the results reported here, showed that the release signal was linearly related to the concentration of releasing agent in the droplet (22). In that case, the release was apparently via hydrofluoric acid generation followed by its irreversible removal due to both droplet concentration and hydrofluoric acid volatility. Comparison of that case with the present one implies diagnostic capabilities of these techniques for droplet evaporation investigations.

LITERATURE CITED

(1) G. M. Berlyne, *Lancet*, 1253 (1970).
(2) D. Waldron-Edward, P. Chan, and C. Skoryna, *Can. Med. Assoc. J.*, 1297 (1971).
(3) V. N. Tikhonov, "Analytical Chemistry of Aluminum", translated by J. Schmorak, Halsted Press, New York, N.Y., 1973.
(4) J. M. Ottaway, D. T. Coker, and B. Singleton, *Talanta*, **19**, 787 (1972).
(5) C. I. Lin and C. O. Huber, *Anal. Chem.*, **44**, 2200 (1970).
(6) J. R. Sand and C. O. Huber, *Anal. Chem.*, **48**, 1331 (1976).
(7) J. R. Sand, J. H. Liu, and C. O. Huber, *Anal. Chim. Acta*, **87**, 79 (1976).
(8) J. Steinbeck and H. Freiser, *Anal. Chem.*, **26**, 375 (1954).
(9) S. Stene, *Tidsskr. Kjemi Bergves.*, **19**, 6 (1939).
(10) M. E. Doty and G. Schrenk, "Developments in Applied Spectroscopy", Vol. 3, J. E. Forrett and E. Laterman, Ed., Plenum Press, New York, N.Y., 1964, pp 196–206.
(11) R. W. Looyenga and C. O. Huber, *Anal. Chem.*, **43**, 498 (1971).
(12) R. W. Looyenga and C. O. Huber, *Anal. Chim. Acta*, **55**, 179 (1971).
(13) J. I. Dinnin, *Anal. Chem.*, **32**, 1475 (1960).
(14) I. Rubesca and B. Moldan, *Anal. Chim. Acta*, **37**, 421 (1967).
(15) W. Slavin, *At. Absorpt. Newsl.*, **6**, 9 (1967).
(16) W. T. Elwell and J. A. Gidley, "Atomic Absorption Spectrometry", Pergamon Press, New York, N.Y., 1966, pp 41–50.
(17) J. W. Robinson, *Anal. Chim. Acta*, **27**, 462 (1962).
(18) J. B. Willis, *Nature (London)*, **207**, 715 (1965).
(19) M. D. Amos and P. E. Thomas, *Anal. Chim. Acta*, **32**, 139 (1965).
(20) M. L. Parsons, *J. Chem. Educ.*, **46**, 290 (1969).
(21) A. J. Blotcky, D. Hobson, J. A. Leffler, E. P. Rack, and R. R. Recker, *Anal. Chem.*, **48**, 1084 (1976).
(22) V. Fong and C. O. Huber, *Spectrochim. Acta, Part B*, **31**, 113 (1976).

RECEIVED for review February 8, 1978. Accepted May 8, 1978.

Determination of Trace Metals by Microwave Plasma Spectrometry with an Atmospheric Pressure Helium Discharge

Andrew T. Zander[1] and Gary M. Hieftje*

Department of Chemistry, Indiana University, Bloomington, Indiana 47401

A recently described resonant cavity for generating microwave-induced helium plasmas (MIPs) at atmospheric pressure has been evaluated for use in the emission spectrometric determination of metallic elements, and has been found to offer several advantages over alternative designs. The new cavity allows self-ignition of an atmospheric pressure helium MIP. In addition, the plasma which is formed exhibits significantly improved operational stability and is considerably less susceptible to disruption by injected aerosol samples. The helium MIP was used in conjunction with a single-shot microarc sample atomizer. With this combination, analytical calibration curves for Zn, Pb, Mn, Mg, Cu, Ca, and Na are linear over 2 to 5 orders of magnitude of concentration; also, detection limits for these elements are equal to or better than those obtainable with other MIPs. As with most MIPs, the ionization of easily ionized elements must either be overcome using ionization suppressants or exploited through use of ion emission lines. Interference from refractory elements is less than that exhibited by most MIPs.

A new design of resonant cavity for the generation of 2450 MHz microwave-induced plasmas (MIPs) has been recently described (*1*). The cavity has a minimal internal volume so that energy density in the plasma chamber at a given input power level is high enough to allow self-ignition of a helium plasma at atmospheric pressure. Subsequent communications (*2, 3*) concerning this cavity have dealt with the theory of its design, probable excitation mechanisms in plasmas formed within it, and its use as a halogen and nonmetallic element detector for gas chromatography.

The high excitation capability and greatly improved stability of atmospheric pressure helium plasmas formed in this cavity suggest its further application as an excitation source for metallic elements in aqueous sample solutions. Accordingly, we have constructed, with minor modification, a version of the cavity described by Beenakker (*1–3*) with a microarc atomization unit (*4*). The microarc atomizer has also been modified, to enable its operation in helium. The operational characteristics of the resulting microarc/MIP excitation source and its usefulness for the atomic emission detection of several metallic elements have been studied.

EXPERIMENTAL

A modified microwave cavity was machined from a single piece of 5-inch (12.7-cm) diameter Cu cylindrical bar stock. The finished cavity, shown in Figure 1, is 1.5 inches (3.8 cm) thick and weighs about 5 pounds (2.3 kg). The cavity is essentially a fixed well 10 mm deep with a removable lid held in place by 12 bolts to ensure good electrical contact. The thickness of the cavity walls and bottom were increased over those of the previous design (*1*) for easier construction and mechanical stability. Also, the microwave power input connector was bolted directly to the cavity, without further modification (*1*). The coupling loop (*1*), constructed of 1-mm diameter Cu wire, extended into the cavity 10 mm and is silver-soldered to the cavity bottom. A 7-mm hole is formed in the center of the well and lid to allow insertion of the quartz plasma chamber into the cavity. Because the introduction of dielectric material such as the quartz chamber into the cavity lowers the cavity resonant frequency (*1, 5*), the internal diameter of the cavity must be less than the resonant $^3/_4$-wave distance calculated to be 93.7 mm at 2450 MHz. Thus, the cavity was constructed with an internal diameter of 92.5 mm, which can be reduced if desired by means of $^1/_4$-in.–40 brass tuning stubs located on the cavity (*1*).

The central discharge chamber for the plasma was fabricated from quartz tubing, 5-mm o.d., 3-mm i.d., and was approximately 3.5 cm long. This chamber fit snugly into a quartz sleeve, 7-mm o.d., 5-mm i.d., which was left in the cavity at all times. This sleeve prevented introduction of any foreign material into the cavity while the chamber was replaced or adjusted during the initial set-up procedures. Presumably, the quartz sleeve would not be required for a plasma system of fixed configuration. A T-shaped chamber extended from the end of the plasma tube (Figure 2) and housed the modified microarc atomizer. The "T" was bent out of the optical path so thermal emission from the microarc was not seen by the detection system.

The microarc atomizer has been described previously (*4*) but was modified in this work to allow its stable and efficient operation in a helium environment. The operating voltage was increased from 900 V, normally used with an argon microarc discharge, to 1800 V to impart higher energy to the lower mass helium atoms. Also, the anode was made of thoriated tungsten (2% Th, Alfa Division, Ventron Corp., Danvers, Mass.) instead of stainless steel; the thoriated tungsten served to stabilize the discharge sooner after initiation. Conveniently, helium provides more rapid and more even heating of the tungsten sample filament than does argon. The filament was V-shaped and constructed of 0.5-mm W wire; it would hold up to 10 μL of sample solution.

The helium support gas for the microarc and plasma was supplied through a 16-gauge stainless steel syringe needle placed parallel to but above the microarc anode, with the tip of the needle back 5 mm from the flat end of the thoriated tungsten anode. The range of flow rates of helium for stable microarc operation, efficient sample transport, and optimum plasma operation was experimentally determined to be between 300 and 450 mL/min. A flow rate of 400 mL/min optimized the time for sample transport through the plasma and provided greatest signal levels.

Figure 3 is a schematic diagram of the instrumental array. The microwave power supply was a continuously variable, 100-W microwave generator (Model HV-15A, Scintillonics, Inc., Fort Collins, Colo.) operating at 2450 MHz. A coaxial cable, type RG/8, (Belden Corp., Richmond, Ind.) transmitted the microwave power to a double-stub tuner (Model 306A, PRD Electronics, Westbury, L.I., N.Y.) which was connected to the UG/58 RF connector (#82-24, Amphenol, RF Division, Danbury, Conn.) located on the cavity. High-purity helium (99.999%) was used for the microarc and microwave plasma. The microarc power supply has been described previously (*4*). A plano-convex lens, of aperture $f/4$, gathered the output radiation from the plasma and focused it on the entrance slit of a medium resolution monochromator (Model EU-70C, Heath Co., Benton Harbor, Mich.). A Hamamatsu R212 photomultiplier tube (HTV Co., Ltd., Middlesex, N.J.) was used. A picoammeter (Model 427, Keithley Instruments, Inc., Cleveland, Ohio) converted the phototube current to a voltage which was output to either a chart recorder (Model SR-204, Heath Schlumberger Instruments, Benton Harbor, Mich.) for recording peak height information or a PDP-12 laboratory minicomputer

[1]Present address, Department of Chemistry, Cleveland State University, Cleveland, Ohio 44115.

0003-2700/78/0350-1257$01.00/0

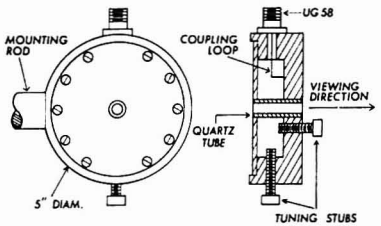

Figure 1. Diagram of 2450-MHz microwave resonant cavity. Inside cavity diameter, 9.25 cm. Cavity material, copper (hatched area). Quartz sleeve, 7-mm o.d., 5-mm i.d

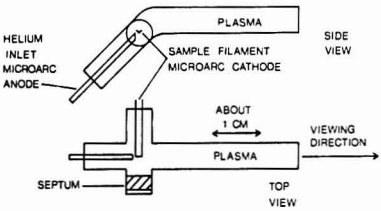

Figure 2. Diagram of quartz plasma chamber. Tubing is 3-mm i.d., 5-mm o.d. and fits inside quartz sleeve of Figure 1

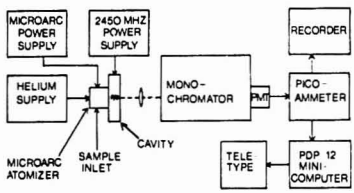

Figure 3. Schematic diagram of instrumental array

(Digital Equipment Corp., Maynard, Mass.). The minicomputer was programmed in FORTRAN IV to calculate the peak area of the output signal, but was not used for control of any part of the experimental system.

DISCUSSION

Ignition of the Plasma. When borosilicate glass tubing is used as the plasma chamber material, the helium plasma is self-igniting at atmospheric pressure, when the reflected power is tuned below 10 W. Presumably, self-ignition occurs because of microwave heating of the glass, which then releases enough charged species to couple with the intense microwave field. The gaseous species act to supply electrons to "seed" the helium and lead to plasma ignition. No attempt was made in this work to identify these "seed" species, since the borosilicate glass was deemed unsuitable for use as a plasma tube material because of its short usable lifetime.

When quartz tubing was employed for the plasma chamber, an insufficient amount of ionizable material was volatilized to enable the plasma to self-ignite. However, it was found possible to ignite the plasma by striking the helium microarc. Enough material is ordinarily ejected from the white-hot microarc cathode filament to "seed" the helium and lead to ignition. Nonetheless, to enhance reliability, routine determinations were performed using a Tesla coil to initiate the helium plasma.

Tuning of the Cavity. Insertion of the quartz plasma chamber into the cavity did not markedly affect the tunability of the cavity. Tuning could be accomplished with either the brass tuning screws on the cavity or with the double-stub tuner on the UG/58 RF connector. Either method produced the same results; consequently, the cavity was regularly tuned using the double-stub tuner, so the holes for the on-cavity tuning screws could be employed for cooling (see below).

The plasma ignited readily whenever the reflected power was tuned below 20 W and 75 W were directed to the cavity. Once the plasma was ignited, the reflected power could be easily tuned to 0 W.

Power Applied. The microwave power supply was generally run at 100 W forward power (FP), although exact measurements of the microwave power dissipated in the plasma were not taken. It is assumed that the power utilized by the plasma was less than the 100 W applied since some of this power was lost as heat by the cavity.

Cooling. The cavity thermally stabilized after approximately 15 min from the time of first plasma ignition. The external skin temperature of the cavity was about 90 °C with 100-W FP applied.

The utility of cooling the cavity was investigated. Using the double-stub tuner for tuning, the on-cavity tuning screws were removed and the holes used for cooling of the cavity, with the hole on the outer edge of the cavity being used as the cooling gas inlet. The cooling gas was passed through a drying trap and a cooling coil (in liquid N_2) before entering the cavity. Plasma operation and signal-to-noise ratio were not significantly affected by cooling with air, nitrogen, argon, or helium, and so no cavity cooling was used.

Plasma Stability. The stability of the plasma was determined by monitoring the 471.3 nm He I line. The time constant of the detection system was 0.3 s. Fluctuation of the emission from this line was less than 1% over 3 h, after a warm-up period of approximately 15 min.

Plasma Positioning. The plasma exists as a filament approximately 8–10 mm long and 1 mm in diameter in the center of the 3-mm i.d. chamber. The helium plasma never extended past the internal cavity walls, at any flow rate, whereas the argon plasmas usually extend about 5 mm out the ends of the cavity. With 50-W FP or less, the plasma always existed exactly in the center of the chamber; intensity of emitted radiation was greatest at the plasma center and decreased smoothly out to the chamber walls. Above 50-W FP, the plasma would rest along the inner wall of the chamber. The plasma never moved in position once it ignited along the wall, resulting in etching of the quartz wall over a period of time. This etched region served as a site for collection of analyte vapor and led to undesired analyte memory effects and broadened signal peaks. Consequently, the chamber must be replaced after about 40 h of plasma operation, if plasma powers over 50 W are employed.

Background Characteristics. MIPs generally exhibit uncomplicated background spectra. However, a wavelength scan (200–600 nm) of the background from the present atmospheric-pressure helium plasma showed a significant number of prominent spectral features of both line and broadband character. The wavelength location and relative intensities of the majority of these features were recorded and compared to those of molecular species expected in such a plasma (*6, 7*). Table I is a compilation of the strongest features found and indicates the species causing each feature. The presence of all of the identified molecular bands and lines can be understood with the aid of the excitation mechanisms for this plasma postulated by Beenakker (*3*). Because most of the observed molecular features originated from excitation of atmospheric species, it was possible to reduce their level by using a modified plasma chamber which is closed to the atmosphere with a quartz end window and has a small aperture gas exit port. It also would be possible to compensate

Table I. Most Prominent Background Spectral Features in the Atmospheric-Pressure Helium MIP

originating species	wavelength, nm	transition
NO		$[A^2\Sigma^+\text{-}X^2\Pi]$
	205.24	(2,0)
	215.49	(1,0)
	226.94	(0,0)
	237.02	(0,1)
	247.87	(0,2)
	259.57	(0,3)
OH		$[^2\Sigma^+\text{-}^2\Pi]$
	281.13	(1,0)
	287.53	(2,1)
	294.52	(3,2)
	306.36	(0,0)
NH		$[A^3\Pi\text{-}X^3\Sigma^-]$
	336.00	(0,0)
	337.09	(1,1)
N_2		$[^3P_u\text{-}B^3P_g]$
	357.69	(0,1)
	375.54	(1,3)
	380.49	(0,2)

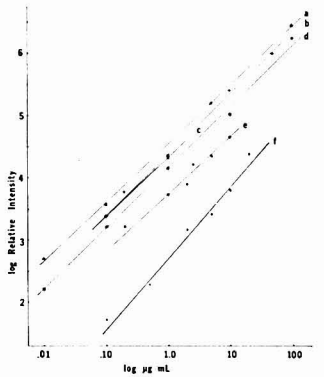

Figure 4. Analytical calibration curves for: (a) Zn I (213.8 nm), (b) Pb I (216.9 nm), (c) Mn I (279.5 nm), (d) Cu I (324.7 nm), (e) Mg I (285.2 nm), and (f) Mn I (403.1 nm)

for many of these features using wavelength modulated detection (8).

Plasma Temperature. A nonrigorous determination of the excitation temperature of the plasma was made for comparative purposes with similar MIPs. The relative intensities of well-documented He I lines were measured and a plot of log $[I_\lambda/g_kA_{ik}]$ vs. E_k was made (9, 10). The slope of this plot yielded an excitation temperature of 7250 K for this plasma. This temperature compares well with other argon and helium MIPs whose excitation temperatures vary between 4500 and 8300 K (11).

Nebulization. It was verified that the new helium MIP can operate continuously during input of a nebulized aerosol, as claimed by Beenakker (1). However, the plasma is obviously weakened by the injected aerosol (about 0.1 mL/min maximum) and becomes less stable. Nonetheless, the resistance of the plasma to extinction by an aqueous aerosol indicates its durability, compared to others which have been reported (4, 11).

Analytical Calibration Curves. Figure 4 shows analytical calibration curves for 5 of the elements (6 analytical lines) studied. The plots for Zn I (213.8 nm), Pb I (216.9 nm), Cu I (324.7 nm), and Mn I (403.1 nm) have slopes of 1.0, within

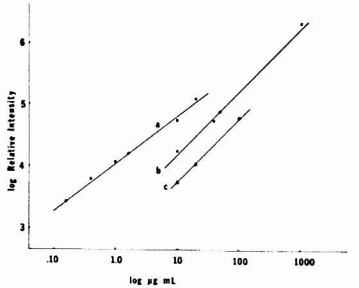

Figure 5. Analytical calibration curves for: (a) Na I (589.0 nm), (b) Ca II (393.4 nm), and (c) Ca I (422.7 nm)

Table II. Detection Limits Obtained with the New MIP, pg

element	wavelength, nm	He MIP[a]	Ar MIP[b]	other systems[c]
Zn	213.8	0.35	9.2	1.0-6.0
Pb	216.9	0.56	3.8	50
Mn	279.5	0.46	-	-
	403.1	20	-	5-40
Mg	285.2	0.85	0.45	50
Cu	324.7	0.42	1.6	5.0
Ca	422.7	1.6	10	50
Na	589.0	0.12	0.01	10

[a] 1-μL sample aliquot. [b] 10-μL sample aliquot, μ-arc Atomizer. Taken from ref. 4. [c] Calculated for 10-μL sample aliquot. Taken from ref. 11 and 12.

experimental error, indicating a linear relationship between emission intensity and concentration. Dynamic ranges for these elements are between 3 and 5 orders of magnitude. Both Mn I (279.5 nm) and Mg I (285.2 nm) were adversely affected by instability of the strong OH spectral background features which overlap these lines, causing decreased log–log plot slopes, decreased dynamic ranges, and degradation in detection limit for both elements.

The analytical calibration curve for Ca I (422.7 nm) (cf. Figure 5) has a slope significantly greater than one and a dynamic range of less than two orders of magnitude. In addition, Ca determination is adversely affected by Ca contamination from the microarc filament, which increases noise on both the baseline and the signal. The sensitivity of Ca at 422.7 nm is lower than expected, presumably because of Ca excitation to higher states and because of Ca ionization. Examination of the Ca II (393.4 nm) line (cf. Figure 5) showed slightly increased sensitivity compared to the Ca I (422.7 nm) line and an analytical calibration plot which was moderately extended toward higher concentration. The slope of this plot was also significantly greater than one. These results suggest that a number of Ca lines must be examined for the optimum SNR and dynamic range to be realized with this MIP.

Emission signals obtained for aqueous Na standards were extremely low and irreproducible for all concentrations. It was assumed that the Na was being ionized, and so 100 μg/mL Rb, as an ionization suppressor, was added to each standard solution. An analytical calibration curve extending almost 3 orders of magnitude was obtained then. This plot, shown in Figure 5, has a slope less than 1.0, presumably because of self-absorption by atoms exiting at the cooler viewing end of the chamber.

Detection Limits. Table II compares detection limits obtained for a number of elements using the new helium MIP

with those cited in recent publications (*11*, *12*). The new MIP detection limits are improved in most cases over those obtained with single-shot sample injection and are improved in all cases over continuous nebulization sample injection systems. Significantly, the detection limits obtained on the present single-shot He MIP system were calculated on the basis of the 1-μL sample aliquot actually used, and therefore represent routinely obtainable values.

Interferences. MIPs have been noted to be affected by the introduction of relatively large amounts of sample material ($\sim$1 μg absolute). However, the new plasma remained ignited during injection of sample material up to the maximum amount atomizable from the microarc used, about 5 μg absolute. Of course, the relative standard deviation of the measured signal degrades as larger and larger amounts of material are atomized into the plasma; however, the plasma remains ignited and, in that sense, proves to be a significantly more durable source than many previous MIPs.

As suggested earlier, ionization interferences are expected in any MIP, and in the new plasma a significant amount of ionization of any easily ionizable element (e.g., Ca, Na, Li) appears to occur. As in most determinations, an ionization suppressant can be employed to overcome such interferences. Further examination of ion emission lines is warranted to determine their analytical utility.

Refractory elements, such as Al and Si, have been found to exert little effect on analyte signals in the plasma. This result is not unexpected in view of the use of the microarc sample atomizer (*4*). However, further investigations of solute vaporization interferences are necessary and are currently under way.

CONCLUSIONS

The atmospheric pressure, helium microwave-induced plasma generated in the cavity designed by Beenakker (*1*) is a durable, stable, and highly efficient excitation source for emission spectrometry of metallic elements. It is easy to ignite and operate and uses low volumes of inert support gas. Moreover, the cavity does not require cooling. Although injected material does lead to reduced excitation efficiency and increased instability, this MIP exhibits a significant improvement over other versions of microwave-induced plasma in its tolerance of sample and solvent material. The high temperature of the new plasma leads to increased ionization and population of higher excited states; this result requires careful choice of emission lines to be used for analytical measurement. Dynamic background correction should prove useful with this plasma for the elimination of broadband molecular emissions.

ACKNOWLEDGMENT

The authors thank C. I. M. Beenakker for useful discussions concerning the use of his new cavity. Also, we greatly appreciated the assistance of Rodney K. Williams in early stages of the investigation.

LITERATURE CITED

(1) C. I. M. Beenakker, *Spectrochim. Acta, Part B*, **31**, 483 (1976).
(2) C. I. M. Beenakker, Paper 305, Pittsburgh Conference on Analytical Chemistry and Applied Spectroscopy, Cleveland, Ohio, March 1977.
(3) C. I. M. Beenakker, *Spectrochim. Acta, Part B*, **32**, 173 (1977).
(4) L. R. Layman and G. M. Hieftje, *Anal. Chem.*, **47**, 194 (1975).
(5) S. Ramo and J. R. Whinnery, "Fields and Waves in Modern Radio", 2nd ed., John Wiley & Sons, New York, N.Y., 1953.
(6) A. G. Gaydon, "The Spectroscopy of Flames", 2nd ed., John Wiley & Sons, New York, N.Y., 1974.
(7) I. Kopp, R. Lindgren, and B. Rydh, "Table of Band Features of Diatomic Molecules by Wavelength Order", Version A, Institute of Physics, University of Stockholm, Stockholm, Sweden.
(8) P. M. Houpt, *Anal. Chim. Acta*, **86**, 129 (1976).
(9) K. Fallgatter, V. Svoboda, and J. D. Winefordner, *Appl. Spectrosc.*, **25**, 347 (1971).
(10) W. L. Wiese, M. W. Smith, and B. M. Glennon, "Atomic Transition Probabilities—Hydrogen Through Neon", NSRDS-National Bureau of Standards, 4, Vol. 1, U.S. Government Printing Office, Washington, D.C., 1966.
(11) R. K. Skogerboe and G. N. Coleman, *Anal. Chem.*, **48**, 611A (1976).
(12) S. Greenfield, H. McD. McGeachin, and P. B. Smith, *Talanta*, **22**, 553 (1975).

RECEIVED for review February 10, 1978. Accepted May 5, 1978. Supported in part by the Office of Naval Research, by the National Institutes of Health through grant PHS GM 17904-05, and by the National Science Foundation through grant CHE 76-10896.

Quantitative Detection of Trace Impurities in Gases by Infrared Spectrometry of Cryogenic Solutions

Samuel M. Freund,* William B. Maier II, Redus F. Holland, and Willard H. Beattie

University of California, Los Alamos Scientific Laboratory, P.O. Box 1663, Los Alamos, New Mexico 87545

A technique for considerably improving the sensitivity and specificity of infrared spectrometry as applied to quantitative determination of trace impurities in various carrier or solvent gases is presented. A gas to be examined for impurities is liquefied and infrared absorption spectra of the liquid are obtained. Spectral simplification and number densities of impurities in the optical path are substantially higher than are obtainable in similar gas-phase analyses. Carbon dioxide impurity ($\sim$2 ppm) present in commercial Xe and ppm levels of Freon 12 and vinyl chloride added to liquefied air are used to illustrate the method.

There are several methods for identifying and determining trace impurities in gases, such as mass spectroscopy, gas chromatography, and infrared spectrometry, or a combination of these methods. Infrared spectrometry has the advantage of being a versatile technique, but it suffers from poor sensitivity and occasionally from poor specificity, i.e., from difficulty in identifying overlapping bands of different compounds when complex mixtures are to be analyzed. Very long pathlengths may be employed to overcome the poor sensitivity, but with certain mixtures, quantitative and often qualitative analyses are still impossible.

In this paper we present a technique for greatly improving the sensitivity and specificity of infrared spectrometry as applied to quantitative determination of some trace impurities in gases by utilizing cryogenic solutions. A gas to be examined for impurities is cooled and pressurized until it becomes a liquid, which is a solvent for the impurities.

Solubilities of trace gases in liquefied carrier gases are often

0003-2700/78/0350-1260$01.00/0

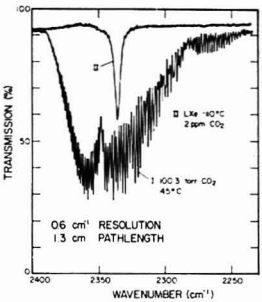

Figure 1. Infrared spectrum of 100.3 Torr of CO_2 vapor at 45 °C (curve I) and that of 2 ppm of CO_2 impurity in liquid Xe at −110 °C (curve II). In the vapor, the $^{12}CO_2$ band overlaps that of $^{13}CO_2$ at the longer wavelengths

sufficiently high to make analyses practical. Since molecular densities in liquids are $\sim 2 \times 10^{22}$ molecules/ cm^3, a 1-ppm level of some impurity translates into $\geq 10^{16}$ molecules/cm^3 of impurity in solution, much above the molecular density in the gas phase. Molecular rotation is suppressed in solution, so that the generally complex rotational structure of a solute vibrational band usually collapses to a single, sharp feature having a peak absorbance (at moderate resolutions) higher than that for the gas at room temperature. Provided that the liquefied carrier gas is essentially free of infrared absorptions at wavelengths where the impurities absorb, detection of low levels (ppm–ppb) of impurities can be performed.

The technique is illustrated with four examples. Vinyl chloride (C_2H_3Cl) and dichlorodifluoromethane (CCl_2F_2) are dissolved at ppm concentrations in liquid air, and commercially available spectroscopic grade Xe is liquefied in order to examine CO_2 and fluorocarbon impurities. Part-per-million levels of impurities are easily and quantitatively observable in cells with about 1-cm optical pathlengths.

EXPERIMENTAL

Infrared spectra were obtained with a Perkin-Elmer Model 180 scanning spectrometer which was continuously flushed with dry nitrogen. Instrumental time constants were of the order of 2 s.

The vacuum insulated, copper cryogenic cells used have been described elsewhere (*1*). Optical pathlengths and cell volumes were 1.3 cm and 2.6 cm^3, respectively, for the experiments conducted in liquid Xe (LXe) and 2.6 cm and 5.0 cm^3 for those in liquid air (LAir). Calcium fluoride windows were utilized in both cases.

All of the gases employed were used as supplied by the manufacturers without further purification.

In order to determine the approximate range of sensitivity of the technique, it was necessary to measure the peak absorption cross sections of the dissolved test gases. Two procedures for dissolution were employed. In the first, a solute gas of interest was mixed with the solvent gas and introduced into the empty, room temperature cell. The lower portion of the cell was cooled and the upper portion heated to condense the solvent gas and additive gas only in the bottom of the cell. During the condensation, a source of solvent gas was kept open to the cell. The second procedure commenced with a cell partly filled with the solvent liquid and maintained at the final temperature of interest. The premixed solute and a small amount of solvent gas were then rapidly swept into the cell with additional solvent gas and condensation was allowed to proceed until the viewing volume was filled—this point is determined by direct observation of the liquid level in the cell. In both procedures, the solution was stirred with a Teflon coated magnetic bar driven by an external source. These mixing procedures cannot put more than the measured amount of additive gas into the cell; therefore, the additive levels quoted herein are upper limits to the concentrations.

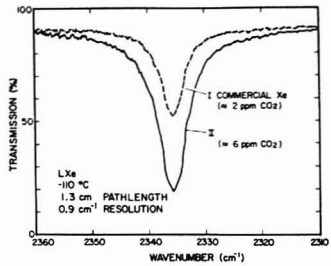

Figure 2. Infrared spectrum of 6 ppm total CO_2 dissolved in liquid Xe at −110°C (curve I) and that of the commercial LXe used, which has about 2 ppm CO_2 impurity (Curve II)

RESULTS AND DISCUSSION

The results from the CO_2 calibration and trace determination experiments are shown in Figures 1 and 2. In Figure 1, we compare the 4-μm vapor phase spectrum of pure CO_2 at 45 °C with a spectrum of the CO_2 impurity in the liquefied (−110 °C) commercial spectroscopic grade xenon used in our laboratory. [Substantial (∼1–100 ppm) fluorocarbon impurities have been found in samples of spectroscopic grade rare gases from several suppliers. Spectra are not given herein. The manufacturer's specifications quote <0.5 ppm CO_2 and levels of fluorocarbons "too low to measure".] The absorption in curve II of Figure 1 corresponds to about 2 ppm of CO_2 in the xenon sample. The absorption feature of dissolved $^{13}CO_2$ in natural abundance is just perceptible at 2271 cm^{-1} and corresponds to ∼0.02 ppm.

Note the almost complete suppression of rotational structure in the liquid phase. Further, the ν_3 band of the solvated CO_2 is broader than the individual rotational features resolved in the vapor phase spectrum, although the instrumental resolution for the two traces is identical. The width of the band in solution may be partly the result of the CO_2 molecules being located in a variety of environments in the liquid xenon. In other cryogenic solvents, the width of the spectral features may be different (*2*). Actually, the width of the CO_2 bands in Xe solution is convenient for quantitative analysis, since for accurate measurement of absorbance, the spectrometer pass band needs to be appreciably narrower than the spectral width of the absorption features. This requirement is easily satisfied in the solutions, with the resolutions indicated in Figures 1 and 2. Considerably higher resolutions than the Model 180 allows would be required to measure accurately the absorbance for the CO_2 gas at the pressure of Figure 1.

Figure 2 shows a spectral scan of approximately 6 ppm total CO_2 dissolved in LXe and a scan of LXe containing CO_2 impurity as in Figure 1. These spectra were obtained at a slower scan speed in order to improve the quantitative determination of the peak heights. The substantial signal-to-noise ratio observed for these CO_2 levels suggests that a factor of 100 reduction in CO_2 concentration could be measured quantitatively with the same apparatus and conditions. Use of a longer optical pathlength and/or sophisticated data averaging and processing techniques would further improve the sensitivity of the method.

The suppression of rotational structure of solvated molecules is a general phenomenon and can be of great value in the analysis of the spectra of complex mixtures. Figure 3 shows an infrared spectrum in the 10-μm region of a mixture of CF_2Cl_2(0.3 ppm; features at 917.5 and 886.5 cm^{-1}) and C_2H_3Cl (2 ppm; features at 943.0 and 899.0 cm^{-1}) dissolved in liquefied bottled air at −188 °C. This spectrum is compared

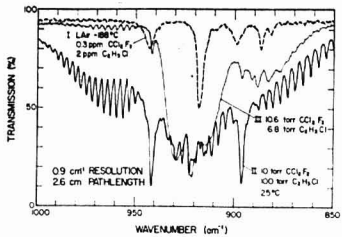

Figure 3. Infrared spectrum (curve I) of the mixture of CCl_2F_2 (0.3 ppm; features at 917.5 and 886.5 cm^{-1}) and C_2H_3Cl (2 ppm; features at 943.0 and 899.0 cm^{-1}) dissolved in liquid air at −188 °C, and spectra of 25 °C mixtures of 10 Torr CCl_2F_2 and 100 Torr of C_2H_3Cl (curve II) and 10.6 Torr of CCl_2F_2 and 6.8 Torr of C_2H_3Cl (curve III)

with those for two gas-phase mixtures of the same compounds. It is apparent that little qualitative or quantitative information can be derived from the vapor phase spectra, whereas the bands of the solvated molecules are completely resolved.

One can test for saturated solutions by raising or lowering the temperature of the liquid and observing the effect on the absorption bands. The additive gases investigated are more soluble at higher temperatures. By maintaining a substantial pressure of solvent gas over the liquid, a broad liquid-phase temperature range is available for a given solvent.

Finally, the liquid-phase features are shifted in energy relative to the origins of vapor phase rotation–vibration bands. For example, gaseous CF_2Cl_2 has band origins at 922 and 882 cm^{-1} (*3*), whereas the observed transitions in solution are at 917.5 and 886.5 cm^{-1}, respectively. The magnitude of this shift is dependent on which solvent is used, but our data suggest that a more reasonable location for the quoted 882 cm^{-1} feature would be somewhat higher than 886.5 cm^{-1}.

CONCLUSIONS

We have demonstrated that conventional infrared spectrometry can be used to analyze trace impurities in some gases with improved sensitivity if the mixture is liquefied. This work utilizes absorption pathlengths of the order of 1 cm, yet achieves sensitivities comparable to pathlengths of many meters under usual vapor-phase conditions. Increasing the effective pathlength by using a multiple traversal scheme or by actually lengthening the absorption cells would further improve the sensitivity of the method. The widths of the features observed in the cryogenic liquids are broader than the resolved rotational lines in low pressure gas-phase spectra but much narrower than those characteristic of high pressure.

Advantages of the technique then are (a) the high densities in the optical path and the higher peak absorption cross sections provide sensitivities which are greatly improved ($>10^3$) over atmospheric pressure gas-phase methodology for similar path lengths; (b) the higher densities of the trace impurities in the liquids mean that errors due to sorption or reaction at the walls of the spectroscopic cell are not as critical as in gases, where extremely small molar concentrations are typical for trace impurities; (c) once absorptivities are known at the liquid temperature, the method gives absolute concentrations independent of the pressure of the original gaseous sample; (d) chemical reactions of species which might be unstable in the gas phase may be suppressed at the very low temperatures used; and (e) the analysis of mixtures may be facilitated by the dramatic simplification of the absorption spectra.

ACKNOWLEDGMENT

The authors thank Bruce Stewart for his technical help and Jack P. Aldridge for his support of this work.

LITERATURE CITED

(1) William B. Maier II, Samuel M. Freund, Redus F. Holland, and Willard H. Beattie, "Photolytic Separation of D from H in Cryogenic Solutions of Formaldehyde", submitted for publication in *J. Chem. Phys.*, 1978.
(2) L. J. Marabella, *Appl. Spectrosc. Rev.*, 7, 313 (1973).
(3) "Tables of Molecular Vibrational Frequencies", T. Shimanouchi, Ed., *Phys. Chem. Ref. Data*, 3, 269 (1974).

RECEIVED for review February 17, 1978. Accepted May 22, 1978. This work was performed under the auspices of the U.S. Department of Energy.

Photoacoustic Spectroscopy Applied to Systems Involving Photoinduced Gas Evolution or Consumption

Robert C. Gray and Allen J. Bard*

Department of Chemistry, The University of Texas at Austin, Austin, Texas 78712

Photoacoustic spectroscopy (PAS) was used to study photoinduced reactions where PAS signals attributable to gas evolution and consumption have been observed in addition to the usual thermally generated pressure fluctuations. Examples of such PAS studies of oxygen consumption in the photooxidation of rubrene and gas evolution in the heterogeneous photocatalytic oxidation of acetic acid to methane and CO_2 at a platinized TiO_2 catalyst are given. The sensitivity of the method and possible further applications are also described.

Recently there has been a resurgence of interest in the theory and applications of the photoacoustic effect and photoacoustic spectroscopy (PAS) (*1–19*). In the usual mode of operation, PAS involves the detection (with a microphone) of a pressure wave induced by thermal changes in a sample upon absorption of light. The sample, enclosed in a leak-tight fixed volume cell, is illuminated with intensity modulated light. If some species in the sample absorbs the light and is promoted to an excited state, relaxation takes place, in part or totally, via radiationless transitions. These radiationless transitions generate heat which diffuses both into the sample and to the sample/gas interface. Heat transferred to the gas at this interface creates a pressure increase in a gas boundary layer at the sample surface which in turn compresses the remaining gas in the fixed volume cell. The amplitude of the pressure wave thus created depends on the incident light intensity, the modulation frequency, the relative thermal properties of the sample and gas, cell geometry, optical ab-

0003-2700/78/0350-1262$01.00/0

sorption coefficient of the sample species, the concentration of the absorbing species in the sample, and the quantum efficiency of the sample for radiative and nonradiative relaxation. Although a high quantum efficiency for radiative pathways leads to lower PAS signals, even in samples with luminescent efficiencies approaching unity a PAS signal may still be observed because of vibrational and solvent relaxation.

An alternate application of PAS, which has not to our knowledge previously been suggested, is to photochemical systems which involve the consumption or evolution of gases. In this case, pressure waves are generated directly by the modulated gas volume changes in addition to any photothermal pressure effects. There are a number of materials in which such effects might be observed, including those which undergo photoinduced reactions with oxygen, heterogeneous photocatalysts which induce gas phase or liquid phase reactions, and materials which show photoinduced adsorption or desorption of gases. In this paper we discuss this novel application of PAS and describe two experimental studies which illustrate this effect.

EXPERIMENTAL

Instrumentation. The spectrometer used in these studies is of the single beam variety similar to that previously described (*13*). The PAS signals detected by the lock-in amplifier, Princeton Applied Research (PAR) Model 186, were digitized and stored in a PAR Model 4101 scan recorder. All spectra were normalized to a carbon powder spectrum recorded under identical conditions and stored in the second channel of the scan recorder. No attempt was made to correct for lamp intensity fluctuations. Our studies indicated that short term lamp noise was primarily of a much higher frequency than the chopping rate and, therefore, was unimportant. Long term lamp drift amounted to no more than 0.5% per hour. Spectral noise was no more than ±2% of full scale for a carbon black signal. This noise was primarily due to quantizing errors in the analog-to-digital converter of the scan recorder and short term lamp fluctuations, these errors being amplified by the normalization process.

A new sample cell design was used with this system, which will be described in detail elsewhere (*20*). This cell provided for easier changing of samples and a smaller gas volume (0.2–0.25 cm^3, depending on sample probe) and increased sensitivity compared to our previous one (*13*). The microphone used with this new cell was a B&K Model 4148 polarized by a highly stabilized 120-V power supply, yielding a sensitivity of 60 mV/Pa. The preamplifier used was identical with that of Munroe and Reichard (*21*).

Chemicals. Rubrene samples were prepared by dry mixing appropriate amounts of rubrene and magnesium oxide and adding a small amount of benzene to dissolve the rubrene. The resulting solution was either allowed to evaporate in air or the solvent was stripped in a Roto-vap to yield a dry powder of magnesium oxide uniformly coated with rubrene. These samples were prepared and stored until use in subdued light. The platinized TiO_2 was prepared by irradiation of a suspension of anatase in a solution of acetic acid and H_2PtCl_6 with a Hg-Xe lamp, as described in a recent communication (*22*). A weighed amount of the powder was introduced into the cell along with quantities of water and acetic acid measured with a microliter syringe.

RESULTS AND DISCUSSION

The thickness of the gas boundary layer (acoustic piston) (*1*, *2*) formed by thermal diffusion in the gas, μ_g, is given by

$$\mu_g \cong (2\alpha_g/\omega)^{1/2} \qquad (1)$$

where ω is the chopping frequency (rad/s) and α_g is the thermal diffusivity of the gas (cm^2/s). For air at chopping frequency of 100 Hz, μ_g is about 0.2 cm. It is this boundary layer which is heated by thermal transfer from the sample surface and which in turn acts as a piston to compress the remaining gas in the cell. While the primary mechanism of motion of this boundary layer is heating and cooling through

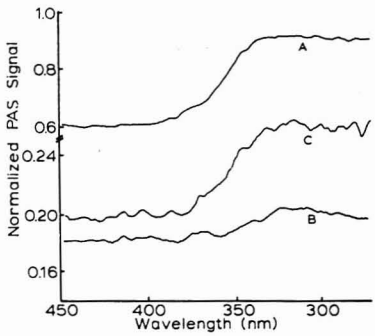

Figure 1. Effect of gas evolution on the PAS signals for platinized doped TiO_2 (anatase) in absence and presence of acetic acid. All spectra are normalized to carbon black. Experimental conditions: 6 nm resolution, 100 nm/min scan rate, 1-s time constant. (A) dry TiO_2 powder; (B) TiO_2 powder wet with benzonitrile; (C) sample in B with 10 μL of acetic acid added

thermal transfer, any other perturbation which affects the pressure of this region will be reflected in the PAS signal. For example, if the sample upon illumination releases a gas, this gas will be added directly to the boundary layer increasing the pressure of the boundary layer above that for simple thermal transfer. The thermal transfer component of the PAS signal can and probably will still be present, however, and thus comparative studies will be necessary to determine the extent of signal enhancement by gas release. When a photoinitiated reaction consumes gas (e.g., O_2) from the boundary layer, the pressure in the boundary layer decreases. Again the boundary layer is still subject to thermal transfer from the sample. Thus, gas consumption may appear as a decrease in the normal PAS signal or even as a negative going signal, depending upon the relative rates of gas consumption and thermal transfer to the gas. Under conditions of coherent detection, phase shifts in the signal (with respect to a carbon black reference) can approach 180°.

Heterogeneous Photocatalytic Decomposition of Acetic Acid on Pt/TiO_2. In a recent report from this laboratory the decomposition of acetic acid containing suspended platinized anatase (Pt/TiO_2) powder under irradiation to form methane and CO_2 was described (*22*):

$$CH_3COOH \xrightarrow[h\nu]{Pt/TiO_2} CH_4 + CO_2 \qquad (2)$$

This reaction was chosen to illustrate the application of PAS to the study of heterogeneous photocatalysis. The usual PAS spectrum of the Pt/TiO_2 catalyst in the dry powdered form is shown in Figure 1A. The onset of light absorption occurs at 380 nm which corresponds to the known band gap energy (E_g) of anatase, 3.25 eV. When the sample is wet with benzonitrile, which does not undergo photodecomposition, the signal level is much smaller (Figure 1B), as is frequently observed with solid samples contacting liquids in PAS. However, when 10 μL of glacial acetic acid are added to the sample, the signal level above E_g is clearly enhanced while the signal at longer wavelengths remains about the same. This clearly indicates an increase of the PAS signal due to gas release from the sample into the gas boundary layer. Similar experiments in which the catalyst was first wet with water, followed by addition of acetic acid have shown the same signal enhancement. The PAS study of heterogeneous photocatalysis clearly allows the action spectrum of the catalyst to be determined and should prove useful in determining the relative

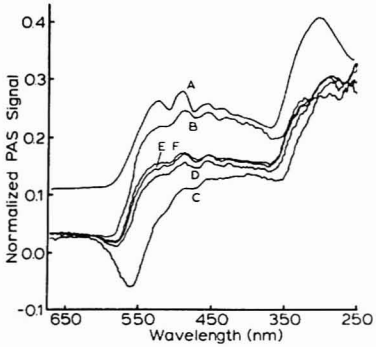

Figure 2. PAS of rubrene supported on MgO powder. Experimental conditions as in Figure 1. (A) reflectance spectrum of 5 wt % rubrene on MgO, dried in Roto-vap (ordinate in arbitrary units); (B) PAS spectrum of sample in A; (C) PAS spectrum of sample in B solvated with benzene, first scan; (D)–(F) are successive scans following C

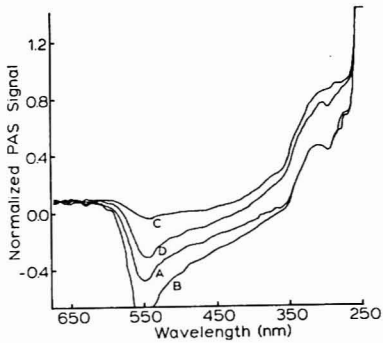

Figure 3. PAS of rubrene supported on MgO powder and dampened with benzene. Experimental conditions as in Figure 1. (A) first scan; (B) after sample in A allowed to stand in dark for 1 h; (C) after exposure of sample to full white light intensity of Xe lamp for 10 min; (D) after sample in C allowed to stand in dark for 15 min

efficiencies of different materials. A study of the PAS signal level as a function of chopping frequency should allow determination of the reaction rates. Studies of this type are currently under investigation.

Rubrene–Oxygen System. The photosensitized reaction of many aromatic hydrocarbons, such as rubrene (tetraphenylnaphthacene), with O_2 to form the endoperoxide has been widely studied [See (*23-25*) and references therein]. The reaction proceeds by the absorption of light by the rubrene, energy transfer to form singlet oxygen and attack of the singlet oxygen on the rubrene. The overall reaction is thus

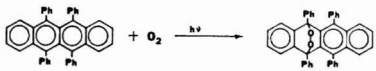

Rubrene in solution shows absorption bands beginning at about 580 nm. Formation of the peroxide destroys the conjugation in one of the interior rings producing a pale yellow product whose absorption spectrum should be similar to that of 1,4-diphenylnaphthalene, with a broad featureless band centered at 300 nm. The PAS spectrum of a sample of 5 wt % rubrene on MgO dried in a Roto-vap is shown in Figure 2B. The PAS spectrum of this sample was close to that obtained by diffuse reflectance (Figure 2A) and was unchanged upon repeated scans. If the rubrene from this sample is redissolved in a small quantity of benzene which is allowed to evaporate in air to apparent dryness, enough benzene is retained on the sample to solvate the rubrene and, on exposure to light of wavelengths shorter than 580 nm in the presence of oxygen, the endoperoxidation reaction proceeds. The first scan from long wavelengths in taking the PAS spectrum of such a sample (Figure 2C) shows a large *negative* going transient due to oxygen uptake from the gas boundary layer which, in this case, is larger than the thermal diffusion signal at wavelengths at the foot of the absorption region. At shorter wavelengths, the absorbance increases and the negative O_2-uptake signal is overtaken by the thermal signal. Figures 2, D–F are scans recorded immediately after 2C. Note that the initial negative-going signal is smaller on the second scan (D) and has disappeared by scan F. Note also the shoulder which grows in at 300 nm. This is the region where the photoproduct is expected to absorb. The final signal (F) looks much like the original one except for a diminished overall intensity in the rubrene band and the presence of a new band at 300 nm. This spectrum can be attributed to unreacted rubrene lying under a layer of the photoproduct. PAS signals due to layers such as this one have been reported previously (*18, 19*). Physical examination of the sample after scan F reveals a yellowish band where the light had fallen. Slightly disturbing the sample surface with a spatula exposed a fresh surface and the same sequence of spectra (2C–F) were obtained: this process could be repeated until all of the powder surface area had reacted.

Since only the slightest trace of benzene solvent was present in the previous sample, diffusional mobility of the rubrene molecule was quite limited. A second, similarly prepared, sample was dampened with benzene to increase the mobility of rubrene. The spectra obtained for this sample are given in Figure 3. The signal in Figure 3A goes negative at the onset of rubrene absorption and remained negative until the onset of the photoproduct absorption band. The strong band in the UV end of the spectrum is due to the benzene absorption band at 260 nm. If the sample was then placed in the dark for 1 h, the spectrum in Figure 3B was obtained. The difference between A and B probably arises because the original sample was loaded in a room illuminated with fluorescent lamps, allowing partial reaction of the surface of the sample before A was run. On standing in the dark, the rubrene could reestablish a fresh homogeneous sample surface. Photolysis of the sample in the full white light intensity of the lamp for 10 min gave rise to spectrum C. In this spectrum, the exposed sample area has been almost totally reacted, as evidenced by the absence of an absorption band by rubrene and the presence of a strong photoproduct band. After this sample stood in the dark for 15 min, spectrum D was obtained. Either unreacted rubrene had diffused into the illuminated area and some of the photoproducts had diffused out or decomposition of the endoperoxide occurred. This would produce an increased negative-going signal at the rubrene wavelengths and a decreased signal at the photoproducts wavelength. Photolysis for a sufficiently long time eventually removed all signals at the rubrene wavelengths leaving only the photoproduct band. Note that this negative-going PAS signal and the observed time dependent behavior were unique to rubrene. Samples of other materials which do not react with oxygen (e.g. anthracene or 9,10-dibromoanthracene) do not show such a response.

Photoinitiated reactions with oxygen (or other gases) are important in several areas, such as the photodegradation of polymers, pharmaceuticals, and foods. PAS measurements could play a useful role in the study of such reactions.

CONCLUSIONS

These examples demonstrate the utility of PAS in the study of photochemical reactions involving gas evolution and consumption. An estimate of the sensitivity of the technique can be obtained by assuming a sinusoidal wave form and a minimum detectable signal level of 1% of that of carbon black powder.

The sensitivity of the microphone is 6 mV/μbar; the cell volume, 0.25 cm^3; and the average signal level found for carbon black powder was 1 mV. This signal level corresponds to an rms pressure change of 0.17 μbar. Assuming an ideal gas, we find this is equivalent to a gas volume change of 4.2×10^{-8} cm^3 rms (or 1.2×10^{-7} cm^3 peak to peak). Thus, detection at 1% represents 1.2×10^{-9}cm^3 (p–p) and at STP this corresponds to 5.3×10^{-14} mol of gas consumed or released per cycle. The average scan time of a PAS spectrum was 200 s, so that at 60-Hz modulation frequency, a maximum of 6.3×10^{-11} mol of gas need be produced or consumed to be detectable in an entire scan. Even if signal levels approaching that of carbon are required, the total amount of gas is only 6.3×10^{-9} mol. Clearly PAS is quite a sensitive technique for studying these types of reactions. Note also that the above calculation assumes irradiation with monochromatic light of rather low intensity (about 1 mW/cm^2). Much larger signals could be obtained using laser excitation or the full output of the xenon lamp. Cells could easily be constructed as well to measure photoeffects directly by sunlight.

While the technique can be used for comparative measurement and for obtaining action spectra for photochemical reactions, careful calibration and a suitable theoretical model may allow the use of PAS in quantitative studies as well. We must stress that this is only a preliminary study and the method requires further investigation. However, the basic concepts described here appear correct and these early successes are quite encouraging.

ACKNOWLEDGMENT

We are indebted to Bernhard Kraeutler for the sample of Pt/TiO_2 and to Michael E. Long for obtaining the reflectance spectrum of rubrene–MgO.

LITERATURE CITED

(1) A. Rosencwaig and A. Gersho, *Science*, **190**, 557 (1975).
(2) A. Rosencwaig and A. Gersho, *J. Appl. Phys.*, **47**, 64 (1976).
(3) A. Afromowitz, P-S. Yeh, and S. Yee, *J. Appl. Phys.*, **48**, 209 (1977).
(4) H. S. Bennett and R. A. Forman, *Appl. Opt.*, **15**, 1313 (1976).
(5) H. S. Bennett and N. A. Forman, *Appl. Opt.*, **15**, 2405 (1976).
(6) H. S. Bennett and R. A. Forman, *J. Appl. Phys.*, **48**, 1432 (1977).
(7) J. G. Parker, *Appl. Opt.*, **12**, 2974 (1973).
(8) L. C. Aamodt, J. C. Murphy, and J. G. Parker, *J. Appl. Phys.*, **48** 927 (1977).
(9) J. C. Murphy and L. C. Aamodt, *J. Appl. Phys.*, **48**, 3502 (1977).
(10) A. Rosencwaig, *Anal. Chem.*, **47**, 592A (1975).
(11) W. R. Harshbarger and M. B. Robin, *Acc. Chem. Res.*, **6**, 329 (1973).
(12) M. J. Adams, S. C. Beadle, A. A. King, and G. F. Kirkbright, *Analyst (London)*, **101**, 553 (1976).
(13) R. C. Gray, V. A. Fishman, and A. J. Bard, *Anal. Chem.*, **49**, 697 (1977).
(14) J. B. Callis, *J. Res. Nat. Bur. Stand., Sect. A*, **80**, 413 (1976).
(15) W. Lahmann and H. J. Ludewig, *Chem. Phys. Lett.*, **45**, 177 (1977).
(16) M. J. Adams, J. G. Highfield, and G. F. Kirkbright, *Anal. Chem.*, **49**, 1850 (1977).
(17) J. A. Burt, *Anal. Chem.*, **49**, 1130 (1977).
(18) M. J. Adams, and G. F. Kirkbright, *Analyst (London)*, **102**, 281 (1977).
(19) M. J. Adams, and G. F. Kirkbright, *Spectrosc. Lett.*, **9**, 255 (1976).
(20) R. C. Gray and A. J. Bard, manuscript in preparation.
(21) D. M. Munroe and H. S. Reichard, Princeton Applied Research, *Appl. Note*, **147**.
(22) B. Kraeutler and A. J. Bard, *J. Am. Chem. Soc.*, **100**, 2239 (1978); **99**, 7729 (1977).
(23) K. Gollnick, in "Advances in Photochemistry", W. A. Noyes, Jr., G. S. Hammond, and J. N. Pitts, Jr., Ed., Vol. 6, Interscience, New York, N.Y., 1968.
(24) B. Munroe, *J. Phys. Chem.*, **81**, 1861 (1977).
(25) B. Stevens and J. A. Ors, *J. Phys. Chem.*, **80**, 2164 (1976).

RECEIVED for review March 9, 1978. Accepted May 15, 1978. The support of this research by the National Science Foundation is gratefully acknowledged.

X-ray Microanalysis of a Natural Mordenite-Containing Rock and Its Ion-Exchanged Derivatives

János Papp,* Erzsébet Czárán, and András Jánossy[1]

Central Research Institute for Chemistry of the Hungarian Academy of Sciences, P.O. Box 17, 1525 Budapest, Hungary

The chemical composition of a natural mordenite and its ion-exchanged derivatives was determined by x-ray microanalysis. In the analysis, crystal particles smaller than 0.5 μm were used, which are thin enough to make ZAF correction unnecessary. Sufficiently accurate quantitative results can be obtained by the revised methods of Russ and of Hall, or by the combination of the two. Interaction with various agents leads to different extents of ion exchange, while treatment with hydrochloric acid leads to a partial dealumination, as well.

Natural zeolites of practical significance are found generally as sedimentary rock which contains other crystalline and amorphous materials as well. The determination of the chemical composition of the zeolite phase is largely impeded since the zeolite phase cannot be separated from the secondary minerals by simple means. Yet the proper knowledge of the chemical composition of the zeolite and its modified, e.g. ion-exchanged, form is essential when using them as catalysts or adsorbents.

There is a convenient method which allows direct chemical analysis without separation: x-ray microanalysis (*1*). In the present paper, we describe our analytical results obtained on the crystalline phase of a natural mordenite mineral of Hungarian origin.

Single mordenite crystals are usually much smaller than the x-ray spatial resolution (governed mainly by electron spreading in the sample) on thick materials, so the conventional microprobe approach had to be rejected. Instead, we analyzed single crystals on carbon-coated electron microscopic grids in the transmission mode where the analyzed thickness was below 0.5 μm. Efforts were made to analyze

[1] Institute of Biophysics, Biological Research Centre, Hungarian Academy of Sciences, P.O. Box 521, 6701 Szeged, Hungary.

0003-2700/78/0350-1265$01.00/0

only the well-defined mordenite crystals and no adhering non-zeolitic phase, but this disturbance cannot be completely eliminated.

EXPERIMENTAL

Specimen Preparation. The mordenite-containing rhyolite tuff from the Tokaj mountains (Hungary) and its modified derivatives were disintegrated in a porcelain mortar, suspended in diethyl ether and, after sedimentation of rough parts (>1 μm), the suspension was poured onto carbon coated Mo grids. (Cu grids could not be employed since the Cu L lines interfere with the Na Kα line). Mordenite crystals in the original form and its NH_4-, Ag-, and H-forms were investigated.

Ion exchange was performed in all cases under static circumstances with 0.1 N, 1 N, 3 N HCl, 2 N NH_4Cl, and 2 N $AgNO_3$ solutions.

One hundred grams of the original sample (grain size between 1.0 and 1.6 mm) was treated with 400 cm^3 solution, by refluxing the mixture 3 times for 4 h, each time with a fresh solution. After treatment, all samples were washed repeatedly till Cl^-- or Ag^+-free with distilled water to remove physically adsorbed HCl, NH_4Cl, and $AgNO_3$.

Carbon replicas were prepared for transmission electron microscopy in the usual way (2).

Transmission electron microscopy was performed on a Zeiss EF instrument with 50-kV accelerating voltage.

X-ray Microanalysis. Analysis was performed with a JEOL 100B transmission electron microscope fitted with an energy dispersive x-ray microanalyzer EDAX 707B at E_0 = 80-kV accelerating voltage exclusively on parts smaller than 0.5 μm for reasons explained above. The electron beam was focused to a spot of approximately 300 nm in diameter. The spectrum was recorded between 0–40 keV with 50 eV/channel sensitivity. For quantitative evaluation, the raw spectrum was background subtracted by the frequency filter method (3) and net peak intensities (1.2 times full width at half maximum) were recorded with an integrated microprocessor (EDIT III). Part of the background spectrum between 30 and 40 keV was also recorded.

QUANTITATION

Intensity and Concentration. The characteristic x-ray intensity, I_i of element i excited by electron beam current i_0 for t s is:

$$I_i = i_0 t \omega_i Q_i L_i T_i N_i \tag{1}$$

with ω_i = fluorescence yield, Q_i = ionization cross section, L_i = fraction of recorded line intensity to total excited intensity, T_i = detector efficiency for observed radiation of element i, N_i = number of atoms i per cm^3. ω_i was taken from the tables of Bertin (4), Q_i was calculated as discussed by Powell (5) and L_i was calculated from the relative line intensity tables of Johnson and White (6) taking into account the proper energy window width on the analyzer. Spectrometer efficiency T_i depends on the detector solid angle $d\Omega/4\pi$ and absorption in the protecting Be window (7.5 μm), the Au contact layer (0.02 μm), and the Si dead layer (0.15 μm). For high energy x-rays (>15 keV), the thickness of the active zone (4.0 mm) has to be considered as well. According to Russ (7), the detector efficiency can be well described by the following empirical equation:

$$T_i = \frac{d\Omega}{4\pi} \exp\left(-\frac{k_1}{E_i^{2.8}}\right)\left[1 - \exp\left(-\frac{k_2}{E_i^{2.8}}\right)\right] \tag{2}$$

where the first exponential term is characteristic of x-ray absorption before the x-ray reaches the active detector zone, and the second term characterizes the process of x-ray penetration through the whole active zone without detection; E_i is the energy of the x-ray in keV. The empirical constants k_1 and k_2 were calculated from the manufacturer's suggested detector data (see above) and also determined by measuring the Lα/Kα intensity ration of Cu (8), yielding in good agreement $k_1 = 1.11 \pm 0.03$ and $k_2 = 20.500 \pm 400$ for our actual system.

The continuum intensity b_ν can be described by a modified Kramers' equation (9, 10)

$$b_\nu = i_0 t \left(\frac{E_0 - E}{E_\nu}\right)^{1.11} Z^n \tag{3}$$

where E_0 = accelerating voltage in kV, E_ν = measured continuum energy in keV, K = empirical constant, Z = atomic number, and $n = f(E_0, E_\nu, Z)$ (11).

In composite materials, the number of atoms N_i in 1 cm^3 will be

$$N_i = \frac{c_i \rho N_0}{A_i} \tag{4}$$

with c_i = weight fraction of element i, ρ = density of composite material, N_0 = Loschmidt's number, and A_i = atomic weight of element i.

Thus, from Equations 1 and 4, the characteristic intensity I_i in a composite material is

$$L_i = i_0 t \omega_i Q_i L_i T_i \frac{c_i}{A_i} \rho N_0 \tag{5}$$

Similarly, the continuum intensity at the particular energy E_ν is

$$b_\nu = i_0 t K \left(\frac{E_0 - E_\nu}{E_\nu}\right)^{1.11} \sum_{i=1}^{i=i} c_i Z_i^n \tag{6}$$

Determination of Elemental Ratios after Russ. Russ (12, 13) has constructed empirical tables which allow direct determination of elemental concentration ratios (elemental or weight fractions) from measured intensity ratios without standards. Since these tables contain many simplifications which affect accuracy, we derived our own values from Equation 5 for weight ratios c_j/c_k of elements j and k:

$$\frac{c_j}{c_k} = \frac{I_j}{I_k} \frac{\omega_k Q_k L_k T_k A_j}{\omega_j Q_j L_j T_j A_k} \tag{7}$$

or with

$$a_i = \frac{c_i}{A_i} \Big/ \sum_{i=1}^{i=i} \left(\frac{c_i}{A_i}\right) \tag{8}$$

(a_i = the atomic fraction) for atomic ratios a_j/a_k:

$$\frac{a_j}{a_k} = \frac{I_j}{I_k} \frac{\omega_k Q_k L_k T_k}{\omega_j Q_j L_j T_j} \tag{9}$$

Determination of Elemental Ratios after Hall. Elemental ratios can be determined with greater accuracy if standards are measured simultaneously which contain the analyzed elements in known concentrations. From Equations 5 and 6 we obtain, after Hall (14), for the atomic ratio a_j/a_k:

$$\frac{a_j}{a_k} = \frac{R_j \left[a_j{}^{\text{std}} \Big/ \sum_{i=1}^{i=j} \left(a_i Z_i^{n+1}\right)\right]_{\text{std "j"}}}{R_k \left[a_k{}^{\text{std}} \Big/ \sum_{i=1}^{i=k} \left(a_i Z_i^{n+1}\right)\right]_{\text{std "k"}}} \tag{10}$$

where

$$R_j = \frac{\left(\frac{I_i}{b_\nu}\right)_{\text{sp}}}{\left(\frac{I_j}{b_\nu}\right)_{\text{std}}}$$

Table I. Atomic Ratios a_i/a_{Al} of a Chabazite Crystal Determined Chemically and by X-ray Microanalysis after Equation 10

a_i/a_{Al}	chemical analysis	x-ray microanalysis
Si/Al	2.191	2.20 ± 0.06
Na/Al	0.085	0.08 ± 0.02
K/Al	0.019	0.02 ± 0.01
Ca/Al	0.426	0.43 ± 0.07
Mg/Al	0.003	0.00
Fe/Al		0.002 ± 0.001

intensity ratio of specimen (sp) and standard (std) and a_j^{std} = atomic fraction of element j in standard "j". For practical measurements, a selected part b_r of the continuum intensity (from 30 to 40 keV in this case) must be measured as well, which, after the theory of Hall, will be characteristic of the total analyzed mass. The exponent n (cf. Equation 3) was ≈1 for all the elements assayed (*15*). The accuracy of such evaluations has been found by various authors to be ±5%.

Evaluation of the Measurements. The methods of Russ and Hall are only valid when no corrections for atomic number, absorption, and fluorescence (ZAF correction) are needed, e.g., the sample is thin enough to prevent these secondary effects.

For checking the quantitation methods suggested here a chabazite crystal of known composition (*8*) has been analyzed and the atomic ratios a_i/a_{Al} calculated. The chabazite single crystal used as standard was pulverized to obtain particles corresponding in size and shape to those of the mordenite to be analyzed (i.e., 0.5 μm thick).

Equation 10 was used with NaCl, KCl, $CaHPO_4 \cdot 2H_2O$, $FeSO_4 \cdot 2H_2O$, SiO_2, and pure Al as standards, and Equation 9 was applied without standards. Both methods yielded similar results within the error limits, except for the most important a_{Si}/a_{Al} ratio, for which only Equation 10 gave satisfactory results.

We decided therefore to evaluate all subsequent analysis by Equation 10 with chabazite as standard for the Si/Al ratio, and by Equation 9 for the remaining cations without standards.

Table I contains the results of chemical analysis and of x-ray microanalysis together with the mean standard errors.

RESULTS AND DISCUSSION

Transmission electron microscopy of the carbon replicas has shown that mordenite crystallites form needles in the range of 0.2 × 0.3 × 10 μm and 0.5 × 1 × 20 μm (Figure 1).

Microanalysis has revealed the elements Na, Al, Si, K, Ca, and Fe in the untreated mordenite phase, whereas the mobile cations Na, K, Ca as well as Fe and Al (the latter two from the "anion part" of the crystal lattice) were more or less removed by the different treatments applied. Analytical results are summarized in Table II.

In Table II, column 1 contains the atomic ratios, a_i/a_{Al} for elements determined in the mordenite crystals in the rock in its untreated state. Columns 2, 3, and 4 refer to the samples treated with 0.1 N HCl, 1 N HCl, and 3 N HCl, respectively, column 5 to the NH_4Cl treated derivative, and column 6 to the Ag^+-ion-exchanged sample.

Figure 1. Transmission electron micrograph of mordenite crystals. Magnification: × 8500

By applying various treatments we intended to exchange the original Na^+, K^+, and Ca^{2+} ions for protons to a high degree. (This process can be affected by an acid treatment in the most direct way, while after ion exchange with NH_4^+ ions a thermal treatment is needed to remove NH_3, and after treating the samples with $AgNO_3$, protons can be produced by reducing the Ag^+ ions in a H_2 atmosphere.)

In the untreated sample, a strict equivalence of the mobile cations to the aluminum has been found, proving the correctness of the results.

According to the data in columns 2, 3, and 4, the acid treatment resulted only in a partial exchange of the cations except for Na^+ ions, which can be exchanged already with a 1 N HCl solution, under the conditions applied.

At higher acid concentrations, the treatment leads, beside cation exchange, to a certain extent to the dissolution of aluminum from the lattice. In the acid treated samples, the iron content considerably decreases, whereas samples ion-exchanged for NH_4^+ and Ag^+—where the other cations are more extensively exchanged—are practically the same as in the original sample. It seems likely that iron—similarly to aluminum—substitutes silicon isomorphously in the crystal lattice.

Upon exchange with NH_4Cl, the Na^+ and Ca^{2+} ions are fully replaced by NH_4^+ ions, while only one half of the K^+ ions are substituted.

All the cations are exchangeable with Ag^+ ions, thus the maximal amount of protons can be generated in the mordenite by ion exchange with $AgNO_3$ and subsequent reduction of the Ag^+ ions.

The formation of the 100% H^+-form from the NH_4^+-form would not be possible even in the case of a total ion exchange, because during the deammoniation of the NH_4^+-form a certain

Table II. Atomic Ratios a_i/a_{Al} of the Crystalline Phase of the Mordenite-Containing Rock[a]

a_i/a_{Al}	untreated	treated with 0.1 N HCl	treated with 1 N HCl	treated with 3 N HCl	NH_4^+-form	Ag^+-form
	1	2	3	4	5	6
Si/Al	5.24 ± 0.50	5.03 ± 0.64	4.94 ± 0.26	5.87 ± 0.21	5.25 ± 0.28	5.34 ± 0.18
Na/Al	0.39 ± 0.02	0.51 ± 0.19	-	-	-	-
K/Al	0.10 ± 0.04	0.11 ± 0.05	0.08 ± 0.04	0.02 ± 0.01	0.05 ± 0.02	
Ca/Al	0.26 ± 0.02	0.19 ± 0.02	0.09 ± 0.02	0.17 ± 0.02	-	-
Ag/Al	-	-	-	-	-	1.14 ± 0.26
Fe/Al	0.07 ± 0.03	0.05 ± 0.03	0.02 ± 0.004	0.01 ± 0.003	0.05 ± 0.01	0.07 ± 0.01

[a] Results are the mean of 6 to 12 measurements.

dehydroxylation takes place at the same time (*16–19*).

ACKNOWLEDGMENT

Thanks are due to H. Beyer for supplying the chabazite standard and the results of chemical analysis. We thank G. Schay for the thorough reading of the manuscript and for helpful discussion.

LITERATURE CITED

(1) D. R. Beaman, and J. A. Isasi, "Electron Beam Microanalysis", **ASTM STP 506**, American Society for Testing and Materials, Philadelphia, Pa. 1972.
(2) C. E. Hall, "Introduction to Electron Microscopy", McGraw-Hill Book Co., New York, N.Y., 1953.
(3) J. C. Russ, *X-Ray Spectrom.*, **6**, 37–55 (1977).
(4) E. P. Bertin, "Theory and Practice of X-Ray Spectroscopy", Academic Press, New York/London, 1975, p 980.
(5) C. J. Powell, *Rev. Mod. Phys.*, **48**, 33–48 (1976).
(6) G. G. Johnson, Jr., and E. W. White, "X-Ray Emission Wavelengths and keV Tables for Nondiffractive Analysis", ASTM Data Series **DS 46**, American Society for Testing and Materials, Philadelphia, Pa., 1960.
(7) J. C. Russ, *EDAX Editor*, **5** (3), 3–6 (1975).
(8) A. Jánossy, E. Czárán, and J. Papp, *Magy. Kém. Foly.*, **83**, 289 (1977).
(9) H. A. Kramers, *Phil. Mag.*, **46**, 836 (1923).
(10) D. G. W. Smith, C. M. Gold, and D. A. Tomkinson, *X-Ray Spectrom.*, **4**, 149 (1975).
(11) A. Jánossy, Unpublished work.
(12) J. C. Russ, "Thin Section Microanalysis", J. C. Russ and B. J. Panessa, Ed., Proc. Symp. St. Louis, 1973.
(13) (a) A. Hendricks, *EDAX Editor*, **5** (3), 7 (1975); (b) *Ibid.*, p. 13.
(14) T. A. Hall, "The Microprobe Assay of Chemical Elements", in "Physical Techniques in Biological Research", G. Oster, Ed., Academic Press, New York, N.Y., Vol. I/A, 1971, pp 157–275.
(15) A. Jánossy, Unpublished work.
(16) H. Beyer, J. Papp, and D. Kalló, *Acta Chim. Acad. Sci. Hung.*, **84**, 7 (1975).
(17) A. P. Bolton, *Exp. Methods Catal. Res.*, **1976**, Vol. 2.
(18) D. W. Breck, "Zeolite Molecular Sieves", John Wiley, New York, N.Y., 1974.
(19) J. A. Rabó, Ed., "Zeolite Chemistry and Catalysis", *ACS Monogr.*, **171**, (1976).

RECEIVED for review December 12, 1977. Accepted May 3, 1978.

Energy-Dispersive X-ray Spectrometric Analysis of Environmental Samples after Borate Fusion

P. A. Pella,* K. E. Lorber,[1] and K. F. J. Heinrich

Institute for Materials Research, Analytical Chemistry Division, National Bureau of Standards, Washington, D.C. 20234

In order to overcome particle-size and sample inhomogeneity effects in the analysis of environmental samples by energy-dispersive x-ray spectrometry, an automated borate fusion procedure was investigated and applied to the analysis of NBS-SRM 1633 Fly Ash and NBS-SRM 1648 Particulate Matter. Twelve elements in each sample were determined and the results are in agreement with NBS certified values and/or those of other workers, usually within ±5 to 10% for most elements over the concentration range from 70 ppm to 15%. Fly Ash samples were fused with the heavy absorbers La_2O_3 or WO_3 and analyzed using a linear calibration curve, assuming no matrix effects. The particulate samples, however, were fused with lithium tetraborate only and the data were corrected for x-ray absorption and K x-ray line interferences by a NBS mathematical procedure. The limits of detection of this procedure for most of the elements analyzed in the sample were between 10 to 100 ppm.

The elemental composition of environmental samples such as particulates collected from urban aerosols can be quantitatively determined by energy-dispersive x-ray fluorescence spectrometry (EDXRF). Such samples have been analyzed by other workers (*1, 2*). Ambient air aerosols can be collected on thin filter substrata and then measured directly by EDXRF, using thin specimens of known elemental composition for calibration. Since particulate matter collected from aerosols can penetrate the filter medium, significant attenuation of both incident and fluorescent x-rays by the filter can take place, especially for light elements. Absorption effects within the larger collected particles may also be significant, resulting in systematic error (*3*). When particle size effects are appreciable, fusion methods of sample preparation with lithium tetraborate become an attractive alternative.

Fusion methods have been applied to the analysis of geological materials (*4–8*). These can be classified as (a) fusion of the sample followed by a separate casting operation to produce a glass disk for direct x-ray analysis, (b) fusion and grinding where the samples are fused, ground, and pelleted, and (c) fusion and direct solidification where the fused sample solidifies directly in the crucible from which the solid glass disk separates. With the availability of the 95% Pt–5% Au alloy crucible, commercial automated fusion devices have recently been developed, and disks can be prepared by method c (*9*).

The present work was performed to determine whether environmental samples could be analyzed with good accuracy with automated fusion as an alternative to nondestructive sample preparation methods. Two samples consisting of NBS-SRM 1633 Fly Ash and NBS-SRM 1648 Particulate Matter were each analyzed for 12 elements. Monochromatic excitation of the sample was provided by three secondary target x-ray emitters. Several workers (*7, 10*) have reported on the use of heavy absorbers such as lanthanum oxide to minimize x-ray absorption effects in thick samples. This technique has been applied mainly to the determination of light elements below atomic number 26 in mineral specimens. Its principal advantage is that the x-ray intensity from the analyte element approaches a linear function of its concentration in the glass disk, and corrections of x-ray absorption effects by digital computations are, in principle, not required. The heavy absorber method was used in this work in the analysis of the NBS-SRM 1633 Fly Ash to determine if acceptable results could be obtained for elements whose x-ray fluorescence lines cover a broad range of energies from 2.0 to 14.0 keV. In order to avoid severe x-ray line interferences between the analyte x-ray lines and lines of the absorber, lanthanum oxide was used in the analysis of zinc, lead, and strontium, and tungsten oxide for all other elements. Interferences by x-ray lines of the analyte were corrected in an

[1] Present address, Technical University of Graz, Graz, Austria.

empirical manner with standards containing noninterfering elements and the heavy absorber.

The NBS-SRM 1648 particulate sample was analyzed with a digital computation procedure developed at NBS (*11*) to correct for x-ray absorption and K x-ray line interferences. The analytical results reported herein are compared to NBS certificate values and/or those obtained by other workers where certified values were not available. The theoretical limits of detection were calculated in order to characterize the sensitivity of this method.

EXPERIMENTAL

Reagents. All materials used to prepare standards were Analytical Reagent quality and dried at 100 °C for 2 h before use, except calcium carbonate which was dried at 260 °C. The compounds used to prepare the standards were finely ground powders of Al_2O_3, SiO_2, KNO_3, $CaCO_3$, Cr_2O_3, MnO_2, Fe_2O_3, NiO, CuO, ZnO, and $Pb(NO_3)_2$. All grinding was performed in a noncontaminating boron carbide mortar. Lithium tetraborate (Spex Industries, Lot 176) was dried at 500 °C for 2 h. The purity of the $Li_2B_4O_7$ blank was determined by EDXRF, and detectable amounts of iron, copper, zinc, and lead were found. However, the concentration of these elements in the blank was low (e.g., <5 ppm) compared to their concentration in fused sample disks so that the signal-tc-background was not seriously affected. It is expected, however, that the detection limits for these elements calculated and tabulated in Table III would change appreciably if their concentration in the blank varied from lot to lot as supplied by the manufacturer.

Apparatus. An automated fusion device (Angstrom, Inc., Belleville, Mich. 48111) was employed to perform the fusions. An energy-dispersive x-ray fluorescence spectrometer (Kevex Corporation) equipped with a modified 16-position sample changer was used for making the x-ray measurements. The sample changer was fabricated at the NBS and consisted of an aluminum alloy plate which was machined so that the positioning of the sample above the x-ray source and detector was maintained constant with a high degree of precision as the changer rotated from sample to sample. A Siemens AG-W61 tungsten target x-ray tube was used with Ti, Ni, and Mo secondary target emitters to provide monochromatic excitation radiation. The x-ray tube powered by a General Electric XRD-6 power supply was operated at 20 kV, 20 mA with Ti and Ni, and 40 kV, 20 mA with the Mo secondary emitters. The count rates observed varied between 2000–3500 counts/s and live time counting intervals ranged from 15 min to 1.5 h per sample. A reduced pressure of 70 Pa (0.5 mm Hg) was maintained during the analysis of elements below atomic no. 24. The Si(Li) detector resolution was about 165 eV (FWHM) at 5.9 keV. The measurement of the x-ray intensities from the analyte was performed within selected energy regions distributed symmetrically about the FWHM of each line. Background intensities were measured using standard disks.

Crucible Pretreatment and Sample Preparation. *Crucible Pretreatment.* In the fusion procedure recommended by the manufacturer of this equipment, HBr wetting agent is added prior to fusion to prevent the stress-cracking of the resultant glass disks. In this work the wetting agent was omitted because of possible volatilization and subsequent loss of lead in the samples. It was necessary however, to prepare the crucibles before each sample or standard was fused to avoid sticking and stress cracking of the fused samples. They were preconditioned by polishing with a 220 grit followed by a 400 grit abrasive paper, and then cleaned by boiling in 6 M HCl. Final cleaning was performed by fusing in each crucible three 6.0-g $Li_2B_4O_7$ blanks. The third blank disk was examined by EDXRF to determine if the crucibles were free from contamination. This process was repeated until the level of trace elements in the blank disks was suitably low.

Fly Ash Samples. Four samples (from 0.25 to 1.0 g) of NBS-SRM 1633 Fly Ash previously dried over P_2O_5 for 8 h were fused with 6.0 g of $Li_2B_4O_7$, 0.5 g of either La_2O_3 or WO_3, and 3.0 g of NH_4NO_3. Standards were prepared by fusing various known amounts of the reagent compounds described above, with 6.0 g of $Li_2B_4O_7$ containing the same amounts of heavy absorber and NH_4NO_3 as the analyte samples. Each sample was fused at 1100–1110 °C for 40 min. The bottom surfaces of the resultant glass disks were ground on a wet diamond abrasive (200 grit), followed by polishing with a 220 and 400 grit abrasive paper, respectively. The disks were rinsed first with distilled water, then with ethanol and dried.

Particulate Matter Samples. Three 0.5-g samples previously dried at 110 °C for 8 h were each fused with 6.5 g of $Li_2B_4O_7$ and 4.0 g of NH_4NO_3 at 1100–1110 °C for 40 min. A sample size of 0.5 g was taken in order to obtain good sensitivity for most elements. Six standard disks were prepared, each containing from three up to twelve elements and prepared as described in the section on "Fly Ash Samples" above.

RESULTS AND DISCUSSION

In the x-ray analysis of elements at low concentrations the uncertainty in the measurements of the background under the analyte x-ray lines in addition to x-ray line interference corrections often influence the accuracy of the final result. Because of the limited energy resolution of the Si(Li) detector, it is difficult to select energy regions of interest on a sample where the background can be determined unambiguously. This is especially true when the sample contains many elements at different concentration levels. Consider an element at low concentration, C_1, whose x-ray line falls on the lower-energy side of an x-ray line of a major constituent, C_2. A major contribution to the background of C_1 is caused by the low energy tailing of C_2 due to incomplete charge collection in the Si(Li) detector. Fortunately, this contribution can be measured. The correction used here requires that additional synthetic standards be prepared which contain only the major constituents present in the analyte sample. The background contribution to the Kα lines of titanium, chromium, and manganese from iron (i.e., a major constituent) in the analyte samples was established from synthetic disks containing iron. The background increases linearly in the respective energy regions for titanium, chromium, and manganese with increasing iron concentration.

The results obtained for the NBS-SRM 1633 Fly Ash are tabulated in Table I, and are compared to NBS certificate values and those obtained by other workers (*2*, *12*). The agreement is within 5 to 10%. It is important, however, that the concentrations of elements such as zinc, lead, and strontium be sufficiently low in the glass disks so that they do not contribute significantly to x-ray absorption, as compared to absorption by the heavy absorber. This points out a major problem of the heavy absorber method: x-ray absorption effects are minimized but not eliminated. Also, because of x-ray line interferences between analyte and absorber lines, more than one absorber is required so that the sample preparation time is substantially increased. However good accuracy can still be obtained as shown in Table I when analyte elements are present at relatively low concentrations in the glass disks.

In Table II, are summarized the results for 12 elements in the NBS-SRM 1648 Particulate Matter using the NBS data reduction procedure. Comparison of these values to those of other NBS workers where results are available shows agreement within ±6%. A relatively high systematic error was assigned to the copper value because of the large variability between standard disks of identical composition prepared with copper oxide. This is believed to be caused by partial reduction to the metal which subsequently alloys with the platinum crucible. The addition of $LiNO_3$ as an oxidizing agent to fusion preparations instead of NH_4NO_3 is currently being investigated in order to overcome the problem.

To characterize the sensitivity of the fusion procedure, the theoretical detection limits (*13*, *14*) were calculated for three secondary target emitters and summarized in Table III. These detection limits expressed in $\mu g/g$ in the glass disk are based only on Poisson counting statistics for the element of interest and assume the absence of systematic and non-

Table I. Comparison of Average Values Found for NBS-SRM 1633 Fly Ash

Element	Concentration found,[a] μg/g	Uncertainty[b] μg/g	Systematic error,[c] μg/g	n[d]	NBS[e]	NAA[f]	LBL,[g] μg/g
Ca	4.62%	0.15%	0.3%	7	···	4.7 ± 0.6%	···
Fe	6.16%	0.30%	0.3%	6	···	6.2 ± 0.3%	···
K	1.67%	0.06%	0.06%	2	(1.72)	1.61 ± 0.15%	···
Ti	7360[h]	344	400	6	···	7400 ± 300	8600 ± 1100
V	200[i]	34	80	6	214 ± 8	235 ± 13	295 ± 156
Cr	131	8	10	4	131 ± 2	127 ± 6	159 ± 115
Mn	500	17	20	6	493 ± 7	496 ± 19	528 ± 104
Ni	95	20	20	6	98 ± 3	98 ± 3	101 ± 7
Cu	125	13	30	7	128 ± 5	···	133 ± 4
Zn	200	10	10	8	210 ± 20	216 ± 25	216 ± 14
Pb	66	12	15	4	70 ± 4	75 ± 5	72 ± 5
Sr	1256	37	40	4	(1380)	1700 ± 300	1342 ± 20

[a] Concentrations are expressed in μg/g except when indicated by wt %. [b] Uncertainty due to random error is the 95% confidence interval for the mean (i.e., mean ± $t s/\sqrt{n}$ where $t_{0.95,5}$ is Student's t for $n - 1$ degrees of freedom, and s is the estimated standard deviation of a single measurement based on n measurements). [c] Estimate of systematic error based on range of values obtained with different standards. [d] Number of replicate measurements. [e] NBS certificate of analysis 1633 Fly Ash. Values in parentheses are not certified values. [f] Instrumental neutron activation analysis (NAA) results from Ondov et al. (*12*). Uncertainty is either one standard deviation or authors' estimate, whichever is larger. [g] Lawrence Berkeley Laboratory (LBL) results from Giauque et al. (*2*) (uncertainties are 2 standard deviations). [h] Corrected for Ba Lα interference. [i] Corrected for Ti Kβ, Ba Lβ interferences.

Table II. Comparison of Average Values[a] Found for NBS-SRM 1648 Particulate Matter

Element	Concentration found,[b] %	Uncertainty,[c] %	Systematic error,[d] %	NBS[e]
Si	14.7	0.3	0.5	···
K	1.04	0.02	0.04	···
Ca	6.10	0.04	0.04	···
Ti	0.426	0.003	0.004	···
Cr	0.044	0.001	0.001	0.0403 ± 0.0012
Mn	0.087	0.003	0.005	0.0851 ± 0.0005[f]
Fe	3.96	0.037	0.04	3.91 ± 0.10
Ni	0.0083	0.0004	0.001	0.0082 ± 0.0003
Cu	0.07	0.01	0.03	0.0609 ± 0.0027
Zn	0.465	0.015	0.02	0.476 ± 0.0014
Pb	0.678	0.006	0.02	0.655 ± 0.008
Sr	0.019	0.001	0.002	···

[a] Mean of six measurements performed on three replicate samples. [b] All concentrations are expressed as wt %. [c] Uncertainty due to random error is 95% confidence interval for mean based on 5 degrees of freedom. [d] Estimate of systematic error based on range of values obtained with different standards. [e] NBS certificate of analysis 1648 Particulate Matter. [f] Value from atomic absorption spectrophotometry (not certified).

Table III. Theoretical Detection Limits in μg/g Calculated from Standard Disks for Selected Elements[a]

[t = 5000 s]

Emitter	Si	K	Ca	Ti	Cr	Mn	Fe	Ni	Cu	Zn	Pb	Sr
Ti	70	···	1.5	···	···	···	···	···	···	···	···	···
Ni	200	7.0	3.0	1.0	0.7	0.7	0.6	···	···	···	···	···
Mo	···	···	···	···	···	···	···	1.0	1.4	1.2	1.1	0.4

[a] The above detection limits should be multiplied by 14 to obtain the detection limits in the original sample.

Poissonian random errors. The expression used for calculation is (see Ref. *13*, *14*)

$$\text{D.L. } (\mu g/g) = C_{STD} \frac{4.65\sqrt{N_0}}{N_{STD} - N_0}$$

where C_{STD} is the known concentration (μg/g) of that element in the standard; N_0 is the number of counts corresponding to the background in 5000 seconds counting time; and N_{STD} is the gross counts for that element also in the same time interval. To obtain detection limits at different time intervals (t in seconds), the above expression should be multiplied by $(t/5000)^{-1/2}$. To convert to concentrations in the sample, these values should be multiplied by the ratio of the disk weight to the sample weight. Assuming the total disk weight to be about 7.0 g and the sample weight to be 0.5 g, the detection limits for samples without a heavy absorber would range from 6 to 100 ppm for most elements investigated except silicon which would be about 1000 ppm. The detection limits calculated for samples with a heavy absorber are not very different which is somewhat surprising since the fluorescence intensity is reduced because of absorber attenuation. However, there is no significant decrease in the signal-to-background ratio because the background intensity is also suppressed to some extent.

CONCLUSION

The results show that acceptable accuracy can be obtained using lithium tetraborate fusion for sample preparation of environmental samples for x-ray analysis. The main purpose of the heavy absorber is to obviate the need for digital computation of x-ray absorption effects. However, this advantage is outweighed by increased sample preparation time because of the need for several absorbers. In the analysis of

major constituents in cement and glass samples, we have found appreciable variations (e.g., 3 to 5%) in replicate disks due to the nonhomogeneous distribution of elements within the disk containing 0.5 g of La_2O_3. Therefore we believe that digital computation of x-ray absorption effects including corrections for x-ray line interferences is preferable. This is especially true in the general application where EDXRF analysis of a wide variety of materials of different matrices is possible. Because of serious losses of analyte elements or compounds which are volatile at fusion temperatures, this technique should be used with caution. For those samples where this presents no major problem, the detection limits of 10–100 ppm are reasonably low, making this technique suitably sensitive for the analysis of environmental samples.

LITERATURE CITED

(1) R. D. Giauque, R. B. Garrett, L. Y. Goda, J. M. Jaklevic, and D. F. Malone, LBL Report 4402 (September 1975).
(2) R. D. Giauque, R. B. Garrett, and L. Y. Goda, *Anal. Chem.*, **49**, 1012 (1977).
(3) J. W. Criss, *Anal. Chem.*, **48**, 179 (1976).
(4) F. Claisse, *Norelco Reporter*, **4**, (1957).
(5) C. O. Ingamells, *Anal. Chim. Acta*, **52**, 323 (1970).
(6) K. Norrish, and J. T. Hutton, *Geochim. Cosmochim. Acta*, **33**, 431 (1969).
(7) H. J. Rose, Jr., I. Adler and F. J. Flanagan, *Appl. Spectrosc.*, **4**, 81 (1963).
(8) G. Andermann and J. D. Allen, *Adv. X-ray Anal.*, **4**, 414 (1961).
(9) C. K. Matocha, "An Automatic Fusion Device for Preparation of Non-Metallic Samples for X-Ray Fluorescence Analysis", 25th Pittsburgh Conference on Analytical Chemistry and Applied Spectroscopy, Cleveland, Ohio, Mar. 4–8, 1974, Paper No. 38.
(10) F. Claisse, Quebec Department of Mines, Preliminary Report 327 (1956).
(11) R. L. Myklebust, C. E. Fiori, D. N. Breiter, and K. F. J. Heinrich, FACSS Abstracts (3rd Annual Meeting) No. 241, Philadelphia, Pa., 1976.
(12) J. M. Ondov, W. H. Zoller, I. Olmez, N. K. Aras, G. E. Gordon, L. A. Rancitelli, K. H. Abel, R. H. Filby, K. R. Shah, and R. C. Ragaini, *Anal. Chem.*, **47**, 1103 (1975).
(13) P. A. Pella, R. L. Myklebust, M. M. Darr, and K. F. J. Heinrich, NBSIR 77-1211 (June 1977).
(14) L. A. Currie, *Anal. Chem.*, **40**, 586 (1968).

RECEIVED for review February 13, 1978. Accepted April 13, 1978. Identification of any commercial product does not imply recommendation or endorsement by the National Bureau of Standards, nor does it imply that the material or equipment identified is necessarily the best available for the purpose.

Calculated X-ray Diffraction Data and Quantitative X-ray Diffractometry

Stephen Altree-Williams

Division of Occupational Health and Radiation Control, Health Commission of New South Wales, P.O. Box 163, Lidcombe, Australia 2141

An equation is derived that relates the quantitation constant for direct quantitative x-ray powder diffractometry, k_{iJ}, to the calculated x-ray powder diffraction data parameters, ASF_J and I_{iJ}^{rel}. The derived equation is tested experimentally and the results confirm the potential usefulness of both the derived equation and, more generally, calculated x-ray diffraction data. A diffractometer constant, κ, is introduced that should allow experimentally determined k_{iJ} values from different laboratories to be directly compared.

As a quantitative technique, x-ray powder diffractometry (XRD) attempts to relate the quantity of an analyte phase to the intensity of one of its diffraction lines. For the conventional Bragg–Brentano parafocusing powder diffractometer (*1*) and the general case of a flat sample of depth less than the penetration depth of the x-ray beam, the quantitation equation is (*2*)

$$I_{iJ} = k_{iJ}\frac{W_J}{\mu}\left(1 - e^{-2\,\mu\bar{M}\,\mathrm{cosec}\,\theta_{iJ}}\right) \qquad (1)$$

For a sample "infinitely" thick to the x-ray beam, Equation 1 becomes

$$I_{iJ} = k_{iJ}\frac{W_J}{\mu} \qquad (2)$$

For a thin-layer sample supported on a diffracting underlay, Equation 1 becomes (*3*, *4*)

$$I_{iJ} = \frac{2\,k_{iJ}}{L\sin\theta_D}\cdot\left(1 - e^{-L\,\sin\theta_D\,\mathrm{cosec}\,\theta_{iJ}}\right)\cdot\bar{M}_J \qquad (3)$$

where I_{iJ} = integrated intensity of diffraction line i of phase J; k_{iJ} = the quantitation constant, its value depending on the diffractometry conditions and on diffraction line i of phase J; W_J = weight fraction of phase J in the sample; μ = mass absorption coefficient of the sample; $\bar{M}$ = weight of sample per unit area; $\bar{M}_J$ = weight of phase J per unit area; θ_{iJ} = angle of incidence of the x-ray beam to the sample for diffraction line i of phase J; θ_D = angle of incidence of the x-ray beam to the sample for a chosen diffraction line from the thin-layer support material; $L = \ln(I^0{}_D/I_D)$; $I^0{}_D$, I_D = integrated intensity of the chosen diffraction line from the material supporting the thin-layer before and after loading, respectively.

The quantitation constant, k_{iJ}, is the same constant in each of Equations 1–3. To date this constant has had to be determined by diffractometry on samples of pure phase J. However, the availability of calculated XRD data (*5–8*) allows the determination of k_{iJ} from such data alone.

Consider the conventional powder diffractometer with a constant divergence slit, without monochromator, and with an "infinitely" thick sample of pure phase J assumed to be at theoretical density. Let the crystallites of phase J be randomly oriented and let them have a particle size such as to eliminate extinction and microabsorption effects without introducing any significant line broadening. Then the integrated intensity of diffraction line i of phase J is theoretically given by (*9–12*)

$$I_{iJ} \propto \frac{I^0\lambda^3}{\Omega r}\cdot\frac{e^4}{m^2c^4}\cdot\frac{1+\cos^2 2\theta_{iJ}}{\sin^2\theta_{iJ}\cos\theta_{iJ}}\cdot p_{iJ}r|F_{iJ}|^2\cdot\frac{1}{V_J{}^2\,\mu^*} \qquad (4)$$

where I_{iJ}, θ_{iJ} are as previously defined; I^0, λ, Ω, r = constants for a given diffractometer run under constant conditions, being the intensity of the primary x-rays used for diffraction, their wavelength, the scan rate used for counting the integrated intensity, and the radius of the goniometer circle, respectively; e, m, c = physical constants, being the charge and rest mass of the electron and the velocity of light, respectively; p_{iJ},$|F_{iJ}|$ = the multiplicity, and the amplitude of the structure factor (including thermal effects) for line i (Miller index, hkl) of phase J, respectively; V_J = volume of the unit cell of phase J; μ^* = linear absorption coefficient of the sample, in this case, phase J at theoretical density.

Equation 4 can be transposed into a more convenient form by considering the following. For a given diffractometer run under constant conditions, the diffractometer constants, the physical constants, and the constant of proportionality can be incorporated into a single constant, κ. For the specific wavelength used in the diffractometer, the combined relative effect of the Lorentz-polarization term, the multiplicity factor, and the structure factor term on the intensity of the diffraction lines of phase J is given by the calculated relative intensities, I_{iJ}^{rel}, for the lines of phase J. The most intense diffraction line of phase J is given an I_{iJ}^{rel} value of 100. The absolute effect of the Lorentz-polarization, multiplicity, and structure factor terms on the diffraction intensities of phase J is a property of phase J and λ. The factor for this absolute effect adjusts the relative intensity data to the absolute scale and is incorporated with $1/V_J{}^2$ to give the absolute scale factor for phase J, designated ASF_J (*6*). Equation 4 can thus be written

$$I_{iJ} = \kappa\cdot ASF_J\cdot I_{iJ}^{rel}\cdot\frac{1}{\mu^*} \qquad (5)$$

Equation 5 refers to a sample of pure phase J at theoretical density. For real samples containing phase J (including pure powdered phase J as packed in a diffractometer), Equations 4 and 5 can be modified by including a term for the volume fraction of phase J in the sample, with μ^* referring to the linear absorption coefficient of the sample. Expressing μ^* in terms of the mass absorption coefficient of the sample and expressing the volume fraction of phase J in terms of the weight fraction of phase J gives

$$I_{iJ} = \kappa\cdot ASF_J\cdot I_{iJ}^{rel}\cdot\frac{W_J}{\rho_J\mu} \qquad (6)$$

where all terms have been previously defined except ρ_J, the density of phase J. Comparison of Equation 6 with its equivalent experimental equation, Equation 2, gives the equation for determining k_{iJ} from calculated XRD data

$$k_{iJ} = \kappa\cdot ASF_J\cdot I_{iJ}^{rel}\cdot\frac{1}{\rho_J} \qquad (7)$$

0003-2700/78/0350-1272$01.00/0

Table I. Comparison of $k_{i,J}$ Values Determined by Calculation[a] and by Experiment

phase, J	line, i, hkl	ASF_J	ρ_J, g cm^{-3}	$k_{i,J}$, net counts cm^2 μg^{-1} calculated	$k_{i,J}$, net counts cm^2 μg^{-1} experimental[c]
corundum (α-Al_2O_3)	113	0.120	3.987	[b]	11.5 ± 0.1
α-quartz (SiO_2)	101	0.321	2.65	46.3	45.3 ± 0.3
calcite ($CaCO_3$)	104	0.250	2.71	35.2	47 ± 1
sylvite (KCl)	200	0.329	1.987	63.3	65 ± 1
zincite (ZnO)	101	0.912	5.68	61.3	53 ± 2
anatase (TiO_2)	101	0.497	3.89	48.8	47 ± 1
eskolaite (Cr_2O_3)	104	0.361	5.21	26.5	22 ± 1
hematite (α-Fe_2O_3)	104	0.56	5.26	40.7	30.2 ± 0.2
Ag	111	5.33	10.5	194	122 ± 1

[a] Values for ASF_J and ρ_J are from Hubbard, Evans, and Smith (7) except for hematite (JCPDS card 24-72A) and are corrected for the use of a graphite crystal monochromator with Cu Kα radiation. [b] The diffractometer constant, κ, was determined as (3.82 ± 0.03) × 10^6 net counts · ASF^{-1} cm^{-1} by equating the experimental measurements and calculated data for corundum. [c] Average value of four sample preparations ± mean deviation.

Equation 7 indicates that $k_{i,J}$ can be determined from calculated XRD data (ASF_J and $I_{i,J}^{rel}$) for all phases except for the one chosen to experimentally determine κ for the diffractometer. With this one limitation, x-ray powder diffractometry can be considered an absolute instrument technique where the quantitation of phase J can be performed without recourse either to a calibration standard of phase J or to an internal standard for each sample. Two further deductions of practical interest can be made from Equation 7. Since κ, ASF_J and ρ_J are constant for a given diffractometer, wavelength, and phase, then the quantitation constant for each diffraction line of a given phase is directly proportional to $I_{i,J}^{rel}$. Again, since for any given diffraction line of any given phase ASF_J, $I_{i,J}^{rel}$ and ρ_J are constant for a given wavelength and independent of the diffractometer, then the quantitation constants for a set of phases determined on one diffractometer will be directly proportional to the quantitation constants for that same set of phases determined on any other diffractometer, subject to the same wavelength being used.

Note that Equation 4 refers to the use of a conventional diffractometer without monochromator. When a monochromator is used (either on the incident beam to the sample or on the diffracted beam) the polarization term, $1 + \cos^2 2\theta_{i,J}$, in Equation 4 needs to be changed to $1 + \cos^2 2\theta_{i,J} \cos^2 2\theta_m$, where θ_m is the Bragg angle for the monochromator crystal reflection and wavelength used (13). This change affects the intensity of all lines depending on their $\theta_{i,J}$ and on θ_m. It necessitates adjustment of the calculated values of ASF_J and $I_{i,J}^{rel}$, which are routinely determined assuming a polarization factor of $1 + \cos^2 2\theta_{i,J}$ (8).

The validity of Equation 7 for determining $k_{i,J}$ has been investigated experimentally, as has the deduction that for lines of the one phase $k_{i,J}$ is proportional to $I_{i,J}^{rel}$. The results are considered below.

EXPERIMENTAL

Phases. All phases used were laboratory chemicals except for corundum (Linde A, Union Carbide Corporation), α-quartz (natural crystal, Kingsgate, New South Wales), and silver (Selas Flotronics silver membrane filter, 0.2-μm pore size).

Diffractometry. A Philips (Eindhoven) x-ray diffractometer was used comprising vertical goniometer (PW 1050/70), diffracted beam monochromator with graphite crystal, sample spinner, xenon filled proportional counter, and copper anode broad focus x-ray tube (PW 2253/20).

The quantitation constant was determined, by the use of Equation 3, from measurements obtained from deposits of <7-μm diameter airborne particles of the phase of interest on Nuclepore filters (4). Silver was used as the diffracting underlay to all phases. The intensity of the corundum (110) and (113) reflections were read on a platinum underlay. Four filters were prepared for each phase and the average $k_{i,J}$ was determined on the line or lines of interest. For silver, the silver filters were used directly in the diffractometer and $k_{i,J}$ was determined using Equation 2 and a theoretical mass absorption coefficient for silver of 218 cm^2/g.

Samples were analyzed at tube conditions of 45 kV, 28 mA with pulse height selection and sample spinning. These tube conditions gave the same external standard count as used in previous work (3, 4). A 1° divergence slit and a 0.3-mm receiving slit was used. The integrated intensity of a diffraction line was measured by counting while scanning the diffraction line at a rate of $^1/_2$° 2θ/min for 2 min. Loadings on the filters were such that the 1° 2θ scan range effectively encompassed the whole diffraction peak for all lines measured. Background was counted at the start and finish angles of the scan and the average value used. Net peak area counts was used as the integrated intensity of the diffraction line. An aluminum blank was used as an external standard to correct for long term instrument drift.

RESULTS AND DISCUSSION

Calculated and Experimental Values of $k_{i,J}$. Calculated XRD data for the most intense line of the phases used in this work were taken from Hubbard, Evans, and Smith (7) or, for hematite, from JCPDS card 24-72A. The data were suitably adjusted for the graphite crystal monochromator used in this work. Using the calculated ASF_J for corundum (113) and determining its $k_{i,J}$ experimentally, the value of the diffractometer constant, κ, was found to be (3.82 ± 0.03) × 10^6 net counts ASF^{-1} cm^{-1}. Using this value for κ, calculated $k_{i,J}$ values were determined from Equation 7 for the most intense line of each of the other phases. These calculated values are given in Table I together with the equivalent $k_{i,J}$ values determined by experiment.

The results provide support for the validity of Equation 7 and, on the wider scene, provide additional evidence of the practical value of calculated XRD data. The experimental results for α-quartz, sylvite, and anatase match the calculated $k_{i,J}$ values to within 4%. The experimental value for zincite was 13% less than the calculated value. Speculation as to the reason for this difference is not advisable in the absence of calculated data for the full diffraction pattern of zincite. The remaining phases investigated also show significant differences between their calculated and experimental $k_{i,J}$ values but these differences can be explained in terms of deviation of the samples from assumptions inherent in Equations 4 and 7. The high experimental value for calcite appears to be due to a combination of preferred orientation and extinction (see below). The low experimental values for eskolaite, hematite, and silver show increasing deviation with linear absorption coefficient and would be explained in terms of microabsorption.

The results given here show a better match between experimental and calculated values than results published previously for the reference intensity ratio determined on bulk samples (7). This is no doubt due to the use of samples of small particle size for the present study. Care would need to be taken in the use of Equation 7 if the samples analyzed were

Table II. Comparison of Experimental $k_{i,J}$ Values for the Lines of a Phase with Their Calculated $I_{i,J}^{rel}$ Values

phase, J	line, i, hkl	experimental $k_{i,J}$, net counts cm^2 μg^{-1}	experimental relative $k_{i,J}$	calculated,[a] $I_{i,J}^{rel}$
corundum	012	5.83 ± 0.07	51	58.8
	104	9.75 ± 0.10	85	90.3
	110	4.21 ± 0.06	37	41.2
	113	11.53 ± 0.10	100	100
	116	11.6 ± 0.3	100	102.9
	124	4.58 ± 0.11	40	41.5
	030	6.76 ± 0.07	59	63.7
α-quartz	100	8.20 ± 0.11	18.1	18.0
	101	45.3 ± 0.3	100	100
	102	3.43 ± 0.05	7.6	7.8
	112	6.92 ± 0.04	15.3	14.5
	211	5.25 ± 0.10	11.6	10.9
calcite	012	3.22 ± 0.05	6.9	26
	104	46.9 ± 1.1	100	100
	202	7.50 ± 0.12	16.0	33
	116	10.1 ± 0.14	21.5	43
	122	4.76 ± 0.11	10.2	22
hematite	012	8.42 ± 0.04	28	29
	104	30.2 ± 0.10	100	100
	110	21.6 ± 0.14	72	73
	116	15.6 ± 0.16	52	48
	214	10.3 ± 0.09	34	33

[a] Calculated data are from Smith (*5*) for corundum and α-quartz and from JCPDS cards 24-27A (calcite) and 24-72A (hematite). The data have been corrected for the effect of the monochromator.

subject to preferred orientation, extinction, or microabsorption.

$k_{i,J}$ Values for Diffraction Lines of the One Phase. Of the phases considered in Table I, the full calculated XRD pattern (integrated intensity) could be found only for corundum (*5*), α-quartz (*5, 6*), calcite (JCPDS card 24-27A), and hematite (JCPDS card 24-72A). Quantitation constants were experimentally determined for the five most intense lines of each of these phases. The relative values of $k_{i,J}$ for the lines of each phase are compared to their calculated $I_{i,J}^{rel}$ values in Table II. The results for α-quartz and hematite show close agreement between the calculated and experimental values. It is reasonable to conclude that both phases, as prepared on the Nuclepore filter, are free of significant orientation and extinction effects.

For corundum, the match is also quite close although there may well be some effect in the experimental work that favors the (113) reflection. A small degree of preferred orientation would be a possible explanation, although corundum is generally regarded as being free of this effect. Another possible explanation of the observed difference is in the choice of the degree of ionization used for Al and O in determining the calculated data. The calculated data for corundum given in Table II are based on partially ionized Al and O (*5*). Calculated data based on fully ionized Al and O would give a better match to the experimental data given in Table II (*7*).

The results for calcite are particularly interesting. Not only are there large deviations between the relative $k_{i,J}$ and the calculated $I_{i,J}^{rel}$ values (Table II), but the absolute value of $k_{i,J}$ for calcite (104) is significantly larger than that found previously for the same sample of calcite deposited on silver filters (*3*). Counting the silver filter deposits for the other calcite reflections showed that these reflections were relatively more intense on the silver filter (although still significantly less than the $I_{i,J}^{rel}$ data). The results can possibly be explained by different degrees of preferred orientation for calcite deposited on Nuclepore and silver filters coupled with a general extinction effect on the calcite (104) reflection.

The Work of Smith, Hubbard, and Co-workers. Smith and Hubbard together with their co-workers have made a practical reality of the theoretically reasonable concept of calculated XRD data (*5–8*). This present paper supports the concept of calculated XRD data as given by these workers and attempts to extend its use to the direct quantitation methods summarized in Equations 1–3. Of the calculated XRD data terminology used here, ASF_J and $I_{i,J}^{rel}$ are as used by Smith et al. (*6, 7*), while κ is equal to $^1/_2K$ (*7*). One minor criticism of the monumental work of Smith, Hubbard and co-workers is their recent use of γ_J as the scale factor for calculated data, where

$$\gamma_J = \frac{ASF_J}{2\,\mu_J^*} \tag{8}$$

The incorporation of μ_J^*, the linear absorption coefficient of phase J at theoretical density, into the scale factor would seem to have little to recommend it, as the calculation of both the quantitation constant, $k_{i,J}$, and the reference intensity ratio, I/I_c, (*7*) are made by the use of ASF_J. If the scale factor is reported in terms of γ_J, then it would be useful if the μ_J^* used was also reported because this parameter must be eliminated from γ_J before either $k_{i,J}$ or I/I_c can be calculated.

General Comment. Equation 7 provides a number of useful alternatives in the application of calculated XRD data to the direct XRD quantitation methods. First, it allows for the determination of $k_{i,J}$ directly from calculated XRD data. When the sample complies with the innate assumptions of Equation 7 (no orientation, extinction, or microabsorption) it is likely that calculated $k_{i,J}$ values of good quality will be obtained.

Second, it provides a theoretical basis for the use of calculated XRD data where interference occurs to those lines of an analyte phase for which experimental $k_{i,J}$ values are at hand. Quantitation could be accomplished from the known experimental $k_{i,J}$ and calculated $I_{i,J}^{rel}$ values of a line together with the calculated $I_{i,J}^{rel}$ value for any line of the phase that was free of interference.

Finally, and perhaps most importantly, Equation 7 introduces the concept of the diffractometer constant, κ. All powder diffractometers operating on the conventional Bragg–Brentano parafocusing principle should obey Equations 1–7. This being the case, the simple expedient of determining κ for a diffractometer (using a suitable standard reference material) should immediately place the experimentally determined $k_{i,J}$ of a given phase at an absolute value that any conventional powder diffractometer in any laboratory could reproduce. The publication of experimental $k_{i,J}$ values determined under standard experimental conditions together with an experimentally determined diffractometer constant, κ, should allow the accumulation of a consistent body of absolute $k_{i,J}$ values that will improve the usefulness of x-ray powder diffractometry as a quantitative analytical technique, particularly if rational explanation can be provided for differences that occur between the experimental set and the equivalent calculated data.

ACKNOWLEDGMENT

I thank John G. Byrnes of the Geological and Mining Museum, Sydney for supplying the α-quartz.

LITERATURE CITED

(1) H. P. Klug and L. E. Alexander, "X-ray Diffraction Procedures", 2nd ed., John Wiley and Sons, New York, N.Y., 1974.
(2) A. J. C. Wilson, *J. Sci. Instrum.*, **27**, 321–325 (1950).
(3) S. Altree-Williams, *Anal. Chem.*, **49**, 429–432 (1977).
(4) S. Altree-Williams, J. Lee, and N. V. Mezin, *Ann. Occup. Hyg.*, **20**, 109–126 (1977).
(5) D. K. Smith, *Norelco Rep.*, **15**, 57–65, 76 (1968).
(6) I. Y. Borg and D. K. Smith, "Calculated X-ray Powder Patterns for Silicate

Minerals", Memoir 122, The Geological Society of America Inc., Boulder, Colo., 1969.
(7) C. R. Hubbard, E. H. Evans, and D. K. Smith, *J. Appl. Crystallogr.*, **9**, 169–174 (1976).
(8) C. R. Hubbard and D. K. Smith, *Adv. X-ray Anal.*, **20**, 27–39 (1977).
(9) "International Tables for X-ray Crystallography", Vol. II, Kynoch Press, Birmingham, England, 1967.
(10) R. W. James, "The Optical Principles of the Diffraction of X-rays", G. Bell and Sons, London, 1962.
(11) B. E. Warren, "X-ray Diffraction", Addison-Wesley, Reading, Mass., 1969.
(12) A. J. C. Wilson, "Elements of X-ray Crystallography", Addison-Wesley, Reading, Mass., 1970.
(13) L. V. Azaroff, *Acta Crystallogr.*, **8**, 701–704 (1955).

RECEIVED for review February 21, 1978. Accepted May 18, 1978.

Resistive-Pulse Particle-Sizing Instrument

A. W. Venolia

Fruit and Vegetable Chemistry Laboratory, Science and Education Administration, U.S. Department of Agriculture, Pasadena, California 91106

A recently assembled resistive-pulse particle-size analyzer is described. The analyzer was tested with Coulter Counter apertures of 30, 50, and 100 μm nominal diameter, and seven latex standards ranging from 1.099 to 25.7 μm nominal diameter. Results were correlated with an equation having two empirical constants in addition to the conventional aperture constant. Twenty groups of particle diameter estimates derived from 239 test runs displayed a mean relative standard deviation of 1.2%. Duplicate counts in regions of overlap of a broad particle size distribution showed an average deviation from the means of 4.2%.

The literature concerned with resistive-pulse instrumentation is extensive; see, e.g., references cited in the present paper. A significant fraction of the reported effort has dealt with problems such as the relationship between aperture dimensions, particle size, particle trajectory, and the character of the resulting electrical pulse. To thoroughly understand instrument performance, it would be necessary to extend such analytical scrutiny to each stage of pulse processing, including the eventual conversion of some pulse parameter(s) to digital form.

In the present work, no direct attention was given to the foregoing type of inquiry. Instead, the approach toward optimal performance was sought via observation of instrument response to a broad range of operating conditions. This approach entailed the generation of a substantial quantity of data and culminated in the development of an equation that is used to represent all the data. The results reported here suggest that progress has been made in the desired direction. Not only do the results seem to be of improved quality, but they may also point toward the resolution of an earlier difficulty—the disparity between standard latex nominal diameters and those found by resistive-pulse examination.

The present work used readily available materials and comparatively simple procedures. Much of the testing exploited the ability of a multichannel analyzer (MCA) to provide a detailed record of the consequences of altering aperture current; the effect upon estimates of aperture constants, in particular, received considerable attention. The final evaluation of performance was made in terms of the quality of overlap replication within a broad particle size distribution. Testing was based upon a moderately large number of latex standards with the intent of: (a) minimizing error due to possibly inaccurate nominal diameters, and (b) making the rather inevitable interpolations and extrapolations of future applied work as reliable as possible.

Table I. Instrument Components

item	model no.	company
teleprinter	ASR-33TZ	Teletype Corp., Skokie, Ill.
H.V. supply	6116A	Hewlett-Packard, Palo Alto, Calif.
L.V. supply	60153D	Hewlett-Packard, Palo Alto, Calif.
digital multimeter	7205	Systron-Donner Corp., Concord, Calif.
multichannel analyzer	8100	Canberra Industries, Meriden, Conn.
preamplifier unit	...	assembled in this laboratory
sample stand	...	Coulter Electronics, Inc., Hialeah, Fla.
control unit	...	assembled in this laboratory

In examining particles having a narrow size range, the question of overlap quality may not arise since a single group of instrument settings permits characterization of the whole distribution. However, when a certain size range is exceeded, runs with several settings of instrument controls become necessary and the widest distributions require more than one aperture for complete characterization. In either case, the description of a broad distribution requires the joining of groups of data that are somewhat disparate due to the influence of a number of sources of error; hence, the present interest in the quality of overlap replication.

Testing of the instrument described here was facilitated by its flexibility and resolution capability. The methodology developed in the course of the testing may help others who use the resistive-pulse method of particle size analysis. If extensive work with an instrument similar to the present one is contemplated, it may be well to consider taking advantage of the computer interfacing options offered by the manufacturer of the MCA.

EXPERIMENTAL

Apparatus. The layout of the instrument is given in Figure 1, and components are identified in Table I. Conventional Coulter apertures were used in a Coulter sample stand that was unmodified except as noted here: (a) the vacuum regulator was discarded, (b) cabling for the manometer control of counting was

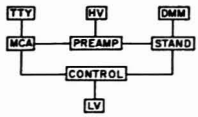

Figure 1. Particle sizing instrument

Table II. Components of Preamplifier Unit

item	quantity	model no.	company
amplifier	1	155N	Ithaco, Inc., Ithaca, N.Y.
capacitor, 0.1 μF	1	X463UW	TRW, Ogallala, Neb.
capacitor, 530 μF	2	WHB 530-150	Cornell-Dubilier Electronics, Newark, N.J.
resistor	1	MS 223	Caddock Electronics, Inc., Riverside, Calif.

replaced to provide compatibility with the control unit, and (c) the coaxial cable was relocated and shortened to about 50 cm.

Up to 120 mL of sample suspension was held in a jacketed borosilicate-glass beaker. The sample was thermostated at 25 °C with a circulating water bath (Neslab TE3, Neslab Instruments Inc., Portsmouth, N.H.). No Faraday cage was employed, but water circulation lines were shielded, in part, with flexible copper braid to facilitate manipulation of the sample beaker. Aperture current was provided by the H.V. supply; the output of this supply is adjustable from 0 to 100 volts. The digital multimeter (DMM) indicates the voltage across the aperture electrodes.

The circuit of the preamplifier unit is shown in Figure 2, and its components are identified in Table II. The 155N amplifier has switch selectable gains of 20 and 40 dB. Power for the 155N comes from the 24-volt supply of the MCA via twinax cable. The two 530-μF capacitors that provide the 1060 μF of capacitance shown parallel an additional 200-μF present in the output circuit of the H.V. supply. The 40-kΩ resistor is rated at 3 watts and has a specified temperature coefficient of 50 ppm/°C. The 0.1-μF capacitor is a metallized polycarbonate type.

The control unit of Figure 1 uses 7400-series integrated circuits to interface the sample stand and the MCA. By allowing the manometer of the sample stand to turn the data collecting function of the MCA on and off, the control unit permits automatic metering of samples of 50, 500, or 2000 μL through the Coulter apertures. The circuit diagram of the control unit may be obtained by writing to the author.

The teleprinter types out the contents of the MCA memory; a punched tape bearing the same information can be obtained during printout. The punched tape option is useful because it permits a data set to be reloaded into the MCA memory for examination and processing.

Except for the use of twinax cable previously referred to, all interconnections were made with coaxial cable: RG-114A/U between the preamplifier unit and the sample stand, and RG-62A/U elsewhere. Conventional grounding (*1*) was provided using appropriate BNC connectors.

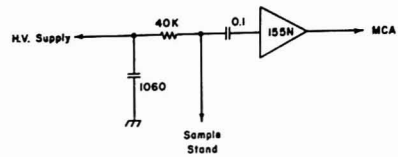

Figure 2. Preamplifier unit

Pulses for gain comparisons were obtained by rectifying the sinewave output of an audio oscillator (IG-18, Heath Company, Benton Harbor, Mich.) with a 1N4148 diode.

Electrolyte Solutions. Distilled, deionized water was used to prepare all electrolytes. Solute concentrations were as follows (g/L, throughout). Standard, low-density electrolyte: NaCl (7.13), NaN_3 (0.20). High-density electrolyte: citric acid monohydrate (133.4), KCl (5.70), $MgCl_2 \cdot 6H_2O$ (0.29), KH_2PO_4 (0.20), $CaCl_2$ (0.15), NaCl (0.033), NaN_3 (0.077). The high-density electrolyte was a multipurpose solution having a density of about 1.05 g/cm³ at 25 °C and an electrical conductivity approximately equal to that of the low density electrolyte. The final step in all electrolyte preparation consisted of passage through a UF-porosity sintered-glass filter or a 0.10-μm Millipore filter.

Latex Standards. Some data pertaining to standards appear in Table III. Standards from Coulter are identified by nominal diameter only. Dow lot numbers for the 2.02- and 25.7-μm standards were LS1078B and 2F8V, respectively, and the stated standard deviations were 0.0135 and 10.0 μm, respectively. The 10.3-μm standard was Duke lot number 2142, catalog number 117, relative standard deviation, 12.5%.

Basic Equation. In the present instrument, the MCA memory is divided into 1024 channels. The first channel records run time in seconds while the rest record pulse counts. Channel number c is nearly proportional to pulse amplitude. The value of c that represents a particle of diameter d depends upon aperture current i and amplifier gain setting g. If d, i, and g are fixed, but an aperture of different size is substituted, then c assumes a new value not necessarily falling within the active range of the instrument. For a given aperture it is approximately true that igd^3/c is constant—the aperture constant k. In the present work the range of experimentally determined values of k, for a given aperture, was reduced by introducing empirical quantities, α and β, such that the expression for the aperture constant became:

$$k = i^{\alpha} g d^3/(c + \beta)$$

Additional comments on the empirical constants appear later.

Calculations. Data were generally processed with a Hewlett-Packard 9100B calculator. In some instances, however, it was most efficient to subject raw count data to preliminary integration. This was done using the MCA option that permits direct readout of the integral of a band consisting of an arbitrary number of channels located anywhere within the MCA memory.

Mode Estimation. The peaks or modes of particle size distributions were located using numerical differentiation. When required by the need for precision, differentiation was preceded by the application of a first-degree, three-point smoothing procedure that was iterated once. Both numerical procedures were taken from Hildebrand (*2*). Direct differentiation was

Table III. Sizing of Latex Standards

nominal diameter, μm	latex source[a]	aperture[b]	no. of detmns	range of series std dev, %	diameter found, μm	deviation from nominal diameter, %
1.099	A	1, 2	17	0.8–1.5	1.20	9.2
1.305	A	1, 2	24	1.0–1.2	1.28	−1.9
1.947	A	1, 2	40	0.5–1.0	1.98	1.7
2.02	B	1, 2	40	0.4–3.3	1.92	−5.0
3.49	A	1, 2	72	0.7–2.8	3.42	−2.0
10.3	C	2	16	1.7	10.1	−1.9
25.7	B	3	14	0.3–0.4	25.4	−1.2

[a] A: Coulter Electronics, Inc. Hialeah, Fa.; B: Dow Diagnostics, Indianapolis, Ind.; C: Duke Standards Co., Palo Alto, Calif. See text for details. [b] 1: 30 μm, 2: 50 μm, 3: 100 μm.

Table IV. Determination of α Values

nominal aperture diameter, μm	no. of latex standards	nominal latex size range, μm	no. of detmns	$\bar{\alpha}^a$	std dev
30	5	1.099-3.49	79	1.005	0.0024
50	6	1.099-10.3	130	1.023	0.0020
100	3	3.49-25.7	30	1.000	0.0017

[a] Linear, unbiased, minimum-variance estimates.

employed when the channel that contained the peak was obvious from inspection of the raw counts; the procedure was simply applied to the three largest counts recorded. When the location was less certain because of the breadth of the peak, low total count, or both, a less direct procedure was used: (a) neighboring channels were combined into groups of uniform width and of sufficient size to yield integral counts that were monotonic on either side of the peak, and (b) before numerical differentiation was applied, the integral counts were smoothed numerically. In either event, c was expressed to four significant figures.

Raw Count Integrals. The allocation of raw count data to bands that represented specified size ranges was based upon linear interpolation. Any fractional count that resulted from the interpolation and subsequent integration was rounded to the nearest integer.

Amplifier Gain. The ability of the MCA to respond to pulse amplitude was used to compare instrument gain settings. Each adjacent pair of gains was tested with 16 different pulse amplitudes. These amplitudes were chosen to provide nearly uniform sampling of the available range of channels: ca. 25 to 1000. The oscillator described earlier provided the pulses. The counting interval was 10 s, and the oscillator frequency was 50 kHz throughout. Peaks registered by the MCA were sufficiently narrow to permit the direct application of numerical differentiation as described.

Nearly all of the work reported here was done with the preamplifier gain set at 40 dB and the fine gain control of the MCA set at its nominal minimum of 0.3. Under these conditions the MCA nominal gain setting of 500 was taken as the base to which all other gain settings would be related. Coarse gain settings of 50 to 2000 are provided on the front panel of the MCA. The nominal gains of 5 and 15 were obtained with the MCA coarse gain set at 50 and the preamplifier gain set at 20 dB; gain 5 then resulted from the 0.3 setting of the MCA fine gain control and gain 15 resulted from the 1.0 setting of the fine gain control.

General Run Procedure. Latex standards were vigorously agitated by hand for 60 s prior to dilution. Sonication was not used since the presence of significant quantities of multiplets would have been obvious on the MCA display.

During any given run, the H.V. supply of the present instrument applies a constant voltage to the preamplifier unit. Consequently, for a particle-sizing run of practical duration, electrode polarization causes the aperture current to decrease continually. Short runs with large apertures are scarcely affected by this characteristic of the instrument, but with long runs or small apertures the effect clearly merits attention. The significance of the decreasing current was minimized by the following procedure: (a) the DMM was observed from the time the aperture current was initiated until immediately before pulse counting started, (b) the voltage was recorded, the DMM was disconnected from the aperture terminals and counting began, (c) counting stopped, the DMM was immediately reconnected, and the aperture voltage was recorded, (d) the sample beaker was lowered to open the path of the aperture current and the power supply voltage was recorded. The first two readings provided the estimate of mean aperture voltage, and the third, using Ohm's law, permitted calculation of the mean aperture current. The DMM was disconnected during counting to suppress noise injection. An incidental benefit of observing the DMM was that partial plugging of the aperture was instantly detected.

Throughout the work reported here, the lower-level discriminator of the MCA was set at 020 to deactivate the first 19 pulse-counting channels; this setting was chosen by trial and error to reduce the effect of pulses that were attributed to powerline noise. The deadtime of the MCA analog-to-digital converter never exceeded 42% in the work reported. Apertures were routinely examined for cleanliness with a microscope set for 100X magnification.

Size Distribution Runs. An eight-run series with dense electrolyte only was used to characterize the size distribution of the 25.7-μm latex. The 100-μm aperture was used throughout, and the runs were made in two series using slightly different latex concentrations. All results were placed on a single concentration basis by using the total count in the region of overlap to define the required normalization factor; the region of overlap was 11–29 μm, and the total counts were 52915 and 44011. All runs were made with the 2000-μL manometer setting.

RESULTS AND DISCUSSION

Effect of Electrolyte Density. Low- and high-density electrolytes were used to nearly the same extent in the work with the 30- and 50-μm apertures, but no dependence of the results upon electrolyte density could be found. However, with 25.7-μm latex in the 100-μm aperture, the low-density electrolyte gave decidedly irreproducible results.

The shape of the pulse generated by a particle passing through the sensing aperture has been reported to affect instrument performance (*3–5*). Such effects may have played a role in the present work. Indeed, the ability of the dense electrolyte to essentially remove the gravity-induced vertical component of particle velocity may have been responsible for needed pulse shape improvement. On the other hand, the comparatively good performance obtained with the dense electrolyte may have been due merely to avoidance of fractional sedimentation.

The α Correction. The results shown in Table IV indicate that α values distinctly different from unity reduced the variance of the aperture constant estimates obtained with the 30- and 50-μm apertures. The origin of the need for such a correction is not clear, but the heat evolved in the particle sensing aperture may be contributory; a discussion of such heating has been published (*6*). Considering the level of uncertainty in particle diameter encountered in the present work, the magnitude of the α correction might appear to be too small to warrant attention. However, with the improvement in determination of particle diameter that can be expected in the future, this type of correction would become distinctly significant.

Amplifier Gain. Apparent gain ratios originally obtained with constant amplitude pulses showed considerable dependence upon channel number c. This dependence was largely removed by calculating the ratios not from c values but rather from $c + \beta$ values, where β is an empirically determined zero-correction. The working value of β was obtained by: (a) successive approximation of the value of β needed to minimize the variance of each set of 16 experimentally defined gain ratios, and (b) averaging the resulting seven estimates of β to provide the working β, mean 14.9, standard deviation 0.3.

Table V shows the individual β estimates and the reduction in the spread of apparent gain ratio estimates that was obtained by introducing the zero-correction. Application of the zero-correction appears to permit reasonable approximation of the true gain ratios; the working gain values, 5.47 and 16.3, are within the manufacturer's stated tolerances.

Table V. Amplifier Gain Calibration and Evaluation of β

nominal gain	β	std dev of gain ratio, % $\beta = 0$	std dev of gain ratio, % $\beta = 14.9$	working gain
5				5.47
	14.94	8.8	0.1	
15				16.3
	15.00	8.7	0.5	
50				51.3
	15.39	8.5	2.7	
100				101
	14.52	8.0	1.6	
200				201
	14.78	9.1	1.4	
500				500
	15.08	8.7	1.5	
1000				1008
	14.75	7.5	0.3	
2000				2017

Electrode Polarization. The importance of the drop in aperture current caused by electrode polarization may be ascertained from the observed differences between initial and final aperture voltage. The ratio of this difference to mean voltage was calculated for each of the 250 runs that provided most of the data for the present report. The mean value of this ratio was 0.11%. In the eight runs used to characterize the particle size distribution of the 25.7-μm latex, the mean ratio was 0.17%. These results, together with the results of the error propagation analysis to be discussed, led to the conclusion that electrode polarization did not contribute significant error to the present work.

Latex Standards. Table III summarizes the results of 20 discrete series of particle size measurement runs. Each series represents a single amplifier gain setting and a variety of aperture currents. Usually the aperture currents were so selected that the series as a whole sampled the range of the MCA nearly completely and uniformly. As may be seen in column five of Table III, the series that displayed the greatest scatter had a particle size relative standard deviation of 3.3%. The mean of the relative standard deviations for all the series was 1.2%. This estimate of overall precision compares favorably with the results of the error propagation analysis to be discussed.

At present, the question of accuracy is difficult to treat, but work in progress at the National Bureau of Standards (7) should help in resolving this problem. It may be appropriate, at this juncture, to note simply that the worst-case deviation from nominal diameter found in the present work was 9.2% and the corresponding mean value for all seven estimates was 3.3%. One source of difficulty in improving the accuracy of size estimation may have been the comparative ease with which resistive-pulse instruments provide estimates of modal diameter, while with optical methods the mean is more accessible; i.e., size distribution skewness may have been a source of disagreement between some estimates of the characteristic size of standard latex particles. Another source of error may reside in the use of arrays of particles to estimate the size of very broad distributions (8). Even if arrays are not used, there may be instances in which small particles that are hidden from view by larger particles or particle clusters will be detected by resistive-pulse instruments. At present it would be difficult to judge how important these, and other unexamined sources of error, may be.

Results obtained by Matthews and Rhodes (8) using electron microscopy agree closely with the present work: differences for the 1.305- and 3.49-μm latexes are 0.8 and 0.6%, respectively. Alliet (9) used a variety of methods to size a large group of standards. For latexes of the same nominal diameter, differences between the present estimates and Alliet's values were 3.49 μm: 1.8 and 3.5%, 10.3 μm: 11.5 to 14.4%.

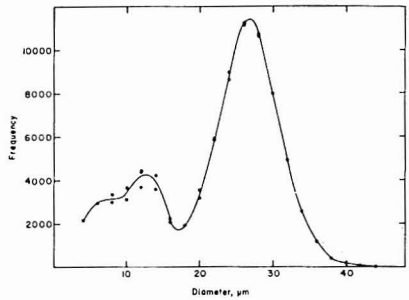

Figure 3. Particle size distribution of 25.7-μm latex

Table VI. Overlap Quality, 25.7-μm Latex

mean diameter, μm	run conditions[a]	mean count	deviation from mean count, %
8	1, 2	3 168	5.3
10	1, 2	3 386	7.8
12	1, 2, 3	4 185	9.4[b]
14	2, 3	3 892	8.0
16	2, 3	2 132	3.4
20	4, 5	3 344	5.8
22	4, 5	5 875	0.7
24	4, 5	8 798	2.0
26	4, 5	11 222	0.4
28	4, 5	10 713	0.5

[a] 1: 0.381 mA, gain 100; 2: 0.903 mA, gain 15; 3: 0.201 mA, gain 15; 4: 0.600 mA, gain 5; 5: 0.165 mA, gain 5. [b] Pairwise deviations of 9.1 and 9.6% were averaged to give the tabulated value.

Particle Size Distribution Overlaps. Figure 3 shows the results of eight particle size distribution runs made to characterize the 25.7-μm latex. Selected data from the same runs also appear in Table VI; the latter data were derived in such a way that no bias was introduced by the concentration normalization referred to earlier. The overlap discrepancies that form the basis of Table VI can be seen as discrete points in Figure 3. Note that for the 12-μm overlap three runs, rather than two, are represented. The extent to which these runs sampled the range of the instrument may be judged from the aperture currents and gain settings detailed in Table VI plus the range of channel numbers represented: 37–994.

The data plotted in Figure 3 yield a mean diameter estimate of 22.3 μm and a mode of 26.5 μm. The mode here represents two determinations while the independent estimate of 25.4 μm shown in Table III represents 14 determinations.

The last column in Table VI shows the deviation of observed particle counts from the means. The average deviation is 4.2%, and the worst-case value is 9.6%. The superior replication found between 19 and 29 μm compared with that found between 9 and 17 μm may reflect the use of a single amplifier gain in the former case vs. the use of two in the latter.

Error of Diameter Estimates. The relative importance of known sources of uncertainty in the estimation of particle diameter was examined. The sources identified were: (a) aperture constant, (b) aperture current, (c) channel number, (d) amplifier gain, (e) the constant α, and (f) the constant β. To make the computation practical, attention was confined insofar as possible to a single run with 3.49-μm latex in the 50-μm aperture. This run was selected to well represent the present work; e.g., the mean deviation of the aperture current

was 0.14%; cf., the earlier discussion of aperture current variability. The basis for estimating the probable error contributed by each source is given here: (a) three estimates of k obtained with the 3.49-μm standard were combined with one estimate from each of the two comparable standards: 1.305 and 10.3 μm; cf., Table III, last column; (b) the manufacturer's specifications for the DMM provided the aperture current estimate; (c) the uncertainty of the modal channel number was estimated by repeatedly making single channel adjustments of the sizes and locations of the channel groups used; (d) the amplifier gain estimate was based on the largest relative standard deviation found in establishing the gain ratios; (e) the α estimate was based on the standard deviation of the 130-run group of Table IV; and (f) the β estimate was drawn from the seven values given in Table V.

Error propagation analysis based on the information just described indicated that the only significant source of error was the aperture constant. The next most significant source was the constant α, but it contributed only 0.5% as much error as the aperture constant. According to the analysis, the error of the diameter estimate when expressed as relative standard deviation was 2.5%. This estimate appears to be consonant with the five experimental estimates of the diameter of the 3.49-μm latex obtained in the present work: mean 3.42 μm, relative standard deviation, 2.5%.

The results obtained by the highly empirical approach adopted in the present work suggest that the method has merit. Furthermore, it appears that numerous improvements are possible. For example, the accuracy of the nominal diameters of size-standards could evidently be improved, better formulas for describing instrument behavior can probably be devised, and larger, more accurate, and more representative data bases might be developed.

ACKNOWLEDGMENT

The helpfulness of comments by Nelson Smith and Alvin Beilby of Pomona College and by Vincent Maier and Carl Vandercook of the Science and Education Administration is gratefully acknowledged.

LITERATURE CITED

(1) R. Morrison, "Grounding and Shielding Techniques in Instrumentation", Wiley, New York, N.Y., 1967.
(2) F. B. Hildebrand, "Introduction to Numerical Analysis", McGraw-Hill, New York, N.Y., 1974.
(3) G. Ruhenstroth-Bauer, G. Valet, V. Kachel, and N. Boss, *Naturwissenschaften*, **61**, 260 (1974).
(4) R. Davies, R. Karuhn, and J. Graf, *Powder Technol.*, **12**, 157 (1975).
(5) J. Schulz and R. Thom, *Med. Biol. Eng.*, **11**, 447 (1973).
(6) R. W. De Blois and C. P. Bean, *Rev. Sci. Instrum.*, **41**, 909 (1970).
(7) W. A. Cassatt, W. T. Yap, W. P. Reed, and S. A. Mills, *Powder Technol.*, **13**, 27 (1976).
(8) B. A. Matthews and C. T. Rhodes, *J. Colloid Interface Sci.*, **32**, 339 (1970).
(9) D. F. Alliet, *Powder Technol.*, **13**, 3 (1976).

RECEIVED for review January 3, 1978. Accepted May 5, 1978. Reference to a company or product name does not imply approval or recommendation of the product by the U.S. Department of Agriculture to the exclusion of others that may be suitable.

Isotopic Determination of Silver in Picomole Quantities by Surface Ionization Mass Spectrometry

William R. Kelly,* Fouad Tera,[1] and G. J. Wasserburg

The Lunatic Asylum of the Charles Arms Laboratory, Division of Geological and Planetary Sciences, California Institute of Technology, Pasadena, California 91125

A microanalytical procedure is described for the quantitative separation of Ag from natural samples by anion exchange and analysis by surface ionization mass spectrometry using silica gel as an emitter. The isotopic composition of 50 pmol of Ag can be measured on a Faraday detector with a precision of 0.1%. Isotopic measurements have been made on as little as 0.15 pmol with a precision of 1% using an electron multiplier detector. The total procedural blank for the anion exchange separation is 0.15 pmol. Using stable isotope dilution 0.5 pmol of Ag, which is 3×10^{11} atoms, can be measured with a precision of better than 1% with only a 30% blank correction. This allows the accurate determination of Ag in natural samples down to concentration levels of 1 pmol per gram. The ionization efficiency for Ag is about 1–2% and the detection limit is 1 fmol. This procedure has been applied to several meteorites, and a standard terrestrial rock.

We report on a new procedure that allows the precise isotopic analysis of picomole quantities of Ag with ion currents of typically 10^{-12} A which corresponds to an ionization efficiency of 1–2%. This is a substantial improvement compared to previously described analytical procedures which required several nanomoles of Ag for ion currents of only 10^{-14} A (*1–4*). The marked increase in ion production is made possible by loading Ag in the presence of silica gel and phosphoric acid on single Re V-shaped filaments. The silica gel technique was first used by Cameron et al. (*5*) to obtain good quality data on nanomole quantities of Pb. Tera and Wasserburg (*6*) extended and applied this technique to the dating of lunar rocks and meteorites by U–Th–Pb systematics. By miniaturizing the chemical separation procedure and thus reducing the blank to acceptable levels, they have demonstrated that high quality data can be obtained on picomole and subpicomole quantities of Pb. The same approach was used for Ag with success comparable to that achieved for Pb. In addition spectral interferences in the Ag mass region due to hydrocarbons and AsS^+ have been eliminated.

There is cosmochemical interest in both the precise isotopic composition and the abundance of Ag. Natural Ag consists of two stable isotopes of almost equal abundance ($^{107}Ag/^{109}Ag = 1.081$). Its potential as a very precise early solar system chronometer has been recognized for some time (*1*). Silver-107 may be produced as a decay product of now extinct ^{107}Pd ($t_{1/2} = 6.5 \times 10^6$ yr). If solids formed in an environment containing ^{107}Pd and remained unaltered, the isotopic composition of Ag as measured today would be altered in a manner directly

[1] Present address, Department of Terrestrial Magnetism, Carnegie Institution of Washington, 5241 Broad Branch Road, Washington, D.C. 20015.

0003-2700/78/0350-1279$01.00/0

Table I. Silver Content of Reagents

reagent	Ag content pg/mL
H_2O[a]	0.4
12 N HCl[b]	1.1
Concd HNO_3[c]	0.28
HF[c]	0.24

[a] Commercially distilled, passed through two series of ion-exchange columns and redistilled in a two-stage quartz still by us. [b] Concentrated HCl made by bubbling HCl gas through H_2O, and dilution to desired concentration. [c] Obtained from NBS (Analytical Chemistry Division).

proportional to the original $^{107}Pd/Ag$ in the material. The abundance of ^{107}Pd can be calculated from the estimated production rate and an assumed nucleosynthetic model. By measuring the bulk Pd/Ag ratio and the $^{107}Ag/^{109}Ag$ ratio a model-dependent age can be calculated. This age would presumably define the time interval between the last event which produced ^{107}Pd and its incorporation into a solid object assuming the system remained closed to both Pd and Ag. This system is analogous to the ^{129}I–^{129}Xe and ^{26}Al–^{26}Mg chronometers, both of which have yielded positive results (*7, 8*). Searches of these kinds have been restricted to meteorites because ages determined by other chronologies show them to be the oldest known objects in our solar system.

In addition to the geochemical and cosmochemical importance of Ag, it is worth noting the well established extreme toxicity of this element to marine organisms. In 1939 J. R. E. Jones systematically studied the toxic effects of many heavy metals on the stickleback fish (*9*). Ag was found to be the most toxic of the elements considered which included Hg, Pb, Cd, and Cu. A concentration of 3 ppb was fatal within 10 days while 10 ppm proved fatal within 25 min. Recent studies have substantiated the extreme toxicity of Ag. In a study of the toxicity of both Ag and Cd to the cunner, a small inshore fish common to the northeast coast, Thurberg and Collier (*10*) found that the lethal (96 h) concentration of Ag was 0.5 ppm. Ag is 100 times more toxic to this fish than Cd. In an investigation of the toxicity of heavy metals to embryos of the American oyster, it was found that Ag was lethal (LC_{50}, 48 h) at 6 ppb (*11*). It was 600 times more toxic than Cd. Only Hg was more toxic. Of even more concern are the possible deleterious effects of Ag at sublethal concentrations that may prohibit normal growth and maturity on eggs and developing embryos. In addition, sublethal concentrations of heavy metals may be more lethal than is currently believed because of synergistic effects.

The concentration of Ag in normal seawater is not well known but is estimated as 1 pmol/mL. At this level, no existing analytical technique has the sensitivity to analyze a small volume of seawater. The stable isotope dilution technique described in this paper fills the need for a very sensitive, accurate, and precise method for the analysis of Ag.

EXPERIMENTAL

Reagents. The reagents used in this study are listed in Table I along with their Ag content as determined by us. One picogram is 10^{-14} mol or 6×10^9 atoms. The ^{109}Ag enriched spike was obtained from the Oak Ridge National Laboratory and was calibrated with a standard made from high purity Ag shot obtained from the Ventron Corporation. The 0.1 N H_3PO_4 was prepared from P_2O_5 which was specially prepared for us by Research Inorganic/Organic Corporation. The high purity silica gel was synthesized by us.

Laboratory Ware. Labware consisted of Teflon (FEP) beakers, quartz pipets, and quartz ion-exchange columns. Quartz columns were 8 cm long with an i.d. and o.d of 2 mm and 4 mm, respectively. Each had a 2-mL reservoir at the top and was fitted with a small plug of Pyrex fiber at the tip. Dissolution and evaporation of samples was done in Teflon beakers mounted within a Teflon pot covered with a quartz disk. The Teflon pot has two small openings which allow the entrance and exit of dry filtered N_2 to prevent condensation (*12*). The Teflon and quartz ware were cleaned by boiling for 1 day in each of the following: 1:1 HCl, aqua regia, 1:1 HNO_3, and 1% HNO_3. The ion-exchange columns were initially cleaned once by the above procedure and all subsequent cleaning between samples was done with 0.5 N HCl and 1 N HNO_3. The anion-exchange resin (Bio-Rad AG1x8, 100–200 mesh) was washed with distilled water (D.W.) and 9 N HCl and then stored in 4 N HCl. The Re filaments were made from zone refined Re ribbon obtained from the Rembar Company. They were formed into a V, which was 3.2 mm long, 0.3 mm wide, and 0.4 mm deep. Filaments were outgassed at 2000 °C for 2 h at $< 2 \times 10^{-6}$ Torr prior to sample loading.

Chemical Procedure. All sample handling was carried out in clean rooms under strictly controlled conditions. Metallic samples were washed in Specpure methanol, etched with 12 N HCl, washed with D.W., and dissolved in 12 N HCl (~5 mL/g of sample). Silicate samples were dissolved in a mixture of 10 parts HF to 1 part HNO_3 (10 mL/0.3 g sample).

The quantitative separation of Ag from other chemical constituents was carried out using common anion-exchange techniques. The whole process, however, has been miniaturized in order to use these techniques to their full potential and reduce the chemical blank to very low levels. This miniaturization was made possible by the disparity in the anion-exchange properties of Ag compared with the majority of the abundant elements.

Early in this study it was discovered that the concentrated HCl contained small amounts of As and S. During mass spectrometry these contaminants give rise to AsS^+ species which appear at masses 107, 108, 109, and 111 corresponding to the S isotopes 32, 33, 34, and 36. These interferences were reduced to negligible levels by eluting Ag from the last column with 1 N HNO_3 instead of 9 N HCl. The separation procedure described herein is designed to accommodate 300 mg of an iron meteorite which consists principally of Fe (80–95%), Ni (5–20%), Co (0.5–1%), and microgram quantities of most of the transition elements. Silicate samples of at least 300 mg can also be processed by this procedure.

Two-Column Procedure. This procedure is used for concentration measurements. An aliquot containing approximately 300 mg of sample is precisely weighed and then spiked with ^{109}Ag. One mL of 12 N HCl is then added to this solution. Because most of the original HCl has been consumed in dissolving the sample, this acid is added to increase the acidity and thus prevent the hydrolysis of Fe^{3+} in the next step. The solution is reduced in volume by evaporation until $FeCl_3$ begins to precipitate. After most of the liquid has evaporated, leaving only a slush containing $FeCl_3$ crystals, the beaker is removed and 10 mL of 0.1 N HCl is added immediately. All of the solids go into solution within 3–5 min. This clear solution, which is close to 0.1 N in HCl, is loaded onto the first column in 2-mL portions. This column contains 0.16 mL of resin which has been conditioned with 3 column volumes of 0.1 N HCl. Under these conditions, Ag is quantitatively retained on the resin with a distribution coefficient of 5000 (*13*) along with differing amounts of Zn, Cd, Pd, and other heavy transition elements. All other elements pass through the column and are discarded. The column bulb and resin bed are washed with 2 mL of 0.1 N HCl added in approximately 0.2-mL portions. The Ag is eluted with 0.5 mL of 9 N HCl.

The eluate, which contains the Ag and a small amount of Fe (<1 μg), is evaporated to 0.1 mL. To this is added 1 mL of 0.1 N HCl and the sample is placed onto a second column containing 0.06 mL of resin which has been conditioned with 10 column volumes of 0.1 N HCl. The sample solution is added in small portions so as to only half fill the column capillary. The column is rinsed with 2 mL of 0.1 N HCl. The column is then rinsed with 1 mL of 0.001 N HCl; this rinsing procedure removes the Fe and most of the HCl from the resin bed. After the column has drained completely and before the Ag is eluted with HNO_3, the bulb and capillary are made free of all traces of HCl in the following manner. The column bulb is filled with D.W. leaving an air gap above the resin bed. The water column then is lowered carefully to within 2–3 mm of the resin bed using a pipet. The D.W. is removed with the pipet and the process repeated two more times. The Ag is eluted with 1 N HNO_3. This is added in very small portions (0.1

Table II. Procedural and Loading Blanks

procedure	Ag, pg
two-column chemistry	13.6, 12.3, 10.2 Av. 12.0 ± 3
three-column chemistry	10.7, 15.2, 12.0 Av. 12.6 ± 2
loading blank	4.3, 3.3 Av. 3.8

mL or less). The first three drops (1 drop = 0.05 mL) to pass contain no Ag and are discarded. The next 15 drops to pass are collected and contain >95% of the Ag. Exactly 2.5 μL of 0.1 N H_3PO_4 is added to the beaker containing the sample and the solution is evaporated until only the hydrated speck of P_2O_5 (~0.1 mm diameter) containing the Ag remains. The sample is now ready for loading onto a Re filament.

Three-Column Procedure. This procedure is used for samples whose isotopic composition is to be determined and is identical to the procedure described above with one exception; a third column is interposed between columns one and two. For precise isotopic measurements, it is desirable to have the largest ion beam intensity possible. In the analysis of picomole quantities of Ag, equivalent amounts of other elements, particularly Fe, seriously suppress the ionization of Ag. The amount of Fe in the final sample can be dramatically reduced by using a three-column procedure. In this procedure, the wide disparity in the distribution coefficients of Fe and Ag are used to great advantage. In 9 N HCl, the distribution coefficients of Fe and Ag are 10^4 and 3, respectively (*13, 14*). A column containing 0.06 mL of resin is rinsed with 15 column volumes of 0.1 N HCl to remove any Fe and then conditioned with 15 column volumes of 9 N HCl. The 0.5 mL of 9 N HCl which was collected from the first column is loaded directly onto the above column. The Fe is held quantitatively while the Ag breaks through and is collected. The column is rinsed free of Ag with 7 column volumes (8 drops) of 9 N HCl which is collected. The eluate quantitatively contains the Ag and is now processed through a third column in a fashion identical to the second column operation described above for the two-column procedure. The resin used for the separations is discarded after use and the columns are cleaned by rinsing them with 20 mL of 1 N HNO_3 and 20 mL of 0.5 N HCl.

Procedural Blanks. Total blanks are determined by adding a small amount of dilute spike (typically 0.3 pmol) enriched in ^{109}Ag to a Teflon beaker. To this is added 1 mL of 12 N HCl and the solution is treated and processed as an actual sample according to the procedures described in the previous two sections. The values determined for these blanks represent the total chemistry blank including filament loading and are tabulated in Table II. These blanks were determined with a precision of about 1% and fluctuations among blanks are less than 30%, which are well within acceptable limits.

To guard against these blanks being spurious, the isotopic composition of the blank was also determined. It had a 107/109 ratio of 1.3 due to a small contribution to the 107 peak from $^{75}As^{32}S^+$. It can be shown from isotope dilution systematics, however, that this will introduce only a 5–10% high bias in the measured blanks. We discovered that the concentrated HCl was the source of the AsS^+ species by mass spectrometric analysis of a small portion of the acid. From the observed peak signatures at masses 107, 108, 109, and 111, AsS^+ was unequivocally identified.

Chemical Yields. Chemical yields were established in two ways. The ion-exchange column yields were calibrated using radioactive ^{110}Ag ($t_{1/2}$ = 260 d) and the total yield on an actual sample was determined by stable isotope dilution. The distribution coefficient of a particular species in a concentrated matrix of other elements can be severely reduced and in some cases enhanced because of column loading. With the radioactive tracer it was determined that 300 mg of Fe in 10 mL of 0.3 N HCl (60 column volumes) could be passed through the first column with negligible breakthrough of Ag (<10%). The two smaller columns were also calibrated and were found to function ideally.

An exact chemical yield was established precisely on an actual sample by stable isotope dilution. A 314-mg aliquot of the Canyon Diablo meteorite (#5A) was spiked with 23.8 pmol of ^{109}Ag and

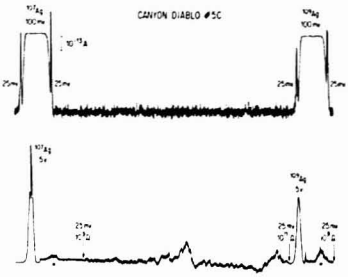

Figure 1. Analog display showing Ag mass region. Top figure was taken on Faraday detector with a defining slit of 0.64 mm. Bottom figure was taken on electron multiplier detector with a defining slit of 0.13 mm. Solid dots indicate hydrocarbon peaks. The spike in the ^{107}Ag peak is due to scale change. The dispersion in this mass region is 28 G/amu

processed through the two-column procedure. The 15-drop eluate from the second column was accurately divided into two equal portions. One portion was analyzed to determine the bulk concentration; the other portion was additionally spiked with 24.7 pmol of ^{109}Ag and its isotopic composition determined. From this experiment, it was determined that the chemical yield was 94.5%.

Filament Loading and Mass Spectrometry. Sample loading is performed with the aid of a Hamilton microsyringe equipped with a 2-cm length of Intermedic polyethylene tubing (i.d., 0.07 mm). Exactly 2.5 μL of D.W. is drawn into the tubing and ~0.5 μL is placed in the V-shaped boat of the filament. The remainder is placed directly on the sample which is in a beaker. Silica gel (~0.1 mg) is added to the V with a tungsten needle. This needle is cleaned before and after use with 1 N HNO_3 and then rinsed with D.W. The sample is then placed in the V in small portions and a low current (0.5–1.0 A) is passed through the filament after each addition to evaporate the sample. After all the sample has been added, the silica gel is bonded to the filament by increasing the current to 1.5–1.8 A for 5–10 s.

The two identical mass spectrometers used in this study have been described in detail by Wasserburg et al. (*15*). These instruments are single focusing mass spectrometers equipped with both Faraday and electron multiplier collectors. A programmable magnetic field power supply allows rapid (500 G/s) steps from peak to peak. The maximum drift in the magnetic field is $|\Delta B/B| \leq 2 \times 10^{-5}$. The equivalent maximum drift in the accelerating potential is $|\Delta V/V| \leq 4 \times 10^{-5}$. These instabilities correspond to an ion beam translation of 0.012 mm. The measurement of a single peak intensity consists of three measurements, two background readings and the peak itself. The backgrounds are typically taken 8–10 gauss on both sides of the peak. In the case of Ag, which has two isotopes, 3 min of data acquisition are required for 1 set of 10 ratios. Data reduction is done both online and offline by a PDP-11 computer.

Analog displays covering the Ag mass region are shown in Figure 1. Both spectra were taken with the same recorder speed and magnetic field sweep rate. The top spectrum was taken on the Faraday cage detector using a feedback resistor of 10^{11} Ω with source and detector slit widths of 0.25 mm and 0.64 mm, respectively. The bottom spectrum was taken on the electron multiplier detector with a defining slit width of 0.13 mm which allows resolution of the satellite peaks from the main peaks. The electron multiplier has a gain of 5000 and feedback resistors of 10^9, 10^{10}, and 10^{11} Ω. With the increased sensitivity of the multiplier hydrocarbon peaks can be clearly seen. All of our samples were run at a filament temperature of 1000 °C. At this relatively low temperature, hydrocarbon peaks are common, particularly when silica gel is used as an emitter. The hydrocarbon intensities are significantly reduced by prolonged pumping of the source (overnight) and the use of the cold finger in the source region at liquid N_2 temperature. At the end of several runs, we have monitored the hydrocarbon peaks at masses 107 and 109 as the cold finger was warmed quickly to room temperature. A

Table III. Precision of Concentration Measurements

sample, weight, mg	Ag content, ng/g[a]
Tlacotepec #1A.1, 259	3.06 ± 0.14
Tlacotepec #1A.2, 211	3.14 ± 0.03
Tlacotepec #1C,[b] 249	3.33 ± 0.03

[a] Errors are 2σ for a single determination. [b] 1.03 ng of normal Ag was added to this solution before chemistry. This value was obtained after subtracting the added amount.

rapid increase in the hydrocarbon intensities of 3–4 orders of magnitude is observed followed by a slow exponential decay. From these observations we conclude that the hydrocarbons are indigenous to the source and presumably vaporize from the source surfaces when high vacuum is attained. Weekly cleaning of the source focusing plates reduces the hydrocarbon intensities considerably.

Regardless of the absolute magnitude of the satellite peaks, it is mandatory to demonstrate that they do not contribute to the main peaks if high precision work is to be considered accurate. This was demonstrated in two ways. The first way was to determine the position of the satellite peak in relation to the detector slit when the main ion beam is centered in the slit opening to the Faraday cage. The spatial relationships of the peaks can be determined from the information provided in Figure 1. It can be shown that when the main peak is centered in the detector slit opening, the satellite peak is completely resolved. More importantly the 10-G offset, which was used for the high field background reading, will translate the hydrocarbon beam 1 G (0.12 mm) beyond the slit edge. This distance is large compared to the drifts in the ion beam because of small instabilities in the magnetic field and accelerating potential. The second way was to plot the measured $^{107}Ag/^{109}Ag$ ratio vs. the measured $^{107}Ag/^{107}$hydrocarbon ratio. The $^{107}Ag/^{109}Ag$ ratio was constant to within 0.1% for $^{107}Ag/^{107}$hydrocarbon ratios of 100–2000. This demonstrates that no functional relationship exists between the satellite peaks and the main peaks to 0.1%.

Ionization Efficiency of Ag. The net ionization efficiency is defined as the number of ions collected divided by the number of atoms initially present. It was determined from the integrated ion current on several normal and sample runs and found to range from 1–2% in typical runs. On occasion, efficiencies as high as 5% were found.

RESULTS AND DISCUSSION

Concentration and isotopic measurements were made on several iron meteorites and the U.S.G.S. standard rock BCR-1 which is a Columbia River basalt. We included the Canyon Diablo and Toluca iron meteorites in our study because the Ag concentration and composition on these two samples have been determined by a number of investigators. This allows meaningful comparisons to be made among a variety of techniques.

Concentration Measurements. All samples whose concentrations were to be determined were spiked with ^{109}Ag before being passed through the two-column separation procedure. The concentration data, therefore, are independent of the chemical yield provided the procedural blank is negligible. Our control of both precision and accuracy is demonstrated in Tables III, IV, and V. In Table III, the replicate analyses on aliquots from the same solution of the Tlacotepec meteorite agree within errors. The last entry in the table is an experiment in which we added 10 pmol of normal Ag and ^{109}Ag spike to an aliquot of Tlacotepec before the chemical separation. After mass spectrometry, the result was corrected by subtraction of the 10 pmol that was added. In spite of this large 60% correction, the result is within 10% of the two replicate values. These experiments demonstrate our ability to aliquot identical solutions but do not demonstrate that these aliquots are representative of the sample as a whole because of the possible precipitation or plating out of Ag. We experienced difficulties in obtaining representative aliquots from concentrated solutions of iron which appeared to be clear and free of precipitate. This problem is considerably reduced if the solutions are at least 6 N in HCl and aliquoted in this form as demonstrated in Table IV. A 3.5-g piece of Tlacotepec (#2) was dissolved in HCl and centrifuged. The solids, consisting mostly of sulfides, were dissolved in aqua regia and centrifuged. A small amount of white residue (~1 mg) was observed. This was identified as silicate material by energy dispersive x-ray analysis in a scanning electron microscope. The supernate was converted to the chloride form and recombined with the main solution. This solution was then totally spiked with 0.1020 nmol of ^{109}Ag. The solution was heated and thoroughly mixed. After cooling to room temperature two aliquots were taken. One (#2) was analyzed for composition, which then allows the number of Ag atoms in the solution to be calculated. The other aliquot (#2B) was additionally spiked and analyzed, which allows the number of Ag atoms in the aliquot to be calculated. A third aliquot (#2C) was taken one week later and treated in the same way as aliquot #2B. The results of these three experiments are shown in Table IV. The degree with which aliquots #2B and #2C agree with aliquot #2A is an indication of how representative they are of the total solution. There is exact agreement between #2A and #2B, but aliquot #2C, which was removed 1 week later, is 5% low. We believe this discrepancy is real and indicates a difficulty in obtaining representative aliquots from concentrated solutions of iron. The cause and solution of this problem are under investigation.

Table IV. Aliquoting Reproducibility Measurements

sample, aliquot weight, mg	Ag, ng/g
Tlacotepec #2A, 254	6.17 ± 0.06
Tlacotepec #2B, 319	6.12 ± 0.15
Tlacotepec #2C, 317	5.79 ± 0.09

Table V. Ag Measurements on Standard Terrestrial Rock BCR-1

sample, weight, mg	Ag content, ng/g
BCR-1, 124	30.7 ± 0.1
BCR-1,[a] 26 determinations, Keays et al., 1974	27.2 ± 6.0

[a] Data obtained by radiochemical neutron activation analysis.

A comparison of the results obtained by our method with those of other workers is shown in Table V. Our value for the standard rock BCR-1 agrees within errors to those obtained by Keays et al. (*16*) who used RNAA. Their value is an average of 26 different determinations made over a period of 8 years as part of their lunar analysis program.

Concentration measurements were made on nine meteorites from three different meteorite classes and a standard terrestrial rock. For the concentration measurements, small aliquots were used in order to conserve the samples. These data are shown in Table VI. Although the absolute amounts of Ag analyzed ranged from 100 down to 5 pmol, the blank corrections were always less than 4% (columns 3 and 4). The contributions to the measured $^{107}Ag/^{109}Ag$ ratios from AsS^+ are less than 1% in most cases (columns 5 and 6).

The sample concentrations are given in the last column. Our values for Canyon Diablo and Toluca fall within the broad range reported by other investigators. These data are summarized in (*17*). Seventeen analyses of Canyon Diablo by three different investigators yield a range of 10–180 ng/g with a median value of 50 ng/g. Five analyses of Toluca by two different investigators yield a range of 10–130 ng/g and an average value of 90 ng/g. Our analyses of two different

Table VI. Summary of Ag Concentration Measurements

sample	sample weight, mg	amount of Ag measured, ng	total blank correction[a] pg (%)	$^{107}Ag/^{107}$hydrocarbon	$^{107}Ag/^{75}As^{32}S^{+}$	Ag concn, ng/g ± 2σ
iron meteorites group 1a						
Canyon Diablo #3A	263	10.2	15 (0.15)			38.8 ± 0.1
Canyon Diablo #5A	314	10.7	15 (0.14)	290	$>8.6 \times 10^4$	33.9 ± 0.1
Toluca #1A	196	9.1	15 (0.16)	1.2×10^3	$>6.0 \times 10^4$	46.2 ± 0.3
Group 4b						
Cape of Good Hope #1C	266	1.7	15 (0.88)	344	2.1×10^3	6.47 ± 0.04
Hoba #2A	161	2.6	14 (0.54)	630	$>7.0 \times 10^3$	15.9 ± 0.1
Klondike #1A	230	1.6	15 (1.9)	220	$>4.9 \times 10^3$	7.15 ± 0.14
Santa Clara #1A	311	0.61	14 (2.3)	31	$>3.0 \times 10^3$	1.91 ± 0.02
Tlacotepec #1A.1	259	0.78	32 (3.9)	53	$>4.8 \times 10^2$	3.06 ± 0.14
Tlacotepec #1A	212	0.66	13 (2.0)	130	$>1.1 \times 10^3$	3.14 ± 0.03
Warburton Range #1A.1	287	3.0	14 (0.47)	1.1×10^3	$>1.1 \times 10^3$	10.5 ± 0.2
standard terrestrial rock BCR-1 #3	124	3.84	20 (0.53)			30.7 ± 0.1

[a] Sum of reagent and total chemistry blanks.

slices of Canyon Diablo give values that are within 15% of each other. We believe both of these values are correct and merely reflect small scale heterogeneities in the distribution of Ag. The extreme variations among other investigators may be due to macroscopic heterogeneities in the meteorite or they may be due to spurious analysis.

Our values for six iron meteorites of Group 4b are the only determinations on this class with the exception of Hoba. The values below 10 ng/g are the lowest reported values on meteorites.

Isotopic Measurements. The normalization techniques normally employed for high precision isotopic measurements cannot be used in the case of Ag because it has only two stable isotopes and no long-lived radioactive isotopes. In previous studies it has been observed that the measured ratio changes with time, becoming progressively enriched in the heavy isotope. This behavior is a general phenomenon which is mass dependent and appears to obey the Rayleigh fractionation equation; thus, the measured ratio differs from the true ratio by an unknown amount. Investigators have attempted to arrive at the true value by using calibrated mixtures of the two enriched isotopes of Ag. By comparing the measured value with a known standard, a fractionation factor is obtained and applied to samples of unknown composition. This approach has been used by Crouch and Turnbull (*18*) and Shields et al. (*19*) at the National Bureau of Standards (NBS). In this study, no correction factors were applied to the data. We report only raw uncorrected ratios.

The same normal chosen by Shields et al. (*19, 20*) was used as the standard in this study. This is a commercial $AgNO_3$ designated NBS 978 which was shown to be identical in composition to Ag extracted from a variety of Ag ore bodies.

In relative determinations, one is not concerned with absolute values; it is only necessary to compare values of samples to measured values of an accepted or arbitrary standard. This latter method has been used in past geochemical studies (*1–4*) and was used in this study. In either approach it is imperative that samples and standards be measured under identical conditions to avoid systematic errors. This must be demonstrated experimentally. In our study, samples and standards were analyzed under identical conditions which included a strict time and filament temperature schedule. The filament was heated by a programable power supply to 990 °C in 1 h. Filament temperatures were obtained with an optical pyrometer and could be determined to better than ±5 °C. Five sets of 10 ratios were taken at this temperature and then the temperature was raised to 1000 °C. Ten sets of 10 ratios were obtained at this temperature which required 30 min.

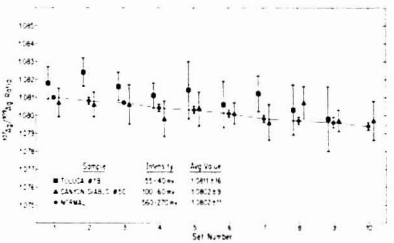

Figure 2. Fractionation behavior of three samples at 1000 °C. Each data point represents the mean of 10 ratios; associated error bars are twice the standard deviation of the mean

The run histories for three samples of differing ion intensities are shown in Figure 2. Here we have plotted the measured ratio vs. time as represented by the set number. The time interval represented by the abscissa is 30 min. The error bars associated with the individual sets are governed by ion counting statistics and beam stability. A systematic decrease of about 0.1% in the measured ratio is clearly seen. The average values and their associated errors for the individual runs are also shown in the figure. These errors are governed by ion counting statistics and beam instabilities, plus the systematic drift in the measured ratio throughout the run. It is this last variation which governs the precision of the average of an individual run. This statement is justified by the observation that the errors associated with the three averages are almost identical in spite of the large variations in ion intensity. The conclusion is that an ion beam of $\sim 5 \times 10^{-13}$A is sufficient to give errors which are small compared to the error introduced by the systematic drift in the measured ratio with time. A 5- to 10-ng sample, therefore, is sufficient for the precise isotopic determination of Ag at the 0.2% level.

Figure 3 shows a histogram for the 12 measured normals. All data were taken at 1000 °C. Each block represents one set of 10 ratios. The highest and lowest measured ratios were 1.083 and 1.079. The errors associated with the averages of the first five and last five sets are identical; thus no gain in precision can be realized by decreasing the data acquisition time. The average fractionation during the 30-min interval was 0.05%. This is based on the difference in the averages

Table VII. Summary of Isotopic Composition Measurements

sample	amount of Ag measured, ng	$^{107}Ag/^{109}Ag$[a]	$^{107}Ag/^{75}As^{32}S^{+}$	$^{109}Ag/^{109}$hydrocarbon
NBS 978 Normals (12)	5-15	1.0810 ± 18[b]		
BCR-1 #1	4	1.0813 ± 16	$>2.8 \pm 10^5$	425
Canyon Diablo #5B	9	1.0799 ± 14	$>2.4 \pm 10^5$	2.8×10^3
Canyon Diablo #5C	11	1.0802 ± 9	$>7.9 \times 10^5$	5.0×10^3
Toluca #1B	15	1.0811 ± 16	$>4.4 \times 10^5$	6.3×10^3
Hoba #2B	5	1.0839 ± 50[c]	3.2×10^4	130
Santa Clara #1B	0.5	*1.106 ± 13*[d]	6.0×10^3	20

[a] Errors are 2σ. All data were taken on Faraday detector with the exception of Santa Clara which was determined on the electron multiplier. These are observed measured ratios; no correction factors have been applied. [b] Grand mean of 12 determinations. [c] Low intensity run. [d] Data obtained on electron multiplier detector.

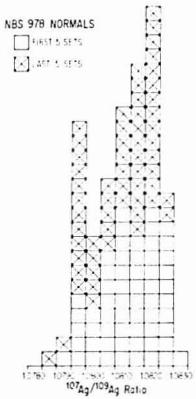

Figure 3. Histogram of all normals. Each block represents the mean of 10 ratios taken at 1000 °C. The grand average is 1.0810 ± 18. The average values for the first five and last five sets are 1.0812 ± 19 and 1.0809 ± 21, respectively

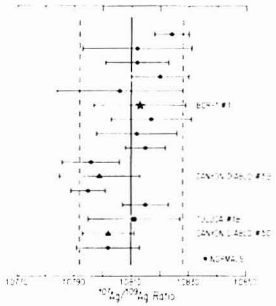

Figure 4. Summary of isotopic measurements taken at 1000 °C on Faraday detector. Symbols represent the means of 10 sets of 10 ratios. These are the raw measured ratios. The associated error bars are twice the standard deviation. The solid vertical bar represents the mean of all normals and the associated dashed lines represent twice the standard deviation

for the first and last sets. This is a factor of 40 smaller than that observed by Chakraburtty et al. (*3*), who used microgram samples, and a factor of 10 smaller than that observed by Shields et al. (*19*), who used 100-μg samples. In these last two studies, data were collected for only 20 min.

The averages of the 10 data sets for both normals and natural samples are displayed in Figure 4. These data are the observed measured ratios; no correction factors were applied. The error bars associated with the individual determinations are 2σ. The grand mean for the 12 normals is 1.0810 ± 0.0018 and is represented by the middle vertical bar. The vertical error bars associated with the grand mean are 2σ and not $2\sigma_m$, which is usually reported by this laboratory. All determinations lie within this envelope and it is probably an accurate representation of the standard deviation of the mean. The precision with which the isotopic composition of Ag can be determined is limited by the inability to initiate data acquisition for all samples at the same point on the fractionation curve.

The isotopic measurements are tabulated in Table VII. The second column gives the actual amounts of Ag loaded. The weights of most of the normals were approximately 10 ng but ranged from 5 to 15 ng in order to bracket the sample sizes. There was no observable relation between the fractionation pattern and the sample size. Measured ratios are given in column three. All of the meteorites analyzed thus far are identical in composition to the standard within the precision of the analyses. The last two entries, Hoba and Santa Clara, were low intensity runs. The large errors associated with these two runs are the result of poor ion statistics. The Santa Clara sample was determined on the electron multiplier. A 1 ng normal determined on the same detector gave a value of 1.0896 ± 26. The last two columns in the table give the $^{75}As^{32}S^{+}$ and $^{109}Ag/^{109}$hydrocarbon ratios, respectively. The $^{107}Ag/^{107}$hydrocarbon ratios are not given but they were always larger than the corresponding ratios at mass 109 In all cases, except the two low intensity runs, the contributions of the AsS^{+} peaks to the Ag peaks are less than 0.05%. It should be noted that in all cases no 108 peak was detected and, therefore, its intensity was taken as $\sim 10^{-17}$ A. This is the noise level of the electron multiplier and its associated electronics with the source high voltage on and the defining slit opened to 0.64 mm.

CONCLUSIONS

An anion-exchange procedure for the separation of Ag from a variety of chemical matrices has been described. It is applicable to a wide variety of materials. The chemical procedure has been miniaturized with an accompanying reduction in blank. The procedural blank is 0.15 pmol. This allows the isotopic measurement of as little as 0.50 pmol of Ag with precision of better than 1% and with only a 30% blank correction. Materials whose Ag concentration is 0.1 ppb or above can be analyzed reliably by this technique.

Isotopic measurements have been performed on 50 pmol of Ag on a Faraday detector with a precision of 0.1% with negligible blank correction. The ionization efficiency was increased to 1–2% and the limit of detection reduced to 1 fmol. We have obtained fractionation control of better than 0.2% as demonstrated by the repeatability of 12 normals. Isotopic measurements on several different samples have been per-

Table VIII. Limits on the Formation Ages of Iron Meteorites

sample	$\delta^{107}Ag$[a]	Pd/Ag[b]	$\Delta_{SUDDEN} \times 10^{-6}$ yr	$\Delta_{CONTINUOUS} \times 10^{-6}$ yr
Canyon Diablo	−1.0 ± 2.0 −0.7 ± 2.0	106	>97	>32
Toluca	+0.09 ± 2.0	65	>87	>21
Hoba	+2.7 ± 5.0	412	>91	>25
Santa Clara	+15.0 ± 12.0	3470	>99	>34

[a] $\delta^{107}Ag = [(^{107}/^{109})SAMPLE/(^{107}/^{109})STD] \times 10^3$. Errors are 2σ and include the error associated with both std and sample. [b] Pd data taken from Smales et al. (*25*). The Pd content of Santa Clara was assumed to the same as Hoba.

formed, including four iron meteorites, one terrestrial basalt, and the NBS $AgNO_3$ standard. Within the limits of the precision, all of the samples have identical Ag isotopic compositions. Our observed 107/109 ratio for the NBS $AgNO_3$ standard is 1.0810 ± 0.0018 which is identical to the observed value of 1.0815 ± 0.0011 obtained by the NBS.

A serious spectral interference due to AsS^+ has been identified and eliminated. Several investigators have alluded to spuriously high 107 beams during the isotopic analysis of Ag. Some workers (*1, 3, 4, 18*) have attributed this to ZrO^+, but this species was never identified by its spectral signature. The well-known difficulty with which Zr is ionized makes this assignment highly improbable. In addition, some investigators loaded Ag as a sulfide (*1–3*) and used As compounds in their chemical procedure (*3*). For these reasons we believe that the AsS^+ species may have been observed in these studies but not identified. In the analysis of Ag, the AsS^+ species can be monitored only at mass 108. All future work on Ag should include the observed $^{107}Ag/^{75}As^{32}S^+$ ratios and monitoring of hydrocarbons. Without this information no meaningful statement as to accuracy can be made.

The group 4b iron meteorites were chosen for analysis because they are known to contain solar abundances of the refractory noble metals and to be severely depleted in volatile elements such as Au, Cu, Ga, and Ge. Their trace element chemistry matches closely that of a high temperature condensate as predicted from thermodynamic calculations (*21*). The Pd contents of several of their members are known and average about 5 ppm; the other members are believed to be within a factor of 2 of this number. For these reasons it was believed these samples might have very high Pd/Ag ratios and thus be good candidates in which to observe isotopic effects produced by ^{107}Pd.

Our results to date have established that the $^{107}Ag/^{109}Ag$ ratio in the samples studied is normal to within 0.2%. Because of the small $^{107}Ag/^{75}As^{32}S^+$ ratios in the case of Hoba and Santa Clara, their Ag ratios can be considered as upper limits. These data can be used to set lower limits on the formation ages of these samples. Two nucleosynthetic models are considered, the sudden synthesis model and the continuous synthesis model of Wasserburg et al. (*22*). From the production equations for radioactive and stable nuclei, the following two equations can be derived giving the formation age, Δ, in terms of measured quantities.

Sudden synthesis:

$$\Delta = \frac{1}{\lambda}\left[\ln\left(\frac{K^{107}}{K^{105}}\right) - \ln\left(\frac{\delta^{107}Ag}{1000}\right) + \ln\left(\frac{^{105}Pd}{^{109}Ag}\right)\right] \quad (1)$$

Continuous synthesis:

$$\Delta = \frac{1}{\lambda}\left[\ln\left(\frac{K^{107}}{K^{105}}\right) - \ln\left(\frac{\delta^{107}Ag}{1000}\right) + \ln\left(\frac{^{105}Pd}{^{109}Ag}\right) - \ln(\lambda T)\right] \quad (2)$$

where K^{107}/K^{105} is the production ratio of the two Pd isotopes, $\delta^{107}Ag$ is defined in Table VII, $^{105}Pd/^{109}Ag$ is the atom ratio of these two isotopes, T is the time interval over which nucleosynthesis occurs, and λ is the decay constant for ^{107}Pd. The production ratio is taken as 0.64 (*23*), the recently determined half life for ^{107}Pd is 6.5 ± 0.3 × 10^6 yr (*24*), and T is assumed to be ~10^{10} yr. Inserting these quantities into Equations 1 and 2 yields lower limits for the formation ages. In the calculations of Δ, the value for $\delta^{107}Ag$ was taken as the sum of the determined value and the absolute value of its associated error. The calculated values for the two models are lower limits only and are given in the last two columns of Table VIII. The sudden synthesis model gives lower limits of about 90 × 10^6 yr, while the continuous synthesis model gives lower limits of about 30 × 10^6 yr.

Iron meteorites are believed to be the products of chemical differentiation of a more primitive material. It is possible that this primitive material was formed immediately after the cessation of nucleosynthesis and that the iron meteorites were formed at some later time during a high temperature process. At this later time, the Pd–Ag clock would be reset partially or completely. The formation ages determined on iron meteorites, therefore, would reflect the time interval between the end of nucleosynthesis and solidification.

Future experiments will include isotopic measurements on additional members of group 4b as well as Pd concentration and composition measurements. These techniques will also be extended to other meteorite classes.

ACKNOWLEDGMENT

This project was conceived by John W. Larimer of Arizona State University and the authors and was carried out as a joint study between ASU and the California Institute of Technology. We are pleased that both institutions allowed communal use of resources. The advice and encouragement of John W. Larimer was greatly appreciated. The encouragement and assistance of colleagues D. A. Papanastassiou and Felix Oberli is acknowledged.

LITERATURE CITED

(1) D. C. Hess, R. R. Marshall, and H. C. Urey, *Science*, **126**, 1291–1293 (1957).
(2) V. R. Murthy, *Geochim. Cosmochim. Acta*, **26**, 481–488 (1962).
(3) A. K. Chakraburtty, C. M. Stevens, H. C. Rushing, and E. Anders, *J. Geophys. Res.*, **69**, 505–520 (1964).
(4) J. R. Dews and R. S. Newbury, *J. Geophys. Res.*, **7**, 3069–3081 (1966).
(5) A. E. Cameron, D. H. Smith, and R. L. Walker, *Anal. Chem.*, **41**, 525–526 (1969).
(6) F. Tera and G. J. Wasserburg, *Anal. Chem.*, **47**, 2214–2220 (1975).
(7) J. H. Reynolds, *J. Geophys. Res.*, **65**, 3843–3846 (1960).
(8) T. Lee, D. A. Papanastassiou, and G. J. Wasserburg, *Geophys. Res. Lett.*, **3**, 109–112 (1976).
(9) J. R. E. Jones, *J. Exp. Biol.*, **16**, 425–437 (1939).
(10) F. P. Thurberg and R. S. Collier, *Mar. Pollut. Bull.*, **8**, 40–41 (1977).
(11) A. Calabrese, R. S. Collier, D. A. Nelson, and J. R. MacInnes, *Mar. Biol.*, **18**, 162–166 (1973).
(12) H. G. Sanz and G. J. Wasserburg, *Earth Planet. Sci. Lett.*, **6**, 335–345 (1969).
(13) Y. Marcus, Bull. *Res. Counc. Israel*, **A8**, 17–26 (1959).
(14) Y. Marcus, *J. Inorg. Nucl. Chem.*, **12**, 287–296 (1960).
(15) G. J. Wasserburg, D. A. Papanastassiou, E. V. Nenow, and C. A. Bauman, *Rev. Sci. Instrum.*, **40**, 228–295 (1969).
(16) R. R. Keays, R. Ganapathy, J. C. Laul, U. Krähenbühl, and J. W. Morgan, *Anal. Chim. Acta*, **72**, 1–29 (1974).

(17) P. R. Buseck, "Handbook of Elemental Abundances in Meteorites", B. Mason, Ed., Gordon and Breach, New York, N.Y., 1971, pp 351–359.
(18) E. A. Crouch and A. H. Turnbull, *J. Chem. Soc.*, **31**, 161–170 (1962).
(19) W. R. Shields, D. N. Craig, and V. H. Dibeler, *J. Am. Chem. Soc.*, **82**, 5033–5036 (1960).
(20) W. R. Shields, E. L. Garner, and V. H. Dibeler, *J. Res. Natl. Bur. Stand., Sect. A.*, **66**, 1–3 (1962).
(21) W. R. Kelly and J. W. Larimer, *Geochim. Cosmochim Acta*, **41**, 93–111 (1977).
(22) G. J. Wasserburg, W. A. Fowler, and F. Hoyle, *Phys. Rev. Lett.*, **4**, 112–114 (1960).
(23) D. D. Clayton and W. A. Fowler, *Ann. Phys.*, **16**, 51–68 (1961).
(24) K. F. Flynn and L. E. Glendenin, *Phys. Rev.*, **185**, 1591–1593 (1969).
(25) A. A. Smales, D. Mapper, and K. F. Fouche, *Geochim. Cosmochim Acta*, **31**, 673–720 (1967).

RECEIVED for review October 17, 1977. Accepted May 2, 1978. W.R.K. was supported by NASA Grant NSG 7040 while a Visiting Associate in Geochemistry at the California Institute of Technology. General support for the Lunatic Asylum laboratory is provided by NSF Grant PHY 76-83685 and NASA Grant NGL 05-002-188. This is Contribution No. 2980 (254) of the Division of Geological and Planetary Sciences.

Characterization of Metal Surfaces by Secondary Ion Mass Spectrometry and X-ray Photoelectron Spectroscopy

R. W. Hewitt,[1] A. T. Shepard,[2] W. E. Baitinger, and Nicholas Winograd*

Department of Chemistry, Purdue University, West Lafayette, Indiana 47907

G. L. Ott and W. N. Delgass

School of Chemical Engineering, Purdue University, West Lafayette, Indiana 47907

The techniques of XPS and SIMS have been combined in the same ultra-high vacuum system for the study of surface reactions. Using a mass spectrometer capable of detecting high molecular weight clusters, we have investigated the behavior of clusters up to Ag_5^+ and In_4^+ ejected from polycrystalline Ag and In surfaces under low flux argon ion bombardment. For lattice-oxide formation on Pb and In surfaces cleaned by ion bombardment, the O 1s peak areas directly relate to the PbO^+ and InO^+ intensities allowing calibration of surface coverages for SIMS studies. The fact that PbO_2^+ emission begins at higher oxygen exposure than PbO^+ suggests that oxygen incorporation into the lattice occurs directly. For In, however, the fact that InO_2^+ emission increases in roughly the same fashion as InO^+ indicates that indium oxide islands grow outward from one or more nucleating sites, allowing for the existence of oxygen–oxygen next-nearest neighbors at low coverage for InO_2^+ formation.

Interest in the chemistry of solid surfaces has rapidly intensified in recent years. The development of new analytical techniques, as well as the refinement of existing methods, has led to significant advances in the understanding of surface-related phenomena. Many approaches have been taken to the problem of gleaning information from the surface region of materials. Most of these methods utilize ions, electrons, or photons as the probing particle, followed by energy or mass analysis of these or secondary particles which are scattered from the surface.

We have chosen to combine the techniques of x-ray photoelectron spectroscopy (XPS) and secondary ion mass spectrometry (SIMS) as complementary tools for elucidation of surface reactions. For this pair of methods, the deficiencies of one are often the strong points of the other. For example, in SIMS, ambiguities may arise due to alterations in the sample surface caused by the incident ion beam. Differential sputtering and atomic mixing under the influence of ion bombardment are phenomena which have been well documented (*1–3*). The photons used in XPS, however, usually do not damage the surface. In addition, the ionization probability of secondary ions may change by orders of magnitude as the surface electronic properties are altered. It would therefore be advantageous to obtain information from the sample with a technique which yields quantitative data concerning the concentration of specific atoms on the surface. XPS has proved to be a valuable tool for yielding quantitative information about the amount and molecular structure of the surface species and for the elucidation of electronic structures of materials. The SIMS technique has a very high sensitivity and is able to detect less than 0.1% of a monolayer of material. The possibility also exists for determining information about short range atomic order via analysis of molecular cluster ions. A comparison of the characteristics of XPS and SIMS is given in Table I.

Table I. Comparison of the Attributes of XPS and SIMS

SIMS	XPS
ultimate sensitivity to 10^{-15} g/cm^2	ultimate sensitivity to 10^{-8} g/cm^2
surface sensitivity to 1 or 2 layers	surface sensitivity from 1 to 10 layers
nonquantitative	quantitative (10–20%)
short range atomic order from analysis of molecular cluster ions	molecular structure from binding energy chemical shifts
destructive	nondestructive
ability to detect hydrogen	

In this paper, we discuss instrumentation appropriate to a combined XPS/SIMS system. Spectra obtained from the clean metal surfaces of Ag and In are compared in detail. In addition, we utilize the chemical shift information in XPS and the nature of the cluster ions found in SIMS to elucidate the mechanism of oxidation of clean Pb and In evaporated metal surfaces. The results are discussed in terms of recent

[1] Present address, Westhollow Research Center, Shell Development Co., Houston, Texas 77001.
[2] Present address, E. I. Du Pont de Nemours, Inc., Parkersburg, W. Va.

0003-2700/78/0350-1286$01.00/0

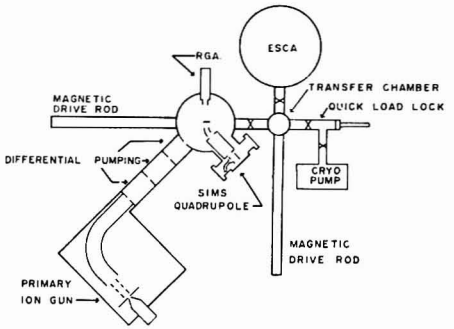

Figure 1. Overall schematic of the XPS/SIMS instrument with associated transfer system

computer simulations of the cluster emission process.

EXPERIMENTAL

Details of the XPS/SIMS system have been described in detail elsewhere (*4*, *5*). The sample can be shuttled between the SIMS (Riber Model 0156) and XPS (Hewlett-Packard 5950A) spectrometers under UHV by a set of magnetically driven transfer devices. The SIMS and XPS experiments were then performed sequentially on the same sample. The base pressure of the system was $1-3 \times 10^{-10}$ Torr. A schematic of the instrumental design is shown in Figure 1.

Materials used in this work were prepared from silver (m3N) and indium (m5N) foils obtained from Alfa Division–Ventron Corporation, which were sputter cleaned with 10 KeV Ar^+ ions at 2 μA cm^{-2} for 3 h. The Pb samples were prepared by evaporation onto a gold substrate at 5×10^{-9} Torr followed by the Ar^+ ion bombardment treatment. Oxygen used in the adsorption experiments was research grade (99.99% purity) obtained from Matheson Gas Products.

RESULTS AND DISCUSSION

The overall performance of our XPS/SIMS instrument on metal surfaces is illustrated in Figure 2. Figure 2a is a wide scan SIMS spectrum of a freshly evaporated silver surface, whose most intense peaks are those of $^{107}Ag^+$ and $^{109}Ag^+$, as expected. Other less intense peaks are of the impurities $^{23}Na^+$, $^{27}Al^+$, and $^{39}K^+$, of which $^{23}Na^+$ and $^{39}K^+$ are present in nearly all positive ion SIMS spectra. The rather large peak at $m/e = 40$ arises from the use of argon as the primary ion. In Figure 2b, we present the XPS spectrum of the same silver surface. Although the characteristic 3s through 4d levels of silver are clearly seen, no peaks are observed to arise from the presence of potassium or sodium. Based on the large secondary ion yield of these two species (*6*), we estimate their surface concentration to be less than 0.1%, below the limit of detection in XPS.

The high mass capability of the quadrupole makes it a valuable tool for studying secondary molecular cluster ions. The potential for obtaining useful information from these clusters about the local atomic ordering of atoms on the surface has already been established (*1*, *7*), although a quantitative interpretation of these observations will require a more thorough understanding of the secondary emission process. In Figure 3 are results obtained for positively charged molecular clusters ejected from clean indium and silver surfaces. Aggregates of up to four indium atoms at $m/e = 460$, and up to five silver atoms at $m/e = 535$–545 are observed with the expected isotopic distributions. Their intensities are denoted by solid lines, while the broken lines are the intensities corrected for the theoretical transmission, T, of the quadrupole, where T is assumed to be proportional to $(\Delta m/m)^2$.

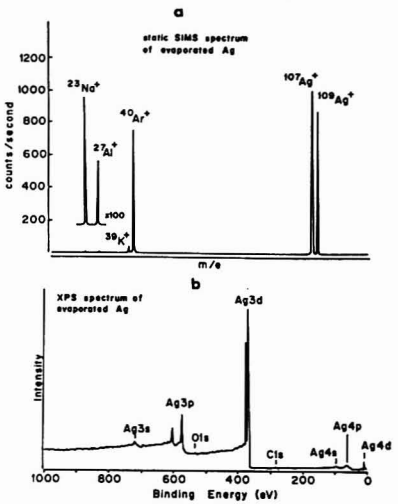

Figure 2. Static SIMS, with $I_p^+ = 2 \times 10^{-10}$ A cm^{-2} of Ar^+ at 2 keV, and XPS spectrum of an evaporated silver surface

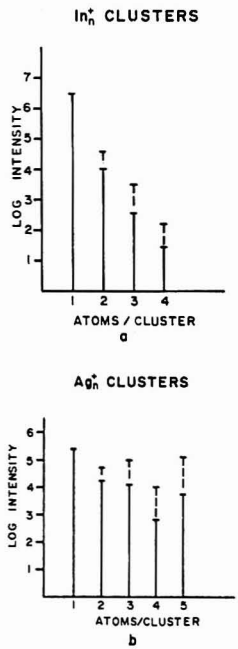

Figure 3. Relative intensity of (a) In^+ clusters with $I_p^+ = 2 \times 10^{-6}$ A cm^{-2} at 10 keV of Ar^+ and (b) Ag^+ clusters with $I_p^+ = 1 \times 10^{-6}$ A cm^{-2} at 20 keV of Ar^+

Of particular interest here is the marked difference in variation of intensity with cluster-size, indium exhibiting a monotonic decrease and silver displaying periodic oscillations. Similar

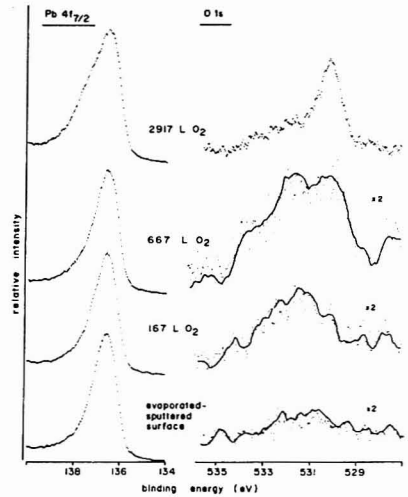

Figure 4. Pb $4f_{7/2}$ and O 1s XPS spectra of an evaporated and sputtered Pb surface before and after oxygen exposure

trends have been observed for transition metal ion clusters using an ion microprobe mass analyzer (*8*), although under more severe bombardment conditions. The cluster data in the present work are obtained in a comparatively lower primary current domain, where each ion impact can be considered as an isolated event. The silver cluster results are of special interest since molecular orbital calculations performed on these species (*9, 10*) yield cluster stabilities displaying oscillations similar to those in the experimental data. The observed alternations in fact may be due to the presence of a lone s electron in the odd numbered clusters and paired electrons in the even numbered clusters. Analogous calculations have not been performed for indium, but nevertheless, it might be qualitatively predicted that the availability of three s and p electrons for bonding and the concomitant large number of closely spaced molecular orbitals could reduce the "even-odd" effect noted in the case of silver. As the theory underlying these calculations becomes more sophisticated and in turn is applied to a greater number of systems, it will be intriguing to correlate experimentally determined cluster intensities with their calculated electronic properties.

The combination of XPS and SIMS is an excellent means of studying metal-adsorbate systems, since XPS, in addition to being a quantitative method, is sensitive to the molecular environment of the species on the surface. Static SIMS can yield information concerning the local atomic order through analysis of secondary molecular cluster ions. The increase in secondary ion yield due to the presence of oxygen is a well documented phenomenon (*7, 11, 12*) although it is at best only qualitatively understood and in need of further investigation. In this work, clean Pb and In surfaces are exposed to several doses of oxygen with successive monitoring by both XPS and static SIMS, ($I_p^+ = 2 \times 10^{-9}$ A cm^{-2} at 2 KeV of argon). In the case of XPS, either the Pb $4f_{7/2}$ or In $3d_{5/2}$ level, in addition to the O 1s signal are recorded after each exposure to O_2. SIMS spectra are also taken sequentially so that correlations can be made between the two data sets. A summary of the XPS results for an Ar^+ sputtered lead film is diagrammed in Figure 4. The lower trace represents the virgin surface, before any exposure to oxygen. Close examination of the O 1s

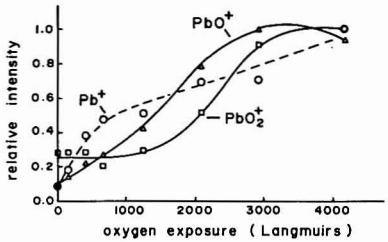

Figure 5. Intensity behavior of Pb^+, PbO^+, and PbO_2^+ cluster ions vs. oxygen exposure. $I_p^+ = 2 \times 10^{-9}$ A cm^{-2} at 2 keV of Ar^+. Relative yields are calculated by normalizing the peak intensity to its highest value in the exposure range to emphasize the curve shape rather than the absolute intensity

spectrum reveals a residual amount of oxygen at 531.5 eV while the Pb $4f_{7/2}$ line shows no clearly discernible indication of binding energy shift due to lead oxide or $PbO_{(adsorbed)}$. The residual oxygen might be attributed either to dissolved oxygen in the lead lattice or an adsorbed oxygen moiety. In either case, the high binding energy peak is not characterisitic of oxide formation. Upon exposure to 167 L O_2, (1 L = 1×10^{-6} Torr s), the O 1s peak at 531.5 eV grows considerably in intensity and the Pb $4f_{7/2}$ trace begins to show a greater degree of asymmetry due to the growth of a small amount of PbO on the surface. The high binding energy O 1s signal is still the predominant species, however, at this exposure. As the oxygen dose is increased, a peak at 529.2 eV, characteristic of rhombic PbO (*13, 14*) rises in the O 1s region, and eventually becomes the predominant species. A high binding energy shoulder on the Pb $4f_{7/2}$ at 137.9 eV is also evident at high PbO coverage. It is interesting that the behavior of a clean Pb surface upon oxygen exposure is strongly dependent upon sample preparation. A freshly evaporated lead film evinces the immediate formation of rhombic PbO, with no traces of initial oxygen adsorption, while an argon-ion bombarded Pb film exhibits an adsorbed oxygen species prior to oxide formation. The surface concentration of oxide can be calculated from the escape depth of the Pb $4f_{7/2}$ photoelectron (*15*) in combination with the rhombic PbO unit cell dimensions, and shows equivalent monolayer concentration to occur at 1200 L O_2 exposure. This result agrees very well with the "effective" monolayer coverage reported by Evans and Thomas (*16*) for a sputtered Pb foil.

The behavior of the positive secondary ions Pb^+, PbO^+, and PbO_2^+, also monitored vs. oxygen dosage, is plotted in Figure 5. The relative yield is calculated by normalizing the peak intensity to its highest value in the exposure range to emphasize the curve shape rather than absolute intensity. As qualitatively expected, the Pb^+ yield increases, with the most dramatic change occurring at less than 0.5 monolayer PbO. Note that the PbO^+ species appears almost immediately, while there is marked delay in the onset of PbO_2^+ emission. The fact that the relative yield of PbO_2^+ emission is higher than that of PbO^+ at low oxygen coverage is a manifestation of the normalization procedure. The actual intensity of the PbO_2^+ emission is an order of magnitude less than that for PbO^+.

The explicit interpretation of these curves awaits theoretical development of the cluster ion emission process. Recent studies, however, have been completed for metals using classical trajectory methods to calculate the positions and momenta of all particles in a model microcrystallite as a function of time subsequent to the ion bombardment process (*17–20*). In these studies metal clusters containing up to 7 atoms have been found to form by formation of ejected atoms within the interaction range, say ~4 Å, of the solid. In

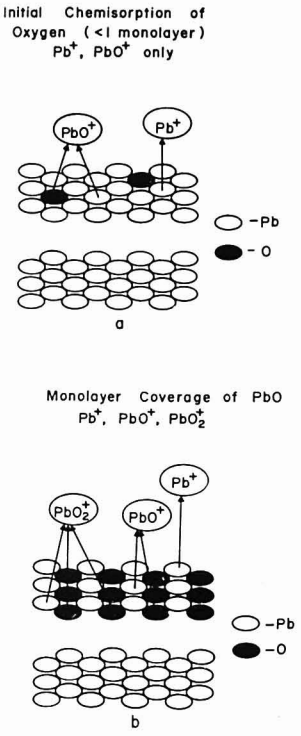

Figure 6. Schematic representation of (a) an oxidized Pb surface at low oxygen coverage and (b) an oxidized Pb surface at monolayer coverage

addition, it was found that most dimers and trimers arise from either nearest-neighbor or next-nearest-neighbor sites on the surface.

In Figure 6, we extropolate this scheme to the formation of metal atoms and oxygen atoms over the solid to test possible oxidation schemes on the Pb surfaces. From Figure 6a, a representation of low PbO coverage, only secondary species like Pb^+ and PbO^+ are possible since there are no oxygen–oxygen next-nearest-neighbors to permit PbO_2^+ formation. In contrast, at monolayer coverage, represented in Figure 6b, Pb^+, PbO^+, and PbO_2^+ are all possible. This representation then suggests that if PbO does indeed grow as a uniform surface layer, the PbO_2^+ emission should exhibit a short delay, and then increase to a maximum intensity when one monolayer is completed.

Returning to Figure 5, the observed PbO_2^+ intensity does not reach a maximum until nearly 3500 L O_2, and does not begin to increase until equivalent monolayer coverage as determined by XPS. This apparently anomalous result can be rationalized in terms of the different information depths for XPS and SIMS. Static SIMS is a true surface technique, while XPS probes the first 10–40 Å of sample, equivalent to several monolayers. If, instead of forming a uniform monolayer, the growth of the PbO progresses by oxygen incorporation into the lattice, the greater sampling depth of XPS would cause it to indicate monolayer coverage of PbO when, in fact, the actual surface coverage was much less. Additional

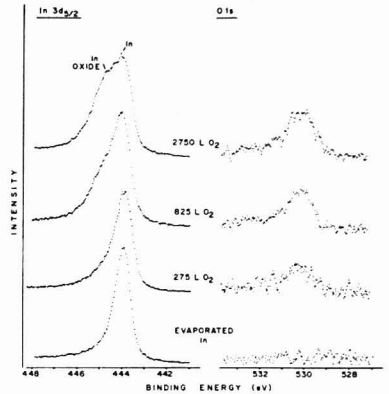

Figure 7. In $3d_{5/2}$ and O 1s XPS spectra of an evaporated In surface before and after oxygen exposure

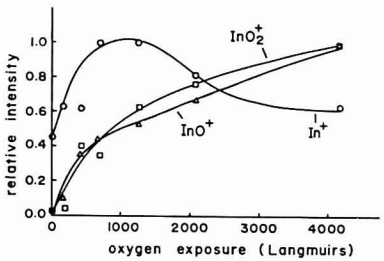

Figure 8. Intensity vs. O_2 exposure behavior of In^+, InO^+, and InO_2^+. $I_p^+ = 2 \times 10^{-9}$ A cm^{-2} at 2 keV of Ar^+

oxygen exposure would eventually promote the formation of a complete monolayer of PbO at the surface, thereby increasing the probability of PbO_2^+ emission, and bringing about a leveling off of the PbO_2^+ intensity as observed. This mechanism is also consistent with the decrease in work function observed in other investigations of the oxidation of sputtered (*16*) and evaporated (*21*) Pb films.

The XPS data for indium oxidation are diagrammed in Figure 7. The O 1s region displays peaks indicative of both adsorbed oxygen at 531.5 eV and an indium oxide species at 530.2 eV. The In $3d_{5/2}$ peak exhibits a high binding energy shoulder at 444.6 eV, which has also been assigned to indium oxide. Other XPS measurements made in our laboratory suggest that the oxide species is In_2O_3, although the wide variation in binding energies reported in the literature for In_2O_3 (22–25) precludes an unequivocal assignment. In contrast to the lead XPS data, the oxide begins to form immediately on indium, and continues to grow with additional exposure. The higher binding energy oxygen, assigned to an adsorbed moiety in this work, is present in all exposures. This peak was also present in the XPS spectrum of bulk In_2O_3.

In^+, InO^+, and InO_2^+ SIMS results are shown in Figure 8. As is observed for Pb, the secondary ion yields increase with oxygen exposure. The In^+ intensity reaches a maximum at 1000 L O_2, then decreases to a steady state value at 3500 L. This behavior can be explained in terms of the number of In sites on the probed surface. At low oxygen coverage, the increase in secondary ion yield is due to the presence of oxygen. As the oxidation process continues, the number of

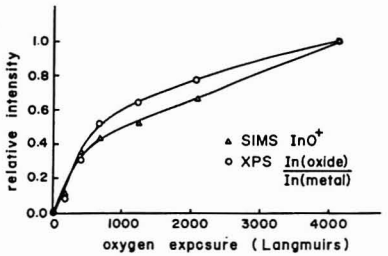

Figure 9. Deconvoluted XPS indium oxide peak areas from the $3d_{5/2}$ peak and the SIMS InO^+ yield vs. oxygen exposure

In metal sites decreases, and the diminishing indium metal concentration at the surface begins to compete with oxygen enhancement as the controlling factor of the measured ion yield.

The immediate appearance of InO_2^+, also in marked contrast to the Pb results, is most likely due to differences in the mechanism of oxide growth. Thus, indium oxide islands probably grow outward from one or more nucleating sites, allowing for the existence of oxygen–oxygen next-nearest-neighbors at low coverage for InO_2^+ formation.

A comparison of the SIMS InO^+ yield and the deconvoluted In(oxide)/In(metal) ratio is represented in Figure 9. The striking similarity of the two curves indicates that the InO^+ yield is directly dependent upon the amount of oxide formed at the surface. A linear relationship would imply that the InO^+ secondary ion yield is a function only of the oxygen concentration, and that the ionization efficiency is a constant independent of any events occurring external to the region of cluster formation. A similar agreement between the XPS O 1s intensity for the PbO component and the SIMS PbO^+ yield was obtained for the case of Pb.

LITERATURE CITED

(1) K. S. Kim, W. E. Baitinger, and N. Winograd, *Surf. Sci.*, **55**, 285 (1976).
(2) K. S. Kim and N. Winograd, *Surf. Sci.*, **43**, 625 (1974).
(3) T. Ishitani and R. Shimizu, *Appl. Phys.*, **6**, 241 (1975).
(4) R. W. Hewitt, A. T. Shepard, W. E. Baitinger, N. Winograd, and W. N. Delgass, *Rev. Sci. Instrum.*, submitted.
(5) T. Fleisch, A. T. Shepard, T. Y. Ridley, W. E. Vaughn, N. Winograd, W. E. Baitinger, G. L. Ott, and W. N. Delgass, *J. Vac. Sci. Technol.*, in press.
(6) A. Benninghoven, *Surf. Sci.*, **53**, 596 (1975).
(7) A. Shepard, R. Hewitt, G. Slusser, W. Baitinger, R. Cooks, N. Winograd, N. Delgass, A. Varon, and G. Devant, *Chem. Phys. Lett.*, **44**, 371 (1976).
(8) P. Joyes, *J. Phys. Chem. Solids*, **32**, 1269 (1971).
(9) R. C. Baetzold and R. E. Mack, *J. Chem. Phys.*, **62**, 1513 (1975).
(10) R. C. Baetzold, *J. Chem. Phys.*, **55**, 4363 (1971).
(11) A. Shepard, R. W. Hewitt, W. E. Baitinger, G. J. Slusser, N. Winograd, G. L. Ott, and W. N. Delgass, "Quantitative Surface Analysis of Materials", *ASTM, STP* **643**, 187 (1978).
(12) P. H. Dawson, *Phys. Rev. B.*, **15**, 5522 (1977).
(13) K. S. Kim and N. Winograd, *Chem. Phys. Lett.*, **19**, 209 (1973).
(14) K. S. Kim, T. J. O'Leary, and N. Winograd, *Anal. Chem.*, **45**, 2214 (1973).
(15) T. A. Carlson and G. E. McGuire, *J. Electron. Spectrosc.*, **1**, 161 (1972/3).
(16) S. Evans and J. M. Thomas, *J. Chem. Soc., Faraday Trans. 2*, **71**, 313 (1975).
(17) D. E. Harrison and C. B. Delaplain, *J. Appl. Phys.*, **47**, 2252 (1976).
(18) B. J. Garrison, N. Winograd, and D. E. Harrison, Jr., *J. Chem. Phys.*, in press.
(19) N. Winograd, D. E. Harrison, Jr., and B. J. Garrison, *Surf. Sci.*, submitted for publication.
(20) D. E. Harrison, Jr., P. W. Kelly, B. J. Garrison, and N. Winograd, *Surf. Sci.*, in press.
(21) J. M. Saleh, B. R. Wells, and N. W. Roberts, *Trans. Faraday Soc.*, **60**, 1865 (1964).
(22) A. W. C. Lin, N. R. Armstrong, and T. Kuwana, *Anal. Chem.*, **49**, 1228 (1977).
(23) C. D. Wagner and P. Biloen, *Surf. Sci.*, **35**, 82 (1973).
(24) V. I. Nefedov, B. F. Fruzsinszkij, N. P. Szergusin, J. V. Szalen, and G. ês Gáti, *Magy. Kem. Foly.*, **81**, 495 (1975).
(25) G. E. McGuire, G. K. Schweitzer, and T. A. Carlson, *Inorg. Chem.*, **12**, 2450 (1973).

RECEIVED for review March 10, 1978. Accepted May 22, 1978. Work supported by the National Science Foundation (Grant No. MPS75-9308), the Materials Research Program (Grants Nos. DMR-72-3-18A04), and the Air Force Office of Scientific Research (Grant No. AF-762974). Nicholas Winograd is a J. S. Guggenheim Fellow on leave at Materials and Molecular Research Division, Lawerence Berkeley Laboratory, Berkeley, Calif. 94720, until Fall 1978.

Effect of Argon Ion Bombardment on Metal Complexes and Oxides Studied by X-ray Photoelectron Spectroscopy

Yoshio Umezawa[1] and Charles N. Reilley*

Department of Chemistry, University of North Carolina, Chapel Hill, North Carolina 27514

The effect of high energy (0.5–2 keV) Ar^+ bombardment on 20 different metal complexes and several metal oxides was studied. Although most of the metal centers in the complexes and oxides were reduced, some were oxidized or exhibited no change depending upon the ligands and central metal atoms present. Some ligands in metal complexes were reduced, such as ClO_4^- and NO_3^- forming Cl^- and NO_2^-, respectively. The nonmetal groups such as NH_3, NO_2^-, CN^-, ClO_4^-, and NO_3^- were found to be sputtered off more efficiently than the central metal ion itself. Finally, the influence of Ar^+ bombardment on the nonstoichiometric nature of metal oxide surfaces is discussed.

Ion bombardment has proved to be a very useful and important technique for obtaining clean and reference surfaces for ESCA, Auger, and other spectroscopic investigations. However, very little information has so far been reported with respect to the explicit chemical effects of ion bombardment. Winogard and co-workers (*1*, *2*) concluded that certain types of metal oxides are reduced by ion bombardment and that the reduction tendency was inversely related to the free energy of formation of the oxides. For the ion bombardment technique to be used rationally as an analytical aid, a knowledge of the various types of phenomena potentially introduced by this technique is desirable.

The purposes of the present study are to examine briefly (i) the types of chemical reactions, such as redox, substitution, and chemical transformation of one functional group to another, introduced by ion bombardment, (ii) the dependence of sputtering efficiency on the kind of elements and functional groups involved, and (iii) the nonstoichiometric nature of compositions at the surface of oxides as characterized by ion bombardment. To obtain meaningful information with respect

[1] Present address, Department of Chemistry, Faculty of Science, University of Tokyo, Hongo, Tokyo, Japan.

0003-2700/78/0350-1290$01.00/0

Table I. Redox Reaction of Metal Centers Produced by Ar^+ Bombardment[a]

Process observed	Compound[b]
Reduction	$K_3[Fe(CN)_6]$, $Cu(dip)(NO_3)_2 \cdot 3H_2O$, $K_3[Fe(C_2O_4)_3]$, $Cu(dip)_3(NO_3)_2$, $Co(o\text{-phen})_3(ClO_4)_3$, $Co(NH_3)_5(NO_2)_3$, $Na_3[Co(CN)_6]$, $Fe(dip)_3(ClO_4)_2$, $Cu(en)_2SO_4 \cdot 2H_2O$, $Co(en)_3(ClO_4)_3$, $K[Co(edta)] \cdot 2H_2O$, *trans*-$[Co(NH_3)_4(NO_2)_2]Cl$, $[Co(NH_3)_5Cl]Cl_2$, $Co(NH_3)_5(NO_3)_3$
Oxidation	$Fe(dip)_3(ClO_4)_2$, $Mn(dip)_2Br_2$, $K_3[Cr(C_2O_4)_3]$
No change (same oxidation state)	$Na_3[Co(NO_2)_6]$, $Pt(dip)Cl_2$, $Pt(dip)_2Cl_2$

[a] Energy for Ar^+ ion is 2 keV for 2 mins. [b] Abbreviations: dip: 2,2'-dipyridyl; *o*-phen: *o*-phenanthroline; edta: ethylenediaminetetraacetate.

to the above items, a variety of types of metal complexes were chosen along with some metal oxides as illustrative examples. Although metal complexes are, of course, more or less subject to decomposition upon ion bombardment, they seem to provide one of the more suitable model systems for the present experimental purpose.

EXPERIMENTAL

The metal complexes were synthesized by usual methods. The metal oxides $LaCoO_3$, $La_{0.5}Sr_{0.5}CoO_3$, $LaNiO_3$, $LaMnO_3$, and $SrMnO_3$ were prepared using a conventional ceramic technique (*3*). The other oxides examined were obtained commercially. ESCA spectra were obtained with a DuPont Model 650B spectrometer (Mg anode). Under optimum conditions, a $^1/_4$-inch gold disk yields a 4f 7/2 peak intensity of 400 000 counts/s with FWHM of 1.2 eV and a typical operating vacuum is 1×10^{-7} Torr. Powder specimens were rubbed onto a gold probe with a round glass rod to achieve good electrical contact. A typical total scan time for the ESCA measurement was 5–15 min. The C_{1s} contamination peak, having in most cases the same order of intensity as the sample peaks, was employed as a reference peak and assigned a binding energy value of 284.4 eV (*4*). For Ar^+ sputtering, the sample was lowered without breaking vacuum to a sample preparation compartment which was equipped with an ion gun attachment made by Physical Electronics Inc. An ion beam of up to 2 keV with beam currents of 35 mA was used; this beam could be focused to about 0.5 cm^2 at normal incidence on the sample probe by an electrostatic lens. The total pressure in this compartment was maintained at 5×10^{-5} Torr during sputtering by introduction of Ar gas.

RESULTS AND DISCUSSION

Ar^+ Bombardment on Transition Metal Complexes. *Redox Reaction by Ar^+ Bombardment.* Table I summarizes the redox reaction behavior produced by Ar^+ bombardment on a variety of transition metal complexes as deduced from the corresponding ESCA spectrum. Changes in binding energies and the appearance of shake-up peaks (*5–7*) provide useful diagnostic criteria for determining the nature of the products produced. For example, Figure 1 shows the effect of 2-keV Ar^+ ion bombardment on the $Co(en)_3(ClO_4)_3$ complex. Upon Ar^+ ion bombardment, the metal center of the complex was reduced and two sets of new Co 2p peaks appeared, one corresponding to a shake-up satellite peak due to Co(II) and the other to Co(0). The above assignments are supported by the following two observations. Cobaltous oxide, CoO, gives shake-up satellite peaks for Co $2p_{1/2}$ and $2p_{3/2}$ and these peaks occur at binding energy values equal to those of the highest binding energy peaks of the sputtered $Co(en)_3(ClO_4)_3$ (see Figure 1b). Among the three peaks of cobalt metal foil (see Figure 1d), the one at the lowest binding energy, which is assigned to Co metal (Co(0)), corresponds very closely to that of the lowest binding energy peak found for the sputtered $Co(en)_3(ClO_4)_3$ complex. This Co(0) peak disappeared by exposing the sputtered sample to air for 2 min (Figure 1c). This corresponds to the reoxidation of Co(0) to Co(II) and/or Co(III) by air. Co(0) was also produced by Ar^+ bombardment

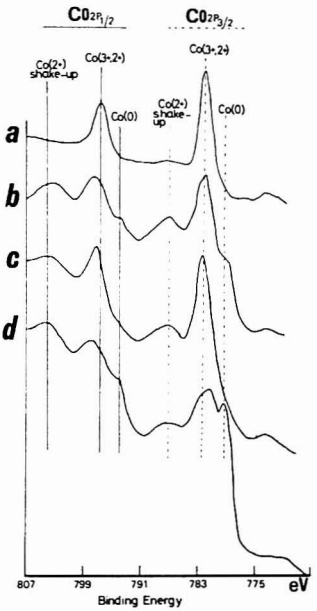

Figure 1. Effect of high energy Ar^+ ion bombardment on $Co(en)_3(ClO_4)_3$. (a) Prior to Ar^+ bombardment, (b) 2 keV Ar^+ bombardment for 2 min, (c) exposed to air after b, (d) cobalt metal foil polished in air immediately before measurement

on NaCo(edta) and $K_3Co(CN)_6$ complexes. The remaining cobalt(III) complexes studied did not form Co(0) ESCA peaks upon Ar^+ bombardment.

In the case of $Cu(dip)_3(NO_3)_2 \cdot 6H_2O$, Cu(II) is reduced to form Cu(I) upon Ar^+ bombardment. This is evidenced by the shift of the Cu $2p_{1/2}$ peak from 955.5 eV to 953.9 eV and Cu $2p_{3/2}$ from 935.7 eV to 934.3 eV and also by the disappearance of large Cu 2p shake-up peaks (964.0 eV, 944.7 eV) upon Ar^+ bombardment (see Figure 2b). The fact that Cu $2p_{3/2}$ and Cu $2p_{1/2}$ peaks of Ar^+ bombarded $Cu(dip)_3(NO_3)_2 \cdot 6H_2O$ occur at binding energy values about 1 eV higher than those of copper metal foil (Figure 2c, d) leads to the conclusion that the oxidation state of copper for Ar^+ bombarded $Cu(dip)_3(NO_3)_2 \cdot 6H_2O$ is 1+ rather than zero.

It should be noted that whereas most of the metal centers in the other metal complexes examined in Table I were reduced to lower oxidation states, those in $Fe(dip)_3(ClO_4)_2$, $Mn(dip)_3Br_2$, and $K_3Cr(C_2O_4)_3$ were oxidized. In the case of

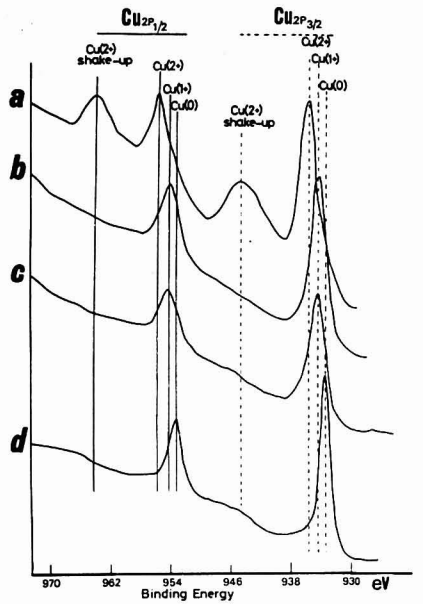

Figure 2. Effect of high energy Ar^+ ion bombardment on $Cu(dip)_3(NO_3)_2 \cdot 6H_2O$. (a) Prior to bombardment, (b) 2 keV Ar^+ bombardment for 2 min, (c) exposed to air after b, (d) copper metal film polished immediately before measurement

Table II. Dependence of "Reduction Yield" on Energy for Ar^+ Bombardment (2 min, 35 mA)

Sputtering voltage, keV	I_S/I_M[a]	I_o/I_M
2	0.41 (0.41: 4 min)	0.44 (0.59: 4 min)
1.5	0.42	0.45
1.0	0.38	0.28
0.5	0.34	0.0

[a] I_S, I_M, and I_o are the satellite, the main, and the zero valent Co peaks, respectively, from Ar^+ bombarded $Co(en)_3(ClO_4)_3$.

$Na_3(Co(NO_2)_6)$, $Pt(dip)Cl_2$, and $Pt(dip)_2Cl_2$, no significant change was observed with respect to the binding energy of spectral shapes of the metal centers (shake-up peaks, appearance of additional peaks, etc.).

Dependence of Reaction Yield on Ar^+ Energy. Table II shows the dependence of reaction "yield" of Co(II) and Co(0) from $Co(en)_3(ClO_4)_3$ on the magnitude of energy of Ar^+ bombardment. Yield is conveniently defined here as (I_S/I_M), and (I_0/I_M), where I_S is the intensity of the shake-up satellite peak appearing at higher binding energy side of Co $2p_{3/2}$ main peak, which is due to the paramagnetic Co(II) species produced by Ar^+ bombardment, I_M the intensity of Co $2p_{3/2}$ main peak at 782.2 eV which overlaps the remaining Co(III) and the newly produced Co(II) peaks, and I_0 the intensity of the cobalt(0) peak at 779.3 eV (see Figure 1b). The "yield" is, in general, increased with increase in sputtering time. This yield for a given time duration (e.g. 2 min) is dependent on the Ar^+ energy. It is interesting to note that the saturation of "yield" occurs at 2-keV energy. At this energy, even prolonged (4 min) bombardment produces no further increase in yield. Reaction yield vs. sputtering time at a given Ar^+ energy is also an interesting point, which remains for further study.

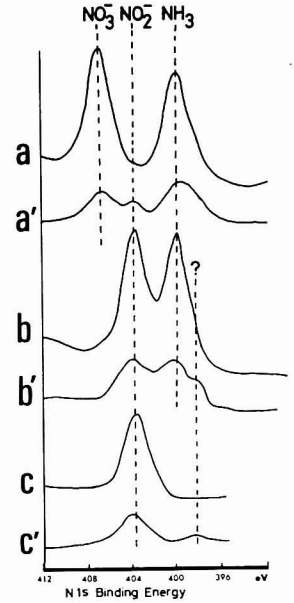

Figure 3. Change in nitrogen is spectra for some Co(III) complexes upon Ar^+ ion bombardment. (a) $Co(NH_3)_3(NO_3)_3$ prior to bombardment, (a') $Co(NH_3)_3(NO_3)_3$ with 2-keV Ar^+ bombardment for 7 min, (b) $Co(NH_3)_3(NO_2)_3$ prior to bombardment, (b') $Co(NH_3)_3(NO_2)_3$ after 2-keV Ar^+ bombardment for 2 min, (c) $Na_3Co(NO_2)_6$ prior to Ar^+ bombardment, (c') $Na_3Co(NO_2)_6$ after 2 min. 2-keV Ar^+ bombardment

Chemical Transformation of Ligands and Counterions. Figure 3 and 4 show the effect of Ar^+ bombardment upon the chemical changes in ligands and counterions of the metal complexes. In the case of $Co(NH_3)_3(NO_3)_3$, two N_{1s} peaks are clearly visible, one at 406.7 (NO_3^-) and one at 399.8 (NH_3). Upon Ar^+ bombardment, a new N_{1s} peak appears at 403.8 eV which is attributed to NO_2^- formed by reduction of NO_3^- by Ar^+ bombardment. $Na_3(Co(NO_2)_6)$ upon Ar^+ bombardment yields an additional N_{1s} peak at 398.5 eV, which is fairly close to NH_3 nitrogen peak. This may also be interpreted in terms of reduction by Ar^+ bombardment of NO_2^- to some lower oxidation state species such as NH_3 or similar species (*4*). $Co(NH_3)_3(NO_2)_3$ which has a 403.5-eV peak for NO_2^- and a 399.5-eV peak for NH_3, also exhibits a new N_{1s} peak upon Ar^+ bombardment indicating the formation of a new nitrogen-containing species of unknown nature. Another example of chemical transformation by Ar^+ bombardment occurs in the case of $Co(o\text{-phen})_3(ClO_4)_3$, where $Cl_{2p_{1/2}}$ and $Cl_{2p_{3/2}}$ peaks (overlapped) for ClO_4^- are decreased to a half of the original intensities and new peaks (overlapped) at around 198.0 eV due to Cl^- appear. Obviously, this is the result of reduction by Ar^+ bombardment of ClO_4^- to Cl^-. Similar behavior was observed with $Fe(dip)_3(ClO_4)_2$, $Co(dip)_3(ClO_4)_3$ and the other ClO_4^- containing species.

Sputtering Efficiency. An interesting example is $Cu(dip)_3(NO_3)_2$. The relative intensity of the N_{1s} peak for NO_3^- to that of dipyridyl (dip) is changed from 1.0:2.82 to 0.0:1.53

Table III. Change in Peak Intensities of Various Elements in Metal Complexes by Ar^+ Ion Bombardment (2 keV, 2 min)

Compound	Peak Intensity Ratio[c]					
$K_3[Cr(C_2O_4)_3]$	Cr	K	O	CO	Au[a]	C[b]
	1.42	1.13	0.68	0.40	1.11	0.92
$Co(NH_3)_3(NO_2)_3$	Co	NO_2	NH_3	O	Au[a]	C[b]
	2.40	0.33	0.35	0.89	1.34	0.90
$Mn(dip)_2Br_2$	Mn	Br	N	Au[a]	O[d]	C[b]
	0.48	0.42	0.40	1.06	0.87	1.18
$Fe(dip)_3(ClO_4)_2$	Fe	N	ClO_4	O	Au[a]	C[b]
	0.70	0.55	0.25	0.35	1.20	1.27
$Pt(dip)Cl_2$	Pt	N	Cl	Au[a]	C[b]	
	0.53	0.33	0.32	1.20	1.27	
$Na_3[Co(NO_2)_6]$	Co	Na	N	O	Au[a]	C[b]
	1.61	2.14	0.45	0.72	1.05	0.95
$[Co(NH_3)_5Cl]Cl_2$	Co	N	Cl	Au[a]	C[b]	
	1.58	0.56	1.04	1.25	0.90	
$Co(en)_3(ClO_4)_3$	Co	N	Au[a]	C[e]		
	2.50	0.67	1.69	0.84		
$Cu(dip)(NO_3)_2$	Cu	N(dip)	NO_3	Au[a]	C[e]	
	0.60	0.68	0.27	1.32	1.12	
$K_4[Fe(CN)_6]$	Fe	K	N	O[d]	Au[a]	C[e]
	0.80	0.71	0.38	2.23	1.00	1.10
$Co(o\text{-phen})_3(ClO_4)$	Co	N	ClO_4	O	Au[a]	C[e]
	0.73	0.50	0.59	0.46	1.36	1.29

[a] Signal from the gold probe. [b] Background carbon. [c] Ratio of peak intensities after (I_a) and before (I_b) bombardment ($= I_a/I_b$); accurate to ±0.05. [d] Adsorbed water. [e] Background carbon plus ligand carbons.

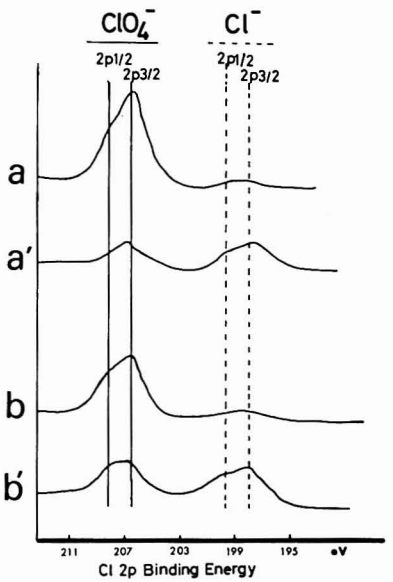

Figure 4. Chemical transformation of ClO_4^- ion into Cl^- ion upon Ar^+ bombardment. (a) $Co(o\text{-phen})_3(ClO_4)_3$ prior to bombardment, (a') $Co(o\text{-phen})_3(ClO_4)_3$ after 2-keV Ar^+ bombardment for 2 min, (b) $Fe(dip)_3(ClO_4)_2$ prior to bombardment, (b') $Fe(dip)_3(ClO_4)_2$ after 2-keV Ar^+ bombardment for 2 min

by Ar^+ sputtering, indicating that the NO_3^- functional group is more easily sputtered away than the dip group. In contrast, the ligands NH_3, NO_2^-, and NO_3^- in $Co(NH_3)_3(NO_2)_3$ and $Co(NH_3)_3(NO_3)_3$ show similar sputtering tendencies upon Ar^+ bombardment. The dependence of Ar^+ sputtering efficiency on various elements and ligands in several other metal complexes is summarized in Table III. The $Au_{4f_{7/2}}$ peak from the sample mounting probe was also measured and the ratio of its intensity after to before sputtering is cited to permit some judgment to be made of the overall Ar^+ sputtering efficiency in each case. Some conclusions may be drawn from the results presented in Table III.

One general tendency observed is that the ESCA peak intensities for the transition and alkali metal ions are increased by Ar^+ bombardment, whereas the intensities for the nonmetal elements are decreased, indicating that the ligand species are sputtered off more easily than the transition and alkali metal ions.

Occasionally, the peak intensity due to the contamination carbon is increased upon Ar^+ bombardment. This increase is observed only with particular ligand species such as dip, *o*-phen, and CN and may be caused by a chemical change in ligand species upon Ar^+ bombardment to produce this type of carbon. In this case, the peak intensities for the transition and alkali metal ions are decreased as well as those attributed to the initial ligand species.

Ar^+ Bombardment on Metal Oxides. The surface composition of solid materials often is not identical to that for the bulk itself because of surface chemical reactions, particularly with typical atmospheric components such as O_2, CO_2, H_2O, H_2S, etc. and because of accidental contamination by contact of the surface with the adsorbable species. Thus the surface composition of a material will depend greatly upon its intrinsic reactivity, mode of preparation, and storage history. For the transition metal complexes described in the previous section, the surface composition probably reflected the bulk composition to a high order. This might be expected since these species were prepared in aqueous solution in the presence of air and hence represented chemical composition states which are stable and resistant to further reaction with atmospheric components. This is less likely to be the case with other reactive species which have to be synthesized under more stringent conditions of temperature and environments. The ESCA spectra for cobalt metal foil (Figure 1d) represents a case of one reactive material whose surface composition differs from the bulk. Ar^+ sputtering is a useful technique for removing the surface layers on metals and creating a surface whose composition reflects that of the bulk material. On the other hand, the Ar^+ bombardment technique applied to materials such as the transition metal complexes described in the previous section clearly leads to changes in surface

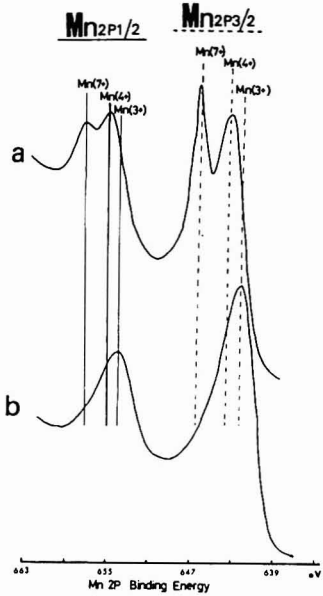

Figure 5. Effect of Ar^+ ion bombardment (2 keV, 2 min) on $KMnO_4$. (a) Prior to and (b) after bombardment, respectively

composition so that it no longer reflects that of the bulk. The new surface composition probably more closely approximates that which would be obtained by heating the bulk sample in vacuum to an elevated temperature equivalent to the surface temperature achieved by Ar^+ bombardment. Thus Ar^+ sputtering is not equivalent to a thin knife blade simply eroding away the surface layers one by one leaving the composition of the sublayers intact. Obviously mechanical fracture techniques under vacuum are more suitable in these cases.

Metal oxides represent a class of material whose surface composition is likely to be different from that of the bulk and it is of interest to determine the effect of Ar^+ bombardment on such materials.

As shown in Figure 5, the Mn 2p spectra of $KMnO_4$ have anomalous doublet structure at 657.5 and 655.4 eV for $2p_{1/2}$ and at 646.6 and 643.5 eV for $2p_{3/2}$. The relative intensity of the doublet peaks depends upon the history of the $KMnO_4$ sample. Upon Ar^+ bombardment, however, both doublet peaks disappear and new peaks are produced at 654.1 eV and 642.4 eV for Mn $2p_{1/2}$ and Mn $2p_{3/2}$, respectively. The change in binding energy of Mn $2p_{1/2}$ and $2p_{3/2}$ for $KMnO_4$ before and after Ar^+ bombardment is summarized in Table IV along with the results obtained by analogous experiments for Mn_2O_3 and MnO_2. From Figure 5 and Table IV, it is clear that the surface of the $KMnO_4$ as obtained from the shelf is already partially reduced to MnO_2, and that both $KMnO_4$ and MnO_2 at the surface are reduced to form Mn_2O_3 upon Ar^+ bombardment:

$$KMnO_4 \xrightarrow{Ar^+} Mn_2O_3 + 2O_2 + K_2O$$

$$4MnO_2 \xrightarrow{Ar^+} 2Mn_2O_3 + O_2$$

Jolly speculated previously that the surface of such highly oxidized metal compounds could be partially reduced to a

Table IV. Effect of Ar^+ Bombardment on $KMnO_4$ and Related Compounds[a]

	Binding energy of Mn peaks prior to bombardment, eV		Binding energy of Mn peaks after bombardment, eV	
Compound	$2p_{1/2}$	$2p_{3/2}$	$2p_{1/2}$	$2p_{3/2}$
$KMnO_4$	657.5 655.4	646.6 643.5	654.1	642.4
MnO_2	654.7	643.0	654.3	642.4
Mn_2O_3	654.1	642.4	654.4	642.5

[a] Energy for Ar^+ beam: 2 keV for 2 min, (C_{1s} = 284.4 eV).

Table V. Influence of Ar^+ Bombardment on Oxygen Excess of Various Metal Oxides

	O/M Ratios[a]		
Compound	Before Ar^+ sputtering	After Ar^+ sputtering[c]	
MnO_2	1.86	0.92	R[b]
Mn_2O_3	2.10	1.20	
$SrMnO_3$	1.96	0.68	R
$LaMnO_3$	2.63	1.70	
Co_3O_4	2.00	0.77	R
$LaCoO_3$	2.75	1.82	R
$La_{0.5}Sr_{0.5}CoO_3$	2.54	0.76	R

[a] Ratio of O_{1s} and $M_{2p_{3/2}}$ peak intensities ($=O_{1s}/M_{2p_{3/2}}$), corrected for stoichiometry of the compound listed and cross section (accurate to ±0.05). [b] R = Reduction of transition metal center by Ar^+ bombardment. [c] Ion beam of 2 keV and 35 mA for 2 min.

lower oxidation state (7). Jolly's speculation was based on the fact that such compounds as $KMnO_4$, K_2FeO_4, and SnO_2 give increadibly low metal core binding energies for such high oxidation state compounds. Previous reports have not claimed the existence of the doublet structure of Mn 2p peaks for $KMnO_4$. Copperthwaite (8), however, found that prolonged x-ray irradiation led to reduction of Mn(VII) to lower valence states.

As shown in Table V, the intensity ratio of oxygen to metal peaks (O/M), after correction for stoichiometry and the photoelectric cross section (9), for some metal oxides is larger than unity. These results suggest that excess oxygen (adsorbed oxygen, water, and so on) exists at the surface of these oxides. However, upon Ar^+ bombardment, the O/M value (corrected) becomes closer to unity for most of the oxides. The above results indicate that the excess oxygen atoms at the surface can be sputtered off relatively easily. Electronic reduction of central metals by Ar^+ bombardment causes a change in stoichiometry and therefore also leads to a decrease in the O/M ratio. It was also found that the absolute intensity of the metal center peak is increased by 30–100% upon Ar^+ bombardment, whereas the absolute intensity of the oxygen 1s peak decreased. The increase in the metal center peak intensity is of course due to the sputtering off by Ar^+ bombardment of the carbon contamination layer on the surface of the oxides.

The O 1s spectrum for transition metal oxides in general contains two peaks, a feature frequently observed by many workers (10, 11). Usually, the appearance and the relative intensity of the higher binding energy peak is dependent on the history and pretreatment of the sample. It is reasonable to assign the lower binding energy peak to "lattice oxygen" and the higher binding energy one to "excess surface oxygen" peak (such as M–OH and/or MO·H_2O). It is therefore in-

teresting to examine the effect of Ar^+ bombardment on each of the oxygen peaks. In the case of $La_{0.5}Sr_{0.5}CoO_3$, $LaCoO_3$, and $LaNiO_3$, the absolute intensity of "excess surface oxygen" peaks decreased greater than that of "lattice oxygen". The opposite however was observed for Mn_2O_3, MnO_2, and Co_2O_3. Although we initially expected that the intensity of "excess surface oxygen" should decrease to a greater extent than that of "lattice oxygen" because of its origin, it became clear from the present study that the situation is not so straightforward. Additional features concerning sputtering of metal oxides are given by Wekner (*12*).

LITERATURE CITED

(1) K. S. Kim and N. Winograd, *Surf. Sci.*, **43**, 625 (1974).
(2) K. S. Kim, W. E. Baitinger, J. W. Amy, and N. Winograd, *J. Electron Spectrosc.*, **5**, 351 (1974).
(3) H. Obayashi, T. Kudo, and T. Gejo, *Jpn. J. Appl. Phys.*, **13**, 1 (1974).
(4) K. Siegbahn, C. Vordling, A. Fahlman, R. Nordberg, K. Hamrin, J. Hedman, G. Jonansson, T. Bergman, S. Karlsson, I. Lindgren, and B. Lindberg, "ESCA—Atomic, Molecular, and Solid State Structure Studied by Means of Electron Spectroscopy", Almquist and Wiksells, Uppsala, Sweden, 1967.
(5) T. Robert and G. Offergeld, *Chem. Phys. Lett.*, **29**, 606 (1974).
(6) K. S. Kim and N. Winograd, *Chem. Phys. Lett.*, **31**, 312 (1975)
(7) W. L. Jolly, *Coord. Chem. Rev.*, **13**, 47 (1974).
(8) R. G. Copperthwaite, *ES News Letter, Case Western Reserve Univ.*, (No. 6, March) 26 (1975).
(9) J. H. Scofield, *Lawrence Livermore Lab.* [*Rep*] **UCRL-51326, 1973.**
(10) W. Dianis and J. E. Lester, *Surf. Sci.*, **43**, 602 (1974).
(11) T. Robert, M. Bartel, and G. Ofergeld, *Surf. Sci.*, **33**, 123 (1972).
(12) G. K. Wekner, in "Methods of Surface Analysis", A. W. Czanderna, Ed., Elsevier Publishing Co., Amsterdam, 1975, p 24.

RECEIVED for review December 1, 1977. Accepted April 10, 1978. This work was partially supported by a grant from the National Science Foundation.

Standards for pH Measurements in Isotonic Saline Media of Ionic Strength $I = 0.16$

Roger G. Bates,* Carmen A. Vega,[1] and D. R. White, Jr.

Department of Chemistry, University of Florida, Gainesville, Florida 32611

Evidence is presented that pH measurements of blood plasma and other clinical media at an ionic strength (I) of 0.16 vs. the NBS standards may involve residual liquid-junction errors amounting to 0.03 to 0.05 unit. Eight dilute buffer solutions to which NaCl had been added in amount sufficient to raise the ionic strength to 0.16 were studied at 25 and 37 °C. Measurements of cells both with and without liquid junction led to the conclusion that errors due to residual liquid-junction effects can be nearly eliminated by matching the ionic strength of the standard to that of the clinical sample. This result was confirmed by calculation of liquid-junction potentials. Standard pH values for four useful reference solutions with pH and ionic strength near those of blood plasma were determined at 10 temperatures from 5 to 50 °C. A phosphate buffer composed of 0.005217 *m* KH_2PO_4, 0.018258 *m* Na_2HPO_4, and 0.1 *m* NaCl (buffer ratio 1:3.5 and $I = 0.16$) is to be preferred to the 1:3.5 phosphate buffer ($I = 0.1$) of the NBS standard scale for pH measurements in saline media of ionic strength near 0.16.

Measurements of the pH of blood and plasma are an important integral part of clinical diagnosis. For the highest accuracy and reproducibility, the glass electrode pH assembly should be standardized at or near the pH of the clinical sample. Furthermore, the reference standard solution (S) should, ideally, have an ionic strength (I) close to that of the "unknown" sample (X), namely about 0.16 mol kg^{-1} for blood plasma. The pH of the sample X is defined in terms of the emf E of the cell

Reference electrode ||Soln. S or X|H_2 (g, 1 atm);Pt (A)

by the operational definition

$$pH(X) = pH(S) - \frac{(E_X - E_S)F}{RT \ln 10} \quad (1)$$

The double vertical line in cell A represents a liquid junction. In practice, the hydrogen electrode is usually replaced by a glass electrode.

It should be noted that, in accord with the preference of the International Union of Pure and Applied Chemistry at its 1977 meeting in Warsaw, and contrary to its earlier recommendation (*1*), cell A is written with the reference electrode on the left and the hydrogen or glass electrode on the right. Consequently, a minus sign appears before the last term of Equation 1.

Standardization of the assembly at a point close to the pH of blood can be achieved within the framework of the NBS standard pH scale. One of the primary reference solutions of this scale, a mixture of KH_2PO_4 and Na_2HPO_4 in the mole ratio 1:3.5 and an ionic strength of 0.1, has a pH (S) value near 7.39 at 37 °C. Other reference solutions of pH near 7.4 must be regarded as secondary standards, useful because their pH values have been compared carefully with the primary standard scale. These include buffers of tris(hydroxymethyl)aminomethane ("Tris") of ionic strengths 0.05 to 0.16 (*2*, *3*), of tris(hydroxymethyl)methylglycine ("Tricine") of $I = 0.02$ (*4*), as well as other mixtures of phosphate salts with $I = 0.13$ (*5*).

Nevertheless, attempts to establish a primary reference standard of ionic strength 0.16 and pH near 7.4 have met with difficulty. Durst and Staples (*2*) studied the solution Tris·HCl (0.05 mol kg^{-1}) + Tris (0.01667 mol kg^{-1}) + NaCl (0.11 mol kg^{-1}) at 25 and 37 °C by means of cells without liquid junction in the manner employed for establishing the primary NBS standards. When the values they assigned to this reference solution were found to be inconsistent with the NBS primary scale (see, for example, ref. 6), it was suggested (*7*) that this solution also be regarded as a secondary standard. The reason for this disparity of 0.03 to 0.05 unit was not clear; it has been

[1] Present address, Department of Chemistry, University of Puerto Rico, Mayagüez, P.R.

0003-2700/78/0350-1295$01.00/0

attributed, at least in part, to the anomalous behavior of Tris in contact with liquid-junction devices incorporated in certain types of commerical reference electrodes (*8*).

The internal consistency of the NBS primary standards, all of which have ionic strengths of 0.1 or below, has been clearly demonstrated (*9*). Pursuant to a study of the dissociation of four substituted ethanesulfonic acids, two of which are suitable for pH control in the physiological range, however, it was discovered that buffer solutions formed from these substances and adjusted to $I = 0.16$ by addition of NaCl displayed departures from the NBS standard scale in much the same manner as earlier observed with Tris buffers. The buffer substances in question were TES, *N*-tris(hydroxymethyl)methyl-2-aminoethanesulfonic acid, and HEPES, *N*-2-hydroxyethylpiperazine-*N'*-2-ethanesulfonic acid (*10*). Both TES and HEPES are zwitterions, while Tris is an uncharged base.

To enhance the reliability of pH measurements in blood plasma and other clinical media, reference standards of ionic strength 0.16 are much to be desired. Secondary standards can fill the need in part, providing reproducibility from time to time and from place to place. Nevertheless, pH values based on these do not bear a simple relationship to chemical equilibria such as that provided by the convention on which the NBS scale is based (*9*). We have, therefore, undertaken a study to reveal the causes of the disparity between the operational pH of buffer solutions at $I = 0.16$, referred to the primary scale, and the pH(S) determined from the emf of cells without liquid junction. Factors investigated were (a) possible failure of the convention for $\log \gamma_{Cl}$ at ionic strengths in excess of 0.1, and (b) an appreciable liquid-junction potential when the relatively dilute NBS reference solutions are replaced by buffer solutions of $I = 0.16$. It is concluded that factor b alone can account for nearly all of the observed discrepancy.

EXPERIMENTAL

The phosphate salts were NBS Standard Reference Materials: KH_2PO_4, SRM186Ic, and Na_2HPO_4, SRM186IIc. TES and HEPES were obtained from Sigma Chemical Co. They were subjected to recrystallization from 80% ethanol–water and assayed by titration with a standard solution of carbonate-free NaOH. Assay values averaged 99.97%. Sodium chloride was recrystallized from water and dried at 110 °C. The buffer solutions were prepared by weighing the buffer substances, NaCl, a standard solution of NaOH, and conductivity water.

Platinum hydrogen electrodes thinly coated with platinum black from a solution of chloroplatinic acid were used in cells of type A and also type B, without a liquid junction:

$$Pt;H_2(g, 1\ atm)|Buffer\text{–}NaCl\ soln.|AgCl;Ag \qquad (B)$$

The standard emf of this cell was found to be 0.22242 V at 25 °C and 0.21440 V at 37 °C by measurements of cells containing 0.01 *m* HCl (*11*). The silver–silver chloride electrodes were of the thermal-electrolytic type, prepared as described elsewhere (*9*). The liquid junction between 3.5 M KCl and the buffer solutions in cell A was formed in a vertical tube (internal diameter about 3 mm) with the heavier KCl solution below.

A short series of emf measurements was made with cells of the type

$$NaISE|Phosphate\ buffer + NaCl|AgCl;Ag \qquad (C)$$

in which a Corning sodium electrode No. 476210 was used. The emf of cells A and B was measured by a Hewlett-Packard digital voltmeter Model 3460B and that of cell C by a Corning pH meter Model 112.

RESULTS

The measurements of cell A were all standardized by a parallel measurement of the emf of the cell containing the NBS phosphate solution with 1:3.5 buffer ratio; its composition is KH_2PO_4 (0.008695 *m*), Na_2HPO_4 (0.03043 *m*), and its ionic strength is 0.1. Inasmuch as the reference emf (E_S) was not always the same, the values given in Table I have been normalized to correspond with values of 0.2501 and 0.2453 V for the potentials of a 3.5 M calomel electrode at 25 and 37 °C, respectively (see p 327 of ref. 9). Other phosphate buffer solutions were prepared either by adding NaCl to this solution to raise the ionic strength or by diluting this solution before addition of NaCl. The buffer ratio 1:3.5 was always maintained. The compositions are identified by listing separately the contributions of the buffer mixture and NaCl to the total ionic strength. Thus, "0.06 phosphate, 0.1 NaCl" (or simply "0.06 P, 0.1 NaCl") signifies a solution in which the 1:3.5 phosphate buffer contributes 0.06 to the ionic strength, while the added NaCl contributes 0.1. As this is six-tenths of the ionic strength of the NBS standard phosphate solution, the molalities of the phosphate salts are evidently 0.005217 (KH_2PO_4) and 0.018258 mol kg^{-1} (Na_2HPO_4) and that of NaCl is 0.1 mol kg^{-1}.

The structures of Tris, TES, and HEPES are as follows:

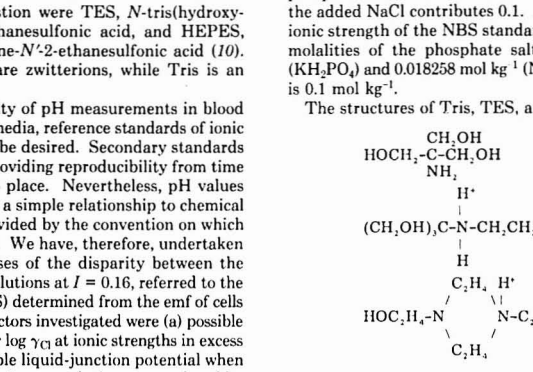

The buffer solutions studied had the following compositions, where the figures in parenthesis are molalities:

1:3 Tris: Tris·HCl (0.05), Tris (0.01667), NaCl (0.11)
1:1 TES: TES (0.04), NaTES (0.04), NaCl (0.12)
1:2 TES: TES (0.02), NaTES (0.04), NaCl (0.12)
1:2 HEPES: HEPES (0.02), NaHEPES (0.04), NaCl (0.12)

The measurements of cells without liquid junction (type B) were more extensive than those of cell A. TES buffers (TES/NaTES of 1:1 and 1:2) and HEPES buffers (HEPES/NaHEPES of 1:2) were studied at several molalities over the temperature range 5 to 50 °C, always with NaCl added to maintain an ionic strength of 0.16. Similar measurements were made with the phosphate–chloride mixture designated 0.06P+0.1NaCl. To conserve space, only the emf at 25 and 37°C for one solution of each series is given in Table II. (Data at the other temperatures are available in microform; see final paragraph of paper.) In addition, emf measurements of cells of type B containing other phosphate-chloride solutions and the Tris-chloride buffer were made at 25 and 37°C and are included in Table II. The results from these latter measurements were in excellent accord with those of Durst and Staples (*2*).

TREATMENT OF DATA

Operational pH values were calculated by Equation 1 from the data of Table I. In each case, the reference solution was the NBS "blood buffer", KH_2PO_4 (0.008695) + Na_2HPO_4 (0.03043 mol kg^{-1}). Although pH(S) values for this reference solution have been determined for the lots of phosphate salts used here, an independent check was made using the data for cells without liquid junction as given in Table II. The procedure, which employed the emf for solutions of the blood buffer containing 0.01, 0.02, 0.04, and 0.06 *m* NaCl, has been set forth elsewhere (*9*). Figure 1 is a plot of $p(a_H\gamma_{Cl})$, defined by

$$p(a_H\gamma_{Cl}) \equiv \frac{(E - E^\circ)F}{RT \ln 10} + \log m_{Cl} \qquad (2)$$

Table I. Electromotive Force of Cells of Type A: $Hg;Hg_2Cl_2$, 3.5 M KCl‖Buffer Soln.$|H_2$(g, 1 atm);Pt, at 25

buffer, ionic strength, I		NaCl, I	$-E_{25}$	pH, 25 °C	$-E_{37}$	pH, 37 °C
phosphate	0.1[a]	0	0.6885	(7.411)[b]	0.6999	(7.387)[b]
phosphate	0.1	0.02	-	-	0.69779	7.353
phosphate	0.1	0.04	-	-	0.69588	7.322
phosphate	0.1	0.06	0.68242	7.308	0.69397	7.291
phosphate	0.08	0.08	0.68159	7.294	0.69324	7.279
phosphate	0.06	0.10	0.68082	7.281	0.69250	7.267
phosphate	0.04	0.12	0.67988	7.265	0.69151	7.251
0.02 TES 0.04 NaTES	0.04	0.12	0.70644	7.714	0.70702	7.503
0.04 TES 0.04 NaTES	0.04	0.12	0.68869	7.414	0.68862	7.204
0.02 HEPES 0.04 NaHEPES	0.04	0.12	0.70939	7.764	0.71490	7.631
0.05 Tris-HCl 0.01667 Tris	0.05	0.11	0.70472	7.685	0.69951	7.381

[a] Each phosphate buffer was composed of KH_2PO_4 and Na_2HPO_4 in the mole ratio 1:3.5. [b] Reference values.

Table II. Electromotive Force of Cells of Type B: $Pt;H_2$(g, 1 atm)‖Buffer Soln.$|AgCl;Ag$, at 25 and 37 °C, in Volts

buffer, ionic strength, I		NaCl, I	E_{25}	pH(S), 25 °C	E_{37}	pH(S), 37 °C
phosphate	0.1	0.02	0.76675	7.385	0.77917	7.360
phosphate	0.1	0.04	0.74775	7.360	0.75945	7.334
phosphate	0.1	0.06	0.73644	7.339	0.74768	7.314
phosphate	0.08	0.08	0.72860	7.331	0.73950	7.306
phosphate	0.06	0.10	0.72232	7.323	0.73295	7.297
phosphate	0.04	0.12	0.71723	7.315	0.72769	7.290
0.02 TES 0.04 NaTES	0.04	0.12	0.74340	7.758	0.74276	7.535
0.04 TES 0.04 NaTES	0.04	0.12	0.72560	7.457	0.72429	7.235
0.02 HEPES 0.04 NaHEPES	0.04	0.12	0.74619	7.805	0.75051	7.661
0.05 Tris-HCl 0.01667 Tris	0.05	0.11	0.73529	7.746	0.72849	7.427
			E° = 0.22242		E° = 0.21440	

Table III. Operational pH Values Calculated by Equation 1 from the emf of Cell A vs. Phosphate–Chloride Standard Reference Solutions at 25 and 37 °C

buffer solution	standard reference solution: NBS 0.1P[a]	0.1P + 0.02NaCl	0.1P + 0.04NaCl	0.1P + 0.06NaCl	0.08P + 0.08NaCl	0.06P + 0.10NaCl	0.04P + 0.12NaCl	pH(S)
			25 °C					
0.02 TES, 0.04 NaTES, 0.12 NaCl	7.714	-	-	7.745	7.751	7.756	7.764	7.758
0.04 TES, 0.04 NaTES, 0.12 NaCl	7.414	-	-	7.445	7.451	7.456	7.464	7.457
0.02 HEPES, 0.04 NaHEPES, 0.12 NaCl	7.764	-	-	7.795	7.801	7.806	7.814	7.805
0.05 Tris-HCl, 0.01667 Tris, 0.11 NaCl	7.685	-	-	7.716	7.722	7.727	7.735	7.746
			37 °C					
0.02 TES, 0.04 NaTES, 0.12 NaCl	7.503	7.510	7.515	7.526	7.530	7.533	7.542	7.535
0.04 TES, 0.04 NaTES, 0.12 NaCl	7.204	7.211	7.216	7.227	7.231	7.234	7.243	7.235
0.02 HEPES, 0.04 NaHEPES, 0.12 NaCl	7.631	7.638	7.643	7.654	7.658	7.661	7.670	7.661
0.05 Tris-HCl, 0.01667 Tris, 0.11 NaCl	7.381	7.388	7.393	7.404	7.408	7.411	7.420	7.427

[a] P = Phosphate buffer (1:3.5); the numbers indicate the respective contributions of phosphate buffer and NaCl to the total ionic strength.

as a function of the molality of NaCl in the phosphate–NaCl mixture. The intercepts $p(a_H\gamma_{Cl})^\circ$ at $m_{Cl} = 0$, found by linear regression analysis, were 7.520 at 25 °C and 7.499 at 37 °C, with a mean deviation slightly greater than 0.001 from the lines drawn. By introduction of the "pH convention" (*12*)

$$-\log \gamma_{Cl} = \frac{AI^{1/2}}{1 + 1.5\, I^{1/2}} \qquad (3)$$

into the identity

$$pH(S) \equiv p(a_H\gamma_{Cl})^\circ + \log \gamma_{Cl} \qquad (4)$$

pH(S) was found to be 7.411 at 25 °C and 7.387 at 37 °C. These values, which differ somewhat from those assigned by the NBS to these lots (7.415 and 7.392, respectively), were used in subsequent calculations. The pH derived with their use appears in the second column of Table III as well as in Table I.

If the pH convention set forth in Equation 3 is valid up to I = 0.16 (above its intended upper limit of 0.1), one can calculate pH values for all of the buffer–chloride solutions from the emf data given in Table II. These values are collected in Table II and in the last column of Table III. The same treatment for the solutions of TES and HEPES from 5 to 50 °C yielded the smoothed values summarized in Table IV. Similar results for the phosphate–chloride solution 0.06 P + 0.1 NaCl are given in Table V. The values derived from cells

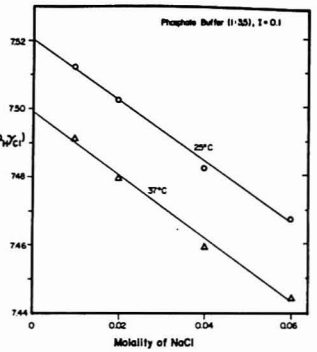

Figure 1. Plots of $p(a_H\gamma_{Cl})$ for the NBS phosphate "blood buffer" as a function of the molality of added NaCl

Table IV. pH(S) Values for TES + NaTES + NaCl and HEPES + NaHEPES + NaCl Buffer Solutions (Ionic Strength 0.16) from 5 to 50 °C

	molality of NaTES or NaHEPES		
t, °C	0.02	0.04	0.06
	TES/NaTES = 1:2		
5	8.170	8.172	8.174
10	8.060	8.062	8.064
15	7.954	7.956	7.957
20	7.851	7.855	7.854
25	7.755	7.758	7.758
30	7.663	7.662	7.664
37	7.534	7.535	7.536
40	7.482	7.483	7.484
45	7.398	7.399	7.398
50	7.316	7.318	7.318
	TES/NaTES = 1:1		
5	7.873	7.872	7.873
10	7.762	7.761	7.763
15	7.656	7.656	7.657
20	7.554	7.554	7.555
25	7.457	7.457	7.457
30	7.362	7.362	7.363
37	7.235	7.235	7.236
40	7.182	7.182	7.183
45	7.100	7.098	7.099
50	7.021	7.017	7.018
	HEPES/NaHEPES = 1:2		
5	8.060	8.066	8.072
10	7.993	7.998	8.003
15	7.927	7.933	7.938
20	7.862	7.868	7.873
25	7.801	7.805	7.810
30	7.741	7.745	7.748
37	7.658	7.661	7.664
40	7.623	7.626	7.629
45	7.567	7.569	7.572
50	7.511	7.514	7.516

without liquid junction have been designated pH(S) to distinguish them from values based on the emf of cell A which involves a liquid-junction potential.

DISCUSSION

There is reason to believe that discrepancies of the sort that appear between column 2 and the last column of Table III are the result of an appreciable residual liquid-junction potential (*13*). Maas (*14*) is of the opinion that this source of error in clinical pH measurements can largely be eliminated by matching the ionic strength of the standard reference solution to that of the clinical samples. This can be accomplished readily by employment of secondary standards. To achieve results congruent with the primary standard scale, however, it is necessary to examine the data for cells without liquid junction and the validity of the convention of Equation 3.

Table V. Emf and pH(S) Values for the Reference Solution: KH_2PO_4 (0.005217m) + Na_2HPO_4 (0.018258m) + NaCl (0.1m) from 5 to 50 °C

t, °C	E, V	pH(S)
5	0.70500	7.406
10	0.70929	7.379
15	0.71362	7.356
20	0.71795	7.337
25	0.72232	7.323
30	0.72665	7.309
35	0.73106	7.298
37	0.73295	7.297
40	0.73544	7.291
45	0.74001	7.289
50	0.74449	7.287

Single Ion Activity Coefficient. Evidence, largely circumstantial, leads one to believe that pH(S) values derived from the emf of cell B with the aid of Equation 3 lie close to the NBS standard scale, based on the same pH convention. This reasoning will now be summarized.

The estimated values for the logarithm of the activity coefficient for chloride ion at 25 °C resulting from Equation 3 are −0.110 at I = 0.1 and −0.128 at I = 0.16. These values are close to the logarithm of the mean activity coefficient (log $\gamma_\pm$) of NaCl at I = 0.1 (−0.109) and at I = 0.16 (−0.126). At 37 °C, log γ_{Cl} at I = 0.16 is −0.130 from Equation 3, while log $\gamma_\pm$ is −0.128. An inconsistency of the order of 0.02 to 0.04 seems extremely unlikely. Furthermore, the hydration convention for single ionic activities at high concentrations (*15*) yields a value of −0.130 for log γ_{Cl} in a solution of NaCl of molality 0.16 mol kg^{-1}.

One expects, of course, that log $\gamma_\pm$ and log γ_{Cl} in a phosphate–NaCl mixture (I = 0.16) will differ from that in 0.16 m NaCl. Furthermore, these quantities will probably vary linearly with molal composition at this constant ionic strength (*16*). In order to estimate the probable change in log $\gamma_\pm$(NaCl) when a part of the NaCl is replaced by a phosphate buffer at a constant ionic strength of 0.16, the sodium glass electrode (NaISE) was utilized in cells of type C at 25 and 37 °C. The following emf data were obtained:

ionic strength		E(V) at	
phosphate	NaCl	25 °C	37 °C
0	0.16	0.0432	0.0465
0.04	0.12	0.0540	0.0574
0.10	0.06	0.0767	0.0814

The standard emf of cell C was derived by use of the known log $\gamma_\pm$ in the 0.16 m NaCl solution, and the activity coefficient in the buffer–chloride mixtures was calculated by

$$-\log \gamma_\pm = \frac{(E - E^\circ)F}{2RT \ln 10} + 1/2 \log (m_{Na} m_{Cl}) \qquad (5)$$

The results, shown in Figure 2, are not of high accuracy. Those at 37 °C, in particular, confirm the expectation that −log $\gamma_\pm$ at I = 0.16 increases in linear fashion with replacement of NaCl by buffer. They show that the increase amounts to about 0.001 in −log $\gamma_\pm$ for each increment of 0.01 in the contribution of phosphate to the total ionic strength. Thus, −log γ_{Cl} calculated by the hydration convention for the solution

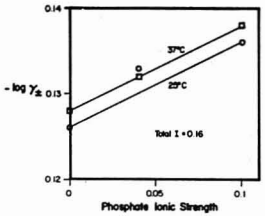

Figure 2. Variation of the logarithm of the mean activity coefficient of NaCl in phosphate–chloride mixtures of $I = 0.16$, as a function of composition at 25 and 37 °C

composed of phosphate ($I = 0.06$) and NaCl ($I = 0.1$) should be higher by 0.006 than the value (0.130) calculated above. It may be concluded that deficiencies in the estimation of the activity coefficient of chloride ion are small compared with the difference of 0.042 at 25 °C and 0.030 at 37 °C between the pH values of this solution derived from cells A and B (see Tables I and II.)

Residual Liquid-Junction Potential. We have now shown that, in all likelihood, the values of pH(S) given in the last column of Table III lie close to the standard scale defined by the NBS primary standards. Thus it is possible to determine the effect of the ionic strength and composition of the standard on the pH of TES, HEPES, and Tris buffers derived from the emf of cell A by Equation 1. For this purpose, one selects from Tables I and II corresponding values of E_S and pH(S) for reference phosphate–chloride solutions. The results of such a calculation are entered in Table III, and the data at 37 °C are shown graphically in Figure 3. The horizontal dotted lines indicate the values of pH(S) determined from cells without liquid junction by applying the convention set forth in Equation 3.

It is clear that the greater part of the discrepancy between the operational pH value from cell A and the conventional activity pH from cell B is removed by matching the ionic strength of standard S with that of the unknown sample X. As far as buffers of TES, HEPES, and Tris with added NaCl are concerned, some further improvement results from an increase in the NaCl molality at the expense of the phosphate. Indeed, a reference standard composed of phosphate ($I = 0.06$) and NaCl ($I = 0.1$) appears to eliminate the residual liquid-junction potential for the TES and HEPES buffers, although a potential difference of about 0.9 mV (0.015 pH unit) persists for the Tris buffer.

Calculations of residual liquid-junction potentials by the Henderson equation lead to expected differences (in pH units) of 0.008 to 0.015 between the NBS blood buffer ($I = 0.1$) and solutions with ionic strength 0.16 (*13*). Using limiting ionic conductances at 25 °C when available and estimating those for HPO_4^{2-}, TES^-, $HEPES^-$, and Tris·H^+ from the conductances of ions of related structures, we find the following values for the potentials across the junction buffer||3.5 M KCl:

buffer solution	I	E_j, mV
1:3.5 Phosphate	0.1	1.9
P(0.10) + NaCl(0.06)	0.16	1.5
P(0.08) + NaCl(0.08)	0.16	1.4
P(0.06) + NaCl(0.10)	0.16	1.3
P(0.04) + NaCl(0.12)	0.16	1.3
1:1TES(0.04) + NaCl(0.12)	0.16	1.3
1:2TES(0.04) + NaCl(0.12)	0.16	1.3
1:2HEPES(0.04) + NaCl(0.12)	0.16	1.3
1:3Tris(0.05) + NaCl(0.11)	0.16	0.8

It is evident that the *residual* liquid-junction potential when the blood buffer ($I = 0.1$) is replaced by a TES buffer ($I = 0.16$), for example, should not exceed 0.6 mV (0.01 pH unit),

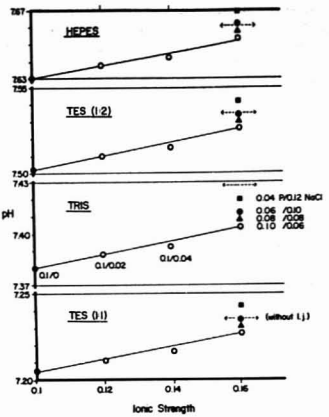

Figure 3. Effect of the ionic strength and composition of the reference standard on the operational pH values of TES, HEPES, and Tris buffer solutions of ionic strength 0.16 at 37 °C

whereas the observed differences are three times this figure. On the other hand, the calculations offer support for the conclusion that the residual liquid-junction potential is small when the pH of TES/NaCl and HEPES/NaCl buffers is measured with phosphate/NaCl standards of a comparable ionic strength. As plasma and other clinical media usually contain NaCl and have an ionic strength near 0.16, the choice of 0.06 phosphate + 0.1 NaCl, pH(S) = 7.297 at 37 °C, as a standard for routine clinical measurements has much to recommend it. Although this reference solution has a pH about 0.1 unit lower than that of blood plasma, errors in the emf/pH slope of commercial glass electrodes are not likely to introduce any significant error, if adequate temperature control is provided. Double standardization, above and below the pH of blood, is possible with the buffers 0.04TES + 0.04NaTES + 0.12NaCl, pH(S) = 7.235 at 37 °C, and 0.02TES + 0.04NaTES + 0.12NaCl, pH(S) = 7.535 at 37 °C. Unfortunately, to prepare these buffer solutions, one needs a standard solution of NaOH. It is worth noting that pH measurements at 37 °C and $I = 0.16$, based on the NBS blood buffer ($I = 0.1$), fall, on the average, 0.03 unit lower than those based on these reference buffers with ionic strength of 0.16.

Finally, the calculations show that the liquid-junction potential for the Tris buffer at $I = 0.16$ probably differs considerably from that of the other buffers studied. Correction for the residual liquid-junction potential of 0.5 mV between 0.06P + 0.1NaCl and the Tris/NaCl buffer adds 0.008 pH unit to the values derived from cell A and given in Table III. The corrected value of 7.419 at 37 °C still falls short of 7.427 found from measurements of cell B.

The low value of E_j calculated by the Henderson equation of Tris/NaCl buffers compared with the other buffer solutions of the same ionic strength is the result of a larger value of $\Sigma c_-\lambda_-^\circ - \Sigma c_+\lambda_+^\circ$, which, in turn, is caused by the fact that the mobility of the Tris·H^+ cation is lower than the mobilities of the cations (Na^+, K^+) of which the other buffer solutions are composed. One may attribute the lowered mobility to the high capability for hydrogen bonding to water afforded by the three hydroxyl groups of the Tris structure.

Supplementary Material Available: Tables (1 page) containing emf data for TES/NaCl and HEPES/NaCl solutions over the temperature range 5 to 50 °C will appear following these pages in the microfilm edition of this volume of the journal.

Photocopies of the supplementary material from this paper or microfiche (105 × 148 mm, 24X reduction, negatives) may be obtained from Business Operations, Books and Journals Division, American Chemical Society, 1155 16th St., N.W., Washington, D.C. 20036. Full bibliographic citation (journal, title of article, author) and prepayment, check or money order for $5.50 for photocopy ($7.00 foreign) or $3.00 for microfiche ($4.00 foreign) are required.

LITERATURE CITED

(1) "Manual of Symbols and Terminology for Physicochemical Quantities and Units", IUPAC, Butterworths, London, 1970, p 33.
(2) R. A. Durst and B. R. Staples, *Clin. Chem.* (*Winston-Salem, N.C.*), **18**, 206 (1972).
(3) R. G. Bates and R. A. Robinson, *Anal. Chem.*, **45**, 420 (1973).
(4) R. G. Bates, R. N. Roy, and R. A. Robinson, *Anal. Chem.*, **45**, 1663 (1973).
(5) S. J. G. Semple, G. Mattock, and R. Uncles, *J. Biol. Chem.*, **237**, 963 (1962).
(6) J. H. Ladenson, C. H. Smith, D. N. Dietzler, and J. E. Davis, *Clin. Chem.* (*Winston-Salem, N.C.*), **20**, 1337 (1974).
(7) R. A. Durst and R. G. Bates, in "Blood pH, Gases, and Electrolytes", R. A. Durst, Ed., *NBS Spec. Publ.*, **450**, Washington, D.C., 1977, p 247.
(8) C. C. Westcott and T. Johns, *Appl. Res. Tech. Rept.*, **542**, Beckman Instruments, Inc., Fullerton, Calif.
(9) R. G. Bates, "Determination of pH, Theory and Practice", 2nd ed., Wiley, New York, N.Y., 1973.
(10) C. A. Vega and R. G. Bates, *Anal. Chem.*, **48**, 1293 (1976).
(11) R. G. Bates, E. A. Guggenheim, H. S. Harned, D. J. G. Ives, G. J. Janz, C. B. Monk, J. E. Prue, R. A. Robinson, R. H. Stokes, and W. F. K. Wynne-Jones, *J. Chem. Phys.*, **25**, 361 (1956); **26**, 222 (1957).
(12) R. G. Bates and E. A. Guggenheim, *Pure Appl. Chem.*, **1**, 163 (1960).
(13) A. H. J. Maas, ref. 7, p 195.
(14) A. H. J. Maas, private communication.
(15) R. G. Bates, B. R. Staples, and R. A. Robinson, *Anal. Chem.*, **42**, 867 (1970).
(16) H. S. Harned and B. B. Owen, "The Physical Chemistry of Electrolytic Solutions", 3rd ed., Reinhold, New York, N.Y., 1958, Chap. 14.

RECEIVED for review March 16, 1978. Accepted April 12, 1978. This work was supported in part by the National Science Foundation under Grant OCE76 24384.

Differential Pulse Polarographic Determination of Molybdenum at Parts-per-Billion Levels

Paula Bosserman and Donald T. Sawyer*

Department of Chemistry, University of California, Riverside, California 92521

Albert L. Page

Department of Soil and Environmental Sciences, University of California, Riverside, California 92521

A new method for the determination of molybdenum at trace levels has been developed, which is based on the electrochemical reduction of dioxobis(8-quinolinolato)molybdenum(VI). The complex is formed and extracted from the sample matrix into chloroform prior to its reduction at −1.08 V vs. SCE in dimethyl formamide. Only tungsten co-extracts and it does not interfere with the analysis. A linear calibration curve is obtained for the concentration range from 0.1 μM (9.6 ppb) to 100 μM (9.6 ppm). The method has been applied to plant samples that have been grown on fly-ash amended soils.

Numerous analytical methods have been developed for the determination of molybdenum (*1*). Among the most common are the spectrophotometric analysis of $Mo(SCN)_5$ (*2*) and flameless atomic absorption spectrometry (*3*). Although these methods are reasonably sensitive, they are subject to numerous interferences. Other sensitive methods for the determination of molybdenum include neutron activation analysis and x-ray fluorescence spectrometry. The detection limit for neutron activation analysis is several nanograms for a 10-h irradiation with a flux of 10^{13} neutrons cm^{-2} s^{-1} (*4*). A detection limit of 72 ng of molybdenum has been reported for x-ray fluorescence spectrometry (*4*). Both of these methods require the use of elaborate and often unavailable instrumentation. Furthermore, sensitive neutron activation methods for molybdenum require long irradiation times. A method based on the EPR spectrum of Mo(V) (*5*) is a variant of the $Mo(SCN)_5$ spectrophotometric procedure. Although it is sensitive, the response is nonlinear and provides poor precision. Inductively coupled plasma emission spectroscopy also offers a sensitive method of molybdenum analysis with a detection limit of 5 ng/mL (*4*). This method also is subject to matrix interferences.

Several polarographic methods for the determination of molybdenum have been developed. These include Mo(VI) by anodic stripping voltammetry at mercury (*6*) and graphite (*7*) electrodes. In both cases, the limit of detection is 5 μM.

The sensitivity of molybdenum determinations can be enhanced by the use of solvent extraction to both isolate and concentrate molybdenum complexes. Molybdenum(VI) forms an especially useful complex with 8-quinolinol (8-hydroxyquinoline, oxine, HQ) in acidic solution which can be quantitatively extracted into chloroform (*8*). This complex also can be extracted into isobutyl methyl ketone and ethyl acetate (*9*). Polarographic studies have established that the bis(8-quinolinolato)molybdenum(VI) complex has a reduction half-wave potential at −0.30 V vs. a Hg pool in isobutyl methyl ketone and ethyl acetate, and at −0.46 V vs. a Hg pool in chloroform. The voltammetric behavior of the Mo(VI)−8-quinolinol complex in dimethyl sulfoxide at a platinum working electrode has been described (*10*). A quasi-reversible peak at −1.15 V vs. SCE is observed for the complex, and free ligand is not reduced in this system at potentials less negative than −1.95 V vs. SCE.

Differential pulse polarography has been demonstrated to be a sensitive voltammetric method for the analysis of many trace metals. Although most differential pulse polarographic methods have been developed for aqueous media, the selectivity and preconcentration of solvent extraction has led to the present study. This has resulted in a method for the

0003-2700/78/0350-1300$01.00/0

determination of the Mo(VI) oxine complex in aprotic solvents that is rapid, selective, and sensitive to trace levels of molybdenum in biological matrices.

EXPERIMENTAL

Apparatus. Differential pulse polarograms were obtained by use of a Princeton Applied Research Model 174A Polarographic Analyzer using a three-electrode system, and a Hewlett-Packard Model 7040A X-Y recorder. The electrochemical cell consisted of a 100-mL electrolytic beaker and a Leeds and Northrup polyethylene electrochemical cell top. The cell top had provision for inserting a dropping mercury electrode, which was used as the working electrode, a reference electrode, an auxiliary electrode, a bubbler used to deaerate the solutions with argon, and a short piece of glass tubing used to flow argon over the cell while the polarograms were recorded.

A tapered dropping mercury electrode capillary tube was connected to a mercury reservoir by means of Tygon tubing. Inserted in the tubing was a platinum wire contact which had been sealed in soft glass. A Princeton Applied Research Model 174/70 drop knocker was used to obtain reproducible drop times. The reference electrode consisted of a silver wire coated with silver chloride in a Pyrex tube closed with an unfired Vycor tip. The electrode was filled with a solution of tetramethylammonium chloride with the concentration adjusted such that the electrode potential was 0.00 V vs. SCE. The auxiliary electrode was a platinum flag sealed in soft glass. Neither an auxiliary compartment nor a Luggin capillary was used. A Leeds and Northrup pH meter equipped with a Broadly James Corp. combination pH electrode was used for all pH measurements.

Reagents. Dioxobis(8-quinolinolato)molybdenum(VI) ($Mo^{IV}O_2Q_2$) was prepared by the method of Isbell (*10*) The product was filtered and washed three times with methanol. It was then dried under vacuum for four days and stored under vacuum. Stock solutions of 1.00×10^{-3}M $Mo^{VI}O_2Q_2$ in dimethyl sulfoxide (DMSO), propylene carbonate (PC), and dimethyl formamide (DMF) were prepared by use of Burdick and Jackson "distilled in glass" solvents. All of the electrochemical studies made use of these solvents. Tetra-*n*-butylammonium perchlorate was obtained from Frederick Smith Chemical Company and was used as the supporting electrolyte. Stock solutions of Mo(VI) were prepared by dissolving in distilled water Mallinckrodt ammonium molybdate ($(NH_4)_6Mo_7O_{24}\cdot 4H_2O$) which had been dried for 2 h at 110 °C. A 1% solution of 8-quinolinol in chloroform was made by use of Matheson, Coleman, and Bell 8-quinolinol and Mallinckrodt reagent grade chloroform. Stock solutions of EDTA were prepared by dissolving J. T. Baker Na_2H_2EDTA in distilled water. Bethlehem triple distilled instrument grade mercury was used for the dropping mercury electrode.

Procedure. The differential pulse polarogram was recorded between an initial potential of −0.80 V and a final potential of −1.40 V. A scan rate of 2 mV/s was used with a modulation amplitude of 25 mV. A drop time of 1 s was obtained by use of the mechanical drop knocker. The low pass filter and the noise filter on the mechanical drop knocker were left off. Calibration curves were prepared by the addition of $Mo^{VI}O_2Q_2$ to a cell that contained 50 mL of solvent with 0.1 M TBAP as supporting electrolyte. For some of the differential pulse polarograms 20 μL of concentrated acetic acid was added to the cell solution. Prior to the polarographic analysis the cell solutions were degassed for 5 min with argon.

RESULTS AND DISCUSSION

Molybdenum in the form of the dioxobis(8-quinolinolato)molybdenum(VI) complex ($Mo^{VI}O_2Q_2$) can be determined effectively by differential pulse polarography in a dimethyl formamide (DMF) solvent system. Figure 1 illustrates the differential pulse polarograms for 0.1 μM and 1.0 μM $Mo^{VI}O_2Q_2$ in DMF. The peak current at −1.08 V vs. SCE is directly proportional to the concentration of molybdenum, as illustrated by the calibration curves of Figure 2. The response is linear from 0.1 μM to 100 μM molybdenum if the sample solution contains 7 μM acetic acid.

Selection of Solvent. Because the Mo(VI) oxine complex is reasonably soluble in dimethyl sulfoxide (DMSO) and this

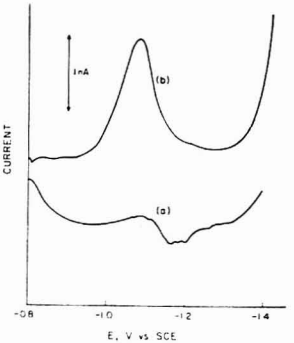

Figure 1. Differential pulse polarograms for dimethylformamide solutions that contain (a) 0.1 μM and (b) 1.0 μM Mo(VI)–8-quinolinol, 0.1 M TBAP, and 7 μM acetic acid

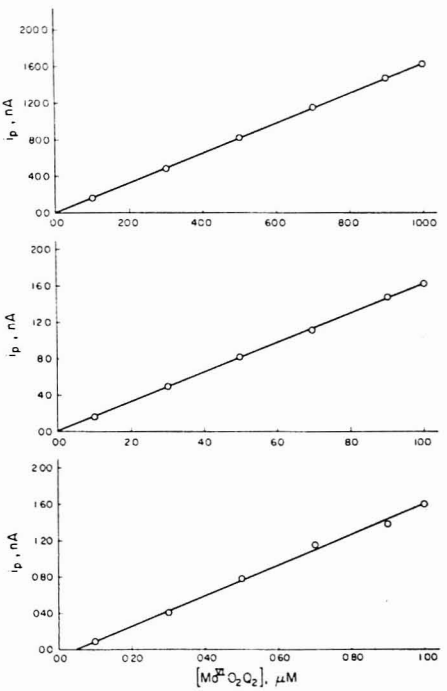

Figure 2. Calibration curves for the peak current of Mo(VI)–8-quinolinol as a function of its concentration in DMF that contains 7 μM acetic acid and 0.1 M TBAP as supporting electrolyte

represented a solvent with known electrochemistry for the complex (*10*), DMSO received first consideration for the determination of molybdenum. For a DMSO solvent with 0.1 M tetra-*n*-butylammonium perchlorate (TBAP) as the supporting electrolyte the detection limit for $Mo^{VI}O_2Q_2$ is 1 μM. However, the calibration curve is not linear because of the appearance of a doublet peak at concentrations of molybdenum above 18 μM. Below this concentration, $Mo^{VI}O_2Q_2$ is reduced at a peak potential of −1.04 V vs. SCE, and for

Table I. Analytical and Extraction Efficiency for Molybdenum as $Mo^{VI}O_2Q_2$ from an Aqueous Solution of $(NH_4)_6Mo_7O_{24}\cdot 4H_2O$

μmol added	μmol found	% recovery
0	0	-
1.0×10^{-3}	1.2×10^{-3}	120
5.0×10^{-3}	5.1×10^{-3}	102
1.0×10^{-2}	1.1×10^{-2}	110
5.0×10^{-2}	4.9×10^{-2}	98
1.0×10^{-1}	1.1×10^{-1}	110
5.0×10^{-1}	4.6×10^{-1}	92

concentrations above 80 μM the complex is reduced at −1.10 V.

Propylene carbonate also received consideration as a solvent system. With it and 0.1 M TBAP as the supporting electrolyte, linear calibration curves are obtained for the concentration range from 0.5 μM to 100 μM $Mo^{VI}O_2Q_2$. Peak splitting does not occur within the concentration range. However, the quality of the Burdick and Jackson propylene carbonate was highly variable. A contaminant often appeared with a reduction peak at −1.09 V. Vacuum distillation did not result in a significant improvement.

The deficiencies of DMSO and propylene carbonate prompted us to try dimethylformamide (DMF) as a solvent for the determination of $Mo^{VI}O_2Q_2$. In DMF with 0.1 M TBAP as the supporting electrolyte, the detection limit for molybdenum is 0.2 μM. For these conditions, the calibration curves are not linear because of the same peak splitting phenomenon that is observed in DMSO. The addition of a small amount of concentrated acetic acid to the cell solution (about 7 μM) eliminates this problem at all concentrations and results in linear calibration curves. Addition of acetic acid increases the peak current for $Mo^{VI}O_2Q_2$ at all concentrations and causes the reduction peak potential to be stable at −1.08 V vs. SCE. Figure 3 illustrates the effect of acetic acid concentration on the peak current for the Mo(VI)-oxine complex in DMF.

Quality of Extraction. To test the extraction procedure, known amounts of ammonium molybdate have been extracted from distilled water according to the method of Morrison and Freiser (*8*). To a beaker that contains known amounts of ammonium molybdate in approximately 50 mL of distilled water is added 5 mL of 0.02 M EDTA solution. The solution is diluted to about 100 mL and the pH adjusted to pH 1.55 by use of concentrated NaOH and 3 M HCl. The solution is then transferred to a 250-mL separatory funnel and extracted twice by shaking for 2 min with 10-mL portions of a 1% solution of 8-quinolinol in chloroform. The chloroform layer is then transferred to an electrochemical cell, and the chloroform removed by evaporation at room temperature. Next, 10 mL of DMF that contains 1 mmol of TBAP and 0.07 mmol of acetic acid is added to the cell. The differential pulse polarogram is recorded after the solution is deaerated with argon for 5 min, and the peak current compared to the calibration curves to determine the percent recovery. Table I summarizes the results. Theoretically, 99% of the molybdenum should be extracted.

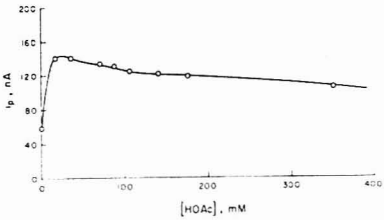

Figure 3. Dependence of peak current for the reduction of $Mo^{VI}O_2Q_2$ in DMF (0.1 M TBAP) as a function of the concentration of acetic acid

Applications. The differential pulse polarographic method has been applied to the determination of molybdenum in plants that have been grown on fly-ash amended soils. Two types of plant materials, alfalfa and fescue, have been analyzed by use of a combustion procedure. Approximately 2.5 g of air-dried plant material are placed in Vycor crucibles and dry-ashed in a muffle furnace at 550 °C for 8 h. (Attempts to wet-ash plant samples failed because of incomplete oxidation of the organic matter.) After ashing, the samples are allowed to cool to room temperature. The ash is then dissolved in 3 M hydrochloric acid and diluted to exactly 50 mL with 3 M hydrochloric acid. Occasionally, a small amount of residue does not dissolve in the acid. In these cases, the sample is centrifuged until all of the particulate matter is separated from the bulk of the solution. For the purposes of evaluating the procedure, each dry-ashed and dissolved sample has been divided into two portions to test for interferences and percent recovery. Ten-mL aliquots of each portion have been extracted by the previously-described procedure. One of these is analyzed by the differential pulse polarographic procedure. Then, by means of the standard addition method, the sample is spiked with a known amount of $Mo^{VI}O_2Q_2$ and reanalyzed for molybdenum. The results confirm that the reduction current only is due to the presence of molybdenum and that interferences are not extracted. These results are in accord with the expectation that only the molybdenum and tungsten oxine complexes are extracted into chloroform at pH 1.55.

The second portion of sample solution has been extracted and analyzed in the usual manner except that, before extraction, a known amount of ammonium molybdate has been added to the sample solution to determine the efficiency of the extraction process.

The results are summarized in Table II and are compared to the results that are obtained by the $Mo(SCN)_5$ spectrophotometric method (*11*). The differential pulse polarographic method provides a sensitive, selective means for the determination of trace levels of molybdenum in environmental samples. By use of a solvent extraction cleanup, interferences are excluded from the electrochemical solution. The latter has a detection limit of 0.1 μM Mo(VI) oxine; a linear peak

Table II. Determination of Molybdenum in Plant Samples

	molybdenum content			
sample	differential pulse polarography, ppm	standard addition, differential pulse polarography, ppm	spectrophotometry, ppm	extraction efficiency, %
fescue 1	6.6	6.6	5.2	94
fescue 2	1.7	1.7	2.4	100
alfalfa 1	5.6	4.8	5.1	112
alfalfa 2	2.1	2.4	1.5	95
alfalfa 3	5.0	4.3	2.7	97

current response is obtained up to concentrations of 100 μM.

ACKNOWLEDGMENT

We are grateful to Tony Gange of the Department of Soil and Environmental Sciences, University of California, Riverside, for supplying the plant samples and the comparison analyses.

LITERATURE CITED

(1) A. I. Busev, "Analytical Chemistry of Molybdenum", Academy of Sciences of the U.S.S.R., Moscow, 1962 (Israel Program for Scientific Translators, Jerusalem, 1964).
(2) I. M. Koltoff, E. B. Sandell, E. J. Meeham, and S. Bruckenstein, "Quantitative Chemical Analysis", 4th ed., Macmillan, New York, N.Y., 1969, p 1136.
(3) D. A. Segar and A. Y. Cantillo, in "Analytical Methods in Oceanography", T. R. P. Gibb, Jr., Ed., Chap. 7, Advances in Chemistry, No. 173, American Chemical Society, Washington, D.C., 1975.
(4) J. J. Dulka and T. H. Risby, *Anal. Chem.*, **48**, 640A (1976).
(5) G. Hanson, A. Szabo, and N. D. Chasteen, *Anal. Chem.*, **49**, 461 (1977).
(6) P. Lagrange and J.-P. Schwing, *Anal. Chem.*, **42**, 1844 (1970).
(7) V. V. Pnev, G. N. Popov, and V. G. Nagarev, *Zh. Anal. Khim.*, **28**, 2050 (1973).
(8) G. H. Morrison and H. Freiser, "Solvent Extraction in Analytical Chemistry", John Wiley and Sons, New York, N.Y., 1957.
(9) R. M. Dagnall and S. K. Hasanuddin, *Talanta*, **15**, 1025 (1968).
(10) A. F. Isbell and D. T. Sawyer, *Inorg. Chem.*, **10**, 2449 (1971).
(11) C. M. Johnson and T. H. Arkley, *Anal. Chem.*, **26**, 572 (1954).

RECEIVED for review March 23, 1978. Accepted May 19, 1978. The study was supported by the National Science Foundation under Grant No. CHE-76-24555, and by the Kearney Foundation of Soil Science, University of California.

Differential Pulse Polarography of Phenylarsine Oxide

J. H. Lowry,* R. B. Smart, and K. H. Mancy

Department of Environmental & Industrial Health, The Environmental Chemistry Laboratory, 2530 School of Public Health I, The University of Michigan, Ann Arbor, Michigan 48109

Differential pulse polarography was applied to analyze for phenylarsine oxide (PAO) in aqueous solutions at different pH values. Optimization of the instrumental artifacts resulted in a detection limit of 10^{-6} M PAO at pH 7.3, a relative standard deviation of 1.7%, and a maximum sensitivity of 450 μA/mM PAO. The polarographic reduction of phenylarsine oxide was found to be pH dependent. Cyclic voltammetry and coulometry were used to characterize the electrode process.

Several studies have been reported on the polarographic reduction of organic arsenic species (*1–5*). This interest is the result of the use of these compounds as herbicides (*6*) as well as the fact that organic arsenic compounds may be produced from inorganic arsenic by natural biological processes (*7*).

The determination of inorganic arsenic by differential pulse polarography (DPP) (*8*) and differential pulse anodic stripping voltammetry (*9*) has been reported previously. The polarographic reduction of dimethylarsinic acid and methylarsonic acid has also been reported (*3*). Bess et al. (*4*) studied the DPP of a series of alkylarsonic and dialkylarsinic acids below pH 2. They found the peak potentials were pH dependent, shifting to more anodic values at lower pH values. Recently, Bess et al. (*5*) reported on the DPP of aromatic arsonic and arsinic acids. They found peak potentials as well as peak currents were pH dependent below pH 2.

Phenyl arsonic acid and phenyl arsonous acid were studied extensively by Watson and Svehla (*1, 2*) using dc polarography at a DME. They suggested that phenylarsine oxide (PAO) existed in aqueous solution as phenyl arsonous acid and the diffusion current was pH independent. Unfortunately, above pH 2 their waves were poorly formed and exhibited broad maxima. No data were presented above this pH, and most of the work was carried out in 0.1 M HCl at concentrations below 1×10^{-4} M, where PAO showed two main reduction processes. The half-wave potentials were shown to be pH dependent as the reduction processes became increasingly irreversible with increasing pH. A reaction scheme for PAO in 0.1 M HCl was proposed, where the reduction product reacts with the electroactive species with the formation of an insoluble polymeric product. The first wave was attributed to the reduction of PAO to phenylarsine, where each mole of phenylarsine combines with an additional two moles of PAO to form the insoluble polymeric product. The second wave was due to an increase in the fraction of PAO molecules that undergoes reduction to phenylarsine and a decrease in the fraction of PAO molecules that reacts with the phenylarsine. At this wave there is a net increase in the average number of electrons consumed per molecule of PAO. Further information on the reaction schemes can be found in their original article.

PAO is used as a titrant for the direct and indirect determination of residual chlorine and ozone in water and wastewater (*10*). Preliminary investigations on the direct measurement of PAO by DPP indicate that this technique is a promising method for lowering the detection limits in the indirect measurement of these oxidants (*11*). Since the control of pH is a necessary consideration in free and combined chlorine analysis with PAO (*10, 12*) as well as the stability and measurement of ozone (*10, 13*), an investigation of the effect of pH on the DPP of PAO was mandatory.

In the following discussion we describe the DPP behavior of PAO and suitable conditions for analysis. For the purpose of analytical method development, the effect of pH on the reduction of PAO was investigated, and the reduction was shown to have strong pH dependence. This is in contrast to earlier findings by Watson and Svehla (*1, 2*), emphasizing the need for a better understanding of the reduction processes. In addition to investigating the reduction processes, we have optimized instrumental artifacts (*14*) for the DPP technique, resulting in a highly reproducible analysis of PAO whose sensitivity is pH dependent.

EXPERIMENTAL

Apparatus. A Princeton Applied Research, Inc. (PAR) Model 174 Polarographic Analyzer and a Model 174/50 drop timer were used. A PAR Model 175 Universal Voltage Programmer was used for cyclic voltammetry. Temperature studies were conducted using the PAR Model 9350 water jacketed cell with a Haake TP-42

0003-2700/78/0350-1303$01.00/0

Table I. Constant Ionic Strength Buffers, $\mu = 0.025$

pH	buffer composition
1-4.8	$HCl-HC_2H_3O_2-KCl$
4.8-5.2	$HC_2H_3O_2-NaOH-KCl$
6.3-7.6	$Na_2HPO_4-KH_2PO_4$
8.3-8.9	$H_3BO_3-Na_2B_4O_7$
10.5	$NaHCO_3-Na_2CO_3$
12	$NaOH-HCl-KCl$

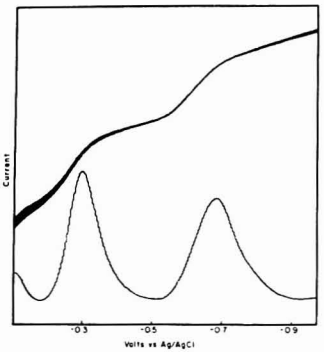

Figure 1. DC and DP polarograms of 2.57×10^{-5} M PAO at pH 1.8

constant temperature recirculating water bath. Coulometric experiments were performed with a PAR Model 379 coulometer and Model 377 cell system using a mercury pool electrode and 5 mL of electrolyte. Current was recorded on either a Houston Omnigraphic Model 200 X-Y recorder or a Honeywell Model 194 strip chart recorder.

A double Vycor junction Ag/AgCl reference electrode with a potential of −40 mV vs. SCE was used for all experiments. A platinum wire was used as the counter electrode. A Metrohm E-410 HMDE was used for cyclic voltammetry, and a DME with a natural drop time of 3 s at 49.5 cm with a flow of 3.05 mg/s was used for all polarograms unless otherwise stated.

Reagents. All chemicals were reagent grade and used without further purification. Triple distilled mercury was used throughout. All water was passed through mixed bed ion-exchange resins and triple glass distilled. Constant ionic strength buffers were prepared according to Perrin and Dempsey (*15*) and are given in Table I. Stock PAO solution (2.5×10^{-3} M) was prepared according to the standard method (*10*).

RESULTS AND DISCUSSION

As a preliminary examination, a dc polarogram of 2.5×10^{-5} M PAO at pH 1.8 was run and is shown in Figure 1. The DPP polarogram of the same solution is also given for comparison. Since Triton-X 100 and a high degree of damping were used to obtain the dc polarogram in Figure 1, Tast polarograms were run for the first reduction wave of 6.25×10^{-6} M PAO at pH values 1.8 and 8.7 ($\mu = 0.025$) to observe the effect of pH on the diffusion current and half-wave potential. The diffusion currents were 0.186 μA with an $E_{1/2}$ of −0.200 V and 0.06 μA with an $E_{1/2}$ of −0.756 V at pH 1.8 and 8.7, respectively.

Since our goal was the development of a sensitive technique for the analysis of PAO, further studies required the use of DPP. Using constant ionic strength buffers (*16*), 3.08×10^{-6} M PAO was examined throughout the pH range 1.8 to 12.5. In general, PAO exhibited three reduction peaks, A, B, and C, with varying pH dependencies, as shown in Figure 2. Two unresolved peaks, B and C, occurred at the more cathodic potential. At low pH, peak B predominates; while at high pH value, peak C predominates. At about pH 4.7, both peaks B

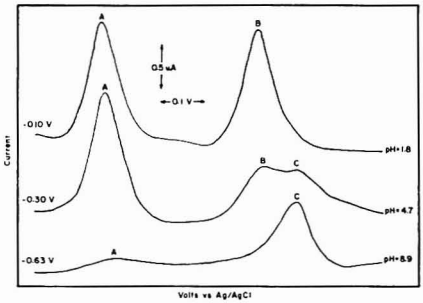

Figure 2. DPP of PAO at various pH values. [PAO] = 3.08×10^{-6} M; scan rate = 2mV/s; drop time = 2 s; pulse amplitude = 100 mV; ionic strength (μ) = 0.025

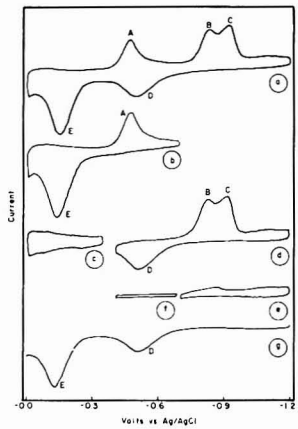

Figure 3. Cyclic voltammograms of PAO at an HMDE. [PAO] = 2.50×10^{-5} M; scan rate = 200 mV/s; HMDE area = 2.22 mm^2; $\mu = 0.025$; pH 4.7

and C approach equal height. Better resolution could not be obtained with decreases in scan rate (0.5 mV/s) or smaller modulation amplitudes (5, 10, 25 mV). The pH dependence of the current is inconsistent with the results reported by previous investigators (*1*, *2*). It is apparent that the pH dependence is not an artifact of DPP since Tast polarograms exhibit the same behavior. To determine if this behavior is characteristic of a DME only, an investigation of the mechanism of reduction of PAO by stationary electrode voltammetry and coulometry was initiated.

Voltammetry. The voltammetric behavior of PAO at an HMDE was investigated to aid in the resolution of the reduction processes. The experimental data reported below are uncorrected for spherical diffusion, charging current, or $1/\sqrt{t}$ decay of reduction current.

Cyclic voltammograms were obtained for 2.5×10^{-5} M PAO at a pH of 4.7 and are shown in Figure 3. It can be seen from this series of voltammograms that peak E represents the oxidation of the product of process A and peak D represents the oxidation of the product of process B and C.

In cyclic voltammetry, the mechanism of an electrode reaction can be studied by analyzing the variation of the experimental data with changes in the scan rate, concentration,

or pH. The peak current function, $i_p/C\sqrt{V}$ is a particularly useful diagnostic parameter in the evaluation of kinetic effects (*17*).

At a concentration of 1.18×10^{-5} M PAO and pH 4.7, the peak current function for A increased by 87% when the scan rate is increased from 0.1 V/s to 1.0 V/s while that for peak E decreased by 8%. On increasing the scan rate, peaks B and C formed a single peak (B) whose peak current function increased 23% over this scan range while that for peak D increased 134%. The peak potentials of peak A and peak B shifted cathodically 43 mV and 50 mV, respectively, over this scan range. The fact that cathodic shifts are observed together with the occurrence of anodic peaks implies that quasi-reversible electron transfers are involved in both reduction processes (*17*). On increasing the PAO concentration to 5.76×10^{-5} M from 1.18×10^{-5} M PAO at a scan rate of 0.2 V/s, the peak current function decreased 42% for A, 28% for B, 42% for C, and 23% for D. Very few processes other than adsorption cause the peak current function to both increase with increasing scan rate and decrease with increasing concentration (*18*).

A brief investigation, involving film stripping voltammetry, confirmed the presence of adsorption. At a given PAO concentration, adsorption and therefore i_p increased with increasing deposition time at a potential of −0.7 V for peak E and peak B in subsequent anodic and cathodic stripping voltammograms, respectively. No effect of the deposition time was observed on either peak A or B and C in cathodic stripping voltammograms after deposition at 0.0 V, or on peak D and E in anodic stripping voltammograms after deposition at −1.2 V (Figure 3E). This implies that the product of process A is adsorbed and is reduced in process B.

The diagnostic parameter, i_a/i_c, for product adsorption should approach unity at low scan rates (diffusion controlled) and increase at higher scan rates (adsorption controlled). For reactant adsorption the i_a/i_c ratio should approach unity at low scan rates and decrease at higher scan rates (*18, 19*). It has already been shown that the product of peak A is adsorbed; however, the i_a/i_c ratio for peak E and A decreased from 3.1 at 0.1 V/s to 1.5 at 1.0 V/s. Where reactant adsorption has been shown (peak B), the i_a/i_c ratio for peaks D and B increased from 0.6 to 1.1. The deviation from the theoretical response could imply that another kinetic component such as a coupled chemical reaction could be involved. In cyclic voltammetric studies of phenylarsonic acid, Bess et al. (*5*) reported that both product and reactant adsorption could occur depending on the concentration examined. They also found that the reduction process was not entirely diffusion controlled and that coupled chemical kinetics did contribute to the total reduction current.

The occurrence of a pH dependent step involved in the reduction of PAO is apparent by examination of the peak current function with changing pH. The peak current function of A decreased 52% on increasing the pH from 1.2 to 7.6, while that for peak B decreased 20%. The E_p for peak A shifted cathodically 0.068 V/pH unit and peak B shifted cathodically 0.073 V/pH unit.

These results indicate that the reduction of PAO is probably the result of stepwise quasi-reversible electron transfers. The adsorption of the product of the first reduction process undergoes reduction at the second electron transfer and this process is further complicated by a pH dependent coupled chemical reaction.

Coulometry. Exhaustive microcoulometry was performed in 0.1 M $HClO_4$ and at a pH of 1.8 in the constant ionic strength buffer. This was done at the dc polarographic plateaus of each wave in order to determine the number of electrons involved in the reduction process. Electrolysis of 2.36×10^{-7} mol of PAO at either −0.35 V or −0.5 V at mercury pool cathode for the first wave was inconclusive because of unexplainable changes in the background current in the pH 1.8 buffer. In contrast, electrolysis at −0.35 V in 0.1 M $HClO_4$ gave very reproducible results, permitting calculation of the number of electrons. Eight replicate experiments of two different stock solutions performed over a two-day period gave an average n value of 2.02 with a standard deviation of 0.02. Electrolysis of three additions of 1.28×10^{-6} mol and four additions of 2.36×10^{-6} mol of PAO in 0.1 M $HClO_4$ resulted in an average n value of 2.01 with a standard deviation of 0.05. During these electrolyses, a precipitate was obtained and mass spectra analysis showed monomeric, dimeric, and trimeric mass units of (C_6H_5As) as well as evidence of higher mass units. No evidence corresponding to a mass unit of $(C_6H_5As)_3O$ or its fragmentation pattern was observed (*1, 2*).

Electrolysis on the plateau of the second wave in the pH 1.8 buffer for seven replicate experiments for 2.36×10^{-7} mol of PAO resulted in a value for n of 3.92 ± 0.05. In 0.1 M $HClO_4$, electrolysis of 2.36×10^{-7} mol of PAO for seven experiments gave a value of 3.96 ± 0.08 for n. No precipitate was observed until the solution was allowed to stand exposed to air.

Electrolysis at −0.35 V in 0.1 M $HClO_4$ followed by electrolysis at −0.8 V for 2.36×10^{-7} mol of PAO resulted in 2 electrons per molecule at −0.35 V and another 1.6 electrons per molecule at −0.8 V. These results confirm the stepwise reduction mechanism indicated earlier by cyclic voltammetry. The fact that a total of only 3.6 electrons were found instead of 4 may be explained by adsorption of the insoluble product on the cell or electrodes, thereby preventing contact with the mercury. After electrolysis at −0.35 V, a differential pulse polarogram was scanned between +0.1 and −1.0 V and neither peak A or peak B was observed. The absence of peak B is due to the adsorption of the product of A on the mercury pool cathode.

A potential of +0.1 V was applied to the mercury pool, after electrolysis at −0.35 V, and a large anodic current flow was observed. A differential pulse polarogram was subsequently run and the reappearance of peak A and peak B was observed. This indicates that the product of the first electron transfer can be oxidized back to PAO and may represent the cyclic voltammetric peak E.

No DPP peaks were observed after electrolysis at −0.8 V followed by electrolysis at +0.1 V. Since cyclic voltammetry indicated that the second reduction is quasi-reversible, the product of that reduction must either be involved in irreversible chemical reaction or form a gas which is removed from solution by effusion.

Differential Pulse Polarography. *Effect of Temperature.* A common way of investigating the nature of the peak current of a reduction process is to observe the effect of temperature. Observing the change in peak currents with temperature can help to evaluate whether kinetic currents are involved. Diffusion controlled currents usually change by less than 2% per degree, while the effect on kinetic current may vary from 2 to 20% (*20*).

The change of i_p in the temperature range of 20–55 °C for all peaks as a function of pH are shown in Table II. These data indicate that most of the current is diffusion limited. Nevertheless, some kinetic current component is evident, which would be expected if a coupled chemical reaction is involved in the reduction mechanism. Increasing the temperature should decrease the peak height of adsorption controlled process; yet some adsorption processes can be diffusion controlled (*21*). Therefore, the temperature coefficients are not inconsistent with the adsorption observed by voltammetry.

Table II. Polarographic Characteristics of PAO

pH	peak A	peak B	peak C
	protons/electron		
1.8-3.8	1.1	1.1	...
4.7-6.8	1.8	...	2.00
	% $\Delta i_p/\Delta$°C		
1.8	+0.6	+4.2	...
7.6	−1.0	...	+4.0
8.9	+0.5	...	+1.1

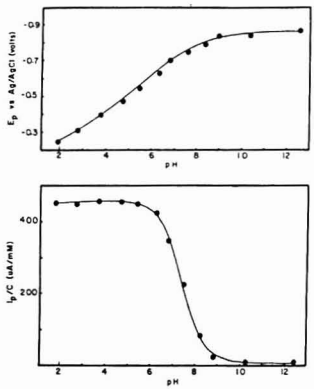

Figure 4. Dependence of peak current and peak potential for peak A on pH. [PAO] = 3.04 × 10^{-6} M; scan rate = 2 mV/s; drop time = 2 s; pulse amplitude = 100 mV; μ = 0.025

Effect of pH. PEAK A. The relationship between i_p and pH is shown in Figure 4 for peak A. The inflection point of this curve occurs at about pH 7.6. The plot of E_p vs. pH is also shown in Figure 4 and exhibits regions of pH dependence and independence. Linear regression analysis of the pH independent and dependent regions with solution of the appropriate equations results in a point of intersection at pH 7.6. The number of protons per electron (P/n) involved in the rate determining step can be determined from the slope of the line for the pH dependent region using the following equation:

$$E_p = \text{const} - \frac{RT}{F}\frac{P}{n}\,\text{pH}$$

The calculated values of P/n ratios are shown in Table II.

PEAKS B AND C. Figure 5 illustrates the dependency of i_p on pH for both peaks B and C. In the pH range 4 to 7, the measurement of peak currents and peak potentials was difficult due to the lack of peak resolution. The inflection point of the rising portion of the curve for peak C is approximately at pH 7.6. Above pH 10.3, no data were obtained because the peak coincided with the cathodic limit of the electrolyte.

The effect of pH on E_p for peaks B and C is also illustrated in Figure 5. Within the pH range where peak C could be distinguished from peak B (above pH 3.8), the effect of pH on E_p for C is the same as observed earlier for peak A. Using the same data analysis procedure, the lines of the pH independent and dependent regions were found to intersect at pH 7.6. The P/n ratios for B and C are given in Table II.

PEAK AREAS. The peak areas of A and the double peak, B plus C, measured with a planimeter, are expressed in

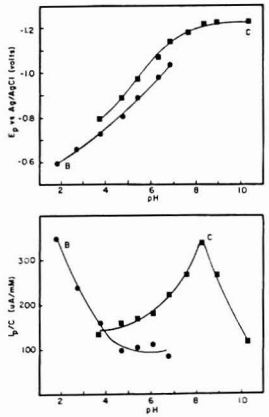

Figure 5. Dependence of peak currents and peak potentials on pH for peaks B and C. [PAO] = 3.08 × 10^{-6} M; scan rate = 2 mV/s; drop time = 2 s; pulse amplitude 100 mV; μ = 0.025

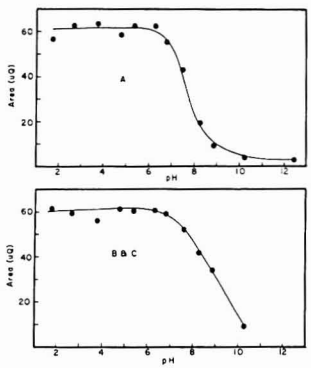

Figure 6. Peak areas as a function of pH. [PAO] = 3.08 × 10^{-6} M; scan rate = 2 mV/s; drop time = 2 s; pulse amplitude = 100 mV; μ = 0.025; μQ = microcoulombs

microcoulombs and illustrated in Figure 6 as a function of pH. The inflection point in the curve for peak A occurs at a similar pH to that reported above. These data correlate well with the pH dependence exhibited by the peak current functions of cyclic voltammetry. The DPP peak area of A decreased 52% over the pH range 1.2 to 7.6 while the cyclic peak current function of A decreased 52% over the same pH range. The area of B and C decreased 17% and the peak current function of B decreased 20%. This indicates that the mechanisms of reduction at an HMDE are similar to that of a DME.

In the pH independent range of 1.8 to 6.8, the ratio of the area of peak A to peak B plus C is 1.00 with a standard deviation of 0.007. In DPP, the increase in current at peaks B and C represents the difference in electron flow rate between that at A and that at B and C. Since the peak area ratio is 1.00, twice as many electrons flow at B and C than at A. This is consistent with the coulometric data of 2 electrons per molecule at A and 4 electrons per molecule at B and C.

Reversibility. For DPP, the peak half-width was shown to be dependent on both the amplitude of the applied pulse and the reversibility of the reduction process (22). The variation

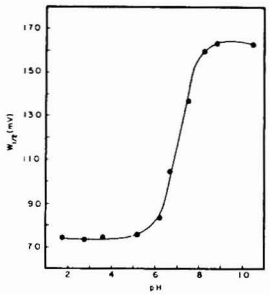

Figure 7. Dependence of peak half width ($W_{1/2}$) for peak A on pH. [PAO] = 3.08 × 10^{-6} M; scan rate = 2 mV/s; drop time = 2 s; pulse amplitude = 100 mV; μ = 0.025

in the reversibility of the reduction process for peak A vs. pH is shown in Figure 7. Smaller values of $W_{1/2}$ indicate a more reversible electrode process. Results shown in Figure 7 illustrate a change from reversible to irreversible conditions with increasing pH, and exhibit an inflection point at pH 7.6. These findings can be used to explain the shape of the i_p–pH curve for peak A (Figure 4). At low pH, high i_p values are indicative of a more reversible reduction; while at higher pH, the low i_p values are indicative of a less reversible reduction.

The change in the slope of the E_p–pH plots reflects this change of reversibility. At low pH, a $P/\alpha n_a$ of 1.1 would result in an α_a of 0.90 and at higher pH a $P/\alpha n_a$ of 1.8 would give α_a = 0.56. In DPP, using small values for the pulse amplitude (<25 mV) the peak half width ($W_{1/2}$) is given by the equation:

$$W_{1/2} = 3.52\,\frac{RT}{\alpha nF}$$

The value of α can be evaluated from this equation and a comparison can be made between the two reduction processes. The calculated values for A and B at pH 1.8 using this equation were 1.4 and 1.1, respectively. Using an n value of 2 for process B, since it represents a change in electron flow rate, the calculated value of α_A is 0.70 and α_B is 0.58. These α values indicate that A is more reversible than B.

The reversibility of the two electrode processes can be assessed by comparing the experimental and theoretical peak currents. For a reversible electrode reaction, the peak current is given by (*23*):

$$i_p = nFAC\sqrt{\frac{D}{\pi t}}\left(\frac{\sigma - 1}{\sigma + 1}\right)$$

where t = the time after pulse application when the current is measured, $\sigma = \exp(-\Delta EnF/2RT)$, and ΔE = the pulse amplitude. Substituting n = 2 and assuming a diffusion coefficient of 1 × 10^{-5} cm^2/s (*21*), an i_p/C value of 46.2 μA/mM was calculated under the conditions employed (t = 48 ms, A = 2.89 mm^2, ΔE = 100 mV). The PAR 174 has a tenfold instrumental gain in the DPP mode. With this consideration, our experimental i_p/C values of 450 μA/mM for peak A and 362 μA/mM for peak B at pH 1.8 were actually 45.0 μA/mM and 36.2 μA/mM. Obviously peak A correlates more closely with the reversible theoretical current. It is of interest to note that ratio of the peak current of A to peak B is 1.2 and the ratio of α_A/α_B is 1.2, both indicating the same difference in reversibility.

Effect of Concentration. Since dc polarography can be used to determine concentrations of PAO as low as 5 × 10^{-5} M (*1*, *2*), it was decided to limit the major portion of this DPP investigation to concentrations lower than 2 × 10^{-5} M. Generally, at a pH of 1.8, both peaks A and B increased linearly over the concentration range 1.23 × 10^{-7} M to 1.23 × 10^{-5} M.

A brief investigation of higher concentrations resulted in the same behavior observed by the previous investigators (*1*, *2*). Increasing the PAO concentration to 2.36 × 10^{-4} M, the current function (i_p/C) for peak A decreased about 20% while that for peak B decreased 30%. It was also observed that a peak 0.08 V cathodic of peak B, assumed to be peak C, started to appear. At a concentration of 2.36 × 10^{-3} M, two peaks situated between peak A and B appeared and the current functioning for peaks A and B continued to decrease. Peak C was now predominant over peak B. Watson and Svehla (*1*, *2*) observed the inhibition of peaks A and B, the predominance of peak C, and determined that the two additional peaks were due to adsorption related to the first reduction process. They also found that the height of peak C was proportional to the concentration even after the inhibition of B.

Reduction Mechanisms. Watson and Svehla found 1.3 electrons per molecule for the first reduction process and 2 electrons per molecule for the second reduction process (*1*, *2*). They proposed the following mechanisms for the reduction of PAO in 0.1 M HCl based on the identification of the suspected products and intermediates:

Process I:

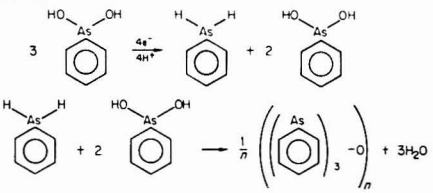

Process II:

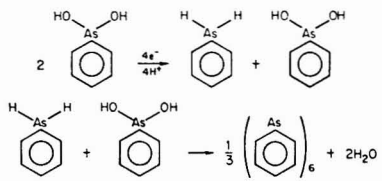

It is evident that the coulometric and mass spectra findings in our paper are not consistent with these mechanisms.

The discrepancy between the number of electrons per molecule found by Watson and Svehla (*1*, *2*) and our results possibly reflects the difference in the coulometric methods used. They performed a prolonged electrolysis of PAO and measured the subsequent decrease in wave height, while we based our interpretation on the exhaustive reduction of PAO. The products observed by Watson and Svehla probably represent intermediates formed in the bulk solution in the presence of PAO and not in the depleted zone at the electrode. These products can be further reduced during the exhaustive coulometry. Thus, the two mechanisms could represent initial and final states of the electroreduction of PAO.

We observed a pH dependence of the peak currents at a DME in contrast to the previous investigators (*1*, *2*). The reason for these differences is not clear. Our pH dependence has been shown not to be due to an artifact of DPP since Tast polarograms as well as cyclic voltammograms indicate a similar behavior. Perhaps the inconsistence can be partially explained by the fact that Watson and Svehla used solutions an order of magnitude more concentrated and the dc waves were poorly

formed and exhibited broad maxima above pH 2 (*1, 2*). It is not unlikely that the reduction mechanisms may change with concentration or media composition. It may appear that the inflection at pH 7.6 observed frequently in our study represents an apparent p*K* for PAO. However, the p*K* value for PAO was reported to be 11 (*24*). Therefore, the pH dependence must represent changing reversibility and/or the effect of coupled kinetics.

Based on our data as well as Watson and Svehla's mechanisms, a possible reaction path for the first wave is postulated:

Process I:

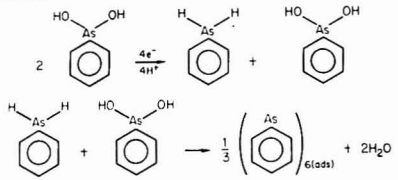

Watson and Svehla indicate that a 4-electron transfer would result in the formation of phenylarsine (gas). Therefore, based on our studies, the reaction path for the second wave would be as follows:

Process IIa:

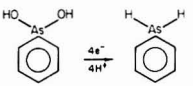

or, for a stepwise reduction:

Process IIb:

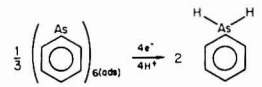

In consideration of our proposed reduction mechanism, it would appear that the fact that peak A is inhibited at higher concentrations while peak C continues to increase proportional to concentration, would be inconsistent with a stepwise reduction. However, the adsorption of the product of Process I is the most probable explanation of the inhibition of peak A and peak B. Coulometry and voltammetry did show that the product of Process I can be reduced at Process II. Therefore, a probable explanation of this observed phenomenon would be that after the product of Process I undergoes reduction (Process IIb) the additional current flow could be due to the direct reduction of PAO (Process IIa).

Analytical Considerations. *DPP.* Since the current–concentration relationships below 2×10^{-5} M PAO are pH dependent, any analytical methodology involving the DPP of PAO will require strict pH control. The optimum sensitivity is obtained by using peak A in the lower pH range. The variation of the sensitivity with instrumental parameters was investigated over a PAO range of 1.23×10^{-6} M to 1.23×10^{-5} M. At a pH of 7.3 and a natural drop time of 3.4 s, the effect of pulse amplitude (MA), artificial drop time (τ), and scan rate (ν) on the sensitivity (i_p/C) are found in Table III. The greatest sensitivity for DPP is obtained with the largest drop, slowest scan rate, and the largest pulse amplitude (*14*). A calibration curve prepared using these conditions (See Table III) over the PAO range of 1.23×10^{-7} M to 1.54×10^{-6} M showed a sensitivity of 234 μA/mM with a relative standard deviation of 1.7% as determined from seven replicates of 1.54×10^{-6} M PAO. The limit of detection was determined by dividing three times the background current by the sensitivity

Table III. Variation of Sensitivity with Instrumental Parameters; pH = 7.3, Initial Potential = −0.350 V, μ = 0.0025

MA, mV[a]	τ, s	ν, mV/s	i_p/C, μA/mM
100	2	2	190
50	2	2	78
25	2	2	33
100	1	2	129
100	0.5	2	77
100	2	5	148
100	2	10	99

[a] MA = pulse amplitude. τ = drop time. ν = scan rate. i_p/C = sensitivity.

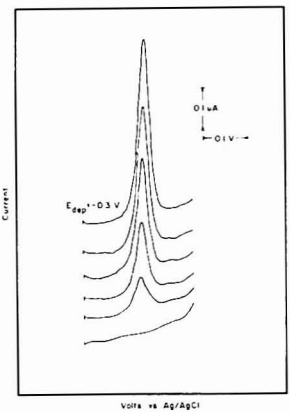

Figure 8. Differential pulse cathodic stripping voltammetry of PAO [PAO] = 2.36×10^{-8} M to 1.18×10^{-7} M; pH 1.2; HMDE area = 2.22 mm^2; τ_{dep} = 30 s; scan rate = 5 mV/s; pulse amplitude = 50 mV; pulse interval = 0.5 s

and was found to be 1.2×10^{-8} M PAO.

As mentioned earlier, this investigation was prompted by a desire to determine free chlorine in water. The standard titrimetric method (*10*) requires a pH range of 6.5 to 7.5 for the reaction of PAO with the free chlorine. This was the reason for choosing pH 7.3 for the above work. However, an even lower detection limit, approximately one-half that at pH 7.3, could be obtained in acidic media.

The analytical performance and versatility of this technique is being investigated by comparison with standard methods of analysis for oxidants in a variety of aqueous samples (*11*).

Stripping Voltammetry. The fact that the product of process A adsorbs and undergoes reduction at the second process at an HMDE suggested the possibility of determining lower levels of PAO by cathodic stripping voltammetry. A few experiments were conducted to investigate the analytical utility of this technique.

The production of the adsorbable species is controlled by the time that the potential at the HMDE is more cathodic than the first reduction process, yet more anodic than the second process. A differential pulse ramp was used because it often provides higher sensitivity using short deposition times. Utilizing a deposition time of 30 s at a potential of −0.3 V with an HMDE area of 2.22 mm^2 in a pH 1.2 buffer, the cathodic peak current was found to be proportional to the PAO concentration over the range 2.36×10^{-8} to 1.18×10^{-7} M PAO (Figure 8). Above this concentration range, the peak current became independent of the concentration. The sensitivity of the linear range was 3520 μA/mM. Seven

replicate determinations of 2.36×10^{-8} M PAO resulted in a relative standard deviation of 3.9%. Utilizing the method of Skogerboe and Grant (25) and the standard deviation of the 2.36×10^{-8} M PAO measurements, a detection limit of 2.3×10^{-9} M PAO was calculated.

The possibility of using the anodic peak E as well as coulometric stripping techniques is now under investigation for determining trace levels of PAO.

LITERATURE CITED

(1) A. Watson and G. Svehla, *Analyst (London)*, 100, 489 (1975).
(2) A. Watson and G. Svehla, *Analyst (London)*, 100, 573 (1975).
(3) R. Elton and W. E. Geiger, Jr., *Anal. Lett.*, **9**, 665 (1976).
(4) R. C. Bess, K. J. Irogolic, J. E. Flannery, and T. H. Ridgway, *Anal. Lett.*, **9**, 1091 (1976).
(5) R. C. Bess, K. J. Irogolic, J. E. Flannery, and T. H. Ridgway, *Anal. Lett.*, **10**, 415 (1977).
(6) E. A. Woolson, Ed., "Arsenical Pesticides", American Chemical Society, Washington, D.C., 1975.
(7) J. M. Wood, *Science*, **183**, 1049 (1974).
(8) D. J. Myers and J. Osteryoung, *Anal. Chem.*, **45**, 267 (1973).
(9) G. Forsberg, J. W. O'Laughlin, and R. G. Megargle, *Anal. Chem.*, **47**, 1586 (1975).
(10) "Standard Methods for the Examination of Water and Wastewater", American Public Health Association, 13th ed., 1971.
(11) J. H. Lowry, R. B. Smart, and K. H. Mancy, *Anal. Lett.*, **10**, 979 (1977).
(12) H. C. Marks and J. R. Glass, *J. Am. Water Works Assoc.*, **34**, 1227 (1942).
(13) W. Stumm, *J. Boston Soc. Civ. Eng.*, **45**, 68 (1958).
(14) J. H. Christie, J. Osteryoung, and R. A. Osteryoung, *Anal. Chem.*, **45**, 210 (1973).
(15) D. D. Perrin and B. Dempsey, "Buffers for pH and Metal Ion Control", John Wiley and Sons, New York, N.Y., 1974.
(16) P. J. Elving, J. C. Komyathy, R. E. Van Atta, C. S. Tank, and I. Rosenthal, *Anal. Chem.*, **23**, 1218 (1951).
(17) R. S. Nicholson and I. Shain, *Anal. Chem.*, **36**, 706 (1964).
(18) R. H. Wopshall and I. Shain, *Anal. Chem.*, **39**, 1514 (1967).
(19) R. H. Wopshall and I. Shain, *Anal. Chem.*, **39**, 1535 (1967).
(20) P. Zuman, "Progress in Polarography, Vol. II", P. Zuman, L. Meites, and I. M. Kolthoff, Ed., Wiley Interscience, New York, N.Y., 1962, Chap. XXIX.
(21) O. H. Muller, in "Physical Methods of Chemistry, Part IIA: Electrochemical Methods", A. Weissberger and B. W. Rossiter, Ed., Wiley Interscience, New York, N.Y., 1971, Chap. V.
(22) E. P. Parry and K. B. Oldham, *Anal. Chem.*, **40**, 1031 (1968).
(23) E. P. Parry and R. A. Osteryoung, *Anal. Chem.*, **37**, 1634 (1965).
(24) H. Eagle, R. B. Hogan, G. O. Doak, and H. Steinman, *J. Pharmacol. Exp. Ther.*, **76**, 221 (1940).
(25) R. K. Skogerboe and C. L. Grant, *Spectrosc. Lett.*, **3**, 215 (1970).

RECEIVED for review September 12, 1977. Accepted May 5, 1978. This work was partially supported by U.S., EPA Grant No. R804834-01-1.

Determination of Ammonia and Other Nitrogen Compounds by Polarography

J. D. McLean,* V. A. Stenger, R. E. Reim, M. W. Long, and T. A. Hiller

The Dow Chemical Company, Analytical Laboratories, Midland, Michigan 48640

A polarographic procedure is described for the determination of ammonia and primary amine compounds at levels below 1 ppm. It has been applied to water and brine samples and to reagent testing, where it can replace a distillation procedure currently employed. The method should also be useful in monitoring air quality. For reagent testing, total nitrogen impurities can be found if nitrate (including nitrite) is also determined polarographically. The determinations can be performed with either a differential pulse polarographic instrument or a recently introduced digital analyzer.

Standard methods (*1*, *2*) for the determination of ammonia nitrogen in water are either colorimetric, based on reaction with Nessler reagent or phenol and hypochlorite; or potentiometric, based on selective ion electrode procedures. A prior distillation is generally recommended to eliminate interfering substances. To determine ammonium compounds as impurities in chemical reagents (*3*), distillation followed by colorimetry with Nessler reagent is also employed. Nitrate or nitrite in reagents may be included as ammonia if a suitable reducing material such as aluminum or Devarda alloy is present during the distillation.

It would be advantageous to have another method for determining ammonia nitrogen, if the method were sufficiently sensitive and free from interferences so that distillation might be avoided. The behavior of ammonia at a dropping mercury electrode (DME) has been investigated by Nyman, Ragle, and Linde (*4*). The sensitivity is limited to concentrations above 10^{-3} M and the half-wave potential is in a region where interferences would be likely. Earlier, Norton and Mann (*5*) had studied a polarographic method based upon condensation of phthalaldehyde with ammonia. Reduction of the aldehyde wave allows detection of ammonia at 10^{-5} M, but a reaction time of 3 h or longer is required and, for practical work, a distillation is considered necessary.

Tur'yan and Zhantalai (*6*) reported the polarographic determination of 10^{-3}–10^{-5} M ammonium ion based on reaction with formaldehyde in an acidic buffer. The method was also applied in determinations of amino acids at the 10^{-2}–10^{-5} M level (*7*, *8*).

More recently, a differential pulse polarographic method for ammonia at 50 to 600 ppb in water has been recommended (*9*). Ammonia is allowed to react with excess formaldehyde, forming a reducible condensation product. A high blank, originally attributed to ammonia in the distilled water used, prevented extension to lower concentrations. In the present study, blanks of similar or even higher magnitude were encountered and were shown to be caused by an impurity in the formaldehyde. Purification is accomplished with a cation-exchange resin. Our tests indicate that with a sufficiently low blank, ammonia in city water can be detected at 25 ppb. The method is applicable also to the analysis of brine samples, to monitoring air quality, and to the testing of reagent grade chemicals.

For completeness in reagent testing for nitrogen compounds, it is desirable to have a simple polarographic method for oxidized forms of nitrogen in addition to that for ammonia. Kolthoff, Harris, and Matsuyama (*10*) have recommended such a procedure for nitrate, based on the catalytic effect of uranyl ion in an acid medium. Keilin and Otvos (*11*) noted that nitrite responds similarly. Various other elements, including several in the rare earth series, can also be employed to catalyze the electrochemical reduction of nitrate and nitrite. The literature has been reviewed by Boese, Archer, and

0003-2700/78/0350-1309$01.00/0

O'Laughlin (*12*), who recommended ytterbium and studied interferences. In the present paper, conditions suitable for applying the Kolthoff uranyl procedure to the testing of several reagent chemicals have been investigated.

EXPERIMENTAL

Reagents. So far as possible, the chemicals used were ACS Reagent Grade. In much of the work reported, 37% formaldehyde was purified by passing 100-mL portions through a 1.5 × 10-cm column of cation-exchange resin (Dowex 50 × 8, 50–100 mesh, hydrogen form) which previously had been washed in succession with 100-mL portions of methanol, deionized water, and 0.1 M acetic acid. The first 20 mL of formaldehyde was discarded and the remainder was stored in a brown glass bottle. Following conversion of the resin to the H^+ form, at least 400 mL of formaldehyde can be passed through the column before regeneration is required. Subsequent tests have shown that the blank can be further lowered by a factor of about 2 if the column length is doubled, and that regeneration with 1 N hydrochloric acid is effective. Even more simply, the impurity can be lowered still farther by adding 10 to 50 g of resin to a 1-lb bottle of formaldehyde and placing the bottle in a shaker for an hour or allowing it to stand overnight.

Acetate buffer was prepared by dissolving 10.4 g of sodium acetate trihydrate and 32 mL of glacial acetic acid in 200 mL of deionized water. Supporting electrolyte for ammonia or amine determination was usually prepared by mixing 5 mL each of this acetate buffer and prepurified formaldehyde.

The supporting electrolyte for nitrate determination contained 0.45 g of uranyl acetate dihydrate, 4.3 mL of hydrochloric acid, and 37.3 g of potassium chloride in water to make 1 L.

All solutions were prepared from water which had been passed through a Millipore deionization system. Deoxygenation was done with pre-purified nitrogen.

Apparatus. Polarograms were recorded using a Princeton Applied Research Model 174 Polarographic Analyzer and a Houston Model 2000 X-Y recorder, employing a drop time of 1 s, a scan rate of 2 mV/s, and a modulation amplitude of 50 mV. The working electrode was dropping mercury, the reference electrode saturated calomel (SCE), and the counter electrode, platinum. All experiments were performed at ambient room temperature, 23 ± 1 °C.

Analyses were also performed using a Brinkmann Model CPA/15 Computing Polarographic Analyzer (which operates as a dc polarograph) and a Metrohm Model E-410 hanging mercury drop electrode (HMDE). The drop size was that produced by a 5-division turn of the micrometer screw (~2.65 mm^2 surface area). The scan range for amine nitrogen was −0.60 to −1.10 V vs. SCE, at the rate of 60 s/scan. Polarograms from this system were recorded by a Heath-Schlumberger Model SR-255B strip-chart recorder with a range of 1 V full scale.

Procedure for Amine Nitrogen. Ten mL of supporting electrolyte and an appropriate amount of sample are transferred to a 25-mL volumetric flask and diluted to volume. The solution is heated on a steam bath 2.5 min, shaken, and heated an additional 2.5 min. Polarograms are recorded after cooling the solution to room temperature and deoxygenating the cell for 5 min with nitrogen. Blanks (reagents plus pure water) are run similarly and subtracted. Standards are run separately and confirmed for each sample system by spiking.

Procedure for Nitrate Nitrogen. Five mL of nitrate supporting electrolyte and an appropriate amount of sample are added to a 25-mL volumetric flask and diluted to volume. Polarographic scans are recorded from −0.60 to −1.10 V vs. SCE after bubbling with nitrogen for 5 min. A similar sample is prepared with the addition of a known amount of nitrate and scanned. Since the uranyl ion contributes some current at the potential of interest, a blank on the electrolyte and water is subtracted. The half-wave potential is pH dependent, but diffusion currents in this electrolyte can usually be measured at approximately −1.0 V vs. SCE. If pH adjustment is needed, it should be to 2.0 ± 0.3.

RESULTS AND DISCUSSION

Reaction. Ammonium ion reacts with excess formaldehyde in pH 4 acetate buffer to form an electroactive species which is reduced at $E_{1/2}$ = −0.88 V vs. SCE as shown in Figure 1.

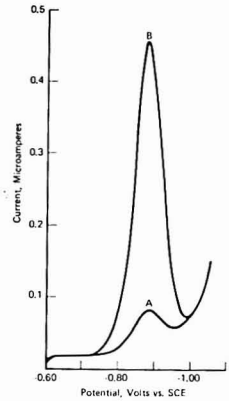

Figure 1. Differential pulse polarogram of ammonia-formaldehyde reaction product. (A) Blank. (B) 11.3 μg NH_4^+

The reactions of formaldehyde with ammonium ion have been reviewed by Walker (*13*). Werner (*14*) concluded that the first step of the reaction in acid solution yields a methylenimine salt;

$$CH_2O + NH_4Cl \rightarrow CH_2OHNH_2{\cdot}HCl \rightarrow CH_2{=}NH{\cdot}HCl + H_2O \quad (1)$$

Tur'yan and Zhantalai (*6*) also indicate that the reaction product is methylenimine (or hydroxymethylamine since formaldehyde is hydrated in aqueous solution). The product is stable in acid, but hexamethylene tetramine is formed when the acid is neutralized:

$$4CH_2{=}NH{\cdot}HCl + 4NaOH + 2CH_2O \rightleftharpoons (CH_2)_6N_4 + 4NaCl + 6H_2O \quad (2)$$

Polley, Winkler, and Nichols (*15*) confirmed the formation of hexamethylenetetramine, finding also that the reaction rate and yield increase with increasing pH. The instrument manufacturer's literature previously cited (*9*) suggested that hexamethylene triamine is formed, but presented no basis for such a conclusion.

Long ago Plöchl (*16*) demonstrated that methylamine can be prepared in a two-step reaction summarized by the equation:

$$2CH_2O + NH_4Cl \rightarrow CH_3NH_2{\cdot}HCl + HCOOH \quad (3)$$

As will be shown later, ammonia and methylamine behave somewhat differently in the polarographic method and it does not appear that the reaction product under our conditions is methylamine (which would react with excess formaldehyde). It should also be noted that while our formaldehyde concentrations are comparable with those of Plöchl, his ammonia concentrations were about a million times greater than those to be determined in the procedure.

In an acetate buffer at pH 4, hexamethylenetetramine (without added formaldehyde) does not yield a polarographic wave, indicating that it is not the electroactive species. In testing for ammonia, the wave height decreases with increasing pH, which is consistent with Equation 2. Further, the half-wave potential of the reaction depends upon the hydrogen-ion concentration. As shown in Table I, $\Delta E_{1/2}/\Delta pH$ is about −50 mV.

To account for the observed electrochemical reducibility of the reaction product, it seems likely that a carbon–nitrogen double bond is present. This would be consistent with Equation 1. If the active compound is an imine, reduction

Table I. Effect of pH on Half-Wave Potential of Ammonia-Formaldehyde Reaction Product

pH	$E_{1/2}$ vs. SCE
3.0	−0.80 ± 0.01
4.0	−0.85 ± 0.01
5.0	−0.90 ± 0.01
6.2	−0.98 ± 0.01

Table II. Repeatability of the Ion-Exchange Procedure for Removing Trace Impurities from Formaldehyde

batch	column length, cm	blank current, μA before	blank current, μA after
A	10	0.43 ± 0.04	0.058 ± 0.005
B	10	0.38 ± 0.04	0.048 ± 0.004
C	10	NA[a]	0.064 ± 0.005
D	10	NA	0.058 ± 0.005
E	10	NA	0.055 ± 0.005
F	20	NA	0.029 ± 0.003
	bottle test, g resin/lb		
G	10	NA	0.021 ± 0.003

[a] NA = not analyzed.

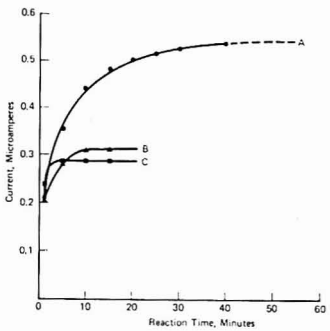

Figure 2. Time dependence of ammonia–formaldehyde reaction. (A) 20 μg NH_4^+ in sodium chloride solution (100 g/L), not heated. (B) 10 μg NH_4^+ in water, not heated. (C) 10 μg NH_4^+ in sodium chloride solution (100 g/L), heated

with two electrons should produce the corresponding amine. A value of $n = 2$ was obtained from the polarographic data, assuming a diffusion coefficient of 1×10^{-5} cm^2/s.

Kinetics. At ambient temperature, at least 15 min are taken for the ammonia–formaldehyde reaction to reach equilibrium (Figure 2). In sodium chloride solution (100 g/L), at least 40 min are required. Such variations in the reaction time would limit the utility of the method; however, by heating the solution on a steam bath the reaction period is reduced to 5 min. Once formed, the electroactive compound is stable for at least 2 h.

Blank. Preliminary tests confirmed the previous report (*9*) of a significant reagent blank. Further work traced this to the formaldehyde, which can absorb ammonia from the air or which may have been treated with a nitrogen-containing stabilizer (*17–19*). Presumably, a basic impurity could be removed by distillation of the formaldehyde from acid, but we chose to make use of cation exchange as described under Reagents. As shown in Table II, considerable purification could be achieved.

The stability of a formaldehyde solution stored in a brown glass bottle after cleanup is shown in Table III. No change

Table III. Stability of Formaldehyde Solution after Ion-Exchange Treatment

elasped time, days	blank current, μA
0	0.058 ± 0.006
21	0.058 ± 0.006
51	0.050 ± 0.005
82	0.063 ± 0.006

Table IV. Polarographic Determination of Ammonia in Sodium Chloride Solution (100 g/L)

sample	ppm NH_3 present	ppm NH_3 found[a]
A	0.25	0.28 ± 0.04
B	0.35	0.36 ± 0.03
C	1.00	0.92 ± 0.07
D	1.25	1.25 ± 0.10
E	2.00	2.05 ± 0.03

[a] Mean of triplicate determinations by pulse polarography.

Table V. Comparative Determination of Ammonia in Brine by Polarography and Selective Ion Electrode

sample	ppm NH_3[a]	ppm NH_3[b]
A	0.20 ± 0.03	0.26 ± 0.03
B	0.12 ± 0.02	0.13 ± 0.02
C	0.22 ± 0.03	0.15 ± 0.02
D	0.09 ± 0.01	0.12 ± 0.02
E	0.20 ± 0.02	0.13 ± 0.02
F	1.7 ± 0.10	1.7 ± 0.2[c]

[a] Pulse polarography. [b] Average results by ammonia-selective electrode on single distillates from alkaline solution. [c] No distillation—direct electrode determination.

was observed over a period of 3 months. However, to avoid possible contamination from the air, it is prudent to keep some cation-exchange resin in the bottle.

Analytical. With the Princeton instrument, the calibration curve is linear up to 30 μg NH_4^+ per 25 mL of final solution. The detection limit in water is about 25 ppb NH_4^+ with a 15-mL sample. Increasing ionic strength decreases the sensitivity of the method, e.g., the response in sodium chloride solution (100 g/L) is 0.81 μA/μg/mL as compared to 1.1 in water.

The accuracy and repeatability of the method were evaluated using sodium chloride solution (100 g/L) containing known amounts of ammonium chloride. Results, summarized in Table IV, show good accuracy and a repeatability of ±8% at the 1 ppm NH_3 level.

Ammonia in a series of process brine streams was determined using the polarographic method and the results were compared with those obtained by distillation followed by use of an ammonia-selective electrode. Results shown in Table V indicate fairly good agreement between the methods.

Recoveries and possible cross interference between NH_4^+ and NO_3^- were tested by adding known amounts of NH_4NO_3 to KBr followed by polarographic determination employing the two procedures. Excellent results were obtained as shown in Table VI.

Interfering Compounds. Various aliphatic, aromatic, and alkanol amines can also react with formaldehyde to form electroactive compounds. The resolution of the half-wave potentials is usually not sufficient, however, to allow qualitative identification. Nevertheless, certain peculiarities in behavior can in some cases reveal whether one is determining ammonia or another compound. The ammonia–formaldehyde

Table VI. Recovery of Ammonium and Nitrate from Pure Potassium Bromide

sample	ppm NH_4^+ [a]	ppm NO_3^- [a]
pure KBr (fused)	none detected at a limit of 1	none detected at a limit of 1
pure KBr + 23 ppm NH_4^+ and 78 ppm NO_3^-	24 ± 2	81 ± 4
pure KBr + 39 ppm NO_3^- and 11 ppm NH_4^+	10 ± 1	38 ± 2

[a] Average of duplicate determinations.

reaction appears to reach a stable equilibrium with time but, if one doubles the formaldehyde concentration, the wave height is also approximately doubled. Under the usual conditions, methylamine can be detected a little more sensitively (on a molar basis) than ammonia, but doubling the formaldehyde produces very little change. For hydrazine, the method is much more sensitive than for ammonia, but increasing the formaldehyde lowers the hydrazine response.

Hydroxylamine shows a double differential pulse wave with peaks at −0.75 and −0.87 V. The former wave gives sensitivity about equal to that of ammonia on a weight basis, while the latter is still more sensitive. Glycine has a single wave at −0.72 V and its molar sensitivity is close to that of ammonia.

Urea does not respond, probably because amides are usually nonreactive toward aldehydes. Thus the method is useful for determining ammonia in the presence of urea.

If the electroactive compound is an imine, no interference from secondary and tertiary amines would be expected. Actually, most commercial amines produce some response, but this can often be shown to be caused by a primary amine impurity. All of the primary amines tested have been found active. In general, as would be expected from diffusion theory, the response decreases as the size of the aliphatic group is increased.

Since sensitivities vary, the procedure is most useful when a single amine predominates. This is often the case in industrial hygiene air-monitoring of production facilities, when a compound in use must be monitored to protect personnel. Monoethanolamine in air has been successfully determined after collection in an impinger system using 0.1 M HCl as the absorber solution and air flow rates less than 1 L/min.

Behavior of Nitrite in the Method for Nitrate. As Keilin and Otvos (*11*) demonstrated, nitrite exhibits about three-fifths the molar response of nitrate in the polarographic method, but because nitrite is easily lost from an acid solution, it is recommended that the polarograms be run promptly. If, as in reagents testing, it is desired merely to report nitrate plus nitrite as nitrate, a single measurement will usually suffice. To obtain values for each component, the quoted authors determined the total response for nitrate plus nitrite, then oxidized the nitrite in a separate portion with hydrogen peroxide and determined the response again. Results for each component are calculated by solving simultaneous equations based on data determined with standards.

We have observed that nearly all nitrite can be expelled from the sample plus supporting electrolyte if purging with nitrogen is continued for about 30 min. Nitrate is not lost under these conditions and no new nitrate is produced. Data illustrating these findings are given in Figures 3 and 4. If the presence of nitrite is suspected and a simple determination of the nitrogen oxide anions as nitrate is desired, one may employ either the Keilin–Otvos oxidation procedure or a direct polarographic nitrate plus nitrite test (which will give a somewhat lower result if nitrite is actually present). In the

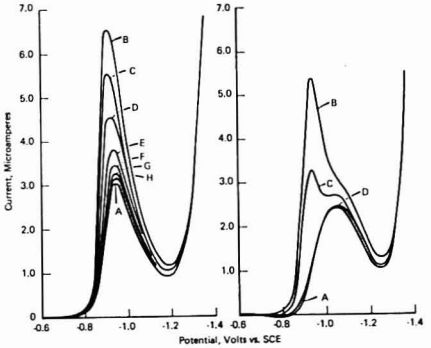

Figure 3. Removal of nitrite by nitrogen purge, 27 ppm NO_2^-. Left side: (A) reagent blank (pre-purged 5 min with N_2). (B) Same + 27 ppm NO_2^-, purged 30 s. (C) same, purged 10 min. (D) Same, purged 20 min. (E) Same, purged 40 min. (F) Same, purged 60 min. (G) Same, purged 80 min. (H) Same, purged 100 min. Right side: (A) Reagent blank + 1 g pure (fused) KBr (pre-purged 5 min with N_2). (B) Same + 27 ppm NO_2^-, purged 30 s. (C) Same, purged 10 min. (D) Same, purged 20 min

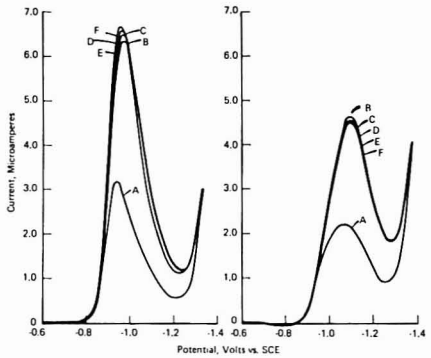

Figure 4. Retention of nitrate under nitrogen purge, 39 ppm NO_3^-. Left side: (A) Reagent blank (pre-purged 5 min with N_2). (B) Same + 39 ppm NO_3^-, purged 30 s. (C) Same, purged 10 min. (D) Same, purged 30 min. (E) Same, purged 60 min. (F) Same, purged 120 min. Right side: (A) Reagent blank + 1 g pure (fused) KBr (pre-purged 5 min. with N_2). (C) Same + 39 ppm NO_3^-, purged 10 min. (B) Same, purged 30 s. (D) Same, purged 30 min. (E) Same, purged 60 min. (F) Same, purged 120 min

latter test, it is desirable to purge the supporting electrolyte and neutral or alkaline sample solutions separately in advance, so that final deoxygenation of the mixture can be done within about 1 min to avoid appreciable loss of nitrous acid.

In the testing of reagents described hereafter, it has generally been assumed that nitrite is absent and that the value obtained directly represents only nitrate.

Reagent Grade Chemical Testing and Quality Control. The original purpose of this work was to make available simple and sensitive procedures for determining various nitrogen impurities in commercial and reagent grade chemicals. For such applications, the use of a simplified computing polarograph recently introduced by Brinkmann Instruments (see Apparatus) is attractive. While it does not have the sensitivity of differential pulse polarography, the hanging mercury drop electrode employed eliminates many of the problems associated with dropping mercury electrodes (*20*). The computing

Table VII. Comparison of Polarographic and Reduction Methods for Total Nitrogen in KBr

sample	total ppm N[a] reduction	total ppm N[b] polarography	ppm NO_3^-,[b] polarography	ppm NH_4^+,[b] differential pulse polarography	ppm NH_4^+,[b] computing polarographic analyzer
#1 ACS grade	37	35 ± 4	1.7 ± 0.2	43 ± 4	46 ± 4
#2 ACS grade	6.1	9.7 ± 1	43 ± 4	<1	<2
#3 not ACS grade	N.A.	34 ± 3	150 ± 10	<1	<2

[a] Current ACS specifications for KBr Reagent Grade not to exceed 50 ppm nitrogen as N. [b] Average of at least duplicate determinations.

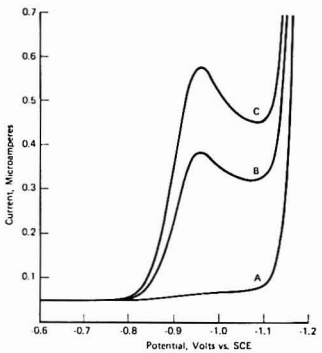

Figure 5. Polarographic scans for ammonia with the Brinkmann Computing Polarographic Analyzer. (A) Ammonia electrolyte (all in 25 mL). (B) Ammonia electrolyte + 1 g KBr Sample #1. (C) Ammonia electrolyte + 1 g KBr Sample #1 + 27 μg NH_4^+

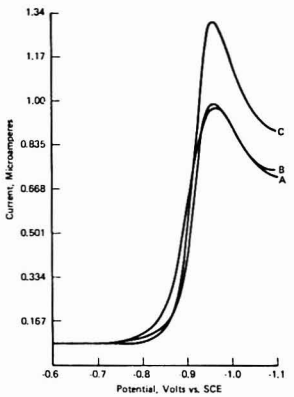

Figure 6. Polarographic scans for nitrate nitrogen with the Brinkmann Computing Polarographic Analyzer. (A) Nitrate electrolyte (all in 25 mL). (B) Nitrate electrolyte + 1 g KBr sample #1. (C) Nitrate electrolyte + 1 g KBr sample #1 + 25 μg NO_3^-

feature provides a direct digital readout in any desired concentration units and saves calculation time. With this instrument, the detection limit for ammonia in water is about 0.2 ppm, based on a 10-mL sample.

The polarographic methods described for ammonia and nitrate both permit the addition of a soluble neutral salt to the electrolyte and are sensitive to about 2 μg of nitrogen using the computing instrument. Thus in many cases 2 ppm can be detected on a 1-g sample. Calibration is performed easily by spiking. As already shown, the method is applicable to ammonium ion in sodium chloride solutions. The ACS requirements for sodium chloride include a limit of 0.003% chlorate and nitrate (as NO_3^-), determined spectrophotometrically with brucine sulfate reagent and a nitrate standard, and a limit of 0.001% nitrogen compounds (as N) determined colorimetrically with Nessler reagent after distillation from an alkaline solution containing aluminum. A typical sample of reagent grade sodium chloride showed the presence of less than 2 ppm of either form of nitrogen, by polarography with the Brinkmann instrument.

Potassium bromide has an ACS limit of 0.005% nitrogen compounds as N by the reduction–distillation method. In this laboratory, the ammonium salt formed by trapping after distillation has usually been determined with an ion-selective electrode. Comparative data by the various methods are presented in Table VII. Since the impurity may be either nitrate, ammonium ion, or both, more information is given by the polarographic tests than by distillation. Curves obtained in testing one of the samples are shown in Figures 5 and 6.

Sodium bromide has an ACS limit of not more than 5 ppm nitrogen compounds as N (*21*). A typical sample was found to contain less than 2 ppm of either ammonium or nitrate nitrogen. Ammonium bromide and ammonium chloride have no ACS limits for nitrate nitrogen, probably because the reduction–distillation procedure is not applicable. The polarographic nitrate procedure has been found to work well on ammonium bromide and should be equally suitable for the chloride.

In testing acids, alkalies, or salts with buffer capacity, care must be taken to maintain the proper pH for polarography (4.0 ± 0.5 for ammonium, 2.0 ± 0.3 for nitrate). Thus, it becomes necessary to have neutralizing reagents available which do not contribute significantly to the blank. The ACS limit for nitrogen compounds in sodium hydroxide is 10 ppm as N, determined by distillation after reduction with aluminum. This would be too high for a satisfactory blank in case the sodium hydroxide were used for neutralizing an acid. However, ammonia can be expelled by boiling a sodium hydroxide solution and the cooled solution can then be used for neutralizing prior to the polarographic ammonia test.

The ACS limit for ammonium ion (NH_4^+) in hydrochloric acid is 3 ppm. There is no limit for nitrate but if any were present, the acid would not pass the iodometric color test for free chlorine, the limit for which is about 1 ppm. It is also possible to expel nitrogen oxides by boiling 6 M hydrochloric acid. In view of these facts, we were able to test both sodium hydroxide and hydrochloric acid polarographically by using a purified or tested solution of one to neutralize the other. One-gram samples of typical reagents were analyzed with the result that less than 2 ppm NH_4^+ or nitrate N appeared to be present in either sodium hydroxide or hydrochloric acid. With a larger sample, 1.4 ppm NH_4^+ was found in one lot of sodium hydroxide. In the case of the acid, the response for ammonia can be increased considerably by evaporating a larger sample.

There is no ACS limit for ammonium or nitrate in acetic acid. Because this acid is used in the buffer for ammonia determination, it was of interest to test the purity. Portions of 11 g and 1 g of sample were treated with 10 mL of water and evaporated to about 1 mL. Each was neutralized with sodium hydroxide solution and tested. The smaller portion served as a blank so that the difference represented a 10-g sample. Less than 0.2 ppm NH_4^+ was found. To test for nitrate, the same quantities were employed but 0.1 g of sodium acetate trihydrate was added to each before evaporation. Less than 0.2 ppm nitrate N was found. Since these quantities are so low, there is no apparent need to establish an ACS test.

Ammonium hydroxide has no ACS limit for nitrate. Using 2-g samples, two lots of reagent showed 1.6 and <1 ppm of nitrate N. If purer material is needed for use in neutralizing acids prior to nitrate testing, it can easily be obtained by distillation or by trapping cylinder ammonia in water.

Sulfuric acid has ACS limits of 2 ppm NH_4^+ and 0.5 ppm nitrate as NO_3^-. The acid can be tested for ammonium after diluting and neutralizing a 2-g sample with freshly boiled 5 N sodium hydroxide solution. Because sodium sulfate suppresses the polarographic wave somewhat, calibration should be done by spiking an equivalent salt solution and making appropriate blank corrections. Duplicate analyses yielded results of 0.6 and 0.4 ppm NH_4^+ on typical reagent grade acid, but the latter figure is about the detection limit. For better sensitivity one might evaporate a larger sample, as was done for acetic acid. At present, the polarographic nitrate method is not sensitive enough for testing sulfuric acid at the 0.5 ppm NO_3^- level, and the nitrogen oxides cannot be concentrated by evaporation.

For magnesium sulfate heptahydrate, the ACS limits are 0.0020% for either NH_4^+ or NO_3^-. In the polarographic test for ammonium, a 1-g sample was dissolved in 15 mL of water and treated with 5 mL each of acetate buffer and purified formaldehyde. Standardization was done with 0.58 g of ACS grade sodium sulfate added to both a blank and a 20-μg NH_4^+ standard, plus reagents. Less than 3 ppm NH_4^+ was found in U.S.P. grade Epsom salt. A recovery of 95% was obtained when this sample was spiked with 14 ppm (0.0014%) of NH_4^+.

In the test for nitrate, a 1-g sample was also employed and the blank and 20-μg NO_3^- standard were treated similarly with 0.58 g of sodium sulfate. Less than 8 ppm NO_3^- was found in the sample. A recovery of 100% was obtained when this sample was spiked with 20 ppm (0.002%) of NO_3^-.

Some difficulty is encountered in testing calcium sulfate for nitrate because of its limited solubility in water. The ACS limit for the dihydrate is 50 ppm NO_3^- and the indigo carmine test in strong sulfuric acid is specified. The polarographic test is applicable under the following conditions: A sample of 0.15 g is heated to 90–100 °C with 15 mL of sodium chloride solution (100 g/L). This converts the dihydrate to hemihydrate, which dissolves upon cooling to room temperature and adding electrolyte plus water to make 25 mL. The quantity of sulfate present does not cause a serious decrease in polarographic sensitivity, but an equivalent quantity of sodium sulfate can be added to a blank and to a 7.5-μg nitrate standard if desired. In the presence of sulfate, a fresh drop of mercury should be used for each scan, as lowered response is found with successive scans on the same drop. Less than 25 ppm NO_3^- was found in natural gypsum from Alabaster, Mich. A recovery of 94% was obtained when this sample was spiked with 25 ppm of NO_3^-.

CONCLUSIONS

A method for the determination of amine nitrogen, based on reaction with excess formaldehyde and polarographic measurement, has been found useful. Blank problems are diminished by ion-exchange treatment of the formaldehyde reagent. Signals corresponding to detection limits of less than 25 ppb ammonia can be achieved in water samples. A method for the polarographic determination of nitrate (plus nitrite) nitrogen, based on the catalytic effect of uranyl ions, was also tested. The two methods have been combined to yield a simple estimate for total nitrogen which compares favorably with the Devarda distillation procedure usually employed. The methods are applicable to water and brine analyses as well as to reagent testing procedures and quality control.

A new Computing Polarographic Analyzer was found to give results in good agreement with data from the differential pulse polarographic procedures.

LITERATURE CITED

(1) "Standard Methods for the Examination of Water and Wastewater", 14th ed., American Public Health Association, Washington, D.C., 1975.
(2) "Methods for Chemical Analysis of Water and Wastes", Methods Development and Quality Assurance Research Laboratory, U.S. Environmental Protection Agency, Washington, D.C., 1974.
(3) "Reagent Chemicals", 5th ed., American Chemical Society, Washington, D.C., 1975.
(4) C. J. Nyman, J. L. Ragle, and P. F. Linde, *Anal. Chem.*, **32**, 352 (1960).
(5) D. R. Norton and C. K. Mann, *Anal. Chem.*, **26**, 1180 (1954).
(6) Y. I. Tur'yan and B. P. Zhantalai, *Zavod. Lab.*, **28**, 1431 (1962).
(7) B. P. Zhantalai and Y. I. Tur'yan, *Zavod. Lab.*, **31**, 668 (1965).
(8) B. P. Zhantalai and N. I. Kobylina, *Zavod. Lab.*, **31**, 668 (1965).
(9) "Ammonia", *Application Brief* **A-3**, Princeton Applied Research Corp., Princeton, N.J., 1974.
(10) I. M. Kolthoff, W. E. Harris, and G. Matsuyama, *J. Am. Chem. Soc.*, **66**, 1782 (1944).
(11) B. Keilin and J. W. Otvos, *J. Am. Chem. Soc.*, **68**, 2665 (1946).
(12) S. W. Boese, V. S. Archer, and J. W. O'Laughlin, *Anal. Chem.*, **49**, 479 (1977).
(13) J. F. Walker, "Formaldehyde", *ACS Monogr.* **159**, 3rd ed., Reinhold Publishing Corp., New York, N.Y., 1964.
(14) E. A. Werner, *J. Chem. Soc.*, **11**, 844 (1917).
(15) J. R. Polley, C. A. Winkler, and R. V. V. Nichols, *Can. J. Res., Sect. B*, **25**, 525 (1947).
(16) J. Plöchl, *Ber.*, **21**, 2117 (1888).
(17) G. Altiei, Italian Patent 509976 (1957).
(18) H. M. Kvalnes, U.S. Patent 2,476,212 (1949), Reissue 23, 174 (1949).
(19) J. F. Walker, U.S. Patent 2,000,152 (1935).
(20) J. D. McLean and J. F. Holland, *Environ. Sci. Technol.*, **9**, 127 (1975).
(21) "Reagent Chemicals", 5th ed., Supplement No. 1, *Anal. Chem.*, **49**, 526 (1977).

RECEIVED for review February 8, 1978. Accepted May 22, 1978.

Electrocatalysis of Dihydronicotinamide Adenosine Diphosphate with Quinones and Modified Quinone Electrodes

Daniel Chi-Sing Tse and Theodore Kuwana*

Department of Chemistry, The Ohio State University, Columbus, Ohio 43210

Solution rates of reaction between several quinones and dihydronicotinamide adenosine diphosphate, NADH, indicated that the ΔG of the reaction and the ortho structure of the quinone were important. The ortho quinones derived from dopamine and 3,4-dihydroxybenzylamine were subsequently covalently bound to carbon electrodes. The NAD^+ generated by the quinones was assayed and found to have high enzymatic activity. The behavior of the quinone-bound electrodes was compared to the oxidation of ascorbic acid and to the "adsorbed" 9,10-phenanthraquinone electrode which did not oxidize NADH catalytically.

Much of the previous electrochemical investigations of the redox cofactors, nicotinamide adenosine diphosphate (NAD^+) and dihydronicotinamide adenosine diphosphate (NADH), has been concerned with the reduction of NAD^+ to NADH. Unfortunately, electroreduction resulted mainly in producing an inactive dimer through a one-electron, free radical mechanism (*1–3*). Recently, attention has been directed to the electrooxidation of NADH to NAD^+ in attempts to develop methods to analyze substrates which can be enzymatically coupled to NAD^+/NADH (*4*), or to electrochemically regenerate NAD^+ for enzymatically coupled substrate turnovers (*5, 6*). The electrochemical oxidation of NADH on solid electrodes has been characterized by poorly defined current–potential (i–E) waves which were complicated partly by electrode fouling at NADH concentrations above 0.1 mM. The oxidative behavior of low concentrations of NADH to eliminate such fouling has been reported by Blaedel and Jenkins (*7*). At platinum (Pt), Coughlin and co-workers (*8*) have suggested improved sensitivity which has been utilized for regeneration of NAD^+ and also for the amperometric assay of oxidoreductase enzymes. Kelly and Kirwan (*9*) have shown that the potential dependent oxidative turnover for NADH at a graphite electrode approached an "activity" of 90–95%.

The NADH electrooxidation at both Pt and carbon electrodes proceeds with considerable overpotential from the reversible potential. Blaedel and Jenkins (*7*) have reported that the overpotential at a glassy carbon electrode could be reduced some 0.2 to 0.25 V by certain "conditioning" pretreatments. These pretreatments were suggestive that perhaps oxygen containing functionalities such as hydroxyls, carbonyls, carboxyls, and quinones, which may be produced on carbon surfaces, participated in catalyzing the NADH oxidation. And our earlier observation that surface quinoidal groups could catalyze the oxidation of ascorbic acid (*10*) stimulated the present work.

The introduction of surface functionalities on electrode surfaces by a chemical reaction route is an exciting research area of recent interest. A variety of attachment schemes have been proposed to fabricate these so-called chemically modified electrodes (CMEs) including strong surface adsorption (*11, 12*), silinization (*13–16*), amidization (*10, 17–21*), ether linkage (*22, 23*), and carbon–carbon bonding (*24*). Our approach to electrocatalysis by CMEs is to covalently bind onto carbon or metal oxide electrodes electron transfer *mediators* which can undergo fast electron transfer with the electrode and also with the substrate (solution species) in question.

In the present case, we have found that *o*-quinoidal structures, such as the catechols, appeared to be rather specific for the fast, homogeneous oxidation of NADH to NAD^+. Thus, the determination of the homogeneous rates of the reaction between NADH and several quinones was undertaken to assess those quinones which might be the best candidates for covalent binding to an electrode surface in the fabrication of a CME. Such a CME would be expected to catalyze NADH oxidation through a surface EC catalytic mechanism:

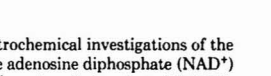

$$\text{---}QH_2 \rightarrow \text{---}Q + 2e^- + 2H^+ \quad (1)$$

$$\text{---}Q + NADH + H^+ \rightarrow \text{---}QH_2 + NAD^+ \quad (2)$$

where

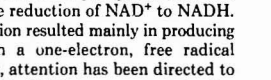

$\text{---}QH_2$ = the surface bound dihydroquinone

and

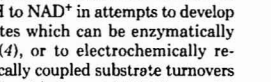

$\text{---}Q$ = the fully oxidized bound quinone

The thermodynamic requirement for the EC catalytic sequence 1 and 2 is that the reversible redox potential of NADH must be less positive in value than that of quinone/dihydroquinone. The assumption, yet to be proved, is whether those quinones (or, in general, mediators) which react rapidly in the homogeneous reaction with NADH (or in general, substrates) will also react favorably once they are bound to an electrode surface. The homogeneous rates of reaction between several quinones and NADH, and the preliminary results for electrocatalysis of NADH using catecholamines bound to graphitic electrodes will be discussed in this paper.

EXPERIMENTAL

Chemicals. The 3-hydroxytyramine (commonly called dopamine, DA) hydrochloride (99% purity), 4-methylcatechol (4-MC, 99% purity), 3,4-dihydroxybenzylamine (3,4-DHBA, 98% purity) hydrobromide, 5-hydroxy-1,4-naphthoquinone (5-OH-1,4-NPQ), and 2-anthraquinonesulfonic acid sodium salt (AQ-2-S) were obtained from Aldrich Chemical Company. Methylhydroquinone (MHQ), 9,10-phenanthraquinone (9,10-PAQ), 1,2-naphthoquinone-4-sulfonic acid sodium salt (1,2-NPQ-4-S) and 1,4-naphthoquinone-2-sulfonic acid potassium salt (1,4-NPQ-2-S) were obtained from Eastman Kodak Company. The 2,5-dihydroxyphenacetic acid (2,5-DHPA, Grade II) and NADH (Grade III) from yeast were obtained from Sigma Chemical Company. All chemicals were stored according to manufacturers direction or in a desiccator at 4 °C and were used without further purification. Buffer solutions were prepared by mixing 0.005 M NaH_2PO_4 and 0.005 M Na_2HPO_4, each containing 0.1 M NaCl, to the desired pH. All solutions were prepared freshly prior to each experiment. Demineralized water was double distilled and stored in a quartz container.

0003-2700/78/0350-1315$01.00/0

Table I. Abbreviations of Compounds and Terms

abbreviation	compound or term
CME	chemically modified electrode
PG	pyrolytic graphite
GC	glassy carbon
CV	cyclic voltammetry
RF	radio frequency
3,4-DHBA	3,4-dihydroxybenzylamine
DA	3-hydroxytyramine
4-MC	4-methylcatechol
5-OH-1,4-NPQ	5-hydroxy-1,4-naphthoquinone
AQ-2-S	2-anthraquinonesulfonic acid
MHQ	methylhydroquinone
9,10-PAQ	9,10-phenanthraquinone
1,2-NPQ-4-S	1,2-naphthoquinone-4-sulfonic acid
1,4-NPQ-2-S	1,4-naphthoquinone-2-sulfonic acid
2,5-DHPA	2,5-dihydroxyphenacetic acid
ADH	alcohol dehydrogenase
NADH	dihydronicotinamide adenosine diphosphate

Electrochemistry. A solid state potentiostat of conventional design utilizing a positive feedback for *iR* compensation (*25*) was employed. Waveforms to the potentiostat were provided by a HP model 3300 A function generator. The cell design was similar to one previously described (*26*). The radio frequency (RF) plasma treatment of pyrolytic graphite (PG), (Ultracarbon Corp., Bay City, Mich.) and glassy carbon electrodes (GC), (Tokai Co., Japan) in oxygen atmosphere was described by Evans and Kuwana (*27*). The RF treatment was 5 min. Unless otherwise stated, all potentials are reported vs. a reference saturated calomel electrode (SCE). The current–time profiles for the double potential step experiments were recorded on a Tektronix Model 564B storage oscilloscope.

Measurement of Rate Constants. The rate constants between various quinones and NADH were determined using three different methods depending on the initial redox state of the mediator and the magnitude of the rate. Double potential step chronocoulometry (DPSC) (*28*, *29*) and cyclic voltammetry were used for mediators in the reduced form such as DA, 4-MC, 3,4-DHBA, MHQ, and 2,5-DHPA. For the DPSC experiments, mediator concentration was 0.1 mM and NADH was 1.0 mM. Increasing the NADH concentration to 2 mM gave the same rate constant after concentration corrections. The potential step times ranged from 5 ms to 5 s. DPSC experiments in buffer solutions alone were run to determine the background charge corrections.

In the cyclic voltammetric experiments, the oxidative and reductive peak currents were monitored in the presence and absence of NADH. The quinone concentrations were 0.1 mM–0.2 mM and NADH, when present, was 0.5 mM or 1.0 mM. The reaction of 1,4-NPQ-2-S, 5-OH-1,4-NPQ, or AQ-2-S with NADH was sufficiently slow that the concentration of NADH could be electrochemically monitored (oxidation) after the addition of an excess of these quinones to the NADH solution.

The rate of the reaction between 1,2-NPQ-4-S and NADH was determined using a Durrum-Gibson stop-flow instrument. Equal volumes of 1.1×10^{-4} M 1,2-NPQ-4-S and 1.98 mM NADH were mixed and the change in the concentration of the naphthaquinone was monitored at wavelength of 400 nm. The optical absorbance vs. time data were recorded and analyzed by a Data General NOVA 1200 minicomputer.

Procedure for Measurement of NAD^+ Activity. The enzymatic activity of the NAD^+ solution electrogenerated through the EC catalytic mechanism utilizing 3,4-DHBA was determined by spectrophotometrically monitoring the NAD^+ to NADH conversion when alcohol dehydrogenase (ADH) and ethanol were added. For example, 10 mL of 1.0×10^{-4} M 3,4-DHBA and 1.0×10^{-4} M NADH solution was electrooxidized at a pyrolytic graphite electrode at a controlled potential of +0.35 V vs. SCE until 70–90% of NADH was oxidized. ADH (0.5 to 0.8 mg) and 100 μL aliquots of pure ethanol were added to 3.0 mL of the electrolyzed, NAD^+ solution. Spectra were taken in the wavelength range of 280 to 400 nm before and after the addition of each aliquot of ethanol. The optical absorbance change at 340 nm was used to calculate the amount of NAD^+ converted to NADH by ADH–ethanol. Controls included unelectrolyzed solutions of NADH and 3,4-DHBA, and NADH electrolyzed under the same conditions but in the absence of 3,4-DHBA. The abbreviations of compounds and other terms used are summarized in Table I.

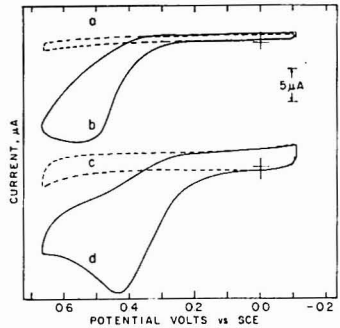

Figure 1. Cyclic voltammograms of PG electrodes in pH 7.0 phosphate buffer (a, c) and in 0.1 mM NADH in pH 7.0 phosphate buffer (b, d). The pyrolytic graphite electrode pretreatments were: (a, b) extracted in methanol for 24 h and vacuum dried. (c, d) first extracted in methanol for 24 h, vacuum dried, then subjected to radio frequency (RF) plasma treatment. The scan rate was 50 mV/s

RESULTS AND DISCUSSION

NADH is involved in many enzymatic reactions. However, nonenzymatically, only certain oxidants can oxidize NADH (*30*, *31*). Kubowitz (*32*), and Nason and co-workers (*33*) have indicated that the quinones and, in particular, the ortho form, reacts with NADH as follows:

$$\mathrm{R{-}Ph{-}(=O)_2 + NADH + H^+ \overset{k_f}{\rightleftharpoons} R{-}Ph{-}(-OH)_2 + NAD^+} \quad (3)$$

where R indicates some substituent group, Ph–$(=O)_2$ is a quinone, and Ph–$(-OH)_2$ is the reduced, dihydro form. In electrochemistry, it is convenient to oxidize the dihydroquinone to quinone which in turn can oxidize NADH in an EC catalytic sequence as discussed earlier. The questions to be answered are: (1) Whether the ortho structure is specific to the oxidation of NADH compared to the para or meta forms; and (2) Whether the ortho or any other quinone which reacts rapidly with NADH can be appropriately attached to an electrode surface for the surface EC catalysis of NADH.

Initially, the electrochemistry of NADH and several quinones (usually in the dihydro form) was examined at PG or GC electrodes so that the electrochemical behavior of each could be understood prior to the EC catalytic studies. In Figure 1, the cyclic voltammetric (CV) current–potential (*i*–*E*) curves are shown for the oxidation of NADH at a PG electrode prior to (trace b) and after (trace d) radio frequency (RF) plasma treatment in O_2 atmosphere ($P_{O/2}$ = 150 mTorr). As may be seen from comparison of these two curves, the peak potential, E_p, for NADH oxidation is ca. 100 mV less positive at the RF treated electrode. This shift in E_p, similar to that observed by Blaedel and Jenkins (*7*), may be due to the presence of oxygen functionalities introduced on the carbon surface by the RF treatment (*10*). However, the decrease here may also be due to the increase in the effective surface area of the electrode. This area increase is manifested clearly by an increase in the background charging current of the treated electrode (see *i*–*E* curve, trace c) over that of the untreated one (trace a). Work is in progress to further quantitate the effect of RF plasma treatment to NADH oxidation.

Table II. Values of Redox Potentials and Kinetic Rates

compound	$E^{\circ\prime}_{\gamma}$, V vs. NHE	rate constant, M^{-1} s^{-1} [a]
3,4-DHBA	0.41 ± 0.02[c]	7.7 (± 0.8) × 10^4 [b]
DA	0.37 ± 0.02[c]	3.6 (± 0.4) × 10^4 [b]
4-MC	0.32 ± 0.04[e]	3.3 (± 0.4) × 10^3 [b]
2,5-DHPA	0.260[f]	0[b]
MHQ	0.24 ± 0.04[e]	0[b]
1,2-NPQ-4-S	0.215[f]	4.4 (± 0.9) × 10^2 [c]
1,4-NPQ-2-S	0.120[f]	0[d]
5-OH-1,4-NPQ	0.033[f]	0[d]
AQ-2-S	−0.225[f]	0[d]
NADH	−0.320[f]	

[a] Temperature 23 ± 1 °C. [b] Determined by DPSC. [c] Determined by stop-flow. [d] No change in NADH concentration after 0.5 h when 10-fold excess of quinone was mixed with NADH. [e] Measured in this work by means of cyclic voltammetry. [f] From ref. 37.

The CV curves for the oxidation of 3-hydroxytyramine (dopamine, DA), 3,4-dihydroxybenzylamine (3,4-DHBA), and 4-methylcatechol (4-MC) at PG electrode in pH 7.0 solution are shown in Figure 2, traces a, c, and e, respectively. All three compounds produced well defined CV curves for the two-electron oxidative conversion of the dihydro to the quinone form. The electrochemical data for these and several other quinones are summarized in Table II. In the case of DA, the oxidation was characterized by a follow-up chemical reaction, a cyclization (*35*), which produces a new wave at ca −0.25 V vs. SCE. Such a chemical follow-up reaction was absent for 3,4-DHBA and 4-MC. The CV curves, b, d, and f in Figure 2 are repeats of the above experiments except in the presence of 1.0 mM NADH. The electrochemical currents are now considerably enhanced by the EC coupled oxidation of NADH, and the potential for NADH oxidation is now governed by the respective quinone couples. Since the experimental conditions are similar, the shape and height of the *i–E* curves reflect the kinetic rates of the quinone oxidation of NADH. The NADH oxidation rate by 4-methyl-*o*-quinone is slower than the corresponding quinone of DA and 3,4-DHBA. One observed not only less catalytic current but also the oxidation of NADH by the electrode at 0.58 V (Figure 2f). It should be noted also that the irreversible, homogeneously coupled quinone/NADH reaction removed the reductive current on reversal of the potential scan.

The values of the kinetic rates of the quinone/NADH reaction 3 are summarized in the last column of Table II. There appears to be two factors in the rate enhancements. First, a larger free energy of reaction 3 as reflected by the more positive redox potential, $E^{\circ\prime}_{\gamma}$, increased the rate. Second, there is a preference for the ortho structure. The generality of these two factors will be further tested in the future.

Since reaction 3 is proton dependent, an increase in the oxidative rate between a quinone and NADH should increase with a decrease in pH. This effect of pH was examined for DA between the pHs of 6.5 to 8.5. The rate constant decreased by ca. 1.2×10^4 M^{-1} s^{-1} per pH.

Enzymatic Activity of NAD⁺. Kelly and Kirwan (*9*) assayed the enzymatic activity of NAD^+ in pH 9 pyrophosphate buffer by determining the acetaldehyde concentration after ADH-ethanol were added to the NADH electrolyzed solution. They reported that a maximum NAD^+ production of 95% occurred at an applied potential of +0.700 V vs. SCE using a carbon electrode (anode grade graphite, Union Carbide). To assess the enzymatic activity of the NAD^+ produced through reaction 3, a similar assay was performed except that the change in the NADH concentration was monitored by spectrophotometry. A 0.1 mM solution of 3,4-DHBA at an applied potential of +0.35 V vs. SCE at a PG electrode in the presence of 0.1 mM NADH (pH 7.0) was used. The coulometric charge (background corrected) was accurately measured so that the amount of NAD^+ produced could be calculated. In all of the runs reported in Table III, more than 90% of the NADH was oxidized. The enzymatic activities ranged from 92 to 98%. In the control experiments where NADH was electrolyzed under the same condition as in the absence of 3,4-DHBA, only 3-4% NADH oxidation was observed.

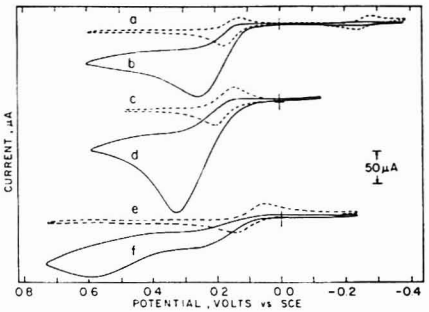

Figure 2. Cyclic voltammograms of (a) 0.1 mM DA, (b) 0.1 mM DA, 1.0 mM NADH, (c) 0.1 mM 3,4-DHBA, (d) 0.1 mM 3,4-DHBA, 1.0 mM NADH, (e) 0.1 mM 4-MC, (f) 0.1 mM 4-MC, 1.0 mM NADH, in pH 7.0 phosphate buffer with a RF plasma treated pyrolytic graphite electrode. The scan rate was 50 mV/s

Electrochemical Activity of Bound *o*-Quinone CMEs. The two quinones exhibiting the highest rate of NADH oxidation in Table II were fortunately those containing a terminal amino group on the substituent side-chain. Thus, the reduced forms of these quinones, DA and 3,4-DHBA, were attached by amidization to carboxylic acid functionalities on RF/O_2 treated PG and air oxidized GC in the presence of dicyclohexylcarbodiimide. The reaction conditions and the GC electrode pretreatments were similar to those described by Fujihira, Tamura, and Osa (*36*). The time of reaction was four days after which the electrodes were extracted in methanol for 24 h to remove adsorbed reactants. Since 3,4-DHBA on GC exhibited the best properties toward surface EC catalysis of NADH, the discussion will be restricted to this CME.

Trace a in Figure 3 is a typical CV curve for a 3,4-DHBA CME. The oxidative E_p is + 0.20 V vs. SCE which is identical to the one obtained for solution 3,4-DHBA (see trace c, Figure

Table III. Enzymatic Activity of NAD^+

NADH concn, 10^{-4}	Final ethanol concn, M	NADH enzymatically generated	
		mg ADH	NAD^+ electrochemically generated[a]
1.00	2.02	0.8	0.963
0.98	1.56	0.7	0.926
0.93	2.02	0.5	0.977
0.92	2.02	0.5	0.969

[a] The decomposition of NADH was corrected by monitoring unelectrolyzed solution of NADH and 3,4-DHBA spectroscopically. Collections ranged from 2 to 3% of the initial NADH concentration.

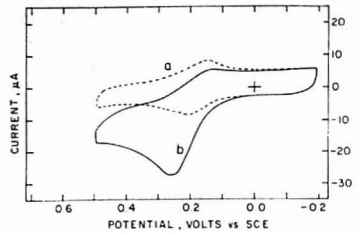

Figure 3. Cyclic voltammograms of a 3,4-DHBA modified GC electrode (a) in pH 7.0 phosphate buffer, and (b) in 0.2 mM NADH, pH 7.0 solution. The scan rate was 50 mV/s

2). This CV changed slightly when repetitively cycled for 10 or more times. The surface coverage by 3,4-DHBA was calculated to be 1.3×10^{-10} mol/cm^2 from the oxidative electrochemical change, assuming $n = 2$ for 3,4-DHBA. Trace b in Figure 3 is the repeat of the CV except in the presence of 0.2 mM NADH. The E_p of the surface EC coupled oxidation of NADH is slightly less positive than the solution EC one (see trace d, Figure 2). This difference in E_p may be due to the higher concentration of NADH in the solution case. The important aspect is the EC surface catalysis of NADH which is being accomplished by a deliberate chemical/structural modification of an electrode surface, i.e., an *o*-quinone CME. Unfortunately, the activity of this electrode could not be maintained for more than a few cycles in the presence of NADH. Because of the previous implication (*7*) that electrode fouling by NADH could be deleterious to an electrode, the activity of the 3,4-DHBA CME was tested by the oxidation of ascorbic acid.

Indeed, a well-defined oxidative *i-E* characteristic of an EC catalyzed wave was obtained for the oxidation of ascorbic acid by this CME. The peak heights were reproducible from run to run for several cycles without loss of activity. It is reasonably safe to conclude that the decrease in the activity of the 3,4-DHBA CME with NADH is not due to loss of the bound 3,4-DHBA but rather the presence of NADH, NAD$^+$, or the presence of small amounts of unknown side products of NADH oxidation. For ascorbic acid, the rate of oxidation by this CME was apparently quite rapid since the E_p was nearly identical to that obtained in the absence of ascorbic acid.

Recently, Brown et al. (*12*) have reported the interesting case of an electrode modification by the strong surface adsorption of 9,10-phenanthraquinone. This molecule is believed to be adsorbed on graphitic surfaces with the plane of the ring lying parallel to the surface. The E_p for the oxidation was observed to be at ca +0.20 V vs. SCE in 1 M trifluoroacetic acid which is the condition of the experiment reported. At pH 7.0 phosphate buffer, the E_p for the oxidation of 9,10-dihydroxyphenanthrene was −0.20 V vs. SCE (0.04 V vs. NHE). Interestingly, this adsorbed *o*-quinone/dihydroquinone electrode did not "catalytically" oxidize NADH (0.2 mM). Although the free energy of this redox couple is not as favorable as, for example, the bound 3,4-DHBA, the total unreactivity is possibly indicative of structural orientation differences between the two "bound" *o*-quinones. The "adsorbed" 9,10-phenanthraquinone may be less accessible to the 4-dihydro position of the NADH for oxidation to occur.

The feasibility of fabricating a CME capable of catalyzing the oxidation of NADH has been demonstrated. For utilizing such CME electrodes for analytical purposes, the deleterious effect of the presence of high concentrations of NADH may be perhaps circumvented by the use of the pulse method described by Lane and Hubbard (*37*). Future studies will more fully explore the molecular/structural aspects which are necessary for the design of CME with redox specificity.

LITERATURE CITED

(1) A. L. Underwood and Robert W. Burnett, "Electrochemistry of Biological Compounds", in "Electroanalytical Chemistry", Vol. 6, A. J. Bard, Ed., Marcel Dekker, New York, N.Y., 1973.
(2) G. Dryhurst, "Electrochemistry of Biological Molecules", Academic Press, New York, N.Y., 1977, Chap. 9.
(3) C. O. Schmakel, K. S. V. Santhanam, and P. J. Elving, *J. Am. Chem. Soc.*, **97**, 5083 (1975).
(4) See Introductory discussion in paper by F. S. Cheng and G. D. Christian, *Anal. Chem.*, **49**, 1785 (1977).
(5) M. Aizawa, R. W. Coughlin, and M. Charles, *Biochem. Biophys. Acta*, **385**, 362 (1975).
(6) R. W. Coughlin and B. F. Alexander, *Biotechnol. Bioeng.*, **17**, 1375 (1975).
(7) W. J. Blaedel and R. A. Jenkins, *Anal. Chem.*, **47**, 1337 (1975).
(8) T. C. Wallace, M. B. Leh, and R. W. Coughlin, *Biotechnol. Bioeng.*, **19**, 901 (1977).
(9) R. M. Kelly and D. J. Kirwan, *Biotechnol. Bioeng.*, **19**, 1215 (1977).
(10) J. F. Evans, T. Kuwana, Mary T. Henne, and G. P. Royer, *J. Electroanal. Chem.*, **80**, 409 (1977).
(11) R. F. Lane and T. Hubbard, *J. Phys. Chem.*, **77**, 1401, 1411 (1973).
(12) A. P. Brown, C. Koval, and F. C. Anson, *J. Electroanal. Chem.*, **72**, 379, (1976).
(13) P. R. Moses and R. W. Murray, *J. Am. Chem. Soc.*, **98**, 7435 (1976); *J. Electroanal. Chem.*, **77**, 393 (1977).
(14) D. G. Davis and R. W. Murray, *Anal. Chem.*, **49**, 194 (1977).
(15) G. J. Leigh and C. J. Pickett, *J. Chem. Soc., Dalton Trans.*, 1797 (1977).
(16) A. F. Diaz and K. K. Kanazawa, *J. Am. Chem. Soc.*, **99**, 5838 (1977).
(17) B. F. Watkins, J. R. Behling, E. Kariv, and L. L. Miller, *J. Am. Chem. Soc.*, **97**, 3549 (1975).
(18) M. Fujihara, T. Matsue, and T. Osa, *Chem. Lett.*, 875 (1976).
(19) C. A. Koval and F. C. Anson, *Anal. Chem.*, **50**, 223 (1978).
(20) N. Oyama and F. C. Anson, *J. Electroanal. Chem.*, **88**, 289 (1978).
(21) N. Oyama, A. P. Brown, and F. C. Anson, *J. Electroanal. Chem.*, **87**, 435 (1978).
(22) A. W. C. Lin, P. Yeh, A. M. Yacynych, and T. Kuwana, *J. Electroanal. Chem.*, **84**, 411 (1977).
(23) A. M. Yacynych and T. Kuwana, *Anal. Chem.*, **50**, 640 (1978).
(24) S. Mazur, T. Matusinovic, and K. Cammann, *J. Am. Chem. Soc.*, **99**, 3888 (1977).
(25) A. A. Pilla, *J. Electrochem. Soc.*, **118**, 702 (1971).
(26) F. Hawkridge and T. Kuwana, *Anal. Chem.*, **45**, 482 (1973).
(27) J. F. Evans and T. Kuwana, *Anal. Chem.*, **49**, 1632 (1977).
(28) J. H. Christie, *J. Electroanal. Chem.*, **13**, 79 (1967).
(29) P. J. Lingane and J. H. Christie, *J. Electroanal. Chem.*, **13**, 227 (1967).
(30) L. Hellerman, F. P. Chinard, and P. A. Ramsdell, *J. Am. Chem. Soc.*, **63**, 2551 (1941).
(31) W. T. Caraway and L. Hellerman, *J. Am. Chem. Soc.*, **75**, 5334 (1953).
(32) F. Kubowitz, *Biochem. Z.*, **299**, 32 (1938).
(33) W. D. Wosilait and A. Nason, *J. Biol. Chem.*, **206**, 255, 271 (1953).
(34) W. M. Clark, "Oxidation-Reduction Potentials of Organic Molecules", The Williams and Wilkins Company, Baltimore, Md., 1960.
(35) D. Tse, R. L. McCreery, and R. N. Adams, *J. Med. Chem.*, **19**, 37 (1976).
(36) M. Fujihira, A. Tamura, and T. Osa, *Chem. Lett.*, 361 (1977).
(37) R. F. Lane and A. T. Hubbard, *Anal. Chem.*, **48**, 1287 (1976).

RECEIVED for review March 27, 1978. Accepted May 15, 1978. This work supported by funds from NSF Grant Number CHE76-81591 and US PHS Grant Number GM19181.

Enzymatic Determination of Nitrate: Electrochemical Detection after Reduction with Nitrate Reductase and Nitrite Reductase

Chih-Hen Kiang,[1] Shia S. Kuan, and George G. Guilbault*

Department of Chemistry, University of New Orleans, New Orleans, Louisiana 70122

A method for the determination of nitrate and/or nitrite using the dual enzyme system: MVH (methyl viologen, reduced form) nitrate reductase (EC 1.9.6.1) and nitrite reductase (EC 1.6.6.4) has been developed. MVH-nitrate reductase was induced and purified from *E. coli* K12. MVH-nitrite reductase was isolated and purified from spinach leaves. Nitrate is reduced by MVH-nitrate reductase to nitrite which is subsequently reduced to ammonia by MVH-nitrite reductase. The ammonia produced is monitored, using an air-gap electrode. Nitrate and/or nitrite are determined in the range of 5×10^{-5}–1×10^{-2} M using either a soluble or an immobilized enzyme system.

The toxicity of nitrite is well known and has two entirely separate aspects: (a) the induction of methemoglobinemia (*1*) by nitrite oxidation of hemoglobin from the ferrous to the ferric form; the ferric form of hemoglobin (methemoglobin) does not reversibly bind oxygen, and death results from anoxias in severe cases (*2*), and (b) the formation of carcinogenic *N*-nitroso compounds by the reaction between nitrite, and secondary or tertiary amines and amides (*3–5*). It is generally accepted that nitrate itself is not toxic. However the reduction of nitrate to nitrite occurs in the presence of microorganisms. As reported by Tannenbaum et al. (*6*), the major part of the nitrite found in the human body actually originates from the reduction of nitrate in the saliva by bacteria within the mouth. Recently the increasing use of nitrate and nitrite in foods, fertilizers, detergents, and other fields of industry has caused serious contamination problems in the environment. These problems have attracted increasing attention, especially since nitrite is suspected of being responsible for some incidence of cancer. Action has already been undertaken by some agencies to prevent such contamination. The U.S. Public Health Service (*7*) has announced that the allowable limits for nitrate and nitrite in potable water are 10 and 0.06 ppm, respectively. Recently, the U.S. Department of Agriculture has proposed to discontinue the use of nitrate in all meat and poultry products and to reduce the allowed level of nitrite added for curing of meat and poultry from 200 to 156 ppm (*8*).

Numerous nonenzymatic methods for the analysis of nitrate and nitrite have been developed and reported elsewhere. However, most of these are nonspecific and are subject to serious interferences from diverse substances. Pretreatment is usually required to eliminate these interferences before measurement. This, of course, is inconvenient and makes the method time-consuming. Since enzymic techniques have been widely used in analytical chemistry because of their high selectivity and sensitivity, several enzymatic methods for the determination of nitrate and nitrite have been reported (*9–12*). The common approach of these methods is to reduce nitrate to nitrite using a nitrate reductase; the nitrite found is subsequently measured colorimetrically. The disadvantage of this approach is that it is subject to the same interferences as the colorimetric method for nitrite and that the whole system is rather complicated. We would like to introduce an entirely different approach here: a new electrochemical enzymatic method, which has the advantages of specificity, rapidity, and simplicity for the determination of nitrate and/or nitrite.

In this electrochemical method, nitrate and nitrite can be specifically and quantitatively reduced to ammonia by nitrate and nitrite reductases in the presence of MVH as electron donor, obtained through the chemical reduction of its oxidized form by dithionite added initially into the reaction mixture (Equations 1, 2, and 3):

$$2H_2O + 2MV^{2+} + S_2O_4^{2-} \rightarrow 2HSO_3^{2-} + 2MV^{+\cdot} + 2H^+ \quad (1)$$

$$2H^+ + NO_3^- + 2MV^{+\cdot} \xrightarrow{\text{nitrate reductase}} NO_2^- + 2MV^{2+} + H_2O \quad (2)$$

$$8H^+ + NO_2^- + 6MV^{+\cdot} \xrightarrow{\text{nitrite reductase}} NH_4^+ + 6MV^{2+} + 2H_2O \quad (3)$$

The ammonia generated during the reaction can be selectively measured using a new air-gap electrode (*13, 14*). This recently developed air-gap electrode is based on the same principle as other gas sensors, except that it does not have any gas-permeable membrane. The membrane is replaced by an air gap which separates the electrolyte layer from the sample solution, the entire system being contained in a gas-tight measuring chamber. The electrolyte itself is adsorbed as a very thin film on the surface of the indicator (pH) electrode. During measurement, the ammonia gas evolved from the sample solution under basic conditions, passes through the air gap and reaches the electrolyte layer on the surface of the electrode, thus increasing the pH value of the electrolyte layer. The amplitude of the pH at equilibrium is directly proportional to the ammonia concentration in the sample solution (Nernstian relationship). The electrolyte layer can be easily renewed after each measurement, by touching the electrode surface on a cone-shaped polyurethane sponge, well soaked with the electrolyte solution, in an electrode holder. The greatest advantage of this design is that the electrode is never in direct physical contact with the sample solution which therefore may contain components that normally affect the function of any electrode. The simplicity of design, the easy renewal of electrolyte, and the fast response and recovery are further advantages of the air gap.

We have reported (*15*) previously the determination of nitrite using MVH-nitrite reductase and air-gap electrode. At this time we describe an extension of this methodology to the determination of nitrate and/or nitrite, using both nitrate and nitrite reductases in a soluble and immobilized form.

EXPERIMENTAL

Apparatus. The Radiometer type 503810 glass electrode was used, and the construction of the air-gap sensor is essentially the same as described by Ruzicka and Hansen (*13, 14*). A Corning

[1] Present address, Department of Chemical Engineering and Nuclear Engineering, Iowa State University, Ames, Iowa 50011.

0003-2700/78/0350-1319$01.00/0

digital 110 pH meter and a Heath Strip chart recorder with dc offset module and potentiometric amplifier were used to record the electrode response.

Reagents and Materials. The electrolyte solution used was 5×10^{-3} M ammonium chloride solution saturated with wetting agent (Victawet 12, Stauffer Chemical Co.).

Methyl viologen, cyanogen bromide, and glutaraldehyde were obtained from Sigma Chemical Co. (St. Louis, Mo.). Alkylamine glass beads were purchased from Corning Glass Co. (Corning, N.Y.).

E. coli K12 PA 601 was obtained from the American Type Culture Collection. Fresh leaves of *Spinacea oleracca* were purchased from a local market.

Preparation of Enzyme. The isolation and purification of nitrite reductase from spinach leaves was carried out according to Ho and Tamara (*16*) up to the DEAE–cellulose chromatography step. The induction, isolation and purification of nitrate reductase from *E. coli* K12 was performed according to Forget (*17*) to the first ammonia fractionation step. The enzyme was solubilized by heat rather than acetone treatment. The main fractions of enzymes were combined, freeze-dried, and stored in a freezer for later use. As a result of the preparation, from 1.0 kg of spinach leaves, about 220 units of nitrite reductase, can be obtained with specific activity of 1.5 units/mg and from 45 g of wet weight *E. coli* cells about 4560 units of nitrate reductase can be obtained with a specific activity of 10.0 units/mg.

Immobilization of Enzyme. The method is based on the procedure of Marshall (*18*), with some modifications. Activate 2 g of glass beads by adding 15 mL of 3% glutaraldehyde, then degas the product under a desiccator vacuum for 10 min at room temperature. After activation for 60 min at atmospheric pressure and room temperature, decant and wash the glass beads at least three times with distilled water. The activated glass beads were added to 15 mL of 0.1 M phosphate buffer containing 50 mg of nitrate reductase or 100 mg of nitrite reductase. The mixture was degassed for 10 min on an ice-bath, and the coupling reaction was carried out for 24 h at 4 °C with gentle shaking. The immobilized material was washed at least three times with 0.01 M phosphate buffer (pH 8.0) and stored in a refrigerator until use.

Measurement of Nitrite or Nitrate with Soluble Enzymes. Fifty μL of Tris buffer, 0.45 M, pH 7.0, containing 3 units of nitrite reductase for nitrite assay, or 3 units of nitrite reductase plus 3 units nitrate reductase for nitrate assay, and 0.75 μmol of methyl viologen, was pipetted into a sample chamber, followed by 200 μL of a nitrate standard solution. The reaction was initiated by adding 50 μL of sodium bicarbonate solution, 0.26 M, containing 3.75 mg of sodium dithionite, which was prepared immediately before use. The sample chamber was put in a water bath at 30 °C, incubated for 5 min, and then placed on a magnetic stirrer, preset at the desired speed. One-hundred μL of 0.05 N NaOH-KCl solution was added, and the chamber was immediately covered with the electrode body. The potential change was recorded until a steady state was reached. The pH of the equilibrium state (pH_e) on the surface of the glass electrode was read directly from the digital pH meter. The stirrer is best preset at a moderate speed, so that all measurements could be accomplished under almost identical conditions. In order to extend the detection limit, a minimal sample dilution should be effected.

Measurement of Nitrite or Nitrate with Immobilized Enzymes. To 0.25 mL of 0.45 M, pH 7.0 Tris buffer, containing 3.75 μmol methyl viologen, add 1.0 mL of sample solution and 0.25 mL of 0.25 M sodium bicarbonate, containing 18.25 mg sodium dithionite; mix. Pass this solution through column A (0.5 × 14 cm), which contains immobilized nitrite reductase for nitrite assay, or column B, which contains a 1:1 mixture of immobilized nitrate and nitrite reductases for nitrate assay, at a flow rate of 0.3 mL/min controlled by a peristaltic pump, so that a 100% conversion can be assured. After 5–6 min, collect 300 μL of the eluent, pipet into the sample chamber, and measure the amount of ammonia released as described above. Since the void volume and dead volume of the column are about 0.9 and 0.1 mL, respectively, this 5–6 min waiting time is necessary to obtain homogeneous sample composition.

Measurement of Nitrate and Nitrite Mixtures with Immobilized Enzymes. The procedure employed is the same as described for the measurement of nitrite or nitrate. The same amount of sample solution and reaction solution are passed through both column A and B and the eluents are measured. The value obtained from column A indicates the amount of nitrite present in the mixture and nitrate can be calculated by subtracting the value of column A from the value of column B.

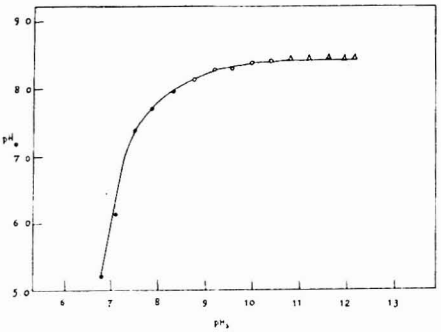

Figure 1. Effect of pH_s upon the evolution of ammonia. NH_4Cl concentration, 0.01 M, 200 μL. Buffer concentration, 0.5 M, 200 μL. (● – ●) Tris buffer (μ = 0.1), (O – O) $NaCO_3$-NaOH buffer (μ = 0.1), (Δ – Δ) Na_2HPO_4-NaOH buffer (μ = 0.1)

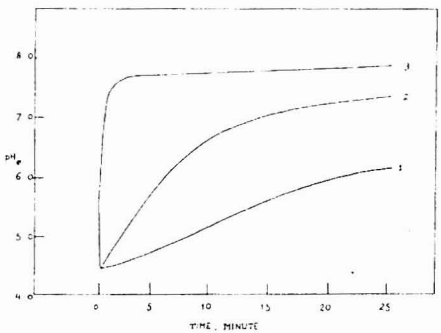

Figure 2. Comparison of the direct and the two-step methods. (For details, see text). Curve 1: blank, no enzyme added; curve 2: direct measurement of substrate method; curve 3: two-step measurement of substrate

RESULTS AND DISCUSSION

Effect of pH_s for Evolution of Ammonia. In general, the pH of the sample solution (pH_s) determines whether a quantitative or partial conversion of ammonia ion occurs. Figure 1 shows the dependence of pH_e on pH_s. At $pH_s > 10.5$, the curve levels off, indicating a total conversion of ammonium ion to ammonia. However, the optimum pH for MVH-nitrate and nitrite reductase is around 7.4–7.8. Within this range only partial conversion of ammonium ion to ammonia takes place. As shown in Figure 2, curve 2, obtained with a KNO_2 concentration of 1×10^{-3} M at pH_s 8.0 (direct method), the response was very slow, taking about 20 min to reach 95% of equilibrium. Furthermore, the sensitivity is very low, and the pH_e drifts badly at equilibrium. As can be seen from Figure 1, any pH_s below 10.5 must be very well fixed in order to obtain good reproducibility. Thus, accurate measurements are difficult to achieve and direct monitoring of the reaction with an air-gap electrode is not practical. Because of difficulties encountered, it was decided to perform the measurement in two separate steps: that is, to let the catalytic

Table I. Effect of Electrolyte Concentration on Sensitivity and Drift

electrolyte solution, $(NH_4^+)_e$, M	detection limit for NH_4^+, M	drift of pH_e: sample concn, $(NH_4^+)_s$, M	drift of pH_e: $\Delta pH_e/5$ min
1×10^{-3}	4.4×10^{-5}	1×10^{-4}	0.08
1×10^{-3}	4.4×10^{-5}	1×10^{-3}	0.04
1×10^{-3}	4.4×10^{-5}	1×10^{-2}	0.007
5×10^{-3}	4.8×10^{-5}	1×10^{-4}	0.02
5×10^{-3}	4.8×10^{-5}	1×10^{-3}	0.007
5×10^{-3}	4.8×10^{-5}	1×10^{-2}	0.002
1×10^{-2}	1.0×10^{-4}	1×10^{-4}	0.01
1×10^{-2}	1.0×10^{-4}	1×10^{-3}	0.005
1×10^{-2}	1.0×10^{-4}	1×10^{-2}	0.001

Table II. Interference Studies of Diverse Substances in the Electrochemical Method

diverse ions	final concn of diverse ions, M	% error observed: NO_2^-	% error observed: NO_3^-
Ca^{2+}	5×10^{-3}	−3.2	+1.9
Zn^{2+}	5×10^{-3}	−2.6	−3.5
Mn^{2+}	5×10^{-3}	+1.9	−4.2
Cu^{2+}	5×10^{-3}	−80.6	−75.4
Co^{2+}	5×10^{-3}	−2.7	−1.6
Ni^{2+}	5×10^{-3}	+1.7	−2.6
Mg^{2+}	5×10^{-3}	−3.4	+1.9
Hg^{2+}	5×10^{-3}	−100.0	−100.0
Na^+	5×10^{-3}	−0.9	−2.8
K^+	5×10^{-3}	−3.1	+1.3
NO_2^-	5×10^{-3}	...[a]	−2.7
NO_3^-	5×10^{-3}	+2.7	...[a]
ClO_4^-	5×10^{-3}	−4.5	−1.9
SO_4^{2-}	5×10^{-3}	+0.6	−4.4
SO_3^{2-}	5×10^{-3}	−1.7	−2.1
Cl^-	5×10^{-3}	+4.0	+0.7
ClO_3^-	5×10^{-3}	−1.8	−2.9
BrO_3^-	5×10^{-3}	−1.2	+3.2
IO_3^-	5×10^{-3}	+3.8	−1.2

[a] Final nitrate and nitrite concentrations: 5×10^{-3} M.

reaction incubate at a suitable pH for a definite time, and then to carry out the actual ammonia measurement by the addition of an excess amount of strong base to secure quantitative conversion. Therefore, pH 7.0 was chosen to minimize loss of ammonia during incubation, and the enzyme in either soluble or immobilized form still shows reasonably high activity, compared with curve 2. Much better results were obtained by the two-step method (curve 3) at the same substrate concentration (compare to curve 2). Curve 1 is a blank, with no enzyme added (*19*).

Effect of Concentration of Electrolyte on the Surface of the Electrode. The concentration of electrolyte was studied to determine which was optimum to achieve the greatest electrode response with the least drift. From Table I, two conclusions were reached. First, the lower the electrolyte concentration, the better the sensitivity. Second, the higher the concentration, the smaller the drift. Therefore, a compromise electrolyte concentration, 5×10^{-3} M, was used for all subsequent measurements.

Response Time and Recovery. The response time varies with substrate concentration. In general, it takes 30 s to 1 min, 2–3 min, and 5–7 min, to reach steady state at concentrations of 10^{-1}, 10^{-3}, and 10^{-4} M, respectively. Although the thickness of the electrolyte layer on the surface of the electrode has essentially no effect on the final pH_e value, it does affect the response time. This effect becomes especially apparent at low substrate concentrations, (5×10^{-6} M to 5×10^{-4} M), where poor response times were obtained (>7 min), if the layer was too thick. To make the layer thinner, a tissue was used to absorb the excess electrolyte. The return of the signal to a steady, well-defined baseline (the recovery time) was almost instantaneous, provided that the electrolyte layer is renewed between measurements.

Calibration Curve of Standard Solutions. According to the procedures described above, standard curves for nitrite and nitrate were obtained and are shown in Figure 3. The linear range is between 5×10^{-5}–1×10^{-2} M NO_3^- and NO_2^-, with a slope of 1.10–1.12 pH units/decade. The fact that the curve levels off at high concentrations is possibly due to (1) the oxidation of reduced methyl viologen by molecular oxygen before completion of the enzyme reaction. (2) The equation by Ruzicka and Hansen (*14*) does not hold at high concentrations, or (3) concentration is plotted and not activity. The leveling off observed at low concentration is due to the detection limit of the electrode. The calibration curves obtained using immobilized enzymes for nitrate, nitrite, and nitrate plus nitrite fall on one single straight line between 1×10^{-4}–1×10^{-2} M substrate with a slope of 1.04, which is close to theoretical value of 1.00.

Interference Study. Theoretically, using the steady-state method and the air-gap electrode, no interference is expected from any ions which do not inhibit the enzymic reaction. This is verified by the data in Table II, which shows that most diverse ions which may cause severe interference in conventional methods do not interfere. However, copper(II) and mercury(II), which immediately precipitate with dithionite ion, do interfere. No interference was observed from any other cations or anions.

Stability of Immobilized Nitrite and Nitrate Reductases. The stability of the immobilized enzyme was studied, based on how many measurements could be made with a 100% conversion of 1×10^{-2} M substrate to product, under standard assay conditions. It was shown that the immobilized nitrite reductase could be used with 100% conversion of nitrite to ammonia for about 100 measurements. After that time, the conversion efficiency decreased to 90% at 120 measurements. The immobilized nitrate reductase gave 100% conversion of nitrate to nitrite up to 150 measurements, with a gradual decrease resulting thereafter. However, the lifetime of the enzyme for 100% conversion can be extended by slowing down the flow rate.

Table III. Determination of Nitrate and/or Nitrite at a 1:1 Ratio

$(NO_3^- + NO_2^-)$ M: added	$(NO_3^- + NO_2^-)$ M: found	SD[b]	CV, %	relative error, %	(NO_2^-) M, found	SD	CV, %	relative error, %	(NO_3^-)[a] M calcd	relative error, %
1×10^{-4}	1.06×10^{-4}	0.081	7.6	6.0	4.55×10^{-5}	0.38	8.3	9.0	6.05×10^{-5}	21.0
5×10^{-4}	5.22×10^{-4}	0.30	5.7	4.4	2.38×10^{-4}	0.15	6.3	4.8	2.84×10^{-4}	13.6
1×10^{-3}	0.96×10^{-3}	0.040	4.2	4.0	4.88×10^{-4}	0.26	5.3	2.4	4.72×10^{-4}	5.6
5×10^{-3}	5.12×10^{-3}	0.17	3.3	2.4	2.51×10^{-3}	0.10	4.0	0.4	2.61×10^{-3}	5.2
1×10^{-2}	1.03×10^{-2}	0.022	2.1	3.0	4.93×10^{-3}	0.18	3.6	1.4	5.37×10^{-3}	7.4
				Av 3.96				Av 3.6		Av 10.56

[a] $(NO_3^-) = (NO_3^- + NO_2^-) - (NO_2^-)$. [b] Average of three measurements.

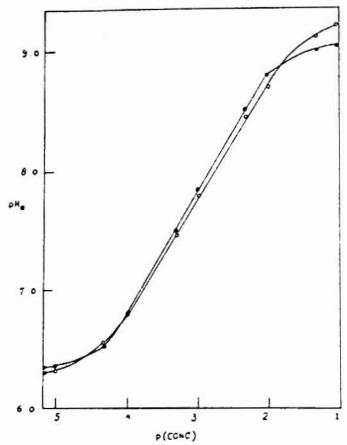

Figure 3. Calibration curve of nitrite and nitrate obtained from the soluble enzyme system. All measurement conditions (see text). (● – ●) nitrate, (O – O) nitrite

The immobilized enzymes are also very stable with temperature. Leaving the immobilized enzymes at room temperature for three weeks, 100% conversion was observed with both enzymes.

Determination of Nitrate and/or Nitrite in a Mixture. With the use of the dual enzyme system, samples of nitrite and nitrate in a mixture were measured (Table III). Poor reproducibility and high errors were observed at low substrate concentrations. This is mostly due to the sensitivity of the electrode to the CO_2 desorption from the electrolyte layer (coated on the surface of the electrode) onto the sample solution which was adjusted to high pH value (11.0). This CO_2 desorption causes an increase in pH value of the electrolyte layer (*19*), thus resulting in a drift of the response curve. This effect becomes obvious at low substrate concentration since at these concentrations the time to reach equilibrium is slow and the pH value at equilibrium, pH_e, is usually lower than those obtained from higher substrate concentrations (which have higher CO_2 desorption rates). The CO_2 desorption rate depends on temperature, the pH value, the volume of the electrolyte layer and of the sample solution, the stirring speed, and the air-gap space. All these factors can be controlled easily, with the exception of the thin electrolyte layer which is difficult to reproduce each time. Since the volume of the electrolyte layer is so small, a slight change will cause a large effect on the CO_2 desorption rate (*19*). Therefore, it is difficult to predict whether the error will be high or low. The assay value for nitrate, or nitrate plus nitrite, has more error than that for nitrite alone, because errors in both measurements are introduced. However, the method is reasonably good for the determination of NO_2^- and NO_3^- at concentrations greater than 5×10^{-4} M. It appears likely that this procedure is not very promising for the accurate assay of nitrate and nitrite mixture in potable water since 5×10^{-4} M is well above the allowable limits as previously described.

LITERATURE CITED

(1) J. Haldane, R. H. Makgill, and A. E. Mavrogordato, *J. Physiol.*, **21**, 160 (1897).
(2) O. Bodansky, *Pharm. Rev.*, **3**, 144 (1951).
(3) P. N. Magee and J. M. Barnes, *Br. J. Cancer*, **10**, 114 (1956).
(4) S. S. Mirvish, *J. Natl. Cancer Inst.*, **44**, 633 (1970).
(5) A. L. Fridmen, F. M. Mukhametshin, and S. S. Novikov, *Russ. Chem. Rev.*, **40**, 34 (1971).
(6) S. R. Tannenbaum, A. J. Sinskey, M. Weisman, and W. J. Bishop, *Natl. Cancer Inst.*, **53**, 79 (1974).
(7) Resources Agency of California "Water Quality Criteria", State Water Quality Control Board Publication No. 3-A, J. E. Mckee and H. W. Wolf, Ed., Sacramento, Calif., 1963, p 224.
(8) *Fed. Regist.*, **40**, No. 218, Tuesday, Nov. 11 (1975).
(9) G. B. Garner, J. S. Baumstark, M. E. Muhrer, and W. H. Pfander, *Anal. Chem.*, **28**, 1589 (1956).
(10) A. L. McNamara, G. R. Meeker, P. D. Shaw, and R. H. Hageman, *J. Agric. Food Chem.*, **19**, 229 (1971).
(11) R. H. Lowe and M. C. Gillespie, *J. Agric. Food Chem.*, **23**, 783 (1975).
(12) D. R. Senn, P. W. Carr, and L. N. Klatt, *Anal. Chem.*, **48**, 954 (1976).
(13) J. Ruzicka and E. H. Hansen, *Anal. Chim. Acta*, **69**, 129 (1974).
(14) E. H. Hansen and J. Ruzicka, *Anal. Chim. Acta*, **72**, 353 (1974).
(15) C. H. Klang, S. S. Kuan and G. G. Guilbault, *Anal. Chim. Acta*, **80**, 209 (1975).
(16) C. H. Ho and G. Tamara, *Agric. Biol. Chem.*, **37**, 37 (1973).
(17) P. Forget, *Eur. J. Biochem.*, **42**, 325 (1974).
(18) D. L. Marshall, *Biotech. Biol.*, **15**, 447 (1973).
(19) E. Hslung, S. S. Kuan, and G. G. Guilbault, *Anal. Chim. Acta*, **84**, 15 (1976).

RECEIVED for review January 10, 1978. Accepted May 17, 1978. The authors thank the NSF-RANN Food Technology Program (Grant No. AER-76-23271) for financial assistance in carrying out this project.

Enzymatic Determination of Nitrate: Fluorometric Detection after Reduction with Nitrate Reductase

Chih-Hen Kiang,[1] Shia S. Kuan, and George G. Guilbault*

Department of Chemistry, University of New Orleans, New Orleans, Louisiana 70122

An enzymatic method for the determination of trace amounts of nitrate in water has been developed. The enzyme, NADH-dependent nitrate reductase (EC 1.6.6.1), has been induced from *Chlorella vulgaris* and was highly purified by affinity chromatography. Nitrate is reduced to nitrite by this enzyme in the presence of NADH as electron donor. At the same time, NADH is oxidized to NAD^+. The rate of disappearance of NADH, indicated by a decrease of fluorescence intensity, is monitored with a newly developed, silicone-rubber pad fluorometric technique. Detection range is 50 ppb to 7.5 ppm.

Recently, the analysis of trace amounts of nitrate in drinking water has become very important. However, as mentioned earlier, most of the current methods are nonspecific, time-consuming and complicated. Therefore, the development of a simple, specific method which is sensitive enough to measure the nitrate content in drinking water is desirable. Fluorometric methods have a sensitivity which is approximately 10^3 times greater than that of most spectrophotometric methods. This method, together with an enzymatic approach, is well suited for this purpose.

NADH(nicotinamide adenine dinucleotide)-dependent nitrate reductase induced from algae can effect the reduction of nitrate to nitrite ion, in the presence of NADH as an electron donor. At the same time, NADH is oxidized to NAD^+; thus the rate of disappearance of NADH fluorescence can be easily monitored using a fluorometer.

$$NO_3^- + NADH_2 + \xrightarrow{\text{nitrate reductase}} NO_2^- + NAD^+ + H_2O \quad (1)$$

Because of its simplicity, sensitivity, and economy, a newly developed silicone-rubber pad fluorometric method (*1*) was used for all measurements.

EXPERIMENTAL

Apparatus. An Aminco Fluoro-Microphotometer (American Instrument Co., Silver Spring, Md.), fitted with Corning 7-60 primary filter, a Kodak-Wratten combination 2A/47B secondary filter, and RCA 1P28 photomultiplier as detector was used to monitor the fluorescent changes. The cell compartment and instrumental set up were the same as described by Lau and Guilbault (*2*). The change in fluorescence with time is measured and equated to the concentration of nitrate to be determined. Silicone-rubber pads used were the same as described by Kuan et al. (*1*).

Reagents and Materials. NADH, purchased from Sigma Chemical Co., was dissolved in 0.5 M phosphate buffer, pH 7.8 to make a final concentration of 2.5 mg/10 mL. Water samples were obtained from Jefferson Water Works (Jefferson, La.).

Chlorella vulgaris was a kind gift from L. P. Solomonson, Department of Biochemistry, College of Medicine, University of South Florida.

[1] Present address, Department of Chemical Engineering and Nuclear Engineering, Iowa State University, Ames, Iowa 50011.

Preparation of Enzyme. The induction, isolation, and purification was carried out as described by Solomonson (*3*). The enzyme has a specific activity of 21 units/mg, after a one-step affinity chromatographic purification from the crude extract.

Measurement of Nitrate. Place a silicone-rubber pad onto the center of the cell. To the pad add 10 μL of distilled water, 50 μL of standard nitrate solution or the sample solution, and 30 μL of enzyme solution; mix thoroughly with the help of a tiny syringe needle. Add 10 μL of NADH buffer solution and mix. Immediately insert the cell with the pad on it into the cell compartment to line up with the incident beam of the fluorometer. Record the change in fluorescence at 460 nm (excitation wavelength, 340 nm) for 2–3 min. Plot the change of fluorescence per min (ΔF/min) vs. the nitrate concentration of a series of standard nitrate solutions for the construction of a calibration curve. The nitrate in a water sample can be read directly from this calibration curve.

RESULTS AND DISCUSSION

Optimization of Measurement Conditions. The assay conditions were optimized, based on the effect of pH, buffer, buffer concentration, and temperature. As shown in Figure 1, the enzyme has higher activity in phosphate buffer than in Tris-HCl buffer. The optimum pH in phosphate buffer is around pH 7.6–8.0. Figure 2 shows that the optimum concentration of phosphate buffer for the rate change is fairly broad with a peak at 0.5 M. The enzyme is quite sensitive to temperature changes. Inactivation of enzyme occurred at temperatures greater than 30 °C; therefore, all measurements were run at room temperature. The effect of enzyme concentration on the rate is shown in Figure 3. A leveling off was observed at 30 μL of enzyme solution (0.0014 unit/μL), at substrate concentrations lower than 10 ppm. The order of reagent addition is also important since the enzyme can be inactivated by NADH in the absence of nitrate (*3*, *4*). It is better to mix enzyme, nitrate solution, and buffer solutions first; NADH is then added to initiate the enzyme reaction.

Calibration Curve of Nitrate. A calibration curve of standard nitrate solution exhibits linearity in the range of 1–7.5 ppm. However, a lower detection limit can easily be obtained by decreasing the amount of NADH used, and by switching the multiplier down to a more sensitive scale. In this case a straight line calibration curve was obtained from standard solutions between 50–1000 ppb. However, in the 50–250 ppb concentration range, the linear range of the reaction rate (ΔF/min) is short (15–30 s). To obtain better, more accurate plots, the use of faster chart speeds is recommended. When measuring a blank solution containing no nitrate ion, a small rate is always observed. This is probably due to the presence of trace amounts of NADH-oxidase which was not removed during the purification steps and to the self-decomposition of NADH at room temperature.

Measurement of Water Samples. Table I shows the value of nitrate obtained by the present method compared with the UV absorbance method (*5*); the agreement is very good. The recovery study showed an average of 98.5% (Table II). In order to evaluate the dynamic range of this method, the water sample was diluted 10-fold, and the percentage recovery was measured in the more sensitive range. The results are shown in Table III.

0003-2700/78/0350-1323$01.00/0

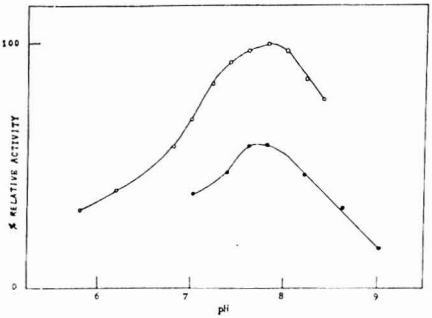

Figure 1. pH profile of NADH-nitrate reductase. KNO_3 concentration, 2×10^{-3} M. Incubation time, 5 min. Temperature, 25 °C. (O - O) Phosphate buffer, 0.075 M, pH 7.8. (● – ●) Tris buffer, 0.075 M, pH 7.8

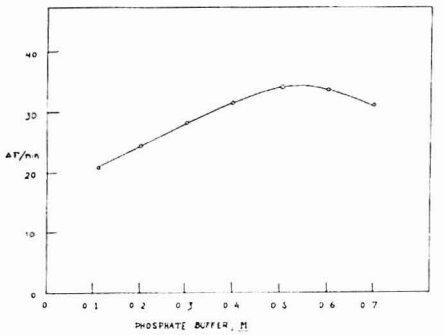

Figure 2. Plot of ΔF/min vs. M of phosphate buffer, pH 7.8. NO_3^- concentration, 5 ppm. All other conditions are the same as described in text

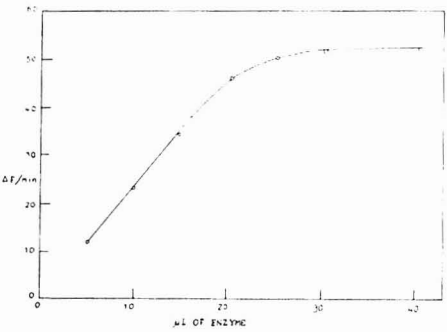

Figure 3. Plot of ΔF/min vs. nitrate reductase added per assay. NO_3^- concentration, 10 ppm. All other conditions are the same as described in text

Interference Study. The interference study is shown in Table IV. Except for copper(II) and mercury(II), most anions or cations do not interfere. The interference from chlorate, iodate, and bromate is because these anions are cosubstrates of the enzyme (*6*). The small interference from nitrite is probably due to product inhibition.

Table I. Determination of Nitrate in Water Samples

sample	UV method,[a] ppm	proposed method,[b] ppm	SD, ppm	CV, %
tap water				
1	3.72	3.77	0.09	2.3
2	5.28	5.41	0.07	1.3
river water				
1	4.37	4.92	0.12	2.4
2	6.23	6.05	0.13	2.1

[a] Data obtained from Jefferson Water Works. Average of three measurements. [b] Average of three measurements.

Table II. Recovery Study of Water Samples

NO_3^- added, ppm	total NO_3^- found, ppm	recovery, %
0.00	3.77	...
0.50	4.14	97
1.00	4.72	99
1.50	5.11	97
2.00	5.88	102
2.50	6.12	98
3.00	6.63	98
		av 98.5

Table III. Recovery Study of Diluted Water Samples[a]

nitrate concn, ppm		recovery, %
reported[b]	found[c]	
tap water		
3.77	3.54	94
5.41	5.30	98
river water		
4.92	5.06	103
6.05	5.74	95
		Av 97.5

[a] All samples were diluted 1:10. [b] Data obtained from Jefferson Water Works, average of three measurements. [c] Value obtained multiplied by the dilution factor (× 10), average of three measurements.

Table IV. Interferences Studies of Diverse Substances in the Fluorometric Method[a]

diverse ions	final concn of diverse ions, M	error observed, %
Ca^{2+}	1×10^{-3}	+2.0
Zn^{2+}	1×10^{-3}	−3.9
Mn^{2+}	1×10^{-3}	−5.2
Cu^{2+}	1×10^{-3}	−89.3
Co^{2+}	1×10^{-3}	+1.3
Ni^{2+}	1×10^{-3}	−18.4
Mg^{2+}	1×10^{-3}	−2.1
Hg^{2+}	1×10^{-3}	−100.0
Na^+	1×10^{-3}	−0.8
K^+	1×10^{-3}	−1.7
NH_4^+	1×10^{-3}	+3.1
NO_2^-	1×10^{-3}	−12.5
ClO_4^-	1×10^{-3}	−2.3
SO_4^{2-}	1×10^{-3}	−1.4
SO_3^{2-}	1×10^{-3}	+3.2
Cl^-	1×10^{-3}	−1.5
ClO_3^-	1×10^{-4}	+94.4
BrO_3^-	1×10^{-4}	+34.2
IO_3^-	1×10^{-4}	+18.7

[a] Nitrate concentration, 8×10^{-5} M.

Reproducibility. Many other factors such as drop shape, sample volume, and pad shape affect the reproducibility as discussed by Guilbault and Vaughan (7). Attention should be paid to placement of the pad inside the cell and to efficient mixing of the reagents before each measurement.

CONCLUSION

A method for the determination of nitrate in water samples at ppb levels has been developed. The advantages of this method over other enzymatic and spectrophotometric procedures are: simplicity—only enzyme, NADH, buffer solution, and substrate are needed for the measurement; rapidity—only 3–5 min is required for each assay; and specificity—most diverse ions do not interfere. Therefore, this procedure can be a very useful method for monitoring of nitrate in contaminated drinking water, as well as in food and other fields. The main disadvantages generally associated with most fluorescence methods, i.e., (1) errors from fluorescing contaminants such as aromatic organic compounds in the water sample and (2) sample matrix effects generally caused by spectral and nonspectral interferences associated with the matrix, are not as important in solid-surface methods such as the one described herein. Any strongly fluorescing compounds present, which absorb or emit at the same wavelengths as NADH, would interfere.

ACKNOWLEDGMENT

The authors thank L. P. Solomonson for his kind and generous supply of *Chlorella vulgaris*.

LITERATURE CITED

(1) J. C. W. Kuan, H. K. Lau, and G. G. Guilbault, *Clin. Chem.*, (*Winston-Salem, N.C.*), **21**, 67 (1975).
(2) H. K. Lau and G. G. Guilbault, *Clin. Chem.*, (*Winston-Salem, N.C.*), **19**, 1045 (1973).
(3) L. P. Solomonson, K. Jetschmann, and B. Vennesland, *Biochim. Biophys. Acta*, **309**, 32 (1973).
(4) J. M. Maldonado, J. Herrera, A. Paneque, and M. Losada, *Biochem. Biophys. Res. Commun.*, **51**, 27 (1973).
(5) "Standard Methods for the Examination of Water and Waste Water", 14th ed., Method 419–A, p 420; published by the American Public Health Association, American Water Works Association, and the Water Pollution Control Association, 1975.
(6) L. P. Solomonson and B. Vennesland, *Plant Physiol.*, **50**, 241 (1972).
(7) G. G. Guilbault and A. Vaughan, *Anal. Chim. Acta*, **55**, 107 (1971).

RECEIVED for review January 10, 1978. Accepted May 17, 1978. The financial assistance of the NSF-RANN Food Technology Program (Grant No. AER-76-23271) is gratefully acknowledged.

Determination of Polypropylene Glycol Extracted from Polymers into Food-Simulating Solvents

Tore Ramstad,* T. J. Nestrick, and R. H. Stehl

Dow Chemical U.S.A., Midland, Michigan 48640

A method for the determination of polypropylene glycol at sub-ppm levels in aqueous and organic media is presented. Combining the classical Zeisel alkoxyl reaction with high-efficiency GLC, the method has been used to determine the amount of polypropylene glycol (P-1200) extracted from several polymers into food-simulating solvents—ethanol/water, acetic acid/water, water, and heptane. Extracted polyglycol is degraded using hydriodic acid to form 2-iodopropane as the major reaction product. The 2-iodopropane is determined either by GLC or by GC-MS. This procedure has produced 75% overall conversion (yield) of polyglycol to 2-iodopropane and ±20% relative standard deviation.

Polypropylene glycol has found use as an additive in a variety of polymers. Its compatibility with the matrix, low volatility, and plasticizing attributes have led to increased use of polypropylene glycols as flexibilizing modifiers. To evaluate the amount of the additive which may migrate from a plastic food package into food, in support of our concerns about product stewardship as well as those of the Food and Drug Administration (*1*), analytical procedures have been developed to measure the concentrations of the additive in food-simulating media.

Several studies have been published on the analysis of polyglycols at high concentrations, including percent levels. These studies include procedures utilizing nuclear magnetic resonance spectrometry (*2*), a modified Zeisel procedure for oxyalkylene groups, including polypropylene glycol, in which evolved iodine was measured (*3*), thin-layer chromatography of various derivatives of polyglycols (*4*), and gas chromatography of polyethylene glycols as their silyl ethers (*5*, *6*).

For low ppm determinations, an alternative approach is required. [Since completion of this work, a sensitive technique for determining polyglycols by a derivative chronopotentiometric procedure has been published (*7*)]. Alkoxyl groups have been determined by the classical hydriodic acid decomposition of Zeisel (*8*). For ethers the Zeisel reaction may be represented as:

$$ROR' \xrightarrow{HI} RI + R'I + H_2O$$

Many modifications of the procedure exist (*9*, *10*), including the use of GLC for determination of the alkyl iodide. The determination of alkoxyl groups in cellulosics by Cobler et al. (*11*) was one of the first such applications. Crippen (*12*) reports a glycol determination on a 0.1-g sample using HI and propionic anhydride followed by gas chromatographic analysis on Poropak Q. Merz (*13*) published a method for the determination of propylene oxide polymers in which the chief reaction product of the Zeisel reaction is isopropyl iodide (68%) with 22% conversion to propionaldehyde. The volatile isopropyl iodide was collected in *m*-xylene in a cold trap and then determined chromatographically. More recently Pfifer (*14*) described the use of Rohm and Haas XAD resins to sorb oxyethylene from water. The oxyethylene was then reacted with HI to produce ethyl iodide with a final determination by GLC. We report here a microscale Zeisel/GLC procedure for the determination of polypropylene glycol of nominal molecular weight 1200 (P-1200) in four food-simulating

0003-2700/78/0350-1325$01.00/0

solvents—water, 1:1 (v/v) ethanol/water, 3:97 (v/v), acetic acid/water, and heptane.

EXPERIMENTAL

The decomposition of polypropylene glycol treated with 57% aqueous HI was investigated. Known amounts of P-1200 were introduced into ampules of ca. 6 cm^3 volume (Kontes Glass Company) along with measured amounts of acid. The sealed ampules were placed in an oven for different periods of time to study conversion efficiencies to the expected halides. Upon removing the ampules, they were cooled, scored, and opened. Using HI the major reaction product is 2-iodopropane (isopropyl iodide). It was established that at the low levels being determined in this work, a small amount of acetic anhydride added to the reaction ampule improved the conversion efficiency.

Nine plates of each plastic material (8.9 cm × 5.1 cm × 0.25 cm), separated by glass rods, were placed in 250–300 mL of food-simulating solvent in 16-oz bottles. Extractions into the food-simulating solvents were conducted at 49 °C (120 °F) for periods up to 21 days. Two or three milliliters each of the heptane, ethanol/water, and acetic acid/water extracts and 5 mL of the water extract were withdrawn at designated intervals and pipetted into the reaction ampules. These solutions were then evaporated to dryness under N_2 @ 55 °C. To each ampule was added, successively, 1 mL *o*-xylene, 100 μL HI, and 50 μL acetic anhydride. Following the addition of reagents, the ampules were sealed and placed in an oven at 150 °C for 1 to 1.5 h.

Upon completion of the reaction, the ampules were cooled first to room temperature, then in dry ice. The upper layer (*o*-xylene) was carefully thawed and the top portion of the ampule was washed with the *o*-xylene by careful tipping. Quickly then, the ampule was scored, opened, and covered with a serum cap. Upon reaching room temperature, most of the *o*-xylene layer (containing the isopropyl iodide) was transferred to a 2-dram vial containing 1 mL of freshly prepared aqueous K_2CO_3 (4 g in 50 mL) and K_2SO_3 (1 g in 50 mL). These reagents neutralize remaining acid and remove any free I_2. An aliquot of the *o*-xylene layer was injected into a gas chromatograph or into a combination gas chromatograph–mass spectrometer.

Reagents. The following reagents were used as received: hydriodic acid (57%), MC&B; acetic anhydride, J. T. Baker Chemical Company; *o*-xylene, Burdick & Jackson; 2-iodopropane, Aldrich Chemical Company, Inc.; and P-1200, Dow Chemical U.S.A.

Gas Chromatography. A Varian 1400 gas chromatograph was used in this work. Columns were packed either with 0.7% OV-275 on 80/100 Carbopack C or with Carbowax 20M bonded to 150/200 Porasil E-AW (internal preparation). Operating conditions are given in the caption of Figure 1. Combined gas chromatography–mass spectrometry was performed on a LKB 9000S. The column packing was either 25% DC-200 on 80/100 Chromosorb W-HP or Carbowax 20M bonded to 115/150 Porasil E-AW (internal preparation). Operating conditions are given in the caption of Figure 2.

The concentration of isopropyl iodide in the *o*-xylene was determined by comparison with isopropyl iodide standards prepared by weight in *o*-xylene. By subtracting any contribution from blanks (i.e., migration solvents alone), the amounts of polyglycols extracted and converted to isopropyl iodide were calculated.

Calculations. P-1200 may be represented as:

$$HO\text{-}\left(\text{CH}(CH_3)\text{-}CH_2\text{-}O\right)_{20}\text{-}H$$

Ignoring the two end groups (OH and H), we have from the Zeisel reaction,

$$\underset{\textbf{58}}{-CH(CH_3)-CH_2-O-} \longrightarrow \underset{\textbf{170}}{I-CH(CH_3)-CH_3}$$

Hence, for 100% conversion, 1 g of P-1200 yields ~(170/58) × 1 = 2.93 g of 2-iodopropane. Since 2-iodopropane standards were available, the actual yield of the Zeisel reaction could be determined and did not require the use of an identical sample of P-1200. The concentration of P-1200 corresponding to a measured amount of 2-iodopropane could then be calculated from the determined yield. The percent conversion of P-1200 to isopropyl iodide was approximately 75% although it ranged from 60–80%. As a check on conversion reproducibility, a known amount of P-1200 was included in each set of Zeisel reactions; all data subsequently reported are corrected for the experimentally-determined conversion yields.

Table I. ppm PPG Extracted[a] from GP Polystyrene[b]

water	0.08
$HOAc/H_2O$	0.10
$EtOH/H_2O$	0.50

[a] ppm (μg/mL) calculated for (10 cm^3 solvent volume)/(in.^{2} surface area) (*15*). These are averages of replicate determinations. [b] Addition of P-1200 at the 5% level.

Table II. ppm PPG Extracted[a] from Tyril[b]

H_2O	$HOAc/H_2O$	$EtOH/H_2O$	heptane
0.079	0.12	0.12	0.054
0.079	0.12	0.13	0.053
0.083	0.10	0.14	0.054
0.076	0.10	0.12	0.053
0.081	0.10	0.14	0.053
av. 0.080	0.11	0.13	0.053

[a] ppm (μg/mL) calculated for (10 cm^3 solvent volume)/(in.^{2} surface area) (*15*). [b] Addition of P-1200 at the 1% level.

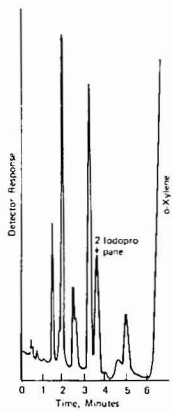

Figure 1. Gas chromatogram of $EtOH/H_2O$ extract of polystyrene. The 2-iodopropane peak is equivalent to 0.5 ppm PPG in the extract. GC conditions: 2 m × 3 mm glass packed with Carbowax 20M bonded to 150/200 Porasil E-AW; helium carrier at a flow of 75 cm^3/min; column temp., 70 °C; injector temp., 150 °C; FID detector temp., 250 °C; sample size, 2 μL; sensitivity, 2 × 10^{-12} afs

RESULTS

In Table I are shown the levels of polypropylene glycol (PPG) found in extracts of General Purpose (GP) polystyrene after 21 days. Figure 1 shows the gas chromatogram of the $EtOH/H_2O$ extract of polystyrene. Table II shows the results of five separate determinations of PPG extracted from Tyril (Trademark of The Dow Chemical Company), a copolymer of styrene and acrylonitrile, after 10 days. The data of Table II show excellent reproducibility for this procedure. Single-ion chromatograms of a $HOAc/H_2O$ blank and a 10-day $HOAc/H_2O$ extract of Tyril are shown in Figure 2; all data are corrected for blanks. Results for high impact polystyrene

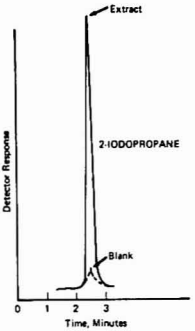

Figure 2. Single-ion mass chromatograms of HOAc/H_2O blank and extract of Tyril, mass = 170. The 2-iodopropane peak is equivalent to 0.11 ppm PPG in the extract. GC-MS conditions: 2 m × 3 mm glass packed with Carbowax 20M bonded to 115/150 Porasil E-AW; helium carrier at a flow of 40 cm^3/min; column temp., 135 °C; injector temp., 175 °C; separator temp., 150 °C; ion source temp., 250 °C; sample size, 2 μL

Table III. ppm PPG Extracted[a] from HIPS[b]

H_2O	HOAc/H_2O	EtOH/H_2O
0.73	0.77	1.76
0.70	0.82	1.73
0.83	0.87	1.78
0.76	0.86	1.81
0.83	0.81	1.80
av. 0.77	0.83	1.78

[a] ppm (μg/mL) calculated for (10 cm^3 solvent volume)/($in.^2$ surface area) (*15*). [b] Addition of P-1200 at the 5% level.

(HIPS) after 25 days are shown in Table III.

DISCUSSION

It was indicated that solvent blanks must be included in the analysis because of possible propylene glycol or propyl iodide contamination. It was discovered that the source of reagents is important: the blank using acetic anhydride catalyst which had been kept in a polyethylene bottle (Nalgon) was four times that of the blank using acetic anhydride kept in a glass bottle. In the latter case, the residual blank may have been due to some propyl iodide in the hydriodic acid. Nevertheless, for these solvents, the magnitude of the blank did not exceed one-tenth the amount of polyglycol originating from the polymer.

Conversions of P-1200 to 2-iodopropane were approximately 75%. Essential to high conversion efficiency is the inclusion of a solvent in the reaction ampule prior to carrying out the reaction. In the early stages of our work, a solvent was added after scoring and opening of the ampule, just prior to determination by GC. It was not until a solvent was added to the ampule before reacting the contents that conversion efficiency to the expected halide exceeded 25%. (We also investigated the decomposition of P-1200 using HBr. In this case, conversion never exceeded 25%). We believe that the effect of this solvent is twofold: to retain the propyl iodide as it is formed, promoting further reaction, and to reduce the chance of disproportionation to propane and propene (*3*). It should also serve to minimize losses of the volatile iodide when the ampule is opened. The use of a solvent in a sealed ampule precludes lower boiling solvents, since their vapor pressure would be excessive at the 150 °C needed for reaction.

The major reaction sequence presumed to occur with HI is as follows (*3*):

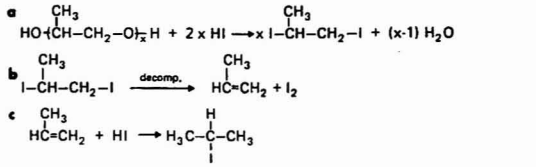

In (a) the oxypropylene units comprising the polymer are cleaved, reacting to form 1,2-diiodopropane (propylene iodide). The latter compound is unstable, being decomposed by both heat and light. Vicinal deiodination leads to propylene (b) which, in the presence of excess HI undergoes largely Markovnikoff addition to 2-iodopropane.

As the conversion efficiency of P-1200 to 2-iodopropane was normally about 75%, side reaction(s) are probably occurring. (Increased reaction time beyond 0.5–1 h did not increase the yield.) Siggia et al. (*3*) postulate the reaction of 1,2-diiodoethane with HI to form ethyl iodide. The equivalent reaction for 1,2-diiodopropane would be:

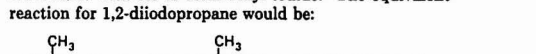

Under conditions where the 1-iodo- and 2-iodopropanes are resolved, there is relatively little 1-iodopropane formed. We conclude from this observation that the formation of 1-iodopropane does not subtract significantly from an overall yield to 2-iodopropane.

In summary, the modified Zeisel/GLC procedure developed yields a total figure for oxyalkylene units. Hence, it should be applicable to the determination of both high and low molecular weight glycols for these kinds of studies. Other possible applications include: (1) traces in waste water; (2) determination in biological materials; and (3) environmental distribution studies.

LITERATURE CITED

(1) Regulation 21 CRF 171.1—"Petitions", Bureau of Foods, Food and Drug Administration, Department of Health, Education, and Welfare, Washington, D.C. 20020.
(2) A. Mathias and N. Mellor, *Anal. Chem.*, **38**, 472 (1966).
(3) S. Siggia, A. C. Starke, Jr., J. J. Garis, Jr., and C. R. Stahl, *Anal. Chem.*, **30**, 115 (1958).
(4) L. Favretto, L. Favretto Gabrielli, and G. Pertoldi Marletta, *J. Chromatogr.*, **66**, 167 (1972).
(5) M. K. Withers, *J. Gas Chromatogr.*, **6**, 242 (1968).
(6) P. Holmqvist, *Anal. Chim. Acta*, **89**, 315 (1977).
(7) J. Törnqvist, *Acta Chem. Scand.*, **21**, 2095 (1967).
(8) S. Zeisel, *Monatsh.*, **6**, 989 (1885).
(9) D. Grün and F. Bochlach, *Ber.*, **41**, 3477 (1908).
(10) P. W. Morgan, *Ind. Eng. Chem., Anal. Ed.*, **18**, 500 (1946).
(11) J. G. Cobler, E. P. Samsel, and G. H. Beaver, *Talanta*, **9**, 473 (1962).
(12) R. C. Crippen, "Identification of Organic Compounds with the Aid of Gas Chromatography", McGraw Hill Book Company, New York, N.Y., 1973, pp 194–196.
(13) W. Merz, *Z. Anal. Chem.*, **82**, 232 (1967).
(14) L. H. Pfifer, 26th Pittsburgh Conference on Analytical Chemistry and Applied Spectroscopy, Cleveland, Ohio, March 3–7, 1975.
(15) "FDA Guidelines for Chemistry and Technology", Requirements of Indirect Food Additive Petitions, Bureau of Foods, Food and Drug Administration, Department of Health, Education, and Welfare, Washington, D.C. 20204, March 1976.

RECEIVED for review January 16, 1978. Accepted May 5, 1978.

Preparation and Chromatographic Applications of an Amide Resin

Gene M. Orf and James S. Fritz*

Ames Laboratory—U.S. Department of Energy and Department of Chemistry, Iowa State University, Ames, Iowa 50011

Synthetic routes are discussed for incorporation of a tertiary aliphatic amide group in a macroporous polystyrene–divinylbenzene resin. The amide resin retains uranium(VI), thorium(IV), and zirconium(IV) selectively from aqueous solution, pH 3.0. A liquid chromatographic separation scheme using the resin is given and quantitative results are obtained for uranium in synthetic and actual samples, and for thorium in synthetic samples. Gold(III) and palladium(II) are selectively retained by the resin from aqueous solutions containing hydrochloric acid. The resin has a capacity for gold of 1.7 mmol/g.

Incorporation of a chelating group of known selectivity into a resin is likely to result in a chelating ion-exchange resin of predictable selectivity. For example, isooctylthioglycolate is known to extract silver(I), gold(III), bismuth(III), copper(II), and mercury(II) selectively from acidic aqueous solution (*1*). A resin containing the thioglycolate functional group retains selectively all of the above metal ions except copper(II) from acidic aqueous solution (*2*).

The success of liquid amides in extracting uranium(VI), and to a lesser extent thorium(IV) and zirconium(IV), from aqueous nitrate solutions (*3*) has inspired us to introduce an amide group into a polystyrene-DVB resin. The resulting resin does indeed sorb selectively uranium, thorium, and zirconium from aqueous solution. It also retains gold(III) and palladium(II) strongly from aqueous chloride solutions.

EXPERIMENTAL

Chromatography. The liquid chromatograph used has been previously described (*4*). A resin column 6.0 cm × 0.6 cm was used for all separations. Uranium(VI), thorium(IV), and zirconium(IV) were determined automatically after addition of an Arsenazo III solution to the eluent stream at pH 0.5. Gold(III) was detected by collecting fractions and analyzing by ICP emission spectrometry.

Resin Synthesis. First, an amide group was introduced into silica gel or Porasil by the following sequence

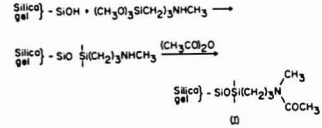

The starting material for resins II and III was Amberlite XAD-4 resin, a macroporous styrene-divinyl-benzene copolymer supplied by Rohm and Haas Co. The resin was Soxhlet extracted with methanol, ground, and sieved before use.

Resin II was prepared by the following reaction sequence:

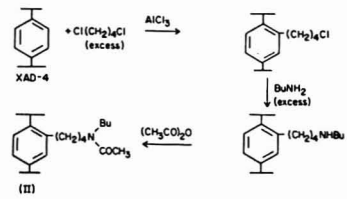

The first product of the synthesis of resin III was prepared as described by Falbe, Paatz, and Korte (*5*). This was accomplished by stirring 28 mL of γ-chlorobutyryl chloride into a solution of 84 mL of dibutylamine in 150 mL of petroleum ether which had been cooled in an ice bath. The reaction mixture was stirred for 2 h in the ice bath and then allowed to stand overnight. The salt was then filtered off and washed with petroleum ether. The ether was distilled from the product by rotovaporization and the product was purified by vacuum distillation at 150 °C, 0.001 mm Hg. The IR and NMR spectra confirm the structure of the first product.

The final resin was prepared by slowly adding 15 mL of the first product to a mixture of 9 g of XAD-4 which had been dried in a vacuum at 120 °C for 24 h, 21 g of anhydrous aluminum chloride, and 200 mL of carbon disulfide. The reaction mixture was then poured into an ice bath and the resin was finally filtered and washed with dilute hydrochloric acid and acetone.

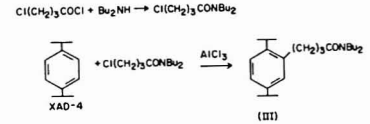

The presence of an amide group on the resin was confirmed by an IR spectra of the final product. The nitrogen content of the resin was determined by the Dumas method. This showed the resin to contain 2.88% nitrogen, which indicates 2.05 mequiv of amide functional group per gram of resin.

RESULTS AND DISCUSSION

Resins. Resin I retains uranium, thorium, and zirconium at pH values greater than 4.0 when nitrate or perchlorate salts are in relatively high concentration. However, unreacted hydroxyl groups on the silica prevented clean elution of the retained metal ions. Attempted deactivation of the hydroxyls by silanization improved the situation only slightly.

Resin II retained uranium, thorium, and zirconium only when 2.0 M (or greater) sodium nitrate or sodium perchlorate was added to the aqueous solution. It is possible that the 1,4-dichlorobutane may have caused some cross-linking between phenyl groups that would hinder complexation of metal ions by the amide groups. Since three different chemical reactions were performed before obtaining the final product, there is the possibility of undesirable functional groups remaining from incomplete chemical reactions.

Resin III was much the most successful. At least two different batches of the resin were prepared successfully. This resin was used for all of the work reported in this paper.

Separation of Uranium(VI), Thorium(IV) and Zirconium(IV). Uranium, thorium, and zirconium are taken up by a column of the resin from pH 3.0 perchloric or nitric acid solutions. The method chosen for the separation of uranium, thorium, and zirconium from each other and from several other heavy metals was as follows. A sample containing uranium, thorium, zirconium, and foreign ions is injected into an eluent stream of pH 3 perchloric acid. Under these conditions, most foreign ions are eluted and the three ions of interest are retained. The uranium is then eluted with pH 2 perchloric acid, the thorium is eluted with pH 0.5 perchloric acid, and the zirconium is eluted with 1 M sulfuric acid. Zirconium could be eluted with any mineral acid with a

0003-2700/78/0350-1328$01.00/0

Table I. Determination of Uranium in the Presence of Foreign Ions

foreign ions	% recovery, av of two trials
10^{-3} M Fe^{3+}, Al^{3+}, and Co^{2+}	99.1
10^{-3} M Mg^{2+}, Pb^{2+}, and Ni^{2+}	99.5
10^{-3} M Zn^{2+}, Cu^{2+}, and Cd^{2+}	99.5
10^{-3} M V^{5+}, 5×10^{-5} M Th^{4+}, and Zr^{4+}	100.0
10^{-3} M Hg^{2+}, 5×10^{-5} M Th^{4+}, and Zr^{4+}	99.0
10^{-3} M NO_3^-, 5×10^{-5} M Th^{4+}, and Zr^{4+}	97.9
10^{-3} M Cl^-, 5×10^{-5} M Th^{4+}, and Zr^{4+}	100.0
10^{-3} M SO_4^{2-}, 5×10^{-5} M Th^{4+}, and Zr^{4+}	99.4
10^{-3} M tartrate	91.5
10^{-3} M citrate	76.0
10^{-3} M phosphate	99.2

Table II. Determination of Thorium in the Presence of Foreign Ions

foreign ions	% recovery, av of two trials
10^{-3} M Fe, Al, Co, 5×10^{-5} M U, and Zr	97.2
10^{-3} M Mg, Pb, Ni, 5×10^{-5} M U, and Zr	99.4
10^{-3} M Zn, Cu, Cd, 5×10^{-5} M U, and Zr	98.9
10^{-2} M tartrate, 5×10^{-5} M U, and Zr	94.6
10^{-2} M citrate, 5×10^{-5} M U, and Zr	85.6
10^{-2} M phosphate, 5×10^{-5} M U, and Zr	0
10^{-3} M Ho, 5×10^{-5} M U, and Zr	83.3
10^{-3} M Ce, 5×10^{-5} M U, and Zr	90.7
10^{-3} M Gd, 5×10^{-5} M U, and Zr	92.6
10^{-3} M V, 5×10^{-5} M U, and Zr	97.2
10^{-3} M Sn, 5×10^{-5} M U, and Zr	77.6
10^{-3} M Hg, 10^{-5} M U, and Zr	100.0
10^{-3} M sulfate, 5×10^{-5} M U, and Zr	127.0
10^{-3} M nitrate, 5×10^{-5} M U, and Zr	104.0
10^{-3} M chloride, 5×10^{-5} M U, and Zr	98.2

concentration of 1 M or greater, but the sharpest elution was obtained with sulfuric acid. A chromatographic separation is shown in Figure 1.

Separations of standard solutions of uranium, thorium, and zirconium of various concentrations gave linear calibration curves (peak height vs. μg of metal ion) for uranium and thorium. However, zirconium could not be determined quantitatively, possibly because of polymerization or lack of complete, reproducible reaction with the color-forming detection reagent.

Uranium and thorium were determined quantitatively in the presence of 20-fold molar excesses of several foreign metal ions and as much as a 200-fold excess of some anions. All separations were performed on a 6.0 cm × 0.6 cm resin column with an eluent flow rate of 1.2 mL/min and a color-forming reagent flow rate of 0.8 mL/min. The sample loop was 54 μL. The results in Tables I and II show the method to be quite selective. Rare earth salts and citrate cause major interference for both uranium and thorium. Phosphate interferes with thorium but not with uranium.

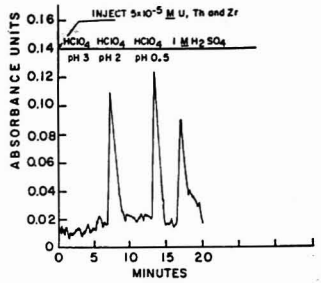

Figure 1. Separation of 5×10^{-5} M uranium(VI), thorium(IV), and zirconium(IV)

Low grade ores were analyzed for uranium and thorium to see if the resin had a practical use for the determination of trace amounts of the metals in real samples. Carnotite samples of 0.1 g were digested in 20 mL of concentrated hydrochloric acid and then digested to dryness in a solution of 15 mL of concentrated hydrochloric acid and 15 mL of concentrated nitric acid. The residue was then dissolved in 100 mL of distilled water. Uraninite samples of 0.1 g were digested in a solution containing 15 mL each of concentrated sulfuric and nitric acids and also diluted to 100 mL. The samples were analyzed in the same way as all previous samples. The results are shown in Table III. Attempted analysis of a monazite sample for uranium and thorium was not successful.

Separation of Gold(III). The amide resin sorbs gold(III) strongly from aqueous hydrochloric acid solutions. The capacity of a resin column for gold was fairly constant from 0.5 M to 4.0 M hydrochloric acid and averaged 1.7 mmol/g. This compares with column capacities of only 0.08 mequiv/g for uranium and 0.04 mequiv/g for thorium under the conditions described earlier.

Column studies with 1.0 M and 5.0 M hydrochloric acid showed that gold(III) and palladium(II) are taken up strongly, but rhodium(III), platinum(IV), and silver(I) are not retained. It is difficult to elute gold and palladium from the resin column with most reagents tried, but elution is readily accomplished with 0.1 M sodium cyanide.

Gold(III) added to deionized water and also to seawater at approximately 1 ppm concentrations was quantitatively recovered after passing 1 L of water through a 6.0 cm × 0.6 cm resin column at 5 mL/min and subsequently eluting with 0.1 M sodium cyanide.

Many resins that are selective for gold(III) cause partial reduction of the gold(III), perhaps to the metal. This does not occur nearly so readily on the amide resin, although the yellow gold band on the resin column does turn black if left for a long period of time. Even then, the black band is removed by elution with cyanide and the resin can be used for many sorption and elution cycles.

Table III. Analysis of Low Grade Uranium and Thorium Ores

sample	species determined	% found	% previously found
Uraninite (International Atomic Energy Survey Reference Sample No. S4)	U_3O_8	0.371 ± 0.053	0.375
Carnotite (USERDA Reference Materials Section, New Brunswick, N.J., Carnotite Sample No. 4)	U_3O_8	0.19 ± 0.02	0.18

LITERATURE CITED

(1) J. S. Fritz, R. K. Gillette, and H. E. Mishmash, *Anal. Chem.*, **38**, 1869 (1966).
(2) E. M. Moyers and J. S. Fritz, *Anal. Chem.*, **48**, 1117 (1976).
(3) J. S. Fritz and G. M. Orf, *Anal. Chem.*, **47**, 2043 (1975).
(4) M. D. Arguello, Ph.D. Thesis, Iowa State University, Ames, Iowa, 1977.
(5) J. Falbe, R. Paatz, and F. Korte, *Chem. Ber.*, **97**, 2544 (1964).

RECEIVED for review December 19, 1977. Accepted May 12, 1978. This work supported by the U. S. Department of Energy, Division of Basic Energy Sciences.

Characterization of the Ion-Exchange Membrane Detector for Liquid Chromatography and Its Application to the Separation of Quaternary Ammonium Compounds

John G. Dorsey, Mark S. Denton,[1] and T. W. Gilbert*

Department of Chemistry, University of Cincinnati, Cincinnati, Ohio 45221

An LC detector which operates by measuring dimensional changes of a strip of ion-exchange membrane has been further characterized and is shown to be useful for the detection of quaternary ammonium ions. The detector has a precision of better than 1% standard error and a linear range for choline and acetylcholine of at least 2.5 orders of magnitude.

Quaternary ammonium ions are commercially used as antiseptics, antistatic agents, in detergent formulations of fabric softeners, as a water treatment biocide, and in secondary-recovery oil wells. They are also prevalent in biological systems, and are of great biomedical interest. The commercial products are usually mixtures, and the determination of individual compounds in them has long been a troublesome analytical problem. Most often only the total tetraalkyl ammonium content is determined. Trace amounts have been determined in both commercial (*1*) and biological (*2*) samples by ion-pair extraction and colorimetry. Larger amounts may be determined and differentiated from amines by nonaqueous titration (*3*). Some degree of selectivity may be achieved by careful control of ion-pair extraction conditions followed by two-phase titration with lauryl sulfate (*4*). However, closely similar quaternary ammonium ions cannot be differentiated by the latter procedure and, for those that can be differentiated, qualitative knowledge of the sample composition is required for proper adjustment of the conditions of extraction (*5, 6*).

For the separation of closely similar quaternary ammonium ions, a chromatographic method is required. Thin-layer chromatography on alumina (*7, 8*) and high voltage electrophoresis (*9*) have been used, and quantitation has been accomplished by spraying with color-forming reagents. Gas chromatography has been applied to the analysis of choline and its esters but, because of the nonvolatility of the compounds, either prior derivatization or pyrolysis techniques must be used (*10–13*). GC-MS, both electron impact ionization and chemical ionization, is also useful (*14, 15*).

Liquid chromatography would be the separation method of choice because of the poor volatility of the compounds. Unfortunately, the lack of useful UV-visible absorption bands has made the detection and quantitation of quaternary ammonium ions difficult. Ion-pair partition chromatography using picrate as the anionic species has permitted the use of UV detection (*16*). However, this method has a very limited concentration range because of changes in the distribution ratios of the individual cations with concentration. Various other methods, all involving collected fractions and subsequent analysis, are still widely used for the detection of quaternary ammonium ions. These include precipitation with sodium triphenylcyanoborate (*17*), ^{14}C labeling of the compounds (*18*), NMR analysis (*19*), and color formation with periodide (*18, 20*).

It is clear that a continuous means of detecting quaternary ammonium compounds is badly needed for such studies.

Recently a new general purpose detector was developed in this laboratory for continuously monitoring the effluent from a liquid chromatography column (*21*). This detector utilizes a phenomenon which is associated with all ion-exchange processes—namely, the volume change of the resin matrix which accompanies all ion-exchange reactions. An osmotically induced volume change also occurs for nonelectrolytes which partition into the resin phase. Thus, it is seen that insofar as only species which are capable of exchanging with the counterions, or partitioning into the resin are considered, the detector is completely general, giving a response for all species. The magnitude of the response will depend on the identity of the pair of ions in the exchange reaction, the physical properties of the resin matrix, and the composition of the external solution.

The effluent flows through a low volume glass tube in which a strip of ion-exchange membrane is suspended and attached to a linear voltage differential transformer (LVDT) in a Du Pont Model 941 thermomechanical analyzer (TMA). Extremely small changes in the length of the ion-exchange membrane during sorption and desorption of ions cause the LVDT core to be displaced from its electrical center, resulting in a signal which is recorded on the Y axis of a strip chart recorder.

This paper describes the application of this detector to the separation and determination of some simple quaternary ammonium ions, and of choline and its esters. The synthesis of an ion-exchange membrane with a greater sensitivity than commercially available membranes is reported. The precision, linearity of response, flow rate sensitivity, and detection limits of this new detector are discussed.

EXPERIMENTAL

Chromatographic System. Delivery of the mobile phase was made with a Chromatronix Model CMP-2 chemically inert piston pump. Samples were introduced into the flowing mobile phase

[1] Present address, Oak Ridge National Laboratories, P.O. Box X, Room B8, Building 4500N, Oak Ridge, Tenn. 37830.

0003-2700/78/0350-1330$01.00/0

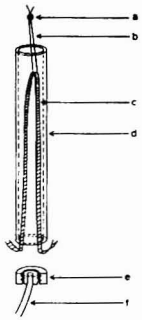

Figure 1. Inverted loop membrane detector. (a) Pb ball; (b) Pt ribbon; (c) ion-exchange membrane; (d) thick walled Pyrex tube; (e) Chromatronix microbore column fitting; (f) Teflon inlet tubing

stream with a Chromatronix R60SV rotary injection valve having replaceable sample loops. An adjustable bed Chromatronix LC-9M column, 9.0-mm i.d., was used throughout. All components were interconnected with 0.79-mm i.d. Teflon tubing. The system was capable of operation up to a maximum pressure of 500 psi.

Aminex A-4 resin (Bio-Rad Laboratories), 16–24 μm, was equilibrated three times with the mobile phase and then slurry packed. When the column was filled, the resin bed was compressed by pumping the mobile phase through the column at maximum flow rate for at least 1 h, and the column adjusted to this final bed height. The mobile phase was 0.025 M ethylene diammonium chloride (en·2HCl) made in distilled water and vacuum degassed.

Reagents. The en·2HCl was made using the procedure of Arguello and Fritz (*23*). The quaternary ammonium salts, tetramethylammonium bromide, ethyltrimethylammonium iodide, diethyldimethylammonium bromide, and triethylmethylammonium iodide (Eastman Chemical, Rochester, N.Y.); and choline and esters, choline chloride, acetylcholine chloride, propionylcholine iodide, and butyrylcholine iodide (all 99%, Sigma Chemical, St. Louis, Mo.) were used as received. Sample solutions were prepared by dissolving the solids in 0.035 M en·2HCl; solutions containing choline and its esters were stored at 4 °C.

Membranes. Strips of polyethylene (12 × 0.15 cm, 26.7 μm thick) were cut from Glad Food Storage Bags (Union Carbide). They were washed overnight with a detergent solution, rinsed with distilled water and ethanol, and air dried. Pyrex tubes (ca. 35 cm long, 15-mm o.d., 12-mm i.d.) were half filled with styrene (Eastman, 98%, stabilized with *tert*-butylpyrocatechol), the polyethylene strips added, and the mixture was bubbled with N_2 for 10 to 15 min. The tubes were flame sealed and irradiated with a 195 kR/h γ-ray source for varying lengths of time. After irradiation, the strips were washed three times with benzene, once with absolute ethanol, and dried. The percent grafting was established by the weight change of a pre-weighed square of the polyethylene film. The samples were sulfonated by immersing the polymer strips in chlorosulfonic acid at room temperature for 25 min. The strips were then placed successively in CCl_4 for 1 h to remove excess chlorosulfonic acid, concentrated H_2SO_4 for 5 min, and finally in 20% NaOH at 70 °C for 20 min.

The capacities of the membranes were determined by titrating the hydrogen ions liberated by the membranes upon the addition of an excess of NaCl to a solution containing the membranes. Each membrane was first converted to the hydrogen form by soaking in 1 M HCl followed by rinsing with water until the effluent was free of chloride ion. The titrations were performed with carbonate-free NaOH to a phenolphthalein end point. The titration volumes were corrected by a blank titration of NaCl.

Monitor and Detector. The monitor and the adjustment of the TMA have been described previously (*21*). The detector design is that of Hansen (*22*) and is different from the one previously used. It is shown in Figure 1. A strip of sulfonated, 4-h irradiated copolymer, 12 × 0.15 cm, was looped in the shape of an inverted V inside a thick walled glass tube, 7.2 cm × 0.27 cm i.d., giving the detector a volume of 412 μL. A piece of Pt ribbon (0.009 × 0.15 mm) was placed through the membrane loop, and a Pb ball was squeezed shut on the ends of the Pt ribbon. The Pb ball then rests in a cradle on the tension probe connected to the LVDT core. By using thick walled glass tubing and the fittings from a Chromatronix microbore column, the bottom of the membrane is easily held in place. A sealing disk with a centered hole holds the two ends of the membrane tightly against the end of the glass tube and the column effluent is pumped directly into the center of the detector body.

Procedures. For the membrane response comparisons, the flow rate study, the calculations of precision of response, and the time constant measurements 0.276-mL samples of 0.1 M NaCl were injected directly into the detector with 1.0 M H_2SO_4 as eluent.

Table I. Percent Polystyrene Grafting and Exchange Capacity of Membranes

radiation time, h	total dose, kR	% grafting, w/w	membrane capacity: μequiv/cm²	membrane capacity: mequiv/g dry membrane
1	188	3.6	1.05	0.508
4	752	34.1	5.25	2.60
8[a]	1504	37.8	6.00	2.78
16.9	3130	63.5	8.34	3.85

[a] A high degree of homopolymerization of this sample was indicated by a very viscous styrene liquid phase.

DISCUSSION

Membranes. The primary considerations for an ideal membrane for this application are: high mechanical strength for resistance to tearing, flexibility for resistance to cracking, thinness for rapid equilibration with the external solution, resistance to inelastic deformation and low cross-linking for maximum swelling or shrinking response to ion-exchange reactions. These characteristics are antagonistic and compromises must be made. Of the many commercial membranes which have been tested, the cation membrane CC-60 and the anion membrane AA-60 (American Machine and Foundry Co.) which were used previously (*21*) continue to be the most responsive. These are of the graft copolymer type, consisting of a polyethylene backbone with grafted polystyrene which is then sulfonated or quaternized. Unfortunately, these are no longer being manufactured, so similar membranes were prepared by a method similar to that of Chen et al. (*24*). Table I shows the percent grafting and capacity data for these membranes. The copolymer films from the 8- and 17-h irradiation times were grainy, showing localized styrene polymerization, and have not been investigated for detector response.

The response of the 4-h irradiated sample was then compared to that of the CC-60. The average probe displacement for the CC-60 was 4.74 μm (15 replicates) while that for the synthesized membrane was 14.0 μm (seven replicates). Thus, for a pure ion-exchange interaction, the newly prepared membrane gave a response about three times greater than that of the commercial membrane.

It is believed that two factors contribute to this improved response. The new membranes are three to four times thinner than the commercial membranes, providing for more rapid equilibration during the exchange process. Second, the extent of cross-linking of the commercial membranes is not known, but the new membranes are not DVB cross-linked, and so are likely to show greater dimensional changes during an exchange reaction.

Detector Design and Response. The new detector cell design is an inversion of that previously reported (*21*). The previous design required very tedious alignment of the detector cell to prevent the TMA probe from binding on the cell walls.

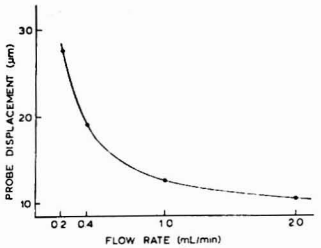

Figure 2. Detector response to NaCl samples vs. flow rate

Table II. Precision Data

injection	peak height,[a] mm	peak width$_{0.5}$, mm	peak area, mm^2 [b]
1	71.5	10.0	715
2	69.5	10.0	695
3	70.5	9.8	691
4	69.5	10.0	695
5	70.5	10.0	705
6	71.5	10.0	715
7	71.0	9.5	675

[a] A peak height of 70 mm corresponds to a probe displacement of 14 μm. [b] Peak area standard and mean deviations. $S = 14.3$ mm^2. $S_m = 5.40$ mm^2.

The inverted loop membrane design is not as critical with respect to alignment, and setup time is on the order of a few minutes. The new design is also much less sensitive to flow pulsations.

Figure 2 shows the response of the inverted loop membrane detector as a function of flow rate. Each data point represents the average of triplicate samples. The slower flow rates allow longer residence time of the solute in the detector cell and, hence a greater response, as more of the solute ions exchange onto the membrane. Present work is being directed toward a design giving more turbulent flow to minimize this diffusion limited response.

Table II shows the peak height and peak area ($A = h \times w_{0.5}$) for seven sequential injections. The average area was 699 mm^2 with a standard deviation of 14.3 mm^2 and a standard error of 5.40 mm^2. Thus, the detector is reproducible during any given period of operation. Day to day variations of 10 to 20% can occur, however, if the detector is dismounted at the end of the day's operation.

Different membrane strips of the same capacity and similar in length show responses within the 10 to 20% variation range. Therefore, if the detector is dismounted, or a new membrane is used, two or more standards must be run to re-establish the calibration curve.

These seven sequential injections were also used to measure the time constant of the membrane, defined as the time required for the membrane to reach 63% of its maximum value at a flow rate of 2.00 mL/min. For the adsorption process, the value is 11 s, while for the desorption process, it is 25 s.

Applications. Figure 3 shows a separation of simple quaternary ammonium ions with a 22.5-cm column of Aminex A-4 resin. The negative peak at 10 min is the "exchange peak" and has been discussed previously (*21*). Analogous to the refractive index detector, both positive and negative peaks can be obtained, corresponding to expansion and contraction of the membrane.

Figure 4 shows the separation of choline and three of its esters with a 19-cm column of Aminex A-4. Two factors had

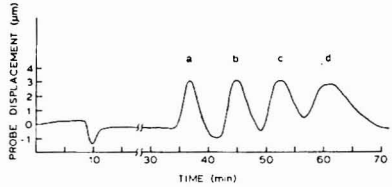

Figure 3. Separation of simple quaternary ammonium ions. (a) tetramethylammonium; (b) ethyltrimethylammonium; (c) diethyldimethylammonium; (d) triethylmethylammonium. Sample: 1.009 mL of 0.035 M en·2HCl which is also 0.015 M in each of (a), (b), (c), (d). Mobile phase: 0.035 M en·2HCl. Flow rate: 1.00 mL/min. Column: 22.5 × 0.90 cm Aminex A-4

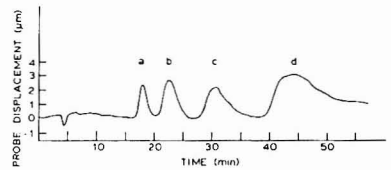

Figure 4. Separation of choline and esters. (a) choline, 0.010 M; (b) acetylcholine, 0.010 M; (c) propionylcholine, 0.0060 M; (d) butyrylcholine, 0.0060 M. Sample: 1.009 mL of (a), (b), (c), (d) at the above concentrations in 0.035 M en·2HCl. Mobile phase: 0.035 M en·2HCl. Flow rate: 2.00 mL/min. Column: 19 × 0.90 cm Aminex A-4

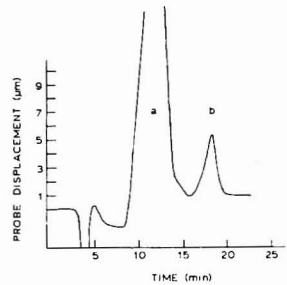

Figure 5. Determination of choline in a soy meal extract. (a) Li^+; (b) choline determined to be 2.6 mg/mL. Sample: 0.456 mL of soy meal extract. Mobile phase: 0.035 M en·2HCl. Flow rate: 2.00 mL/min. Column: 17 × 0.90 cm Aminex A-4

to be considered in the selection of the mobile phase for this separation. First, it has been shown that the identity of the mobile phase and the sample affect the response of the detector (*21*, *25*). Second, the stability of the choline esters had to be considered. It has been shown that the maximum stability of acetylcholine with respect to hydrolysis at room temperature was obtained at pH 4.7 (*26*). The rates of hydrolysis of the other choline esters should be similar. The pH of 0.035 M en·2HCl is 4.4 at 22 °C and the greatest membrane response to choline was obtained with this mobile phase.

The linear range for choline under these conditions is from 10^{-1} M to 5×10^{-4} M. The average peak heights of triplicate samples of 1.009 mL were converted to probe displacement and a plot of log displacement vs. log concentration gave a slope of 1.00. This method for obtaining a quantitative estimation of detector linearity has been described by Fowliss and Scott (*27*). The lower end of the linear range is limited by the sensitivity of the detector and could probably be extended somewhat at a slower flowrate. With a mobile phase of 0.035 M en·2HCl and a flow rate of 2.00 mL/min, the

minimum detectable quantity, defined as the concentration of sample that produces a signal equal to twice the baseline noise, is about 3×10^{-5} g/mL for choline or acetylcholine. While this detector is significantly less sensitive for these compounds than GC (*10–13*), no lengthy sample pretreatment is necessary.

Figure 5 shows an application of the membrane detector to the determination of choline in a soy meal extract. The large, off-scale peak is Li^+, from LiOH, used to raise the pH of the extract. The second peak is choline, determined to be 2.6 mg/mL of extract. Details of this analysis, including extraction conditions and comparisons with other methods will be presented elsewhere.

LITERATURE CITED

(1) M. E. Auerbach, *Ind. Eng. Chem., Anal. Ed.*, **15**, 492–493 (1943).
(2) S. Eksborg and B. A. Persson, *Acta Pharm. Suec.*, **8**, 605–608 (1971).
(3) St. J. H. Blakeley and V. J. Zatka, *Anal. Chim. Acta*, **74**, 139–146 (1975).
(4) S. O. Jansson, R. Modin, and G. Schill, *Talanta*, **21**, 905–918 (1974).
(5) R. Modin and S. Back, *Acta. Pharm. Suec.*, **8**, 585–590 (1971).
(6) B. A. Persson, *Acta Pharm. Suec.*, **8**, 217–228 (1971).
(7) C. Radecka, K. Genest, and D. W. Hughes, *Arzneim.-Forsch*, **21**, 548–550 (1971).
(8) W. F. H. McLean and K. Jewers, *J. Chromatogr.*, **74**, 297–302 (1972).
(9) S. E. Brooker and K. J. Harkiss, *J. Chromatogr.*, **89**, 96–98 (1974).
(10) P. I. A. Szilagyi, D. E. Schmidt, and J. P. Green, *Anal. Chem.*, **40**, 2009–2013 (1968).
(11) D. J. Jenden, R. A. Booth, and M. Roch, *Anal. Chem.*, **44**, 1879–1881 (1972).
(12) D. E. Schmidt and R. C. Speth, *Anal. Biochem.*, **67**, 353–357 (1975).
(13) J. L. W. Pohlmann and S. L. Cohan, *J. Chromatogr.*, **131**, 297–301 (1977).
(14) I. Hanin and R. F. Skinner, *Anal. Biochem.*, **66**, 568–583 (1975).
(15) C. G. Hammar, I. Hanin, B. Holmstedt, R. J. Kitz, D. J. Jenden, and B. Karlen, *Nature (London)*, **220**, 915–917 (1968).
(16) S. Eksborg and G. Schill, *Anal. Chem.*, **45**, 2092–2100 (1973).
(17) J. S. Hayes, M. A. Alizade, and K. Brendel, *Anal. Chim. Acta*, **80**, 361–367 (1975).
(18) D. Speed and M. Richardson, *J. Chromatogr.*, **35**, 497–505 (1968).
(19) F. Chastellain and P. Hirsbrunner, *Fresenius' Z. Anal. Chem.*, **278**, 207–208 (1976).
(20) W. K. Gourley, C. D. Haas, and S. Bakerman, *Anal. Biochem.*, **19**, 197–200 (1967).
(21) T. W. Gilbert and R. A. Dobbs, *Anal. Chem.*, **45**, 1390–1393 (1973).
(22) Larry C. Hansen, Ph.D. Thesis, University of Cincinnati, Cincinnati, Ohio, 1973.
(23) M. D. Arguello and J. S. Fritz, *Anal. Chem.*, **49**, 1595–1598 (1977).
(24) W. K. W. Chen, R. B. Mesrobian, D. S. Ballantine, D. J. Metz, and A. Glines, *J. Polym. Sci.*, **23**, 903–913 (1957).
(25) Richard A. Dobbs, Ph.D. Thesis, University of Cincinnati, Cincinnati, Ohio, 1973.
(26) D. J. Jenden and L. B. Campbell, in "Methods of Biochemical Analysis, Supplemental Volume", D. Glick, Ed., Interscience, New York, N.Y. 1971.
(27) I. A. Fowliss and R. P. W. Scott, *J. Chromatogr.*, **11**, 1 (1963).

RECEIVED for review December 19, 1977. Accepted May 8, 1978. J.G.D. gratefully acknowledges the University of Cincinnati Research Council for support from a Summer Fellowship. M.S.D. gratefully acknowledges the University of Cincinnati for support through a Twitchell Fellowship. Partial support of this work in the form of a Frederick Gardner Cottrell Grant from the Research Corporation is also gratefully acknowledged.

Evaluation of a Computer-Controlled Stopped-Flow System for Fundamental Kinetic Studies

Glen E. Mieling and Harry L. Pardue*

Department of Chemistry, Purdue University, West Lafayette, Indiana 47907

This paper describes the application of a computer-controlled stopped-flow system for a kinetic study of the Fe(III)–thiocyanate reaction. Kinetic equations are developed for a proposed mechanism involving two parallel pathways, and results of some 456 experiments run under computer control are interpreted and processed to provide explicit values for forward and reverse rate constants for the proposed mechanism as well as activation and thermodynamic parameters. Of the 456 experiments run, three were rejected as being inconsistent with other data and only nine were lost completely because of an inadequate supply of stock reagent. The imprecision was about 0.03 s^{-1} for rate constants in the range of 1.8 to 5 s^{-1}.

The stopped-flow mixing method represents one of the most useful techniques for kinetic studies involving reactions with half-lives in the range from a few milliseconds to a few seconds. Because the method generates data at a relatively rapid rate, some investigators have used small laboratory computers on-line with stopped-flow instrumentation (*1–3*). While these innovations have greatly improved the convenience and reliability of stopped-flow studies, most of them do not take full advantage of the capabilities of the computers because they are used only for data acquisition and processing. Coupled with automatic reagent and sample handling equipment, a small computer can also control and execute most of the operations required to carry out major phases of stopped-flow kinetic studies.

An earlier report from this laboratory described a unique sampling/mixing system that permitted control of the sampling and mixing steps via electrical switches (*4*). A more recent report described a reagent preparation system that could mix up to five solutions and one diluent in a wide range of proportions and deliver many such solutions in sequence to the sampling/mixing system (*5*). The total integrated system is controlled by a computer system so that after stock reagents are supplied and the conditions for several experiments are entered into the computer via Teletype, then all steps required to perform the desired experiments and process the data are carried out automatically under computer control and without operator intervention. Although data were presented to illustrate some features of the quantitative performance of the system, no data were presented to evaluate performance for a detailed kinetic study and that is the subject of this paper.

In this work, the Fe(III)–SCN^- reaction is used as a model system to further evaluate the performance of the computer controlled stopped-flow instrument. Although the thermodynamic and spectral properties of the monothiocyanato complex of Fe(III) in acid solution have been well characterized (*6–8*), there are significant discrepancies among kinetic rate constants reported for the system (*9–13*). Therefore, in

0003-2700/78/0350-1333$01.00/0

addition to evaluating the automated stopped-flow system, this study also has provided useful information related to the model reaction.

GENERAL CONSIDERATIONS

The rationale for experiments performed in this study is best described in terms of a proposed mechanism and rate equation for the reaction. Earlier work provided evidence for a reaction between $Fe^{3+}_{(aq)}$ and SCN^- (*14*). Later work that demonstrated increases in reaction velocity with pH (*9*) suggests the probable involvement of a hydroxy complex of Fe(III). An overall reaction scheme that accounts for these observations is

$$\begin{array}{ccc} Fe^{3+}_{(aq)} + SCN^- & \underset{k_{-1}}{\overset{k_1}{\rightleftharpoons}} & FeSCN^{2+} \\ \Big\Updownarrow K_{h1} & & \Big\Updownarrow K_{h2} \\ Fe(OH)^{2+} + SCN^- & \underset{k_{-2}}{\overset{k_2}{\rightleftharpoons}} & Fe(OH)SCN^{1+} \\ + & & + \\ H^+ & & H^+ \end{array} \quad (1)$$

where K_{h1} and K_{h2} are equilibrium constants for hydrolysis steps that are assumed to be very fast in comparison with the other processes. Starting with a rate equation in terms of forward and reverse rate constants and concentrations of all species in Equation 1, and applying conservation of mass equations, it can be shown that this reaction scheme leads to a rate equation of the form

$$-\frac{d[SCN^-]}{dt} = (k_1 + k_2K_{h1}/[H^+])[Fe^{3+}][SCN^-] - (k_{-1} + k_{-2}K_{h2}/[H^+])[FeSCN^{2+}] \quad (2)$$

If the Fe^{3+} concentration is maintained at least 20 times larger than the SCN^- concentration ($C_{Fe(III)} \geq 20$ [SCN]), then reactions 1 can be treated as two competing first-order reactions, and the integrated form of the rate equation under this set of conditions is

$$\ln\left(\frac{[FeSCN^{2+}]_\infty}{[FeSCN^{2+}]_\infty - [FeSCN^{2+}]_t}\right) = [(k_1 + k_2K_{h1}/[H^+])[Fe^{3+}] + (k_{-1} + k_{-2}K_{h2}/[H^+])]t \quad (3a)$$

where $[FeSCN^{2+}]_\infty$ represents the concentration of this species when the reaction is at equilibrium. In the discussion that follows it will simplify notation to refer to the quantities in parentheses on the right side of Equation 3a as the forward and reverse constants ($k_f \equiv k_1 + k_2K_{h1}/[H^+]$ and $k_r \equiv k_{-1} + k_{-2}K_{h2}/[H^+]$).

It has been observed that the absorbance at 450 nm is proportional to $[FeSCN^{2+}]$ ($\epsilon_{450} = 4.6 \times 10^3$ L/mol cm). Therefore, Equation 3a can be rewritten in the simplified form

$$\ln(A_\infty - A_t) = -(k_f[Fe^{3+}] + k_r)t + \ln \Delta A \quad (3b)$$

where ΔA is the total change in absorbance from $t = 0$ to equilibrium ($\Delta A = A_\infty - A_0$).

It is apparent from Equation 3b that plots of $\ln(A_\infty - A_t)$ vs. t should be linear if the previously proposed mechanism and simplifications are correct. Also, the slope should have the form of an apparent first-order rate constant

$$k_a = k_f[Fe^{3+}] + k_r \quad (4)$$

If values of k_a are evaluated at different values of Fe^{3+} concentration for fixed values of $[H^+]$, then plots of k_a vs. Fe^{3+} for each $[H^+]$ concentration should be linear with slope equal to k_f and intercept equal to k_r. Noting the quantities represented by k_f and k_r, it follows that a plot of k_f vs. $1/[H^+]$ should be linear with slope equal to k_2K_{h1} and intercept equal to k_1, and a plot of k_r vs. $1/[H^+]$ should be linear with slope equal to $k_{-2}K_{h2}$ and intercept equal to k_{-1}. Previously determined values of K_{h1} and K_{h2} can be used to compute explicit values for k_2 and k_{-2} (*7*, *15*).

Clearly, all of the rate constants included in reactions 1 can be determined by the procedures outlined above. However, in order to avoid large uncertainties that can arise from the data processing procedure alone, especially those involving extrapolated intercepts, it is important that all determinations be based upon several data points over a relatively wide range of the independent variable in each case. One set of experiments designed to evaluate these rate constants at 25 °C involved triplicate runs at seven different Fe^{3+} concentrations at each of eight perchloric acid concentrations (see Table I) corresponding to a total of 168 experiments. A second set of experiments designed to evaluate the temperature dependence of the rate constants and associated information involved duplicate runs on each of 48 solutions at each of three temperatures corresponding to 288 experiments. These types of studies that involve large numbers of experiments run under well defined conditions are ideally suited to automation and serve as excellent examples for evaluation of the computer controlled stopped-flow system.

EXPERIMENTAL

Apparatus. Details of the stopped-flow system including computer hardware and software concepts have been presented earlier (*5*) and are not discussed here.

Reagents. All solutions were prepared in distilled water that had been passed through a mixed cation-anion exchange resin bed.

Iron(III) Perchlorate. A 0.077 mol/L iron(III) perchlorate stock solution in 0.200 mol/L $HClO_4$ was prepared from reagent grade $Fe(ClO_4)_3$ (G. Frederick Smith Chemical Co., Columbus, Ohio) and standardized potentiometrically at pH ~ 2 with 0.010 mol/L standard EDTA containing no NTA (J. T. Baker Chemical Co., Phillipsburg, N.J. 08865).

Perchloric Acid. A 2.354 mol/L perchloric acid stock solution was prepared from reagent ACS grade $HClO_4$, 70% (Fisher Scientific Co., Fair Lawn, N.J. 07410) and standardized against weighed amounts of Baker Analyzed Reagent grade anhydrous Na_2CO_3 (J. T. Baker Chemical Co., Phillipsburg, N.J. 08865) using methyl orange as indicator.

Sodium Perchlorate. A 1.413 mol/L sodium perchlorate stock solution was prepared by diluting 2.354 mol/L perchloric acid stock solution with water. The pH of the stock $NaClO_4$ solution was adjusted to 7.0 with analytical reagent grade anhydrous Na_2CO_3 (Mallinckrodt, Inc., St. Louis, Mo. 63147) and the solution was heated to remove dissolved carbon dioxide.

Sodium Thiocyanate. A 2.0×10^{-4} mol/L sodium thiocyanate stock solution in 1.000 mol/L $NaClO_4$ was prepared from dried Baker Analyzed Reagent grade NaSCN (J. T. Baker Chemical Co., Phillipsburg, N.J. 08865) and the appropriate amount of 1.413 mol/L $NaClO_4$ stock solution.

Procedure. The reagent preparation system was calibrated by dispensing water into preweighed vials for different amounts of time, weighing the vials, and computing the least squares slope and intercept of the mass vs. time data. Stock solutions of iron(III) perchlorate, perchloric acid, sodium perchlorate and water are placed in containers with delivery tubes to the reagent preparation system and are adjusted to and maintained at 25 °C in a water bath. Desired volumes of these three solutions and water are dispensed into 30-mL vials on a turntable and each solution is mixed with a magnetic stirring bar placed in each vial at the start of a series of experiments. The turntable delivers each different reagent to the sampler/mixer feed line. A stock solution of sodium thiocyanate maintained at 25 °C is connected to the sample side of the sampler/mixer via a delivery tube. For the temperature study, solutions prepared with the reagent preparation system were adjusted to the desired temperature prior to being run on the stopped-flow.

When all reagents are in place, all instrumental and photometric adjustments are complete, and all pertinent information related to the desired experiments is entered into the computer, then the

Table I. Effects of $[H^+]$ and $[Fe^{3+}]$ upon Apparent First-Order Rate Constant at 25 °C

C_{HClO_4}, mol/L	$C_{Fe(ClO_4)_3}$, (mol/L) 0.0050	0.0075	0.0100	0.0125	0.0150	0.0175	0.0200
	Apparent first-order rate constants (s^{-1})						
0.200	2.29 ± 0.03[a]	2.79 ± 0.03	3.23 ± 0.06	3.73 ± 0.03	4.03 ± 0.03	4.47 ± 0.03	4.99 ± 0.05
0.225	2.17 ± 0.01	2.58 ± 0.03	3.11 ± 0.04	3.49 ± 0.01	3.84 ± 0.02	4.28 ± 0.02	4.76 ± 0.02
0.250	2.07 ± 0.03	2.58 ± 0.03	2.94 ± 0.04	3.30 ± 0.02	3.71 ± 0.07	4.09 ± 0.03	4.52 ± 0.01
0.275	2.01 ± 0.02	2.42 ± 0.03	2.85 ± 0.03	3.20 ± 0.04	3.54 ± 0.02	[3.90 ± 0.01][b]	[c]
0.300	1.91 ± 0.02	2.35 ± 0.03	2.74 ± 0.02	3.07 ± 0.04	3.49 ± 0.04	3.87 ± 0.07	4.16 ± 0.02
0.325	1.89 ± 0.02	2.27 ± 0.01	2.67 ± 0.02	2.99 ± 0.03	3.38 ± 0.01	3.71 ± 0.02	4.08 ± 0.04
0.350	1.85 ± 0.02	2.23 ± 0.02	2.62 ± 0.02	2.90 ± 0.05	3.27 ± 0.05	3.70 ± 0.02	[c]
0.375	1.81 ± 0.01	2.18 ± 0.02	2.51 ± 0.003	2.81 ± 0.02	3.19 ± 0.01	3.56 ± 0.01	[c]

[a] Standard deviation of three replicate runs. [b] Point not used. [c] Stock reagent depleted.

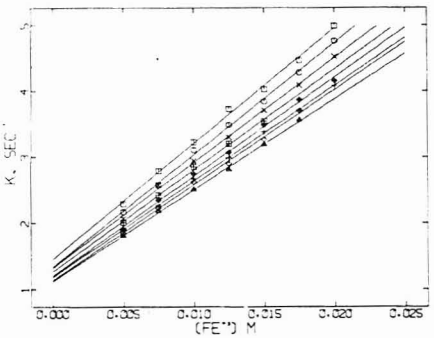

Figure 1. Plots of apparent rate constant vs. Fe^{3+} concentration. $[H^+]$: (□) 0.200; (○) 0.255; (×) 0.250; (■) 0.275; (♦) 0.300; (+) 0.325; (◇) 0.350; (△) 0.375.

system is activated and the experiments are carried out automatically except for a manual 100% T adjustment during the first experiment.

RESULTS AND DISCUSSION

In the study at 25 °C, data were obtained for all but three of the 56 sets of conditions represented in Table I. Each experiment included a trial run during which the computer selected a data rate that was appropriate for the range of reaction rates for that set of conditions. After the trial run, then three replicate runs were made on one solution prepared for each set of conditions. The 162 runs represented by the data in Table I required approximately 7 h for completion after all stock reagents and program information were set up. The only operational problem encountered during that period was related to an insufficient supply of some of the stock solutions (see Table I).

Each datum in Table I represents the average of three values of the apparent first-order rate constant based upon the slope of $\ln (A_\infty - A_t)$ vs. t plots (See Equation 3b). The uncertainties quoted in the table represent the standard deviation ($\pm 1S$) of the three results averaged in each case. Standard deviations of individual least squares slopes of the $\ln (A_\infty - A_t)$ vs. t plots from which the averages were computed ranged between 0.002 and 0.005 s^{-1}. Therefore, most of the uncertainty included for each datum is related to differences among runs and very little of it is related to within run variations.

Figure 1 shows the observed rate constants at each acid concentration plotted vs. Fe^{3+} concentration at 25 °C. These plots exhibit the linear relationship predicted by Equation 4. The least squares slopes and intercepts that represent K_f and K_r are included in Table II along with standard deviations

Table II. Regression Data for Apparent First-Order Rate Constant vs. Fe^{3+} Concentration

C_{HClO_4}, mol/L	slope, k_f, L/mol·s	intercept, k_r, s^{-1}	std error of estimate, s^{-1}
0.200	175 ± 3	1.46 ± 0.04	0.06
0.225	170 ± 2	1.34 ± 0.03	0.05
0.250	159 ± 2	1.32 ± 0.03	0.04
0.275	154 ± 1	1.27 ± 0.03	0.04
0.300	150 ± 2	1.20 ± 0.03	0.05
0.325	145 ± 1	1.19 ± 0.02	0.03
0.350	144 ± 2	1.14 ± 0.03	0.04
0.375	138 ± 1	1.12 ± 0.02	0.02

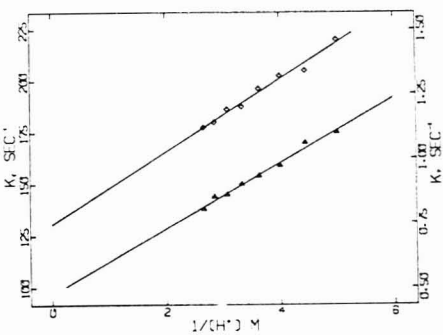

Figure 2. Plots of k_f and k_r as functions of $[H^+]^{-1}$. (△) k_f vs. $[H^+]^{-1}$; slope = 15.9 ± 0.8; intercept = 97 ± 3. (◇) k_r vs. $[H^+]^{-1}$; slope = 0.140 ± 0.008; intercept = 0.75 ± 0.03.

of slopes and intercepts and the standard errors of estimate. The standard errors of estimate indicate that the upper limit for the scatter in the rate constants imposed by the total system including reagent preparation, sampling and mixing, measurement, temperature control, etc. is in the range of 0.02 to 0.06 s^{-1}.

The individual values of k_f and k_r in Table II are plotted vs. $1/[H^+]$ in Figure 2 producing linear plots as predicted by Equation 3a. Least-squares values of the intercepts correspond to $k_1 = 97 \pm 3$ L/mol·s and $k_{-1} = 0.75 \pm 0.03$ s^{-1}. Values of $K_{h1} = 1.65 \times 10^{-3}$ mol/L (*15*) and $K_{h2} = 6.5 \times 10^{-5}$ mol/L (*7*) are used with the slopes to compute $k_2 = (9.6 \pm 0.5) \times 10^3$ L/mol·s and $k_{-2} = (2.2 \pm 0.1) \times 10^3$ s^{-1}.

These values of rate constants are summarized in Table III along with values obtained by other workers using a variety of methods. The value for k_{-2} included from an earlier paper (*11*) is based on a different mechanism that uses the dissociation constant for water where we used K_{h2} to compute k_{-2}. The slope of the k_r vs. $1/[H^+]$ from that paper is 0.19 mol/L·s

Table III. Compilation of Rate Constants at 25 °C from Several Studies

method (ref.) (ionic strength)	k_1, L/mol·s	k_2, L/mol·s	k_{-1}, s^{-1}	k_{-2}, s^{-1}
stopped-flow (*9*) (μ = 0.4)	127 ± 10	(1.0 ± 0.1) × 10^4		
pressure jump (*10*) (μ = 0.5)	150 ± 50	(2.6 ± 0.2) × 10^4		
stopped-flow (*11*) (μ = 0.5)	90 ± 5	(5.1 ± 0.5) × 10^3	1.6 ± 0.2	(1.0 ± 0.1) × 10^{13}
pressure jump (*12*) (μ = 0.2)	132 ± 50	(4.2 ± 0.5) × 10^4		
temperature jump (*13*) (μ = 0.5)	130 ± 40	(1.3 ± 0.2) × 10^4		
present work (μ = 1)	97 ± 3	(9.6 ± 5) × 10^3	0.75 ± 0.03	(2.2 ± 0.1) × 10^3

Table IV. Regression Data for Apparent First-Order Rate Constant vs. Fe^{3+} Concentration

C_{HClO_4}, mol/L	T, °C	slope, k_f L/mol·s	intercept, k_r s^{-1}	std error estimate, s^{-1}
	20 ± 0.1	106.1 ± 0.4	0.826 ± 0.003	0.005
0.200	25 ± 0.1	172 ± 4	1.37 ± 0.03	0.04
	30 ± 0.1	271 ± 4	2.71 ± 0.03	0.04
	20 ± 0.1	99.6 ± 0.2	0.799 ± 0.002	0.002
0.225	25 ± 0.1	165 ± 2	1.27 ± 0.03	0.02
	30 ± 0.1	254 ± 4	2.00 ± 0.04	0.04
	20 ± 0.1	97.0 ± 0.4	0.759 ± 0.003	0.004
0.250	25 ± 0.1	158 ± 1	1.23 ± 0.01	0.008
	30 ± 0.1	238 ± 2	1.94 ± 0.02	0.03
	20 ± 0.1	94.1 ± 0.4	0.735 ± 0.003	0.004
0.275	25 ± 0.1	151 ± 3	1.20 ± 0.03	0.04
	30 ± 0.1	227 ± 2	1.86 ± 0.02	0.03
	20 ± 0.1	91.1 ± 0.3	0.713 ± 0.003	0.01
0.300	25 ± 0.1	148 ± 1	1.14 ± 0.01	0.01
	30 ± 0.1	215 ± 4	1.79 ± 0.04	0.06
	20 ± 0.1	88.8 ± 0.2	0.696 ± 0.003	0.01
0.325	25 ± 0.1	141 ± 3	1.13 ± 0.03	0.04
	30 ± 0.1	212 ± 2	1.71 ± 0.02	0.04
	20 ± 0.1	86.8 ± 0.3	0.679 ± 0.003	0.004
0.350	25 ± 0.1	142 ± 2	1.07 ± 0.02	0.03
	30 ± 0.1	205 ± 2	1.68 ± 0.02	0.02
	20 ± 0.1	84.6 ± 0.2	0.668 ± 0.002	0.003
0.375	25 ± 0.1	133 ± 3	1.10 ± 0.03	0.02
	30 ± 0.1	204 ± 1	1.60 ± 0.01	0.02

compared with a value of 0.14 mol/L·s obtained in this work, and when that slope is used with $K_{h2} = 6.5 \times 10^{-5}$ mol/L to compute k_{-2}, a value of 2.9×10^3 is obtained in comparison with the value of 2.2×10^3 obtained in this work. Little can be said about the other differences among the constants except to note the large quoted uncertainties associated with some values of k_1 and to mention that the earlier stopped-flow data were evaluated manually from oscilloscope traces.

One other comparison involving k_1 and k_{-1} can be made. The ratio $k_1/k_{-1} = 129 \pm 6$ should represent the equilibrium

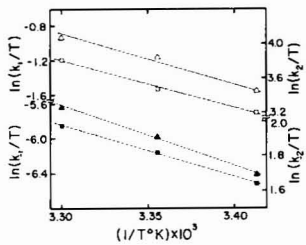

Figure 3. Replots of temperature dependent rate constant data. (△) k_1, (□) k_2, (▲) k_{-1}, (■) k_{-2}

constant for the hydroxide independent step in reaction 1. This value compares favorably with values of 125 ± 2 and 132 ± 1 determined by potentiometric (*16*) and spectrophotometric (*7*) procedures, respectively. The equilibrium constant for the second step in reactions 1 can be estimated as $k_2/k_{-2} = 9.6 \times 10^3/2.2 \times 10^3$ or 4.4 ± 0.1 mol/L.

The second set of data involved measurements at 20, 25, and 30 °C for similar conditions represented for the 25 °C data in Table I. Individual values of rate constants at several Fe(III) concentrations were used to evaluate k_f and k_r as described earlier, and the results are presented in Table IV.

Values of ΔH_{h1} = 10.2 kcal/mol (*15*) and ΔH_{h2} = 12 kcal/mol (assuming the same ΔS for both K_{h1} and K_{h2} and estimating ΔH_{h2} from its free energy) were used with values of k_f and k_r in Table IV to compute the forward and reverse rate constants for reactions 1. Results are included in Table V. The activation parameters included in Table V were computed from weighted least squares slopes and intercepts of the ln (k/T) vs. $1/T$ plots shown in Figure 3. The thermodynamic constants were evaluated from the differences between the forward and reverse activation parameters for the two reaction pathways in Equations 1 above. Literature values for the thermodynamic constants under similar conditions for the pH independent reaction vary from −1.5 (*8*)

Table V. Resolved Rate Constants at Various Temperatures

T, °C	k_1, L/mol·s	k_{-1}, s^{-1}	k_2(L/mol·s) × 10^{-3}	k_{-2}(s^{-1}) × 10^{-3}
20 ± 0.1	62 ± 1	0.481 ± 0.006	7.2 ± 0.3	1.50 ± 0.03
25 ± 0.1	93 ± 3	0.75 ± 0.03	9.7 ± 0.5	1.8 ± 0.1
30 ± 0.1	120 ± 0.6	1.09 ± 0.05	13.6 ± 0.5	2.2 ± 0.2
		Activation parameters		
ΔH, kcal/mol	11.8 ± 0.6	13.9 ± 0.6	10.8 ± 0.8	6.0 ± 0.1
ΔS^*, eu	−9 ± 2	−13 ± 2	−3.5 ± 2	−23.4 ± 0.4
		Thermodynamic constants		
ΔH, kcal/mol	−2.1 ± 0.8		4.8 ± 0.8	
ΔS, eu	4 ± 3		20.2 ± 2	

to −1.3 (*17*) kcal/mol for ΔH and from 4 (*8*) to 5 (*17*) eu for ΔS, and these values are within the 95% confidence level uncertainties of values reported in Table V.

Some checks for internal consistency can be made between the two data sets run several months apart. The standard errors of estimate for the data in Tables II and IV reflect the maximum scatter in the data imposed by the total system. The standard errors at 20 °C are consistently lower than those at 25 and 30 °C, and this may reflect better temperature control for the experiments nearer room temperature. When the rate constants in Table I are regressed against rate constants for the same conditions for the other data set at 25 °C, the slope and intercept were 0.95 ± 0.01 and 0.03 ± 0.03, respectively, with a standard error of estimate of 0.04 s^{-1} and a correlation coefficient of 0.997. The slope shows that the combined effects of chemical and instrumental variables contribute a difference of only 5% between the two data sets.

We believe the results presented above represent convincing evidence that the computer controlled stopped-flow system has much to offer for aspects of fundamental kinetic studies that involve large numbers of experiments under reasonably well defined conditions. Results presented elsewhere (*18*) described the performance for routine kinetic analyses.

LITERATURE CITED

(1) R. J. Desa and O. H. Gibson, *Comput. Biomed. Res.*, **2**, 494 (1969).
(2) B. G. Willis, J. A. Bittikofer, H. L. Pardue, and D. W. Margerum, *Anal. Chem.*, **42**, 1340 (1970).
(3) P. M. Beckwith and S. R. Crouch, *Anal. Chem.*, **44**, 221 (1972).
(4) D. Sanderson, J. A. Bittikofer, and H. L. Pardue, *Anal. Chem.*, **44**, 1934 (1972).
(5) G. E. Mieling, R. W. Taylor, L. G. Hargis, J. English, and H. L. Pardue, *Anal. Chem.*, **48**, 1686 (1976).
(6) G. S. Lawrence, *Trans. Faraday Soc.*, **52**, 236 (1956).
(7) M. W. Lister and D. E. Rivington, *Can. J. Chem.*, **33**, 1572 (1955).
(8) V. E. Mironov and Yu. I. Rutkovskii, *Zhur. Neorg. Khim.*, **10**, 2670 (1965).
(9) J. F. Below, R. E. Connick, and C. P. Coppel, *J. Am. Chem. Soc.*, **80**, 2961 (1965).
(10) H. Wendt and H. Strehlow, *Z. Elektrochem.*, **66**, 228 (1962).
(11) S. Funakaski, S. Adachi, and M. Tanoka, *Bull. Chem. Soc. Jpn.*, **46**, 479 (1973).
(12) F. P. Cavasino and M. Eigen, *Ric. Sci., Part 2, Sez. A*, **4**, 509 (1964).
(13) D. M. Goodall, P. W. Harrison, M. J. Hardy, and C. J. Kirk, *J. Chem. Educ.*, **49**, 675 (1972).
(14) H. E. Bent and C. L. French, *J. Am. Chem. Soc.*, **63**, 568 (1941).
(15) R. M. Milburn, *J. Am. Chem. Soc.*, **79**, 537 (1957).
(16) R. Portanova et al., *Gazz. Chim. Ital.*, **98**, 1290 (1968).
(17) "Critical Stability Constants, Vol. 4: Inorganic Complexes", R. M. Smith and A. E. Martell, Plenum Press, New York and London, 1976.
(18) H. L. Pardue et al., *Clin. Chem. (Winston-Salem, N.C.)*, **23**, 1230 (1977).

RECEIVED for review December 28, 1977. Accepted May 12, 1978. This work was supported by Grant No. CHE 75-1550 A01 from the National Science Foundation.

In-Situ Chemically-Modified Surfaces for Normal-Phase Liquid Chromatography

R. K. Gilpin* and W. R. Sisco

Research Division, McNeil Laboratories, Camp Hill Road, Fort Washington, Pennsylvania 19034

In this paper, the preparation of three short-chainlength trichlorosilane (*n*-butyl, 2-carbomethoxyethyl, and 3-cyanopropyl) modified silica gels by a totally in-situ process is reported. Detailed investigations of efficiency and selectivity of these modified materials along with unmodified silica have been carried out in a normal-phase mode using a series of 14 test solutes with water-saturated *n*-hexane as the mobile phase. All compound retentions have been examined on a relative basis using aniline as the reference solute. Columns have been found to vary in polarity in the order: silica, *n*-butyl, 2-carbomethoxyethyl, 3-cyanopropyl. In addition, column-to-column reproducibility of these packings has been evaluated for multipreparations. Typical average deviations of relative retention for the 14 test solutes have ranged between 4–8%.

In recent years the number of commercially available high-efficiency liquid chromatographic packings has grown at a remarkable rate (*1, 2*). This has been especially true for the chemically modified materials (*3, 4*). In parallel growth has been the number of literature references of the application of these materials to analytical problems. In addition a number of reports have appeared describing the experimental preparation and characterization of various bonded-phase materials for liquid chromatographic application. These have been extensively reviewed in the literature (*3–8*).

In a majority of the reported studies and applications, bonded-phase materials have been used in the reversed-phase mode (*4*), with a combination of either water or an aqueous buffer and either methanol or acetonitrile as the mobile phase. Another application for bonded phases is as adsorptive (i.e., normal-phase mode) packings. A few workers have reported normal-phase studies on bonded materials (*9–14*). In this mode, even greater potential in selectivity may eventually be realized.

The feasibility of forming bonded siloxane phases totally in-situ on porous layer materials and on completely porous small-particle silica has been demonstrated (*15, 16*). These materials were evaluated for use in a reversed-phase mode. In this paper, three short-chain trichlorosilane modified silica gels for use as normal-phase high pressure liquid chromatographic packings have been prepared by a similar in-situ approach.

Detailed investigations of efficiency and selectivity on these short-chain packings have been carried out using a series of 14 test solutes. All compound retentions have been examined on a relative basis using aniline as the reference compound.

EXPERIMENTAL

Column Preparation. The 2.4-mm i.d. by 25 cm stainless steel columns were slurry-packed with LiChrosorb SI 50 silica (av. dp $\simeq$10 μm) as previously described (*16*). Following packing, each column was conditioned with 100 mL of water, methanol, isopropanol, diethyl ether, 1,2-dichloroethane, and at least 500 mL of water-saturated *n*-hexane. After conditioning, all columns were characterized in terms of efficiencies using nitrobenzene as the test solute and a mobile phase of water-saturated *n*-hexane. In addition, capacity factors for each test solute were calculated using benzene as the unretained peak. These data were obtained from duplicate injections using 6 to 8 different linear velocities covering a range from 0.11 to 1.1 cm/s (0.3 to 3.0 mL/min).

Following packing and evaluation, suitable columns were bonded in-situ as described (*16*). In each case, 100 mL of

0003-2700/78/0350-1337$01.00/0

water-saturated toluene followed by 200 mL of dry toluene were used to establish pre-reaction conditions. These solutions were pumped through at a rate of 5.0 mL/min. Immediately following this procedure, the pump was stopped and a reaction reservoir ($^3/_8$ in. o.d. × 2 ft stainless steel tube) containing 30 mL of a 50% solution of trichlorosilane monomer in dry toluene was inserted into the system between the column and pump. The reaction solution was then pumped through the column at a rate of 1.0 mL/min, followed by 500 mL of dry toluene at the maximum attainable flow. The reaction reservoir was removed from the system, and 100 mL of water-saturated toluene, followed by 100 mL of water:acetonitrile (5:95) were pumped through the modified columns. Each column was subsequently conditioned using the same solvent series listed above for the uncoated silica.

Equipment. Either a Waters Model 6000 pump, or an Altex Model 100 pump were used for the bonding reactions. Chromatographic experiments were performed on a Perkin-Elmer Model 1220 liquid chromatograph equipped with a Schoeffel Model 770 variable wavelength detector. All measurements were made at 254 nm. Retention measurements were made with the aid of a Hewlett-Packard Model 3352 data system. Injections were made on-column using Precision Sampling syringes. All column evaluations were carried out at ambient temperature (ca. 25–27 °C).

Reagents. The *n*-hexane and toluene used were distilled in glass from Burdick and Jackson and analytical reagent grade from Mallinckrodt, respectively. The dry toluene was prepared by refluxing over calcium hydride for at least 4 h and then stored over calcium hydride until used. Both the water-saturated *n*-hexane and water-saturated toluene were prepared by stirring overnight at ambient temperature in the presence of distilled water. These solvents were then stored under static conditions prior to use. *n*-Butyltrichlorosilane, 2-carbomethoxyethyltrichlorosilane, and 3-cyanopropyltrichlorosilane were obtained from Petrarch Systems and were used in the condition received.

RESULTS AND DISCUSSION

Columns modified with *n*-butyltrichlorosilane, 2-carbomethoxyethyltrichlorosilane, and 3-cyanopropyltrichlorosilane were prepared in-situ using optima pre-reaction and reaction conditions based on previous studies (*16*). After preparation, columns were conditioned with a solvent series of decreasing polarity (*17*) and chromatographically characterized as normal-phase packings. In addition to selectivity and efficiency studies, reproducibility for multicolumn preparations was evaluated. The reproducibility studies were carried out on a relative basis using aniline as the reference compound.

Changes in column efficiency between the modified and unmodified surfaces were examined using nitrobenzene as the test compound. In each case, water-saturated *n*-hexane was used as the mobile phase.

Selectivity was investigated using a series of 14 test solutes which are listed in Table I and water-saturated *n*-hexane as the mobile phase. Capacity factors for these test solutes ranged from ~0.1 for biphenyl to ~100 for phenol. From these data, relative retention ($\alpha_a{}^i$) data were calculated using aniline as the reference compound. The $\alpha_a{}^i$ (ratio of capacity factor of each component to the capacity factor of aniline) was determined using the relationship

$$\alpha_a{}^i = \frac{k'_{\text{component}}}{k'_{\text{aniline}}} = \frac{t_{r_1} - t_{r_0}}{t_{r_0}} \Big/ \frac{t_{r_a} - t_{r_0}}{t_{r_0}}$$

where (t_{r_1}) was the retention time of the component of interest, (t_{r_0}) the retention time of the unretained compound, benzene, and (t_{r_a}) the retention time of the reference compound, aniline. Aniline was chosen as the reference compound, since it was the parent structure of a majority of the test solutes studied. Additionally the retention of aniline was intermediate among the test compounds investigated.

Reproducibility. Listed in Table I are mean relative retention data and resulting coefficients of variation in these data for the series of 14 test compounds obtained on three

Table I. Variation in Relative Retention for Unmodified and for Modified Micro-Silica Columns[a]

	silica columns		*n*-butyl columns		2-carbomethoxyethyl columns		3-cyanopropyl columns	
test compounds	mean relative retention, $\alpha_a{}^i$	relative av. deviation, %	mean relative retention, $\alpha_a{}^i$	relative av. deviation, %	mean relative retention, $\alpha_a{}^i$	relative av. deviation, %	mean relative retention, $\alpha_a{}^i$	relative av. deviation, %
naphthalene	$3.6 \times 10^{-3} \pm 3.5 \times 10^{-4}$	9.7	$3.6 \times 10^{-3} \pm 2.5 \times 10^{-4}$	6.9	$4.6 \times 10^{-3} \pm 3.5 \times 10^{-4}$	7.6	$8.2 \times 10^{-3} \pm 1.8 \times 10^{-3}$	22.0
biphenyl	$7.0 \times 10^{-3} \pm 7.2 \times 10^{-4}$	10.3	$6.7 \times 10^{-3} \pm 6.1 \times 10^{-4}$	9.1	$7.8 \times 10^{-3} \pm 4.6 \times 10^{-4}$	5.9	$10.8 \times 10^{-3} \pm 1.6 \times 10^{-3}$	14.8
anthracene	$9.1 \times 10^{-3} \pm 7.1 \times 10^{-4}$	7.8	$8.9 \times 10^{-3} \pm 4.6 \times 10^{-4}$	5.2	$1.1 \times 10^{-2} \pm 5.8 \times 10^{-4}$	5.3	$2.1 \times 10^{-2} \pm 4.0 \times 10^{-3}$	19.0
nitrobenzene	$8.4 \times 10^{-2} \pm 8.7 \times 10^{-3}$	10.4	$8.3 \times 10^{-2} \pm 2.3 \times 10^{-3}$	2.8	$8.6 \times 10^{-2} \pm 2.9 \times 10^{-4}$	3.4	$8.8 \times 10^{-2} \pm 7.1 \times 10^{-3}$	8.1
N,N-dimethylaniline	0.26 ± 0.0058	2.2	0.22 ± 0.023	10.7	0.18 ± 0.021	11.4	0.12 ± 0.020	16.7
N-methylaniline	0.42 ± 0.015	3.6	0.38 ± 0.010	2.6	0.35 ± 0.012	3.3	0.31 ± 0.010	3.2
2,6-dimethylaniline	0.70 ± 0.012	1.7	0.67 ± 0.029	4.3	0.67 ± 0.021	3.1	0.55 ± 0.059	10.7
aniline	1.00 ± 0.0 (k' = 54.2)	0.0	1.00 ± 0.00 (k' = 35.3)	0.0	1.00 ± 0.00 (k' = 30.8)	0.0	1.00 ± 0.00 (k' = 35.8)	0.0
o-chloroaniline	0.18 ± 0.015	8.3	0.19 ± 0.0058	3.1	0.20 ± 0.00	0.0	0.22 ± 0.015	7.1
m-chloroaniline	0.47 ± 0.012	2.6	0.50 ± 0.025	5.0	0.57 ± 0.017	3.0	0.68 ± 0.038	5.5
p-chloroaniline	0.71 ± 0.017	2.4	0.71 ± 0.012	1.7	0.85 ± 0.010	1.2	0.97 ± 0.036	3.7
2,6-dimethylphenol	0.35 ± 0.020	5.7	0.36 ± 0.010	2.8	0.38 ± 0.0058	1.5	0.41 ± 0.00	0.0
2,4-dimethylphenol	1.19 ± 0.087	7.3	1.25 ± 0.068	5.4	1.32 ± 0.087	6.6	1.52 ± 0.097	6.4
phenol	1.92 ± 0.058	3.0	2.12 ± 0.21	9.9	2.40 ± 0.21	8.6	3.01 ± 0.14	4.5

[a] Mobile Phase: Water-saturated *n*-hexane. All single column relative retention results were obtained from an average of 5 to 10 experimental determinations. Mean relative retention ($\alpha_a{}^i$) represent triplicate column determinations. k' for aniline determined from a representative column per modification type.

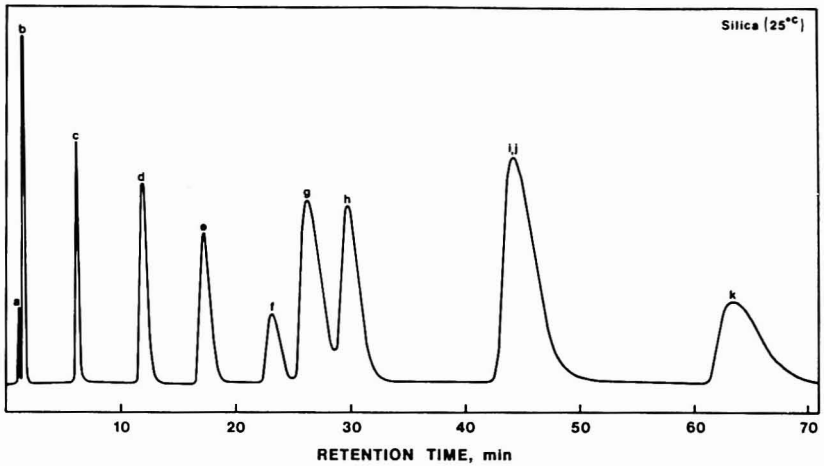

Figure 1. Representative chromatogram obtained on an unmodified silica column. Conditions: mobile phase, water-saturated *n*-hexane; flow rate, 1.6 mL/min; column temperature, ambient. Test solutes: (a) benzene, (b) biphenyl, (c) nitrobenzene, (d) *o*-chloroaniline, (e) *N,N*-dimethylaniline, (f) 2,6-dimethylphenol, (g) *N*-methylaniline, (h) *m*-chloroaniline, (i) 2,6-dimethylaniline, (j) *p*-chloroaniline, (k) aniline

replicate unmodified micro-silica columns. Also listed in Table I are inter-column variations reported as percent relative average deviation ($\sigma_{\alpha_a}{}^i/\bar{\alpha}_a{}^i$) (100). All relative values for a given test solute are averages obtained from 5 to 10 experimental determinations per column. The inter-column variation for triplicate column preparation was typically less than 8% with a significant portion of these data falling between 1% and 4%; in a few cases, higher values were obtained for those test solutes which eluted early.

Also shown in Table I are mean relative retention ($\alpha_a{}^i$) data for the same test series obtained on three replicate column preparations for each of the column types: *n*-butyltrichlorosilane, 2-carbomethoxyethyltrichlorosilane, and 3-cyanopropyltrichlorosilane. As in the case of the unmodified columns, overall inter-column variations for a particular type of modification were less than 8% with many test solutes showing smaller relative deviations.

Absolute retention data for aniline reported as k' are listed in Table I. These data were determined from a representative column of each modification as shown in Figures 1 and 2. In terms of absolute retention, column-to-column variations were found to be similar to those reported in earlier studies (*16*); this was true when the batch of monomer and lot of silica remained constant. Changes in either resulted in higher coefficients of variation in reproducibility.

When comparing the overall variation in $\alpha_a{}^i$ data between column types, no statistically significant differences ($p < 0.05$ by ANOVA) were noted between modified and unmodified materials. These results indicate that most inter-column variation within a particular modification type was the result of experimental factors other than those arising from the bonding process. One such factor is fluctuation in temperature of the column and mobile phase. Temperature has been found to affect significantly compound retention under the conditions studied (*18*); this has been attributed to changes in water content of the mobile phase and resulting adsorbed surface water.

The three in-situ 3-cyanopropyltrichlorosilane modified columns were compared to a similar commercially available column (ES Industries), using the 14 test compounds. Relative retention data are listed in Table II. As in the case of the

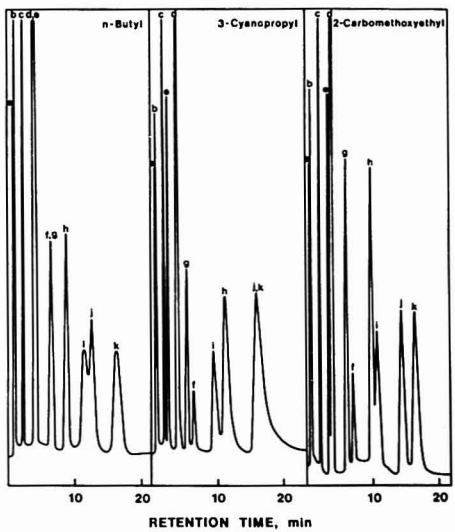

Figure 2. Representative chromatograms obtained on the various surface types: *n*-butyl, 3-cyanopropyl, 2-carbomethoxyethyl. Conditions: mobile phase, water-saturated *n*-hexane; flow rate, 2.0 mL/min; column temperature, ambient. Test solutes: same as Figure 1

in-situ modifications, the $\alpha_a{}^i$ data on the commercially available column are mean values obtained from 5 to 10 experimental determinations for each solute. When comparing $\alpha_a{}^i$ values, the columns were found to be similar in selectivity even though the capacity factor for each solute was approximately four times larger on the in-situ prepared surfaces. The smaller k' values obtained on the commercially available surface are reconcilable in terms of differences in surface area and monomer loading between the packings (*19*). Of particular

Table II. Variation in Relative Retention for In-Situ and Commercially Available 3-Cyanopropyl Columns

test compounds	relative retention, α_a^i A[a]	B[a]
naphthalene	8.2×10^{-3}	1.2×10^{-2}
biphenyl	1.1×10^{-2}	1.6×10^{-2}
anthracene	2.1×10^{-2}	3.1×10^{-2}
nitrobenzene	8.8×10^{-2}	11.0×10^{-2}
N,N-dimethylaniline	0.12	0.13
N-methylaniline	0.31	0.32
2,6-dimethylaniline	0.55	0.49
aniline	1.00 (k' = 35.8)	1.00 (k' = 9.21)
o-chloroaniline	0.22	0.24
m-chloroaniline	0.68	0.73
p-chloroaniline	0.97	0.98
2,6-dimethylphenol	0.41	0.37
2,4-dimethylphenol	1.52	1.19
phenol	3.01	2.53

[a] A, in-situ prepared columns. α_a^i results are mean values obtained from three replicate columns. B, commercially available column (ES Industries). α_a^i results are values obtained from one column.

interest is the excellent agreement between relative data, which supports the argument that the observed selectivities are primarily the result of bonded functionality and not due only to differences of bonded polymer bulk or matrix effects. Thus relative retention has been used to examine surface selectivity and to characterize the surface types in terms of varying polarity.

Efficiency. Tabulated in Table III are calculated mean ratios of column efficiency before (H_{before}) to column efficiency after (H_{after}) chemical modification. These ratios (H_{before}/H_{after}) are listed for each of the modification types for linear flow velocities of 0.38 and 0.76 cm/s. All H_{before} and H_{after} values were determined from plots of efficiency vs. linear velocity of the mobile phase over an operating range of 0.11 to 1.1 cm/s. Data were collected using a mobile phase of water-saturated *n*-hexane and the test solute, nitrobenzene. Representative plots before and after modification are shown in Figure 3. These data were obtained on an *n*-butyl modified surface but reflect the general trend for all modifications. H_{before}/H_{after} ratios of approximately 0.8 (Table III) were obtained for each modification type.

A ratio of 1.0 at both linear velocities would indicate the superimposition of efficiency curves before and after modification over the 0.38 to 0.76 cm/s range. However, since the H_{before}/H_{after} ratio was <1.0, the modified columns were judged to be slightly less efficient than the unmodified surfaces. Although all evaluations were carried out using the same test solute and mobile phase, this argument neglects differences in k' for nitrobenzene between the modified and unmodified surfaces.

Selectivity. Tabulated in Table I are α_a^i values as a function of column modification. Of particular interest are changes in α_a^i as a function of surface modification and test solute type. All of the test solutes, within experimental variability, demonstrate consistent trends in relative retention

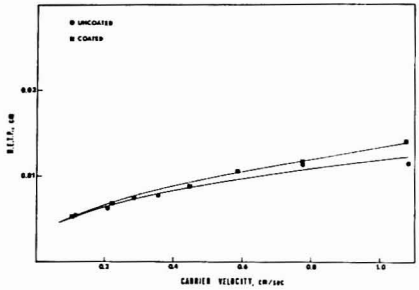

Figure 3. Effect of mobile phase velocity on plate height for a typical micro-silica column before and after modification. Modified in-situ using *n*-butyltrichlorosilane. Chromatographic conditions: mobile phase, water-saturated *n*-hexane; test solute, nitrobenzene

(Table I) when the surfaces are ordered: silica, *n*-butyl, 2-carbomethoxyethyl, and 3-cyanopropyl (A to D, respectively). The observed discrepancies in the four earliest eluting compounds (naphthalene, biphenyl, anthracene, and nitrobenzene) on the silica and *n*-butyl surfaces are reconcilable in terms of their large coefficients of variation of α_a^i. These consistent trends are explainable in terms of varying surface polarity and the nature of the solute.

The column types studied vary in polarity from the unmodified silica surface, which is the most positive due to surface hydroxyl groups, to 3-cyanopropyl which is the surface with the greatest peripheral electron density. The *n*-butyl and 2-carbomethoxyethyl are intermediates of these extremes, respectively.

The nonbonded electrons of the amine groups of aniline and the substituted anilines studied have been found to contribute significantly to solute–surface interaction. This is consistent with other reported studies of the interaction of compounds containing $-NH_2$ groups with silica gel (*20–22*). Aniline and various mono-substituted aromatics have been shown to primarily interact with unmodified silica surfaces through a one-point interaction (*20–22*). The solutes chosen in this work likewise exhibit one-point interaction with the surface of the packings. Alteration of the attachment site by either electronic or steric means affects the degree of solute–surface interaction. These alterations included stationary phase modifications as well as solute changes. The resulting effect from these changes was either increased or decreased retention relative to the parent compound as seen in Figure 4.

The chloroanilines when referenced to aniline showed greater affinity for increasingly electron-rich surfaces while *N*-methyl- and *N,N*-dimethylaniline showed greater affinity for increasingly electron-deficient surfaces. These trends are explainable in terms of the electronic nature of the solutes.

Addition of a chlorine atom to the benzene ring of aniline effectively delocalizes the nonbonding pair of electrons of the nitrogen by virtue of its electron-withdrawing nature. This

Table III. Reproducibility of In-Situ Prepared Columns[a] Based on HETP Data

modification	H_{before}/H_{after} A[b]	B[b]	relative av deviation, % A[b]	B[b]
n-butyl	0.73 ± 0.049	0.77 ± 0.0071	6.8	0.92
2-carbomethoxyethyl	0.88 ± 0.13	0.86 ± 0.11	14.8	12.8
3-cyanopropyl	0.80 ± 0.057	0.75 ± 0.042	7.1	5.7

[a] Mobile phase: water-saturated *n*-hexane. Test solute: nitrobenzene. [b] Linear flow velocity: A, 0.38 cm/s; B, 0.76 cm/s.

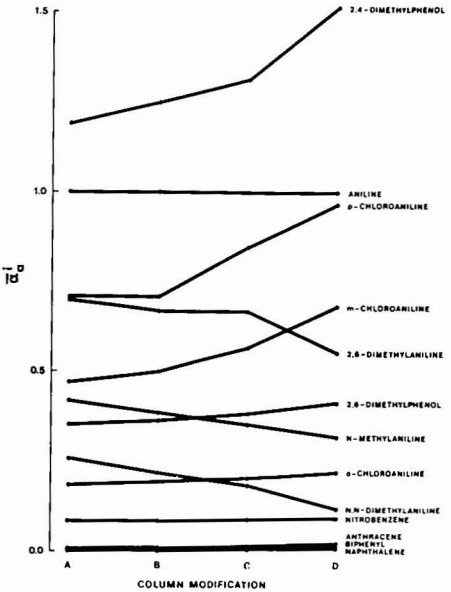

Figure 4. Variations in average relative retention ($\bar{\alpha}_a^i$) as a function of column modification: (A) unmodified, (B) *n*-butyl, (C) 2-carbomethoxyethyl, (D) 3-cyanopropyl

results in the nitrogen atom of the chloroaniline having more positive character than the nitrogen atom of aniline, thus favoring electron-rich surfaces which can interact more readily with the less basic nitrogen. This is shown in Figure 4 as an increase in relative retention for the column modifications A to D. The methyl substituent, on the other hand, when placed on the nitrogen atom of aniline affects a localization of charge about the nitrogen atom by virtue of the electron donating nature of the group. This situation causes the nitrogen atom to possess greater negative character than aniline, thus favoring electron-deficient surfaces which can interact more readily with the more basic nitrogen atom as illustrated by a decrease in α_a^i for the column modifications A to D.

Within each column modification, the elution order of the test compounds depended on the degree of hindrance of the solute's site of interaction. This is seen in Table I as a decrease in α_a^i as the solute becomes increasingly hindered by substituents. This effect was seen on all columns investigated and found to be dominant over electronic considerations.

From steric considerations, the availability of the nonbonded electrons of the methyl substituted anilines to interact with the surfaces is greatest in 2,6-dimethylaniline; the electronic availability decreases as the nitrogen atom is increasingly hindered by methyl groups. This situation is seen in Figure 4, where 2,6-dimethylaniline is retained longest on all columns investigated, while *N*,*N*-dimethylaniline is the least retained methylaniline on all columns. Although the electronic character of the methylanilines is opposite from the chloroanilines, as reflected in their reversed trends (Figure 4), the proximity of a bulky chlorine group to the solute's point of interaction alters retention in the same way as the methyl substituent in the methylanilines. These steric considerations are illustrated as a large difference in retention between *o*-chloroaniline and *p*-chloroaniline (Table I). Since electronically these solutes should have similar α_a^i values, their wide separation is attributed to steric effects (*23*).

The phenolic solutes' interactions with the various stationary phases are consistent with the above arguments. However, in order to better visualize the electronic and steric effects of the methyl substituents it is necessary to normalize the relative retention data to phenol. The mean relative retentions, α_p^i, (where α_p^i is defined analogously to α_a^i except relative to phenol instead of aniline) of 2,6-dimethylphenol are 0.18, 0.17, 0.16, and 0.14 for surfaces A to D respectively. Likewise, α_p^i values of 0.62, 0.59, 0.55, and 0.51 are obtained for 2,4-dimethylphenol.

The electron donating effect of the methyl groups on the phenol ring effects an increased localization of the nonbonded electron about the oxygen atom. This results in the oxygen atom having greater negative character than phenol, thus favoring electron deficient surfaces which interact more readily with the more basic oxygen atom. Although this situation is similar to the case of methyl substituted anilines, it may not be apparent from Figure 4. However, plots of α_p^i vs. column modification, would show similar trends for methyl substitution on phenol as seen for aniline. These results, in terms of steric arguments, are consistent with those of the substituted anilines. As the methyl groups block the site of interaction α_p^i decreases. Since the 2,6-dimethylphenol has the most hindered oxygen atom, it shows the lowest affinity for the stationary phases studied, while the 2,4-dimethylphenol has a more available oxygen atom and exhibits greater retention.

The four surface types examined form a useful set with varying polarity. High pressure liquid chromatography using columns packed with these surfaces can offer unique and selective separations; representative chromatograms obtained on the four surface types using selected test solutes are illustrated in Figures 1 and 2 for unmodified and modified packings, respectively. The changes in selectivity and resolution of solutes seen in these figures offer an alternative to modifying solvent composition.

LITERATURE CITED

(1) R. E. Majors, *Am. Lab.*, **7** (10), 13 (1975).
(2) R. E. Majors, *J. Chromatogr. Sci.*, **15**, 334 (1977).
(3) E. Grushka and E. J. Kikta, Jr., *Anal. Chem.*, **49**, 1004A (1977).
(4) C. Horvath and W. Melander, *J. Chromatogr. Sci.*, **15**, 393 (1977).
(5) D. C. Locke, *J. Chromatogr. Sci.*, **11**, 120 (1973).
(6) A. Pryde, *J. Chromatogr. Sci.*, **12**, 486 (1974).
(7) V. Rehak and Smolkova, *Chromatographia*, **9**, 219 (1976).
(8) I. Sebestian and I. Halasz, *Adv. Chromatogr.*, **14**, 75 (1976).
(9) E. Grushka and E. J. Kikta, Jr., *Anal. Chem.*, **46**, 1370 (1974).
(10) M. Novotny, S. L. Bektesh, K. B. Denson, K. Grohmann, and W. Parr, *Anal. Chem.*, **45**, 971 (1973).
(11) M. Novotny, S. L. Bektesh, and K. Grohmann, *J. Chromatogr.*, **83**, 25 (1973).
(12) K. K. Unger, N. Becker, and P. Roumeliotis, *J. Chromatogr.*, **125**, 115 (1976).
(13) R. E. Majors and M. J. Hopper, *J. Chromatogr. Sci.*, **12**, 767 (1974).
(14) J. H. Knox and Pryde, *J. Chromatogr.*, **112**, 171 (1975).
(15) R. K. Gilpin, J. A. Korpi, and C. A. Janicki, *Anal. Chem.*, **47**, 1498 (1975).
(16) R. K. Gilpin, D. J. Camillo, and C. A. Janicki, *J. Chromatogr.*, **121**, 13 (1976).
(17) L. R. Snyder and J. J. Kirkland, "Introduction to Modern Liquid Chromatography", J. Wiley and Sons, New York, N.Y., 1974, p 197.
(18) R. K. Gilpin and W. R. Sisco, IV FACSS, Detroit, Mich., Nov. 1977.
(19) M. J. Telepchak, ES Industries, private communication, 1977.
(20) E. Soczewinski and W. Golkiewicz, *Chromatographia*, **5**, 431 (1972).
(21) E. Soczewinski, W. Golkiewicz, and W. Markowski, *Chromatographia*, **8**, 13 (1975).
(22) E. Soczewinski, *J. Chromatogr.*, **130**, 23 (1977).
(23) H. C. Brown and A. Cahn, *J. Am. Chem. Soc.*, **72**, 2939 (1950).

RECEIVED for review January 9, 1978. Accepted May 23, 1978.

Determination of 5-Hydroxyindole-3-acetic Acid in Urine by High Performance Liquid Chromatography

Nermin Fornstedt[1]

Department of Clinical Chemistry, University Hospital, S-750 14 Uppsala, Sweden

A combination of aromatic adsorption chromatography with high performance liquid chromatography (HPLC), using UV-absorbance detection, provides a selective, sensitive, and simple determination of 5-hydroxyindole-3-acetic acid (5-HIAA) in urine. The adsorbent, dinitrophenyl-coupled thiolated Sephadex G-25, retains 5-HIAA to such an extent that the interfering compounds of urine are completely excluded from 5-HIAA-containing fractions before injection onto the reverse-phase column, which fully resolves accompanying UV-positive urine compounds. By preventing 5-HIAA decomposition, checking accuracy in calibration curves, and maintaining intact adsorbent capacities, a detection limit of 0.1 μg/mL and a recovery of 99.9% of added 5-HIAA (0.5% RSD) are obtained.

The side pathway in tryptophan metabolism leading to 5-hydroxyindole-3-acetic acid (5-HIAA) is well known, since serotonin (5-hydroxytryptamine, 5-HT) was isolated in 1948 (*1*) and the breakdown of 5-HT into 5-HIAA was discovered in 1954 (*2, 3*). At the same time, in 1953–55, the malignant carcinoides (tumors originating from cells of the small intestinal tract) were reported (*4*) to contain large amounts of 5-HT (*5*) and 5-HT was also found in blood from patients with metastatic malignant carcinoids (*6*). Additionally, abnormally high values of 5-HIAA were measured in urine from such patients (*6–8*).

Most of the presently available methods developed for the determination of 5-HIAA in urine are based on a number of extraction stages followed by some identification and quantification technique, such as paper chromatography (*7–9*), colorimetry (*7–9*), thin-layer chromatography (*10–12*) or fluorometry (*13*). However, all these methods are laborious and may be subject to gross errors by losses in extractions, by simultaneous extraction of interfering urine compounds and/or by low specificity of the color reagents *p*-dimethylaminobenzaldehyde in diluted hydrochloric acid (*7, 10*), α-nitroso-3-naphthol-nitrous acid (*8*), diazotized *p*-nitroanilin (*9*), tetracyanoethylene, picric acid (*12*) or 2,4,7-trinitro-9-fluorenone (*14*). The colorimetric method (*8*) of 1955 (average recovery: 85%) is still widely used for clinical purposes. However, interference was pointed out recently after using the method in the presence of reducing urine metabolites (*15*) and of basic phenothiazine derivates (*16*). The high performance liquid chromatography (HPLC) with fluorometric detection was applied to the analysis of indoles in deproteinizated urine (*17*) and high recovery, sensitivity, and rapidity was reported. Unfortunately the selectivity, which is diagnostically important, does not seem to be fully satisfactory for 5-HIAA, especially at low concentrations; the normal peak in urine from healthy individuals is partially masked, and there will be a risk of greater masking by reason of the variety of large fluorescence compounds occurring in varying urine samples. In general, several problems are caused by directly injected urine onto the column, such as clogging, irreversible adsorptions, and simultaneous elution of interfering compounds (*18*).

In this paper, a two-step chromatographic determination of urinary 5-HIAA will be presented. The method consists of a combination of mini-column adsorption chromatography on a dinitrophenyl-coupled gel carrier to isolate the compound from urine with reversed phase HPLC using UV detection to determine it in the isolated fraction. The paper also includes stability conditions for 5-HIAA solutions (pure as well as urinary ones) and preparing conditions for true calibration curves. No study on decomposition of 5-HIAA was found in the literature except a report in 1956 (*19*), warning of instability at high pH, in air and in light.

EXPERIMENTAL

Apparatus. Absorbance measurements were made on a Hitachi-101 Spectrophotometer (1-cm absorption cells). A peristaltic 3-channel pump, P 3 (Pharmacia Fine Chemicals, Uppsala, Sweden), and a fraction collector, FR 3 (Stål Produkter, Uppsala, Sweden), were used for the adsorption chromatographic separation on the isolation columns. As isolation columns (4 mm i.d. × 11.3 cm) graduated 2-mL pipets were utilized; their upper part was cut off, and a rubber cork with an entrance capillary was inserted into the top of the remainder (16 cm) of the pipet, and a small glass-wool plug was placed in the bottom.

The HPLC-UV system consisted of a high pressure pump, Pulse Dampener Model 709, equipped with an in-line filter with a 2-μm frit (LDC, Riviera Beach, Fla.), a sample injection valve, Model 70-10, and a loop filler port, Model 70-11, with a standard sample loop, 20 μL (Rheodyne, 2809 Tenth St., Berkeley, Calif. 94710), a reverse-phase column, Partisil-10 ODS, 4.6 mm i.d. × 25 cm (Whatman, Clifton, N.Y.), and a variable-wavelength UV-VIS detector, Spectro Monitor II 1202 (LDC). The flow rate was maintained at 0.94 ± 0.01 mL/min. The detector sensitivity was usually set at 0.02 AUFS and the wavelength at 280 nm. The detector output was recorded at a chart speed of 10 in/h.

Reagents. (1) 0.1 M ammonium formate buffer, pH 3; (2) mobile phase: 110 mL acetonitrile/890 mL distilled water/0.4 mL concentrated sulfuric acid/0.1 g sodium lauryl sulfate, pH 2. Both buffer and mobile phase were prepared from spectro grade chemicals and from glass distilled and degassed water and were filtered. (None of the solutions showed any absorbance at 280 nm.) (3) 5-HIAA (Sigma Chemical Co., St Louis, Mo. 63178) stock standard solution, 1 mg/mL in the buffer, was stored as 1–2 mL aliquots at −20 °C in small, tinfoil-wrapped amber bottles (stable for months). UV tests of stock solution, diluted with buffer to 20 μg/mL, resulted in $A_{280} = 0.565$ (2.5% RSD; $N = 10$) for each of the lots 53C-1790 and 26C-0152. The working standards 40, 20, 10, 5, 2.5, and 1.25 μg/mL were prepared as a 1:2 dilution series, checking the standards 20 and 10 μg/mL at 280 nm.

Procedure. After initial studies considering 5-HIAA photodecomposition (Figure 1 and Table I), the need of preventing breakdown in each moment of the procedure became evident, by which reason light was excluded throughout, low pH was preferred, and addition of chloride ions was avoided.

Preparation of the Isolation Columns. The adsorbent, dinitrophenyl-coupled thiolated Sephadex G-25 (DNP-S-Seph.G-25), was synthesized in the following stages: by reaction with epichlorohydrin, Sephadex G-25 (Pharmacia) was converted into epoxide-activated gel (*20*), and, by treatment with sodium

[1] Present address, Institute of Biochemistry, Biomedical Center, University of Uppsala, Box 576, S-751 23 Uppsala, Sweden.

0003-2700/78/0350-1342$01.00/0

Table I. Influence of pH and Anions on Photodecomposition of 5-HIAA

storage time in transparent bottles at room temperature	percentage of remaining 5-HIAA[a]								
	in bright daylight at pH 3 in different anions			in ordinary laboratory light at different pH					
					buffer				
	0.1 M ammonium formate	diluted acetic acid	diluted hydrochloric acid	0.1 M formic acid, pH 2.3	0.1 M ammonium formate, pH 3	0.1 M ammonium formate, pH 4	0.1 M ammonium formate, pH 5	0.1 M sodium acetate, pH 6	0.1 M Tris-hydrochloric acid, pH 7
1 week	69	54	42	92	96	97	96	88	79
2 weeks				82	88	88	90	62	49

[a] From 20 μg/mL solutions; determination as described in Figure 1 legend but without dilution.

thiosulfate and reductive cleavage of the alkyl thiosulfate structures by dithiothreitol, thiolated gel was obtained (*21*), to which dinitrophenyl groups were coupled via the thioether bonds (*22*). The dried product contained 1.49% S and 0.42% N. Dinitrophenyl groups were then calculated to 150 μmol/g dry gel. The adsorbent was suspended in the buffer (See Reagents, (1)), and the suspension was degassed before packing. After equilibrating with 10–15 mL buffer, using the peristaltic pump at a flowrate of 3 mL/h, and after readjusting the bed height, the packings were capped and stored in a refrigerator until use.

5-HIAA Calibration Process. Sets of three columns were placed on the fraction collector over sets of 12 test tubes. The buffer above the bed was sucked off by a disposable Pasteur pipet, and 250 μL of a 20 μg/mL standard solution was added by a capillary pipet without disturbing the bed surface and was allowed to drain completely into the adsorbent, whereupon the empty space was refilled with buffer. Bright light was avoided by wrapping tinfoil around the columns and the test tubes. After being connected with the pump, the columns were eluated at a flowrate of 3 mL/h and 1-mL fractions were collected. The absorbance of the individual fraction was monitored at 280 nm. Each of the UV-positive fractions, No. 7–12, were then injected onto the reverse-phase column for identification, and a peak appeared at 6.5-min retention time. This was also obtained by directly injection of 5-HIAA standards at the same HPLC conditions.

Determination of 5-HIAA in Urine. Human urine was collected during a 24-h period in an amber bottle, containing glacial acetic acid (AA) as preservative (about 30 mL glacial AA/L urine to keep pH between 3–4) and kept in a cool place; the total volume was measured, and about 2 mL was kept, adjusted to pH 3 with glacial AA and filtered; the sample usually was analyzed immediately or, in any case, within 2 weeks (stored at −20 °C in a tinfoil-wrapped amber bottle).

The determination was carried out as described for the 5-HIAA calibration above with some modification as follows. Sets of three columns were placed on the fraction collector over sets of two test tubes. On the aromatic adsorbent, isolation of 5-HIAA from urine was effected as a group separation; the samples (250 μL) were run on isolation columns as described, except that two 6-mL fractions were collected. After the first fractions had been discarded (first tubes: no tinfoil), the second ones, corresponding to the elution fractions of 5-HIAA, were injected onto the reverse-phase column for identification and quantification. The 5-HIAA concentration in urine was obtained via calibration curve (peak height vs. μg/mL) constructed on working standard solutions run in the same way as urine samples.

RESULTS AND DISCUSSION

Studies on 5-HIAA Instability. Figure 1 illustrates that, at −20 °C, the standard solutions stored in tinfoil-wrapped bottles remained stable for at least 6 months, whereas the standards stored in transparent bottles, broke down into half after 3 months. These findings made clear that conventional storing may cause misinterpretations of analysis results and that solutions and samples containing 5-HIAA should be kept in the dark in order to prevent photodecomposition. As is seen in Table I, photodecomposition runs much faster in hydrochloric acid than in ammonium formate, and in ammonium formate most slowly at pH between 3–5. The

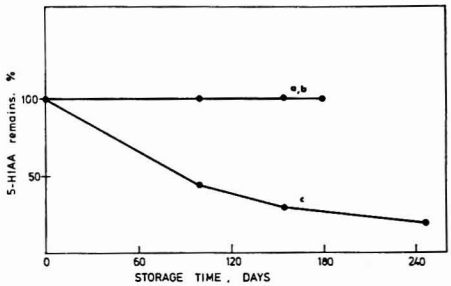

Figure 1. Storage condition influence on 5-HIAA solution stability. Stock standard solutions, 1 mg/mL in 0.1 M ammonium formate buffer, stored at −20 °C in a daily used freezer; in tinfoil-wrapped amber bottles at pH 3 (a) and at pH 7 (b) and in transparent bottles at pH 3 (c). 5-HIAA determination by directly injecting onto ODS of working standards and of the solutions above, diluted 1:50 (HPLC conditions as in Apparatus)

breakdown product was colored (A_{max} at 530-540 nm). The color appeared in the concentrated solutions already after 2–3 days exposing to bright daylight at room temperature.

On HPLC-UV (directly injected) unstably stored 5-HIAA solutions showed several peaks, whereas stably stored or freshly prepared (concentrated) solutions showed only one extra peak (t_r = 5.8 min), interpreted as some minor impurity in the compound. Since all these solutions had almost identical UV-absorption curves, the 5-HIAA breakdown product seems to consist of an easy dissociable complex of components, probably in oxidized states and with intact aromatic skeletons (*23*).

The efficiency of the storage technique was also tested on urinary 5-HIAA by comparing stored urine samples with those analyzed immediately after collecting. While after 2 weeks 5-HIAA still remained intact, 11% of it was destroyed after 3 months under the specified conditions (Table II). As pure stock solutions, stored in the same way for 6 months, proved fully intact, it seems that urine may contain some influencing compound. However, 2 or 3 weeks storing is long enough for practical purposes, so the selected conditions may be sufficient. On the other hand, drastic changes were reported to occur in urine samples stored and manipulated without any particular consideration to the risk of photodecomposition (*24*); in that case, the workers found no 5-HIAA at all in a sample from a malignant carcinoid patient but found instead 2 large peaks on fluorometric detection, which they interpreted as breakdown compounds. Another report described substance losses approaching 77% at determining tryptophan (and 50% for kyurenin) in urine, stored at −11 °C without any other preservative factor (*25*).

Calibration Curves. Altogether, almost identical linear calibration curves, passing through the origin by extrapolating,

Table II. Comparison between the Presented Method and a Reference Method (7)

	presented method				reference method			
storage time, days	5-HIAA concentration, μg/mL urinary	added	found	recovery, %[a]	5-HIAA concentration, μg/mL urinary	added	found	relative recovery, % (Ref./Pres.)
		9.5	15.5	100.0		9.5	13.2	81.5
		9.5	15.4	99.4				
		19.9	26.0	100.0		19.9	20.8	80.3
		19.9	26.0	100.0				
0	6.0[b]	24.8	31.0	100.6	1.5[b]			
		29.8	35.6	99.4		29.8	28.9	81.2
		29.8	35.5	99.3				
		49.7	56.1	100.7		49.7	44.5	79.3
		59.8	65.3	99.2				
		74.5	80.6	100.1		74.5	69.6	86.3
		99.4	105.2	99.8		99.4	89.6	85.2
0	120.0				104.0			86.6
14[d]	120.8 [c]				[c]			
14[e]	98.7							
90	107.0				90.7			84.7

[a] 0.5% RSD. [b] Subject No. 4 in Table IV. [c] Subject No. 11 in Table IV. [d] Storage conditions as described in Procedure. [e] Conventional storage conditions (in transparent bottle at +4 °C and exposed to electric light).

Table III. Retention Behavior of Some Aromatic Compounds Run on DNP-S-Seph. G-25 and on ODS, Respectively[a]

	HMMA	HVA	T	5-HT	IAA	5-HIAA
E_v/E_{vt} on DNP-S-Seph. G-25	1.7	2.4	2.8	3.6	5.0	5.7
t_r, min on ODS	4.1	7.0	106.1	31.4	13.3	6.5

[a] Conditions as described in text.

were obtained when made on analyzed dilutions of freshly prepared stock solutions or of stock solutions, stored under stable conditions in different periods. The curves arising from stock solutions, stored under unstable conditions, were also linear over the investigated range (1.25–40 μg/mL), but, as expected, showed lower inclination. Since the latter curves refer in fact to the respectively remaining 5-HIAA quantities only, they vary and are false, as distinguished from the former reproducible curves.

Urinary 5-HIAA Analysis. Application of HPLC to urine analysis, even when combined with more selective and sensitive detectors than UV, requires effective isolation of the compound before injection, also in order to maintain performance ability and reproducibility of the column. Working up samples by extractions or precipitation of proteins usually results in complex chromatograms. Ion-exchange chromatography as an isolation step involves regeneration problems and requires completing isolation stages as well. These difficulties were overcome by the present procedure, utilizing aromatic adsorption chromatography for isolation of 5-HIAA from urine.

On the adsorbent DNP-S-Seph.G-25, 5-HIAA was retarded to the degree that the fractions containing this compound were separated from the other UV-absorbing urine compounds with only little masking, and usually all UV-absorbing endogenous urine compounds were eluated within 4 h (Figure 2). No regeneration was required but, if more retarding compounds were present, such as drugs or drug metabolites based on strong aromatic components, the column had to be eluated additionally with the buffer.

The aromatic compounds, 4-hydroxy-3-methoxymandelic acid (HMMA = VMA), 4-hydroxy-3-methoxyphenylacetic acid (HVA), tryptamine (T), 5-HT and indole-3-acetic acid (IAA), were all checked by running pure solutions separately at each step; none of them showed any interference risk with regard to the whole 5-HIAA analyzing procedure: the first four of these normal urine metabolites would be fully separated on the aromatic adsorption column, while IAA, which partly accompanies 5-HIAA, would be fully resolved on the reverse-phase column (Table III). E_v/E_{vt} (which is the elution volume to total bed volume ratio) of these compounds points out their retardation on DNP-S-Seph.G-25 (Table III) in an order corresponding to both the number of their aromatic rings and to their electron-donating ability. Inasmuch as there was no molecular sieving effect, the various retardations seem to be mainly due to different properties in forming a charge-transfer complex with the DNP-S groups.

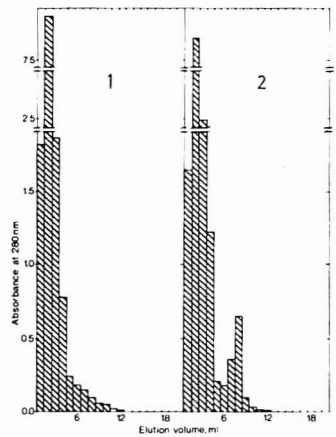

Figure 2. Elution profiles of urine samples run on DNP-S-Seph.G-25. 24-h urine samples from (1) a healthy subject and (2) a malignant carcinoid patient. Chromatography conditions as for isolation in Procedure but 1-mL fractions

By reversed-phase HPLC, the simultaneously isolated urine compounds (Figure 3: peaks X_2–X_4; likewise peak X_1, appearing in urine from some individuals, see Table IV) were completely separated from 5-HIAA and thus did not disturb.

Table IV. Determination of 5-HIAA in Urine Collected from Healthy Individuals and from Malignant Carcinoid Patients

no.[a]	sex	age	weight, kg	urine volume, mL/24 h[b]	5-HIAA concentration[b] μg/mL	mg/24 h	μg/kg per 24 h	endogenous peaks on HPLC chromatogram x_1: 5.5[c]	x_2: 9.4[c]	x_3: 11.0[c]	x_4: 14.4[c]
1[d] a	female	49	57	1300	4.0	5.2	91	+	+	+	+
b				1235	3.7	4.5	79	+	+	+	+
c				905	4.1	3.7	65	+	+	+	+
d				1300	4.5	5.8	101	+	+	+	+
e				113	2.8			+	+	+	+
2	male	61	79	725	6.2	4.5	57	–	+	+	+
3	female	17	60	1010	4.0	4.0	67	–	+	+	+
4	female	45	73	1270	6.0	7.6	104	–	+	+	+
5[e]	male	56	77	1920	3.1	5.9	77	–	+	+	–
6[e]	female	55	76	1105	5.1	5.6	74	++	++	+++	+
7	female	26	58	920	6.1	5.6	96	++	+	+	+
8	male	36	79	1000	1.0	1.0	13	–	+	+	+
9[f]	male	47	114	2530	6.1	15.4	135	–	–	–	+
10[f]	female	42	57	1500	4.1	6.1	107	–	+	+	+
11	female	65		2000	120.0	240.0		–	+	+++	+
12	female	61		780	26.0	20.3		–	–	++	–
13	female	44		1320	21.3	28.1		–	–	++	–
14	male	53		1040	200.1	208.1		–	–	–	–
15	male	59		1180	345.6	407.8		–	–	–	–

[a] No. 1-10 healthy individuals and 11-15 malignant carcinoid patients. [b] Corrected for acetic acid. [c] Retention time in minutes. Peak heights: + = 0-5 mm; ++ = 6-10 mm; +++ = 11-15 mm. [d] Urine from same subject: (a-d) 24-h collections on different days; (a) in the absence of acetic acid, (e) fresh urine sample, immediately analyzed. [e] Subjects on the same diet. (No. 6 takes daily medicine containing levothyroxinnatrium.) [f] Subjects on the same diet.

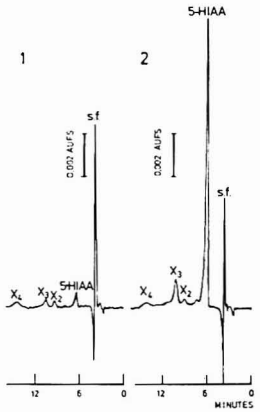

Figure 3. Typical HPLC chromatograms obtained by the presented method. (1) A healthy subject (No. 2 in Table IV) and (2) a malignant carcinoid patient (No. 11 in Table IV). 10 mV full scale recorder deflection

The mobile solvent, containing detergent, was prepared as described for separation of catecholamines and their metabolites (26) and was used throughout the study without any modification.

Once prepared with the aromatic adsorbent and calibrated, the isolation columns were very simple to manipulate, and the adsorbent maintained its capacity and was still self-regenerating after being utilized extensively. Also the ODS column performance proved intact after at least 1000 injections under daily washing with methanol.

Normal 5-HIAA excretions in urine were earlier reported to range from 2 to 8 mg per 24 h (8). The new method indicated an excretion of maximum 15 mg per 24 h in urine specimens from the healthy individuals investigated (Table IV). The lowest detectable amount of 5-HIAA in urine was 0.1 μg/mL. A comparison was made with a colorimetric method (7) based on ether extractions. That method resulted in a lower recovery as well as in a reduced recovery of added 5-HIAA (Table II).

CONCLUSION

The known difficulty in detecting cancer in its early stages, especially in hidden tracts of the body, via available medical diagnostic techniques, might indicate the importance of development of specific, simple, and sensitive analytical methods for determination of cancer metabolites in body fluids.

This paper made clear that, despite today's high sensitive instrumentation, the possibilities to ascertain true values in determining a compound from body fluids would be reduced, if any basic condition were neglected: if compound stability were not ensured, if accuracy in making calibration curves was omitted, if there were compound losses in the isolation step, or if interfering compounds were allowed to pass through.

The qualities of the new method make it suitable for biomedical research as well as for diagnostic routine application without any modification and, furthermore, applicable for fully automatic processing. Additionally, the experiences of the decomposition study may probably be of use for studies on other unstable phenols and indoles too.

ACKNOWLEDGMENT

The author is indebted to Jerker Porath of the Biomedical Center, Uppsala, for being supplied with DNP-S-Seph.G-25 and to Carl-Henrik de Verdier for being permitted to use patient samples and laboratory equipment at the Department of Clinical Chemistry, University Hospital, Uppsala.

LITERATURE CITED

(1) M. M. Rapport, A. A. Green, and I. H. Page, *J. Biol. Chem.*, **176**, 1243 (1948).
(2) V. Erspamer, *J. Physiol.*, **127**, 118 (1955).
(3) E. Titus and S. Udenfriend, *Fed. Proc.*, **13**, 411 (1954).
(4) J. Waldenström, *Nord. Med.*, **51**, 891 (1954).
(5) F. Lembeck, *Nature (London)*, **172**, 910 (1953).
(6) Å. Szoerdsma and S. Udenfriend, *J. Clin. Invest.*, **34**, 914 (1955).
(7) A. Hanson and F. Serin, *Lancet*, **2**, 1359 (1955).
(8) S. Udenfriend, E. Titus, and H. Weissbach, *J. Biol. Chem.*, **216**, 499 (1955).
(9) S. Subrahmanzan, *Curr. Med. Pract.*, **17**, 46 (1974).

(10) D. J. Byrd, W. Kochen, D. Idzko, and E. Knorr, *J. Chromatogr.*, **94**, 85 (1974).
(11) G. H. Schenk, G. L. Sullivan, and P. A. Fryer, *J. Chromatogr.*, **89**, 49 (1974).
(12) O. Hutzinger, *J. Chromatogr.*, **40**, 117 (1969).
(13) I. K. Genefke, *Acta Pharmacol. Toxicol.*, **31**, 554 (1972).
(14) H. T. Gordon and M. J. Huraux, *Anal. Chem.*, **31**, 302 (1959).
(15) J. M. Feldman, S. S. Butler, and B. A. Chapman, *Clin. Chem.* (*Winston-Salem, N.C.*), **20**, 607 (1974).
(16) J. J. Vallon, A. Badinand, and C. Bichon, *Ann. Biol. Clin.* (*Paris*), **32**, 359 (1974).
(17) A. P. Graffeo and B. L. Karger, *Clin. Chem.* (*Winston-Salem, N.C.*), **22**, 184 (1976).
(18) J. P. Sharma, E. G. Perkins, and R. F. Bevill, *J. Chromatogr.*, **134**, 441 (1977).
(19) F. J. Scandrett, *Lancet*, **270**, 967 (1956).
(20) J. Porath and N. Fornstedt, *J. Chromatogr.*, **51**, 479 (1970).
(21) R. Axén, H. Drevin, and J. Carlsson, *Acta Chem. Scand. Ser. B*, **29**, 471 (1975).
(22) J. Porath and K. Dahlgren Caldwell, *J. Chromatogr.*, **133**, 180 (1977).
(23) N. Fornstedt, Department of Clinical Chemistry, University Hospital, Uppsala, Sweden, unpublished work, 1977.
(24) D. D. Chilcote and J. E. Mrochek, *Clin. Chem.* (*Winston-Salem, N.C.*), **18**, 778 (1972).
(25) E. Grushka and E. J. Kikta Jr., *J. Chromatogr.*, **143**, 51 (1977).
(26) J. Jurand, in "High Pressure Liquid Chromatography in Clinical Chemistry", P. F. Dixon, C. H. Gray, C. K. Lim, and M. S. Stoll, Ed., Academic Press, New York, N.Y., 1976, pp 125–130.

RECEIVED for review December 12, 1977. Accepted May 2, 1978. This work was supported by a grant from the Swedish Natural Science Research Council (K-0220-045).

High Performance Liquid Chromatography with Metal-Solute Complexes

Francis K. Chow and Eli Grushka*

Department of Chemistry, State University of New York at Buffalo, Buffalo, New York 14214

Cu(II) was coordinated to two ligands, dithiocarbamate and diketone, which were chemically bonded to silica gel. Twenty-two aromatic amines were used as test solutes to study the chromatographic behavior of the copper-loaded packings. Both systems proved to be highly selective and stable. The presence of Cu(II) was found essential for separation to occur. The dependence of capacity ratios on the concentration of methanol modifier in the mobile phase suggests that the modifier affects the retention by competing for the solutes, and by changing the amount of Cu on the column. Optimum concentration of methanol in the mobile phase allows the separation of 12 aromatic amines in less than 13 min. The effect of Cu(II) concentration in the mobile phase on the capacity ratios was also studied.

The use of metal ions in high pressure liquid chromatography for the enhancement of the resolution is drawing more and more attention. For example, silver ions have been used previously for the separation of unsaturated compounds (see ref. 1 and citations therein). Although in most cases the solid support was impregnated with silver ions, the use of Ag(I) in the mobile phase has also been reported (viz., *2*, *3*). Cations other than silver have been used in ligand-exchange chromatography to achieve selective separation (viz., *4–6*). Kunzru and Frei (*7*) have utilized silica impregnated with Cd(II) for the separation of some aromatic amines. Yasuda (*8*, *9*) has also separated aromatic amines on TLC plates loaded with metal ions. Sternsen and DeWitte (*10*, *11*) have used Ni(II) in the mobile phase to facilitate the separation of amino phenols.

Previous works have indicated the usefulness of metal ions in controlling solute retention behaviors and in improving the selectivity of chromatographic systems. To capitalize on the advantage offered by such systems, Chow and Gruskha (*12*) have recently discussed the possibility of using metal ions which are bonded via a ligand to the support particles. Cooke et al. (*13*) have also discussed such an approach. In addition, Cooke et al. have described the use of metal ions coordinated to an hydrophobic chelating agent in the mobile phases in conjunction with a reversed phase packing.

In our previous paper (*12*), propylamine covalently bonded to silica gel was used to retain Cu(II) as part of the stationary phase. The potential of such a chromatographic approach in achieving selective separations was clearly demonstrated. However, due to the fact that the alkylamine has only one site which can coordinate the metal ion, Cu(II) can be leached from the support rather easily. To overcome this difficulty, a bidentate bonded ligand can be used to ensure a stronger attachment of the metal ion. The present work describes two such bidentate chelating agents: (1) a dithiocarbamate and (2) a diketone. Both of these ligands have been studied extensively in the extraction of metal ions, and both can complex Cu(II) quite strongly. Therefore these chelating agents, when covalently bonded to the support, should retain Cu(II) and provide a stable and selective system for certain chromatographic separations.

It might be anticipated that the retention behavior would also be affected by the presence of the metal ion in the mobile phase, (i.e., over and above the metal ion in the stationary phase). One of the aims of this study was to determine the selectivity of the bonded-Cu(II) columns with excess copper in the mobile phase. An additional benefit of such a study is in investigating the stability of the copper columns with and without copper ions in the mobile phase.

EXPERIMENTAL

Apparatus. The liquid chromatograph consisted of an Altex Model 110 solvent metering pump (Berkeley, Calif.), and LDC (Riviera Beach, Fla.) UV detector model 1285 (254 nm) and a Rheodyne (Berkeley, Calif.) model 7120 injection valve. Columns were made of 316 stainless steel, 25 cm × 0.31 cm i.d. and 20 cm × 0.31 cm for the "Dithiocarbamate" and the "Diketone" columns, respectively.

Reagents. Partisil-10 porous silica support was obtained from Whatman Inc., (Clifton, N.J.). γ-Aminopropyltrimethoxysilane was purchased from Silar Labs (Scotia, N.Y.). Ethyl benzoylacetate, fluorenes, and fluorenones were bought from Aldrich Chemical Co. (Metuchen, N.J.). All other amines were obtained

0003-2700/78/0350-1346$01.00/0

Table I. Table of Solutes Tested

	compound	symbol
1.	naphthalene	N
2.	1-aminonaphthalene	1N
3.	2-aminonaphthalene	2N
4.	1-aminoanthracene	1A
5.	2-aminoanthracene	2A
6.	2-amino-9-fluorenone	2,9
7.	4-amino-9-fluorenone	4,9
8.	2-amino-9-hydroxyfluorene	2AOH
9.	9-fluorenone	9F
10.	fluorene	F
11.	2-aminofluorene	2AF
12.	*o*-chloroaniline	OCA
13.	*m*-chloroaniline	mCA
14.	*p*-chloroaniline	PCA
15.	*o*-nitroaniline	ONA
16.	*m*-nitroaniline	mNA
17.	*p*-nitroaniline	PNA
18.	*o*-Toluidine	OT
19.	*m*-Toluidine	mT
20.	*p*-Toluidine	PT
21.	*o*-Anisidine	OA
22.	*p*-Anisidine	PA

from various other sources. The solutes used are shown in Table I. Methanol was distilled before use; all other solvents were reagent grade and used without further purification.

Procedure. (I) Preparation of the alkylamine bonded phase: 30 mL of 10% γ-aminopropyltrimethoxysilane in dry toluene was added to 5.0 g of Partisil-10 which had been vacuum dried at 150 °C for 6 h. The mixture was then refluxed under anhydrous conditions for 6 h. It was then washed with dry toluene, isopropanol, acetone, methanol, and acetone again, and vacuum dried at 100 °C for 1 h. CHN analysis showed 2.9 μmol/m^2 surface coverage as calculated by the method suggested by Unger (*8*). N analysis was used for the calculation.

(II) Preparation of the "Dithiocarbamate" System: 2.5 g of the alkylamine-bonded Partisil-10 prepared previously were added to 10 mL dry toluene, 2 mL isopropanol, 2 mL carbon disulfide, and 1 mL of 10% methanolic solution of ammonium hydroxide. The mixture was stirred for 20 min at room temperature as suggested by Leyden and Luttrel (*14*). The reaction is as follows:

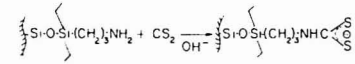

The presence of carbon disulfide in the bonded phase was tested qualitatively by adding concentrated hydrochloric acid to some of the packing (*15*).

(III) Preparation of the "Diketone" System: 2.5 g of previously bonded-amine Partisil-10 were added to 30 mL of 10% ethyl benzoylacetate solution in dry toluene. The mixture was refluxed for 6 h. It was expected that the reaction will yield the β-diketone, compound 1. However NMR studies of the reaction between an alkyl amine and ethyl benzoylacetate indicated that most likely compound 2 is also present on the silica gel:

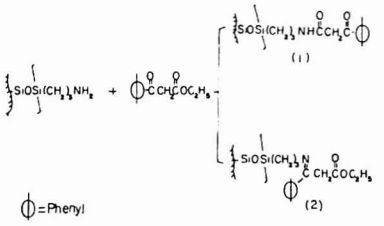

CHN analysis showed that about 50% of the amine sites have reacted with the reagents. Both 1 and 2 can coordinate Cu(II). Although the reactions between ethyl benzoylacetate and the bonded propylamine did not yield just the expected diketone (see reaction scheme), that column will be referred to as the "diketone" column.

(IV) Chromatographic Studies: k' value was collected before loading the columns with Cu(II). Then a 5.0×10^{-3} M $CuSO_4$ solution in methanol was passed through the columns in order to load them with copper. k' value was collected again with the same batches of mobile phases. The mobile phases used are: (1) 20% v/v cyclohexane in methanol (mobile phase A) without and with Cu^{2+}, and (2) a mixture of hexane:methylene chloride: methanol having the ratio 7:1:0.5 (mobile phase B). In one study, the relative ratios of hexane to methanol were changed. Columns were washed with HCl solution (pH ~1.5) and the concentration of Cu(II) was determined by titration as discussed by Belcher and Nutten (*16*). Mobile phases were tested in an increasing order of polarity.

Hold-up times were measured by injecting 10 μL of a solvent having a slightly different composition than that of the mobile phases. The flow rate used throughout the whole study was 1.0 mL/min.

RESULTS AND DISCUSSIONS

The concentration of complexed Cu(II) on the "dithiocarbamate" and "diketone" columns was found to be 0.35 μmol/m^2 and 0.42 μmol/m^2, respectively. These values were obtained after the columns were equilibrated with methanol, and in essence they represent the lower limit of copper loading. Our studies show, as will be discussed later, that mobile phases lean in methanol allowed larger amounts of Cu(II) to be retained on the column. The amount of Cu(II) bonded to the support in the present study is about 1.5 to 2 times larger than that reported by us previously. Still, this amount of Cu(II) is small compared to the total number of sites available for bonding. Several solutions differing in the concentration of Cu(II) were used to bond copper to the support; yet the capacity ratios of the solutes studied here remained constant when the $CuSO_4$ concentration in the loading solution was above about 5×10^{-3} M.

Table II shows the k' values of 22 solutes on the "diketone" and the dithiocarbamate columns with and without Cu(II), using mobile phases A and B. With the dithiocarbamate–Cu(II) column, mobile phase A contained $CuSO_4$ (2.2×10^{-4} M).

The capacity ratios of all the solutes on both columns were very small when Cu(II) was not present and mobile phase A was used. The presence of copper on the stationary phase causes longer retention for all but a few solutes. Those solutes which do not have an amine group, naphthalene, 9-fluorenone and fluorene, eluted faster on the bonded copper columns when mobile phase A was used. The complexed Cu(II) seems to prevent the interaction between the above three solutes and the stationary phases. The increase in the capacity ratio values of the less basic aniline isomers (e.g., *o*-chloroaniline) in the presence of Cu(II) was rather small. Using mobile phase A, separations not possible on the diketone or the dithiocarbamate columns alone can be achieved when Cu(II) is added to the support. As an example, Table III shows some selectivity factors, α, using mobile phase A on both columns with and without Cu(II).

The retention behavior is different when a mobile phase "lean" in methanol is used: see Table II, mobile phase B. With such a mobile phase, the separations of some of the aromatic amines are possible even without the presence of Cu(II); (e.g., nitroanilines, or aminofluorenones). Still, many solutes are not separated; e.g., the aminonaphthalenes or the toluidines. With the copper bonded phase the capacity ratios and the selectivity factors, α, increase, as illustrated in Table III. Even though the capacity ratios are much larger when mobile phase B is used, in general the α values do not differ greatly between the mobile phases. However, because of the very rapid elution of solutes with mobile phase A, errors in measuring k' values, and hence, α, can be significant.

Table II. k' Values with and without Cu(II) Bonded to the Support

		dithiocarbamate column				diketone column			
		no Cu(II)		Cu(II) bonded		no Cu(II)		Cu(II) bonded	
	solutes	mobile phase A[c]	mobile phase B[c]	mobile phase A[a]	mobile phase B	mobile phase A	mobile phase B	mobile phase A	mobile phase B
1.	N					0.7	0.89	0.11	0.56
2.	IN	0.40	1.60	0.90	2.78	0.17	0.89	0.36	4.16
3.	2N	0.40	1.60	1.94	7.36	0.17	0.89	0.73	9.58
4.	1A	0.38	1.78	1.06	2.39	0.18	1.11	0.46	5.08
5.	2A	0.38	1.86	1.84	3.39	0.18	1.32	0.79	9.32
6.	29	0.44	2.71	0.97	6.24	0.18	1.60	0.45	7.46
7.	49	0.44	3.48	0.39	3.78	0.18	1.72	0.25	4.34
8.	2AOH	0.21	6.73	2.68	*b*	0.086	2.42	0.82	38.7
9.	9F	0.36	0.20	0.16	0.03	0.18	0.36	0.11	0.56
10.	F	0.36	0.04	0.16	0.00	0.18	0.14	0.11	0.22
11.	2AF	0.40	1.35	2.74	8.06	0.18	0.92	1.31	13.6
12.	OCA	0.28	0.73	0.26	0.85	0.17	0.58	0.11	1.40
13.	mCA	0.28	1.40	0.71	3.70	0.17	1.00	0.25	4.76
14.	PCA	0.28	1.40	1.29	6.85	0.17	1.00	0.44	7.88
15.	ONA	0.34	2.13	0.31	2.58	0.11	1.53	0.21	2.84
16.	mNA	0.35	3.53	0.53	6.67	0.14	2.28	0.25	6.68
17.	PNA	0.35	7.53	0.42	11.8	0.14	9.88	0.21	10.7
18.	OT	0.20	0.67	0.84	2.06	0.027	0.53	0.34	3.12
19.	mT	0.20	0.87	1.61	5.70	0.027	0.53	0.71	7.56
20.	PT	0.20	0.87	2.29	9.94	0.027	0.53	1.04	12.36
21.	OA	0.20	0.77	0.87	2.63	0.070	0.50	0.45	4.44
22.	PA	0.20	1.48	3.45	*b*	0.070	0.84	2.07	33.6

[a] Mobile phase A contained 2.2×10^{-4} $MCuSO_4$. [b] Retention too long. [c] A = 20% v/v cyclohexane in methanol. B = Hexane:methylenechloride:methanol) (7:1:0.5).

Table III. Comparison of Selectivity Factors, α, of Some Solutes with and without Cu(II) Bonded to Stationary Phases

	mobile phase B			mobile phase A		
Column	$\frac{k'_{2N}}{k'_{1N}}$	$\frac{k'_{2,9}}{k'_{4,9}}$	$\frac{k'_{PCA}}{k'_{mCA}}$	$\frac{k'_{2N}}{k'_{1N}}$	$\frac{k'_{2,9}}{k'_{4,9}}$	$\frac{k'_{PCA}}{k'_{mCA}}$
dithiocarbamate column	1.00	1.28 $(k'_{4,9}/k'_{2,9})$	1.00	1.00	1.00	1.00
"diketone" column	1.00	1.08 $(k'_{4,9}/k'_{2,9})$	1.00	1.00	1.00	1.00
dithiocarbamate-Cu(II) column	2.65	1.65	1.85	2.16[a]	2.49[a]	1.82[a]
"diketone"-Cu(II) column	2.30	1.72	1.65	2.03	1.80	1.76

[a] The mobile phase contained 2.2×10^{-4} M $CuSO_4$. A and B same as Table II.

Some retention reversal should be noted. Without copper, 2-amino-9-fluorenone elutes before the 4-amino isomer. When Cu(II) is bonded to either ligand, the 2-amino isomer is retained longer than the 4-amino isomers. The interaction between the Cu(II) and the 2-amino isomer is stronger than the interaction with the 4-amino isomer. It might be possible that the 2-amino isomer can form a bidentate complex with the bonded copper whereas the 4-amino isomer cannot.

The retention order of the nitroanilines with mobile phase A as compared to B is also of interest. The meta nitroaniline isomer is the most basic of the three, and with the Cu(II) columns and mobile phase A, this isomer elutes last among the three. With mobile phase B, the retention order, which depends most likely on the solubility, is ortho < meta < para, irrespective whether or not Cu(II) is present in the stationary phase. The basicity influence on the retention is still evident, however, and the capacity ratio of *m*-nitroaniline shows largest change when the Cu(II) is introduced to the support.

Figure 1 shows the separation of several solutes on the diketone column without copper using mobile Phase B. Figure 2 is a chromatogram of the same solutes under the same conditions, with the exception that Cu(II) is bonded to the diketone. The solute 2-amino-9-hydroxyfluorene, not shown in the figure, elutes after about 30 min. With the Cu(II) column, 2-aminofluorene elutes after 2-amino-9-fluorenonone and 4-amino-9-fluorenone, and as mentioned before, the elution of the 2-amino and the 4-amino is the reverse of that shown in Figure 1. Apparently, the ketone group of the phenone delocalizes the electrons in the aromatic rings. Consequently the aminofluorene is a stronger base than the two aminofluorenones, and forms a stronger complex with the bonded copper. The aminohydroxyfluorene can form a strong bidentate complex with the copper and it is therefore retained the most. Although the selectivity is higher on the Cu(II)-loaded column, the efficiency, especially as measured from the more retained solutes, is decreased. This decrease presumably is due to the slow dissociation of the solute–Cu(II) complex (*12*, *13*). Table IV shows the plate heights for the columns with and without copper, measured with 1-aminonaphthalene and 2-amino-9-fluorenone. Future research

Table IV. Comparison of Plate Height (mm) of Two Solutes for Columns with and without Cu(II) in the Stationary Phase. Mobile-Phase B[a]

	solutes	
column	1N	2,9
dithiocarbamate column	0.15	0.17
"diketone" column	0.21	0.23
dithiocarbamate column-Cu(II)	0.31	0.58
"diketone" column-Cu(II)	0.28	0.31

[a] Conditions same as Table I.

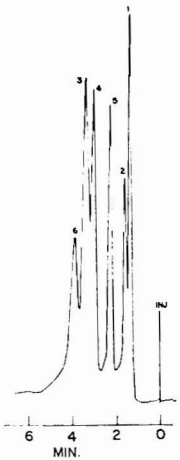

Figure 1. Separation of some fluorenes and fluorenones. No Cu(II) in stationary phase. Mobile phase: Hexane/methylene chloride/methanol (7/1/0.5). Flow rate: 1.0 mL/min. Diketone column. (1) fluorene, (2) 9-fluorenone, (3) 4-amino-9-fluorenone, (4) 2-amino-9-fluorenone, (5) 2-aminofluorene, (6) 2-amino-9-hydroxylfluorene

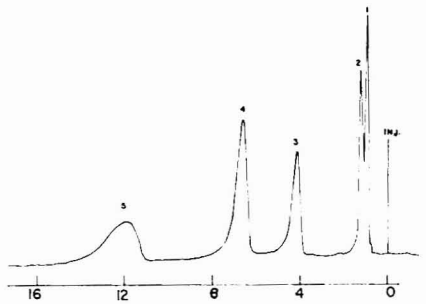

Figure 2. Separation of some fluorenes and fluorenones. Cu(II) bonded to support. Mobile phase: Hexane/methylene chloride/methanol (7/1/0.5). Flow rate: 1.0 mL/min. Diketone column. Solutes are the same as in Figure 1

should be directed at improving the plate height of the bonded-metal system.

Figure 3 shows a chromatogram of the aminonaphthalenes on a copper column. Although the efficiency is rather poor for present day LC technology, the selectivity is so large that the column can be overloaded and used as a preparative one for the separation of these isomers. The same can be said about the separation of various substituted anilines.

Some band tailing was observed in the Cu(II)-loaded column. This tailing might be due to the slow rate of dissociation and association of the Cu(II)–amine complexes.

Effect of Cu(II) Ions in Mobile Phase. Metal cations in the mobile phase, in addition to those in the stationary phase, can have a pronounced effect on the retention behavior and on the separation. Table V shows that the capacity ratios, in general, increase with the concentration of Cu(II) in the mobile phase. Cooke et al. (*13*) found that with Zn(II) in the mobile phase above a certain concentration, the capacity ratios decrease with further increase of the metal ion concentration. Unfortunately in the present study, higher concentration of

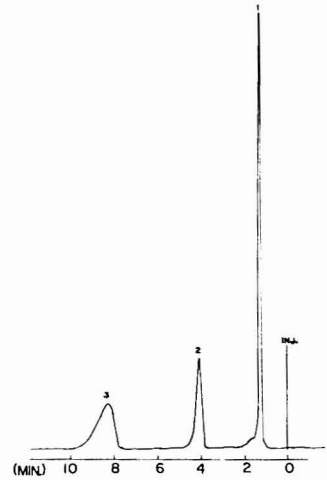

Figure 3. Separation of isomeric aminonaphthalenes on the diketone column with bonded Cu(II). Mobile phase: Hexane/methylene chloride/methanol (7/1/0.5). Flow rate: 1.0 mL/min. (1) naphthalene, (2) 1-aminonaphthalene, (3) 2-aminonaphthalene

Table V. Effect of Concentration of Cu(II) in Mobile Phase A. Diketone–Cu(II) Column (Flow Rate, 1.0 mL/min)

solutes	no. Cu(II)	2.2×10^{-4} M Cu^{2+}	5.5×10^{-4} M Cu^{2+}
N	0.11	0.10	0.14
1N	0.36	0.61	0.83
2N	0.73	1.51	2.14
1A	0.46	0.75	0.97
2A	0.79	1.49	2.09
29	0.45	0.78	1.02
49	0.25	0.27	0.30
2AO4	0.82	1.63	2.11
9F	0.11	0.10	0.083
F	0.11	0.10	0.083
2AF	1.31	2.43	3.05
OCA	0.11	0.13	0.23
mCA	0.25	0.54	0.77
PCA	0.44	1.01	1.49
ONA	0.21	0.10	0.26
mNA	0.25	0.27	0.43
PNA	0.21	0.10	0.26
OT	0.34	0.58	0.89
mT	0.71	1.43	1.97
PT	1.04	2.19	2.89
OA	0.45	0.81	1.14
PA	2.07	4.31	4.71

Cu(II) could not be used because of strong UV absorbance at 254 nm. The increase in the retention time probably is due to the fact that Cu(II) from the mobile phase is being taken up by the support, resulting in a greater probability of forming solute-bonded copper complex. Complexation with the bonded Cu is more favorable (or more probable) than with the metal ion in the mobile phase. Figure 4 shows that effect of Cu(II) in the mobile phase on the retention times and the separation of the aminonaphthalenes. In general, k' values increased with concentration of Cu(II) at least in the concentration range we studied.

Effect of Methanol Concentration. Table II shows that the concentration of methanol in the mobile phase affects

Table VI. Effect of Amount of Methanol in Mobile Phase[a] on k' Values

	k' values									
	diketone column–Cu(II)					dithiocarbamate column–Cu(II)				
solutes	B	B_1	B_2	B_3	B_4	B	B_1	B_2	B_3	B_4	B_5
N	0.56	0.17	0.25	0.27	0.11						
1N	4.16	2.07	1.56	1.40	0.50	2.78	1.93	1.54	1.30	0.70	0.33
2N	9.58	5.42	3.39	3.40	1.22	7.36	4.30	3.88	3.31	1.60	0.79
1A	5.08	2.61		1.60	.67	2.39	1.34	1.14		0.79	0.45
2A	9.32	5.36		3.27	1.22	3.39	1.78	1.57		1.49	0.80
29	7.46	3.48	2.24	1.83	0.58	6.24	2.89	2.37	1.70	0.81	0.47
49	4.34	1.50	1.30	0.86	0.27	3.78	1.62	1.41	0.93	0.41	0.24
2AOH	38.6	11.40	6.16	5.40	1.19		14.80	11.03	6.81	2.29	1.06
9F	0.56	0.38	0.45	0.27	0.083	0.03	0.32	0.072	0.30	0.16	0.076
F	0.22	0.23	0.30	0.27	0.083	0.00	0.14	0.072	0.30	0.16	0.076
2AF	13.6	8.60	4.98	5.07	2.17	8.06	5.76	5.20	4.70	2.23	1.30
OCA	1.40	0.65	0.82	0.47	0.083	0.85	0.74	0.67	0.54	0.27	0.11
mCA	4.76	2.13	1.60	1.33	0.44	3.70	2.35	1.93	1.53	0.71	0.68
PCA	7.88	3.94	2.51	2.43	0.78	6.85	4.00	3.31	2.73	1.25	1.01
ONA	2.84	1.03	0.88	0.63	0.17	2.58	1.32	1.17	0.81	0.33	0.17
mNA	6.68	2.39	1.67	1.21	0.22	6.67	2.80	2.28	1.62	0.61	0.29
PNA	8.84	2.39	1.67	0.97	0.22	11.8	3.54	3.01	1.62	0.61	0.29
OT	3.12	1.75	1.33	1.17	0.37	2.06	1.46	1.36	1.14	0.59	0.25
mT	7.56	4.44	3.05	2.85	0.94	5.70	3.58	3.35	2.79	1.47	0.74
PT	12.36	6.78	4.88	4.67	1.41	9.94	6.25	5.61	4.69	2.40	1.24
OA	4.44	2.10	0.22	1.60	0.57	2.63	1.64	1.41	1.23	0.70	0.29
PA	33.6		1.02	11.27	2.77		18.86	16.04	12.40	5.07	2.37

[a] Mobile phase: hexane/methylene chloride/methanol: 700/100/50, B; 600/100/150, B_1; 550/100/200, B_2; 450/100/300, B_3; 200/100/550, B_4; 50/100/700, B_5.

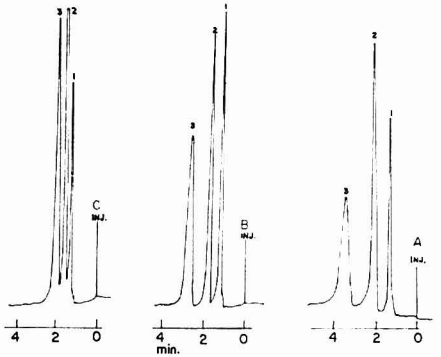

Figure 4. Separation of isomeric aminonaphthalenes on diketone–Cu(II) column with various Cu(II) concentrations in mobile phase A. Flow rate: 1.0 mL/min. Chromatogram A: 20% cyclohexane/methanol with 5.5×10^{-4} M Cu(II). Chromatogram B: 20% cyclohexane/methanol with 2.2×10^{-4} M Cu(II). Chromatogram C: 20% cyclohexane/methanol with no Cu(II). (1) naphthalene, (2) 1-aminonaphthalene, (3) 2-aminonaphthalene

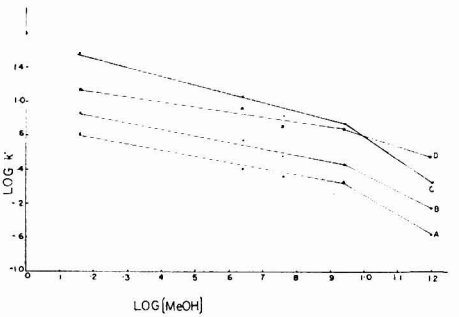

Figure 5. Correlation of log [methanol] to log k' for some fluorenes and fluorenones. Diketone column loaded with Cu(II). (A) 4-amino-9-fluorenone, (B) 2-amino-9-fluorenone, (C) 2-amino-9-hydroxyfluorene, (D) 2-aminofluorene

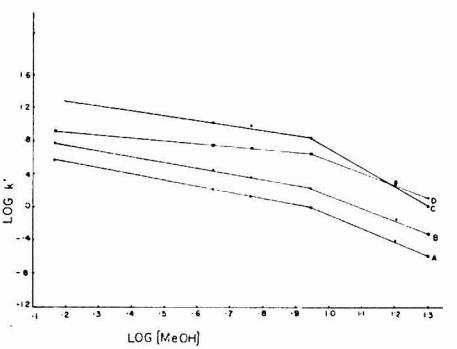

Figure 6. Correlation of log [methanol] to log k' for some fluorenes and fluorenones. Dithiocarbamate column loaded with Cu(II). Solutes are the same as in Figure 5

greatly the retention times of the solutes. To better understand the effect of methanol, a series of mobile phases made of various ratios of hexane:methylene chloride:methanol were prepared. Table VI shows the capacity ratios of the solutes on the two Cu(II)-loaded columns with various amounts of methanol. As expected, the k' values decreased as the amount of methanol is increased. This decrease, however, is not linear. Figures 5 and 6 show plots of log k' vs. log of the concentration of MeOH. For the sake of clarity, the behavior of only four solutes is shown in the figures. Increasing the methanol content of the mobile phase changes the capacity ratios via two mechanisms: (1) better solvation of the solutes and (2) leaching out some of the bonded copper (This effect will be discussed shortly). The change in the retention of the amino-9-fluorenones and the amino-9-hydroxyfluorene seems to

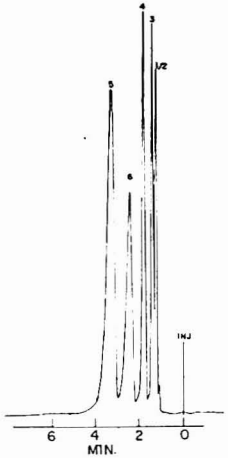

Figure 7. Separation of some fluorenes and fluorenones in a methanol-rich mobile phase. Mobile phase: Hexane/methylene chloride/methanol (2/1/5.5). Flow rate: 1.0 mL/min. Diketone–Cu(II) column. Solutes are the same as in Figure 1

be the same, on each column, as the concentration of methanol is increased from ≃0.2 M to about 0.9 M. The change in k' of the aminofluorene is less than that of the other solutes, as judged by the slope of the plots of Figures 5 and 6. Aminofluorene has only one site which can hydrogen bond with methanol, and perhaps the major cause for the decrease in the retention of that solute is due to the loss of copper from the column as the alcohol content is increased. The other aromatic amines can form H-bonds with the methanol, and solvation by the polar modifier might be the major contribution to the decrease in the k' values. Once the amount of methanol in the mobile phase exceeds a certain limit, the change in the k' values is more pronounced, especially with the amino-9-hydroxyfluorene. As can be seen in Figures 5 and 6 and in Table VI, reversal in some retention order occurs. The increase in the rate of change of the capacity factors is probably a result of the greater extent of Cu(II) stripping from the column by the higher concentration of methanol in the mobile phase.

Comparison of chromatograms shown in Figure 2 and 7 presents a graphical illustration of the effect of the methanol. The mixture and the column are the same in either case. However, in the case of Figure 7, the mobile phase is richer in methanol. Under these conditions, the amino-9-hydroxyfluorene elutes before the aminofluorene.

Using plots such as those shown in Figures 5 and 6, an optimum mobile phase can be found for the separation of a large number of aromatic amines. Figure 8 shows the separation of 12 solutes on the diketone–Cu(II) column in less than 13 min. The use of capacity ratio plots vs. the concentration of the mobile phase to obtain an optimum resolution is similar to the utilization of stationary phase composition as developed by Purnell and Laub in gas chromatography (viz. *17* and references therein). Figure 9 shows a separation of eight substituted anilines on the dithiocarbamate–Cu(II) column.

Column Equilibration and Stability. After the columns were loaded with Cu(II) (by passing 5×10^3 M $CuSO_4$ in MeOH through the columns), the mobile phase was introduced. At that time, monitoring of the volume of mobile phase

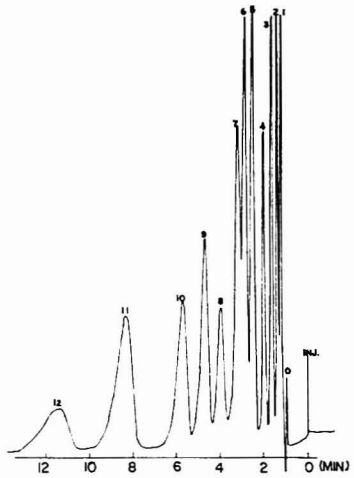

Figure 8. Separation of a mixture of 12 aromatics and aromatic amines. Mobile phase: Hexene/methylene chloride/methanol (6/1/1.5). Flow rate: 1.0 mL/min. Diketone–Cu(II) column. (1) fluorene, (2) 9-fluorenones, (3) *o*-chloroaniline, (4) *o*-nitroaniline, (5) 4-amino-9-fluorenone, (6) 1-aminonaphthalene, (7) *m*-nitroaniline, (8) 2-amino-9-fluorenone, (9) *p*-chloroaniline, (10) 2-aminonaphthalene, (11) 2-aminofluorene, (12) 2-amino-9-hydroxyfluorene

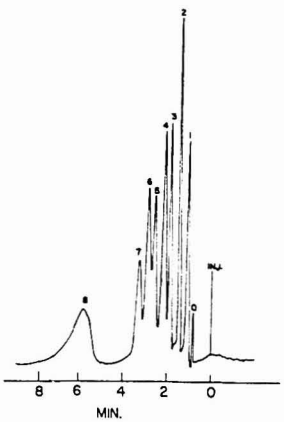

Figure 9. Separation of a mixture of eight anilines on the Dithiocarbamate–Cu(II) column. Mobile phase: Hexane/methylene chloride/methanol (5.5/1/2). Flow rate: 1.0 mL/min. (1) benzene, (2) *o*-chloroaniline, (3) *o*-nitroaniline, (4) *o*-anisidine, (5) *m*-chloroaniline, (6) *m*-nitroaniline, (7) *p*-nitroaniline, (8) *p*-toluidine

passing through the column was started. Injections of several solutes were made as soon as enough UV light was transmitted through the cell (at 5×10^{-3} M Cu^{2+} the absorbance was much too high). Figure 10 shows typical behavior of the k' values of these solutes as a function of time on the diketone–Cu(II) column. When mobile phase A was used, it took about 600 min (flow rate 1 mL/min) before the capacity ratio of the amino-9-hydroxyfluorene stabilized at 0.84. On the other hand, with the solutes which are less sensitive to small variations in the amount of Cu(II), equilibration is much

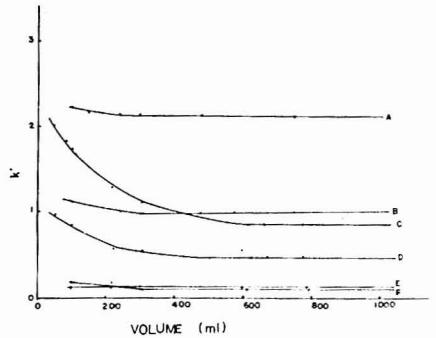

Figure 10. Column equilibration curves for the Diketone column after bonding Cu(II). Mobile phase flow rate, 1 mL/min. Curves C, D, and F are for 2-amino-9-hydroxyfluorene, 2-amino-9-fluorene and 9-fluorenone, respectively using mobile phase A. Curves A, B, and E are for the same solutes with mobile phase A containing 5.5×10^{-4} M $CuSO_4$

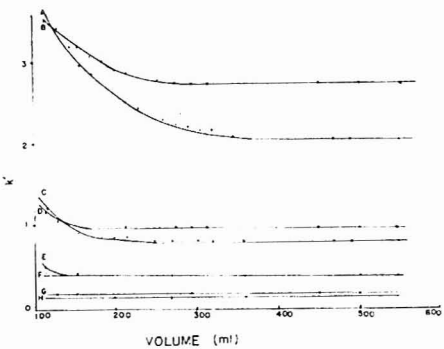

Figure 11. Column equilibration curves for Dithiocarbamate column after bonding Cu(II). Mobile phase flow rate, 1 mL/min. Curves A, C, E, and G are for solutes: 2-amino-9-hydroxyfluorene, 2-amino-9-fluorenone, 4-amino-9-fluorenone, and a fluorenone with mobile phase A. Curves B, D, F, and H are for the same solutes with mobile phase A containing 5.5×10^{-4} M $CuSO_4$

faster. For example, the fluorenone retention time is constant, within experimental error, almost immediately. When the mobile phase contained 5.5×10^{-4} M $CuSO_4$, the equilibration period is much shorter; about 200 min for the amino-9-hydroxyfluorene and 2-amino-9-fluorenone. As expected, k' values at equilibrium are higher when the mobile phase contains copper. Figure 11 shows a similar behavior with the dithiocarbamate–Cu(II) column. In general, however, the equilibrium time is faster with the dithiocarbamate–Cu(II) column.

Column Reproducibility. Reproducibility studies were carried out with the diketone–Cu(II) column. In one case, after using the column with mobile phase A containing Cu(II) (2.2×10^{-4} M), several other mobile phases were employed over a period of several days. Upon returning to the original mobile phase it was found that, within experimental errors, the capacity ratios were constant. Some of the results are shown in Table VII.

Study of column reproducibility is shown in Table VIII with a mobile phase made of hexane:methylene chloride:methanol (4.5:1:3). The first column in the table shows the original data.

Table VII. Reproducibility Test for Diketone Column–Cu(II)[a]

solute	k' values: original run	k' values: return after several days
F	0.10	0.12
9F	0.10	0.12
29	0.78	0.81
49	0.27	0.30
2AF	2.43	2.65
2AOH	1.63	1.76

[a] Mobile phase: 20% cyclohexane/methanol 2.2×10^{-4} M Cu(II), flow rate = 1.0 mL/min.

Table VIII. Reproducibility Test for Diketone Column–Cu(II)—k' Values[a]

solute	original run	return after using more polar mobile phases	values after adding 5.0 mL of 10^{-2} M Cu(II) in MEOH into system and re-equilibrating
F	0.27	0.27	0.25
9F	0.27	0.27	0.26
29	1.83	1.70	1.90
49	0.86	0.67	0.82
2AF	5.07	3.68	5.12
2AOH	5.40	4.00	5.68

[a] Mobile phase: hexane/methylene chloride/methanol (4.5:1:3). Flow rate = 1.0 mL/min.

The second column shows the capacity ratios with the same mobile phase but after several days of use with more polar mobile phases (more MeOH). The capacity ratios of the amine-containing solutes decreased noticeably. However, as seen in the third column of Table VIII, after passing 5.0 mL of 10^{-2} M Cu(II) in MeOH and equilibrating with the original mobile phase, the capacity ratios, within experimental error, are the same as initial values. Column reproducibility, then, can be maintained and controlled rather easily. Tables VII and VIII indicate that the amount of Cu(II) bonded is dependent upon the mobile phase used.

CONCLUSIONS

Chromatography with bonded-metal ions can yield selective separations not attainable without the metals. Proper choice of the ligand to which the metal ion is bonded can affect the stability of the chromatographic column. Of course the ligand may also affect chromatographic behavior. The differences in the column efficiencies, the k' values, and the rate of equilibration between the two ligands used in the present study may be due not only to the higher Cu(II) content but also to the different structure of the ligands. More exotic ligands can be used, and indeed have been used for the separation of amino acid enantiomers (*18*).

Since the amine–Cu complex formation constants are fairly large, the efficiency of the system herein described is limited by poor mass transfer. Other metals which form weaker complexes can be used to improve efficiency. Such an approach was studied by Cooke et al. (*13*). They also found that complexation with metal ions in the mobile phase, in conjunction with reversed phase columns, can yield efficient separations. In our studies, the very large selectivity factors due to the presence of bonded Cu(II) largely overcome the limited column efficiency in producing effective separations.

Clearly, the potentials of using metals in chromatography show great promise, and we are now studying methods of improving column efficiency in order to apply such columns to the difficult separation of biopolymers.

LITERATURE CITED

(1) S. Lam and E. Grushka, *J. Chromatogr. Sci.*, **15**, 234 (1977).
(2) D. J. Weber, *J. Pharm. Sci.*, **66**, 744 (1977).
(3) G. Schomburg and B. Vanach, 3rd International Symposium on Column Liquid Chromatography, Sept. 27–30, 1977, Salzburg, Austria.
(4) F. G. Helfrich, *Nature (London)*, **189**, 1001 (1961).
(5) H. F. Walton, *Sep. Purif. Methods*, **4**, 189 (1975).
(6) A. V. Semechkin, S. V. Rogozhin, and V. A. Davankov, *J. Chromatogr.*, **131**, 65 (1977).
(7) D. Kunzru and R. W. Frei, *J. Chromatogr. Sci.*, **14**, 381 (1974).
(8) K. Yasuda, *J. Chromatogr.*, **60**, 144 (1971).
(9) K. Yasuda, *J. Chromatogr.*, **72**, 413 (1972).
(10) L. A. Sternson and W. J. DeWitte, *J. Chromatogr.*, **137**, 305 (1977).
(11) L. A. Sternson and W. J. DeWitte, **138**, 229 (1977).
(12) F. K. Chow and E. Grushka, *Anal. Chem.*, **49**, 1756 (1977).
(13) N. H. C. Cooke, R. L. Viavattene, R. Eksteen, W. S. Wong, G. Davies, and B. L. Karger, Submitted to *J. Chromatogr.*
(14) D. E. Leyden and G. W. Luttrel, *Anal. Chem.*, **47**, 1612 (1975).
(15) F. A. Cotton and G. Wilkinson, "Advanced Inorganic Chemistry", Interscience, New York, N.Y., 1962, p 229.
(16) R. Belcher and A. J. Nutten, "Laboratory Manual of Quantitative Inorganic Analysis", Butterworth, London, 1955, p 244.
(17) W. K. Al-Thamir, R. J. Laub, and J. H. Purnell, *J. Chromatogr.*, **142**, 3 (1977).
(18) V. A. Davankov and A. V. Semechkin, *J. Chromatogr.*, **141**, 313 (1977).

RECEIVED for review February 13, 1978. Accepted May 12, 1978. We thank NIH for supporting the present work under grant GM-20846.

High Performance Liquid Chromatographic Study of the Retention and Separation of Short Chain Peptide Diastereomers on a C_8 Bonded Phase

Eugene P. Kroeff[1] and Donald J. Pietrzyk*

Chemistry Department, The University of Iowa, Iowa City, Iowa 52242

The effects of peptide structure and stereochemistry and eluent pH and composition on the retention of short chain peptides and peptide diastereomers on a C_8 bonded phase are evaluated by HPLC. The peptides are highly retained in acidic and basic solution and are at a minimum retention at the isoelectric pH. Peptide retention is influenced by the hydrophobicities of the amino acid subunits and by the position of the hydrophobic amino acid subunits in relation to the charged sites. It is suggested that the different conformations for peptide diastereomers have slight differences in hydrophobicity, and this influences their retention order. Several examples which illustrate these parameters and the scope of separating peptide diastereomer mixtures by HPLC are described.

The separation of short chain peptides has traditionally been accomplished by ion-exchange or thin-layer chromatography (*1*). During the past year, high performance liquid chromatography (HPLC) employing nonpolar (reverse) stationary phases has been shown to be very effective in bringing about these separations (*2–6*). Reverse phase HPLC is particularly attractive since it is fast, highly reproducible, and requires a minimum of sample preparation. Easily prepared eluting solvents such as buffered aqueous or aqueous–alcohol or –acetonitrile mixtures are used. Furthermore by using a variable wavelength detector (200 to 220 nm) detection of any amino acid or peptide is possible without resorting to derivitization.

Several nonpolar stationary phases have been used to effect peptide separations. Short chain peptides containing as many as six nonpolar amino acid (AA) subunits, as well as larger hormone peptides were separated on a 5-μm octyl-silica bonded phase type stationary phase (*2*). Retention studies of pharmacologically important nonapeptides were performed on microparticulate octyl- and octadecyl-silica columns (*3*). An HPLC procedure for their determination in dosage forms on these columns has also been reported (*4*).

Peptide retention and separation studies have been carried out on columns containing organic copolymers as the stationary phase. In this laboratory, Amberlite XAD-2 and 4 (polystyrene–divinylbenzene copolymers) have been used to study the retention and separation of AA, peptides, and AA derivatives (*5, 6*). Retention of several dipeptides on XAD-2 was also reported in gravity flow column chromatography (*7*). Other copolymer stationary phases used in AA and peptide retention studies were Poropak Q (*8*) and Poragel PN and PS (*9*).

Procedures have been reported for the separation of certain diastereomeric peptides and their derivatives by paper (*10*), thin-layer (*11, 12*), and ion-exchange chromatography (*13*). A tripeptide chemically bonded to silica was used as a stationary phase in HPLC for the separation of peptides (*14, 15*) and diastereomeric peptides (*16*). Recently, ion-exchange columns were used to separate diastereomeric tetrapeptides (*17*) and D- and L-amino acids as the L–D and L–L dipeptides after reaction with *tert*-butyloxycarbonyl-L-leucine-*N*-hydroxysuccinimide ester (*18*). XAD-2 and XAD-4 columns have also been used to separate diastereomeric peptides (*6, 7*).

Although the XAD copolymers showed promise as stationary phases for the separation of diastereomeric peptides and are stable over the entire pH range unlike the bonded stationary phases, they do not generally provide efficiencies that are comparable to those readily achieved with the bonded stationary phases (*5, 6*). This is particularly true when compared to the microparticulate bonded phases. Therefore, the purpose of this paper is to describe results of our experiments which were designed to illustrate those factors which influence the retention of diastereomeric di- and tripeptides on a bonded reverse stationary phase of the C_8 type. With

[1] Present address, Eli Lilly and Company, Indianapolis, Ind. 46206.

0003-2700/78/0350-1353$01.00/0

Table I. Effect of Eluent pH on the Capacity Factors of Glycine Based Peptides

peptide	capacity factor, k'[a] pH 3.38	pH 5.82	pH 7.91
Gly-Gly	0.00	0.00	0.00
L-Ala-Gly	0.00	0.00	0.00
L-Val-Gly	0.23	0.11	0.27
L-Tyr-Gly	0.58	0.35	0.57
DL-Leu-Gly	0.99	0.60	1.10
L-Phe-Gly	2.21	1.30	2.69
Gly-L-Ala	0.01	0.00	0.00
Gly-L-Val	0.57	0.09	0.16
Gly-D-Val	0.58	0.09	0.16
Gly-L-Tyr	0.90	0.19	0.28
Gly-DL-Leu	2.45	0.56	0.82
Gly-DL-Phe	3.09	1.08	1.56
L-Phe-Gly-Gly	1.64	1.06	2.53
Gly-Gly-L-Phe	3.73	1.10	1.31

[a] 250 × 3.2 mm, 10 μm, LiChrosorb C_8 at a flow rate of 1 mL/min using 5% EtOH–95% H_2O with phosphate buffers at $\mu = 0.1$ and detection at 208 nm.

this type of background, optimum conditions for the separation of mixtures of diastereomeric peptides should be readily predicted. Furthermore, these data provide a basis for selecting the eluting conditions for mixtures of more complex diastereomeric peptides.

EXPERIMENTAL

Reagents. Peptides were obtained from Sigma Chemical Company, Chemical Dynamics Corp., and Research Plus Laboratories, Inc. and were used as received. Inorganic salts and acids were analytical reagent grade. Distilled water for the eluting agents was purified by passing it through a mixed bed ion exchange column, activated charcoal column, and finally through a 0.2-μm filter. Ethanol (95%) and HPLC reagent grade acetonitrile (J. T. Baker) were used.

Equipment. The chromatographic instrumentation consisted of an Altex M-100 pump, an Altex 905 injector fitted with a 175-μL sample loop, and a Tracor 970 variable wavelength detector equipped with an 8-μL Teflon flow cell. The column used was a 3.2 × 250 mm, 10-μm, octyl-silica bonded phase column (LiChrosorb C_8) obtained from Altex.

Procedures. Peptide solutions were prepared by dissolving 3 to 6 mg of a given peptide in 3 mL of water (0.1 M HCl for Leu-Phe and Leu-Gly-Phe) in 6-mL Hypovials fitted with Hycar septa and sealed with aluminum caps (Pierce Chemical). The solutions were refrigerated when not in use. Samples of 2 to 5 μL of the desired peptide solution were injected with a 10-μL Pressure Lok Series B110 syringe (Precision Sampling Corporation).

All eluting agent water–organic solvent mixtures were made as per cent by volume and were buffered with phosphate salts (0.02 M) or HCl. Appropriate quantities of NaCl were added to give an ionic strength of 0.1.

Flow rates ranged from 1.0 to 2.0 mL/min and resulted in column inlet pressures of 900 to 1500 psi depending upon the eluting mixture composition. The detector was operated at 208 nm and an attenuation setting of 0.16 or 0.08 AUFS was used.

Capacity factors, k', were calculated and the column void volume was determined as described previously (*5*, *6*). The precision for k' measuremnt was ±0.03.

RESULTS AND DISCUSSION

Effect of Peptide Structure. Table I lists the k' values for two series of Gly-based peptides as a function of pH. In one series, the first amino acid (AA) subunit is varied while in the second, the second AA subunit is varied. These data show that the retention order is determined by the non-Gly AA subunit. As the carbon content of the non-Gly subunit is increased, the retention is also increased. This retention order follows that observed for the simple AA on an octyl silica column (*2*) and is similar to the AA retention order found on porous copolymer columns (*6*), the one exception being that Tyr shows a higher retention than Leu on the porous copolymers.

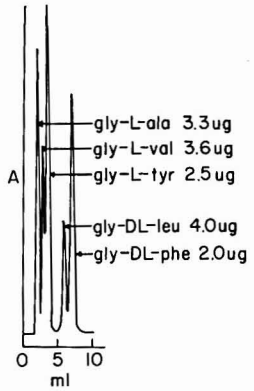

Figure 1. Separation of a series of glycyl dipeptides. 250 × 3.2 mm, 10 μm, LiChrosorb-C_8 at a flow rate of 1 mL/min using 5% EtOH–95% H_2O with pH 3.4 (phosphate) and $\mu = 0.1$ and detection at 208 nm and 0.16 AUFS

Table II. Effect of Peptide Structure and Eluent pH on Capacity Factors

dipeptide	capacity factors, k'[a] pH 3.38	pH 5.82	pH 7.91
L-Ala-L-Val	0.55	0.09	0.29
L-Val-L-Val	1.20	0.22	2.79
L-Leu-L-Val	3.71	1.12	9.24
L-Ala-L-Val	0.55	0.09	0.29
L-Ala-L-Leu	2.52	0.49	1.22
L-Ala-L-Phe	3.57	1.12	2.67
L-Leu-L-Val	3.71	1.12	9.24
L-Leu-L-Tyr	5.17	1.53	>10
L-Leu-L-Leu	>10	6.45	>10

[a] Same column conditions as in Table I.

The retention order in Table I is also consistent with the hydrophobicities and accessible surfaces areas reported for the AA (*19*). If the non-Gly subunit is a polar AA, retention would be reduced. The effect of polar groups in the simple AA on retention has been discussed before (*2*, *6*, *8*) and a similar effect should occur with the dipeptides.

A change in a single subunit of the dipeptide produces a significant change in retention. Thus, separation of many dipeptide mixtures are possible. One example is listed in Figure 1 where a mixture of five glycyl dipeptides are separated using 95% water–5% ethanol buffered at pH 3.4.

It is significant to note that the Gly-Gly dipeptide shows no retention under the eluting conditions used in Table I. Even when using 100% water, the mildest eluting agent, this dipeptide still shows no retention. This is additional evidence which supports the conclusion that retention results from the interaction of the non-Gly AA subunit and the stationary phase and that the Gly subunit and the peptide backbone are not involved in the retention process. Similar results were found when studying a series of Gly peptides on a C_{18} column (*2*).

Table II shows the effect of replacing the Gly subunit for the dipeptides in Table I with a nonpolar AA subunit. In the first group, the glycine subunit is replaced by a valine subunit. Comparison of the k' data to those in Table I clearly indicates a marked increase in the retention of the dipeptide. In the second group of dipeptides in Table II, the glycyl subunit of the peptides in Table I is replaced by an alanyl subunit. The increase in k' values for this series was found to be nominal, the largest being observed for the dipeptide showing the highest retention. In the third group, the glycyl subunit of the peptides in Table I is replaced by a leucyl subunit. This change produced a sharp increase in the retention of the dipeptides.

In all three series, the order of retention of the dipeptides follows that observed for the individual AA subunits that is being varied. Also, unlike the Gly peptides, the AA subunit that is held constant contributes to the retention, and the overall retention is due to both AA subunits in the dipeptide. This additive effect and the ability to quantitatively or qualitatively predict it is being explored further.

Effect of Eluent pH. Controlling the pH of the eluting mixtures used in the separation of AA and peptide mixtures on columns of XAD-2 and -4 has shown that retention is minimal in the region of the isoelectric pH where zwitterion formation occurs (*5, 6*). Retention is markedly increased in acidic eluents (pH <3), where a singly charged protonated amine species exists, and in basic eluents (pH >9), where a singly charged dissociated carboxyl species predominates.

Although the useful pH range of the C_8 column is limited to eluting agents of pH 2 to 8, limited pH studies on this column show similar trends. These data are listed in Tables I and II. In all cases, the minimum is observed near or at the isoelectric pH value.

In Table I, the k' values are larger in basic solution than in acidic solution for the Gly dipeptides in which the Gly subunit provides the terminal carboxyl group. When it provides the terminal amine group, the k' values are larger in acid solution in comparison to the basic solution. Since the non-Gly subunit is primarily responsible for the retention, the position of this subunit relative to the charge sites has a strong influence on the retention.

In the first series of dipeptides in Table I, the retention will be higher in the basic eluent because the nonpolar AA subunit is removed from the vicinity of the highly charged carboxyl site. Therefore, it can interact with the nonpolar stationary phase more strongly than in the acidic eluent where the closeness of the charged protonated amine group would diminish the interaction.

In the second group of dipeptides listed in Table I, where the nonpolar AA subunit contributes the terminal carboxyl group, the highest retention is observed when using the acidic eluent. Under these conditions, the nonpolar AA subunit is removed from the charged, protonated amine site.

The data in Table I indicate that the retention order of the dipeptide can be altered by a change in the pH of the eluent. Consider the Leu containing dipeptides. For example, DL-Leu-Gly will elute before Gly-DL-Leu under acidic eluting conditions, while the reverse is found when using a basic eluent. Other examples have been reported previously (*6*).

The effects of pH on the retention and the retention order for the tripeptides listed in Table I are consistent with the observations found for the dipeptides.

The dipeptides listed in Table II show similar trends. In these dipeptides retention will be dominated by the more nonpolar of the two AA subunits and, therefore, its position in relation to the charged site will determine the retention behavior. When the more nonpolar AA subunit contributes the terminal amine group, which will be uncharged in basic solution, the highest retention is observed for the basic eluent. Examples of this are L-Leu-L-Val, and L-Leu-L-Tyr. In contrast, when the more hydrophobic AA subunit contributes the free carboxyl group, which will be uncharged in acidic solution, highest retention is found in the acidic eluent. Examples of this are L-Ala-L-Val, L-Ala-L-Leu, and L-Ala-L-Phe. Similar pH trends were observed for dipeptide retention on XAD-2 and XAD-4 porous copolymers (*6*).

Table III. Capacity Factors for Alanine Dipeptides as a Function of pH

	capacity factor, k'[a]			
	pH			
dipeptide	2.10	3.32	5.75	7.89
L-Ala-L-Ala	0.28	0.17	0.00	0.08
D-Ala-D-Ala	0.29	0.18	0.00	0.07
L-Ala-D-Ala	1.13	0.65	0.16	0.21
D-Ala-L-Ala	1.11	0.64	0.17	0.20
Gly-Gly	0.00	0.00	0.00	0.00
L-Ala-Gly	0.14	0.07	0.00	0.04
D-Ala-Gly	0.14	0.08	0.00	0.04
Gly-L-Ala	0.26	0.15	0.00	0.03
Gly-D-Ala	0.26	0.15	0.00	0.03

[a] Same column and flow rate as in Table I using water, and HCl and phosphate buffers, $\mu = 0.1$, as the eluting mixture.

Ionization constants for the dipeptides examined in this study lie between $pK_{a_1} = 3.1$ to 3.3 and $pK_{a_2} = 8.1$ to 8.3 (*20*). This means that for the pH range used in this study, the degree of ionization in the acidic and basic eluents is essentially the same for a given dipeptide. Therefore, the difference in the k' values in the acidic or basic eluent must be due to the difference in the position of the charge sites and is not due to the difference in the degree of ionization of the amine or carboxyl group. This further supports the contention that the position of the more nonpolar AA subunit relative to the charge sites is the major factor in determining the level of retention.

Solvent Composition. Although not studied systematically, the data reported here (see Tables I to V) indicate that as the concentration of ethanol is increased in the aqueous–ethanol mixture the k' values decrease. Furthermore, acetonitrile is a stronger eluting agent than ethanol. These observations are consistent with more detailed studies on the effect of solvent composition on the retention of other acids and bases reported elsewhere (*2, 3, 5, 6*).

If a high concentration (>20%) of organic solvent is required to act as a modifier, acetonitrile would be preferred. First, for a comparable elution condition, less acetonitrile than ethanol is needed. Second, the acetonitrile–water mixtures are less viscous and, thus, column inlet pressures are minimized.

Stereochemical Effects. The previous experiments demonstrated the significance of each AA side chain in influencing the degree of retention. To evaluate the effect of an AA subunit's stereochemistry on retention, the stereoisomers of Ala-Ala were studied. These data are shown in Table III where retention on the C_8 column was studied as a function of pH.

As with the previous peptides, retention is low in the region of the isoelectric pH and high in the acidic and basic eluents regardless of the stereoisomeric form. However, at a given eluent condition, retention for the diastereomers is different. At all pH values L-Ala-L-Ala and its enantiomer D-Ala-D-Ala have identical capacity factors. Similarly, L-Ala-D-Ala and its enantiomer D-Ala-L-Ala also have identical capacity factors, but the value is larger than that for the L–L and D–D enantiomers.

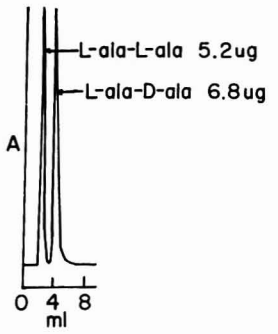

Figure 2. Separation of alanyl–alanine diastereomers. 250 × 3.2 mm, 10 μm, LiChrosorb-C_8 at a flow rate of 1 mL/min using 100% H_2O with pH 2.2 (HCl) and μ = 0.1 and detection at 208 nm and 0.16 AUFS

The fact that enantiomers have equal k' values was shown in Table I. For example, compare Gly-L-Val to its enantiomorph Gly-D-Val. Similarly, the Gly-L-Ala and Gly-D-Ala enantiomers and the L-Ala-Gly and D-Ala-Gly enantiomers (Table III) have equal k' values. However, when the symmetric Gly subunit is replaced with the asymmetric Ala subunit (Table III), the resulting diastereomers exhibit differing k' values.

The difference in the k' values for the diastereomers is not constant throughout the pH range; as the pH decreases, the difference increases. Thus, by choosing the optimum pH for the eluting mixture, a baseline separation of the diastereomers is readily achieved. This is illustrated in Figure 2.

Differences in the physical properties of peptide diastereomers have been attributed to differences in molecular conformations (*21*). A peptide can assume several conformations. However, investigation of molecular size (*11*, *22*), dipole moments (*22*), ionization constants (*23*), and nuclear magnetic resonance studies (*7*, *24–26*) have led workers to conclude that the AA sidechains in a dipeptide are cis to one another (with respect to the peptide bond) for the L-D and its D-L enantiomer (*7*, *21*, *24–26*). In the L-L and its D-D enantiomer the sidechains are therefore trans to one another.

These structures are shown below looking down the di-

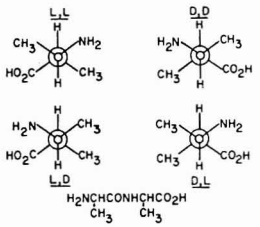

peptide bond for Ala-Ala emphasizing the orientation of the sidechain methyl groups on the asymmetric carbons, which are indicated by the circles.

In the L-D and D-L forms, the methyl groups for the two Ala subunits will be on the same side of the peptide bond and in close proximity to one another. This should produce a higher overall hydrophobic surface area and increase the retention of the L-D and D-L enantiomers in comparison to the L-L and D-D enantiomers where the methyl groups are on opposite sides. As seen in Table III, the retention order is consistent with the predicted hydrophobic characteristics of the Ala-Ala diastereomers.

Table IV. Capacity Factors for Dipeptide Distereomers

dipeptide	capacity factor, k'[a] pH 3.45	pH 5.98
L(D)-Ala-L(D)-Val[b]	0.30	0.03
L(D)-Ala-D(L)-Val[b]	0.69	0.21
L-Ala-L-Leu	1.37	0.30
D-Ala-L-Leu	2.51	0.88
L-Ala-L-Phe	1.65	0.61
D-Ala-D-Phe	1.65	0.61
L-Ala-D-Phe	2.83	1.48
D-Ala-L-Phe	2.84	1.46
L-Leu-L-Tyr	1.74	0.62
D-Leu-L-Tyr	2.63	1.38
L-Val-L-Val	0.59	0.12
D-Val-D-Val	0.58	0.11
D-Val-L-Val	3.50	1.55
D-Leu-D-Leu	7.35	2.71
D-Leu-L-Leu	>10	>10

[a] Same conditions as in Table I except at 10% EtOH–90% H_2O. [b] Obtained as D,L-D,L mixture.

Table V. Capacity Factors for Di- and Tripeptide Diastereomers

peptide	capacity factor, k'[a]
L-Leu-L-Leu	0.92
D-Leu-D-Leu	0.92
L-Leu-D-Leu	4.78
D-Leu-L-Leu	4.79
L(D)-Leu-L(D)-Phe[b]	2.16
L(D)-Leu-D(L)-Phe[b]	6.94
L(D)-Leu-Gly-L(D)-Phe[b]	1.12
L(D)-Leu-Gly-D(L)-Phe[b]	1.58

[a] Same conditions as in Table I except at 20% EtOH–80% H_2O, pH 6.14. [b] Obtained as D,L-D,L mixture (see text).

The study was expanded to include many other diastereomeric dipeptides and tripeptides. These data are shown in Tables IV and V.

The general trends observed for these diastereomeric dipeptides are similar to those for the Ala-Ala dipeptides listed in Table III. That is, the L-L and D-D enantiomers have an identical k' value which is less than the identical k' values found for the L-D and D-L enantiomers. This difference is large enough so that separations of the two pairs are possible. Although not shown, retention differences for a given set of diastereomers are enhanced by using a lower pH and/or reducing the amount of ethanol in the eluting mixture.

The type of the AA subunits present in the diastereomers has an effect on the retention. In dipeptides in which there is a significant difference in the size and polarity of the AA subunits, the difference in the k' values for the diastereomers is large enough to permit their separation. Typical examples are the L-L (and D-D) and L-D (and D-L) diastereomers of Ala-Leu, Ala-Phe, and Leu-Tyr. The differences in the k' values for these diastereomers is minimal however, when compared to dipeptides in which the AA subunits are of equal or similar size and polarity. Examples of this are the L-L (and D-D) and L-D (and D-L) diastereomers of Val-Val, Leu-Leu, and Leu-Phe.

From these observations it can be concluded that for dipeptides having AA subunits of similar size and polarity, there is a significant increase in the peptide's hydrophobic surface area in going from the L-L (or D-D) to the L-D (or D-L) form. This is illustrated in Figure 3. Note that in the time interval required to separate L-Val-L-Val from its D-L diastereomer L-Leu-L-Tyr can be separated from its D-L diastereomer.

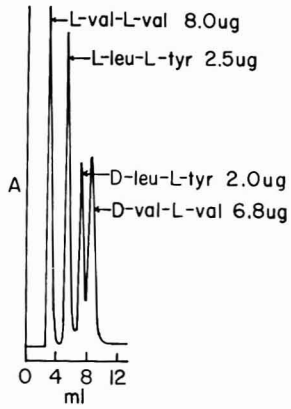

Figure 3. Separation of a mixture of dipeptide diastereomers. 250 × 3.2 mm, 10 μm, LiChrosorb-C_8 at a flow rate of 1 mL/min using 10% EtOH–90% H_2O with pH 3.4 (phosphate) and μ = 0.1 and detection at 208 nm and 0.16 AUFS

Similar results are obtained by substituting the diastereomers of Ala-Leu or Ala-Phe for the Leu-Tyr diastereomers used in Figure 3.

The Leu-Tyr diastereomers were separated on an optically active bonded tripeptide stationary phase (*16*). It should be noted from Figure 3 that the optically bonded phase is not necessary for the separation and that the elution order found in Figure 3 is the reverse of that for the optically bonded phase.

The peptides listed in Table V contain highly hydrophobic AA subunits and it was necessary to increase the concentration of the ethanol in the eluting mixture, as well as to adjust the eluent pH close to that of the isoelectric pH, in order to elute the peptides from the column in a reasonable amount of time. As with the other diastereomeric peptides, the retention for the L–L and D–D enantiomers is the same and considerably less than that for the L–D and D–L enantiomers.

Introduction of a polar group into one of the AA subunits has a significant effect on the retention of the peptides. Compare the k' data for the L–L, and D–L Leu-Tyr stereoisomers in Table IV to the corresponding Leu-Phe stereoisomers in Table V. The latter dipeptide differs in that the Phe does not have a *p*-OH group in the aromatic ring. Retention is not only greater for the more nonpolar Phe-containing peptide but the difference in retention between the L–L and D–D enantiomers and the L–D and D–L enantiomers is much greater.

The introduction of the glycyl subunit into the dipeptide Leu-Phe at position 2 to yield the tripeptide, markedly decreases the retention of the peptide and also decreases the difference in the k' values for the diastereomers (see Table V). Apparently the insertion of the Gly subunit has the effect of breaking up the large hydrophobic surface area which results when the two nonpolar AA subunits (Leu and Phe) are directly adjacent as in the case of the dipeptide Leu-Phe. Note however, even though the chiral centers are separated from one another in the Leu-Gly-Phe tripeptide, the separation of the diastereomers is still possible (see Table V). Additional model peptides in which the chiral centers are even further separated by the addition of glycyl subunits were not readily available. Thus, the question of whether the degree of retention continues to decrease as this distance increases, cannot be answered.

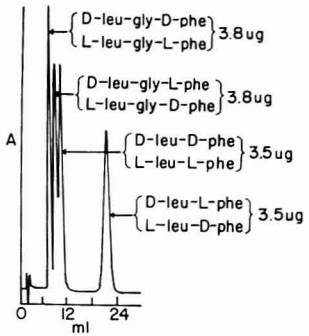

Figure 4. Separation of di- and tripeptide diastereomers. 250 × 3.2 mm, 10 μm, LiChrosorb-C_8 at a flow rate of 1.5 mL/min using 15% CH_3CN–85% H_2O with pH 3.5 (phosphate) and μ = 0.1 and detection at 208 nm and 0.16 AUFS

Table VI. Capacity Factors for Trialanine Diastereomers as a Function of pH

	capacity factor, k'[a]			
	pH			
tripeptide	2.10	3.32	5.75	7.83
L-Ala-L-Ala-L-Ala	0.68	0.62	0.09	0.26
D-Ala-D-Ala-D-Ala	0.69	0.63	0.09	0.27
L-Ala-L-Ala-D-Ala	1.59	1.14	0.22	0.59
L-Ala-D-Ala-L-Ala	3.32	2.58	0.69	1.18
Gly-Gly-Gly	0.05	0.00	0.00	0.00

[a] Same conditions as in Table III.

The Leu-Phe and Leu-Gly-Phe peptides were available only as the D,L–D,L mixtures and based on the elution characteristics of the diastereomers in Tables III and IV, the first peak eluted for such a mixture was assigned the L–L(D–D) configuration, while the second was assigned the L–D(D–L) configuration. A chromatogram for the separation of the Leu-Gly-Phe and Leu-Phe diastereomers is shown in Figure 4.

Table VI lists the k' data for four of the eight stereoisomers of the tripeptide Ala-Ala-Ala which contains three chiral centers. In comparison to the tripeptide $(Gly)_3$, which provides only the peptide backbone, retention is very high for the $(Ala)_3$ peptides. This indicates that the more hydrophobic character of the alanine sidechains plays the major role in determining the level of interaction between the stationary phase and the tripeptide. This is consistent with the observations made for the dipeptides.

The retention of the $(Ala)_3$ tripeptide as a function of pH follows the same trends as those observed for the dipeptides. That is, retention is high in acidic and basic solutions and is at a minimum at the isoelectric pH. It is difficult to experimentally evaluate whether retention is larger in acid or base solution for the symmetrical $(Ala)_3$ peptides since the measurements are limited on the basic side to approximately pH 8. If the k_1, k_0, and k_{-1} values, the capacity factors for retention of the cation, zwitterion, and anion forms, respectively, are calculated according to Equation 4 in reference (*5*), retention for all four $(Ala)_3$ diastereomers is found to be slightly higher in acidic solution than in basic solution.

It is evident in Table VI that not only does the introduction of a D AA subunit alter the retention of the $(L\text{-}Ala)_3$ peptide, but also that the position of the D AA subunit is important. Construction of models using the criteria discussed before for

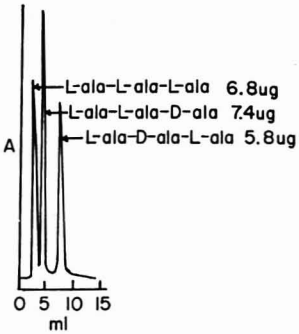

Figure 5. Separation of alanyl-alanyl-alanine diastereomers. 250 × 3.2 mm, 10 μm, LiChrosorb-C_8 at a flow rate of 1.3 mL/min using 100% H_2O with pH 2.2 (HCl) and μ = 0.1 and detection at 208 nm and 0.16 AUFS

the dipeptides (*7*, *21*, *24–26*) yields structures similar to those previously shown for the $(Ala)_2$ dipeptides except that one more sidechain methyl group (from the additional Ala subunit) must be accounted for. For the LLL form, the methyl groups of the Ala subunits are seen to alternate about the peptide backbone; for the LLD form, two adjacent methyl groups are on the same side and the third is on the other side; and finally for the LDL form all three methyl groups are on the same side. It would be predicted that the hydrophobic nature of the side chain groups should increase in this order, that is, LLL < LLD < LDL. This should also be the order in which the retention increases. As seen in Table VI, this was observed experimentally.

The retention of the diastereomeric $(Ala)_3$ tripeptides are sufficiently different enough in acid solution so that mixtures of the LLL (or DDD), LLD, and LDL $(Ala)_3$ tripeptides can be separated. This is shown in Figure 5 where a pH 2.2 aqueous solution is used as the eluting mixture.

Applications. The data in the figures and tables indicate that k' values are sufficiently different so that separation of many different peptide and diastereomeric peptide mixtures are possible. Awareness of those factors which cause the difference in k' values can be used to predict optimum eluting conditions for separation of mixtures of larger peptide diastereomers. For example, the size and polarity of the AA subunits and their relative position determine the optimum solvent composition, while the position of the stereochemical differences indicates the optimum eluent pH. If the stereochemical difference is near the terminal amine, a basic eluent should be used, since it would allow the free amine to interact most strongly with the stationary phase. Thus, differences in retention for the diastereomers would be maximized.

From a fundamental standpoint, the chromatographic properties of peptide diastereomers on reverse stationary phases, offers valuable insight into peptide conformations. In addition to analytical separations, the method should be useful in studying racemization in peptide synthesis, for determining a peptide's stereochemical purity, and in larger scale, preparative separations. It is also important to note that the retention trends of the peptides and peptide diastereomers on the bonded stationary phase are similar to those observed on the porous copolymer packings (*5–7*).

LITERATURE CITED

(1) H. F. Walton, *Anal. Chem.*, **50**, 52R (1976).
(2) I. Molnar and C. Horvath, *J. Chromatogr.*, **142**, 623 (1977).
(3) K. Krummen and R. W. Frei, *J. Chromatogr.*, **132**, 27 (1977).
(4) K. Krummen and R. W. Frei, *J. Chromatogr.*, **132**, 429 (1977).
(5) D. J. Pietrzyk, E. P. Kroeff, and T. D. Rotsch, *Anal. Chem.*, **50**, 497 (1978).
(6) E. P. Kroeff and D. J. Pietrzyk, *Anal. Chem.*, **50**, 502 (1978).
(7) H. Joshua and C. M. Deber, "Chemistry and Biology of Peptides", Ann Arbor Science Publishers, Ann Arbor, Mich., 1972, p 67.
(8) A. Niederwieser, *J. Chromatogr.*, **61**, 81 (1971).
(9) J. J. Hansen, T. Greibrokk, B. L. Currie, K. Nils-Gunnar Johansson, and K. Folkers, *J. Chromatogr.*, **135**, 155 (1977).
(10) F. Sokolowski and J. F. Biernat, *J. Chromatogr.*, **13**, (1964).
(11) T. Wieland and H. Bende, *Chem. Ber.*, **98**, 504 (1965).
(12) A. Arendt, A. Kotodziejczk, and T. Sokotowska, *Chromatographia*, **9**, 123 (1976).
(13) J. M. Manning and S. Moore, *J. Biol. Chem.*, **243**, 5591 (1968).
(14) E. J. Klkta, Jr., and E. Gruska, *J. Chromatogr.*, **135**, 367 (1977).
(15) G. Wing-Kin Fong and E. Gruska, *J. Chromatogr.*, **142**, 299 (1977).
(16) E. Grushka and E. Klkta, Jr., *Anal. Chem.*, **49**, 1004A (1977).
(17) S. B. H. Kent, A. R. Mitchell, G. Barany, and R. B. Merrifield, *Anal. Chem.*, **50**, 155 (1978).
(18) A. R. Mitchell, S. B. H. Kent, I. C. Chu, and R. B. Merrifield, *Anal. Chem.*, **50**, 637 (1978).
(19) C. Chothia, *Nature (London)*, **248**, 338 (1974).
(20) D. D. Perrin, "Dissociation Constants of Organic Bases in Aqueous Solutions", Butterworth, London, England, 1965.
(21) S. Lande, *Biopolymers*, **7**, 879 (1969).
(22) P. Flory and P. Schimmel, *J. Am. Chem. Soc.*, **89**, 6807 (1967).
(23) E. Ellenbogen, *J. Am. Chem. Soc.*, **74**, 5198 (1952).
(24) C. Deber and H. Joshua, *Biopolymers*, **11**, 2493 (1972).
(25) R. Lemieux and A. Barton, *Can. J. Chem.*, **49**, 767 (1971).
(26) B. Weinstein, "Proceedings of the First American Peptide Symposium", B. Weinstein and S. Lande, Ed., Marcel Dekker, New York, N.Y., 1970, p 371.

RECEIVED for review April 18, 1978. Accepted May 22, 1978. This investigation was supported by Grant Number CA 18555 awarded by the National Cancer Institute, DHEW. This work was presented at the 29th Pittsburgh Conference on Analytical Chemistry and Applied Spectroscopy, Cleveland, Ohio, 1978, Paper No. 499.

Distribution Coefficients and Anion Exchange Behavior of Some Elements in Hydrobromic–Nitric Acid Mixtures

F. W. E. Strelow

National Chemical Research Laboratory, P.O. Box 395, Pretoria 0001, Republic of South Africa

Anion exchange distribution coefficients with Bio-Rad AG1-X8, a quaternary amine resin on polystyrene basis, are presented for the elements Bi(III), Cd, Pb(II), Zn, and In(III) in hydrobromic–nitric acid mixtures ranging from 0.03 to 1 M hydrobromic and nil to 2 M nitric acid. The results are discussed and some possible separations are pointed out. The versatility of these eluting mixtures is demonstrated by sequential elution of Zn, Pb(II), Cd, and Bi(III) from a 11.5-mL resin column using appropriate eluting agent concentrations.

Some elements such as Bi(III), Cd, and Pb(II) are considerably more strongly adsorbed by anion exchange resins from dilute hydrobromic than from dilute hydrochloric acid solutions (*1*). Separation factors between these elements and most others are as a result considerably larger in bromide than in chloride solutions, and considerably smaller columns should be required for separations of the same amounts of elements. Unfortunately it has been found that more serious tailing often occurs when elements are eluted with dilute hydrobromic acid (*2, 3*) as compared with dilute hydrochloric acid. An effective method to eliminate this tailing is to add to the eluting agent, a noncomplexing mineral acid containing a relatively strongly adsorbed anion which effectively competes for exchange sites (*2, 3*). Nitric acid is almost tailor-made for this purpose. As an additional advantage, it also is easily volatile. Its only disadvantage is that bromine is formed by oxidation in mixtures of hydrobromic and nitric acid above certain concentrations. Fortunately, these critical concentrations are safely above those relevant for separations.

In the literature, only a very limited amount of information about distribution coefficients in hydrobromic–nitric acid mixtures with strongly basic anion exchange resins can be found. Data are presented for a single hydrobromic acid concentration (0.03 M) with various concentrations of nitric acid (*2*). Because it appeared likely that more favorable conditions for some separations would be found at higher bromide concentrations, a more complete study of distribution coefficients was carried out varying the bromide concentration up to 1 M. The results of this study and their discussion are presented.

EXPERIMENTAL

Reagents and Apparatus. Chemicals were of analytical reagent-grade purity. "Indium(III)–chloride tetrahydrate puriss", was obtained from Fluka AG., Buchs, Switzerland, and converted to the nitrate by repeated evaporation with nitric acid. Water was distilled and then passed through an Elgatat deionizer. The resin was AG1-X8, a quaternary amine anion exchanger on polystyrene base, marketed by Bio-Rad Laboratories, Richmond, Calif. Resin of 100 to 200 mesh particle size was used for batch-equilibrium and resin of 200 to 400 mesh particle size for column experiments. Borosilicate glass tubes of 15-mm i.d. and about 250-mm length were used as columns, fitted with a No. 2 porosity glass sinter and a buret tap at the bottom and a B14 joint at the top. Atomic absorption measurements were carried out either with a Varian-Techtron AA-5 or with a Perkin-Elmer 303 instrument, and a Zeiss PMQ II was used for spectrophotometry.

Table I. Distribution Coefficients in 0.03 M HBr

element	molarity of HNO_3					
	nil	0.1 M	0.2 M	0.5 M	1.0 M	2.0 M
Bi(III)[a]	>10⁴	>10⁴	>10⁴	>10⁴	6800	4800
Cd[a]	680	191	91	33	14.4	2.7
Fb(II)[a]	14.4	8.2	5.0	4.1	1.3	1.1
Zn	<0.5	<0.5	<0.5	<0.5	<0.5	<0.5
In	<1	<1	<1	<1	<1	<1

[a] Published previously (*2*) but included for sake of completeness.

Distribution Coefficients. The resin was converted to the nitrate form in a large column by passing through a solution of about 2 M nitric acid until a silver nitrate test for chloride became negative. After the excess nitric acid had been removed by washing with deionized water, the resin was dried at 60 °C in a Gallenkamp vacuum pistol with magnesium perchlorate (anhydrone) as drying agent, and kept in a desiccator over the same drying agent. Residual water was determined by drying at 120 °C and the weights of resin were corrected accordingly (normally about 4 mg correction for 2.7125 g of resin).

The coefficients were determined by equilibrating 2.7125 g of dry resin in the nitrate form (equivalent to 2.5000 g of dry resin in the chloride form) with 250 mL of solution of shaking for 24 h in a mechanical shaker at 20 °C. The solutions contained the concentrations of hydrobromic and nitric acid shown in Tables I to VI and one of the following elements as the nitrate:1 mmol of either Cd, Zn, or In(III); 0.2 mmol of bismuth(III), or 0.02 mmol of lead(II). The smaller amounts of bismuth and lead were used because of the limited solubility of the oxybromides or bromides, respectively, in some of the equilibrium solutions. After equilibration, the resin was separated from the aqueous phase by filtration and the amounts of the elements in the aqueous and in the resin phase (except for bismuth) were determined by appropriate analytical methods. From the results, weight equilibrium distribution coefficients

$$D = \frac{\text{mol of element on resin}}{\text{mol of element in solution}} \times 100$$

were calculated. The coefficients for 0.03, 0.05, 0.1, 0.2, 0.5, and 1.0 M HBr with various concentrations of nitric acid are presented in Tables I to VI, respectively. Those for 0.03 M HBr have been published previously (*2*) but have been included for sake of completeness. The analytical methods used are summed up in Table VII.

Elution Curve. A column containing 11.5 mL (5 g dry weight) of AG1-X8 resin of 200 to 400 mesh particle size was prepared and converted to the bromide form by passing through 100 mL of 1 M hydrobromic acid. The column in the chloride form was 65 mm in length and 15 mm in diameter and shrank about 5 mm on conversion. A solution containing 0.1 mmol of zinc and 0.02 mmol each of cadmium, lead(II), and bismuth(III) as the bromides in 25 mL of 1 M hydrobromic acid was prepared and passed through the column. The elements were washed onto the resin with small portions of 0.2 M hydrobromic acid containing 0.5 M nitric acid and then eluted with the following sequence of reagents: 200 mL of 0.2 M hydrobromic containing 0.5 M nitric acid for zinc (including wash solution); 200 mL of 0.05 M hydrobromic containing 0.5 M nitric acid for lead(II); 200 mL of 0.02 hydrobromic containing 2 M nitric acid for cadmium; and 200 mL of 0.05 M EDTA in 0.1 M ammonium nitrate for bismuth(III).

0003-2700/78/0350-1359$01.00/0

Table II. Distribution Coefficients in 0.05 M HBr

element	molarity, HNO_3 nil	0.1 M	0.2 M	0.5 M	1.0 M	2.0 M
Bi(III)	400 000	200 000	115 000	54 000	24 000	7 800
Cd	3 030	935	329	148	79	65
Pb(II)	52	23.5	13.5	11.3	10.7	10.4
Zn	<0.5	<0.5	<0.5	<0.5	<0.5	<0.5
In	<1	<1	<1	<1	<1	<1

Table III. Distribution Coefficients in 0.10 M HBr

element	molarity, HNO_3 nil	0.1 M	0.2 M	0.5 M	1.0 M	2.0 M
Bi(III)	500 000	400 000	210 000	83 000	40 000	15 600
Cd	16 200	5 910	2 540	1 320	705	445
Pb(II)	242	103	65	32.9	20.6	15.4
Zn	1.4	1.0	0.7	0.5	<0.5	<0.5
In	1.0	1.1	1.2	1.0	1.1	1.2

Table IV. Distribution Coefficients in 0.20 M HBr

element	molarity, HNO_3 nil	0.1 M	0.2 M	0.5 M	1.0 M	2.0 M
Bi(III)	$>10^4$	$>10^4$	$>10^4$	$>10^4$	$>10^4$	$>10^4$
Cd	50 000	31 000	17 500	9 100	5 250	3 450[a]
Pb(II)	635	354	228	106	56	33.8
Zn	5.4	3.7	2.3	1.5	1.5	1.4
In	2.5	2.3	2.2	2.1	1.9	1.8

[a] Published previously (2) but included for sake of completeness.

Table V. Distribution Coefficients in 0.50 M HBr

element	molarity, HNO_3 nil	0.1 M	0.2 M	0.5 M	1.0 M
Bi(III)	$>10^4$	$>10^4$	$>10^4$	$>10^4$	$>10^4$
Cd	$>10^4$	$>10^4$	$>10^4$	$>10^4$	$>10^4$
Pb(II)	821	583	442	350	279
Zn	21.0	18.2	14.3	11.4	8.2
In	3.6	3.2	3.0	2.8	2.5

Table VI. Distribution Coefficients in 1.0 M HBr

element	molarity, HNO_3 nil	0.1 M	0.2 M	0.5 M
Bi(III)	$>10^4$	$>10^4$	$>10^4$	$>10^4$
Cd	$>10^4$	$>10^4$	$>10^4$	$>10^4$
Pb(II)	620	491	395	270
Zn	100	89	81	58
In	5.8	4.7	4.2	2.6

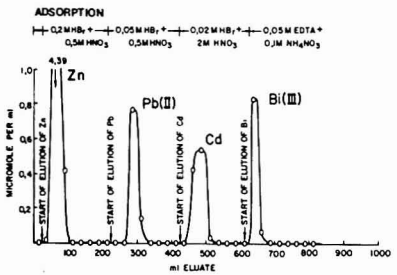

Figure 1. Elution curve Zn–Pb(II)–Cd–Bi(III), column of 11.5 mL (5 g) AG1-X8 resin, 200–400 mesh (65 × 15 mm). Flow rate 2.5 ± 0.5 mL/min

Table VII. Analytical Methods Used for Determinations

element	method
Bi(III)	Complexometric titration with EDTA, xylenol orange as indicator, or spectrophotometry as thiourea complex at 470 nm. Atomic absorption spectrometry at 223.1 nm, using air–acetylene flame for elution curve.
Cd	Complexometric titration with EDTA in slight excess ammonia with methylthymol blue as indicator. Atomic absorption spectrometry at 228.8 nm. using air-acetylene flame for small amounts and elution curve.
Pb(II)	Atomic absorption spectrometry at 217.0 nm. using air–acetylene flame.
Zn	Complexometric titration with EDTA at pH 5.5, xylenol orange as indicator. Atomic absorption spectrometry at 213.9 nm, using the air-acetylene flame for small amounts and elution curve.
In	Addition of excess EDTA and back-titration with zinc sulfate at pH 5.5; xylenol orange as indicator. Atomic absorption spectrometry at 303.9 nm. using the air-acetylene flame for small amounts and elution curve.

The flow rate was 2.5 ± 0.5 mL per minute and the solution always was allowed to drain to the level of the resin bed before eluting agents were changed, and also between washings. Aliquots of 25 mL were taken with an automatic fractionator, and the amounts of the elements in the fractions were determined by atomic absorption spectrometry, after suitable dilution when required, using the methods indicated in Table VII. The experimental curve is shown in Figure 1.

DISCUSSION

Bismuth(III). The distribution coefficients for bismuth(III) are very high over the whole range investigated.

Generally they increase with increasing hydrobromic and decrease with increasing nitric acid concentration. In 0.03 or 0.02 M hydrobromic acid containing 2 M nitric acid, bismuth can be easily separated from Cd, Pb(II), zinc, and indium. Most other elements are even less strongly adsorbed from dilute hydrobromic acid solutions than zinc and indium and their separation therefore should be even more easy. Au(III), Hg(II), Pt(IV), Pd(II), Tl(III), and probably Ir(IV) and Rh(III) are the only elements retained together with bismuth(III). The separation factor for the Bi(III)–Pb(II) pair with a value of over 4000 seems to be the largest one known so far and is considerably larger than anion exchange separation factors in hydrochloric acid (*4*, *5*) nitric acid–organic solvent mixtures (*6*, *7*), or cation exchange separation factors in hydrobromic acid (*8*, *9*) and in acid–EDTA mixtures (*10*). Separation of traces of bismuth from very large amounts of lead (up to several grams) therefore should be possible on quite small columns provided the sample is dissolved in nitric acid, diluted to about 2 M, and the solution contains only about 0.02 to 0.03 M bromide. After elution of lead, elution of bismuth can be carried out with 2 M nitric acid, but is very much more effective with 0.05 M EDTA in 0.1 M ammonium nitrate.

Cadmium. Distribution coefficients for cadmium follow the same pattern as indicated for bismuth, but are somewhat lower. At the lowest concentration of hydrobromic, the differences become quite large and the coefficients of cadmium small enough for elution.

A mixture of 0.1 M hydrobromic and 0.5 M nitric acid is an extremely effective eluting agent for zinc and indium while cadmium is very strongly retained. The separation factor is larger than 1000 and the very strong tailing observed when indium is eluted with 0.1 M hydrobromic acid alone disappears almost completely. Elements such as Ga, Fe(III), Mn(II), Co(II), U(VI), Ni(II), and many others are even less strongly adsorbed from bromide solutions than zinc and should easily be separated. Bismuth and the elements forming stable bromide complexes named in the previous paragraph are retained together with cadmium. When cadmium is eluted with 0.02 M hydrobromic acid containing 2 M nitric acid, bismuth and most of these elements are still retained. For large amounts of cadmium which are already adsorbed as bromide complexes, this eluting agent is not suitable because it leads to very large elution volumes. About 1 M ammonium hydroxide containing 0.1 M ammonium nitrate and 0.02 M ammonium bromide then becomes much more attractive. When on the other hand adsorption is carried out from 2 M nitric acid containing 0.02 or 0.03 M hydrobromic acid and a column equilibrated with the same reagent is used, separation of trace amounts of bismuth from large amounts of cadmium should become easy. Most of the cadmium should pass unadsorbed through the column. Because of the very large separation factors and the large distribution coefficients of cadmium, only very small columns are needed for separations even when gram amounts of elements such as zinc and copper are present. This has been utilized for the development of an improved method using a column of only 4 mL resin for the separation of trace amounts of cadmium-109 from cyclotron targets (*11*). Details for the separation of larger amounts of cadmium from many other elements also have been described (*12*). Lead(II) accompanies cadmium partially when 0.1 M hydrobromic containing 0.5 M nitric acid is used as eluting agent, but good separations are possible by using somewhat larger columns and 0.05 M hydrobromic containing 0.5 M nitric acid for the elution of lead (*12*). The separation factor still has a value of about 14 in this case.

Lead(II). Distribution coefficients for lead increase with concentration of hydrobromic acid to a maximum value of about 800 at about 0.5 M hydrobromic acid and then start to decrease slowly again. They decrease with increasing nitric acid concentration. Good separations from zinc and indium seem to be possible in 0.2 M hydrobromic acid containing between 0.2 and 0.5 M nitric acid. Most other elements including Cu(II), Fe(III), Ga, Al, Co(II), Mn(II), Ni(II), the alkali metals, and alkaline earths have less tendency to form bromide complexes than zinc and should also be easily separated. When lead is eluted selectively with 0.05 M hydrobromic acid containing 0.5 M nitric acid, cadmium, bismuth(III), and the elements forming stable bromide complexes are retained by the column (Figure 1).

Zinc, Indium and Other Elements. Zinc and indium show almost no adsorption up to 0.2 M hydrobromic acid and only weak adsorption in 0.5 M hydrobromic acid. In 1 M hydrobromic acid, the adsorption of zinc becomes fairly strong while that of indium remains rather weak. Higher concentrations of hydrobromic acid are not of interest as far as hydrobromic–nitric acid mixtures are concerned because mixtures containing significant amounts of nitric acid become unstable and, with increasing hydrobromic acid, the nitric acid becomes progressively less effective in depressing tailing effects.

Other elements such as Cu(II), Fe(III), Ga, Co(II), Ni(II), Mn(II), U(VI), Al, Ti(IV), Zr, Hf, Th, Sc, Y, the lanthanides, Be and the alkaline earths, and the alkali metals have even lower distribution coefficients in hydrobromic acid solutions than zinc and indium.

General. Severe tailing effects observed for some elements on elution with dilute hydrobromic acid up to 0.3 M disappear almost completely when about 0.5 to 2.0 M nitric acid is added to the eluting agent. Selectivities of elements in hydrobromic acid–nitric acid mixtures up to 2 M nitric acid follow the sequence:

$$\mathrm{Bi(III) > Cd > Pb(II) > Zn > In(III) > Cu(II)}$$

similar to the sequence in pure hydrobromic acid. The elements are less strongly adsorbed from the mixed acid, but separation factors are often as large and sometimes even larger than in the pure acid.

LITERATURE CITED

(1) T. Andersen and A. B. Knutsen, *Acta Chem. Scand.*, **16**, 849 (1962).
(2) F. W. E. Strelow and F. von S. Toerien, *Anal. Chem.*, **38**, 545 (1966).
(3) F. W. E. Strelow, W. J. Louw, and C. H. S. W. Weinert, *Anal. Chem.*, **40**, 2021 (1968).
(4) F. Nelson and K. A. Kraus, *J. Am. Chem. Soc.*, **76**, 5916 (1954).
(5) S. Onuki, *Jpn. Anal.*, **12**, 844 (1963).
(6) F. Feik and J. Korkisch, *Talanta*, **11**, 1585 (1964).
(7) S. S. Ahluwalia and J. Korkisch, *Z. Anal. Chem.*, **208**, 414 (1965).
(8) J. S. Fritz and R. G. Greene, *Anal. Chem.*, **35**, 811 (1963).
(9) J. S. Fritz and B. B. Garralda, *Anal. Chem.*, **34**, 102 (1964).
(10) Z. Sulzek, P. Povondra, and V. Kratochvil, *Collect. Czech. Chem. Commun.*, **34**, 3711 (1969).
(11) F. W. E. Strelow, *Anal. Chim. Acta*, in press.
(12) F. W. E. Strelow, *Anal. Chim. Acta*, accepted for publication.

RECEIVED for review February 21, 1978. Accepted May 18, 1978.

Algorithm for Recognition and Quantitation of Chromatograms of a Pesticide Mixture by a Microprocessor-Based Integrator

S. M. McCown, H. H. Land, and C. M. Earnest*

Department of Chemistry, Northeast Louisiana University, Monroe, Louisiana 71209

Strobane is a pesticide mixture consisting of polychlorinated terpenoids which contain about 70% chlorine by weight. Some 250 compounds have been identified from the mixture, using capillary GC/MS systems. An algorithm is proposed whereby chromatograms of the pesticide Strobane may be recognized and quantitated by automatic data-handling devices. The method is suitable for adaptation to the chromatographic analysis of any mixture whose chromatogram is known to contain a recognizable, reproducible pattern of retention times and peak intensities. A new concept, relative valley intensity, is introduced and its use is demonstrated.

McCown et al. (*1*) proposed a series of algorithms which could be used to identify and quantitate Chlordane, toxaphene, and polychlorinated biphenyls (PCB). Unstated, but strongly implied in their work, was the idea that the identities of the compounds which produce a set of chromatographic peaks need not be known, provided that a characteristic and reproducible set of phenomena occur. Included in this set of phenomena are relative retention times of peak maxima, relative retention times of minima, and relative intensities of maxima and minima. Relative retention time patterns are reported for Chlordane, Toxaphene, Strobane, and PCB (*2*), using only their peaks. The experienced pesticide residue analyst depends as much on baseline aberration, in the case of toxaphene (*3*) and Strobane (Figure 1), to identify the mixtures as on the relative retention times of the peaks. Since the use of baseline aberrations was somewhat subjective, it was desirable to develop methods to deal with reproducible baseline phenomena produced by the analyte.

The concept of a nonzero valley seemed to be the most straightforward method of obtaining information about the baseline. In the development of this parameter, it is important to realize that in any chromatograph/integrator dialog, two baselines are involved—one for each instrument. The baseline of the integrator is fixed by the manufacturer at some convenient potential (−2.0 mV in the CDS-111c) and that of the chromatograph is usually determined to a greater or lesser extent by the chromatographer. The two baselines are usually different, and it is this difference which allows the microprocessor to track the various fluctuations in the signal from the chromatograph. The trend in the signal determines whether the microprocessor recognizes a peak, a valley, or instrumental baseline (*4*).

A nonzero valley must then be discussed in terms of three points in time: t_1, a time slightly before the occurrence of the suspected valley; t_2, the time of occurrence of the suspected valley; and t_3, a time slightly later than t_2 ($t_1 < t_2 < t_3$). If the chromatogram is considered as the graph of some function $y(t)$, the condition for a minimum in $y(t)$, (y as a function of t), are (*5*): at t_1, dy/dt is negative; at t_2, $dy/dt = 0$; and at t_3, dy/dt is positive. At t_2, Y may be positive, negative, or zero with respect to the prevailing chromatographic baseline. $Y(t_2) = 0$ indicates a well-resolved peak ($R_{j,j+1} \geq 1.5$) (*6*), $y(t_2) < 0$ defines the minimum of a negative peak. $Y(t_2) > 0$ indicates a nonzero valley (Figure 2). The retention times and intensities of these nonzero valleys can be used to help identify a particular mixture and distinguish it from similar mixtures. A combination of the better-known relative peak retention time and relative peak intensity programs with the relative valley intensity programs proposed here, should make identification of complex mixtures easier (*2*, *7*). It is not the objective of this work to identify any of the compounds of the mixtures, but only the mixture itself.

EXPERIMENTAL

Apparatus and Reagents. All chromatograms presented here were obtained from a Varian Model 3700 Gas Chromatograph equipped with a Hewlett-Packard 7671A Automatic Liquid Sampler and a pulse-modulated constant-current electron-capture detector. The chromatographic process took place in an all-glass system. The signal from the electrometer was passed to a Varian CDS-111c computing integrator. The output of the integrator was displayed on a Varian A-25 dual-pen recorder.

The chromatographic column was 6 ft × 2 mm i.d. glass packed with 1.5% OV-17 + 1.95% OV-210 on 100/120 Chromosorb W-HP operated isothermally at 175 °C. A nitrogen carrier gas flow rate of 33 mL/min was employed. A glass-lined injection port was maintained at 200 °C and the detector was held at 310 °C. Control of the instrument and data systems was given to the CDS-111c integrator insofar as this was practical. All pesticide standards were injected into the gas chromatograph from a solution of isooctane. The isooctane was Mallinckrodt nanograde.

Procedure. A pattern recognition program was constructed for the major peaks of Strobane, by a procedure which has become standard in this laboratory (*1*). Standards of all compounds of interest having retention times very similar to those of the components of Strobane were chromatographed. The retention time and the weight of each compound were entered in the memory of the microprocessor. The compounds included were: hexachlorobenzene (HCB), Heptachlor, Aldrin, Heptachlor Epoxide, Dieldrin, Endrin, Mirex, the DDT group of compounds, toxaphene, and the Chlordane group of compounds. Quantitation of these compounds was accomplished by two programs each consisting of a control file and three sub-routine files in the integrator using methods described by McCown et al. (*1*). The difference between the two programs is that one program is constructed for normal operation of the microprocessor integrator and the second program is constructed for operation of the integrator with the input polarity opposite to that of normal operation. The program corresponding to the normal integrator operating polarity is termed the "primary integration program" and the reversed polarity program is called the "secondary integration program". When using the "secondary integration program" with the input polarity reversed, the inverted chromatogram is integrated. Thus, the "secondary integration program" integrates the normal valleys as peaks and views the normal peaks as valleys (Figure 3). The data processing files are constructed from data obtained from chromatograms of various pesticides. Aldrin, hexachlorobenzene, Heptachlor, Heptachlor Epoxide, Dieldrin, Endrin, Mirex, and Methoxychlor are included in the "control" file, File 1. These compounds are identified by their absolute retention times, and are quantitated by the familiar "external standardization" method. Retention times and response factors for the standards are stored in the integrator memory, together with chromatograph and integrator control parameters. The other files in this program are set up as sub-routines of the control file.

0003-2700/78/0350-1362$01.00/0

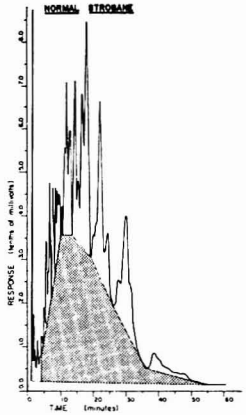

Figure 1. Normal Strobane chromatogram

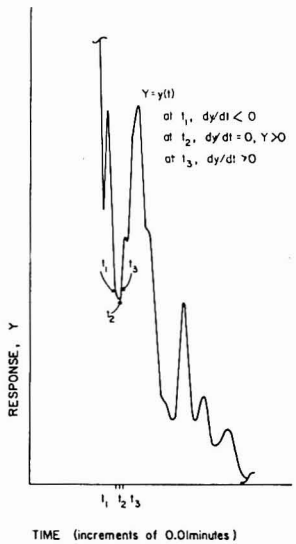

Figure 2. Operating definition of a nonzero valley

File 2 identifies the DDT group of compounds (DDE, DDD, DDT) by their retention times relative to p,p'-DDE, which is identified by its absolute retention time. Quantitation is achieved by external standardization.

File 3 identifies the technical Chlordane mixture (a mixture containing some 15 compounds) on the basis of the retention times of γ-chlordene and α-chlordane relative to the retention times of α-chlordene and γ-chlordane. γ-Chlordane is used as the principal reference peak. These compounds were chosen because of the ready availability of authentic standards and because they form two doublets characteristic of technical Chlordane. Quantitation of the technical mixture is accomplished by quantitation of the four compounds by external standardization. The results are summed and multiplied by a conversion factor, which is the reciprocal of the weight fraction of the four compounds in the technical mixture. The product of this multiplication is the weight of technical Chlordane in the sample.

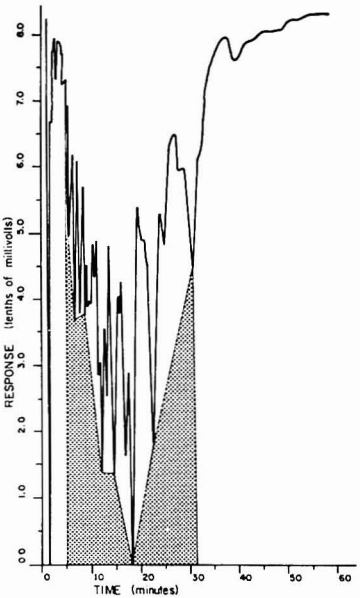

Figure 3. Inverted Strobane chromatogram. This chromatogram was obtained by inverting the signal to the integrator. Each peak is an inverted nonzero valley

File 4 identifies toxaphene on the basis of the retention times of ten peaks relative to two references. The toxaphene chromatogram is very similar to that of Strobane, and the techniques used to deal with one are usually successful in dealing with the other. Quantitation is accomplished by the construction of a pattern quantitation method analogous to the one presented here (vide infra).

It can be seen from Figure 3 that the inverted integration is not exactly the same as relative valley intensity, but there is a close similarity. The CDS-111c is not equipped to make the calculations necessary for true relative valley intensity, nor will it report minima. The secondary integration will report minima, but only when the chromatograms are presented to the integrator in inverted form. In this mode, normal maxima are presented as minima.

After treating the other compounds in the manner described above, a standard solution of Strobane was chromatographed. Its peaks were processed through the routines for single peak compounds (Tables I and II), and finally an area percent report was obtained (Table III). Each table shows the mistaken identification of one or more Strobane peaks for other compounds. The identified peaks are those in Tables I and II which have identification numbers printed in the column headed "*PK*". Twelve of the 28 peaks in Strobane exhibit no interferences. Eleven of the remaining peaks are identified in the toxaphene file, File 4 (Table II).

The retention times of the peaks in the Strobane chromatogram which were identified as other compounds of interest were noted. These peaks were immediately excluded from consideration by dropping their retention times from the data compilation. Their area percents were summed. The sum is known in our nomenclature as $A\%_E$, the total excluded area percent:

$$A\%_E = \Sigma_i A\%_i \quad (1)$$

where i is the ith peak whose retention time (t_r) is identified in another file, and $A\%_i$ is the area percent of the ith excluded peak. The remaining peaks were assigned identification numbers

Table I. Strobane Data Processed through Cyclodiene Pesticide File[a]

RACK 1 VIAL 28
V# 4 INJ. 1
FILE 1 ID# 28

PK #	TIME	AREA	EXT. STD
P	2.55	23108	.00
P	2.73	15368	.00
P	2.97	64272	.00
3P	3.69	210114	29.43
P	4.39	314596	.00
P	4.87	172864	.00
P	5.24	493872	.00
4P	6.15	730164	108.92
P	6.95	489680	.00
P	7.40	640584	.00
P	8.02	514216	.00
P	8.63	478552	.00
P	9.38	557064	.00
5P	9.80	1117408	160.82
P	10.68	1334600	.00
6P	11.99	1491432	262.20
P	13.03	715640	.00
P	13.99	1453064	.00
P	15.19	2389168	.00
P	16.84	570864	.00
P	18.74	2940852	.00
P	20.72	1550664	.00
P	23.65	656032	.00
7P	25.73	2629024	584.21
P	33.30	437328	.00
T	36.66	10464	.00
8T	39.01	9472	7.70
T	41.14	22496	.00
TOTAL		22032962	1153.28

SAMP 1.000000
SCALAR 1.000000

[a] Peaks of Strobane have been identified as: 3, Aldrin; 4, Heptachlor Epoxide; 5, Dieldrin; 6, Endrin; 7, Mirex; 8, Methoxychlor.

Table II. Strobane Data Processed through Toxaphene File

RACK 1 VIAL 28
V# 4 INJ. 1
FILE 4 ID# 14

PK #	TIME	AREA	EXT. STD
1P	2.55	23108	13.03
P	2.73	15368	.00
P	2.97	64272	.00
P	3.69	210114	.00
2P	4.39	314596	249.26
P	4.87	172864	.00
3P	5.24	493872	427.98
P	6.15	730164	.00
P	6.95	489680	.00
P	7.40	640584	.00
P	8.02	514216	.00
5P	8.63	478552	434.77
P	9.38	557064	.00
P	9.80	1117408	.00
6P	10.68	1334600	815.47
P	11.99	1491432	.00
7P	13.03	715640	469.45
8P	13.99	1453064	935.21
P	15.19	2389168	.00
9P	16.84	570864	352.70
P	18.74	2940852	.00
10P	20.72	1550664	964.72
11P	23.65	656032	427.44
P	25.73	2629024	.00
12P	33.30	437328	415.87
T	36.66	10464	.00
T	39.01	9472	.00
T	41.14	22496	.00
TOTAL		22032962	5605.90

SAMP 1.000000
SCALAR 1.000000

(subscript j) corresponding to their position in the chromatogram. These numbers correspond to the identification numbers in the data table of the integrator. The area percent corresponding to each remaining peak was converted into a normalized area fraction by multiplying by the normalization factor:

$$N = \frac{0.01}{1 - (0.01\ A\%_E)} \qquad (2)$$

where $0.01\ A\%_E$ converts the percent to a decimal fraction. In our symbolism, this normalization would appear:

$$A\%_j \left\{ \frac{0.01}{1 - (0.01\ A\%_E)} \right\} = NA\%_j = A_j{}^n \qquad (3)$$

where $A\%_j$ is the area percent of the jth peak and $A_j{}^n$ is the normalized area fraction of the jth peak.

It was then necessary to make the twin assumptions that each peak was produced by only one compound and that each of these compounds exhibited exactly the same response to the detector in use. Both of these assumptions are patently false, but useful in this context, provided that chromatographic resolution remains constant. Having made these two assumptions, the differences in peak areas could only be attributed to different weights of the hypothetical compounds.

These weights were computed (Table IV) and used to calibrate the integrator in the familiar "external standard" mode. The weight of the mixture attributable to each peak was computed by multiplying the weight of Strobane injected by the normalized area fraction ($A_j{}^n$) corresponding to each peak. Thus:

$$W_j = W_T x A_j{}^n \qquad (4)$$

where W_j is the weight assigned to the jth peak; W_T is the total weight of Strobane injected; and $A_j{}^n$ is the normalized area fractions of jth peak. Finally, the retention time of each peak and its assigned weight were entered into the data table of the CDS-111c. The integrator was instructed to calculate response factors for each peak (Table IV). (A check on previous computations can be made by noting the response factors. If they are not all very similar, previous computations contain errors. A standard deviation of 6.70×10^{-4} is routine for 12 factors.)

The construction of the file, as the analytical method is termed, is completed by suppressing the integrations of the solvent front and by forcing a baseline approximately 0.2 min before the end of the program. These two commands assure uniform integration at the beginning and end of each chromatogram. The data table is completed by naming two reference peaks so that the remaining peaks can be identified by retention times relative to the reference peaks.

It is possible to use this method, in its present form, as a data collection file, and chromatograph control file, because it has few constraints placed on its data acquisition. It is important not to use this file as a subroutine to a highly constrained file, as much useful data may be lost because of the restrictions placed on data acquisition.

If the routine proposed here is used as a subroutine, it can be improved by forcing a baseline (suppressing integration) in the regions where no information useful to the file is to be obtained. This has the additional effect of resetting the baseline (*4*); thus the sequence of events at the integrator will now be:

1. Collect data in the data collection file.
2. Apply the routine from the data collection file.
3. Branch to other routines.
4. Close the loop to the data collection file.

The data collected for the secondary integration are treated in exactly the same way as those obtained in the primary integration, i.e., they are normalized, and weights and response factors for each peak are computed, using the methods and assumptions reported above (Table V). The qualitative parameter in this case is based on the retention time of the nonzero valley.

Table III. Strobane Data Processed through Area Percent File

RACK 1 VIAL 28
INJ. 1
FILE 5 ID# 55

PK	*	TIME	AREA	AREA %
1	P	2.55	23108	.10
2	P	2.73	15368	.07
3	P	2.97	64272	.29
4	P	3.69	210114	.95
5	P	4.39	314596	1.43
6	P	4.87	172864	.78
7	P	5.24	493872	2.24
8	P	6.15	730164	3.31
9	P	6.95	489680	2.22
10	P	7.40	640594	2.91
11	P	8.02	514216	2.33
12	P	8.63	478552	2.17
13	P	9.38	557064	2.53
14	P	9.80	1117408	5.07
15	P	10.68	1334600	6.06
16	P	11.99	1491432	6.77
17	P	13.03	715640	3.25
18	P	13.99	1453064	6.59
19	P	15.19	2389168	10.84
20	P	16.84	570864	2.59
21	P	18.74	2940852	13.35
22	P	20.72	1550664	7.04
23	P	23.65	656032	2.98
24	P	25.73	2629024	11.93
25	P	33.30	437328	1.98
26	T	36.66	10464	.05
27	T	39.01	9472	.04
28	T	41.14	22496	.10
		TOTAL	22032962	99.97

Table IV. Data Tabulation for Normal Strobane

j	T_r, min	A%	$A_j{}^n$	W_j, pg	response factor × 104
1	4.39	1.43	0.0362	217 30	6.927610
2	4.87	0.78	0.0198	118.80	6.852210
3	5.24	2.24	0.0568	340.80	6.907050
4	8.02	2.33	0.0590	354.00	6.891850
5	8.63	2.17	0.0550	330.00	6.890580
6	10.68	6.06	0.1535	921.00	6.908290
7	13.03	3.25	0.0823	593.80	6.911720
8	13.99	6.59	0.1670	1002.00	6.899420
9	16.84	2.59	0.0656	393.60	6.905150
10	20.72	7.04	0.1788	1069.80	6.905110
11	23.65	2.98	0.0755	453.00	6.904240
12	33.30	1.98	0.0502	301.20	6.890250
			0.9992	5995.20	

Total injected: 5.0 μL × 1200.00 pg/μL = 6000.00 pg
$A\%_E = 60.53\%$
$\{0.01/[1 - (0.01\ A\%_E)]\} = 2.5336 \times 10^{-2}$

When the signal is inverted, the minimum of the nonzero valley becomes the maximum of a new peak. Between peaks which are resolved to the baseline ($R \geq 2.5$), there are several points at which $dy/dt = 0$, thus the integrator can be forced to ignore them by integration suppression (forced baseline).

It was found useful to reset the instrument baseline after each peak by forcing a baseline for 0.01 min (the smallest available division of the time base) at the beginning and end of each peak (*4*). This technique allows better tracking of the negative baseline aberration common to inverted Strobane and toxaphene. Furthermore, the baseline of the secondary integrator had to be offset by +10 mV through the electrometer bucking potential, in order to allow integration of all peaks. Failure to use this offset led to consistent failure of the program because of the extreme negative excursions of the inverted peaks. This failure can be explained on the basis of the signal crossing below the integrator reference voltage. It is interesting to note that the baseline reset, noted above, suppressed the integration of many of the peaks which otherwise might have interfered with the program (*8*).

Table V. Data Tabulation for "Inverted" Strobane

j	T_r, min	$A_j{}^n$	W_j, pg	response factor
1	1.05	0.0029	17.40	9.7698
2	1.21	0.0064	38.40	9.9010
3	1.30	0.0063	37.80	9.8032
4	1.40	0.0162	97.20	9.8779
5	1.62	0.0145	87.00	9.8316
6	2.03	0.0279	167.40	9.8520
7	2.28	0.0187	112.20	9.8359
8	2.42	0.0191	114.60	9.8425
9	2.76	0.0476	285.60	11.2788[a]
10	3.36	0.0430	258.00	9.8445
11	4.01	0.0271	162.60	9.8644
12	4.61	0.0090	54.00	9.9003
13	4.94	0.0024	14.40	9.8482
14	5.57	0.0118	70.80	9.8287
15	22.64	0.0848	508.80	9.8566
16	24.09	0.0298	178.80	9.8649
17	31.63	0.3562	2137.2	9.8521
18	36.07	0.1351	810.60	9.8492
19	38.54	0.0791	474.60	9.8553
20	40.25	0.0392	235.20	9.8618
21	44.41	0.0275	165.00	9.8552

[a] $W_t = 6000.00$ pg. No areas excluded in this tabulation.

RESULTS AND DISCUSSION

Until recently, the entire emphasis of data acquisition from chromatographic separations has been on complete resolution of all peaks and subsequent identification by any available means. Many efforts have been made to deconvolute fused or partially fused peaks so that their retention times or volumes could be determined (*9–11*).

Many of these techniques are theoretically applicable to the analysis of gas chromatographic data. The drawbacks associated with the use of these techniques are that often complex and costly equipment is required and the operators usually must be highly trained. The algorithm suggested here can be used by relatively inexperienced persons and requires a smaller initial investment. An additional advantage is its ability to deal with convoluted data. Like other more sophisticated techniques, it can be adapted to any pattern which can be described as a function of time. Among the contemplated applications are the interpretation of spectra of mixtures in which one or more components are sought, and for which standards are available, the analysis of thermograms of mixtures, and pyrograms of mixed polymers. In these qualitative analyses, it has been found useful to confirm the original identification by means of a complementary pattern. This complementary pattern can be obtained by the electronic inversion of sets of data in which nonzero valleys occur. The loci of nonzero valleys will become the loci of peaks in the complementary pattern. Distinction between toxaphene and Strobane, whose chromatograms are very similar, has been facilitated through the use of this technique which provides an objective method for the treatment of baseline aberration inherent in the chromatogram of the mixture.

Quantitation, in the cases where the algorithm has been applied, is demonstrably good (Table VI). It has been found that a well-constructed, properly standardized file gives quantitative errors of ±0.1% or less and that errors of ±0.04% are routine. Considering the fact that these analyses are performed at the nanogram level, these techniques represent an improvement upon the existing technology.

The conclusions available from this study are, inter alia, that any set of data which contains a recognizable and re-

Table VI. Recomputation of Strobane through Normal Strobane File

```
                        RACK   1 VIAL 28
                        V#     1 INJ.  1
                        FILE   5 ID#   0

PK #    TIME      AREA     EXT.   STD
  P     3.69    210114              .00
 1P     4.39    314596       217.94
 2P     4.87    172864       118.45
 3P     5.24    493872       341.12
  P     6.15    730164              .00
  P     6.95    489630              .00
  P     7.40    640584              .00
 4P     8.02    514216       354.39
 5P     8.63    478552       329.75
  P     9.38    557064              .00
  P     9.80   1117408              .00
 6P    10.68   1334600       921.98
  P    11.99   1491432              .00
 7P    13.03    715640       494.63
 8P    13.99   1453064      1002.53
  P    15.19   2389168              .00
 9P    16.84    570864       394.19
  P    18.74   2940852              .00
10P    20.72   1550664      1070.75
11P    23.65    656032       452.94
  P    25.73   2629024              .00
12P    33.30    437328       301.33
    TOTAL     21887782      6000.00

              SAMP              1.000000
              SCALAR            1.000000
```

producible pattern of voltages as a function of time can be isolated in whole or in part from a larger set of data. The isolated portions of the pattern can be used to provide a basis for identification and quantitation of a compound or a mixture in the presence of other compounds or mixtures whose spectra, chromatograms, pyrograms, or thermograms are not completely and mutually resolved. Baseline aberrations, if they are an integral part of the data and not instrumental artifacts, can be used as additional patterns or sub-patterns. A pattern can be inverted to give a complementary pattern, which can then be used qualitatively and quantitatively. Furthermore, if the analysis is concerned with the quantitation of a mixture, the compounds of the mixture need not be identified and some interferences can be tolerated. The techniques described have been successfully applied to the analysis of pesticide residues in water, tissue, and soil, as well as to the analysis of solvent residues in oilseed meals and packaging materials. The methods are suitable for inclusion in larger data processing packages and, when this is done, the calculations presented here can be made to take place automatically.

LITERATURE CITED

(1) S. M. McCown, E. S. Greer, R. B. Davey, and C. M. Earnest, *Am. Lab.*, **9**, 16-30 (1977).
(2) J. Sherma and G. Zweig, Ed, "Handbook of Chromatography", C.R.C. Press, Cleveland, Ohio, 1972.
(3) J. Burke et al. "Pesticide Analytical Manual", U.S. Dept. of Agriculture, Beltsville, Md., 1974.
(4) CDS-111c Operation Manual, Varian Instruments, Inc., Palo Alto, Calif., 1976.
(5) M. H. Protter and C. B. Morrey, "College Calculus with Analytical Geometry", Addison-Wesley Publishers, New York, N.Y., 1964.
(6) G. Guiochon and C. Pommier, "Gas Chromatography in Inorganics and Organometallics", Ann Arbor Science Publishers, Ann Arbor, Mich., 1973.
(7) S. M. McCown and C. Dempsey, unpublished data, 1975.
(8) S. M. McCown, *Proc. Louisiana Acad. Sci.*, Vol. XLI (1978).
(9) S. P. Perone and Q. V. Thomas, *Anal. Chem.*, **49**, 1369 (1977).
(10) S. P. Perone, Q. V. Thomas, and R. A. DePalma, *Anal. Chem.*, **49**, 1376 (1977).
(11) S. P. Perone and M. A. Pichler, *Anal. Chem.*, **46**, 1790 (1974).
(12) N. J. Nilsson, "Learning Machines", McGraw-Hill, New York, N.Y., 1968.
(13) K. Tukanaga, "Introduction to Statistical Pattern Recognition", Academic Press, New York, N.Y., 1972.
(14) B. R. Kowalski and C. F. Bendur, *Anal. Chem.*, **44**, 1405 (1972).

RECEIVED for review December 22, 1977. Accepted April 28, 1978. This work was presented, in part, at the 33rd Southwest Regional Meeting of the American Chemical Society, Little Rock, Arkansas, December, 1977.

Computerized Pattern Recognition for Classification of Organic Compounds from Voltammetric Data

D. R. Burgard[1] and S. P. Perone*

Purdue University, Department of Chemistry, West Lafayette, Indiana 47907

Pattern recognition techniques have been used to characterize the electrochemical data obtained from electroactive organic compounds. The studies included compounds belonging to four different electroactive group/skeleton combinations. Peak potentials, features derived from scan rate dependence, and curve shape features were all used for characterization of the compounds. The studies indicated that differences in the peak potentials and curve shapes were the most useful for classification of the different compounds.

Electroanalytical techniques are not normally considered very useful tools for qualitative identification. This is due to the lack of specificity in the polarographic halfwave or voltammetric peak potentials, the complex dependence of the current on many variables, and the fact that systematic studies to characterize a large number of systems under similar conditions have not been performed. The purpose of this work was to see if the application of pattern recognition and visual cluster analysis methods could identify information indicative of the electroactive group, the skeleton, or both, contained in voltammetric data from electroactive organic compounds.

Functional groups commonly found in organic compounds that are highly polar or unsaturated are often reducible at a mercury electrode. Some of these functional groups are: azo, carbonyl, cyano, nitro, nitroso, unsaturated carbon–carbon bonds, and carbon–halogen bonds. Reductions of these groups are generally irreversible electrochemically (k_s is small) and chemically. They often proceed by multiple step mechanisms involving the formation of short-lived intermediates.

Systematic studies of reduction mechanisms (*1*, *2*) and shifts in polarographic halfwave potentials (*3*) with changes in

[1] Present address, Procter & Gamble Company, Miami Valley Laboratories, P.O. Box 39175, Cincinnati, Ohio 45257.

0003-2700/78/0350-1366$01.00/0

substituents have determined that the reduction mechanism depends on the compound skeleton, the position and type of substituents on the skeleton, and the experimental conditions, as well as the electroactive group. Since the electroactive form may be a function of pH, and hydronium ions may be involved in the reduction process, it is necessary to buffer solutions. Similar mechanisms and values of αn (α is the electrochemical transfer coefficient and n is the number of electrons transferred in the rate determining step) can be expected for compounds with the same skeleton and electroactive group under the same experimental conditions. Unfortunately, deviations often result, depending on the position and type of substituents. The studies mentioned above (*1*, *3*), have identified groups of structurally similar compounds and the experimental conditions where the mechanisms and the values of αn are reasonably constant. This information was used to define the compounds and experimental conditions used in the studies reported here. Staircase voltammetry (SCV) was chosen as the electroanalytical technique to be used here.

Staircase Voltammetry. Staircase voltammetry is similar to stationary electrode polarography. Rather than a linear voltage ramp, the applied waveform is a staircase. The current is sampled at time t_m after each step. The effective scan rate is determined by the size (ΔE) and the length (τ) of each step. The sampling parameter, α', as defined by Equation 1, is usually used when referring to the time delay (t_m) after each step before the current is sampled.

$$\alpha' = 1 - \frac{t_m}{\tau} \tag{1}$$

α' is zero when sampling at the end of each step, and α' approaches unity when sampling is near the beginning of each step. SCV theory (*4*, *5*) for reversible and irreversible processes points out the dramatic effect of α' on peak shape. Because existing SCV theory assumes that the electrode process is uncomplicated, direct interpretation of voltammetric data for the organic compounds used in these studies is questionable. However, the same general experimental correlations should be observed, and it is expected that different electrode processes should exhibit different dependencies on α' and scan rate, as predicted for linear sweep voltammetry (*6*). Staircase voltammetry is the method of choice here because it is directly computer compatible and charging current contributions are minimized, while the dynamics of the electrode process can be reflected in the voltammetric behavior by varying α'.

EXPERIMENTAL

Reagents and Solutions. The previously mentioned studies (*1–3*) were used as a guide for the choice of the compounds to be used. The compounds were chosen to represent the four skeleton/electroactive group combinations: aromatic–nitro, aliphatic–nitro, aromatic–aldehyde, and aromatic–aliphatic–ketone. The one exception was benzophenone which belongs to a separate class but was included because of availability and for comparison with the two other carbonyl classes. The 30 compounds used are listed in Table I.

The solvent system consisted of a pH 7.1 buffer in 30% ethanol/70% distilled-deionized water. This McIlvaine type buffer contained 0.165 M Na_2HPO_4 and 0.018 M citric acid (*7*). The supporting electrolyte was 0.5 M KCl. All the chemicals in the solvent system were reagent grade.

Stock solutions, 0.002 M, for each compound were made from fresh bottles of high purity chemicals. The chemicals were used as obtained from the manufacturer. Further dilutions of the stock solutions were made as required.

Instrumentation. The staircase voltammograms were secured using a general purpose electrochemical instrument with computerized data acquisition and control (*8*). The computer was programmed to generate the staircase waveform that was applied to the cell through the internal digital-to-analog converter and the general purpose potentiostat. The cell consisted of a microburet-type hanging mercury drop working electrode (Metrohm E410), a coiled platinum wire counter electrode, and a saturated calomel reference electrode with a Luggin capillary.

Table I. Compounds Used in These Studies

compound reference no.	name	class assignment
1	nitrobenzene	1
2	*p*-nitroaniline	1
3	*p*-nitroacetophenone (first peak)	1
4	*p*-nitrophenol	1
5	*m*-nitrobenzaldehyde (first peak)	1
6	*m*-nitrotoluene	1
7	*p*-nitrotoluene	1
8	*o*-nitrotoluene	1
9	*o*-nitroanisole	1
10	*p*-chloronitrobenzene	1
11	benzaldehyde	2
12	*p*-hydroxybenzaldehyde	2
13	*p*-anisaldehyde	2
14	*m*-tolualdehyde	2
15	*p*-tolualdehyde	2
16	*o*-tolualdehyde	2
17	*p*-chlorobenzaldehyde	2
18	*o*-chlorobenzaldehyde	2
19	nitromethane	3
20	nitroethane	3
21	*sec*-nitropropane	3
22	3-nitro-2-pentanol	3
23	nitrocyclohexane	3
24	acetophenone	4
25	benzophenone	5
26	isobutyrophenone	4
27	*m*-nitrobenzaldehyde (second peak)	2
28	propiophenone	4
29	*n*-butyrophenone	4
30	*o*-methoxyacetophenone	4

Table II. Experimental Conditions for Set of Six Staircase Voltammograms Obtained for Each Compound

scan rate, mV/s	α'
(1) 2678	0.7, 0.3
(2) 695	0.7, 0.3
(3) 347	0.7, 0.3

The computer used for instrumental control and data acquisition was a Hewlett-Packard 2115A with 8K words of core memory. Peripherals included a general purpose interface, paper tape reader and punch, a Teletype, and a Tektronix 601 storage display monitor. Data acquisition and control subroutines were written in Hewlett-Packard assembly language and called by main programs written in BASIC.

The computer system used for the data analyses is described elsewhere (*9*).

Data Acquisition. Prior to data acquisition, all solutions were deoxygenated with high purity nitrogen. Oxygen traces were removed by passing the nitrogen through two gas washing bottles containing chromous chloride and zinc amalgam (*10*). All solutions were deaerated a minimum of 15 min and then blanketed by the same stream of nitrogen.

Each compound was characterized by a set of six cyclic staircase voltammograms that covered a range from 200 mV anodic to 260 mV cathodic of the peak potential. The voltammograms were obtained by sampling twice on each step for three different scan rates (Table II). The step size was 3.64 mV for each scan rate. The scan rates were chosen to cover a wide range of experimental conditions. The starting potential for each scan was found by a preliminary scan from 0 to −1.8 V vs. SCE to locate the peak potential. The step size was 14.6 mV for the preliminary scans.

To obtain the optimum voltammograms under each set of experimental conditions, the working electrode size and/or the

Table III. Curve Shape Features Defined by Sybrandt and Perone (*11*)

feature no.	feature definition
1	$E_p - E(0.75\ i_p)$
2	$E_p - E(0.5\ i_p)$
3	$E_p - E(0.25\ i_p)$
4	feature 2/feature 3
5	feature 2/feature 1
6	feature 3/feature 1
7	Area under curve between data points 44-64
8	A 49-59
9	A 34-54
10	A 44-54
11	A 34-74

sample concentrations were adjusted. The voltammograms saved for analysis were the average of 10 scans with a new drop being used for each scan. Care was taken to reproduce the drop size as precisely as possible for each scan. The raw voltammograms were punched on paper tape for transfer to the other computer system for analysis.

Feature Definition and Extraction. Traditionally, electrochemical systems have been characterized by quantities such as the peak potential, changes in the peak potential that result from changes in scan rate, and the peak current or changes in the peak current (*6*). Each of these were used to characterize the systems studied here.

Several of the voltammetric features related to curve shape defined by Sybrandt and Perone (*11*) were calculated, autoscaled, and tested for their ability to discriminate between the four classes of compounds. The features tested were peak areas, potential differences, and ratios of potential differences. They are defined in Table III.

Thomas and Perone (*12*, *13*) have shown that the coefficients obtained from the discrete Fourier Transform of voltammetric curves are useful for curve shape analysis. This approach was also used to define shape features. Three preprocessing steps are required when this approach is used: Each curve is normalized to the peak maximum to remove differences in absolute magnitudes. This results in a range of current values from 0 to 1.0 for each curve. To avoid introducing extraneous shape information into the transform, each curve must have the same peak location. This is accomplished by shifting the curve so that its peak maximum is at data point 54, for those curves whose maximum did not originally occur there. Finally, each curve is rotated and translated prior to transforming to retain the most fidelity in the transform (*14*). The discrete Fourier Transform is then calculated and the autoscaled Fourier Coefficients (*12*, *13*) are used as features.

Data Analysis Techniques. The interactive feature selection approach described by Pichler and Perone (*15*) was used to identify good feature combinations. This consisted of a one-dimensional k-nearest neighbor (kNN) analysis followed by multidimensional kNN analyses of all possible combinations of the best features that were identified by the one-dimensional analysis. Feature space plots and nonlinear mappings (*16*) of the best combinations were used to verify clustering of the different classes. For all kNN analyses, $k = 1$ was used.

Q-type principal components analyses using correlation about the mean (R_m) as the dispersion matrix were also used (*17*). This type of analysis identifies compounds with similar patterns of variation in their features. Interpretation of the results was based on a comparison of the factor loadings for each compound. Similar compounds were identified by similar loadings.

RESULTS AND DISCUSSION

Two of the compounds included in the data set contained multiple electroactive groups. These were *p*-nitroacetophenone and *m*-nitrobenzaldehyde. Since the peak for the reduction of the keto group in *p*-nitroacetophenone was so cathodic that it appeared as a shoulder on the solvent reduction, only the peak for the nitro group was included in the data set. Both of the peaks for *m*-nitrobenzaldehyde were in a usable range and were included in the data set. These compounds were included in the data set for comparison to compounds containing only one of the electroactive groups. It was expected that there would be distortion of the second peak by the tail of the first in *m*-nitrobenzaldehyde. Benzophenone did not fall into any of the electroactive group/skelton combinations, but was included in the data set for comparison with classes 2 and 4 which contain carbonyl functional groups.

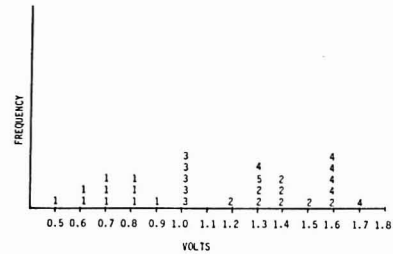

Figure 1. Histogram display of the peak potentials for the curves obtained at 695 mV/s, $\alpha' = 0.3$ for each compound. The numbers refer to the classes defined in Table I

A preliminary visual inspection of the reproduced voltammograms was used to identify any obvious differences in the curves. Two obvious deviations from the normally expected shapes were apparent. Five of the compounds (3, 5, 6, 7, and 10 in Table I) that belonged to the aromatic–nitro group had one or two small shoulders imposed on the main peak in the voltammograms obtained at the slowest scan rate. The extraneous shoulders were probably related to either reactant or product adsorption. Data analysis was based on the main peak. Also, several of the compounds that belonged to the aromatic–aliphatic–ketone class had reduction potentials so cathodic that the solvent reduction was observed in the latter portion of the curve. This was kept in mind when curve shape features were defined.

Three basically different approaches were used to characterize the compounds. They were: (a) comparison of peak potentials, (b) analyses designed to identify systematic differences that resulted from changes in the scan rate, and (c) analyses of features believed to be representative of curve shape. Since no peaks were observed in the reverse scan of each voltammogram, only the forward scan was used for calculation of features.

Comparison of Peak Potentials. Since the voltammetric peak potential depends not only on the electroactive group but also on the skeleton and the position and type of substituents on the skeleton, considerable overlap in the peak potentials for compounds belonging to different classes could exist. To evaluate the discriminatory power of the peak potential for this particular data set, one-dimensional kNN analysis was performed.

The peak potential, in volts, for the curve obtained at 695 mV/s and $\alpha' = 0.3$ for each compound was included in the analysis. One hundred percent predictive accuracy was obtained for the prediction of whether the electroactive group was either nitro or carbonyl. When the compounds were classed according to their electroactive group/skeleton combination, 93.1% predictive accuracy was obtained. The aromatic–nitro and the aliphatic groups were completely resolved. Benzophenone appeared more similar to the aromatic–aldehydes than to the aromatic–aliphatic–ketones. Figure 1 is a histogram display of the distribution of the E_p values for all the compounds in the data set (listed according to class).

Table IV. Peak Potential Difference Features

feature no.	definition[a]
1	$E_{p_3} - E_{p_2}$
2	$E_{p_1} - E_{p_2}$
3	$E_{p_1} - E_{p_3}$

[a] E_{pi} refers to the peak potential for the curve obtained at scan rate i (Table II).

It should be emphasized here that, although peak potential alone is sufficient to classify the compounds in this particular data set with high accuracy, this is an usual situation. That is, Figure 1 shows that nearly the entire working potential range of a mercury electrode is spanned by the E_p values of these four classes. Not only is it fortuitous that the E_p values do not overlap much, but the addition of other classes would necessarily result in overlapped E_p values. Thus, although it is certainly important to utilize E_p values for classification purposes, it is essential that additional class information be provided from the voltammetric behavior. Therefore the classification studies reported below utilizing waveshape and other information were necessary to develop a generally useful method.

Analyses of Features Derived from Scan Rate Dependence. Uncomplicated, irreversible electrochemical systems are often characterized by changes in the peak potential with changes in the scan rate. Even though the systems here may not be completely activation controlled, and the reduction mechanism or its effect on the peak potential may not be known, it is expected that compounds with similar electrode processes might show similar scan rate dependence. Thus, the shift in the peak potential with change in scan rate may be indicative of each class of compounds.

Since the peak potential for the two voltammograms obtained at each scan rate for each compound were essentially identical, only the potential for the voltammogram obtained for $\alpha' = 0.3$ was used in calculation of potential difference features for the three scan rates (Table IV). One-, two-, and three-dimensional kNN analyses of the potential difference features were performed. The results were generally not very good, with the best result being 60% classification accuracy.

For comparison, a Q-type principal components analysis (*17*), using correlation about the mean (R_m) as the dispersion matrix, was performed. The six peak potentials obtained from the set of six voltammograms for each compound were used as features. This type of analysis should identify systematic differences that result from changes in the scan rate. As evidenced by the loadings on the first two factors obtained from the analysis (Table V), most of the compounds had high loadings on factor number 1, indicating a similar scan rate dependence. Compounds 4, 5, 6, 10, 16, 25, and 27, all had high loadings on factor 2 indicating that they had similar scan rate dependence but were different from the others. Apparently, the range of scan rates was not large enough to make any class differences obvious, or the peak potentials for these compounds do not exhibit much scan rate dependence.

Changes in the peak current with changes in scan rate may also be characteristic of the mechanism of reduction for the compounds. To identify any systematic differences, a Q-type principal components analysis (R_m as the dispersion matrix) was performed, using the six values of i_p/CA for each compound, where A is the electrode area and C is the sample concentration. The results again suggested that all compounds, except for *m*-tolualdehyde, were very similar in their scan rate dependence. Apparently, under the conditions used here, there is no dependence of the peak current on the scan rate that can be used to distinguish between the different classes of compounds.

Table V. Loadings on the First Two Factors Resulting from the Principal Components Analysis of the Six Peak Potentials for Each Compound

compound reference no.	loadings	
	factor 1	factor 2
1	0.99	0.13
2	0.92	0.37
3	0.96	−0.3
4	0.37	0.92
5	−0.4	0.91
6	−0.5	0.88
7	−0.9	0.45
8	0.96	0.27
9	0.98	−0.2
10	−0.2	0.97
11	0.99	0.07
12	0.99	0
13	0.99	0.15
14	0.73	0.68
15	0.90	0.36
16	0.66	0.74
17	0.96	0.23
18	0.99	−0.1
19	0.99	−0.1
20	0.98	0.18
21	0.98	0.11
22	0.97	0.20
23	0.99	0.09
24	0.95	0.27
25	0.32	0.93
26	0.92	0.33
27	0.50	0.85
28	0.98	−0.2
29	0.99	−0.1
30	1.0	0.04

Table VI. Classification Accuracy for Fourier Coefficient Ratio Features[a]

class 1	60.0%
class 2	77.8%
class 3	80.0%
class 4	66.7%
overall	70.0%

[a] Ratio features No. 24, 27, 53 (*18*).

The last set of analyses of systematic differences that resulted from a change in scan rate involved the ratios of Fourier coefficients obtained from the voltammograms at different scan rates. This type of feature would be indicative of changes in curve shapes with scan rate. Such changes should be different with different mechanisms of reduction.

The ratios were formed from the coefficients obtained from the discrete Fourier Transform of the portion of the curve between data points 11 and 74. This portion of the curve was chosen because it contained the least amount of extraneous information, as discussed in later sections. There were six ratios derived from each of the first 50 coefficients. The six ratios for each coefficient were the ratio of the value of that coefficient for each curve obtained at each scan rate to the values of that coefficient for each curve obtained at a different scan rate. One-, two-, and three-dimensional kNN analyses were performed. The classification accuracies for the best combination of features are shown in Table VI. As shown in Figure 2, there is some clustering of the members of each class. The obvious outliers were compounds 3, 6, 7, 13, 26, and 27. Most of the class 1 compounds that show significant scatter were those that had multiple peaks in the voltammograms obtained at the slowest scan rate.

The clustering of the different classes was better for these features than for those previously defined and tested. However, because there is a significant amount of scatter in

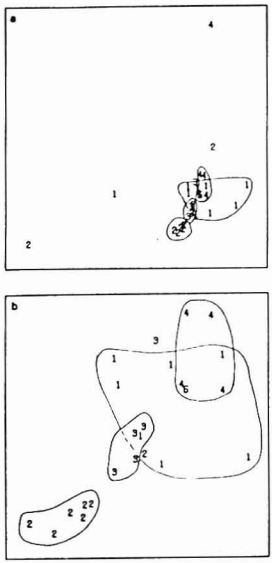

Figure 2. (a) Nonlinear map of Fourier coefficient ratio features 23, 39, and 59 (*18*). All compounds are included. The numbers refer to the classes defined in Table I. Overall kNN classification accuracy was 67% for this feature set. (b) Expanded scale for the main cluster in Figure 2a

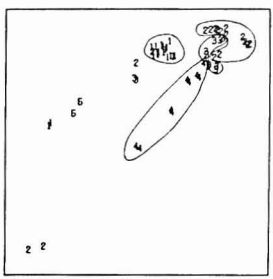

Figure 3. Nonlinear map of voltammetric shape features 7, 8, and 11 (Table III) for the curves obtained at 695 mV/s for all compounds. The numbers refer to the classes defined in Table I

the class 1 compounds, the reported kNN classification accuracies are not as good as the visual clustering would suggest. That is, the clustering of classes 2, 3, and 4 is a strong indication that reproducible differences actually do exist between the different classes.

Analyses of Curve Shapes. The first set of shape features to be tested were the voltammetric features defined by Table III. The data set was divided into three groups according to scan rate. Features 7, 8, and 11 (Table III) were found to give the best classification for each set. The best clustering occurred for the curves taken at 695 mV/s (Figure 3). The obvious outliers are compounds 3, 18, 23, 27. In most cases the nearest neighbors are the two curves obtained at $\alpha' = 0.7$ and $\alpha' = 0.3$ for each compound. Thus, to obtain a realistic estimate of the classification accuracy, kNN analyses were performed using only the curve obtained at 695 mV/s and $\alpha' = 0.3$ for each compound. Analyses were done on two data sets. The first set included all the compounds (except benzophenone), while the obvious outliers were removed from this data set for the second analysis. The results are shown in Table VII, illustrating that removal of the outliers greatly improves the classification accuracy.

Table VII. kNN Classification Results for Voltammetric Shape Features 7, 8, and 11 (Table III)

class	classification accuracy, %
all compounds included	
1	70.0
2	66.7
3	40.0
4	50.0
overall	63.3
optimized data set (Compounds 3, 18, 23, 25, 27 removed)	
1	88.9
2	85.8
3	50.0
4	80.0
overall	80.0

Table VIII. kNN Classification Results for Fourier Coefficient Features

class	classification accuracy, %
all compounds included (except no. 25)	
1	50.0
2	44.5
3	40.0
4	66.7
overall	50.0
optimized data set (compounds 3, 6, 10, 18, 23, 25, 27 removed)	
1	71.4
2	57.1
3	50.0
4	80.0
overall	65.2

The next set of features to be analyzed was the Fourier coefficients obtained from the discrete Fourier Transform of the voltammetric curves. It was found that the portion of the curve between data points 11 and 74 yielded the coefficients with the better discriminatory power, based on one-, two-, and three-dimensional kNN analyses. (No information after data point 74 was reliable since the solvent reduction began to appear at that point in some of the class 4 curves.) Several 3-dimensional combinations of Fourier coefficients 4, 5, 7, 25, 36, and 41 provided overall classification accuracy between 71.7 and 73.4% (*18*). Inspection of the nonlinear maps for these combinations indicated that, again, there was a considerable amount of scatter in the class clusters when all the curves were included.

Further comparisons were made by dividing the data set into the three scan rate groups used earlier. The best results were for the curves obtained at 695 mV/s. kNN analyses were then performed on a data set consisting of one curve (695 mV/s, $\alpha' = 0.3$) for each compound (except benzophenone) and a data set with the obvious outliers removed. The results for the best combination of features (coefficients 4, 5, 36) are summarized in Table VIII.

The type of classification deviations seen with the Fourier coefficients was similar to those observed with the voltammetric features. For example, the class 2 compounds all showed significant differences in the shapes of the two curves obtained at the fastest scan rate. Many of the same outliers

were identified by both sets of features.

CONCLUSIONS

While the analysis of peak potentials yielded the most accurate classification results for the data set used here, these are not generally reliable, and other features must be considered. Curve shape features were very useful for classification of the voltammograms obtained here. Both the voltammetric features and the Fourier coefficients appeared to contain similar class information and were reasonably good features. Classification based on scan rate dependence of Fourier coefficients was also significant.

The fact that the best class clusters were obtained for the curves taken at 695 mV/s indicates that a scan rate in this range may provide the most reliable information. At this scan rate, and the α' values used, data were obtained with negligible charging current contributions. Since some of the curves taken at $\alpha' = 0.7$ for the fastest scan rate had different shapes from those taken at $\alpha' = 0.3$, charging current may have been a contributing factor. Problems with extraneous shoulders on the main peaks obtained at slow scan rates for some compounds were mentioned earlier. These deviations observed at the fastest and slowest scan rates were partially the cause for errors in classification based on scan rate dependence.

The results indicate that benzophenone (No. 25) probably belongs to a different class of compounds than the four that were represented in the data set. The peak for the reduction of the carbonyl group in *m*-nitrobenzaldehyde (No. 27) was obviously distorted by the tail of the first reduction peak. The reasons for the other outliers are not obvious. They are probably different because of a change in the reduction mechanism, a change in the value of αn, or complications such as adsorption.

Considering the limited data set used, the results obtained here were very encouraging. It does appear that functional group and some structural information can be identified in voltammetric waveforms by the application of empirical pattern recognition methods. Thus, further studies are warranted, utilizing a more extensive data base. This study has provided a basis for further work by identifying useful data acquisition conditions, analysis approaches, and features.

ACKNOWLEDGMENT

The authors thank Lars Kryger for his contributions in the early stages of this project.

LITERATURE CITED

(1) P. Zuman, "Topics in Organic Polarography", Plenum Press, New York, N.Y., 1970.
(2) B. Kastening in "Progress in Polarography", Vol. 3, P. Zuman, I. Kolthoff, and L. Meites, Ed., Wiley-Interscience, New York, N.Y., 1972.
(3) P. Zuman, "Substituent Effects in Organic Polarography", Plenum Press, New York, N.Y., 1967.
(4) J. J. Zipper and S. P. Perone, *Anal. Chem.*, **45**, 452 (1973).
(5) D. R. Ferrier and R. R. Schroeder, *J. Electroanal. Chem., Interfacial Electrochem.*, **45**, 343 (1973).
(6) R. S. Nicholson and I. Shain, *Anal. Chem.*, **36**, 704 (1964).
(7) H. Clark, "Determination of Hydrogen Ions", Williams and Wilkins Co., Baltimore, Md., 1928.
(8) Q. V. Thomas, Lars Kryger, and S. P. Perone, *Anal. Chem.*, **48**, 761 (1976).
(9) D. R. Burgard, S. P. Perone, and J. L. Wiebers, *Biochemistry*, **16**, 1051 (1977).
(10) L. Meites, *Anal. Chim. Acta*, **18**, 364 (1958).
(11) L. B. Sybrandt and S. P. Perone, *Anal. Chem.*, **44**, 2331 (1972).
(12) Q. V. Thomas and S. P. Perone, *Anal. Chem.*, **49**, 1369 (1977).
(13) Q. V. Thomas, R. A. DePalma, and S. P. Perone, *Anal. Chem.*, **49**, 1376 (1977).
(14) J. W. Hayes, D. E. Glover, and D. E. Smith, *Anal. Chem.*, **45**, 277 (1973).
(15) M. A. Pichler and S. P. Perone, *Anal. Chem.*, **46**, 1790 (1974).
(16) K. Fukunaga, "Introduction to Statistical Pattern Recognition", Academic Press, New York, N.Y., 1972, Chapter 10.
(17) R. W. Rozett and E. M. Petersen, *Anal. Chem.*, **47**, 1301 (1975).
(18) D. R. Burgard, Ph.D. Thesis, Purdue University, 1977.

RECEIVED for review February 21, 1978. Accepted May 22, 1978. Work supported by the Office of Naval Research.

Optoacoustic Spectrometry in the Near-Infrared Region

M. J. Adams,* B. C. Beadle, and G. F. Kirkbright

Chemistry Department, Imperial College of Science and Technology, London S.W.7., U.K.

A single-beam optoacoustic spectrometer is described for operation in the near-infrared spectral region. Correction for variations in source emission intensity with wavelength is achieved sequentially with the aid of a digital scan recorder. The instrument has been employed for the examination of the absorption bands observed from a variety of sample types.

In recent years there has been considerable interest in the optoacoustic effect and its applications for analysis in optoacoustic spectrometry (OAS) for the study of the ultraviolet and visible absorption spectra of solid and solution samples. Several OAS spectrometers have been described in the literature for studies in this spectral region (*1–3*). OAS monitors the heating effect produced by the absorption of electromagnetic radiation and the corresponding rise in pressure of a filler gas contained with the sample in a sealed cell of constant volume. The periodic pressure variations within the cell, achieved by modulation of the incident radiation, are measured with the aid of a sensitive microphone. Several advantages of the technique over conventional optical transmission and reflectance spectrometric methods of analysis have been proposed, including the ability to examine a wide variety of sample types and optically opaque materials. Rosencwaig has reported the use of OAS in studies of inorganic (*4*) and biochemical (*5*) samples, and Adams et al. (*6*) have recently employed the technique as a calorimetric method for the determination of absolute fluorescence quantum efficiencies.

As a pressure transducer is employed to monitor indirectly the periodic temperature changes occurring within a sample following the absorption of radiation, no photometric detector is required and, provided the incident radiation is of sufficient power to produce a measurable signal, the optoacoustic effect may be employed in any spectral region. To date, the majority of the studies undertaken with condensed phase samples have been concerned with the ultraviolet-visible region. Adams et al. (*1*), however, have recently described a double-beam optoacoustic spectrometer employing a high-pressure xenon arc continuum source capable of operation within the spectral range, 250 nm to 2.5 μm. Unfortunately, rare-gas continuum sources exhibit intense line emission in the near-infrared, thus making difficult the correction of spectra for the variation in

0003-2700/78/0350-1371$01.00/0

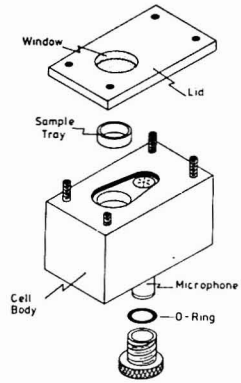

Figure 1. The optoacoustic cell

source emission intensity with wavelength.

Absorption bands observed in the near-infrared spectral region, 0.75 to 2.5 μm may usually be attributed to low-energy electronic transitions or the harmonics (overtones) and combinations of fundamental vibrational modes observed in the molecular species examined. The overtone bands arise from the anharmonicity of the molecular vibrations and combination bands are observed in polyatomic species due to interactions between functional group vibrations. The overtone vibrational frequencies most commonly examined in the near-infrared region are hydrogenic systems, particularly those of -CH and -OH.

This paper reports the use of a single-beam optoacoustic spectrometer in the near-infrared spectral region; a tungsten filament source is employed and sequential correction of spectra for variation in source emission intensity with wavelength is undertaken with the aid of a digital storage scan-recorder. The application of this spectrometer to the study of a variety of sample types is described.

EXPERIMENTAL

Apparatus. The source employed is a 250-W quartz-halogen, tungsten-filament bulb (Type Al/233, Wotan Lamps Ltd., London, U.K.) operated at 25 V/dc. The radiation from the source is focused, using a concave, front-surfaced mirror, through a variable speed rotating sector mounted at the entrance slit of a $f/4$ monochromator. The optical system employed has been described previously (2). Studies in the near-infrared region were undertaken with a plane (300 lines mm^{-1}, 50 mm × 50 mm) grating, blazed at 2.0 μm and with fixed, 2.5-mm wide, entrance and exit slits. This arrangement provided for a reciprocal linear dispersion at the exit slit of 12 nm (0.012 μm) mm^{-1}. To prevent overlapping spectral orders of diffraction being transmitted to the optoacoustic cell, low-wavelength cut-off filters were positioned at the exit slit of the monochromator. The spectral transmission range of the two filters employed was 0.8–1.5 μm and 1.5–2.7 μm. The radiation from the exit slit of the monochromator was focused into the optoacoustic cell by means of a concave mirror.

The optoacoustic cell employed is shown in Figure 1 and is similar to that described by McClelland and Knisely (7). The cell was constructed from aluminum with a 20-mm diameter silica entrance window. A type 4166 capacitor microphone (Bruel and Kjaer Ltd., Hounslow, U.K.) was employed as the pressure transducer. The polarization voltage (240 V) and preamplifier voltage (25 V) for the microphone were supplied from a dry-battery source. Samples were placed in highly polished aluminum cups (16-mm i.d., 3–5 mm deep) and sealed within the cell by means of four locking-nuts.

The optoacoustic signal at the microphone transducer was led directly to a lock-in amplifier (model 186, Princeton Applied Research Corp., Princeton, N.J.); the reference signal was derived from the rotating sector. The output from the lock-in amplifier was led to a digital scan-recorder system (Model 4101, PAR Corp., Princeton, N.J.). This recorder was employed in the two-channel mode to store the reference (lamp emission) spectrum and a sample spectrum. Spectral correction was achieved with the aid of the internal ratiometer unit. The corrected optoacoustic spectra were displayed on a conventional potentiometric chart recorder. All the optoacoustic spectra reported were obtained with a wavelength scan-rate of 300 nm min^{-1} and an amplifier time constant of 1 s.

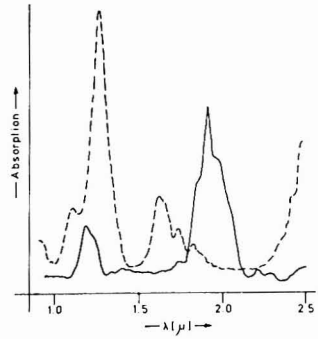

Figure 2. The near-infrared optoacoustic spectra of (—) holmium oxide and (- - -) dysprosium oxide

Reagents. The rare-earth oxides were obtained as high purity, fine powders (Johnson Matthey Ltd., London, U.K.). Type 60 silica gel, TLC grade, was employed for the -OH studies (Merck, Darmstadt, Germany). The *n*-hexane and benzene mixtures were prepared with laboratory grade reagents and the crude oil samples were supplied by Shell Research Ltd. (Thornton, U.K).

Procedure. The source emission spectrum (reference) was obtained by recording the OAS spectrum of a silica plate coated with carbon black; the blackbody absorption characteristics of this sample were confirmed by comparison of the spectrum with the source emission spectrum obtained with a calorimeter detector as described previously for ultraviolet-visible studies (8).

Samples were examined by placing the powder (ca. 100 mg) or solution (ca. 100 μL) into the alumimum sample cup and sealing this into the optoacoustic cell.

RESULTS AND DISCUSSION

Low Energy Electronic Transitions. Electronic transitions in molecular species characteristically occur in the ultraviolet-visible region of the spectrum. However, many inorganic compounds exhibit low-energy transitions which may be examined by their near-infrared absorption spectra. Figure 2 shows the absorption spectra of two rare-earth oxides in the 1 to 2.7 μm spectral region. As with the UV-visible spectra of these materials, the electronic transitions are observed as intense, narrow absorption bands due to the shielding of the 4f electrons (9). The rare-earth oxides absorption bands are well defined and may be employed for wavelength calibration of the spectrometer.

-OH Absorption Bands. The fundamental oxygen–hydrogen vibrations of a nonbonded hydroxyl group (water) occur at ca. 2.7 to 2.8 μm and the first overtone at ca. 1.4 μm; the combination band is observed at 1.9 μm. For bonded hydroxyl groups, the first overtone is apparent also at 1.4 μm but the combination band occurs at 2.2 μm. Thus, near-infrared absorption studies may be employed to characterize the nature of -OH groups present in a sample.

Figure 3 shows several optoacoustic spectra obtained from samples of TLC grade silica gel. The activity of this material for thin-layer chromatography depends on the surface hy-

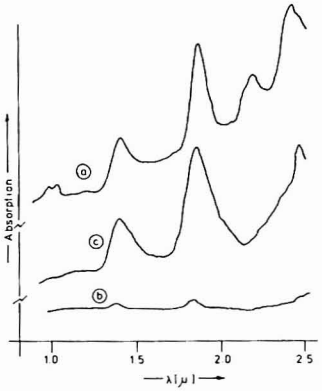

Figure 3. The near-infrared optoacoustic spectra of TLC grade silica gel; (a) untreated, (b) after drying at 1000 °C, and (c) after drying at 1000 °C and exposure to water vapor

droxyl groups bound to the silica. It is evident from the spectrum of the untreated sample (Figure 3a) that both bound hydroxyl groups (1.4 and 2.2 μm) are present as well as surface water (1.4 and 1.9 μm). After drying this sample at ca. 1000 °C, the activity of the silica gel is destroyed and, as shown in Figure 3b, this is accompanied by a loss in –OH absorption bands. Figure 3c demonstrates how, upon exposure to water vapor, the preheated silica gel may adsorb water (1.4 and 1.9 μm) but does not regain the bonded hydroxyl groups necessary for TLC activity.

–CH Absorption Bands. The fundamental carbon–hydrogen stretching vibration absorption band is observed normally at ca. 3.3–3.5 μm, and the first overtone at ca. 1.7 μm. In practice, however, numerous absorption bands are observed in the near-infrared due to C–H bending overtones and the many combination bands possible. As the separation of C–H overtones is greater than that between the fundamentals from which they arise, the near-infrared region may be employed for their identification and characterization.

The optoacoustic spectra of a series of aromatic samples are shown in Figure 4 and compared with an aliphatic system, *n*-hexane. The similarities in the aromatic hydrocarbons are evident and the differences may be attributed to physical nature of the sample, i.e., its solid or liquid nature.

The aromatic C–H absorption band at 2.2 μm was observed not to occur in aliphatic systems and was employed as a means of quantitive analysis for aromaticity in organic mixtures. The absorption band intensities have been shown to be additive, according to the number of absorption centers in a molecule (*10*). Mixtures of benzene in *n*-hexane were prepared and 100-μL aliquots of these examined by OAS. A linear relationship was observed between peak-height, at 2.2 μm, and benzene concentration between zero and 100% benzene in the samples. Figure 5 shows the OAS spectra of undiluted Iranian crude oil samples to which standard additions of benzene have been made; linear plots were obtained for peak-height, at 2.2 μm vs. concentration of benzene present.

CONCLUSION

The single-beam optoacoustic spectrometer described enables the study of absorption spectra in the near-infrared region. Unlike the majority of spectrometers described in the literature, the system discussed employs a relatively low power tungsten filament continuum source. While rare-gas filled arc-lamps have a greater radiant flux and are suitable for use

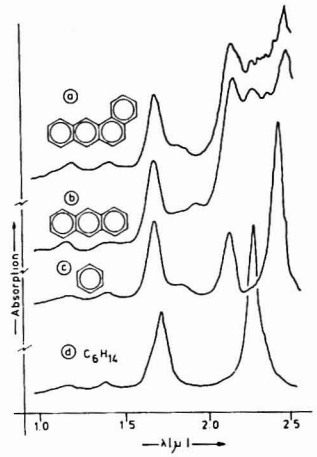

Figure 4. The near-infrared optoacoustic spectra of (a) benzanthracene, (b) anthracene, (c) benzene, and (d) *n*-hexane

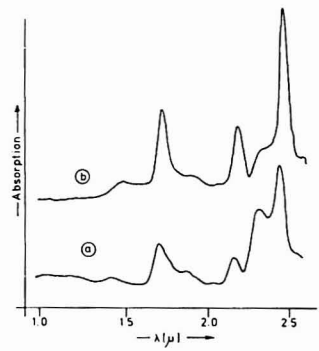

Figure 5. The near-infrared optoacoustic spectra of Iranian crude oil with standard additions of (a) 10% benzene, (b) 30% benzene

in the ultraviolet regions, their use is limited in the near-infrared because of the intense narrow line emission superimposed on the continuum background, thus making double-beam operation difficult to achieve. The tungsten filament source described above provides a near blackbody emission spectrum with an emission wavelength maximum, with the above spectrometer, at ca. 1.4 μm.

The use of the spectrometer to examine a variety of sample types has been described and clear spectra have been obtained from solid powder, solution, and thixatropic oil samples. The near-infrared spectral region may be employed for the examination and characterization of inorganic and organic materials by the absorption bands in this region because of low energy electronic transitions, overtone bands, and combination bands. With the advantages already proposed for OAS, the extension of the working spectral range to include the near-infrared, as described above, should provide for many further applications of the technique in the examination of materials which are normally difficult to study. Quantitative analysis is possible in the near-infrared and, as described, may be employed for the determination of aromaticity in organic mixtures.

ACKNOWLEDGMENT

We are grateful to the Department of Industry for the provision of a studentship to one of us (B.C.B.).

LITERATURE CITED

(1) M. J. Adams, B. C. Beadle, and G. F. Kirkbright, *Analyst (London)*, **102**, 569 (1977).
(2) D. M. Munroe and H. Reichard, *Am. Lab.*, **9**, 119 (1977).
(3) A. Rosencwaig, *Rev. Sci. Instrum.*, **48**, 1133 (1977).
(4) A. Rosencwaig and E. Pines, *Biochim. Biophys. Acta*, **493**, 10 (1977).
(5) A. Rosencwaig, A. P. Grisberg, and J. W. Koepke, *Inorg. Chem.*, **15**, 2540 (1976).
(6) M. J. Adams, J. G. Highfield, and G. F. Kirkbright, *Anal. Chem.*, **49**, 1850 (1977).
(7) J. F. McClelland and R. N. Knisely, *Appl. Opt.*, **15**, 2967 (1976).
(8) M. J. Adams, A. A. King, and G. F. Kirkbright, *Analyst (London)*, **101**, 73 (1976).
(9) W. B. White, *Appl. Spectrosc.*, **21**, 167 (1967).
(10) O. H. Wheeler, *Chem. Rev.*, **59**, 629 (1959).

RECEIVED for review March 13, 1978. Accepted May 24, 1978.

Evaluation and Optimization of the Standard Addition Method for Absorption Spectrometry and Anodic Stripping Voltammetry

J. P. Franke* and R. A. de Zeeuw

State University, Laboratory for Pharmaceutical and Analytical Chemistry, Department of Toxicology, Ant. Deusinglaan 2, 9713 AW Groningen, The Netherlands

R. Hakkert

State Unversity, Mathematical Institute, Groningen, The Netherlands

For the determination of the concentration of a substance by standard addition linear regression, which may be applied when the measurements have a common variance, is compared with other regression techniques based on the assumption of a common coefficient of variation. The latter assumption may be more realistic for atomic absorption spectrometry and anodic stripping voltammetry. For the optimization of the standard addition method, assuming a common coefficient of variation, formulas are given to calculate, for a desired precision, the amount of standard to be added and the required number of replicate measurements. Optimum precision is obtained by applying a single addition of the largest possible amount of standard within the linear range of the response concentration curve.

The method of standard addition is often used (*1–3*) to determine the unknown concentration, ξ_o, of a substance in a solution: new solutions are made from the original one by adding successive, known amounts of that substance. Thus, solutions with concentrations ξ_o, $\xi_o + x_1$, ..., $\xi_o + x_k$ are obtained, where $x_1 < x_2 < ... < x_k$ are known positive constants. For each solution several response-readings can be obtained, leading to a set of data $[y_{ij}; j = 1, ..., n_i; i = 0, ..., k]$, where y_{ij} represents the jth response-reading on the sample with concentration ξ_o (if $i = 0$) or $\xi_o + x_i$ (if $i \neq 0$). The statistical analysis will be based on the idea that the response-readings y_{ij} are the outcome of corresponding random variables Y_{ij}, whose joint distribution is such that (1) all Y_{ij} are mutually independent; (2) Y_{i1}, ..., Y_{in_i} is a random sample from the normal distribution with $EY_{ij} = \mu_i$ and $\mathrm{Var}(Y_{ij}) = \sigma_i^2$; (3) after appropriate corrections have been made for any background signal, the concentration–response curve is a straight line passing through the origin, or, more precisely, for some unknown regression coefficient, β, it is assumed that $\mu_i = \beta(\xi_o + x_i)$.

Apart from these basic assumptions, various additional ones can be made with respect to the variances σ_o^2, ..., σ_k^2. Most authors, using standard regression methods to estimate ξ_o (*4, 5*), implicitly assume homoscedasticity, i.e., $\sigma_o^2 = \sigma_1^2 = ... = \sigma_k^2$.

However, theoretical considerations of Mann et al. (*6*) and our own experimental data contain evidence (Section 4) that this assumption is not always relevant. It rather looks as if $\sigma_o^2 < \sigma_1^2 < ... < \sigma_k^2$. If sufficient replicate measurements in $o, x_1, ..., x_k$ are available, it is possible to estimate σ_o^2, ..., σ_k^2 separately. If, however, no such replications are available, one has to make some sort of model-assumption. It might be more realistic to assume equality of the coefficients of variation, i.e., $\sigma_o/\mu_o = \sigma_1/\mu_1 = ... = \sigma_k/\mu_k$.

Mann et al., dealing with absorption spectrometry (*6*) and Larsen et al. (*4*), whose data are presented in Section 4, suggested that the latter assumption approximately holds true in the absorption range between 0.2 and 1.0 (*6*).

The basic assumptions 1, 2, and 3 mean in practice that: (1) Each addition of standard should be made to the original sample, without appreciable error, and for each solution the response-readings should be obtained independently. (2) Response-readings, Y_{i1}, ..., Y_{in_i} are an independent random sample from a normal distribution. Generally speaking this will be valid for atomic absorption spectrometry and anodic stripping voltammetry (*7*). Fortunately, small deviations from normal distributions will not have a large effect on the merits of the statistical procedures. (3) The linearity of the concentration-response curve should be checked by experiments over a wide concentration range. By application of standard addition, one should check that the highest concentration is still within the linear part of the curve and the slope of the curve should remain unaffected by the addition of standard.

Figure 1 summarizes the necessary terminology. Here, $k = 3$; $n_o = 3$; $n_1 = 3$; $n_2 = 4$; $n_3 = 3$ and the individual response-readings y_{ij} are represented by the open circles. The dotted regression line is specified by the unknown parameters ξ_o and β, or, alternatively, by the usual regression-parameters, $\alpha = \mu_o$ and β. Note that $\xi_o = \alpha/\beta$.

In the next section the two existing calculation methods, the graphical method and standard linear regression are evaluated. So far, little or no attention has been paid to the effects of replicating the response-measurements on the

0003-2700/78/0350-1374$01.00/0

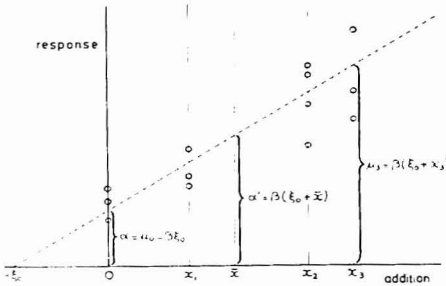

Figure 1. Graphic representation of the standard addition method. ξ_o is the concentration of the sample without addition of standards with response readings $Y_{o,1}$, ..., $Y_{o,n}$. X_1, X_2, X_3 are the added concentrations with $Y_{1,1}$, ..., Y_{1,n_1}, $Y_{2,1}$, ..., Y_{2,n_2}, and $Y_{3,1}$, ..., Y_{3,n_3} response measurements, respectively. Each open circle represents a single response measurement. The dotted line represents the regression line, described by the Equation $Y = \alpha + \beta x$

precision of the obtained estimate for ξ_o. These effects will be evaluated for the graphical method, assuming equality of the coefficients of variation.

In Section 3 some approximate regression-methods will be presented for the case of equal constants of variation, and again the effects of replications on the precision of the obtained estimate will be evaluated.

In Section 4 the two different regression models are discussed in the context of data, presented by Larsen et al. (*4*), and our own data.

2. Existing Techniques. A. The case $k = 1$ is of special interest as it can be shown that this case represents the optimum design, provided x_i is chosen as large as possible within the linear range of the response-concentration curve. Suppose that

$$Y_{i.} = \frac{1}{n_i}\sum_{j=1}^{n_i} Y_{ij}$$

($i = 0,1$) with $n = n_o + n_1$. According to the graphical method, an estimate x_o for ξ_o can be calculated from the relation

$$x_o/(x_o + x_1) = Y_{o.}/Y_{1.} \tag{2.1}$$

which leads to

$$x_o = x_1\, Y_{o.}/(Y_{1.} - Y_{o.}) \tag{2.2}$$

Similarly, β can be estimated by

$$\beta = (Y_{1.} - Y_{o.})/x_1 \tag{2.3}$$

Assuming equality of the constants of variation, an approximation for the variance of the estimator can be calculated as follows. According to Reinmuth (*8*), $\mathrm{Var}(x_o)$ can be approximated by

$$\mathrm{Var}(x_o) \simeq \left(\frac{\partial x_o}{\partial Y_{o.}}\right)^2 \mathrm{Var}(Y_{o.}) + \left(\frac{\partial x_o}{\partial Y_{1.}}\right)^2 \mathrm{Var}(Y_{1.}) \tag{2.4}$$

Substituting (2.2) in (2.4) we obtain

$$\mathrm{Var}\,(x_o) \simeq \left(\frac{x_1 Y_{1.}}{(Y_{1.} - Y_{o.})^2}\right)^2 \mathrm{Var}\,(Y_{o.}) + \left(\frac{-x_1 Y_{o.}}{(Y_{1.} - Y_{o.})^2}\right)^2 \mathrm{Var}(Y_{1.}) \tag{2.5}$$

Denoting the common coefficient of variation by θ, and applying the following approximation,

$$\mathrm{Var}(Y_{1.})/Y_{1.}^2 \simeq \theta^2/n_i \tag{2.6}$$

one obtains:

$$\mathrm{Var}(x_o) \cong x_o^2\,\theta^2\left(1 + \frac{x_o}{x_1}\right)^2\left(\frac{1}{n_o} + \frac{1}{n_1}\right) \tag{2.7}$$

This equation shows that the relative error in x_o decreases with increasing x_1, n_o, and n_1, and, for fixed values of $n(n_o + n_1)$ and x_1, reaches a minimum for $n_o = n_1$. This agrees with the statements of Meites (*1*): optimum precision is obtained by applying a single addition of the largest possible amount of standard within the linear range of the response–concentration curve, and dividing the replications equally among this sample and the original one.

B. Alternatively, if $k > 1$, ξ_o may be estimated by standard linear regression. Ideally, this procedure requires homoscedasticity, i.e., $\sigma_1^2 = \sigma_2^2 = \ldots = \sigma_k^2 = \sigma^2$. In order to be able to carry out generalizations in Section 3, a more general approach will be presented here, namely, weighted standard regression.

Suppose that $\mathrm{Var}(Y_{ij}) = \sigma^2/w_i$, where w_o, ..., w_k are known constants, then the standard estimators a', b, and S^2 for α', β, and σ^2 are somewhat modified. Suppose that $C = 1/\sum_i n_i w_i$, $\bar{x} = C\sum_i n_i w_i x_i$, $x_i' = x_i - \bar{x}$, $D = 1/\sum_i n_i w_i (x_i')^2$ and $\alpha' = \alpha + \beta\bar{x}$, then a_i', b, and S^2 are given by:

$$a' = C\sum_{i,j} w_i Y_{ij} \sim N(\alpha', C\sigma^2) \tag{2.8}$$

$$b = D\sum_{i,j} w_i x_i' Y_{ij} \sim N(\beta, D\sigma^2) \tag{2.9}$$

$$S^2 = \frac{1}{n-2}\sum_{i,j} w_i (Y_{ij} - a' - bx_i')^2 \sim \frac{\sigma^2}{n-2}\chi^2_{n-2} \tag{2.10}$$

Furthermore a', b, and S^2 are independent and, since $\xi_o = \alpha/\beta$, it can be inferred from Equations 2.8–2.10 that $(a' - b(\bar{x} + \xi_o))/(S\sqrt{C + D(\bar{x} + \xi_o)^2})$ is t_{n-2}-distributed. This formula is known as Fieller's Theorem (*9*). Substituting the confidence limits $\pm t_{n-2,1/2\alpha}$ and solving for ξ_o yields the following well-known confidence interval:

$$\xi_o = \frac{a'b}{b^2 - Dt^2S^2} - \bar{x} \pm \frac{tS}{b^2 - Dt^2S^2}\sqrt{D(a')^2 + C(b^2 - Dt^2S^2)} \tag{2.11}$$

Larsen et al. (*4*), in an atomic absorption study, gave an estimate of the confidence interval for ξ_o by using a simplified version of Equation 2.11.

In the simple case where w_o, ..., w_k are all independently known, Equation 2.11 yields an exact confidence interval. The situation becomes more complicated when w is some function of α and β, as happens in the case of a constant coefficient of variation: $w = 1/(\alpha + \beta x)^2$.

Approximate solutions for this problem will be dealt with in Section 3, but first there are a few general observations to be made about Equation 2.11. Figure 2 depicts the estimation procedure, the dotted line being the estimated regression line and the two enveloping curves the confidence limits for $\alpha + \beta x$ for a given x. It can be proved that the confidence interval for ξ_o is the interval AB. As can be seen in Figure 2, a disadvantage of the use of standard linear regression, even if all prerequisites are fulfilled, is that it results in a large confidence interval for ξ_o. This is particularly true in the case of a relatively low number of measurements, and a large standard error of regression: in this case the use of Equation 2.11 may even result in half-infinite intervals.

A second practical objection to Equation 2.11 is that this equation is difficult to work with. This is particularly disturbing when it has to be applied a number of times in a sequence, as will turn out to be necessary in the next section.

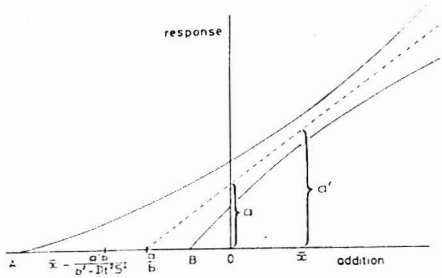

Figure 2. Estimation procedure by standard addition, the dotted line being the estimated regression-line and the two enveloping curves the confidence limits for $\alpha + \beta x$ for a given x. The interval AB is the confidence interval for ξ_o

3. Approximate Solutions for the Case of Constant Coefficient of Variation. A. Supposing that $w_i = 1/(\alpha + \beta x_i)^2$, it is clear that the method of Section 2B can not be applied directly, since the weights w_i are no longer deterministically known. It is possible to obtain a first-order approximation though, using ordinary regression ($w_o = w_1 = \ldots = w_k = 1$) in order to get preliminary estimates for α and β.

These estimates lead to estimates of $w_o, \ldots, w_k$, which, again, can be applied to get a second-order approximation for α and β, and so on. This is a rapidly converging process and, although it is not an exact procedure, it can be shown (lower middle column of Table I) that the results are quite satisfactory. In most circumstances, a second-order estimate will do, as was applied in Table I.

B. A particularly simple solution is obtained by assuming a slightly modified measurements model. Suppose that the experiments could be carried out in such a manner that, instead of adding known amounts of the substance and reading the responses, increasing amounts of substance could be added until the response-readings would reach certain predetermined values, y_{ij}. The appropriate model then seems to be

$$X_{ij} \sim N\left(\frac{1}{\beta}(y_{ij} - \alpha), \left(\frac{\sigma_r}{\beta} y_{ij}\right)^2\right) \qquad (3.1)$$

where $\sigma_r^2 = \mathrm{Var}(X_{ij})/y_{ij}^2$. However, as the experiments are not performed in this way, the method is based on the assumption that the actual data are "not too different" from those wanted in the above mentioned hypothetical manner. What is meant by "not too different" will be explained at the end of this Section.

The calculation of estimators and confidence intervals on the basis of model 3.1 can be carried out as follows. Rewriting the Equation 3.1 with $u = 1/y$, $V = X/y$, $\gamma = 1/\beta$ and $\tau = \sigma_r/\beta$ yields:

$$V_{ij} \sim N(\gamma - \xi_o u_{ij}, \tau^2) \qquad (3.2)$$

Since the problem has now been reduced to the standard homoscedastic form with ξ_o as one of its parameters, the estimators c', x_o and T^2 can be solved directly by means of ordinary regression techniques, analogous to Equations 2.8–2.10 with $C = 1/n$ and $D = 1/\sum_{i,j}(u'_{ij})^2$:

$$c' = C\sum_{i,j} V_{ij} \sim N(\gamma', C\tau^2) \qquad (3.3)$$

$$x_o = -D\sum_{i,j} u'_{ij} V_{ij} \sim N(\xi_o, D\tau^2) \qquad (3.4)$$

$$T^2 = \frac{1}{n-2}\sum_{i,j}(V_{ij} - c' + x_o u'_{ij})^2 \sim \frac{\tau^2}{n-2}\chi^2_{n-2} \qquad (3.5)$$

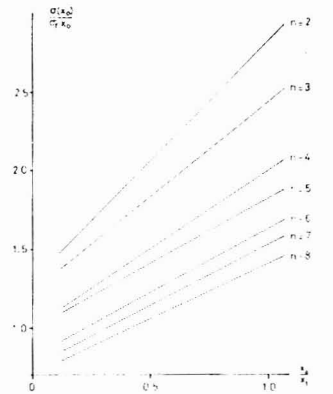

Figure 3. Graphic representation of Equation 3.10 where x_o/X_1 is the ratio of the estimated original concentration and the concentration of added standard, n represents the total number of measurements

For the confidence interval the following simple expression, corresponding to Equation 2.11, is found:

$$\xi_o = x_o \pm DtT \qquad (3.6)$$

For this method, which will be referred to as the transformation method, calculations can be made, similar to the ones in Equations 2.4–2.7. Assuming that $k = 1$, the variance of x_o, Equation 3.4, can be written as follows:

$$\mathrm{Var}(x_o) = \tau^2 \Big/ \left(\sum_{i,j}\frac{1}{y_{ij}^2} - \frac{1}{n}\left(\sum_{i,j}\frac{1}{y_{ij}}\right)^2\right) \qquad (3.7)$$

With the approximations

$$\sum_{i,j}\frac{1}{y_{ij}^2} \cong \frac{n_o}{y_{o.}^2} + \frac{n_1}{y_{1.}^2} \text{ and } \sum_{i,j}\frac{1}{y_{ij}} \cong \frac{n_o}{y_{o.}} + \frac{n_1}{y_{1.}} \qquad (3.8)$$

Equation 3.7 can be transformed into

$$\mathrm{Var}(x_o) = n\tau^2/n_o n_1\left(\frac{1}{y_{o.}} - \frac{1}{y_{1.}}\right)^2 \qquad (3.9)$$

Substituting $\tau = \sigma_R/\beta$ and approximating β by $(y_1 - y_o)/X_1$, Equation 2.3 leads to

$$\mathrm{Var}(x_o) = x_o^2\,\sigma_r^2\left(1 + \frac{x_o}{X_1}\right)^2\left(\frac{1}{n_o} + \frac{1}{n_1}\right) \qquad (3.10)$$

as in Equation 2.7. This equation is graphically reproduced in Figure 3 for some values of n.

Similar equations for $k = 2$ can be derived with the same approximations mentioned above. If $X_2 = 2X_1$, Equation 3.4 can be transformed into

$$\mathrm{Var}(x_o) = x_o^2\sigma_r^2\left(2\frac{x_o}{X_2} + 1\right)^2\left(\frac{x_o}{X_2} + 1\right)^2 n \Big/ \left(n_o n_1\left(\frac{x_o}{X_2} + 1\right)^2 + n_o n_2\left(\frac{2x_o}{X_2} + 1\right)^2 + n_1 n_2\left(\frac{x_o}{X_2}\right)^2\right) \qquad (3.11)$$

This equation is graphically reproduced in Figure 4. The distribution of the replications was carried out in such a manner, for fixed n, $\mathrm{Var}(x_o)/x_o^2$ was minimized.

The Equations 3.10 and 3.11, as reproduced in the Figures 3 and 4 show that:

a. For a fixed value of added standard (X_1,X_2) better

Table I. Outcome of the Three Estimators When Applied to Six Sets of Simulated Data

simulated data $n = 12; N = 1000$	using Fieller's theorem, $w = 1$ (2.B)[e]	using Fieller's theorem, estimated weights (3.A)[e]	using a transformation (3.B)[e]
A. $\alpha = 0.1; \beta = 10; \xi_o = 0.01$	0.00993	0.01034	0.00710[a]
constant var.: $\sigma = 0.05$	0.00231	0.00296	0.00497[b]
$x_1 = 0.5; x_2 = 1.0;$	0.00973	0.00600	0.00350[c]
$x_3 = 2.0$	95%	62.9%	28.5%[d]
B. $\alpha = 2.7; \beta = 15; \xi_o = 0.18$	0.17966	0.18744	0.14346
constant var.: $\sigma = 1$	0.02755	0.04381	0.06558
$x_1 = 0.4; x_2 = 1.85;$	0.11520	0.10014	0.07297
$x_3 = 5.75$	94.8%	70.7%	45.7%
C. $\alpha = 0.2; \beta = 0.18; \xi_o = 1.11111$	1.12116	1.12710	1.07701
constant var.: $\sigma = 0.015$	0.07217	0.08487	0.08902
$x_1 = 0.5; x_2 = 1.0$	0.29971	0.29500	0.28348
$x_3 = 2.0$	95.1%	90%	86.2%
A. $\alpha = 0.1; \beta = 10; \xi_o = 0.01$	0.01125	0.01002	0.01000[a]
constant rel. error:	0.01496	0.00157	0.00034[b]
$\sigma_r = 0.05; x_1 = 0.5; x_2 = 1.0;$	0.10433	0.00224	0.00146[c]
$x_3 = 2.0$	100%	95.2%	94.5%[d]
B. $\alpha = 2.7; \beta = 15; \xi_o = 0.18$	0.18347	0.18081	0.17944
constant rel error:	0.03099	0.00683	0.00683
$\sigma_r = 0.05; x_1 = 0.4; x_2 = 1.85;$	0.23709	0.02930	0.02921
$x_3 = 5.75$	99.9%	94.6%	94.2%
C. $\alpha = 0.2; \beta = 0.18; \xi_o = 1.111$	1.12831	1.12734	1.08796
constant rel. error:	0.08760	0.07157	0.07123
$\sigma_r = 0.05; x_1 = 0.5; x_2 = 1.0;$	0.37219	0.29652	0.28965
$x_3 = 2.0$	96.3%	95.3%	92.7%

[a] Mean estimated ξ_o. [b] Root-mean-square deviation from real ξ_o. [c] Mean length of estimated confidence intervals. [d] Observed percentage of cases where true ξ_o was found to lie within estimated confidence interval. [e] The notation in parentheses refers to the respective paragraphs in the text.

precision of x_o is reached by increasing the total number of measurements (n).

b. With higher values of n, the lines approach each other, thus reducing the effect of an extra measurement.

c. The choice of the amount of added standard is of paramount importance, especially when a low number of response measurements is carried out. High concentrations of X_1 and X_2 within the linear range of the response concentration curves give low ratios of x_o/X_1 or x_o/X_2 and will thus result in smaller relative errors of x_o.

d. For a fixed value of n, (Figure 4) the number of determinations in X_1 (n_1) should be 1 whereas the number of determinations in X_o (n_o) and X_2 (n_2) should be equally divided.

e. For higher values of n, the single determination in X_1 in Figure 4 hardly contributes to obtaining better precision. However, it may serve as a check on the linearity of the response concentration curve between x_o and X_2.

The practical advantages of Figures 3 and 4 are that they allow estimation of the relative error of x_o for those analyses that have a common relative error in the measurements, Y, such as in absorption spectrometry, in which the latter is approximately 0.5% (8). For example, if one wishes to obtain an estimate of the original concentration of solute with a relative error in x_o smaller than 1% ($\sigma(x_o)/\sigma_r x_o < 2$) Figure 3 shows that n should be 4, equally divided over x_o and X_1, provided $x_o/X_1 < 1$. Another possibility is three measurements but then x_o/X_1 should be <0.5. Prerequisites are, of course, that X_1 is still within the linear range of the response concentration curve and that $\sigma_r = 0.005$. The latter condition is valid in the absorption range 0.2–1.0. It should be noted that the method with three measurements has the advantage of saving time.

It still remains to be shown that the transformation method does not lead to serious distortions. Therefore, six sets of normal data, corresponding to three sets (A, B, and C) of actual parameter values and two types of scedasticity (equal variances and equal coefficients of variation) were simulated

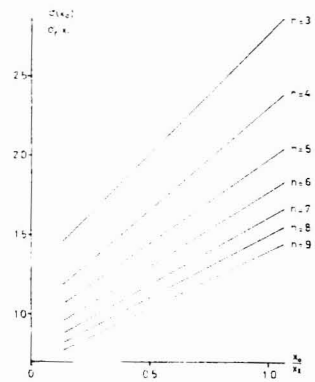

Figure 4. Graphic representation of Equation 3.11, where x_o/X_2 is the ratio of the estimated original concentration and the concentration of the added standard. $X_2 = 2X_1$ and n represents the total number of measurements. The total number of measurements is distributed as follows: $n = 3$: $n_o = n_1 = n_2 = 1$; $n = 4$: $n_o = 2$, $n_1 = n_2 = 1$; $n = 5$: $n_o = n_2 = 2$, $n_1 = 1$; $n = 6$: $n_o = 3$, $n_1 = 1$, $n_2 = 2$; $n = 7$: $n_o = n_2 = 3$, $n_1 = 1$; $n = 8$: $n_o = 4$, $n_1 = 1$, $n_2 = 3$; $n = 9$: $n_o = n_2 = 4$, $n_1 = 1$

1000 times each in order to find out whether these data would be "too different" from the hypothetical data-structure outlined in Equation 3.1. The parameter sets B and C were chosen because of their resemblance to the actual experimental values in Tables II and III. In each of the four points 0, x_1, x_2, and x_3, three "measurements" were simulated and from the thus obtained 12 values, ξ_o was estimated in three different ways.

Inspection of Table I allows a number of conclusions:

Using the wrong estimator, i.e., an estimator requiring

Table II. Evaluation of Common Variance, Common Relative Error and Precision of Atomic Absorption Spectrometry Measurements[a]

concn of added standard, ppm Zn	instrument response readings, absorbance							$Y_{i\cdot}$	$\mathrm{Var}(Y_{ij})$
0	0.197	0.195	0.199	0.195	0.197	0.195	0.197	0.1964	0.00151
0.5	0.291	0.289	0.289	0.287	0.293	0.288	0.287	0.2891	0.00219
1.0	0.381	0.384	0.383	0.382	0.384	0.380	0.384	0.3826	0.00162
2.0	0.556	0.553	0.551	0.561	0.559	0.551	0.553	0.5549	0.00393

Bartlett test on the hypothesis $\sigma_0^2 = \sigma_1^2 = \sigma_2^2 = \sigma_3^2$ (common variance)

$$B = 7.08 > \chi^2_{3,0.90} \text{ and } B < \chi^2_{3,0.95} = 7.81$$

Bartlett test on the hypothesis $\tau_0^2 = \tau_1^2 = \tau_2^2 = \tau_3^2$ (common relative error)

$$B = 1.59 < \chi^2_{3,0.90} = 6.25$$

split F-test for large X values (1.0; 2.0) and small X values (0; 0.5)

$$F = 2.55 > F_{12,\,12,0.90} = 2.15 \text{ and } F < F_{12,\,12,0.95} = 2.69 \text{ (common variance)}$$

$$F = 1.46 < F_{12,\,12,0.90} = 2.15 \text{ (common relative error)}$$

	regression lines;	x_O	±	$t_{26,0.975} \cdot S(x_O)$
standard linear regression:	$Y = 0.199 + 0.179x$	1.110		0.0237
weighted linear regression:	$Y = 0.197 + 0.181x$	1.088		0.0181
using transformation method:	$X/y = 5.511 - 1.087\ 1/y$	1.087		0.0179

[a] Data from Larsen et al. (*4*).

Table III. Evaluation of Common Variance, Common Relative Error and Precision of Differential Pulse Anodic Stripping Voltammetry Measurements[a]

concn of added standard, ppm Tl	instrument response readings, peak current, μA							$Y_{i\cdot}$	$\mathrm{Var}(Y_{ij})$
0	2.53	2.50	2.70	2.63	2.70	2.80	2.52	2.63	0.114
0.387	8.42	7.96	8.54	8.18	7.70	8.34	7.98	8.16	0.297
1.851	29.65	28.70	29.05	28.30	29.20	29.95	28.95	29.11	0.557
5.734	84.8	85.6	86.0	85.2	84.2	86.4	87.8	85.71	1.177

Bartlett test on the hypothesis $\sigma_0^2 = \sigma_1^2 = \sigma_2^2 = \sigma_3^2$ (common variance)

$$B = 24.80 > \chi^2_{3,0.999} = 16.3$$

Bartlett test on the hypothesis $\tau_0^2 = \tau_1^2 = \tau_2^2 = \tau_3^2$ (common relative error)

$$B = 8.50 > \chi^2_{3,0.95} = 7.81$$

split F-test for large X values (1.851; 5.734) and small X values (0; 0.387)

$$F = 16.77 > F_{12,\,12,0.999} = 7.00 \ (\sigma_0^2 = \sigma_1^2 = \sigma_2^2 = \sigma_3^2)$$

$$F = 6.03 > F_{12,\,12,0.99} = 4.16 \ (\tau_0^2 = \tau_1^2 = \tau_2^2 = \tau_3^2)$$

	regression lines;	x_O	±	$t_{26,0.975} \cdot S(x_O)$
standard linear regression:	$Y = 2.508 + 14.499x$	0.1727		0.02466
weighted linear regression:	$Y = 2.605 + 14.300x$	0.1820		0.00560
using transformation method:	$X/y = 0.0695 - 0.1814\ 1/y$	0.1814		0.00555

[a] Data obtained by the method of Franke et al. (*10*).

constant coefficient of variation on homoscedastic data or vice versa, may lead to serious errors.

These errors are particularly spectacular when ξ_o is small (A and B); C does not seem to be very sensitive in this respect. It should be noted, however, that a rigorous research on the sensitivity of different parameter-sets to choosing the wrong estimator has not been undertaken.

Applying an estimator requiring constant coefficient of variation to homoscedastic data leads to underestimating the interval-length, the opposite mistake leads to overestimating the interval-length.

Approximation by means of the transformation model yields reasonable satisfactory estimators and confidence intervals for ξ_o, especially when ξ_o is small.

It should be noted that the risks of applying a homoscedastic estimator to experimental data of unknown scedasticity are smaller than those of applying one of the estimators outlined in this section. When, however, there is a reason to believe that the data are in fact characterized by (nearly) equal coefficients of variation, the latter type of estimation turns out to be superior, as is clearly demonstrated by the simulation-outcomes. Therefore the following rule of thumb seems appropriate:

When the scedasticity of the data is unknown, first test equality of the variances in one of the manners outlined in Section 4.

If this null-hypothesis can be rejected, test the requirements of common coefficient of variation, as is also illustrated in Section 4.

If this null-hypotheses can also be rejected, a homoscedastic estimator is probably safer, especially for large values of ξ_o.

If, however, the latter null-hypothesis (constant coefficient

of variation) seems attractive, it is recommended to use an estimation procedure based on constant coefficient of variation.

4. Actual Experiments. In Tables II and III, the results of experiments by Larsen et al. (*4*) and our own data are displayed. The assumption of equal variances was tested in two ways:

a. By applying a Bartlett-test (*10*), which is possible because of the existence of repeated measurements.

b. By means of a split *F*-test: the data are divided into two groups, one group with low x-values, and one group with high x-values. The error-variances are then estimated for both groups separately and the estimates are compared by means of a *F*-test. This method allows a test of equal variances against a one-sided alternative. Another advantage of this procedure is that it does not require repeated measurements although it does require a minimum of six measurements and at least two standard additions. The assumption of equal constants of variation can be tested in a somewhat similar manner:

a. Dividing the estimated variances of the $k + 1$ groups of repeated measurements by their corresponding group averages $Y_o, \ldots, Y_k$, one arrives at $k + 1$ statistics that may, at least approximately, be taken as a basis for the Bartlett-test.

b. Alternatively one may test the hypothesis that the data are "not too different" from the hypothetical data-structure, Equation 3.1, by applying a split F-test to the transformed variables $u = 1/y$ and $V = X/y$, Equation 3.2. The two tests were applied to the experimental atomic absorption data of Larsen et al. (*4*), the results of which are given in Table II, and to our own data obtained by differential pulse anodic stripping voltammetry (see Table III) (*11*).

For both sets it was observed that the assumption of a common coefficient of variation results in a better fit than the assumption of common variance. For the atomic absorption spectrometry data of Larsen et al., the latter assumption proves to be barely acceptable at a 5% level. At a 10% level, it has to be rejected. The assumption of a common coefficient of variation can be maintained at both levels though.

For our data (Table III) there seems to be no common coefficient of variation. Since, however, the *B*- and *F*-values are much larger when testing common variance than when testing common coefficient of variation, and as ξ_o is relatively small, we may expect the transformation method to yield more accurate results than standard linear regression.

The real scedasticity is probably somewhere in between: no common variance and no common coefficient of variation either.

From the above two sets of experimental data, an estimate, x_o, for ξ_o and for $\mathrm{Var}(x_o)$ have been computed using standard linear regression, weighted linear regression, $w_i = 1/(a + bx)^2$, and the transformation method. The latter two methods yielded the shortest confidence interval for ξ_o, as should be expected according to Table I. Furthermore the transformation model is in good agreement with the weighted linear regression.

CONCLUSIONS

For both atomic absorption spectrometry and anodic stripping voltammetry, more accurate results can be obtained using a linear regression method based upon a common coefficient of variation: weighted linear regression or the transformation model.

Figures 3 and 4 allow optimization of the standard addition method for a given problem and for a desired relative error in the analysis by a proper choice of the total number of measurements and of the amount of added standard. Although this paper deals mainly with absorption spectrometry and anodic stripping voltammetry, being the areas in which standard addition is most frequently applied, it should be emphasized that the above principles can be used equally well for standard addition applications in other areas of analytical chemistry.

List of Symbols

ξ_o, (x_o)	(estimated) unknown concentration of the untreated sample
k	number of additions made
n_i $(i = o, \ldots, k)$	number of replicate measurements in o $(i = o)$ or x_i $(i > o)$.
n	total number of measurements
N	number of simulations
x_i or x $(i = 1, \ldots, k)$	amount of added standard
X_{ij}, X_i, or X $(i = 1, \ldots, k; j = 1, \ldots, n_i)$	amount of added standard, interpreted as a random variable in section 3.B
$\bar{x}$	$= C\sum_{i=1}^{k} n_i w_i x_i$
y_{ij} or y $(i = o, \ldots, k; j = 1, \ldots, n_i)$	jth response-reading in o $(i = o)$ or x_i $(i > o)$
Y_{ij} or Y $(i = o, \ldots, k; j = 1, \ldots, n_i)$	random variable associated with y_{ij} or y
$y_{i\cdot}$ $(i = o, \ldots, k)$	$= (1/n_i)\sum_{j=1}^{n_i} y_{ij}$
$Y_{i\cdot}$ $(i = o, \ldots, k)$	$= (1/n_i)\sum_{j=1}^{n_i} Y_{ij}$
u_{ij}	$= 1/y_{ij}$
$\bar{u}$	$= u - (1/n)\sum_{i,j} u_{ij}$
V_{ij}	$= X_{ij}/y_{ij}$
μ_i $(i = o, \ldots, k)$	$= EY_{ij}$ $(j = 1, \ldots, n_i) = \alpha + \beta x_i$
σ_i^2 $(i = o, \ldots, k)$	$= \mathrm{Var}(y_{ij})$ $(j = 1, \ldots, n_i)$
α, (a)	(estimated) intercept of the regression-line with the Y-axis
β, (b)	(estimated) slope of the regression line
α' (a')	(estimated) $\alpha + \beta\bar{x}$
γ, (c)	(estimated) $1/\beta$
γ', (c')	(estimated) $\gamma - \xi_o\bar{u}$
θ	coefficient of variation, assumed to be equal for all Y_{ij} $(i = o, \ldots, k; j = 1, \ldots, n_i)$
w_i $(i = o, \ldots, k)$	regression-weights
σ^2, (S^2)	(estimated) $\sigma_i^2 w_i$, where w_i $(i = o, \ldots, k)$ are chosen such as to make σ^2 a constant
σ_r^2	$= \mathrm{Var}(X_{ij})/y_{ij}^2$
τ^2, (T^2)	(estimated) σ_r^2/β^2
$\sigma^2(x_o)$, $[S^2(x_o)]$	[estimated] standard-error in x_o
C	$= 1/\sum_{i=o}^{k} n_i w_i$ (weighted regression) $= 1/n$ (transformation method)
D	$= 1/\sum_{i=o}^{k} n_i w_i (x_i')^2$ (weighted regression) $= 1/\sum_{i,j} (u'_{ij})^2$ (transformation method)
x_i' $(i = o, \ldots, k)$	$= x_i - \bar{x}$ $(i > o)$ or $-\bar{x}$ $(i = o)$
t	$= t_{n-2,\ 1/2\,\alpha}$
B	test-statistic of the Bartlett-test
F	test-statistic of the split F-test

ACKNOWLEDGMENT

The authors thank W. Schaafsma (Mathematical Institute,

State University, Groningen) for his interest and advice in this study.

LITERATURE CITED

(1) L. Meites, "Polarographic Techniques", 2nd ed., Interscience Publishers, New York, N.Y., 1965.
(2) H. H. Willard, L. L. Merritt, and J. A. Dean, "Instrumental Methods of Analysis", 5th ed., D. van Nostrand Co., New York, N.Y., 1974.
(3) A. A. Cernik, *Chem. Br.*, **10**, 58–61 (1974).
(4) I. L. Larsen, N. A. Hartmann, and J. J. Wagner, *Anal. Chem.*, **45**, 1511–1513 (1973).
(5) J. Mandel and F. J. Linnig, *Anal. Chem.*, **29**, 743–749 (1957).
(6) Ch. K. Mann, Th. J. Vickers, and W. M. Gulick, "Instrumental Analysis", Harper & Row, New York, N.Y., 1974.
(7) B. A. Kubrak, A. A. Kaplan, and V. N. Polyakova, *Sb. Tr. Molodykh. Uch., Tomsk. Politekh. Inst.*, 11–13 (1973); *Chem. Abstr.*, **82**, 50922 (1975).
(8) W. H. Reinmuth, *Anal. Chem.*, **28**, 1356–1357 (1956).
(9) E. C. Fieller, *J. R. Stat. Soc., Suppl.*, **7**, 1–64 (1940).
(10) P. D. Lark, B. R. Craven, and R. C. L. Bosworth, "The Handling of Chemical Data", Pergamon Press, New York, N.Y., 1968.
(11) J. P. Franke, P. M. J. Coenegracht, and R. A. de Zeeuw, *Arch. Toxicol.*, **34**, 137–143 (1975).

RECEIVED for review January 26, 1978. Accepted May 17, 1978.

CORRESPONDENCE

Effect of Gas Burner Conditions on Lithium Tetraborate Fusion Preparations for X-ray Fluorescence Analysis

Sir: Automated instruments are now available which perform fusions of one or more samples with a suitable fluxing agent such as lithium tetraborate. This procedure produces a glass disk(s) which after grinding and polishing can be directly analyzed by x-ray fluorescence spectrometry. The heat source in these instruments is usually a modified Meker burner fed with either natural gas/air or propane/air gas mixtures. The purpose of this communication is to report some results we have obtained when fusing mixtures consisting of various concentrations of calcium and iron with a constant amount of flux under conditions where the flow rates of propane and air fed into the burner were varied.

EXPERIMENTAL

Apparatus. An automated fusion device was employed to perform the fusions (Angstrom, Inc., P.O. Box 248, Belleville, Mich. 48111). An energy-dispersive x-ray spectrometer was used in these experiments and has been described elsewhere (*1*).

Procedure. Samples were prepared for fusion by adding known amounts of $CaCO_3$ (previously dried @ 260 °C) and Fe_2O_3 (dried at 110 °C) to 6.7 g of lithium tetraborate and 1.5 g of ammonium nitrate. All materials were of analytical reagent quality. The samples were then fused under two different gas burner conditions for 40 min each in platinum–5% gold alloy crucibles (Matthey Bishop Inc., Malvern, Pa. 19355). The resultant glass disks were then ground and polished and analyzed directly by energy-dispersive x-ray spectrometry.

Temperature calibration of the glass melt was performed with an NBS calibrated Pt–10% Rh thermocouple. The temperature of the fusion mixture was set at 1125 °C by varying the flow rates of propane and air entering the burner by adjustment of the respective flow controllers. The air-to-propane ratio was the highest that could be obtained without causing the flame to extinguish (condition I). After a number of glass disks were prepared, the propane flow was increased and the air decreased so that a temperature of 1100–1110 °C was obtained (condition II). Under these conditions, several glass disks were prepared. A summary of the concentrations of calcium and iron in the disks prepared under the two gas burner conditions is tabulated in Table I.

Table I. Concentrations of Ca and Fe Added in Standard Disks

Gas burner conditions	Bead No.	% Ca	% Fe
I (1125 °C)	1	2.91	1.01
	2	2.89	1.01
	3	5.85	0.51
	4	5.85	0.52
	5	7.26	0.25
	6	7.28	0.25
II (1100 °C)	1	1.44	2.00
	2	1.44	2.00
	3	2.89	1.01
	4	2.99	1.01
	5	2.88	1.01
	6	2.89	0.99
	7	7.25	0.26
	8	7.25	0.26

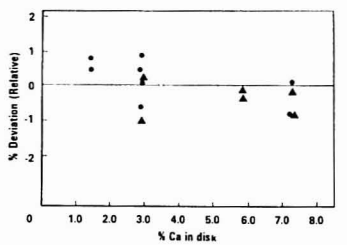

Figure 1. Effect of burner conditions on calcium in standard disks. (▲) Condition I. (●) Condition II

RESULTS AND DISCUSSION

The relative differences found in the determination of calcium and iron obtained under the two sets of fusion conditions are plotted in Figures 1 and 2, respectively. Three replicate measurements of each binary glass disk were made with relative standard deviations of a single measurement of 0.3 to 1.0%. The results shown were corrected for x-ray absorption in the glass disks using an NBS data reduction procedure (*2*). Figure 1 shows that the difference in fusion conditions had no effect on calcium. However, Figure 2 illustrates that under condition I, iron was markedly affected. The low values obtained are believed to be due to the partial chemical reduction of iron to the metal which subsequently alloys with the platinum crucibles (*3*). It was also found that glass disks could not be prepared without cracking under condition I when the iron concentration was greater than 1.5% in the disk. These disks usually appeared very dark brown

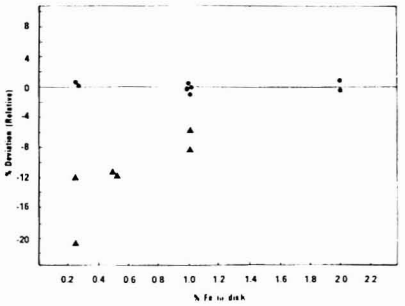

Figure 2. Effect of burner conditions on iron in standard disks. (▲) Condition I. (●) Condition II

and opaque. At lower iron concentrations, the disks exhibited a greenish blue coloration in contrast to the yellowish brown obtained with disks having the same iron content prepared under condition II. The addition of more NH_4NO_3 prior to fusion under condition I did not appear to prevent reduction. These results illustrate the importance of maintaining proper oxidizing flames for accurate sample preparation by fusion. It has been suggested that a nickel crucible of the same size as the platinum crucible be used in an identical position in the flame to determine the oxidizing or reducing conditions of the flame. We found that the use of a nickel crucible for determining these conditions was not always satisfactory. This work suggests that observation of the color of a few fused samples of mixtures containing calcium and iron may serve as a more sensitive test of flame conditions.

LITERATURE CITED

(1) P. A. Pella, R. H. Myklebust, M. M. Darr, and K. F. J. Heinrich, NBSIR 77-1211, June 1977.
(2) R. L. Myklebust, C. E. Fiori, D. N. Breiter, and K. F. J. Heinrich, FACSS Abstracts (3rd Annual Meeting) No. 241, Philadelphia, Pa., 1976.
(3) C. O. Ingamells, *Anal. Chim. Acta*, **52**, 323 (1970).

P. A. Pella

National Bureau of Standards
Washington, D.C. 20234

RECEIVED for review February 12, 1978. Accepted April 13, 1978.

Solvent Extraction of Coal-Derived Products

Sir: The recent interest in separating and characterizing coal-derived oils has revealed an intriguing problem. There is, at present, no standard method or technique that is widely used to separate and characterize liquefied or solvent refined coal products. Most investigators in the field, and those just getting started, are however using a host of similar terms to define dissimilar fractions from coal products. For example, the word asphaltene(s), as it pertains to coal-derived products, can mean a solvent separated material that is benzene or toluene soluble and pentane insoluble (*1*), or hexane insoluble (*2*), or cyclohexane insoluble (*3*) or even derived by specific mixtures of toluene and pentane (*4*). Beside all of these differences, there are a host of techniques being used to characterize coal-derived products by solubility distribution analysis (*5, 6*), chromatographic analysis (*7–9*), and by the use of distillation (*10*). Finally, there is also a redefinition of asphaltenes as being specific chromatographic fractions with one functional group present per molecule (*8*). The situation for the analyst is one of mass confusion. When a chemist wishes to separate coal-derived oils for the first time, he can find two, three, and in the case of "asphaltenes" as many as ten different methods, all of which arrive at supposedly the same product. A common separation method should be used on all coal-derived products to serve as a guide post for comparison by process engineers, chemists, and management. The method we present here should be used only as a guide to the development of a standard separation analysis of coal-derived material. We feel it is important that the finally accepted method be rapid (hours), suitable to analytical (1–10 g) and preparative (10–100 g) batch size, and not require sophisticated instrumentation.

Our procedure can provide an analytical separation of three or four major solvent-defined solubility fractions from the multicomponent coal-derived oil. Separation is carried out at just below room temperature with solvents of increasing orientation solubility (polarity) parameter as defined by Hildebrand (*11*). Each fraction is also defined with respect to the volume of solvent used. We have found that 1 liter of solvent per fraction per 3 grams of starting material is sufficient to define the separation. It has also been our experience that Soxhlet extraction at elevated temperatures requires days to complete and the "soluble" final product of each extraction contains some insoluble material.

Finally we wish to introduce a pre-treatment step of the coal-derived oil prior to solvent extraction. By freezing the oil in liquid nitrogen, one can grind the solid pieces into a fine powder of great surface area. This contributes to rapid and efficient extraction of the pentane soluble material at the onset of the procedure.

EXPERIMENTAL

A coal-derived product is chosen and mixed well if it has been standing for more than 1 h after processing. Most liquefaction products may be warmed to 60 °C and stirred to obtain a uniform mixture. Solids may be chipped or broken. Three to four grams of the product are weighed into a tared 250-mL Pyrex heavy wall or a 315-mL stainless steel (DuPont No. 00522) centrifuge tube to ±5 mg or less.

Add liquid nitrogen to the centrifuge tube slowly until 100 mL can remain as a quiet solution—no rapid evaporation. The now frozen product is ground with a thick glass rod into a fine powder. As the liquid nitrogen nears complete evaporation, place the centrifuge tube in a 50-watt ultrasonic bath and sonicate while adding 240 mL pesticide grade *n*-pentane and stirring rapidly with a glass or Teflon rod. Continue to sonicate and stir until no large particles are present—only a fine powder—approximately 5 min. When sonication is complete, centrifuge for 10 min at 2500 rpm (up to 10 000 rpm have been used), 25 °C. The resulting supernatant is decanted into a tared 250-mL round bottom flask and pentane removed under dry nitrogen flush on a Rotovap from a warm (50 °C) water bath until 5 min after the last drop of pentane is observed to condense. The centrifuge tube is washed with 200 mL *n*-pentane, sonicated, stirred, and centrifuged again, decanting the supernatant into the same distilling flask. The solvent recovered from the Rotovap should be used as part of the next wash to reduce loss. Washing is continued until 1 L of *n*-pentane is used. After the last wash, pesticide grade benzene is added to the residue and the sonication and washing process repeated for a total of 1 L of solvent decanting into a second distilling flask. The water bath temperature is raised to 80 °C. The final benzene wash may be followed by a 50-mL *n*-pentane

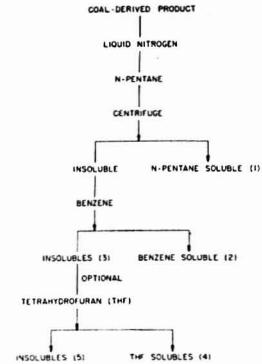

Figure 1. Solvent extraction scheme for coal-derived products

Table I. Suggested Nomenclature for Coal-Derived Materials

fraction	solvent solubility, soluble/insoluble	name
1	pentane/—	oils
2	benzene/pentane	asphaltenes
3	—/benzene	benzene insolubles
4	THF/benzene	preasphaltenes
5	—/THF	THF insolubles-residue

wash, whereupon this last pentane supernatant is discarded and the centrifuge tube residue (benzene insolubles) dried at 50 °C in a vacuum oven for 15 min. The vacuum oven is backfilled with dry nitrogen. As an option to drying the benzene insolubles from the step above, tetrahydrofuran (THF) or methylene chloride–methanol (90–10) may be used as the final solvent extractor. If THF is used, it must be freshly distilled to remove the BHT and any water. Repeat the washing, sonication, and centrifugation steps for five 200-mL washing cycles. After the final THF wash, rinse the residue with *n*-pentane, centrifuge, decant, and dry in a vacuum oven at 50 °C for 15 min. At no other time should the centrifuge residue be allowed to dry or come in direct contact with the open atmosphere.

The benzene washings should not be taken to dryness but brought to about 20 mL, and this solution is freeze-dried at $\sim 10^{-1}$ Torr for 1 to 2 h. To sublime the benzene and leave a solvent-free asphaltene a 20–30 mL solution is swirled in a 250-mL round bottom flask while submerging it in a 2-L Dewar of liquid nitrogen. Care should be taken to achieve a smooth distribution of the solution inside the flask walls. When the solution appears to be solid, allow the flask to remain in the liquid nitrogen 3 min longer for complete thermal equilibrium. Remove the flask from the liquid nitrogen and attach with greaseless fittings to a vacuum pump. Allow the flask to remain undisturbed until all the benzene has been sublimed. This will be noticed by light tan flakes gathering at the bottom of flask and adhering to the walls. Heating in vacuo to remove the residual benzene may change the chemical nature of the fraction and reduced benzene solubility will ensue. Toluene may be substituted for benzene, but solvent removal is more difficult. A scheme of the procedure is given in Figure 1.

DISCUSSION

We suggest the common and operationally defined names in Table I be applied to the solvent separated fractions. The term preasphaltenes is used here to reflect a class of solvent defined substances.

This procedure has been effective in our research efforts to provide reliable results of solvent separated fractions from coal-derived oils in less than $6^1/_2$ hours on 3–4 grams of material. Table II lists solvent separation results of a number of coal liquefaction products. These products have a wide range of viscosities from 100 to greater than 3000 centistokes (70 °C). Samples of this kind are also known to age (*12*) under certain conditions of temperature and excess oxygen, causing changes in the relative amounts of oils:asphaltenes:benzene insolubles. With these considerations, a measure of precision from a limited series of samples cannot be stated.

Table II. Solvent Separated Fractions

coal liquid	oils[a]	weight percent asphaltenes	weight percent benzene insolubles
A	74.2	18.4	7.4
	73.3	22.0	4.7
	72.0	23.2	4.8
B	74.5	18.2	7.3
	72.0	19.3	8.7
C	62.7	20.8	16.5
	62.4	20.9	16.7
D	62.6	19.4	18.0
	61.9	20.8	17.3
E	57.5	29.8	12.7
	57.3	30.4	12.3
F	57.6	34.0	8.4
	55.8	34.5	9.7
	55.7	35.8	8.5
G	58.9	32.9	8.2
	57.9	34.5	7.6
	57.5	34.8	7.7

[a] By difference. Direct measurement gave recoveries of >95%.

This summary should be used only as a guide for future development of a common method of separation and characterization of coal liquids.

ACKNOWLEDGMENT

The authors acknowledge the cooperation of Sayeed Akhtar and Nestor Mazzocco for providing the coal liquefaction products and associated process data.

LITERATURE CITED

(1) M. J. Mima, H. Schultz., and W. E. McKinstry, **ERDA/PERC/RI-76/6**, 1976.
(2) S. Weller, M. G. Pelipetz, and S. Friedman, *Ind. Eng. Chem.*, **43**, 1575 (1951).
(3) T. Aczel, EXXON Research, Baytown, Texas, April 1978, private communication.
(4) F. Steffgen, K. Schroeder, and B. Bockrath, manuscript in preparation.
(5) I. Schwager and T. F. Yen, *Fuel*, **57**, 100 (1978).
(6) H. Sternberg, R. Raymond, and F. K. Schweighardt, *Div. Pet. Chem., Prepr.*, **21** (1), 198 (1976).
(7) J. G. Bendoraitis, A. V. Cabal, R. B. Calen, T. R. Stein, and S. E. Voltz, *EPRI Rep.*, **RP-361**, January 1976.
(8) M. Farcasiu, *Fuel*, **56**, 9 (1977).
(9) R. G. Ruberto and D. M. Jewell, presented at the National Science Foundation Workshop "Analytical Needs of the Future as Applied to Coal Liquefaction", Greenup, Ky., August 21-23, 1974.
(10) J. E. Dooley and C. J. Thompson, *Am. Chem. Soc., Div. Fuel Chem., Prepr.*, **21** (6), 243 (1976).
(11) R. A. Keller, B. L. Karger, and L. R. Snyder, in "Gas Chromatography 1970", Stock and S. G. Perry, Ed., Institute of Petroleum, London, 1971, p 125.
(12) F. S. Karn and F. R. Brown, **ERDA/PERC/TPR-76/2**, 1976.

F. K. Schweighardt*
B. M. Thames

U.S. Department of Energy
Pittsburgh Energy Research Center
4800 Forbes Avenue, Pittsburgh, Pennsylvania 15213

RECEIVED for review October 17, 1977. Accepted May 18, 1978.

Comments on the Savitzky–Golay Convolution Method for Least-Squares Fit Smoothing and Differentiation of Digital Data

Sir: In 1964 a paper by Savitzky and Golay (*1*) describing a technique of smoothing and obtaining smoothed derivatives using convolution arrays derived from the coefficients of least-squares-fit formulas was published in this journal. That paper has become a classic judging by the number of citations (*2*)—well over 350 in more than 100 different journals—since its publication despite the fact that the paper contained numerous errors in the tables of convolution arrays. These errors were first pointed out and almost completely corrected by Steinier, Termonia, and Deltour (*3*) in 1972. The purpose of this letter is threefold: (1) to present two simple equations that may be used to check for errors in the arrays; (2) to note the simplicity involved in generating arrays wider than 25 points (the maximum width in the Savitzky–Golay tables), giving equations that may be used to easily expand the widths of all the convolution arrays discussed in the Savitzky–Golay paper; and (3) to call attention to examples that illustrate the beneficial use of smoothing techniques in extracting information other than simply peak position, height, and width from spectral data made up of peaks of known profile. More detailed discussions of least-squares-fit smoothing, than will be given here, may be found in the review papers of Nernst (*4*) and of Willson and Edwards (*5*).

The Savitzky–Golay convolution smoothing technique is based on fitting an array of n (= $2m + 1$, with m a positive integer from 1 to 12) equally-spaced data points to a polynomial,

$$U(x) = c_0 + c_1x + c_2x^2 + \cdots + c_jx^j = \sum_{q=0}^{j} c_qx^q \quad (1)$$

These n points are normally a subgroup of a larger group of N points $\{u_i(x_i)\}$ ($x_{i+1} - x_i$ = constant) and to smooth the entire set of points (except for m points at each end of the data array that must be treated separately) one takes a moving average. General formulas for smoothing by moving-average fits to a polynomial may be found in textbooks on the statistical handling of data (*6*). Savitzky and Golay pointed out that application of these smoothing formulas is equivalent in digital computers to convoluting a uniformly-spaced data array with a set of smoothing coefficients derived from the least-squares-fit formulas. They further pointed out that, while the coefficient c_0 in Equation 1 gives the smoothed value of the data point at the middle of the n-point array being fitted to the polynomial (= $\bar{u}_i$), the other coefficients c_1, c_2, ..., and c_q in Equation 1 correspond to the smoothed values of the 1st, 2nd, ..., and qth derivatives at the midpoint of the array, divided by 1!, 2!, ..., and q!, respectively. They showed that these simple convolution arrays could be determined from the general equations for the c_q's ($q \neq 0$), and could be simply used to obtain smoothed derivatives in a single convolution operation.

The object of the digital least-squares-fit convolution procedure is thus the determination of a set of n coefficients, $\{p_s^{(0)}\}$, that may be used with a set of uniformly spaced digital data points centered around a data point u_i to obtain a smoothed value for the ith point,

$$\bar{u}_i = \sum_{s=-m}^{m} p_s^{(0)}\, u_{i+s} \quad (2)$$

or a different set of coefficients, $\{p_s^{(q)}\}$, that give the smoothed value of the qth derivative according to

$$\frac{d^q\bar{u}_i}{dx^q} = \sum_{s=-m}^{m} p_s^{(q)}\, u_{i+s} \quad (3)$$

$i = m + 1, ..., N-m-1$. N = the number of points in the array to be smoothed.

Savitzky and Golay give tables of $\{p_s^{(0)}\}$ and $\{p_s^{(q)}\}$ for fitting to polynomials up to degree 6. Errors in those tables may be detected by two simple tests. First, the coefficients must be normalized such that

$$\sum_{s=-m}^{m} p_s^{(q)}\, s^q = (q!) \quad (4)$$

q = 0, 1, 2, 3, 4, or 5. Second, if $q \neq 0$

$$\sum_{s=-m}^{m} p_s^{(s)} = 0 \quad (5)$$

The corrections given by Steinier et al. (*3*) have been checked and found to be correct except for a value given in the first row of their Table I. The correct value for the ±5 point in column 25 of Savitzky–Golay Table I should be 342 instead of 343 as given by Steinier et al.

In recent model calculations to study the effects of random noise on an iterative deconvolution scheme (*7*), it was found that the 25-point smoothing arrays of Savitzky and Golay could be too narrow for the "best results" of smoothing where the buildup of the noise, remaining after smoothing, in the deconvolution process, must be balanced against the signal broadening that results from the smoothing. For single least-squares-fit smoothing, Edwards and Willson (*8*) have found, in a study of the effects of such smoothing on noise-free Gaussian lines, that the optimum width of the smoothing array is 0.7 times the full width at half maximum (FWHM) of the narrowest Gaussian line of their spectra. In a similar study considering Lorentzian- as well as Gaussian-shaped lines, Enke and Nieman (*9*) conclude that the best signal-to-noise enhancement from a single-pass (quadratic-cubic) smoothing occurs for a smoothing array that is twice as wide as the FWHM of the peak being smoothed. Thus the optimum width of a single-pass smoothing array will depend on the criteria set by the user. As found in our deconvolution studies, however, that optimum width can sometimes be greater than 25 points; and the choice is then between iterative, or repetitive, smoothings and generation of wider, single-pass smoothing arrays. Considering the Slutzky–Yule oscillatory distortions (*10*) that can build up with multiple smoothing, and the question of aesthetics—single-pass least-squares-fit smoothing involves exact fits of the original data to a known polynomial while multiple smoothing does not—use of a single least-squares-fit smoothing array of appropriate width may arguably be the more desirable method of smoothing data.

General formulas for the smoothing coefficients $p_s^{(0)}$, for fitting to polynomials of degree from 2 through 5, have already been published (*4*, *5*, *6a*). Similar formulas for calculating the $p_s^{(q)}$, q = 1 thru 5, have been derived and are presented in Table I together with the formulas for $p_s^{(0)}$ using Roman numerals to label the eleven equations in accordance with the Savitzky–Golay tables of coefficients (*1*). With these eleven equations one can easily extend all of the tables of the Savitzky–Golay paper (*1*) for least-squares-fit convolution arrays with no limit to the number of points in an array.

The coefficients given in the Savitzky–Golay tables (*1*) are all integers. They correspond to the numerators of Equations I through XI in Table I (sometimes divided by a factor that

0003-2700/78/0350-1383$01.00/0

Table I. Equations for Calculating Savitzky-Golay Smoothing-Array Coefficients, $p_s^{(q)}$

equation no.	order of smoothed derivative (q)	order of polynomial (j)	equation for $p_s^{(q)}$
I	0	2 or 3	$p_s^{(0)} = \dfrac{3(3m^2 + 3m - 1 - 5s^2)}{(2m + 3)(2m + 1)(2m - 1)}$
II	0	4 or 5	$p_s^{(0)} = \left(\dfrac{15}{4}\right)\dfrac{(15m^4 + 30m^3 - 35m^2 - 50m + 12) - 35(2m^2 + 2m - 3)s^2 + 63s^4}{(2m + 5)(2m + 3)(2m + 1)(2m - 1)(2m - 3)}$
III	1	2	$p_s^{(1)} = \dfrac{3s}{(2m + 1)(m + 1)(m)}$
IV	1	3 or 4	$p_s^{(1)} = \dfrac{5\{5(3m^4 + 6m^3 - 3m + 1)s - 7(3m^2 + 3m - 1)s^3\}}{(2m + 3)(2m + 1)(2m - 1)(m + 2)(m + 1)(m)(m - 1)}$
V	1	5 or 6	$p_s^{(1)} = \left(\dfrac{21}{4}\right)\{7(25m^8 + 100m^7 - 50m^6 - 500m^5 - 95m^4 + 760m^3 + 180m^2 - 300m + 72)s - 105(6m^6 + 18m^5 - 15m^4 - 60m^3 + 17m^2 + 50m - 12)s^3 + 33(15m^4 + 30m^3 - 35m^2 - 50m + 12)s^5\} \div \{(2m + 5)(2m + 3)(2m + 1)(2m - 1)(2m - 3)(m + 3)(m + 2)(m + 1)(m)(m - 1)(m - 2)\}$
VI	2	2 or 3	$p_s^{(2)} = \dfrac{30\{3s^2 - m(m + 1)\}}{(2m + 3)(2m + 1)(2m - 1)(m + 1)(m)}$
VII	2	4 or 5	$p_s^{(2)} = \left(\dfrac{-105}{2}\right)\dfrac{15(6m^2 + 6m - 5)s^4 - 21(4m^4 + 8m^3 - 4m^2 - 8m + 5)s^2 + 5m(2m^5 + 6m^4 - m^3 - 12m^2 - m + 6)}{(2m + 5)(2m + 3)(2m + 1)(2m - 1)(2m - 3)(m + 2)(m + 1)(m)(m - 1)}$
VIII	3	3 or 4	$p_s^{(3)} = \dfrac{210\{5s^3 - (3m^2 + 3m - 1)s\}}{(2m + 3)(2m + 1)(2m - 1)(m + 2)(m + 1)(m)(m - 1)}$
IX	3	5 or 6	$p_s^{(3)} = \left(\dfrac{-945}{2}\right)\{7(6m^6 + 18m^5 - 15m^4 - 60m^3 + 17m^2 - 50m - 12)s - 15(12m^4 + 24m^3 - 28m^2 - 40m + 39)s^3 + 77(2m^2 + 2m - 3)s^5\} \div \{(2m + 5)(2m + 3)(2m + 1)(2m - 1)(2m - 3)(m + 3)(m + 2)(m + 1)(m)(m - 1)(m - 2)\}$
X	4	4 or 5	$p_s^{(4)} = \dfrac{(1890)\{3m(m^3 + 2m^2 - m - 2) - 5(6m^2 + 6m - 5)s^2 + 35s^4\}}{(2m + 5)(2m + 3)(2m + 1)(2m - 1)(2m - 3)(m + 2)(m + 1)(m)(m - 1)}$
XI	5	5 or 6	$p_s^{(5)} = \dfrac{(20790)\{(15m^4 + 30m^3 - 35m^2 - 50m + 12)s - 35(2m^2 + 2m - 3)s^3 + 63s^5\}}{(2m + 5)(2m + 3)(2m + 1)(2m - 1)(2m - 3)(m + 3)(m + 2)(m + 1)(m)(m - 1)(m - 2)}$

is common to the denominator of those equations). It should be noted, however, that the $p_s^{(q)}$ coefficients are all less than unity. Thus, before using the integer coefficients from the Savitzky–Golay tables, those integers must be divided by a normalizing factor, also given as an integer, in order to obtain the correct $p_s^{(q)}$ that satisfy the normalization condition, Equation 4. The denominators of Equations I through XI give the integer normalizing factors of the Savitzky–Golay tables. In calculating the integer entries in corrected Savitzky–Golay tables (*11*) with a PDP-10 computer, double-precision techniques were needed. When it was realized that the precision needed in calculating the integers of Savitzky and Golay was much greater than needed for most applications of least-square-fit smoothing, the $p_s^{(q)}$ were computed directly with less precision leading to considerable simplification in the computer program (*11*).

There are at least two data-processing procedures in which least-squares-fit smoothing/differentiation techniques are found to be potentially beneficial. In these cases, a buildup of random noise is inherent in the procedure and smoothing is found useful in ameliorating the signal-to-noise ratio in the final result. In both cases the experimental spectra which are smoothed do *not* consist simply of lines of known lineshape (e.g., Voigt) but rather of step- or Heaviside-like signals on a large, slowly-varying background. The object of the processing in the first case, Auger electron spectroscopy on solid surfaces, is to deconvolute the broadening and loss features from the background-corrected signal to obtain the "true" Auger line shape. In the second case, Rutherford backscattering spectroscopy from thick solid targets, it is the height, shape, and location in energy of the threshold signals that are to be determined by the data-processing.

Auger transitions that involve the valence electrons of a solid result in signals whose line shapes contain information on the valence-band density-of-states of the solid. These signals are, in general, distorted in shape because of the inelastic interactions that some of the Auger electrons undergo before exiting the solid; and deconvolution is necessary to extract the undistorted Auger line shape from the measured signal. In the iterative (van Cittert) deconvolution technique that we use, random noise is found to build up rapidly with the number of iterations (*7*). This buildup can eventually offset any improvement in the shape of the convolution-distorted signal brought about by the deconvolution. Judicious use of smoothing techniques is found to significantly shift the "break-even" number of iterations at which the noise buildup begins to offset the benefits of deconvolution-shape improvement on the signal. Results of model calculations investigating the buildup of noise in deconvolution have been published (*7*).

The application of nuclear scattering techniques to elemental analysis of solids was first discussed by Rubin, Passell, and Bailey in an article in this journal (*12*). Since that pioneering work, extensive use has been made of Rutherford backscattering spectroscopy for analysis of the near-surface regions of solids. The threshold energy for backscattering is directly relatable to the mass of the scattering nucleus, and the height of the threshold signal is related to the surface concentration of the scattering element in the sample. Using least-squares-fit smoothing coefficients, Peisach (*13*) has investigated the use of differentiation to obtain energy-location and step-height information from backscattering data and has found that such techniques of data analysis can lead to "improved definition of spectral energies and improved precision in determining elemental surface concentrations". Potential-modulation techniques that are commonly used in many other spectroscopies to obtain directly measured derivative spectra are not practical with the experimental

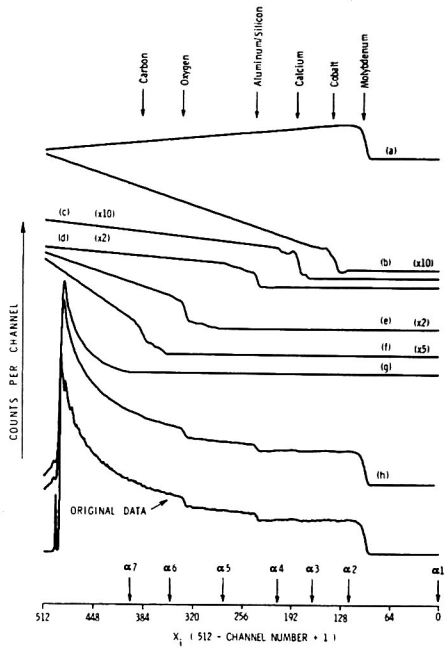

Figure 1. Spectral decomposition of Rutherford backscattering data. Curves a through f—resolved thresholds for molybdenum, cobalt, calcium, aluminum (and/or silicon), oxygen and carbon, respectively. Curve g—residual signal after subtracting curves a through f from the complete spectrum. Curve h—sum of curves a through g, all with unit scaling. The lowest curve gives the backscattering spectrum before decomposition

systems currently used for backscattering spectroscopy, thus making it necessary to mathematically differentiate the measured spectra using a computer. Unfortunately, for some unexplained reason, Peisach used two different arrays for smoothing and differentiation, thus somewhat blurring the utility of using least-squares-fit arrays to obtain smoothed derivatives in a single convolution.

In a similar study of differentiated backscattering data in our laboratory (*11*), single convolution arrays were used to obtain smoothed derivatives. Our conclusions as to the advantages of using smoothed derivatives in analyzing Rutherford backscattering data were similar to those reached by Peisach (*13*). In an extension of these differentiation techniques, it was found possible to easily decompose the backscattering spectrum into separate threshold components. The data used in this study were obtained with singly-charged, 2-MeV helium ions incident on the surface of an alumina-supported, silica-promoted, cobalt-molybdate catalyst (*14*), and are shown as the lowest curve in Figure 1. Plotted in this curve are the numbers of helium ions backscattered into a fixed detector as a function of the energy (which is proportional to channel number) of the backscattered ions. Because the threshold signals in these data turn on as one goes from high to low energy, the data are plotted here against a new abscissa parameter x_i (= 512 − channel number + 1).

Spectral decomposition of these data was carried out using a variation of a background correction scheme devised by Houston (*15*). One can calculate a background-corrected

spectrum $R_2(x_i, \alpha_j)$, using Houston's notation, where the subscript 2 indicates that the second derivative of the original data is first taken, and then this second derivative is integrated twice to recover the original spectrum minus the constant and linear components lost during differentiation. Using a least-squares-fit smoothed-derivative array, the smoothing operation occurs automatically in the process of determining the second derivative. x_i is the independent variable used in the integration, and α_j is the lower limit of integration. Then calculating $R_2(x_i, \alpha_j)$ and $R_2(x_i, \alpha_{j+1})$, where α_j and α_{j+1} are two x_i values in the spectrum below and above the threshold feature to be extracted, respectively, the extracted threshold signal is given by $R_2(x_i, \alpha_j) - R_2(x_i, \alpha_{j+1})$. The locations of the threshold signals are indicated by arrows at the top of Figure 1. The values of x_i that were chosen for the α_j's in the decomposition of the original spectrum were $\alpha_1 = 1$; $\alpha_2 = 118$; $\alpha_3 = 165$; $\alpha_4 = 210$; $\alpha_5 = 280$; $\alpha_6 = 349$; and $\alpha_7 = 400$. These α_j's were chosen to lie in regions of the spectrum assumed to contain only background, and no threshold-signal, information. There were 512 data points in the spectrum and a 19-point convolution array (Equation VII of Table I) was used to determine the second derivative.

The seven spectral components resulting from the decomposition are plotted as curves (a) through (g) in Figure 1. In the original data, three thresholds are clearly discernible while the other three are less so. In the component spectra (curves a through g), all six thresholds are clearly seen. As this example calculation was performed for illustrative purposes only, linear extrapolation of the signals below the threshold energy (in the direction of increasing x_i values) was made instead of using the more correct reciprocal-energy dependence (*14*). Note that the decrease in counts-per-channel below threshold for the molybdenum signal indicates an enhancement of the molybdenum concentration at the solid surface. This result was corroborated by backscattering data taken with 1.4-MeV protons incident on the sample (*14*). Curve h gives the sum of curves a through g, all with unit scaling, and is seen to be essentially a smoothed version of the original data. Thus, the differentiation techniques demonstrated by Peisach (*13*) as useful in analyzing backscattering spectra can be simply extended to give component threshold signals. Least-squares-fit smoothing is beneficial in this operation in ameliorating the noise buildup in the differentiation. It provides a simple one-operation method of obtaining the smoothed derivative.

The Savitzky–Golay convolution method of least-squares-fit smoothing and differentiation of digital data is versatile and extremely simple to use. Using only the coefficients given in the Savitzky–Golay tables (*1*), one is limited to a 25-point smooth, however. Wider smoothing arrays are sometimes desirable and may be simply generated using the eleven equations given in Table I of this letter. Relaxing the condition that integer numerator and denominator values for the $p_s^{(q)}$ be calculated separately leads to further simplification in the computer program. Smoothing has been shown in data processing involving deconvolution (*7*) and/or differentiation (*11*, *12*) to be beneficial. Peak position, height, and width—of lines of known profile—are not the only information that may be sought in some spectroscopies. The smoothing techniques of Savitzky and Golay offer an extremely simple aid in extracting additional lineshape information.

LITERATURE CITED

(1) A. Savitzky and M. J. E. Golay, *Anal. Chem.*, **36**, 1627 (1964).
(2) "Citations Index" (1965–1976).
(3) J. Steinier, Y. Termonia, and J. Deltour, *Anal. Chem.*, **44**, 1906 (1972).
(4) R. R. Nernst, *Adv. Magn. Reson.*, **2**, 39 (1966).
(5) P. D. Willson and T. H. Edwards, *Appl. Spectrosc. Rev.*, **12**, 1 (1976).
(6) (a) E. Whittaker and G. Robinson, "The Calculations of Observations", 4th ed., Blackie and Son, Ltd., London, 1944, pp 291–296. (b) P. G. Guest, "Numerical Methods of Curve Fitting", Cambridge University Press, 1961, pp 349–353. (c) M. G. Kendall and A. Stuart, "The Advanced Theory of Statistics", Hafner Publishing, Inc., New York, N.Y., 1966, Vol. 3, "Design and Analysis, and Time-Series", pp 366–375.
(7) H. H. Madden and J. E. Houston, *Adv. X-Ray Anal.*, **19**, 657 (1976); *J. Appl. Phys.*, **47**, 3071 (1976).
(8) T. H. Edwards and P. D. Willson, *Appl. Spectrosc.*, **28**, 541 (1974).
(9) C. G. Enke and T. A. Nieman, *Anal. Chem.*, **48**, 705A (1976).
(10) M. G. Kendall and A. Stuart, ref 6c, pp 375–379.
(11) H. H. Madden and D. G. Schreiner, "Convolution Method for Least-Squares-Fit Smoothing and Differentiation of Digital Data", Report No. SAND76-0283, Sandia Labs., Albuquerque, N.M., 1976, unpublished work.
(12) S. Rubin, T. O. Passell, and L. E. Bailey, *Anal. Chem.*, **29**, 736 (1957).
(13) M. Peisach, *Thin Solid Films*, **19**, 297 (1973).
(14) J. A. Borders and G. D. Peterson, "Ion Backscattering Studies of Syntholl Catalyst Materials", Report No. Sand77-0479, Sandia Labs., Albuquerque, N.M., 1977, unpublished work.
(15) J. E. Houston, *Rev. Sci. Instrum.*, **45**, 897 (1974).

Hannibal H. Madden

Sandia Laboratories,
Albuquerque, New Mexico 87185

RECEIVED for review April 18, 1977. Accepted May 22, 1978. This work was supported by the U.S. Department of Energy under Contract AT(29-1)789.

Extension of the Rasberry-Heinrich Equation for X-ray Fluorescence Analysis

Sir: For an "infinitely" thick sample, the x-ray fluorescence intensity is shown to be given by the following expression:

$$I_j^Q = K_j C_j \int_{\lambda_{min}}^{\lambda_{Kab}} \frac{I_0(\lambda)\,\mu_j(\lambda)}{\mu_Q(\lambda) + \mu_Q(\lambda_j)}\,d\lambda \qquad (1)$$

where K_j is a factor to take care of the geometrical arrangement of the sample-detector and of fundamental parameters of element j. C_j is weight fraction of element j. $\mu_Q(\lambda)$ is mass absorption coefficient of the sample (denoted by Q) at the incident wavelength, λ. $\mu_Q(\lambda_j)$ is mass absorption coefficient of the sample for the primary fluorescence radiation of element j. $\mu_j(\lambda)$ is mass absorption coefficient of element j for the incident wavelength, λ. λ_{min} is minimum wavelength of the generator tube as given by the excitation voltage. λ_{Kab} is wavelength of the K-absorption edge of element j.

Equation 1 does not include higher order fluorescence effects (secondary, tertiary, etc.) that occur when the sample contains more than one chemical element. Furthermore, we consider monochromatic incident radiation in order to make the physical processes therein easier to understand. This would lead to a better understanding of what happens when the incident spectra is polychromatic, as it is in most of the practical cases.

0003-2700/78/0350-1386$01.00/0

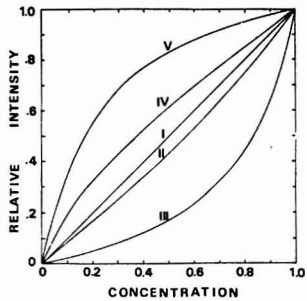

Figure 1. Possible cases of calibration curves for binary samples, I: $A_{AB} = 0$, $B_{AB} = 0$; II: $A_{BA} > 0$, $B_{BA} < 0$, ($|B_{BA}| < A_{BA}$); III: $A_{AB} > 0$, $B_{AB} = 0$; IV: $A_{BA} >$ or < 0, $B_{BA} < 0$, ($-1 < A_{BA} + B_{BA} < 0$); V: $A_{AB} < 0$, $B_{AB} = 0$

For a binary sample containing two elements, denoted by A and B, expression 1 reduces to:

$$I_A^Q = I_0 K_A C_A \frac{\mu_A(\lambda)}{C_A(\mu_A(\lambda) + \mu_A(\lambda_A)) + (1 - C_A)(\mu_B(\lambda) + \mu_B(\lambda_A))} \quad (2)$$

Dividing this intensity by the one from a pure sample of element A we get:

$$R_A = \frac{I_A^Q}{I_A} = \frac{C_A}{C_A + (1 - C_A)\alpha_{AB}}$$

where:

$$\alpha_{AB} = \frac{\mu_B(\lambda) + \mu_B(\lambda_A)}{\mu_A(\lambda) + \mu_A(\lambda_A)} \quad (3)$$

in the case in which both the incident and take off angles are equal (cosecant factors are cancelled out).

Defining:

$$A_{AB} = \alpha_{AB} - 1 \quad (4)$$

we arrive at a more generally used expression:

$$R_A = \frac{C_A}{1 + A_{AB}(1 - C_A)} \quad (5)$$

ANALYSIS OF THE EMPIRICAL EXPRESSION

Equation 5 has been used by many authors (*1–6*) as a relationship between the relative fluorescence intensity of one element and its concentration. It is valid whenever the element of interest is not affected by characteristic radiation emitted by the other element in the sample.

In Figure 1, curves III and V illustrate the behavior of R_A as a function of C_A for different values of the coefficients, A_{AB}. The corresponding range of values of A_{AB} are shown for each case, correcting those ranges initially given by Rasberry and Heinrich (*1*). These authors gave the values $0 < A < 1$ ("negative absorption") and $A > 1$ ("positive absorption") when it should be $-1 < A < 0$ and $A > 0$, respectively. However, this error does not affect the method proposed by them, neither was the interpretation given to their results, because the samples of Cr–Fe–Ni they studied do not show "negative absorption" effects. Negative absorption occurs, for example, in an Al–Cd sample, when it is irradiated with the Fe Kα line and the emitted Cd Lα_1 line is observed.

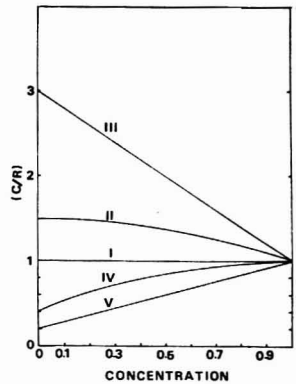

Figure 2. C/R as a function of C for binary samples. The numbering has the same meaning as in Figure 1

When the characteristic radiation intensity from the element of interest is enhanced by fluorescence from the other element, an additional term shoud be included in Equation 5 to represent such enhancement; in this case the shape of the curve will no longer be hyperbolic.

The semiempirical formula proposed by Rasberry and Heinrich (*1*) is:

$$\left(\frac{C}{R}\right)_i = 1 + \sum_{k \neq i} A_{ik} C_k + \sum_{k \neq i} \frac{B_{ik} C_k}{1 + C_i} \quad (6)$$

In this expression the coefficients A_{ik} represent absorption, while the B_{ik} represent enhancement effects. Only the A_{ik}'s have a theoretical justification and they could be determined this way as well as experimentally. The B_{ik}'s can only be determined experimentally since a closed theoretical expression for them does not exist.

Denoting the components of a binary sample by A and B, expression 6 reduces to:

$$\left(\frac{C}{R}\right)_A = 1 + A_{AB} C_B \quad (7)$$

and

$$\left(\frac{C}{R}\right)_B = 1 + A_{BA} C_A + \frac{B_{BA} C_A}{1 + C_B} \quad (8)$$

Element A is the one capable of exciting with its characteristic line the absorption edge of interest in element B. Figure 2 shows curves of C/R vs. C.

Five cases are now possible: I: $A_{AB} = 0$, $B_{AB} = 0$ (linear calibration curve); II: $A_{BA} > 0$, $B_{BA} < 0$ (absorption effects overcome enhancement); III: $A_{AB} > 0$, $B_{AB} = 0$ (preferential absorption); IV: $A_{BA} >$ or < 0, $B_{BA} < 0$, ($-1 < A_{BA} + B_{BA} < 0$) (enhancement effects overcome absorption); V: $A_{AB} < 0$, $B_{AB} = 0$ ("negative absorption" effects dominate).

Case II was not considered by Rasberry and Heinrich even though it is possible; while case V is not completely dealt with. Cases I, III, and IV are discussed by them but the ranges of the coefficients were erroneous.

A few comments about Equation 6 are in order at this point. First, this formula does not take into account tertiary and higher order fluorescence effects, always present in multicomponent system. Thus, if one tries to apply it to these

systems, the B_{ik}'s will be slightly dependent on the concentration of the elements. To overcome this, Hawthorne and Gardner (7), found an additional empirical term to take into account tertiary contributions, while keeping the coefficients B_{ik} independent of the concentrations. Secondly, A_{ik} cannot be zero when enhancement is the predominant effect, as was proposed by Rasberry and Heinrich (1), mainly because absorption effects are always present, as noted by Budesinsky (8), Tertian (9), and Hawthorne and Gardner (7). If one takes $A_{ik} = 0$, then the B_{ik}'s would again be dependent (linearly) on the concentration of the elements.

DISCUSSION

We wish to point out that the importance of Equation 6 in the analysis by x-ray fluorescence of multicomponent samples, resides in the fact that coefficients A and B should be independent of the concentrations C_A and C_B. This is achieved when the only effects present in the spectral line of interest are of secondary order. When higher order effects (tertiary, quaternary, etc.) of relative importance are present, an additional term should be added for each of them.

Suppose now that in the analysis of a binary sample Equation 6 is used and $B_{AB} = 0$, then two cases are possible: (i) $A_{AB} > 0$, in this case $A_{AB}C_B$ represents a loss of fluorescent x-rays since the matrix absorbs more incident and/or fluorescent radiation than a standard of element A. (ii) $A_{AB} < 0$, in this case $A_{AB}C_B$ represents an excess of fluorescent radiation as compared with a standard of element A. This effect could be thought of as a case of "negative absorption" since its net result is similar to an enhancement.

Let us further suppose that in Equation 8 the element B be such that the terms $A_{BA}C_A$ are negligible compared with $B_{BA}C_A/(1 + C_B)$. Then the predominant effect is enhancement of fluorescent radiation. This last term takes into account the net excess of x-rays in the characteristic radiation of element B, due to the fact that radiation emitted by element A is energetic enough to produce secondary fluorescence in element B (note that B_{BA} is always negative).

Finally, if the coefficient B_{BA} is such that: $|B_{BA}| < A_{BA}/2$ we have curves above the line $(C/R)_B = 1$ in Figure 2. For this relation the curve $(C/R)_B$ vs. C_B will show a maximum in the range $0 < C_B < 1$. This fact is of no physical significance, since the curve we always use to determine the unknown element concentration is R_B vs. C_B.

APPENDIX

Consider a binary sample composed of chemical elements denoted by indices A and B such that $Z_A > Z_B$ and $\lambda^A{}_K < \lambda^B{}_{Kab}$, then we can write:

$$\left(\frac{C}{R}\right)_B = 1 + A_{BA}(1 - C_B)\left[1 + \frac{B_{BA}}{A_{BA}(1 + C_B)}\right] \quad \text{(A-1)}$$

Hyperbolic curves will lie above (below) the line $(C/R) = 1$, if the factor between brackets in Equation A-1 is greater than zero (less than zero).

Curves of type II in Figure 2 occur when the second term in Equation A-1 is positive. Since A_{BA} is a positive constant, $1 + B_{BA}/A_{BA}(1 + C_B)$ must be positive too. Because B_{BA} is always negative, the relation between B_{BA} and A_{BA} is $A_{BA}(1 + C_B) > -B_{BA}$ or $A_{BA} > |B_{BA}|$ since $(1 + C_B) \geq 1$.

Curves of type V in Figure 2 are given by Equation 5, namely, $(C/R)_A = 1 + A_{AB} - A_{AB} \cdot C_A$ with $A_{AB} < 0$.

LITERATURE CITED

(1) S. D. Rasberry and K. F. Heinrich, *Anal. Chem.*, **46**, 81 (1974).
(2) J. W. Criss and L. S. Birks, *Anal. Chem.*, **40**, 1080 (1968).
(3) R. Tertian, *Spectrochim. Acta, Part B*, **24**, 447 (1969).
(4) A. Guinier, *Rev. Univers. Mines*, **17**, 143 (1961).
(5) H. J. Beattie and R. M. Brissey, *Anal. Chem.*, **26**, 980 (1954).
(6) G. R. Lachance and R. J. Traill, *Can. Spectrosc.*, **11**, 43 (1966).
(7) A. R. Hawthorne and R. P. Gardner, *Anal. Chem.*, **48**, 14 (1976).
(8) B. W. Budesinsky, *X-Ray Spectrom.*, **4**, 166 (1975).
(9) R. Tertian, *X-Ray Spectrom.*, **2**, 95 (1973).

Jose A Riveros
Rita D. Bonetto
Raul T. Mainardi*
Instituto de Matemática, Astronomía y Física, IMAF,
Universidad Nacional de Córdoba
5000 Córdoba, Argentina

RECEIVED for review January 11, 1978. Accepted April 28, 1978. The authors acknowledge financial assistance from the Comisión Nacional de Estudios Geoheliofísicos (CNEGH) and the Universidad Nacional de Córdoba of Argentina.

Seven-Nanosecond Time-Resolved Resonance Raman Spectrometry of Cytochrome *c*

Sir: Knowledge of the structures of transient chemical species, for example, reaction intermediates or excited states, is essential to adequate understanding of chemical dynamics. Yet few techniques yield such information on short-lived species, particularly in condensed phases. Resonance Raman spectrometry represents an attractive probe for transient structures, inasmuch as the Raman scattering process itself is extremely fast, the vibrational spectra obtained are directly structure-related, and the resonance Raman effect can lead to high sensitivity (detection limits $<10^{-7}$ M) and selectivity for a given chromophore. The resonance Raman effect and its applications are covered in numerous recent reviews, for example, ref. 1.

In practice, however, the *instrumentally-imposed* time-scale of minutes to hours ordinarily required to obtain resonance Raman spectra using a conventional Raman spectrometer, consisting of a scanning monochromator with CW laser excitation, has generally prevented the application of this technique to transients. In this report we describe the successful acquisition of time-resolved resonance Raman (TR^3) spectra of the heme protein cytochrome *c* in dilute (5.5×10^{-4} M) aqueous solution, excited by a *single* seven-nanosecond laser pulse. This result represents a ten order of magnitude improvement over conventional techniques in the time required to obtain spectra with comparable signal-to-noise ratios (S/N), and a two order of magnitude improvement over the best time resolution previously reported for single-pulse resonance Raman spectra.

EXPERIMENTAL

The key device which allows the rapid detection of Raman spectra is the vidicon Raman spectrograph, which combines the spectral multiplex advantage of photographic spectrography with the speed, sensitivity, and linearity of photoelectric detection. The details of vidicon Raman spectrography are discussed elsewhere (*2, 3*). In the present study, we employed an apparatus comprising a SPEX 1870 0.5-m spectrograph incorporating a 1800 groove/mm holographically recorded diffraction grating, and a Princeton Applied Research 1250I Optical Multichannel Analyzer detection system. The vidicon screen was located in the image plane of the spectrograph. This vidicon spectrograph allowed a 345 cm^{-1} segment of a Raman spectrum to be recorded in a single exposure, with laser excitation at 5318 Å.

Pulsed-laser excitation was provided by the second harmonic of a Quanta-Ray DCR-1 Q-switched Nd:YAG oscillator, which produced a maximum per-pulse energy of 75 mJ at 5318 Å. The measured pulsewidth of this laser is 7 ns (FWHM) and the repetition rate is variable from single-shot to 25 Hz. For comparison to the 5318 Å-excited TR^3 spectra, conventional CW resonance Raman spectra were obtained using 5309 Å excitation from a Kr^+ laser, and a Cary 82 spectrometer with a cooled ITT FW-130 photomultiplier tube and photon counting signal processing.

RESULTS AND DISCUSSION

The spectral multiplex advantage of a vidicon Raman spectrograph, in conjunction with pulsed-laser excitation of Raman scattering, allows time-resolved Raman spectrometry to be performed with time resolution equal in principle to the laser pulsewidth (*2–9*). For *normal*, nonresonant Raman samples, vidicon spectrometry has been used to acquire time-resolved spectra using both single laser pulses (*3, 6–9*) and repetitive pulses with signal averaging (*3, 7, 8*). However, because of the feeble nature of normal Raman scattering, exploitation of the resonance Raman effect is necessary to render time-resolved Raman techniques generally applicable to dilute chemical transients. Yet only two groups (*4, 5*) have reported time-resolved *resonance* Raman spectra employing pulsed-laser excitation. Another group has reported resonance Raman spectroscopy of transients in electrochemical reactions, using CW laser excitation and phase-sensitive detection (*10, 11*).

Formidable experimental difficulties, in addition to those encountered in *normal* Raman spectroscopy, are encountered in the time-resolved *resonance* Raman case. In the normal Raman case, the sample generally does not absorb light at the laser wavelength, while in the resonance Raman case it is typical for virtually all the light at the laser wavelength to be absorbed within the scattering volume of the sample. When pulsed-laser excitation is employed with an absorbing sample, which is the usual TR^3 requirement, complications can be expected from sample heating and photochemistry. Furthermore, optical requirements coupled with high peak laser power can lead to damage to sample and cell material. The two previous TR^3 studies minimized these problems either by employing many repetitive excitation pulses at rather low per-pulse energy to gain 5-ns time resolution (*4*), or by using relatively long-duration (0.6 μs) single-pulse excitation to minimize peak pulse power at relatively high per-pulse energy. In the present study, we sought to obtain TR^3 spectra with time resolution of a few nanoseconds while retaining the ability to acquire a spectrum excited by a single laser pulse.

Figure 1 shows spectra of the heme protein cytochrome *c* at 5.5×10^{-4} M concentration in aqueous solution, recorded using conventional scanning with 5309 Å CW excitation, and the TR^3 apparatus with 5318 Å pulsed excitation in both repetitive and single-pulse modes. Comparing the CW spectrum to the repetitive-pulsed one, several points can be made. First, the spectra are essentially the same, feature for feature, indicating that the per-pulse energy which we employ, 11 mJ in the present case, does not degrade or significantly perturb the photolytically-stable heme chromophore of this protein. The shoulder on the low-frequency side of peak C is a spectrograph artifact, and the difference in relative areas of peaks D and E is due to a slightly different resonance condition between 5309 Å and 5318 Å excitation. Second, considering the improved S/N in the pulse-excited spectrum and the laser powers employed in each case, the vidicon Raman spectrograph realizes approximately a factor of 50 improvement over conventional scanning in spectral acquisition time *per scattered photon*, without regard to whether the Raman experiment is CW or time-resolved. This is partially due to the spectral multiplex advantage, and partially due to the greater luminosity, of the vidicon spectrograph. It should be noted that the Cary 82, because of its triple monochromator configuration, suffers a luminosity disadvantage of a factor of perhaps 2 or 3 compared to current scanning instruments. Third, it is clear that repetitive-pulse TR^3 spectra can be obtained with excellent S/N. The middle spectrum was obtained by excitation from 1300 pulses of 7-ns duration, at a repetition rate of 10 Hz. Thus the sample was exposed to laser radiation for only 1.3×10^{-5} s out of a total spectral acquisition time of 130 s, and time resolution of 7 ns is possible for any process which can be repetitively initiated the required number of times.

To obtain TR^3 spectra in processes which cannot be repetitively initiated, single-shot acquisition of TR^3 spectra is required. The bottom spectrum in Figure 1 was obtained using a single excitation pulse from the Nd:YAG oscillator, delivered

0003-2700/78/0350-1389$01.00/0

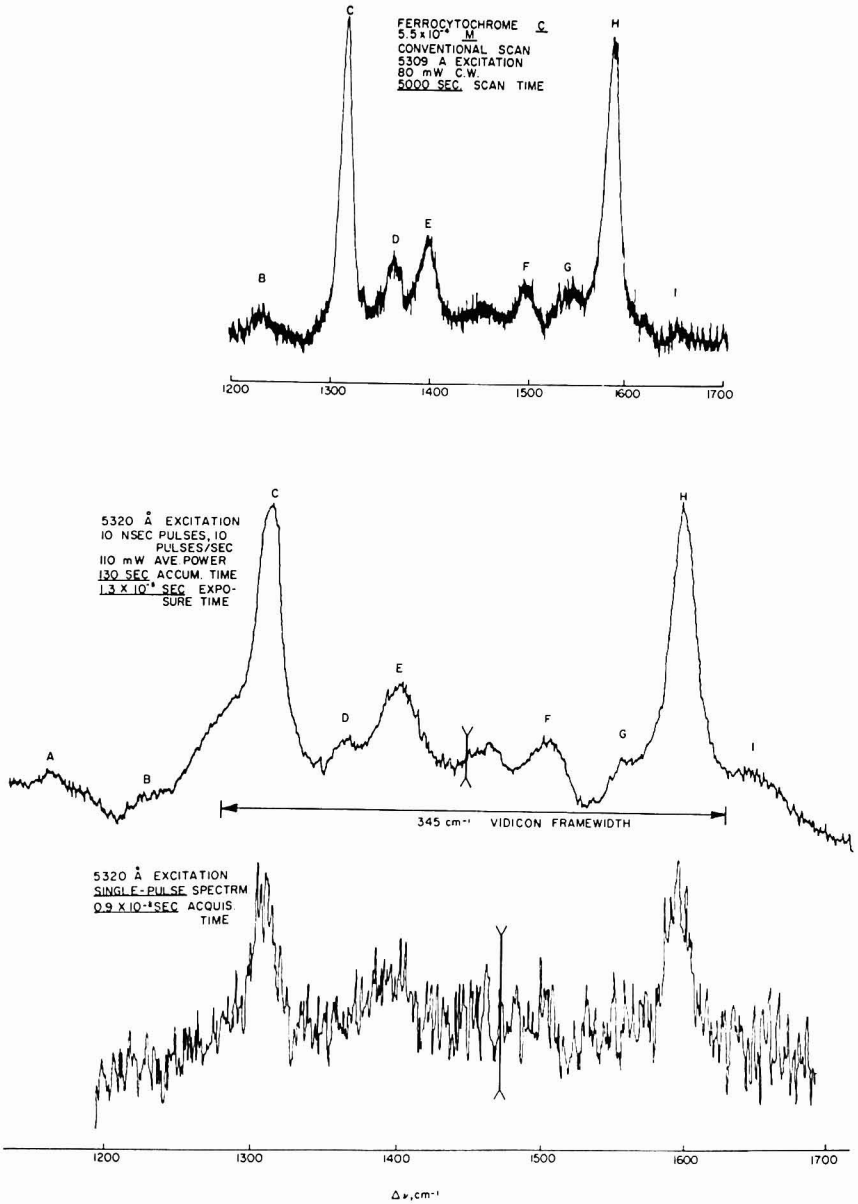

Figure 1. Conventional (CW scanned) and time-resolved resonance Raman spectra of cytochrome c. Top, CW excitation by 5309 Å Kr^+ laser line, scanning spectral detection by Cary 82 spectrometer; middle, 5318 Å (Nd:YAG second harmonic) repetitive-pulse TR^3 spectrum, vidicon spectrographic detection; bottom, single-pulse spectrum. See text. The double-headed arrows in the vidicon spectra denote the points where two vidicon exposure frames were spliced together

during the 0.6-μs retrace time of the OMA detector. Otherwise the conditions were identical to those employed for the repetitive-pulse spectrum. The S/N of the single shot spectrum, 3.5 for peaks C and H, is the expected factor of 36 poorer than for the repetitive-pulse spectrum, and approximately a factor of 8 poorer than the CW-scanned spectrum. Nevertheless, the main features, peaks C, E, H, and perhaps F, are visible in the single-shot spectrum. The acquisition time for the single-shot spectrum is a flat factor of 7×10^{11} shorter than that for the CW-scanned spectrum in Figure 1. Considering the S/N deficit suffered by the single-shot spectrum, allowing the CW spectrum to be acquired 64 times faster than that in Figure 1 to give S/N equal to the single-shot spectrum, this represents a real improvement of ten orders of magnitude over the conventional Cary 82 spectrometer in the temporal acquisition of comparable spectra. We feel that the S/N of the single-shot spectrum can be improved by a factor of three to ten by improving the present scattering geometry, without changing other experimental parameters.

Compared to the previous TR^3 studies (*4*, *5*), the present report represents a conspicuous improvement in S/N for repetitive-pulse TR^3 for comparable time resolution, and an improvement of two orders of magnitude in time resolution over the only previously reported single-shot TR^3 spectra (*5*). We are presently pursuing in these laboratories applications of TR^3 and related techniques to the dynamics of heme protein ligation and electron transfer reactions.

LITERATURE CITED

(1) T. G. Spiro and T. M. Loehr in "Advances in Infrared and Raman Spectroscopy", Vol. 1, R. J. H. Clark and R. E. Hester, Ed., Heyden, London, 1975, Chapter 3.
(2) William H. Woodruff and George H. Atkinson, *Anal. Chem.*, **48**, 186 (1976).
(3) William H. Woodruff and S. Farquharson in "New Applications of Lasers in Chemistry", G. M. Hieftje, Ed., American Chemical Society, Washington, 1978, in preparation.
(4) A. Campion, J. Terner, and M. A. El-Sayed, *Nature (London)*, **265**, 659 (1977).
(5) R. Wilbrandt, P. Pagsberg, K. B. Hansen, and C. V. Weisberg, *Chem. Phys. Lett.*, **39**, 538 (1976).
(6) M. Bridoux, A. Delfontaine, and C. Reiss, *C. R. Hebd. Seances Acad. Sci., Ser. C*, **282**, 771 (1976).
(7) M. Delhaye in "Proceedings of the 5th International Conference on Raman Spectroscopy", E. E. Schmid et al., Schulz, Freiburg, 1976, p 747.
(8) W. L. Peticolas, ref. 7, p 163.
(9) K. B. Lyons, H. L. Carter, and P. A. Fleury in "Light Scattering in Solids", M. Balkanski, R. C. C. Leite, and S. P. Porto, Ed., Flammarion Sciences, Paris, 1976, p 244.
(10) D. L. Jeanmarie, M. R. Suchanski, and R. P. Van Duyne, *J. Am. Chem. Soc.*, **97**, 1699 (1975).
(11) D. L. Jeanmarie and R. P. Van Duyne, *J. Am. Chem. Soc.*, **98**, 4029 (1976).

William H. Woodruff*
Stuart Farquharson

Department of Chemistry,
The University of Texas at Austin,
Austin, Texas 78712

RECEIVED for review February 27, 1978. Accepted May 19, 1978. The authors are grateful for support of this work by NSF Grant CHE77-15220, by Research Corporation Cottrell Grant 7557, and by an instrumental setup grant from The University of Texas at Austin. This work was presented at the Symposium on New Applications of Lasers in Chemistry, 175th National Meeting, American Chemical Society, Anaheim, California, March 14, 1978.

Fast Fourier Transform Based Interpolation of Sampled Electrochemical Data

Sir: The expanding use of on-line, computerized digital data acquisition in scientific measurements has many demonstrated benefits. However, one apparent disadvantage of this measurement approach is the fact that the acquired data are sampled, rather than continuous. If sampling rates cannot be made sufficiently large, resolution problems can arise which are not encountered with continuous analog data. For example, precise identification of magnitude and position of peak-type responses, as well as recognition of peak-shoulder combinations, in chromatography, spectroscopy, and electrochemistry may be hindered by inadequate resolution of sampled data. These difficulties can be overcome somewhat by drawing a smooth curve through the sampled data. However, this form of manual interpolation is too subjective to provide an adequate solution. A more objective interpolation approach, based on a firm mathematical foundation, is needed. One of the most appealing of these is Fourier domain (FD) interpolation, which has been successfully implemented in processing spectroscopic data by Griffiths (*1*), and Horlick and Yuen (*2*). FD interpolation is a convenient, simple, and mathematically rigorous technique whereby the FD spectrum of the data array to be interpolated is computed, extended by a factor of 2^n (n = positive integer) by "zero filling" (*1*), and inverse Fourier transformed. The resulting interpolated array contains 2^n times the number of points in the original array. The procedure validity rests upon the assumption that the original data array, while possibly providing insufficient resolution to satisfactorily serve its intended purpose, is adequate to define its FD spectrum. Assuming that an on-line minicomputer is the element which controlled the original data sampling, it is convenient to implement the FD interpolation approach using the FFT algorithm as the basis for data domain–Fourier domain transforms.

Electrochemical measurements represent a field where sampled data interpolation can be quite useful in assisting evaluation of parameters such as peak magnitude and position, peak full-width at half-height, half-wave potentials, peak separations, and the like, yet we are unaware of published work in this area. Because FFT software or hardware already is required in FFT faradaic admittance measurements (*3*, *4*), the FD interpolation concept is particularly convenient and appealing in this context, especially when the ac cyclic voltammetric (*5*) and rapid dropping mercury electrode (*6*) modes are invoked with rapid dc potential scan rates. If FD interpolation can be shown to be precise and accurate in an electrochemical context, the concept of reducing total measurement time and computer memory requirements by acquiring fewer-than-normal points along the dc potential, time, or frequency axes can be entertained. Rather than increasing data density by special sampling techniques (*7*), which put significant demands on measurement repeatability, the data density may be enhanced by FD interpolation. Because of the foregoing considerations, we have evaluated the FD interpolation procedure in the context of faradaic admittance voltammograms, polarograms, and frequency spectra, as well as dc cyclic voltammetry. We believe these data types to be reasonably representative of the response types encountered

0003-2700/78/0350-1391$01.00/0

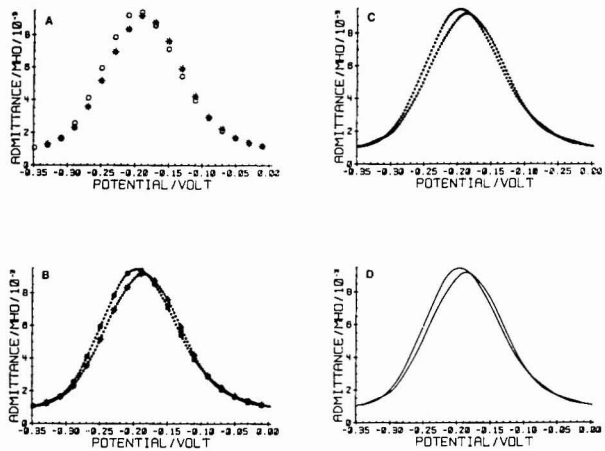

Figure 1. Fourier domain interpolation of FFT ac cyclic voltammogram. System: 8.0×10^{-4} M $TMPD^+$ at Pt–0.1 M tetrabutylammonium perchlorate, CH_3CN interface, 25 °C. Applied: Pseudo-random, odd-harmonic ac waveform (*3*) with 1.5 mV/frequency component, 40 components, superimposed on a staircase dc scan with triangular envelope whose scan rate = 150 mV/s. Dc potentials are in volts vs. Ag/0.010 M $AgClO_4$, CH_3CN. Measured: faradaic admittance magnitude at 488 Hz, obtained with a single measurement pass without FFT digital filtering (39 other frequency components also measured, but not shown); (A) original data only, (B) original and interpolated ($\times 2^3$) data, (C) interpolated data only, and (D) continuous curve constructed by drawing straight lines between interpolated data points (Figure 1C). Notation: O, * = original sampled data, forward and reverse scans, respectively; o, x = interpolated data, forward and reverse scans, respectively

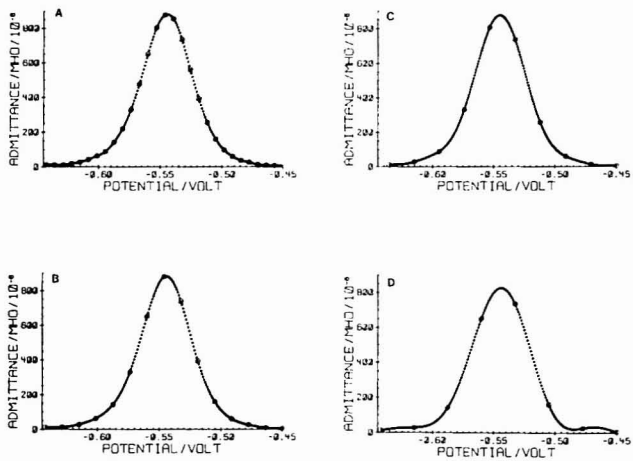

Figure 2. Effects of reducing original admittance polarogram data density on accuracy of FD interpolation. System: Hg–aqueous 1.0 M Na_2SO_4, 1.0×10^{-3} M Cd(II) interface, 25 °C. Applied: Same as Figure 1, except 34 frequency components, staircase dc scan synchronized to rapidly dropping mercury electrode of 0.25-s drop life, and dc potentials are vs. Ag/AgCl (sat'd NaCl). Measured: 10 replicate average of in-phase faradaic admittance magnitude at 585.9 Hz., without FFT digital filtering; (A) original 30 sampled data points, and interpolated ($\times 2^3$) result, (B) 15 points from original data set and interpolated ($\times 2^4$) result, (C) 10 points from original sampled data and interpolated ($\times 2^5$) result, (D) 8 points from original sampled data and interpolated ($\times 2^5$) result. Notation: O = original data, o = interpolated data

in electrochemical relaxation measurements. Some typical results are presented here.

The software routine we have written to invoke FD interpolation utilizes the FFT algorithm. It also allows one to invoke FFT digital filtering (*8*) to smooth the data sets prior to (or after) interpolation. Whether or not digital filtering is invoked, the software fits a polynomial to several points on each extremity of the original data array and subtracts this polynomial from the original array before interpolation and/or filtering. This data domain modification ensures that the data domain array will begin and terminate at zero magnitude, with a negligible first derivative, effectively suppressing truncation error (*8–10*) which can arise in either the filtering or interpolation step. A suitably interpolated version of the polynomial is added to the interpolated data domain array as the final step, producing the enhanced version of the original data

Table I. Parameters Obtained from Interpolated Data of Figure 2

no. of sampled data points in initial array	interpolation factor	peak dc potential, V	peak admittance, mho × 10^4	peak full-width at half-height, mV
30[a]	$\times 2^0$	−0.544	8.80	47
30	$\times 2^3$	−0.5442	8.827	47.4
15	$\times 2^4$	−0.5444	8.828	48.7
10	$\times 2^5$	−0.5444	8.753	48.8
8	$\times 2^5$	−0.5437	8.284	53.9

[a] Best estimates from original data.

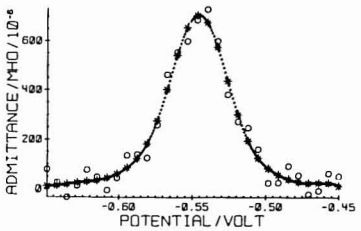

Figure 3. Effect of FFT digital filtering and interpolation on a noisy in-phase faradaic admittance polarogram. System, applied, and measured as in Figure 2, except frequency is 195.3 Hz., O = original sampled data, * = original data after digital filtering, and + = interpolated ($\times 2^3$), filtered data

array. When a data domain set does not contain 2^n (n = integer) points, as required by the FFT algorithm, the data set is zero-filled to the nearest 2^n-point value, following the polynomial subtraction routine. As long as preceded by polynomial subtraction, zero-filling causes no errors. The program is interactive, allowing the operator to enter appropriate parameters for the data domain polynomial modification, the optional FFT filtering, and the FFT interpolation. We call attention to a recently presented interpolation algorithm (*11*) which is equivalent to the FFT approach described here, but uses significantly fewer calculations. However, significant time savings are not realized with the small transforms used in this work.

Figure 1 shows interpolation results with some ac cyclic faradaic admittance voltammograms on the $TMPD^+/TMPD$ couple (TMPD = tetramethylphenylenediamine) at a Pt electrode in a nonaqueous electrolyte. An essentially perfect match between the interpolated and original data trend results (Figure 1B), and identification of the forward and reverse scan "crossover point" (*12*), peak potentials, and peak magnitudes is significantly assisted by the FD interpolation (Figure 1C). Points are sufficiently close-spaced in the interpolated voltammogram that the ultimate interpolation, a continuous curve, can confidently be generated by the expedient of a straight line fit between adjacent data points (Figure 1D).

An important question when considering use of FD interpolation is how many sampled data points are required to accurately define the data array FD spectrum. This question is addressed in Figure 2, where a relatively narrow two-electron reduction faradaic admittance polarogram is considered. The original polarogram, composed of 30 sampled data points, is interpolated to 232 points in Figure 2A. Figure 2, B–D show results of deleting data points from the original data set, followed by interpolation to approximately 232 points. Casual examination of the results clearly indicates that beginning with only 8 data points (Figure 2D) leads to qualitative distortion of the polarogram. However, such distortion is not evident for the 15 and 10 sampled data point cases (Figure 2, B and C). Indeed, careful inspection of admittance magnitude printouts indicates that, although systematic error in the

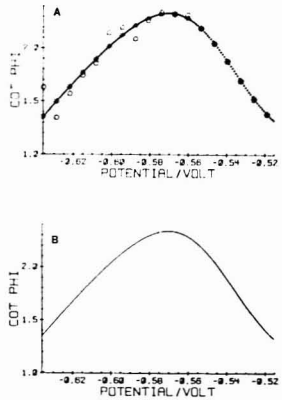

Figure 4. Effect of FFT digital filtering and interpolation on a typical cot ϕ polarogram. System and applied as in Figure 2. Measured: cot ϕ vs. dc potential at 585.9 Hz., where (A) uses same notation as Figure 3, and (B) is continuous curve obtained as in Figure 1D

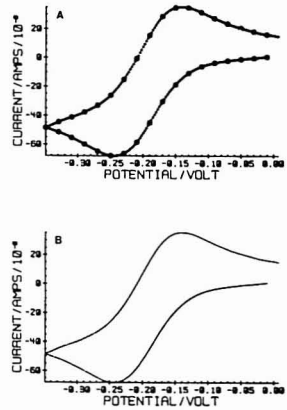

Figure 5. FD interpolation applied to a dc cyclic voltammogram. System, applied, and measured as in Figure 1, except dc component measured, (A) shows original (O) and interpolated (o) data, and (B) is a continuous curve obtained as in Figure 1D

admittance magnitude becomes detectable with 10 points, the FD interpolation results with this sparse data set still yield satisfactory peak parameters (Table I).

Figures 1 and 2 eschew FFT digital filtering because the raw data are relatively noise-free. This is not the case in Figure 3, which shows results of combining digital filtering and

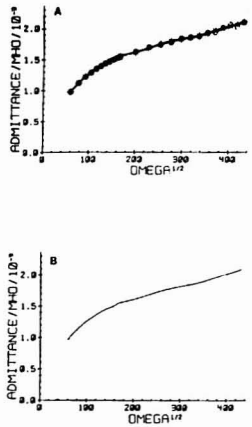

Figure 6. Application of FD interpolation on admittance spectral data. System and applied as in Figure 2. Measured: peak admittance vs. $\omega^{1/2}$. Notation: as in Figure 4

interpolation when a distressingly noisy admittance polarogram is presented. The peak potential (−0.545 V) and full-width at half-height (49 mV) obtained from the filtered, interpolated data are in excellent agreement with the values obtained from the more reliable raw data of Figure 2 and Table I.

Figures 4 and 5 illustrate typical interpolation results for a cot ϕ polarogram and a dc cyclic voltammogram, respectively. Figure 6 depicts an attempt to apply the FD interpolation procedure to admittance spectra data, where the sampled data array is not equally spaced along the abscissa, as the FFT algorithm assumes. Because of this, interpolated data point separations along the abscissa are nonuniform. Nevertheless, this not-strictly-valid procedure yields satisfactory results, including an only slightly flawed continuous spectral response (Figure 6B).

The results shown in Figures 1–6 demonstrate that FD interpolation of electrochemical data can be performed with precision, and to the point of allowing generation of a continuous analog readout, the ultimate interpolation. Ease of identification of peak potentials, widths, and magnitudes are greatly assisted. When FFT digital filtering and FD interpolation are combined, rather substantial data enhancement can be realized, allowing one to recover from a relatively noisy and/or sparse data array quite satisfactory electrochemical response parameter values. The concept of reducing sampled data density to conserve computer memory and/or measurement time, and recovering the lost resolution via FD interpolation is supported by the above results.

ACKNOWLEDGMENT

We are indebted to Richard Schwall for developing the polynomial modification software.

LITERATURE CITED

(1) P. R. Griffiths, *Appl. Spectrosc.*, **29**, 11 (1975).
(2) G. Horlick and W. K. Yuen, *Anal. Chem.*, **48**, 1643 (1976).
(3) D. E. Smith, *Anal. Chem.*, **48**, 221A (1976).
(4) R. J. Schwall, A. M. Bond, R. J. Loyd, J. G. Larsen, and D. E. Smith, *Anal. Chem.*, **49**, 1797 (1977).
(5) A. M. Bond, R. J. Schwall, and D. E. Smith, *J. Electroanal. Chem.*, **85**, 231 (1977).
(6) R. J. O'Halloran, J. C. Schaar, and D. E. Smith, *Anal. Chem.*, **50**, 1073 (1978).
(7) S. C. Creason, R. J. Loyd, and D. E. Smith, *Anal. Chem.*, **44**, 1159 (1972).
(8) J. W. Hayes, D. E. Glover, D. E. Smith, and M. W. Overton, *Anal. Chem.*, **45**, 277 (1973).
(9) G. Horlick, *Anal. Chem.*, **44**, 943 (1972).
(10) R. de Levie, S. Sarangapani, P. Czekaj, and G. Benke, *Anal. Chem.*, **50**, 110 (1978).
(11) M. L. Forman, *Appl. Opt.*, **16**, 2801 (1977).
(12) A. M. Bond, R. J. O'Halloran, I. Ruzic, and D. E. Smith, *Anal. Chem.*, **48**, 872 (1976).

Roger J. O'Halloran
Donald E. Smith*

Department of Chemistry
Northwestern University
Evanston, Illinois 60201

RECEIVED for review March 20, 1978. Accepted May 9, 1978. Work supported by the National Science Foundation (Grant No. CHE77-15462).

Fluorescence Line Narrowing Spectrometry in Organic Glasses Containing Parts-per-Billion Levels of Polycyclic Aromatic Hydrocarbons

Sir: The fact that carcinogenic and mutagenic properties of polynuclear aromatic hydrocarbons (PAHs) can be strongly dependent on isomeric structure (*1*) has prompted us to develop new laser based methodologies characterized by resolution sufficient to distinguish between structural isomers. In addition to very high selectivity, the requirements that our techniques be quantitative, sensitive (≲1 ppb), nondestructive, and rapid have limited the scope of our investigations.

Given the critical dependence of the electronic structure of polyatomic molecules on nuclear geometry and the substantial fluorescence quantum efficiencies of PAHs (*2*), fluorescence based methods for PAH measurements seem very attractive. However, the aforementioned selectivity requirement presents real difficulties and precludes, for example, liquid solution or conventional gas phase fluorescence spectrometry as viable starting points. In the latter case, overlapping rotational structure produces broad rovibronic bands while in the former case, solute–solvent interactions also afford broad bandwidths (FWHM ~200 cm^{-1}). (All bandwidths stated below are "full-width half maximum" or FWHM.)

Although it appears that the problem of overlapping rotational structure can be eliminated (*3*), we wish to report here on a solid state fluorescence based technique which we believe satisfies all the requirements delineated above. Before describing it, we note that it has been known for over 20 years that the low temperature electronic absorption and luminescence spectra of PAHs imbedded in crystalline matrices can be sharp (≲5 cm^{-1}) (*4*). This degree of sharpness satisfies the selectivity requirement. For *any* matrix, selectivity can also be enhanced temporally (*5*) since PAH fluorescence lifetimes are known to vary by several orders of magnitude (*2*). Possible matrices include host PAH crystals, Shpol'skii (*n*-paraffin) solvents, and, to a lesser extent, "inert" gases like

0003-2700/78/0350-1394$01.00/0

Ar. The first and last matrices do not seem very attractive, partly because of lengthy (~several hours) sample preparation time. Quantitative measurements on and characterization of PAHs in Shpol'skii matrices are being pursued (*6*). It should be noted that mismatch of the PAH and *n*-paraffin lengths leads to broad fluorescence bandwidths when excitation is provided with broad band or high energy sources. The multiplet structure (due to energetically inequivalent impurity sites) characteristic of Shpol'skii matrices poses another problem since the multiplet fluorescence pattern depends on the sample cooling rate (*7*). In our opinion, these problems are soluble but at the expense of sample analysis time (for example, resolution of a complex mixture of PAHs would require the use of several different Shpol'skii matrices).

Fluorescence line narrowing spectroscopy (FLNS) of PAHs in organic glasses is the alternative solid state approach to be described here (*8*). Although low temperatures (~4 K) electronic molecular absorption spectra in glasses are severely broadened (FWHM of vibronic bands ~200 cm^{-1}) due to site inhomogeniety, narrow laser line excitation near (vide infra) the absorption origin of the fluorescent state affords sharp lined fluorescence spectra. This effect in glasses was first observed by Personov and co-workers (*9*). The same effect in mixed molecular crystals was observed using incoherent monochromatic excitation as early as 1967 (*10*). FLNS is simply a manifestation of the fact that only impurity sites whose excitation profiles overlap with the laser frequency profile are able to fluoresce. It is most pronounced at low temperature (~4 K) where impurity site interconversion rates are not competitive with fluorescence. Frequently, the reported vibronic linewidths in line narrowed spectra are laser limited, i.e., the homogeneous fluorescence linewidth is narrower than the laser linewidth.

Organic glasses were the media of choice for our FLNS studies for the following reasons: PAH solubility and concentration gradient problems are minimized, high optical quality which minimizes laser scattering, broad impurity absorption linewidths which facilitate PAH excitation, and their potential for accepting water. The latter property allows for direct analysis of contaminated water samples, vide infra. At the outset, we realized that the applicability of FLNS for PAH measurements would be limited primarily by the glass characteristics. After surveying several different glasses, the 1:1 glycerol:H_2O system was found to be almost ideal. Glass formation at $T \lesssim 4.2$ K is facile (15-min cool down time from room temperature with *no* glass cracking), the glass has a high water content, and the high glass quality is *reproducible*. These properties will be emphasized in what follows.

A full description of the FLNS system will be given at a later date. Briefly, it consists of a 3-L Pope Scientific double nested glass liquid He Dewar with quartz optical windows (hold time ~6 h), and a Control 553 U Ar-ion laser with UV output at 363.8, 351.4, 351.1, 335.8, 334.5, and 333.6 nm. Laser powers delivered at the sample are typically 100, 30, 110, 20, 20, and 20 mW, respectively. Spatial separation of the laser lines is achieved with external prisms. Saturation effects at these power levels are negligible. The detection electronics include a photon counting system, although the data presented here were obtained using conventional analog detection with a cooled EMI 9558 QB PMT. A McPherson Model 218 1/3-meter spectrometer was utilized, unless otherwise stated, at a 0.1-nm resolution with slits collinear to the laser beam. Thin walled plastic culture tubes (1-cm o.d.) are used for glass formation and are at least 85% transmitting at all excitation wavelengths.

It is worth noting that molecular absorption spectra of species imbedded in organic glasses can be subject to the phenomenon known as laser induced nonphotochemical hole burning (*11*). The hole burning does affect fluorescence intensities but only to a small extent and, fortunately, in a way that would not affect the analytical capabilities of FLNS in organic glasses (*12*). Glycerol was found to exhibit sufficiently low background fluorescence to permit its use without further purification. For example, we were unable to detect pyrene and anthracene in blank glycerol:H_2O glasses.

Table I. Comparison of the Line-Narrowed Fluorescence Spectrum of Pyrene in a 1:1 Glycerol–Ethanol Glass at 4.2 K with the Fluorescence Spectra of Pyrene in Biphenyl and Fluorene at ca. 10 K[a]

fluorene[b]	biphenyl[b]	glass[c]	analysis
26690 vs	26734 vs	26902 vs	origin
410 s	408 vs	408 ms	408, A_g
459 m	456 m	460 w	456, B_{1g}
597 m	596 s	592 w	596, A_g
738 m	736 s	734 m	736, B_{1g}
805 ms	801 s	805 ms	801, A_g
820 m	816 m		2 × 408
1066 ms	1063 s	1068 w	1063, A_g
1116 ms	1111 ms	1110 ms	1111, B_{1g}
1213 m	1208 mw	1210 vw	408 + 801 − 1
1246 ms	1240, 1246 s	1243 mw	1240, A_g
1335 w	1332 vw	1330 mw	596 + 736
1409 vs	1408 vs	1410 s	1408, A_g
1476 m	1471 w	1476 vw	408 + 1063
1555 ms	1552 s	1550 mw	1552, A_g

[a] The position of the origin is given in cm^{-1} and is vacuum corrected for the mixed-crystal spectra. All other entries show differences from the origin. [b] Lines of "medium" strength, or greater, have been taken from reference 15 as has the analysis above. [c] Spectrum excited by λ_{ex} = 363.8 nm, 90 mW at the sample.

The greatest amount of fluorescence line narrowing is obtained when λ_{ex} (excitation wavelength) lies within the absorption origin of the fluorescent state, S_1. As the excess vibrational energy in S_1 provided by λ_{ex} increases, the probability of exciting different vibrational sublevels belonging to different sites of a given impurity increases. Ultimately, when excitation is into a very spectrally congested region, the fluorescence line narrowing effect is essentially completely lost. This behavior is shown in Figure 1 for pyrene in a 1:1 glycerol:ethanol glass. The prominent band near 372 nm in the upper spectrum is the principal fluorescence origin. The 363.8-nm laser line corresponds to excitation ca. 560 cm^{-1} above the zero-point level of S_1. The origin's linewidth is 0.16 nm (instrument limited). The fluorescence spectrum is quite detailed and can be compared with the very sharp fluorescence spectra of pyrene obtainable in mixed crystals at low temperature, see Table I. The weak but sharp band to lower energy of the principal origin (at 370.6 nm) is a secondary pyrene fluorescence origin due to different pyrene sites than those which contribute to the major origin. In the middle spectrum, the excess vibrational energy provided by the λ_{ex} = 351.1, 351.4 nm doublet is ~1600 cm^{-1}. Note that the principal fluorescence origin exhibits a prominent doublet (splitting = 0.3 nm) due to excitation with the two different laser lines. The doublet component linewidths are 0.3 nm. Finally, in the lower spectrum, the average excess vibrational energy is ~3000 cm^{-1} and no sharp structure is observed. The origin linewidth is 1.7 nm, and this width equals the fluorescence linewidths due to any one of the three laser lines (as verified by spectra obtained using each of these three laser lines individually). Behavior similar to that depicted in Figure 1 has been reported previously (*8, 9*). The spectra suggest the potential advantage to be gained by using a tunable dye laser to generate the FLNS of PAHs. Only then can one be assured of generating sharp line fluorescence spectra for all species. The additional advantage of tunability is that it provides a

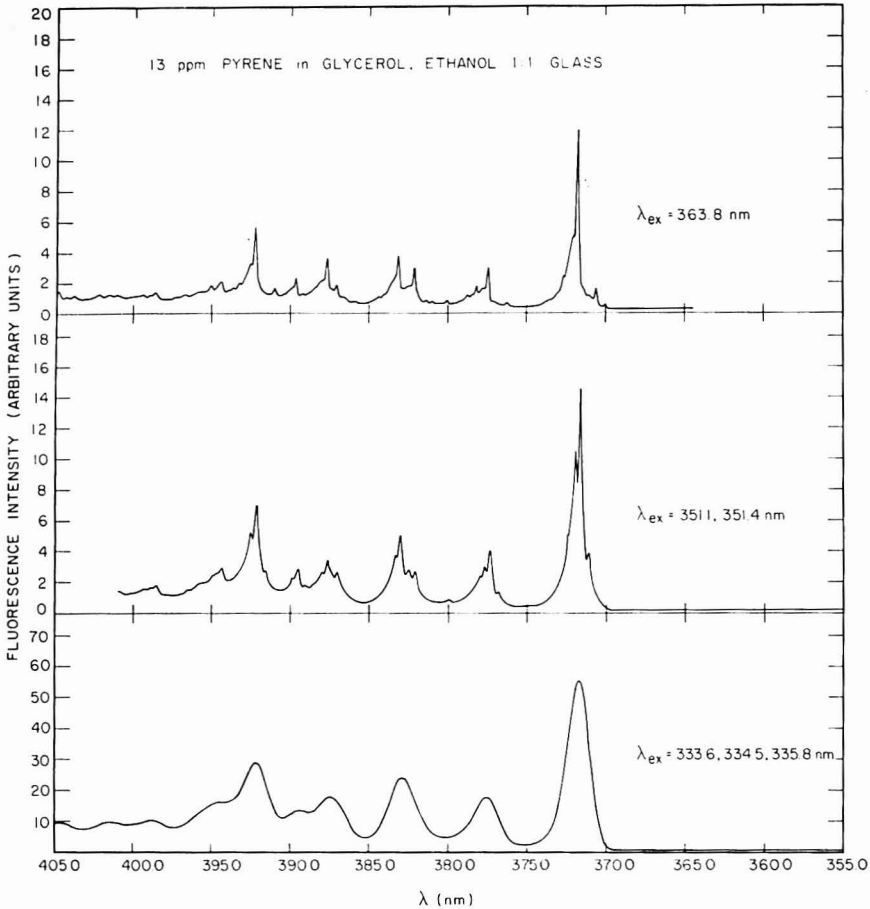

Figure 1. Relationship between the fluorescence linewidth and the excess energy content of the exciting light quantum

degree of *selective excitation* which will greatly simplify the analysis of complex mixtures. When λ_{ex} lies above the absorption origin of a constitutent molecule, that molecule will not be electronically excited and will not fluoresce. Thus in a mixture of two isomers, e.g., anthracene and phenanthrene, which are known to be difficult to resolve using conventional GC-MS techniques (*13*), the excitation wavelength may be chosen to excite anthracene while being too low in energy to excite phenanthrene, thereby resolving the mixture.

With our existing laser, sharp line spectra in glycerol:water glasses have been obtained for many PAHs including pyrene, anthracene, phenanthrene, azulene, 9-methylanthracene, triphenylene, and chrysene. Attention has been focused on pyrene and anthracene since their absorption spectra are quite compatible with the 363.8-nm laser line. Representative spectra are shown in Figure 2. The upper spectrum is that of anthracene (as verified by vibrational analysis) with the principal fluorescence origin near 380 nm. The broader feature built on the origin and displaced 0.5 nm (35 cm^{-1}) to lower energy is a phonon side band. Similar structure can be seen on the intramolecular zero-phonon vibrational bands. While the matrix used for these studies is formally a *glass*, we observe structures in our spectra which are similar to ones observed in crystal spectra. We use the term "phonon" broadly for we cannot envision the effective delocalization of a vibrational mode throughout the glass matrix. The side bands may be intimately connected with the solvent cage–excited molecule interaction and, in fact, the relative magnitude of the phonon wing to the O–O line varies from one glass to another. The 363.8-nm excitation wavelength is ~1100 cm^{-1} above the fluorescence origin and at least partially explains why the anthracene zero-phonon linewidths are somewhat broader than those of pyrene (lower spectrum). The lower spectrum agrees well with that in Figure 1 particularly since the glasses are different. The lower two spectra in Figure 2 were obtained at a sensitivity 5× greater than the upper one. We note that the middle spectrum corresponds to an equal mixture of anthracene and pyrene (100-ppb concentration). Comparison of the pyrene fluorescence intensities in the two lower spectra gave us the first indication that the glycerol:water glass quality

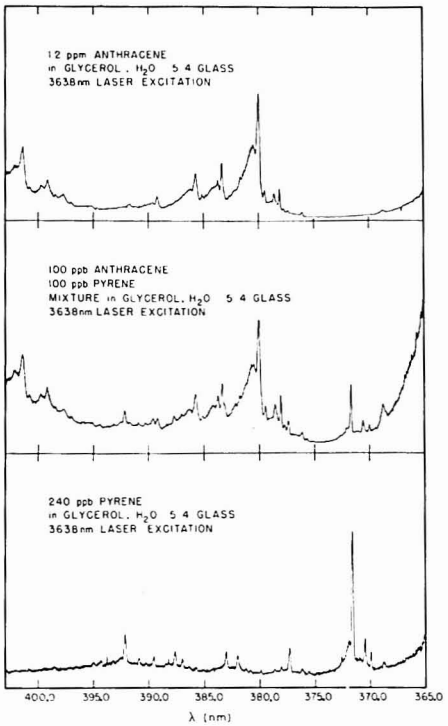

Figure 2. Resolution of a mixture of two PAHs through fluorescence line narrowing spectrometry. All spectra were measured at 4.2 K and excited by λ_{ex} = 363.8 nm

might be sufficiently reproducible to permit quantitative measurements on PAHs without having to resort to internal standards.

That this is the case has been firmly established for both pyrene and anthracene. The data for concentrations ranging between 3 ppm and 1 ppb are contained in Table II. For both, the principal fluorescence origin peak height was used for calibration. The linearity between peak height and concentration expected in the low concentration regime is observed, cf. caption to Table II. The following points deserve emphasis. (i) Data in Table II were obtained using mixtures of pyrene and anthracene with the concentration of the PAH of interest varying between 0.2 and 5.0 times the concentration of the other component. (ii) Data were collected over a 3-day period so that more than three liquid helium Dewar preparations and liquid helium transfers were involved. (iii) Facile glass formation of glycerol:H_2O permitted analysis of ~15 samples during a 6-h period.

In regard to the first point, one would not expect Förster energy transfer (*14*) for the concentration levels used in our studies to be operative and the linearity of our data is consistent with this assertion. We have prepared quite complex multicomponent PAH samples containing known amounts of pyrene and anthracene and have found their analysis to be unaffected by the other species. At the present time, real samples are being analyzed for PAHs such as phenanthrene, anthracene, chrysene, and pyrene.

Table II. Calibration Data

pyrene		anthracene	
concn, ppb	peak height, μA[a]	concn, ppb	peak height, μA[a]
5	0.006	1	0.0024
10	0.014	5	0.010
50	0.061	10	0.021
100	0.120	50	0.098
500	0.560	100	0.170
1000	1.0	500	1.0
3000	2.8	1000	1.8
		3000	3.9
least squares correlation coefficient = 0.993		least squares correlation coefficient = 0.989	

[a] The origin, zero phonon, line was measured (background corrected). Between two and five points were taken at each concentration with an average precision, calculated as the average deviation, of 8%.

Within the near future, the FLNS system will be expanded to include a tunable N_2-pumped dye laser, a gated detection system, and a rapid scan intensified diode array spectrometer. In this way, the resolution (selectivity) will be significantly enhanced, both through selective excitation and temporal discrimination. The addition of a diode array spectrometer promises to ensure that a convenient analysis time for even complex multicomponent samples can be maintained.

In summary, it is our belief that laser induced FLNS of fluorescing organic pollutants such as the PAHs in organic glasses will develop into a practical analytical tool possessing the attributes discussed earlier. The high selectivity (resolution of structural isomers) and ability to analyze contaminated water samples directly (without preseparation of the contaminants) are particularly noteworthy.

LITERATURE CITED

(1) M. L. Lea, M. Novotny, and K. D. Bartle, *Anal. Chem.*, **48**, 405 (1976) and references therein.
(2) J. B. Birks, "Photophysics of Aromatic Molecules", Wiley-Interscience, London, 1970.
(3) R. E. Smalley, L. Wharton, and D. Levy, *J. Chem. Phys.*, **64**, 3266 (1976).
(4) D. S. McClure, *J. Chem. Phys.*, **22**, 1668 (1954); E. V. Shpol'skii, A. A. Il'ina, and L. A. Klimova, *Dokl. Akad. Nauk SSSR*, **87**, 935 (1952).
(5) J. H. Richardson and M. E. Ando, *Anal. Chem.*, **49**, 955 (1977).
(6) G. F. Kirkbright and C. G. deLima, *Analyst (London)*, **99**, 338 (1974).
(7) C. Pfister, *Chem. Phys.*, **2**, 181 (1973); E. V. Shpol'skii and T. N. Bolotnikova, *Pure Appl. Chem.*, **37**, 183 (1974).
(8) J. H. Eberly, W. C. McColgin, K. Kawaoka, and A. P. Marchetti, *Nature (London)*, **251**, 215 (1974).
(9) R. I. Personov and B. M. Kharlamov, *Opt. Commun.*, **7**, 417 (1973).
(10) G. J. Small, Ph.D. dissertation, University of Pennsylvania, Philadelphia, Pa., 1967.
(11) B. M. Kharlamov, R. I. Personov, and L. A. Bykovskaya, *Opt. Commun.*, **12**, 191 (1974).
(12) J. M. Hayes and G. J. Small, *Chem. Phys.*, **27**, 151 (1978).
(13) H. Svec, Ames Laboratory—USDOE and Department of Chemistry, Iowa State University, Ames, Iowa, private communication.
(14) R. C. Powell and Z. G. Soos, *J. Lumin.*, **11**, 1 (1975).
(15) A. Bree and V. V. B. Vilkos, *Spectrochim. Acta, Part A*, **27**, 2333 (1971).

J. C. Brown
M. C. Edelson
G. J. Small*
Ames Laboratory—USDOE and Department of Chemistry
Iowa State University
Ames, Iowa 50011

RECEIVED for review March 20, 1978. Accepted May 1, 1978. Work performed and supported by the Division of Biomedical and Environmental Research (Physical and Technological Programs) of the U.S. Department of Energy.

Fluorescence Labeling of Dicarboxylic Acids for High Performance Liquid Chromatographic Separation

Sir: Easy and efficient methods are needed for the separation and detection of dicarboxylic acids in urine or in blood serum. Present methods frequently involve the derivatization of the acids for separation and identification by GC or GC-MS. Jellum (*1*) has recently reviewed the use of GC-MS in the analysis of organic acid in body fluids.

The analysis of dicarboxylic acids and α-keto acids by HPLC is not yet widespread. One of the major reasons for that fact lies in the lack of a suitably sensitive detector for all but the aromatic acids. Some attempts have been made to use the quinoxalone derivatives of α-keto acid (viz., *2*) in HPLC. The quinoxalone reagent is highly selective toward α-keto acids, and the derivative can be detected by UV or fluorescence. Phenacyl derivatives of dicarboxylic acids have been used in HPLC in conjunction with a UV detector (*3*).

Recently Dünges (*4*) has reported the use of 4-bromomethyl-7-methoxycoumarin (Br-Mmc) as a fluorescence labeling reagent in the TLC analysis of fatty acids. Dünges et al. (*5*) have reported an improved procedure using crown ether. Lam and Grushka further improved the methodology by using a crown ether catalyst (*6*) and they have separated the derivatives using reversed phase HPLC. Dünges, in his work (*4*, *5*), reported that the dicarboxylic acids could not be derivatized with Br-Mmc.

Fluorescence labeling in conjunction with HPLC is attractive since the detection limits are quite low. To the best of our knowledge, however, the preparation and separation of fluorescing derivatives of dicarboxylic acid have not been attempted. This is somewhat surprising in view of the physiological importance of these compounds. The present paper described the procedure by which the Mmc derivatives of dicarboxylic acids and α-keto acids can be formed. Use is being made of the fact that the potassium salts of the acids can be transferred to an aprotic solvent with crown ethers. The carboxylate ions in an aprotic solvent are rather reactive, thus facilitating alkylation reactions. The derivatives of the acids can then be separated by HPLC and detected with a fluorometer.

EXPERIMENTAL

Apparatus. The liquid chromatograph consisted of a model 396 Milton Roy Minipump (LDC, Riveria Beach, Fla.), and a Gilson (Middletown, Wis.) Spectra/Glo fluorometer. The excitation filter had a maximum transmittance at 360 nm and the emission filter had a cut-off valve of 400 nm. The samples were introduced via a Rheodyne injection valve model 70-10 purchased from Altex Scientific Co. (Berkeley, Calif.). The stainless steel column, 22.3 cm × 4.2 mm i.d., was packed by the conventional slurry technique with C_{18} bonded Partisil 10.

Regents. Partisil 10 was obtained from Whatman Co. (Clifton, N.J.). The dicarboxylic acids, 18-crown-6, DNS (5-dimethylamino-1-naphthalenesulfonyl chloride), and solvents were obtained from various sources and used without further purification. 4-Bromomethyl-7-methoxycoumarin (Br-Mmc) was prepared according to Secrist et al. (*7*). The α-keto acids were obtained from Sigma Chemical Co. (St. Louis, Mo.) and were used without further purification. The mobile phase consisted of various ratios of reagent grade methanol and distilled, deionized water.

Procedure. The derivatives were prepared by adding 4–6 mg samples of the acids, 3–4 mg of K_2CO_3, and 1–2 mg of crown ether to a 50-mL round bottom flask, and dissolving the mixture in 10 mL of a previously prepared solution of 4-bromomethyl-7-methoxycoumarin in acetone (0.15 g in 100 mL acetone). The reaction flask was placed in a preheated oil bath at 80–90 °C where it was allowed to reflux for 1 h. Samples for injection were obtained directly from the product solution without further treatment.

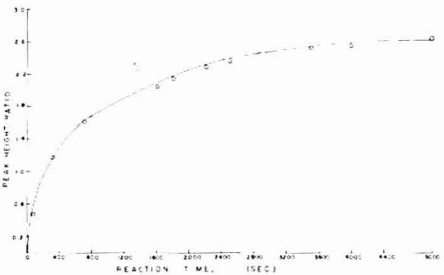

Figure 1. Study of the rate of derivative formation. The acid being derivatized is suberic acid

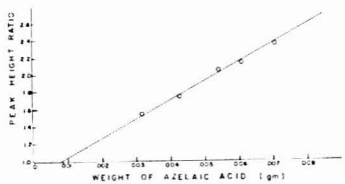

Figure 2. Relationship between the detector response and the amount of acid (azelaic) used in the reaction

The injection was made with a 25-μL syringe. The chromatograms are given in terms of relative intensity. Capacity ratios for the α-keto acids were measured relative to DNS. All the chromatographic runs were made at ambient temperatures.

RESULTS AND DISCUSSION

The excitation and emission spectra of the Mmc derivatives are described elsewhere (*5*, *6*). Lam and Grushka (*6*) have studied various derivatization schemes of mono acids with Br-Mmc. They have shown that the use of K_2CO_3 to form the salt prior to the phase transfer yields an excellent compromise between the ease of the procedure and the rate of derivative formation. Using crown ether, the reaction time was reduced drastically from that reported by Dünges (*4*). As indicated earlier, Dünges could not derivatize dicarboxylic acids. It was felt that with the crown ether transferring the dicarboxylate to an organic solvent, the derivatization reaction with Br-Mmc can be accelerated. Figure 1 shows the result of a reaction rate study. The amount of suberic acid–Mmc ester is plotted vs. the reaction time. The amount of ester formed is proportional to the peak height ratios, i.e., the height of the suberic ester relative to that of the anthracene internal standard. The figure shows that derivatization can take place and that the reaction is essentially completed in 1 h. However, sufficient acid is derivatized in a 15- to 30-minute period to give reproducible response with the fluorescence detector.

The products of the derivatization procedure should be proportional to the amount of the starting acids. Figure 2 shows a typical result. A plot of the peak height of azelaic acid–Mmc derivative relative to anthracene vs. the amount of the acid introduced to the reaction varied yields a straight line. Each experimental point was obtained after a reaction

0003-2700/78/0350-1398$01.00/0

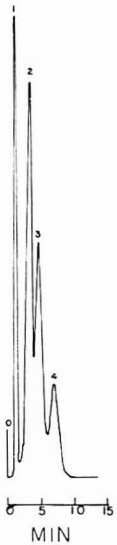

Figure 3. Separation of dicarboxylic acid derivatives on a C_{18} column. Detector: fluorometer. Mobile phase: 55% water/methanol; flow rate: 2.33 mL/min. (1) malonic, (2) succinic, (3) glutaric, (4) adipic

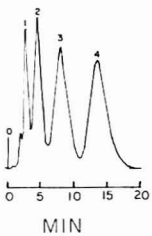

Figure 4. Separation of dicarboxylic acid derivatives on a C_{18} column. Detector: fluorometer. Mobile phase: 50% water/methanol; flow rate: 3.30 mL/min. (1) pimelic, (2) suberic, (3) azelaic, (4) sebacic

period of 1 h. The straight line indicates that the procedure is suitable for quantitative purposes.

Figures 3 and 4 show some chromatographic separations of several dicarboxylic acids. Although no attempts were made to optimize the resolution and maximize the number of acid separated, it is clear from the figures that a methanol gradient can be used to separate the C_2 to C_{10} dicarboxylic acids with little difficulty. Oxalic acid, not shown in the figure, can be derivatized rather easily.

To ascertain the detection limits, two different samples of azelaic acid were derivatized. The resultant derivative solutions were diluted successively and injected into the chromatograph until the signal was twice the noise level. The detection limit was found to be about 2×10^{-10} mol.

Table I. k' Capacity Ratios (Relative to DNS) of Some α-Keto Acids[a]

α-keto acids	k'
glyoxalic	4.25
pyruvic	4.72
α-ketobutyric	7.01
oxalacetic	5.97
α-ketoglutaric	1.99

[a] C_{18}-Partisil 10 column, 50% water/methanol mobile phase. Flowrate: 0.71 mL/min.

α-Keto acid can also be derivatized using the above procedure. Table I shows the capacity ratios, k', of several such acids. DNS was used as the inert peak in the calculations of the k' values. The large differences in the k' values indicates that the acids show in Table I can be resolved easily. The retention order of oxalacetic acid and α-ketoglutaric acid should be compared with that of succinic and glutaric acid. It is not clear to us why the shorter oxalacetic acid should elute before the longer α-ketoglutaric acid. Note that the keto monoacids elute according to the chain length: the longer the chain, the larger the k' value.

It is clear from the results shown above that a crown ether can be used to catalyze the formation of Mmc derivatives of dicarboxylic acids as well as α-keto acids. The derivatization reaction is simple, straightforward, and it can be used in quantitation studies. The reagent Br-Mmc is attractive for the following reason. In the analysis scheme used here, the reagent itself does not fluoresce, thus eliminating possible interferences from unreacted Br-Mmc. The disadvantages of the method are minor: (1) the Mmc derivatives slowly hydrolyze in the presence of water; (2) the reagent and the derivatives decompose when exposed to light over a long period of time. Consequently, all solutions should be prepared within a short time before analysis. These minor disadvantages are compensated for by the ease of preparation and sensitive detection.

LITERATURE CITED

(1) E. Jellum, *J. Chromatogr.*, **143**, 427 (1977).
(2) J. C. Liao, N. E. Hoffman, J. J. Barboriak, and D. A. Roth, *Clin. Chem. (Winston-Salem, N.C.)*, **23**, 802 (1977).
(3) E. Grushka, H. D. Durst, and E. J. Kikta, Jr., *J. Chromatogr.*, **112**, 673 (1975).
(4) W. Dünges, *Anal. Chem.*, **49**, 442–445 (1977).
(5) W. Dünges, A. Meyer, K. H. Müller, M. Müller, R. Pietschmann, C. Plachetta, R. Sehr, and H. Tuss, *Fresenius' Z. Anal. Chem.*, **288**, 361 (1977).
(6) S. Lam and E. Grushka, *J. Chromatogr.*, accepted for publication.
(7) J. A. Secrist III, J. R. Barrio, and N. J. Leonard, *Biochem. Biophys. Res. Commun.*, **45**, 1267 (1971).

Eli Grushka*
Stanley Lam
John Chassin

Department of Chemistry
State University of New York at Buffalo
Buffalo, New York 14214

RECEIVED for review March 20, 1978. Accepted May 26, 1978.

AIDS FOR ANALYTICAL CHEMISTS

Chemiluminescence Method for Atmospheric Monitoring of Nitric Acid and Nitrogen Oxides

Darrell W. Joseph and Chester W. Spicer*

Battelle, Columbus Laboratories, 505 King Avenue, Columbus, Ohio 43201

The determination of gaseous nitric acid in the lower atmosphere has frustrated atmospheric scientists for many years. Measurement of nitric acid is important to our understanding of the fate of nitrogen oxides in the atmosphere, the mechanisms of particulate nitrate formation, and the potential health and ecological (e.g., acid precipitation) effects of the acid.

In 1973, we described (*1*) a coulometric monitor for gaseous nitric acid which we subsequently employed in both smog chamber (*2*) and field (*3*) studies of the kinetics of NO_x reactions and the fate of nitrogen oxides in the atmosphere. We have recently reconfirmed the validity of the coulometric monitor in smog chamber comparisons with a long path Fourier Transform infrared spectrophotometer (*4*). Unfortunately, however, the coulometric monitor is not ideally suited to all sampling requirements. Its detection limit of a few parts per billion and its long response time (due to the subtractive nature of the analysis) make it particularly unsuitable for either remote tropospheric measurements or aircraft studies of plumes. To accommodate these situations, we have recently developed two new techniques for atmospheric nitric acid monitoring. The first is a dual filter technique (*5, 6*) which makes use of a quartz prefilter and a Nylon backup filter to simultaneously separate and collect particulate nitrate and gaseous nitric acid. This technique is applicable to very low nitric acid concentrations and has been employed for both urban studies and airborne plume investigations. A related procedure has been employed by Okita et al. (*7*) to study nitric acid in the atmosphere in Japan, and Lazarus and Gandrud (*8*) to collect stratospheric nitric acid.

The second technique involves a rapid and sensitive method for simultaneously monitoring NO_x and nitric acid by chemiluminescence. This method has a sufficiently rapid response that it can be employed for airborne plume studies, and it has the potential to be significantly more sensitive than the coulometric procedure. The remainder of this paper will be devoted to a description of this new monitor and its operating characteristics.

EXPERIMENTAL

A Thermo Electron Corporation Model 14-D chemiluminescence nitrogen oxides monitor was employed for these studies. This is a dual channel monitor which, in its normal configuration, provides simultaneous measurement of both NO and NO_x. A molybdenum catalyst operating in the 400–500 °C temperature range is employed in the NO_x channel to reduce NO_2 to NO for measurement.

We have modified the chemiluminescence instrument to simultaneously monitor NO_x and HNO_3 by reorganizing the instrument as shown in Figure 1. A second molybdenum catalyst was installed in what was originally the NO flow system of the instrument. Both catalysts are maintained in an oven where they are held at the same constant (350–400 °C) temperature. A 47-mm nylon filter in a Teflon filter holder was inserted just ahead of the Mb catalyst in the NO flow system. We have previously shown that the nylon filter quantitatively scrubs HNO_3 while passing NO and NO_2. The sample line orifice was moved to the front of the Teflon sample line so that most of the sample tubing is maintained under partial vacuum. A Teflon filter ahead of the orifice removes ambient particulate matter.

In operation, the sample gas is split after entering the instrument, part of the sample passing through a Mb catalyst and on to the reaction cell, the remainder passing first through the nylon filter and then through a second catalyst to the reaction cell. The former flow path produces a continuous signal which represents the total NO_x concentration of the sample, including HNO_3. The sample which passes through the nylon filter yields a signal which represents the concentration of total NO_x less HNO_3. The instrument electronics automatically subtract the two channels to generate a signal proportional to the concentration of nitric acid in the sample gas.

RESULTS AND DISCUSSION

Several criteria must be met if the modified chemiluminescence instrument is to serve as a gaseous nitric acid monitor. The catalytic converter must quantitatively reduce nitric acid to NO, the nylon filter must quantitatively remove nitric acid, and the filter must not remove other atmospheric species which yield a chemiluminescent response. Results which demonstrate that these three criteria are met are described below, followed by a discussion of instrument characteristics.

Response to Gaseous Nitric Acid. In order to test the response of the chemiluminescence monitor to gaseous nitric acid, low ppm concentrations of the acid were prepared in the Battelle–Columbus 17 m^3 smog chamber. Dry N_2 was saturated with gaseous nitric acid by bubbling through a HNO_3/H_2SO_4 mixture. After passing through a quartz fiber filter, the N_2 stream was then diluted in the smog chamber at 50% relative humidity. After dilution of the nitric acid, the chamber was found to be essentially particle-free by an electrical aerosol analyzer; all the nitric acid was in the gas phase. The resulting nitric acid concentration was simultaneously monitored with the chemiluminescence monitor and the Battelle microcoulometric nitric acid monitor described elsewhere (*1, 4*). The microcoulometric instrument was calibrated with ppm concentrations of both HCl and HNO_3. It has been validated by both a colorimetric method (*3*) and long path Fourier transform infrared spectroscopy (*4*).

The results of simultaneous measurements by the microcoulometric instrument and the chemiluminescence monitor are shown in Figure 2. The chemiluminescence monitor was calibrated prior to these experiments with a NBS NO_2 permeation tube. The agreement between the two instruments is quite good except at the highest concentration, where the operating range of the microcoulometer is exceeded (*9*). The agreement between the two monitoring techniques confirms the quantitative response of the chemiluminescence monitor to gaseous nitric acid. Studies recently conducted at the California Air Industrial Hygiene Laboratory (*10*) also demonstrate good agreement for nitric acid measurements among a chemiluminescence instrument, a coulometric

0003-2700/78/0350-1400$01.00/0

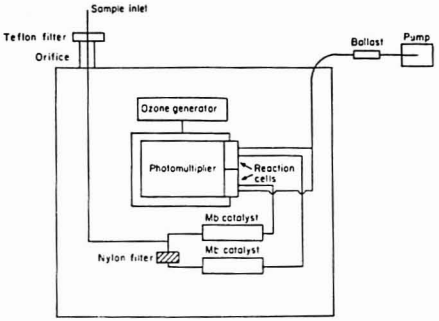

Figure 1. Schematic of chemiluminescent instrument modified for simultaneous NO_x/HNO_3 monitoring

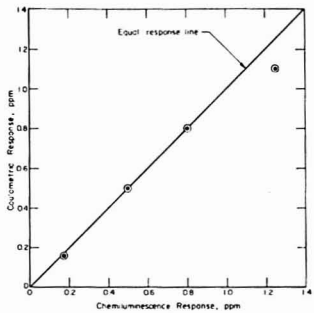

Figure 2. Coulometric vs. chemiluminescent response to gaseous nitric acid

monitor, and a wet chemical analysis method.

We have noticed a decay in the chemiluminescence response to nitric acid after long exposures to high (ppm) concentrations. The catalytic converter apparently loses efficiency under these conditions because of poisoning. However, a few hours of sampling clean air at an elevated catalyst temperature usually restores efficiency. The response also appears variable at high relative humidities (>80%). This seems to be due to adsorption/desorption effects within the instrument and sampling lines. Heating the sampling lines and placing the sample orifice as close to the sampling point as possible minimizes this phenomenon.

Removal of Nitric Acid by the Nylon Filter. The quantitative removal of gaseous nitric acid from air by nylon has been discussed elsewhere (*1–4*). Further confirmation of nitric acid scrubbing by nylon filters is presented in Figures 3 and 4. In both of these figures the solid line represents the total chemiluminescence signal ($NO_x + HNO_3$) after catalytic reduction; the dashed line represents the signal obtained when the sample passes through a nylon filter prior to the catalytic converter. The dashed line has been offset slightly in the figures so that it is distinguishable from the solid line.

In Figure 3, both channels of the monitor respond equally to NO_x in the chamber. Equal response is also evident after nitric acid is added to the chamber. When the nylon filter is inserted in the NO_x sample stream however, the response of the NO_x channel drops back to the original NO_x level in the chamber. This signifies quantitative removal of the nitric acid by the filter. After some loss of the nitric acid to the chamber walls, the filter was removed and the responses of both channels were again equivalent.

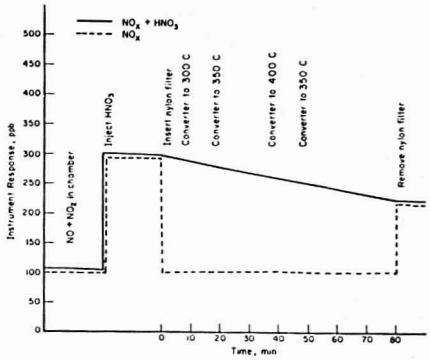

Figure 3. Chemiluminescence response under varying conditions

Table I. Effect of Nylon Filter on Chemiluminescence Response to NO and NO_2 (RH ~ 50%)

Gas concentration upstream of nylon filter	Concentration downstream of nylon filter
0.030 ppm NO	0.031 ppm
0.074 ppm NO	0.074 ppm
0.550 ppm NO	0.552 ppm
3.20 ppm NO	3.20 ppm
0.068 ppm NO_2	0.067 ppm
0.600 ppm NO_2	0.598 ppm
1.2 ppm NO_2	1.20 ppm
0.074 ppm NO, 0.068 ppm NO_2 mixture	0.142 ppm

The same effect is observed in the experiment represented by Figure 4. The responses of both channels of the monitor are equivalent for NO, NO_2, and a mixture of NO_2 and HNO_3. When the nylon filter is inserted in one channel however, the response of that channel falls back to the NO_2 concentration. When the filter is removed, the signals become equal once again.

The results of these experiments agree with our earlier work (*1, 4*) and confirm the quantitative removal of gaseous nitric acid from air by nylon filters.

Interferences. In order to interfere with nitric acid measurement by the modified chemiluminescence monitor, a substance must be reduced to NO by the catalytic converter and must be wholly or partially scrubbed by the nylon filter. Potentially significant interferences are NO, NO_2, and PAN. The concentration of gases such as N_2O_5, HONO, and $HOONO_2$ are not expected to reach high enough concentrations under normal atmospheric conditions to cause interference, even if they met the above criteria.

All three of the potentially interfering gases, NO, NO_2, and PAN yield a chemiluminescence response after passing through the catalytic converter. Therefore, these gases will interfere with nitric acid measurements if they are removed by the nylon filter. The removal of NO and NO_2 by nylon filters has been discussed in our earlier work (*1–4*). Nitric oxide is not affected by the nylon filter, even at high concentrations. This is confirmed in Figure 4, where no difference was observed between the signals of the filtered and unfiltered channels for 3.2 ppm NO. The results of some additional NO experiments are shown in Table I.

Table I also demonstrates that the nylon filter does not remove NO_2 at concentrations up to at least 1.2 ppm. Figure 4 shows an experiment with 1.2 ppm NO_2 at ~55% relative humidity. The presence or absence of the filter has no effect on the chemiluminescence signal. The data presented in Table

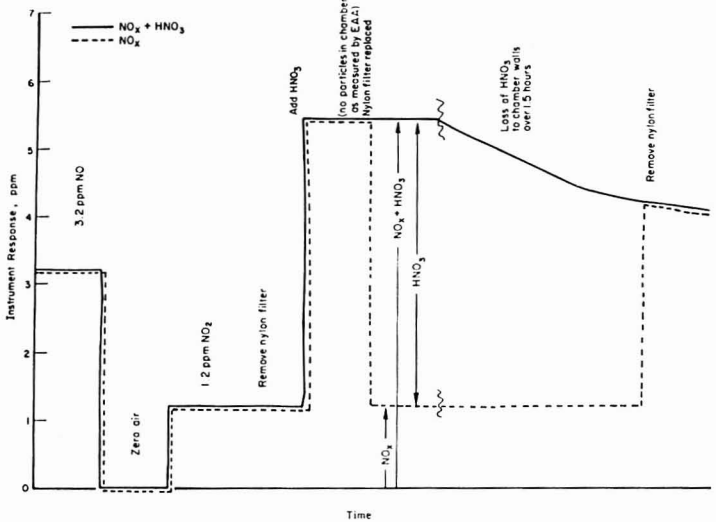

Figure 4. Chemiluminescence response

I and Figure 4 agree with our previous results and confirm that NO_2 is not removed by nylon filters (up to at least 1.2 ppm) and therefore does not interfere with nitric acid monitoring by the modified chemiluminescence monitor.

To determine whether PAN is removed from air by nylon filters, we conducted an experiment to measure PAN removal directly. PAN was generated in a 200-L Pyrex smog chamber by the photolysis of ethyl nitrite. An electron capture gas chromatograph was used to monitor PAN. Once the PAN concentration had stabilized, a known flow rate of chamber air was passed through a nylon filter and the PAN concentration monitored behind the filter. After an induction period, during which PAN is adsorbed by the filter, PAN breaks through the filter and the downstream concentration ultimately reaches the upstream concentration. A plot of downstream PAN concentration vs. time describes an "S" curve. After integration, the area above the curve up to the source concentration can be used along with the flow rate to compute the capacity of the filter to adsorb and remove PAN. The capacity of nylon filters is similar to Teflon filters and is extremely low. Our results indicate that only about 8 ng of PAN can be removed by the nylon filter. Other studies (*11*) have confirmed the lack of significant nitrate collection by nylon filters exposed to PAN.

Since neither NO nor NO_2 nor PAN are affected by the nylon filter employed in the chemiluminescence nitric acid monitor, none of these gases constitute an interference to nitric acid measurement.

Characteristics of the Chemiluminescence Nitric Acid Monitor. A number of important operating characteristics of the chemiluminescence monitor are discussed in the following paragraphs.

Conversion Temperature. One of the important variables affecting the operation of the modified chemiluminescence monitor is catalyst temperature. Figure 3 shows the variation in chemiluminescence output when the catalytic converter temperature is varied from 300 °C. The figure shows a steady loss of nitrogen compounds (due to dilution and wall losses of HNO_3) which is unaffected by converter temperature. Our studies suggest that the conversion of HNO_3 and NO_2 to NO is quantitative above 300 °C. In practice we operate our instrument at 350 °C, to provide a margin of safety.

Response Time. For many practical applications of the instrument described here, response time can be quite important. For example, the use of the instrument for airborne monitoring (the monitor has now been employed for both power plant and urban plume monitoring by aircraft) requires relatively rapid response in order to resolve spatial variations in NO_x and HNO_3 concentrations. We have determined the response time of the monitor by increasing the NO_x concentration in a step change while following the instrument output at a high recorder speed. With the instrument electronics set for a 5-s time constant (via an internal switch provided by the manufacturer), we observed 90% response to the step change in concentration in 14 s. While this response time is adequate for many applications, a more rapid response would be useful for certain types of studies (e.g., power plant plume traverses). Future work will concentrate on improving this response.

Noise. The instrumental "noise" of the output signal is a function of the time constant setting mentioned above. With a time constant of 10 s, we observe noise in the output signal equivalent to ±8 ppb NO_x. Using a time constant of 60 s, the noise drops to ±4 ppb. Chemiluminescence monitors are now being built with significantly lower noise levels. The minimum detectable concentration of these improved instruments should be on the order of tenths of a ppb.

Protection. A 5-μm Teflon filter in a Teflon filter holder at the inlet to the monitor has no effect on the response of the instrument to NO_x or HNO_3 and does not influence operating characteristics. In order to protect the sample orifice and other delicate components of the system, we recommend the use of such a prefilter.

LITERATURE CITED

(1) D. F. Miller and C. W. Spicer, "Measurement of Nitric Acid in Smog", *J. Air. Pollut. Control Assoc.*, **25**, 940 (1975).
(2) C. W. Spicer and D. F. Miller "Nitrogen Balance in Smog Chamber Studies", *J. Air Pollut. Control Assoc.*, **26**, 46 (1976).

(3) C. W. Spicer, "The Fate of Nitrogen Oxides in the Atmosphere", in *Adv. Environ. Sci. Technol.*, **7**, 163–261 (1977).
(4) C. W. Spicer, G. F. Ward, and B. J. Gay, Jr., "A Further Evaluation of Microcoulometry for Atmospheric Nitric Acid Monitoring", *Anal. Lett.*, **11** (1) (1978).
(5) C. W. Spicer, "Photochemical Atmospheric Pollutants Derived from Nitrogen Oxides", *Atm. Environ.*, **11**, 1089 (1977).
(6) C. W. Spicer, P. M. Schumacher, and D. F. Miller, "A Integrated Method for Sampling Atmospheric Nitric Acid", manuscript in preparation, January 1978.
(7) T. Okita, S. Morimoto, S. Izowa, and S. Kouno, "The Measurement of Gaseous and Particulate Nitrates in the Atmosphere, *Atm. Environ.*, **10**, 1085 (1976).
(8) A. L. Lazarus and B. W. Gandrud, "Progress Report on Distribution of Stratospheric Nitric Acid", *Proc. Third CIAP Conf.*, 161 (1974).
(9) Mast Development Co. product brochure, Mast Development Co., Davenport, Iowa, 1968.
(10) B. Appel and J. Tokiwa, AIHL, personal communication, January 1978.
(11) C. W. Spicer, P. M. Schumacher, J. A. Kouyoumjian, and D. W. Joseph, "The Collection and Analysis of Atmospheric Particulate Nitrate", Battelle–Columbus final report to EPA (Contract No. 68-02-2213), January 1978.

RECEIVED for review February 13, 1978. Accepted April 12, 1978.

Switchboard for Experimental and Computer Networking

Steven B. Schram and David H. Freeman*

Department of Chemistry, University of Maryland, College Park, Maryland 20742

The use of computer compatible equipment in analytical laboratories is becoming very prevalent. Laboratory experiments and computer components are usually coupled together using teletype-compatible communications links. This technique is limited if more than two devices are to be coupled in parallel. In that case, it is advantageous to connect them in a network that is conducive for full automation, so that data input, analysis, control, and output can be performed automatically. This process would tend to be viewed as data bus architecture in terms of computer engineering, while the logic of component interconnection is of principal concern to the flow of analytical data. When the latter becomes complicated, the use of switchboard networks become advantageous.

Such networks have been described in the analytical and engineering literature (*1–6*). For example, a recent article by Dessy (*7*) discusses many of the options that are available.

In this article, we will present one possible solution to the problem of connecting serial communications devices together in a versatile fashion. This is a real problem, and although this solution is not the only one possible (and indeed it may not be useful in some circumstances), this represents a simple, strictly mechanical approach that can be easily implemented by any interested party. The problem can be approached quite simply in the following way.

Teletype compatible devices send on one wire, and receive on another. The signals are encoded in current (20-mA current loop) or voltage (RS-232 in USA; CCITT in Europe) changes. Current devices appear less frequently in newer equipment, and these can be modified to the voltage format using simple transistor circuiting (*8, 9*). Voltage signals are easily networked provided that the transmission characteristics are standardized between all of the connected devices.

Standardization between devices must include the transmission rate (Baud rate) and the transmission language. The usual languages are ASCII (American Standard Code for Information Interchange), BAUDOT (similar to ASCII), or EBCDIC (Extended Binary Coded Decimal Interchange Code). After the devices are rate and code compatible, network interfacing can be achieved in a convenient way.

The most frequently encountered serial connector is the standardized 25-pin EIA-RS-232 interface (Cannon DP-25, M or F) as shown in Figure 1. Figure 2 diagrams the closed loop that is formed if this connector is used to link two devices. Note that the two devices can communicate only with each other. Although 25-pin connections are involved, it should be noted that only three of the connections are actually used.

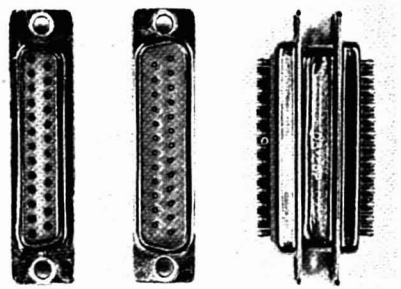

Figure 1. Picture of EIA-RS-232 interface plug

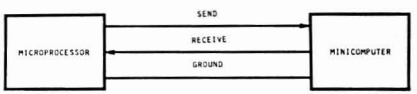

Figure 2. The standard connector allows two devices to communicate with each other

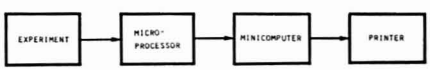

Figure 3. The modified connector allows a device to receive from one device, and transmit to another. The arrow (→) refers to the direction of signal transmission. The ground connection is not shown

It may be desirable to link several devices serially, as shown in Figure 3. However, this requires that the connector be modified to carry out this initial use of a network arrangement.

We have modified our connectors by attaching a mating plug that has been altered by shorting pins 5, 6, 8, and 20 together. This process provides pins 5, 6, and 8 (clear to send; data set ready; carrier detect) with a positive voltage from pin 20 (data terminal "ready"); this is normally provided by the conventional connection. Information flow depends on two other data pins plus a ground connection pin: pin 2 is used for received data; pin 3 for transmitted data, and pin 7 is the ground. Broad flexibility can now be achieved if wires from these three pins are brought from each mating plug, one for

0003-2700/78/0350-1403$01.00/0

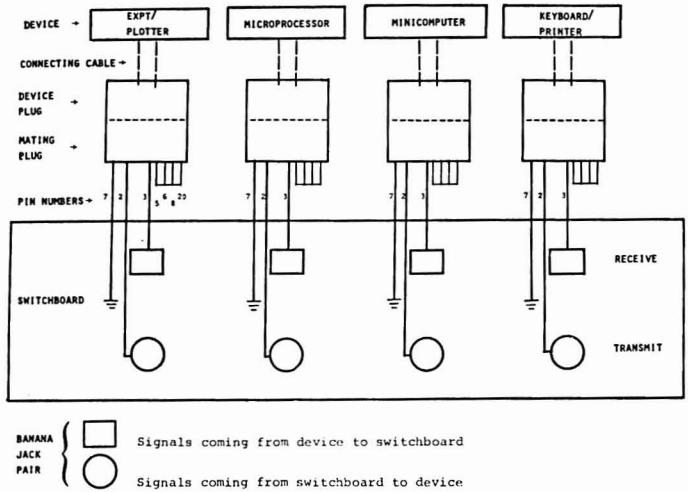

Figure 4. Plug from each device is connected to a mating plug. Pins 5, 6, 8, and 20 are shorted on the mating plug. Pins 2 and 3 are communication lines. Pin 7 is the common ground

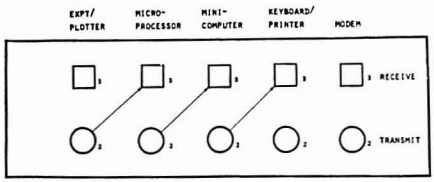

Figure 5. The lines signify jumper cables. The direction of data is indicated by the arrow. Data comes from the experiment, to the microprocessor, from the microprocessor to the minicomputer, and from the minicomputer to the printer

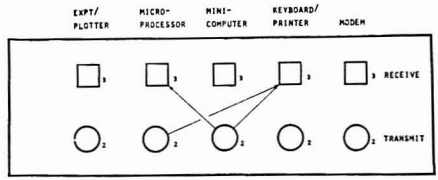

Figure 6. The printer sequentially monitors instructions sent by the minicomputer to the microprocessor, and the microprocessor's response to the instruction

each device, to an interface switchboard.

In the switchboard, all grounds from pins 7 are tied together. Paired input–output sets of banana jack receptacles, one pair for each device, are located on the switchboard panel. Lines from pins 2 connect to one side of the receptacles while lines from pins 3 connect to the other side (Figure 4). A short jumper cable can now be used to carry an input signal to one or more of the desired output terminals. To illustrate this, the configuration in Figure 3 is obtained using the switchboard as shown in Figure 5.

Other configurations are easily visualized. Figure 6 shows how a Texas Instruments printer can sequentially monitor the output of two different devices. Note that no buffering or handshaking capability is included, which means that if there is a lack of suitable control or priority, then there could be a mixture of data and subsequent jumble of output. In this case, our Wang 2200 minicomputer output is sent simultaneously to our Technico 9900 microprocessor and printer. Since the microprocessor does not respond until the entire instruction is received (and hence completely printed), the response to the printer is not mixed, and is printed separate from the original instruction. Thus, provided that only one signal, at one time, is sent to the printer, any number of output devices can be monitored. Since this operation implies a logical "or", all devices must have a reasonably high output impedance (most do) for this to work as described. Any

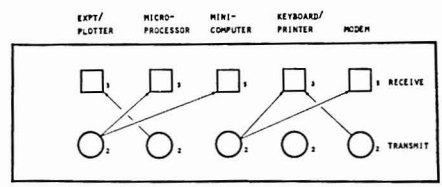

Figure 7. Experiment data are sent to the microprocessor and minicomputer. The microprocessor sends averaged data to a plotter. The minicomputer sends reduced data to a modem and a printer. The modem sends it to another computer. The returned data is received by the modem and also sent to the printer

other RS-232 serially interfaced output device, (plotter, oscilloscope) could also be used instead of the printer.

Various combinations of signal transfers can be achieved. We have used the switchboard to provide the configuration shown in Figure 7.

This configuration is not possible with an unmodified connector. Use of the modification with switchboard provides both reliability and flexibility. Since all signals are present at one location, design changes are easy to adapt. New configurations are easy to test and implement. This represents a great savings in time, and offers the user expanded versatility with regard to signal processing.

LITERATURE CITED

(1) R. E. Dessy and J. A. Titus, *Anal. Chem.*, **45**, 124A (1973).
(2) T. J. Williams, *Chimia*, **27**, 669 (1973).
(3) R. E. Dessy and J. A. Titus, *Anal. Chem.*, **46**, 291A (1974).
(4) P. Lykos, Ed., ACS Symposium Series, Vol. 19 (1975).
(5) J. M. McQuillan and D. C. Walden, *Comput. Networks*, **1** (5) 1 (1977).
(6) W. Greene and U. W. Pooch, *Computer*, **10** (11) 12 (1977).
(7) R. E. Dessy and J. A. Titus, *Anal. Chem.*, **49**, 1100A (1977).
(8) H. V. Malmstadt, C. G. Enke, and S. R. Crouch, "Electronic Measurements for Scientists", W. A. Benjamin Inc., Menlo Park, Calif., 1974, pp 226–262.
(9) D. G. Larson, P. R. Rony, and J. A. Titus, *Am. Lab.*, **7** (6), 78 (1975).

RECEIVED for review February 27, 1978. Accepted April 24, 1978.

Variable-Temperature Cryogenic Trap for the Separation of Gas Mixtures

David J. Des Marais

Extraterrestrial Biology Division, Ames Research Center, NASA, Moffett Field, California 94035

Cryogenic traps offer a clean, simple, and relatively rapid means for resolving simple gas mixtures. This report describes a continuously variable-temperature cold trap which can both purify vacuum-line combustion products for subsequent stable isotopic analysis and isolate the methane and ethane constituents of natural gases. Murakami and Okamoto (*1*), Crosmer et al. (2), and Stump and Frazer (*3*) have previously described variable-temperature cold trap designs for specific applications. I feel the trap described here embodies all the important capabilities of these former designs, yet is generally easier and less expensive to build and operate.

EXPERIMENTAL

Figure 1 is a schematic drawing of the cold trap. The trap is U-shaped and consists of two 0.635-cm (0.25-in.) diameter by 8-cm long pieces of stainless steel tubing (C) welded to a 30-cm segment of Cajon flexible tubing (G) (part no. 321-4-X-12, Cajon Company, 32550 Old South Miles Road, Cleveland, Ohio 44139). A 20-cm long, welded stainless steel canister (D) surrounds the lower portion of the trap, generating a 3-mm annular air space between the canister and the flexible tubing. Asbestos-insulated 25-gauge chromel A resistance wire (E) is wrapped around the flexible tubing and brazed to Fiberglas-insulated copper wires which emerge from the enclosure via a 0.635-cm (0.25-in.) stainless steel tube (F) and a vacuum epoxy feedthrough (B). A 30-gauge chromel–alumel thermocouple (J) is brazed to the bottom of the U-trap, and the wire leads also emerge from the housing via the steel tube (F) and the feedthrough (B). During use, the canister is almost totally immersed in liquid nitrogen. A rubber stopper (A) is inserted in the aperture near the vacuum feedthrough (B) to prevent the condensation of liquid oxygen inside the enclosure. The stopper is preferred to a more permanent closure for reasons of safety. Should a leak permit condensation to occur inside the canister, the stoppered aperture would serve as a pressure release valve for the confined gas.

In operation, a gas mixture to be resolved enters the evacuated U-trap at room temperature. The trap canister is then almost totally immersed in a liquid-nitrogen bath, cooling the U-trap as heat flows across the 3-mm annular air space between the flexible tubing and the canister wall. As the trap cools, the gas mixture components condense sequentially according to their relative vapor pressures. As Table I shows, about 12 min is required for the bottom of the U-trap to attain liquid-nitrogen temperature. Measurements made using traps with additional thermocouples located at positions G and H (Figure 1) describe a thermal gradient along the length of the trap. This gradient reflects the steady-state balance between heat flow from the flexible tube to the canister, and heat flow into the tube from the warmer upper portions of the trap assembly. As discussed by Crosmer et al. (2), such a thermal gradient promotes the fractionation of gas mixture components. After the bottom of the trap (J) has attained liquid-nitrogen temperature, the passage of current through the resistance wire (E) warms the U-trap and permits the distillation of successive gas components at trap temperatures optimal for their resolution. Table I lists the power requirements as a function of temperature for a properly constructed trap. The consumption rate of liquid nitrogen is typically low, even at "warmer" trap temperatures. For example, when trap thermocouple J is at -110 °C, 8 W of heater power is being balanced by a liquid-nitrogen evaporation rate of approximately 4 mL/min.

Table I. Variable-Temperature Trap Thermal Behavior and Power Consumption

power input (W)	temp. (°C) at location G	H	J	time (min) after LN_2 immersion
0	25	25	25	0
0	*a*	*a*	−50	1
0	*a*	*a*	−108	2
0	*a*	*a*	−160	4
0	*a*	*a*	−190	8
0	−163	−190	−195	12
1	−153	−167	−175	*b*
2	−137	−153	−165	*b*
4	−103	−125	−145	*b*
8	−40	−78	−110	*b*
12	+9	−38	−75	*b*

[a] Not measured. [b] The trap usually requires about 1 min to increase its temperature 30 °C and attain a new steady-state thermal profile.

RESULTS AND DISCUSSION

The ability of the variable-temperature trap to separate gas mixtures is shown in Table II. The first mixture represents typical vacuum-line combustion products of geochemical samples such as rocks or marine sediments. Separation of the individual gases of this mixture by the cold trap, facilitates the measurement of their abundance and stable isotopic compositions. CO_2 and SO_2 aliquots of known isotopic composition were used in this demonstration. The gas fractions distilled from the trap were quantified using a mercury manometer, and subsequently analyzed for their purity and isotopic composition using a Nuclide 6-60 RMS mass spectrometer. The gas mixture was condensed in the variable-temperature trap in the manner described earlier. The trap was then warmed to −143 °C and the volatilized CO_2 was distilled for 5 min from the variable-temperature trap to a liquid-nitrogen trap incorporated into the mercury manometer. Despite the substantially greater abundance of SO_2 in the original gas mixture, the CO_2 recovered by this distillation was more than 99% pure, and had sustained little isotopic fractionation. The trap was warmed to −85 °C and the SO_2 was distilled for 10 min into the mercury manometer. The SO_2 fraction also exhibited a very high purity and had sustained negligible isotopic fractionation. The variable-temperature trap was then warmed to room temperature to recover the H_2O. The somewhat lower recovery achieved

Table II. Variable-Temperature Trap Separation of Gas Mixtures

	initial mixture	fraction 1	fraction 2	fraction 3
combustion products				
temp. at pt. J, °C		−143	−85	24
CO_2, μmol	6.4 ± 0.2[c]	6.4 ± 0.2	0.2 ± 0.04	0 ± 0.01
$\delta^{13}C$, ‰[a]	0	−0.2 ± 0.2	*d*	*d*
SO_2, μmol	59 ± 1	0.04 ± 0.01	58 ± 1	0.5 ± 0.05
$\delta^{34}S$, ‰[b]	0	*d*	+0.1 ± 0.2	*d*
H_2O, μmol	16 ± 1	*d*	*d*	14 ± 1
natural gas				
temp. at pt. J, °C		−195	−172	25
CH_4, μmol	228 ± 5	228 ± 5	0.16 ± 0.01	0.06 ± 0.01
C_2H_6, μmol	24 ± 1	0.19 ± 0.01	24 ± 1	0.10 ± 0.01
C_3H_8, μmol	9.1 ± 0.4	0.12 ± 0.01	0.26 ± 0.01	8.8 ± 0.4
$>C_3H_8$, μmol	1.9 ± 0.1	0.15 ± 0.01	trace	1.7 ± 0.1

[a] $\delta^{13}C,‰ = [(^{13}C/^{12}C)_{sample}/(^{13}C/^{12}C)_{reference} - 1]1000$, where $(^{13}C/^{12}C)_{reference}$ is taken to be that of the CO_2 in the initial mixture. [b] Analogous to $\delta^{13}C$ in *a*. [c] Uncertainties expressed as one standard deviation. [d] Not measured.

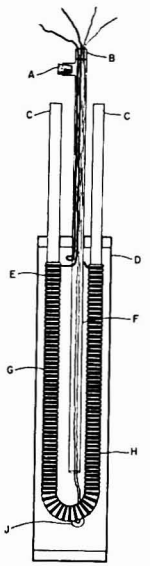

Figure 1. Schematic drawing of the variable-temperature cryogenic trap

probably reflects adsorption of this gas onto the unheated glass surfaces of the vacuum line.

Table II also shows the results of an attempt to separate a natural gas sample. The gas fractions were analyzed using a Hewlett-Packard Model 5830A gas chromatograph fitted with a flame-ionization detector. A 50-m glass capillary column was coated with *n*-octanol and temperature programmed from 10 to 100 °C at 10°/min. As the trap cooled, a Toepler pump circulated the gas mixture through the cold trap. After thermocouple J attained liquid-nitrogen temperature, the uncondensed gas was removed from the vacuum line and analyzed. This gas was found to be almost pure methane. The gas fraction harvested from the trap at −172 °C was 98% ethane. The fraction obtained when the trap was warmed to ambient temperature constituted 95% by volume of the propane and higher molecular weight components in the original gas mixture. These data show that the variable-temperature trap could facilitate the isolation and isotopic analysis of relatively pure methane, ethane, and higher molecular weight fractions of natural gas. Also, because such a procedure could remove the large methane and ethane components of the gas sample, the gas chromatographic analysis of the higher molecular weight residue would achieve a higher sensitivity for minor components in this residue.

The present variable-temperature cold trap design compares favorably with other gas separation techniques in terms of expense, simplicity, and versatility. The trap can be fabricated from easily obtainable materials at a cost of less than $250. Although a sophisticated temperature-control system could be interfaced with the cold trap, a 20-W power supply and a thermocouple readout device are sufficient for its operation. A typical three-component gas mixture can be separated in about 40 min. The trap can handle 100 μmol amounts of gases such as SO_2 and H_2O, a feat well beyond the capabilities of conventional gas chromatographs. Therefore, although the cold trap resolution is substantially lower than those of gas chromatographic systems, the trap is still quite useful for a variety of useful applications requiring the separation of simple gas mixtures.

ACKNOWLEDGMENT

The encouragement of I. R. Kaplan is gratefully acknowledged.

LITERATURE CITED

(1) Y. Murakami and H. Okamoto, "Transactions of the Tenth National Vacuum Symposium of the American Vacuum Society", 1963, Macmillan, New York, N.Y., 1963, p 93.
(2) W. E. Crosmer, N. C. Thomas, P. H. S. Tsang, and R. J. Duckett, *Rev. Sci. Instrum.*, **44** (7), 837 (1973).
(3) R. K. Stump and J. W. Frazer, Lawrence Livermore Laboratory, Rept. UCRL-50318 (1967).

RECEIVED for review March 24, 1978. Accepted May 8, 1978. This work was supported by NASA Grant No. NGR 05-007-221.

Potentiometric Determination of Phenoxyalkylcarboxylic Acids in Pesticides

N. Ciocan

Central Laboratory for Pesticides Control, Sos. Afumati 11, Bucharest 72964, Romania

G. E. Balulescu*

National Institute of Chemistry, Spl. Independentei 202, Bucharest 77208, Romania

It is well known that attachment of $-OCH_2COOH$, $-OCH(CH_3)COOH$, and $-O(CH_2)_3COOH$ groups to aromatic rings leads to an important class of herbicides.

The repeated extractions of these herbicides with diethyl ether in acid medium, followed by the gravimetric and volumetric analyses, constitute a method used for the determination of phenoxyalkylcarboxylic acids in pesticide formulations.

This method is recommended by FAO and CIPAC and used by all producers and users in spite of its disadvantages, such as lack of specificity, reduced sensitivity, consumation of a great quantity of ether, etc. The method and its various modifications (*1–4*) necessitate the use of macrosamples (10–80 g) and determinations of equivalent weights and melting points to prove the purity of the ethered extract. The analysis of pesticides that contain mixtures of phenoxyalkylcarboxylic acids with other extractable compounds in diethyl ether becomes even more complicated. We propose below a method that eliminates the disadvantages mentioned above.

EXPERIMENTAL

Apparatus. The potential was measured vs. a double-junction Orion electrode (No. 90-02-00) with potassium nitrate solution in the other compartment using an Orion Research Digital Ionalyzer 801 A. The solutions were magnetically stirred.

Membrane Electrode. As indicator electrode, a Hg_2^{2+} sensitive extractive electrode was used. This electrode has been described elsewhere (*5, 6*).

Reagents. Analytical grade reagents were used, supplied by Chemapol: 2,4-dichlorophenoxyacetic acid (2,4-D), Bayer: 4-chloro-2-methylphenoxyacetic acid (MCPA), Serva: 2,4,5-trichlorophenoxyacetic acid (2,4,5-T), VEB Electrochemisches Kombinat Bitterfeld: dimethylamine salt of 2,4-dichlorophenoxyacetic acid. All other reagents were from Reactivul Bucharest.

The $Hg_2(NO_3)_2$ solution, ~0.1 N, was prepared by grinding mercurous nitrate with metallic mercury. Then 20 mL of 2 N HNO_3 and 500 mL of distilled water were added. The solution was filtered and diluted to 1000 mL with distilled water. Metallic mercury was added as a preservative.

Procedure. The following procedure was used for all determinations: weigh precisely *A* g of substance corresponding to 0.1–0.8 g of phenoxyalkylcarboxylic acid. Add 10–20 mL of methyl alcohol and 40–60 mL of distilled water. Neutralize with 0.1 N HNO_3 vs. methyl red (addition of excess acid leads to precipitation of organic acid). A solution of 0.1 N $Hg_2(NO_3)_2$ is added. The amount added depends on the amount of phenoxyacetic acid presumed to be in the sample. An excess of about 1–30 mL should be present. The less excess present, the more rapid the washing of the precipitate mentioned below. Leave the sample for 10 minutes with occasional shaking. Filter through wide pore filter paper and wash the precipitate with distilled water until complete elimination of Hg_2^{2+} (the wash water does not react with KBr or diphenylcarbazone). The precipitate is transferred quantitatively with 100–250 mL of 1–2 N HNO_3 into the beaker in which the

Table I. Analysis of 2-Methyl-4-chlorophenoxyacetic Acid (MCPA), 2,4-Dichlorophenoxyacetic Acid (2,4-D), 2,4,5-Trichlorophenoxyacetic Acid (2,4,5-T) and Dimethylamine Salt of 2,4-Dichlorophenoxyacetic Acid (DMA)

Sample No.	MCPA, g		2,4-D, g		DMA, g		2,4,5-T, g	
	Taken	Found	Taken	Found	Taken	Found	Taken	Found
1	0.1000	0.0998	0.1105	0.1100	0.1250	0.1247	0.1010	0.1013
2	0.1404	0.1408	0.1547	0.1543	0.1750	0.1754	0.2222	0.2220
3	0.1805	0.1800	0.1989	0.1987	0.2250	0.2256	0.1414	0.1418
4	0.2206	0.2206	0.2431	0.2433	0.2750	0.2750	0.2805	0.2811
5	0.2610	0.2607	0.2873	0.2871	0.3250	0.3257	0.2930	0.2925

Table II. Some of the Herbicides Analyzed by Potentiometric Titration (For Each Product Five Analyses Were Performed)

No.	Commercial name	State	Taken, g	Active ingredients	Results
1	DMA[a]	Liquid	0.35–1.10	33% dimethylamine salt of 2,4-dichlorophenoxyacetic acid	29.5 ± 0.1
2	Dikotex 40[b]	Liquid	0.30–1.20	40% ammonium salt of 2-methyl-4-chlorophenoxyacetic acid	37.2 ± 0.2
3	Butyrac 175[c]	Liquid	0.50–1.90	23% dimethylamine salt of 4-(2,4-dichlorophenoxy)butyric acid	23.1 ± 0.1
4	Kuron[d]	Solid	0.30–0.80	45% 2-(2,4,5-trichlorophenoxy)-propionic acid	45.0 ± 0.1
5	Banvel M[e]	Liquid	0.40–1.00	25% 2-methyl-4-chlorophenoxyacetic acid, 2% 3,6-dichloro-o-anisinic acid	24.8 ± 0.15
6	Aniten M[f]	Liquid	0.40–1.20	250 g/L 2-methyl-4-chlorophenoxyacetic acid, 80 g/L 9-hydroxyfluoren-9-carboxylic acid	250 ± 1.5
7	DM 68[g]	Liquid	0.30–1.00	25% (4-chloro-2-methylphenoxy)-2-propionic acid, 13.5% 2,4-dinitro-6-*tert*-butyl phenol	25.0 ± 0.1

[a] Romanian product; [b] Czechoslovakian product; [c] Amchem, USA; [d] Dow-Chemical, USA; [e] Chemie Linz, Austria; [f] Cela Merck, W. Germany; [g] Pepro, France.

0003-2700/78/0350-1407$01.00/0

precipitation was done. Titrate potentiometrically with B mL of 0.1 N KBr standard solution. The phenoxyalkylcarboxylic acid content with the molecular weight, mol wt, is given by:

$$\% \text{ Acid} = \frac{\text{mol wt} \cdot B}{100A}$$

RESULTS AND DISCUSSION

The method is based on the fact that phenoxyalkylcarboxylic acids react with Hg_2^{2+} giving insoluble precipitates, $(ArOCOO)_2Hg_2$.

The determination of mercurous mercury contained in the precipitate leads to the evaluation of the concentration of phenoxyalkylcarboxylic acids in the sample.

The titration curve allows a very accurate localization of the equivalence point, with potential jumps exceeding 150 mV (Figure 1). The method is particularly precise. As an illustration, Table I shows the results obtained with analytical standards. The method can be extended to the analysis of samples with a minimum content of 0.01 g of phenoxyalkylcarboxylic acid using 0.01 N KBr solutions as titrant. The method is applicable to the determination of phenoxyalkylcarboxylic acids in all commercial products.

Table II presents some products analyzed using the method previously described as well as the analytical results.

Halides, pseudohalides, sulfides, carbamates, amines, oxidants and reductants, different cations, etc. do not interfere.

Organic acids that give precipitates with Hg_2^{2+} in slightly acidic medium (phthalic, oxalic) are not found in herbicides.

Because of its selectivity, the method is applicable to the analysis of a wide range of herbicides containing phenoxyalkylcarboxylic acids alone or in a mixture with other acidic organic compounds extractable in diethyl ether. If the acid group is esterified, it becomes necessary to hydrolyze it beforehand with hydroxides (*1–4*).

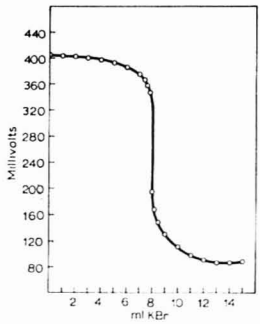

Figure 1. Titration curve of mercurous 2,4-dichlorophenoxyacetate in 250 mL of 2 N HNO_3 with 0.1 N KBr

Because of the performances of the method in which the precision, selectivity, and rapidity is concerned, it has been used by us to establish the quality of all commercial products containing phenoxyalkylcarboxylic acids.

LITERATURE CITED

(1) *FAO Plant Prot. Bull.*, **11**, No. 2–5, 1963.
(2) "CIPAC Handbook", G. R. Raw, Ed., Vol. I, "Analysis of Technical and Formulated Pesticides", 1970.
(3) "Pesticides Plant Growth Regulators and Food Additives", Vol. IV, V, Gunter Zweig, Ed., Academic Press, New York, N.Y., 1967.
(4) The Dow Chemical Company, Analytical Method No. 20959, 1974.
(5) N. Ciocan, Rom. Patent 81211 (1975).
(6) G. E. Baiulescu and N. Ciocan, *Talanta*, **24**, 37 (1977).

RECEIVED for review November 23, 1977. Accepted April 20, 1978.

Author Index

Future Articles

Chlorinated Benzyl Phenyl Ethers: A Possible Interference in the Determination of Chlorinated Dibenzo-*p*-dioxin in 2,4,5-Trichlorophenol and Its Derivatives

W. W. Blaser, L. A. Shadoff, and C. W. Kocher

Simultaneous Determination of Arsenic, Antimony, Cadmium, Chromium, Copper, and Selenium in Environmental Material by Radiochemical Neutron Activation Analysis

M. Gallorini, R. R. Greenberg, and T. E. Gills

Influence of the Instrumental Contributions on the Apparent Column Efficiency in High Speed Gas Chromatography

G. Gaspar, R. Annino, C. Vidal-Madjar, and G. Guiochon

Determination of Trace Elements on Small Geological Samples Fused in Lithiumtetraborate with X-ray Fluorescence Spectrometry

E. Jagoutz and C. Palme

Titration of Diprotic Acids in Alcohols and Intramolecular Hydrogen Bonding in Monoanions with Emphasis on Isopropanol and *tert*-Butanol

I. M. Kolthoff and M. K. Chantooni, Jr.

Isotope-Ratio-Monitoring Gas Chromatography–Mass Spectrometry

D. E. Matthews and J. M. Hayes

Isolation of Polycyclic Organic Compounds by Solvent Extraction with Dimethyl Sulfoxide

D. F. S. Natusch and B. A. Tomkins

Radiochemical Determination of Protactinium-231 in Environmental and Biological Materials

C. W. Sill

Specific Enzyme Electrode for Determination of Lysine in Grains and Foodstuffs

C. White and G. G. Guilbault

Mass Discrimination Effects in a Quadrupole Mass Spectrometer

K. V. Wood, A. H. Grange, and J. W. Taylor

Statistical Analysis of Titration Data

L. M. Schwartz and R. I. Gelb

The only rotary evaporator with an air hose instead of an electrical cord.

The explosion-proof Rotavapor 115EX is Büchi/Brinkmann's innovative solution to the hazard posed by sparking electrical motors when working with highly-volatile materials.

The Rotavapor 115EX has no electrical components whatsoever. Instead, its high-torque, variable speed motor is powered by compressed air. Simply connect the 115EX to any air source of 20-100psi and evaporate in safety at speeds from 15 to 270 rpm. Like the electrically-driven Büchi/Brinkmann standard models, the 115EX comes equipped with 1 liter evaporating and receiving flasks and is available with V-stand, quick-action jack, heating bath and a wide selection of other accessories.

Büchi/Brinkmann Rotary Evaporators are unsurpassed in versatility, durability, and safety of operation. In addition to the 115EX, there are eleven electrically-powered models to meet every concentrating need, from 5ml to 50 liters or more (Pilot Plant models). Our new brochure describes them all. Just write: Büchi Division, Brinkmann Instruments, Inc., Cantiague Road, Westbury, N.Y. 11590. In Canada: 50 Galaxy Blvd., Rexdale, Ont. M9W 4Y5.

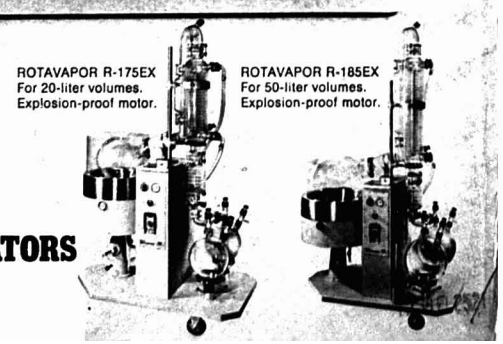

ROTAVAPOR R-175EX
For 20-liter volumes.
Explosion-proof motor.

ROTAVAPOR R-185EX
For 50-liter volumes.
Explosion-proof motor.

Büchi/Brinkmann
EXPLOSION-PROOF EVAPORATORS

CIRCLE 23 ON READER SERVICE CARD